STUDIES ON SURFACTANT-POLYMER INTERACTION IN PRESENCE OF DIFFERENT ADDITIVES

THESIS SUBMITTED IN FULFILLMENT OF

REQUIREMENTS FOR THE DEGREE OF

DOCTOR OF PHILOSOPHY (SCIENCE)

OF

JADAVPUR UNIVERSITY, INDIA

by

BIPIN BIHARI MONDAL, M.Sc.

2025

Department of Chemistry

Jadavpur University

Kolkata-700032

India

Prof. Soumen Ghosh, M. Sc., Ph. D.
Professor of Chemistry & Co-ordinator,
Centre for Surface Science
Department of Chemistry, **Jadavpur University**
Kolkata – 700 032, West Bengal, India
Awards of Prof. B. N. Ghosh from ICS, Dr. B. C. Deb from ISCA, Bronze Medal from CRSI, Visiting Chair Professor of St. F. X. University, Canada &
Selected as Top 2% World Ranking Scientist in Chemical Physics by Scientists of Stanford University, USA.

Phone : +91-33-2457 2503
Fax : 91-33-2414 4266
Mob - 9432 075 363
E-Mail – gsoumen17@yahoo.co.in/
soumen.ghosh@jadavpuruniversity.in

CERTIFICATE FROM THE SUPERVISOR

This is to certify that the thesis entitled **"STUDIES ON SURFACTANT-POLYMER INTERACTION IN PRESENCE OF DIFFERENT ADDITIVES"** submitted by **Sri. Bipin Bihari Mondal,** who got his name registered on 14.08.2019 for the award of **Ph.D. (Science) degree** of **Jadavpur University**, is absolutely based upon his own work under the supervision of **Prof. Soumen Ghosh** and that neither this thesis nor any part of it has been submitted for any degree/diploma or any other academic award anywhere before.

Soumen Ghosh. 28.08.25

Soumen Ghosh
Centre of Surface Science
Department of Chemistry
Jadavpur University
Kolkata-700032

Prof. Soumen Ghosh
Department of Chemistry
Jadavpur University
Kolkata-700 032, W.B., India

“Do not pray for an easy life; pray for the strength to endure a difficult one.”

Bruce Lee (1940-1973)

This thesis is dedicated, with deepest love and gratitude,
to those whose presence, guidance, and affection have shaped my life and journey.

To my late grandfather, EK KARI MONDAL (Dadu), whose wisdom and values continue to illuminate my path,
and to my grandmother, SULEKHA MONDAL (Thakumoni), whose patience and strength inspire me every day.

To my late maternal uncle, ATUL MONDAL (Boro mama), whose memory remains a source of encouragement.

To my father, BADRI BISHAL MONDAL (Baba), and my mother, SOVANA MONDAL (Ma), whose unconditional love, sacrifice, and blessings sustain me always.

To my uncles, SHYAMAL MONDAL (Mejho kaku) and AMAL KUMAR MONDAL (Choto kaku),
and my aunts, Thakurani Mondal and Kanchan Mondal, for their constant affection and support.

To my brothers—BIJAN BIHARI MONDAL (Dada), SANTU MONDAL (Dada), APURBA MONDAL (Vai), and ARPAN MONDAL (Vai)—for standing by me with care and encouragement.

To my nephew, BIHAN MONDAL (Vaipo), and my nieces, SRIJA MONDAL (Vaiji) and ADRIJA MONDAL (Vaiji), whose laughter and innocence bring light and joy to our lives.

Each of you has, in your own way, strengthened me and enriched my journey.

It is to you that I lovingly dedicate this work.

DECLARATION

I hereby declared that the work incorporated in the present dissertation was carried out by me at the centre for surface science, Department of Chemistry, Jadavpur University, Kolkata-700032, India. The entire work or any part of it has never been submitted before for any prize or degree anywhere.

Bipin Bihari Mondal 28.08.2025

(BIPIN BIHARI MONDAL)

ACKNOWLEDGEMENT

With deep gratitude, I acknowledge the invaluable support and contributions of those who have played a pivotal role in the successful completion of this dissertation, ***"Studies on Surfactant-Polymer Interaction in the Presence of Different Additives,"*** undertaken at the Centre for Surface Science, Department of Chemistry, Jadavpur University, Kolkata, India.

I am deeply thankful to Prof. Dr. Soumen Ghosh, Department of Chemistry, Jadavpur University, for his expert guidance, continuous support, and encouragement, which have been vital in the successful execution of this research.

My deepest gratitude to Prof. Dr. Kajal Krishna Rajak, Head of the Department of Chemistry, Jadavpur University, for his generous support in granting access to key research facilities and resources, which were vital to the success of this work.

I wholeheartedly acknowledge the unwavering academic guidance and intellectual rigor imparted by the esteemed faculty of the Department of Chemistry at Jadavpur University, alongside the administrative efficiency demonstrated by the university administration.

A sincere thank you to Dr. Rajesh Banik, along with other colleagues—Mr. Sumanta Bandyopadhyay, Mrs. Sudipta Chakraborty, Mrs. Tanaya Saha, Mr. Raju Sardar, Mr. Rabindranath Pal, and Dr. Jayabrata Maity, for their technical excellence, collaborative spirit, and encouragement throughout this study.

I am truly thankful to the Council of Scientific and Industrial Research (CSIR), Government of India, for the financial backing that made this research endeavor possible.

My heartfelt gratitude goes to my parents and family members for their constant love, encouragement, and sacrifices throughout my academic path.

Center for Surface Science
Department of Chemistry
Jadavpur University
Kolkata-700032
India

Bipin Bihari Mondal
28.08.2025

(Bipin Bihari Mondal)

PREFACE

Polymers constitute a vast class of macromolecular materials composed of numerous repeating monomeric units, intricately linked to form extended molecular architectures. Their vast structural diversity and distinct physicochemical properties render them indispensable across a multitude of technical, pharmaceutical, biomedical, and industrial applications. These macromolecules exhibit profound interactions with surfactants, a phenomenon of paramount significance in diverse domains such as colloidal stabilization, controlled drug delivery, interfacial science, formulation chemistry, and nanostructured material design.

To optimize formulations for advanced functional applications, a variety of surfactant classes—including cationic, anionic, nonionic, and gemini surfactants—can be employed in conjunction with distinct polymeric systems. The interaction between polymers and surfactants induces conformational and configurational modulations in the polymeric backbone, thereby influencing its thermodynamic stability, enthalpic and entropic contributions, self-assembly behaviour, interfacial activity, and microenvironmental polarity in the presence of amphiphilic aggregates.

These intricate molecular interactions can be elucidated through a suite of sophisticated analytical methodologies, including tensiometry, viscometry, conductometric analysis, isothermal titration calorimetry (ITC), fluorescence spectroscopy, and high-resolution electron microscopy techniques such as scanning electron microscopy (SEM) and transmission electron microscopy (TEM). Furthermore, the modulation of interaction dynamics by external physicochemical parameters—including pH, ionic strength, solvent polarity, thermal conditions, and electrolyte concentration—provides deeper mechanistic insights into polymer-surfactant complexation, paving the way for precision-engineered functional materials.

.

INTRODUCTION

Surfactants

A surfactant is a substance that reduces the surface tension of water and/or the interfacial tension between water and oil, causing it to accumulate at the liquid/vapor and liquid/liquid (oil/water) interfaces. Surfactants deliver exceptional benefits, significantly improving the efficiency and quality of textile wet processing. The chemical interactions between fibres and water are crucial, frequently determining the effectiveness or inefficacy of the process. The term "surfactant" can also refer to substances that are only slightly soluble, but reduce a liquid's surface tension by spreading naturally across its interface.

A soap is a surface-active agent made from the salt of a naturally occurring long-chain fatty acid, either saturated or unsaturated. A detergent is a blend of one or more surfactants, typically of synthetic origin, formulated to deliver effective cleaning performance. A syndet [1] is a detergent composed entirely of synthetic ingredients. An emulsifier [2], typically a surfactant, helps to form or stabilize an emulsion in small amounts by reducing the tendency for particle clustering and droplet fusion, thereby enhancing its colloidal stability. A foaming agent [3] is a surfactant that in small quantities, facilitates foam formation and improves its stability by reducing bubble coalescence.

Surfactants [4-7] are amphiphiles that feature both polar and nonpolar regions within a single molecule, imparting hydrophobic (water-repelling) and hydrophilic (water-attracting) characteristics. These molecules typically have a hydrophobic "tail" and a hydrophilic "head." Such inherent properties give rise to significant behaviour in terms of solubility and dispersion, depending on concentration in aqueous solutions. The hydrophobic tail of a surfactant is typically an alkyl chain, while the hydrophilic head can either be charged or uncharged.

Classification: Surfactants can be classified as anionic, cationic, non-ionic, amphoteric (or zwitterionic), and gemini according to the charge on the hydrophilic head of the surfactant.

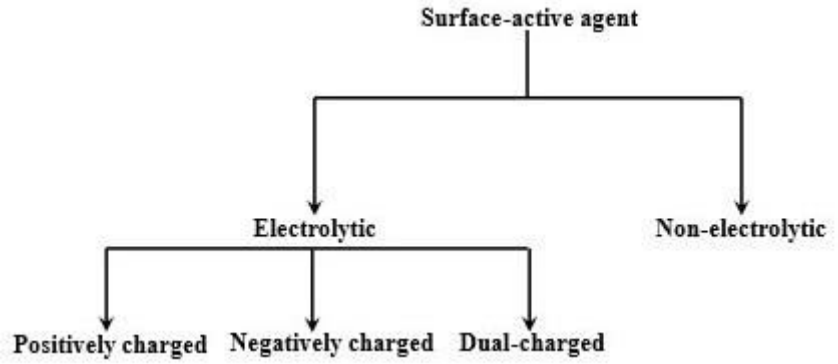

Figure 1. Schematic overview of amphiphile classification based on molecular features.

(i) Anionic surfactants: These surfactants carry a negative charge on their hydrophilic head. This class of surfactants includes alkali carboxylates, sulfonates, sulfates, and certain alkoxy compounds of amino acids.

(ii) Cationic surfactants: These surfactants have a hydrophilic head that carries a positive charge. The quaternary ammonium salts, amine oxides, amine salts, quaternary phosphonium salts, etc., are included in this group.

(iii) Non-ionic surfactants: These surfactants are neutral, as they do not carry any electrical charge. In aqueous medium, they are highly soluble, the polar functional groups can form strong hydrogen bonds with water molecules. This category comprises a range of compounds, including polyoxyethylenes, alkylpolyglucosides, polyglycidols, and others of a similar nature.

(iv) Amphoteric (zwitterionic) surfactants: According to the pH level of the medium, these surfactants can carry a positive or negative charge [8-10]. This class of compounds includes imidazoline compounds, phosphatides, betaines, and other related substances.

(v) Gemini surfactants: Unlike conventional surfactants, this type of surfactant has two hydrophobic (water-repelling) and two hydrophilic (water-attracting) groups that are connected by a short alkyl chain spacer [11, 12]. The dual long hydrophobic chains enable them to exhibit significantly higher surface activity than conventional surfactants. The head groups of gemini surfactants feature both positively charged components, like tetramethylene-1,4-bis(dimethyltetradecylammonium bromide) (14-4-14), and negatively charged entities, such as N,N′-ethylene(bis(sodium N-dodecanoyl-β-alaninate)) (212). The classification of surfactants depends on the specific configuration and polarity of their head group and the composition of their hydrophobic tail, as demonstrated in Figure 2.

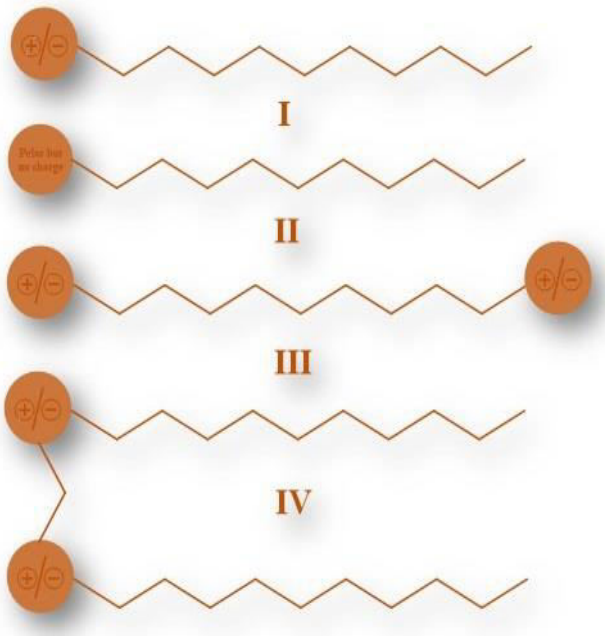

Figure 2. Schematic layout categorizing amphiphiles into four types: (I) charged (cationic/anionic), (II) uncharged, (III) zwitterionic, and (IV) gemini.

Ionic liquids (ILs), often referred to as unconventional surfactants, are exceptional surface-active agents [13, 14]. These compounds, consisting entirely of ions, are typically characterized by melting points below 100 °C. The first ionic liquid, ethyl ammonium nitrate, was introduced by Paul Walden in 1914 [15]. The unique physicochemical properties of ILs,

particularly their surface activity, are strongly influenced by the length of their hydrophobic chains and the chemical nature of their head groups.

Fundamental idea of micelle formation

Surfactant molecules naturally migrate to the air-water interface, driven by their dual nature of having both hydrophilic and hydrophobic moieties. Surfactants preferentially align at the air-water interface, where the conflicting forces of attraction and repulsion with water molecules are in equilibrium. Once the surfactant concentration reaches a critical point, resulting in the complete saturation of the air/water interface, surfactants spontaneously organize into an ordered self-assembled structure to balance their intrinsic attractive and repulsive forces. This formation of aggregates, known as micelles, occurs when the concentration reaches a specific threshold position, referred to as the critical micelle concentration (CMC) [16-19], under the given experimental conditions. A micelle is structured with a hydrophobic core, in which the nonpolar tails of the surfactant molecules interact and cluster together. This central hydrophobic region is enveloped by a layer of hydrophilic, polar head groups that interact with the surrounding water, stabilizing the structure. Amphiphiles spontaneously form micelles, where their nonpolar tails are sequestered in the interior, creating a hydrophobic core, while the hydrophilic polar head groups orient outward, interacting with the aqueous environment, as depicted in Figure 3.

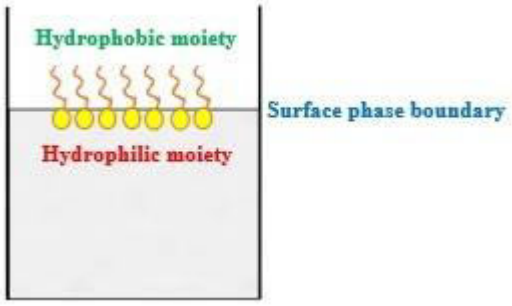

Figure 3. Schematic depiction of the mechanism involved in the initiation of micelle formation.

In a homologous series, surfactants must have at least eight methylene (-CH_2) groups in their alkyl chain to form stable micelles. With fewer methylene groups, the nonpolar tails cannot associate effectively enough to counteract the repulsion between the head groups. Therefore, surfactants with longer alkyl chains tend to be more hydrophobic and surface active, facilitating micelle formation. Their presence in solution, either as individual monomers or as a combination of monomers and micelles, known as "self-assembled colloids [20, 21]," is influenced by the mutual interactions and dynamics between the surfactant and solvent molecules.

The CMC is a key chemical-physical parameter for characterizing pure surfactants, providing valuable insights into their interfacial behaviour, self-assembly mechanisms, and the initiation of micelle formation. The value of CMC differs for each surfactant. Accurate determination of the CMC is therefore an essential and indispensable undertaking. A range of experimental techniques are employed to measure the CMC with high precision. The most widely adopted methods are tensiometry, electrical conductivity, spectrofluorimetry [22], ultraviolet spectrophotometry [23], dynamic light scattering [24], isothermal titration calorimetry [25], and nuclear magnetic resonance [26], which monitor the changes in physical characteristics as surfactant concentration increases. However, the conductometric approach is unsuitable for non-ionic surfactants due to their minimal impact on the solution conductivity. It is important to highlight that the CMC values can exhibit moderate variation depending on the method employed, with an acceptable deviation limit of ±10%. The molecular structure of surfactants is a fundamental factor that governs the magnitude of CMC. Moreover, the CMC is highly sensitive to several external conditions, such as

temperature, medium polarity, pH, and the inclusion of substances like electrolytes or other chemical agents that can alter the solution environment.

Micelles can adopt different shapes and structures depending on the surrounding environment and the diversity of amphiphiles:

(1) Normal micelle: Amphiphiles in polar environments form normal micelles when their hydrophilic heads point outward, interacting with the water surrounding them. At the same time, the hydrophobic tails cluster inward, creating an oily environment within the micelle's core.

(2) Reverse micelle: Surfactants are also capable of self-assembling in nonpolar or organic solvents, including benzene, hexane, toluene, chloroform, and diethyl ether. In these environments, they adopt a reverse configuration, with their hydrophilic heads facing inward to create a core, while their nonpolar tails extend outward to interact with the surrounding solvent. In many instances, a small amount of water can promote the assembly of reverse micelles. The result is a microscopic polar water droplet encased in a surfactant tail and immersed in a nonpolar medium.

(3) Mixed micelle: In aqueous environments, multiple surfactants can combine to form mixed micelles under optimal conditions, driven by either synergistic (cooperative) or antagonistic (competitive) interactions. These interactions are evident from the value of the CMC of the mixture, which differs significantly from the CMC of the individual components. The assembly of mixed micelles is facilitated when the surfactant head groups carry similar charges or when the mixture consists of ionic and non-ionic surfactants or a combination of non-ionic surfactants. Combining two surfactants with opposite charges [27, 28] in a nearly 1:1 ratio usually results in liquid-liquid phase separation, a phenomenon called 'coacervation.' An excessive amount of one of the surfactants may inhibit phase separation or precipitation

by dissolving the micelles of the excess component. The use of mixed surfactants, leading to the formation of mixed micelles, is widespread in domains, such as, chemical engineering, pharmacology, and environmental technology [29, 30]. From a physicochemical viewpoint, they perform more effectively compared to individual surfactants in solution. A natural example of a mixed micelle occurs in the digestive system, where bile salts (like sodium taurocholate) [31, 32] and phospholipids (such as, lecithin) [33] combine. Mixed reverse micelles can also readily form under suitable conditions.

Surfactant Micelles: A Physicochemical Overview

Micelles: Structure and Shape. Micelles typically vary in size from 1 to 10 nanometers [34]. In aqueous solutions, surfactant molecules can spontaneously self-assemble into a wide range of micellar structures, including spherical [35], cylindrical [36], rod-like [37], lamellar [38], disc-shaped [39], worm-like [40], and ellipsoidal [41] forms, and others. Spherical micelles are infrequently observed in most common surfactants. Hartley [42, 43] found that their diameter is roughly twice the length of the hydrocarbon chain, a finding that was later corroborated by McBain [44, 45]. Tanford [46, 47] argued that oblate ellipsoidal micelles are far more thermodynamically stable compared to prolate ellipsoids. Israelachvili et al. [48, 49], accounting for the geometric requirements of amphiphile packing, challenged Tanford's proposed model. They put forward a spheroidal concept, arguing that Tanford's model was flawed due to the overly curved peripheral regions and the excessive thickness of the central core. In Hartley's model, micelles have a hydrophobic, oil-like core encased in a hydrophilic, aqueous outer layer. The hydrophobic core of the micelle is predominantly oil-like, yet it allows some degree of water penetration. This behaviour is comprehensively supported by nuclear magnetic resonance (NMR) and fluorimetric data, which are explained within the framework of the "porous cluster" model [50, 51]. The dynamic light scattering (DLS) technique provides valuable insights into the particle size and distribution of aggregates in

solution. Techniques, such as, small-angle X-ray scattering (SAXS), small-angle neutron scattering (SANS), cryo-transmission electron microscopy (cryo-TEM), atomic force microscopy (AFM), and static light scattering (SLS) offer superior capabilities for accurately characterizing the shape and size of micelles. Among all the techniques mentioned, cryo-TEM is the only one capable of differentiating between linear and complex micelles [52]. External additives can be used to modify and influence the properties of micellar environments. The shape of micelles has been extensively studied and documented in previous literature. Recent advancements in research have offered a clearer, more detailed understanding of the microscopic structure of surfactant-generated micelles. Hartley's concept of modern dynamic micelles emphasizes the rapid interchange of molecules between the solution phase and the micellar aggregates. A high-speed photographic image of a micelle captured by arresting the movement of surfactant molecules provides a sharp and precise visualization of its intricate structure. The presence of a solvent significantly hinders micelle formation, whereas a salt facilitates the process by modifying the structure and composition of the micelles. Salts weaken the repulsive forces between the hydrophilic head groups of surfactant molecules, resulting in transitions that significantly boost the viscoelastic properties and increase the micellar mass of the solution. The packing parameter (P), as proposed by Israelachvili, offers a precise approach for differentiating between the various structural forms of amphiphilic assemblies. P provides an effective means to predict the amphiphilic packing behaviour and the geometry of micelles, as described by the following relation [53].

$$\mathrm{P} = \frac{v}{l\,\mathrm{A}} \qquad [1]$$

Here, v refers to the volume of the hydrophobic chain (in nm^3), assumed to be fluid and incompressible, while l represents the longest effective length of the hydrophobic (nonpolar)

chain in a surfactant molecule (in nm). The term, A represents the overall surface area occupied by the hydrophilic head group in the micellar interfacial region (in nm^2 per molecule). The effective length (l) and volume (v) of the hydrophobic segment are determined based on Tanford's formula [54] for pure amphiphilic substances.

$$l = (0.154 + 0.1265\ C_n)\ nm \quad [2]$$

$$v = (0.0274 + 0.0269\ C_n)\ nm^3 \quad [3]$$

Where C_n denotes the number of carbon atoms in the hydrocarbon chain of surfactant monomers. The parameter 'A' does not represent the geometrical area but instead indicates the maximum effective surface area, considering the repulsive interactions between the polar head groups. The different self-association shapes of amphiphiles, determined by varying packing parameters, are categorized and presented in Figure 4.

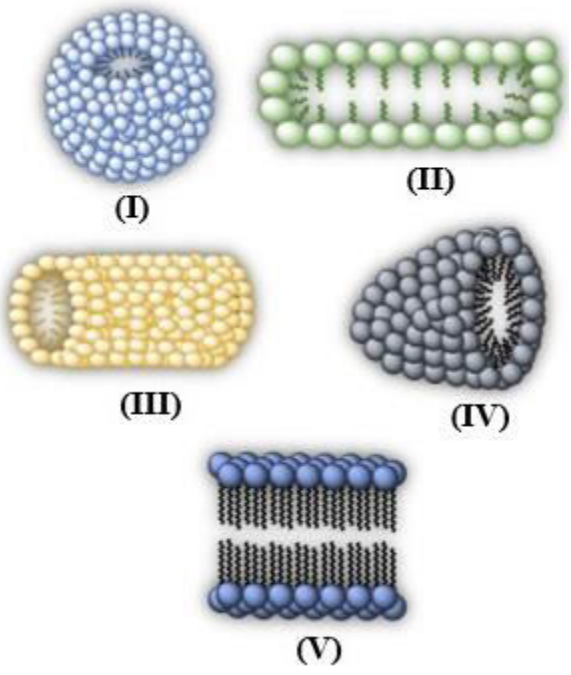

Figure 4. Different geometric shapes proposed for micellar structures include: (I) spherical, (II) cylindrical or wormlike, (III) rodlike, (IV) bisected oblate ellipsoid, and (V) bilayer or lamellar.

Mechanisms of Micellar Stability. Micelles naturally assemble into a thermodynamically stable structure. They are characterized by a hydrophobic core, formed by the self-aggregation of nonpolar hydrocarbon chains, while the polar ionic head groups extend outward, interacting with the surrounding aqueous environment. An electrical double layer [55] develops at the interface of an ionic micelle. When subjected to an electric field, the micelle undergoes electrophoretic movement, driven by its zeta potential and surface electric charge. The 'stern layer' [56] refers to the region directly surrounding the micelle core, where a substantial portion of counterions is tightly bound, effectively reducing the charge distribution at the micellar interface. The micellar stability of surfactants is enhanced when the polar head groups are partially neutralized by counterions through coulombic attraction [57, 58]. This process causes the stern layer to serve as a key stabilizing element of the micellar structure. The ‘Gouy-Chapman layer’ [59] refers to the outermost diffused layer that accommodates the surplus counter ions. Together, the stern layer and the Gouy-Chapman layer form what is known as the ‘electrical double layer.’ The surface region of the stern layer corresponds to the dynamic boundary of the micelle, which is why the interaction between the hydrophobic interior and the stern layer is essential to the micelle's kinetic behaviour. The inclusion of polar groups at the micelle interface induces ion-dipole interactions, facilitating the solvation of the micelles by water molecules and thereby enhancing their stability. Within polyoxyethylated non-ionic surfactant clusters, the core is enveloped by a sheath of polyoxyethylene chains, which can capture solvent molecules via hydrogen bonding [60]. This micellar zone is referred to as the ‘palisade layer’ [61].

Aggregation Number. The aggregation number (n_{Agg}), which denotes the number of surfactant monomers assembling to form a micelle, is a vital indicator of micellar size. Understanding this parameter is crucial for evaluating micellar stability and maximizing its effectiveness in various applications. Many factors influence the aggregation number,

including the molecular structure of the surfactant, temperature, the nature and concentration of salts, and organic additives. Essentially, it depends on the balance between hydrophobic and hydrophilic segments in surfactant monomers as well as the ionic properties of counterions. The aggregation number of a given surfactant is likewise influenced by its concentration. Non-ionic surfactants usually aggregate into larger structures compared to ionic surfactants [62]. The more pronounced the 'polarity disparity' between the surfactant and the solvent, the higher the aggregation number. Higher ‘polarity disparity’ between the surfactant and the solvent medium correlates with a higher aggregation number. As temperature increases, the aggregation number of ionic surfactants generally decreases, while for non-ionic surfactants, it rises significantly. The transformation of micellar structure from spherical to rod-like and ultimately to wormlike is often marked by a substantial increase in their aggregation number [63].

Various techniques have already been applied to evaluate aggregation numbers, including dynamic light scattering (DLS) [64], small-angle neutron scattering (SANS) [65], static fluorescence quenching [66], and fluorescence lifetime quenching [67]. Fluorescence quenching (FQ) relies on the interaction between a probe molecule and a quencher agent to accurately assess the aggregation number, surrounding polarity, and the dynamics of the probe-quencher distribution. Fluorescence quenching is frequently induced using probes such as pyrene [68], fluorescein [69], safranine T [70], and anthracene sulfonate [71], alongside quenchers including cetyl pyridinium chloride (CPyC) [72], thiourea [73], and transition metal ions like Co^{2+}, Ni^{2+}, and Cu^{2+} [74]. For optimal fluorescence quenching, the probe must be excited at a specific wavelength that is not absorbed by any other components in the system, thereby avoiding any distortion from absorption interference. The probe concentration is deliberately kept low to prevent complications from excimer formation and

to maintain the stability of the micellar structure. The following equation [75] has been used to determine the aggregation number (n_{Agg}).

$$\ln\left(\frac{I_0}{I_1}\right) = \frac{n_{Agg}\,[Q]}{[\text{Surfactant}]-CMC} \qquad [4]$$

Here, I_0 and I_1 represent the fluorescence intensities of the probe in the absence and presence of the quencher, respectively. The quencher concentration is denoted by $[Q]$, while the total surfactant concentration is expressed as [Surfactant]. A linear relationship between $\ln\left(\frac{I_0}{I_1}\right)$ and $[Q]$, measured at a constant [Surfactant], yields the aggregation number (n_{Agg}) from the slope of the plot.

Factors influencing micellar aggregation number

In aqueous medium, it has been found that as the hydrocarbon chain length of surfactants in a homologous series increases, the n_{Agg} also rises. Increased concentrations of neutral electrolytes enhance n_{Agg} by diminishing the hydrophilicity of the head group. Temperature variations affect non-ionic and ionic surfactants in different ways. For ionic surfactants, an increase in temperature generally causes a slight reduction in the n_{Agg} value [76, 77]. In contrast, for non-ionic surfactants, the rise in temperature leads to a significant increase in n_{Agg}, primarily due to the cloud point phenomenon [78]. The addition of trace quantities of surface-inactive organic substances with low water solubility generally results in the appearance of larger micelles. However, this observation is likely due to solubilization effects rather than an actual increase in the concentration of surfactant molecules within the micelle. The n_{Agg} of conventional surfactants usually ranges from 20 to 200 [79], with bile salt micelles having a notably lower n_{Agg}, typically between 10 and 15 [80, 81].

Counterion Binding (β). The nature of counterions plays a crucial role in shaping the structure and behaviour of charged micelles. When counterions bind, they reduce the overall charge of the micelle and the area occupied by each surfactant molecule, effectively minimizing the repulsion between the head groups. Once micelles begin to form, a portion of counterions accumulates on the charged micellar surface. The phenomenon of counterion binding is essential for comprehending the behaviour of the surrounding ionic layer and plays a key role in accurately evaluating the thermodynamics and energetics associated with the micellization process. The degree of binding can range widely, from 20% to more than 80% [82], depending on the specific ionic surfactant and the surrounding medium.

Among the various methods available, conductometry [83-86] stands out as the most widely adopted method for precisely quantifying the degree of counterion binding. In conductometry, when the specific conductance of an ionic surfactant solution is monitored at stepwise increasing concentration and plotted, the resulting graph demonstrates the intersection of two straight lines. The surfactant concentration at the point of intersection represents the CMC, and the proportion between the slopes of the straight lines after (S_2) and before (S_1) the micellization indicates the extent of counterion dissociation (α). The degree of counterion binding can therefore be determined as

$$\beta = (1 - \alpha) \text{ or } \left(1 - \frac{S_2}{S_1}\right) \qquad [5]$$

Potentiometry is also a precise and reliable method for determining the value of counterion binding [87]. In this approach, β is quantified by monitoring the counterion activities with an ion-selective membrane electrode. This electrode works in conjunction with a standard reference electrode, such as Ag/AgCl or a calomel electrode, forming an electrochemical cell that ensures accurate measurements. β can also be evaluated using the old-fashioned method of analysing the CMC of a surfactant at different counterion concentrations (C). By plotting

log (CMC) against log C, the slope of the curve yields an estimate of counterion binding, based on a time-honoured theoretical relationship [88],

$$\log (CMC) = \text{Constant} - \beta \log C \quad [6]$$

Factors Controlling Micelle Formation

Molecular nature of amphiphile. The fundamental attributes of amphiphiles are essential in governing their self-aggregation in solution, a well-documented and profoundly impactful phenomenon in surface chemistry. Non-ionic surfactants are characterized by relatively simpler physicochemical properties, while ionic surfactants exhibit more complex and diverse behaviours in solution. The presence of electrical charges in ionic surfactants gives rise to enhanced interactions through electrostatic forces, thereby influencing their behaviour. The CMC of ionic surfactants is significantly higher than that of non-ionic surfactants with equivalent functional groups in aqueous solutions [89]. Zwitterionic surfactants, on the other hand, typically exhibit a CMC comparable to that of ionic surfactants with an equivalent carbon chain length. The propensity for micelle assembly diminishes as the head group moves closer to the chain, due to the partial screening of the chain's two branches from each other, which minimizes interface energy dynamics. In a homologous series, the micellization process becomes more favourable for surfactants with higher hydrophobicity or longer chain lengths [90]. The correlation between the CMC and alkyl chain length within a specific homologous series can be described by the equation [91, 92]:

$$\log_{10}CMC = a - b\, C_n \quad [7]$$

where a and b are constants determined by the specific experimental setup, and C_n represents the number of carbon atoms in the hydrophobic tail.

Effect of salt electrolyte. In aqueous solutions, the addition of an electrolyte reduces the CMC of ionic surfactants, whereas the effect on zwitterionic surfactants is comparatively

minimal. The impact of adding an electrolyte with a charge identical to that of the associated counterion on the CMC of ionic surfactants can be quantitatively characterized by the following expression [93, 94]:

$$\log_{10} CMC = - m \log_{10} C_i + n \quad [8]$$

where m and n are constants specific to a hydrophilic head at a certain temperature, and C_i represents the molar concentration of univalent counterions. Likewise, the effect of salt electrolyte on non-ionic or zwitterionic surfactants can be quantified using the following equation:

$$\log_{10} CMC = - P C_{el} + Constant \ (C_{el} < 1) \quad [9]$$

where P is a constant that depends on the specific surfactant, electrolyte, and temperature, whereas C_{el} represents the concentration of the added salt electrolyte in molarity. As the electrolyte concentration rises, the repulsive forces between the charged micellar head groups are notably reduced, promoting the formation of micelles. The specific nature of the ions present is a key factor in determining the extent of this effect. Organic substances influence the CMC by either incorporating into the micellar structure or altering the interactions between the solvent and the micelle or between the solvent and the monomer [95]. The addition of non-electrolytes, including alcohols, amides, and esters, can cause the CMC to either rise or fall, depending on the specific characteristics of the compound. The value of the CMC is affected by both the length of the hydrocarbon chain in the organic compound and the nature of the hydrophobic moiety attached to the chain. Nonpolar compounds, like hydrocarbons, that integrate into the hydrophobic interior cause only a slight reduction in the CMC [96].

Temperature. Micelle formation is highly sensitive to temperature, which influences the solubility and other molecular behaviours of surfactants in solution. For ionic surfactants,

rising temperatures in the lower range generally promote micelle formation, whereas at higher temperatures, the process becomes less favourable [97, 98]. At higher temperatures, the de-solvation of the head groups increases electrostatic repulsion, which can impede micelle formation. Accordingly, the CMC should exhibit a minimum value as a function of temperature. However, for non-ionic surfactants, this de-solvation promotes micellization, typically causing a decrease in the CMC as the temperature rises [99]. The process is further complicated by changes in the polarity of the surrounding medium at elevated temperatures.

Pressure. Research has been conducted on how pressure influences the micellization of ionic and non-ionic surfactants. The CMC rises with increasing pressure, reaching its peak at approximately 1000 atmospheres, then gradually decreasing as pressure continues to climb [100, 101]. It has been proposed that amphiphiles in the interior of the micelle are more spread out than in their monomeric form in the bulk phase. As pressure increases, it compacts the micelle, restricting the increased mobility of the monomers within, which in turn causes the CMC to intensify. However, the reduction in CMC as pressure exceeds 1000 atmospheres results from the enhanced medium polarity, which lowers the energy barrier for monomers to integrate into micelles.

Solvent polarity. The polarity of the solvent encourages surfactant association, as polar environments enhance this interaction. In contrast, a nonpolar medium, resembling the surfactant hydrophobic tail, diminishes the propensity for self-association. In a non-polar solvent, reverse micelles are formed rather than the typical micelles [102, 103]. These structures have an inverted arrangement as opposed to regular micelles, with the surfactant tails directed inward and the head groups located at the centre of the micelle. The presence of a small quantity of water aids in their formation.

Role of counterions. In aqueous solutions, the magnitude of the CMC of ionic surfactants drops with a reduction in the hydrated size of the counterion. The effect of various ions with the same charge on the aggregation behaviours, such as CMC, counterion binding, etc., is known as the specific ion effect or Hofmeister effect [104]. The cations (0.015 M) are arranged in order of their decreasing effectiveness in reducing the CMC of the anionic SDS surfactant as follows: $Mg^{2+} > K^{+} > NH_4^{+} > Na^{+} > Li^{+}$. For the cationic surfactant CTAB [105], the anions (0.002 M) are ranked by their diminishing impact on the CMC in this order: $NO_3^{-} > Br^{-} > Cl^{-} > F^{-}$. Both sequences above can be seen as the inverse of the Hofmeister series, which was originally established to describe the salting-out phenomena in hydrophilic colloids. A detailed overview of this topic is available in recent review articles.

Polymers

Polymers are a versatile category of compounds made up of repeating molecular units called monomers, which bond together to create long, continuous chains known as macromolecules. A polymer is like a necklace strung together with countless small beads, each representing a monomer. The exceptional spectrum of their molecular configurations and inherent properties makes polymers highly adaptable, allowing for their extensive application across engineering, medicine, biotechnology, and industrial manufacturing sectors. Ongoing advancements in polymer science and technologies are continuously expanding the horizon of new opportunities and possibilities. In various industries, a polymer must retain its strength, shape, and properties when exposed to varying thermal conditions and environmental influences after being fabricated as a product. Recently, there has been increasing focus on the ability to instantly and repeatedly modify the structure or configuration of a molecule without causing any residual effects through external stimuli like electricity, light, or mechanical stress [106-108]. These ‘multifunctional materials’ are designed for advanced applications in data

processing, preservation, and extraction, as well as biochemical sensing, closely emulating the functions of biological systems [109, 110].

Classification of Polymers. Polymers are available in different forms, including both manufactured and naturally occurring types. Natural polymers [111] include proteins (such as collagen, elastin, fibrin, and keratin), carbohydrates (such as pectin, inulin, chitin, cellulose, and starch), DNA, and others. Polyethylene, nylon, polyvinyl chloride, polyester, and polytetrafluoroethylene are prime examples of synthetic polymers [112], whereas rayon, cellulose nitrate, vulcanized rubber, and cellophane are well-known semisynthetic polymers [113].

It is possible to classify polymers according to their chemical structure and composition. Homopolymers are composed of chains where each monomer unit is identical and connected by the same type of chemical bond. Copolymers are composed of chains that feature two or more distinct monomer units, typically linked in varying arrangements. Moreover, copolymers are classified based on the specific arrangement of their monomers within the polymer chain, as described below: (a) Random copolymers [114] consist of two or more distinct monomers distributed unpredictably along the chain, resulting in a random sequence; (b) Alternating copolymers [115] feature a regular, repeating pattern in which two different monomers alternate along the chain; (c) Block copolymers [116, 117] are composed of large segments (blocks) of one type of monomer adjacent to segments of another; (d) Graft copolymers [118, 119] consist of a main polymer backbone made of one monomer type, with branches of a different monomer type attached to it.

(i)-A-A-A-A-A-A-A-A-A-A-A-A-A-A-

(ii)-A-B-A-A-B-A-B-B-A-A-A-B-A-B-B-

(iii)-A-B-A-B-A-B-A-B-A-B-A-B-A-B-A-

(iv)-A-A-A-B-B-A-A-A-B-B-A-A-A-B-B-

Figure 5. (i) homopolymer, (ii) random copolymer, (iii) alternating copolymer, and (iv) block copolymer.

Polymers are also classified based on the type of polymerization reaction employed during their formation. In addition polymers, the individual monomers link together without the elimination of any atoms. Alkenes are the most prevalent type of monomers in this category. In condensation polymers, two distinct monomers chemically bond to form an extended polymer chain, with the simultaneous elimination of a byproduct, most commonly water. Polyamides (nylon-6,6) and polyesters (polyethylene terephthalate) belong to this category of polymers.

Average Molecular Weight of Polymer. Polymer molecules lack a defined molecular weight because of their inherent heterogeneity. Instead, their molecular weights are characterized by different averages, such as number-average ($\overline{M_n}$), weight-average ($\overline{M_w}$), and viscosity-average ($\overline{M_v}$) molecular weights. The details are as follows:

$$\overline{M_n} = \frac{\sum_i N_i M_i}{\sum_i N_i} \qquad [10]$$

where N_i represents the number of molecules, each with a molecular weight of M_i.

$$\overline{M_w} = \frac{\sum_i N_i M_i^2}{\sum_i N_i M_i} \qquad [11]$$

The value of $\overline{M_w}$ is always greater than $\overline{M_n}$. The ratio of $\overline{M_w}$ to $\overline{M_n}$ known as the polydispersity index, reflects the distribution of molecular weights within a sample. For a monodisperse polymer, the molecular weights are uniform, M≡ $\overline{M_w}$ ≡ $\overline{M_n}$. $\overline{M_n}$ can be determined through osmometry, while $\overline{M_w}$ can be evaluated using light scattering technique.

Another significant measure of molecular weight is the viscosity average molecular weight, symbolized as $\overline{M_v}$.

$$\overline{M_v} = \left(\frac{\sum_i N_i M_i^{1+a}}{\sum_i N_i M_i}\right)^{\frac{1}{a}} \quad [12]$$

Here, 'a' is a constant ranging from 0.5 to 2.0. In general, the relationship follows $\overline{M_w} > \overline{M_n} > \overline{M_v}$. In the case of a monodisperse polymer, M, $\overline{M_n}$, $\overline{M_w}$, and $\overline{M_v}$ are all equal.

Polymer-Surfactant Interaction

The integration of amphiphiles with polymers creates a dynamic synergy, effectively addressing the growing requirements in pharmaceutical and medical sciences, as well as in various industrial formulations. In industrial sectors, surfactants primarily function as detergents, emulsifiers, or spreading agents, while polymers perform the specific purpose of thickening in aqua-based products, such as paints, coatings, and construction fluids. Surface interactions are essential for numerous purposes, including particle dispersion, surface adhesion, wetting behaviour, and other related processes. The incorporation of polymers into surfactant-rich formulations significantly impacts solution viscosity, a key factor in the design of personal care products. This increasing demand highlights the need for deeper exploration of the interaction behaviour, driving advancements in both practical applications and the core principles of colloid science. The previous experimental findings provide compelling evidence supporting the widespread presence of this interaction. In combined polymer-surfactant systems, three main types of interactions are observed: (i) interactions between surfactant molecules, (ii) interactions among polymer chains, and (iii) interactions between polymers and surfactants. The first two types can occur as either intermolecular or intramolecular interactions. Depending on the relative strengths of these three interactions, each polymer-surfactant pairing can exhibit distinct physicochemical properties.

The interaction between surfactants and polymers is both sophisticated and highly dynamic, characterized by continuous structural changes. A comprehensive review of the literature

uncovers a substantial amount of research focused on the interactions between non-ionic polymers and charged surfactants. The interaction behaviour of physicochemical phenomena can be evaluated precisely through thermodynamics, as these processes are inherently governed by their principles. In the early stages, the surfactant molecules interact with the polymer backbone through hydrophobic forces. This induces the premature aggregation of the surfactant monomers at concentrations significantly below the CMC. The concentration at which the formation of small micelle-like aggregates initiates is referred to as the 'critical aggregation concentration' (CAC). These micelles bind in a synchronized fashion along the polymer backbone, and once all binding sites are saturated, excess surfactant molecules spontaneously organize into free micelles in the surrounding solution. The initial attachment of smaller surfactant aggregates to polymer adsorption sites is mainly driven by hydrophobic interactions, which are subsequently strengthened by ionic interactions between the hydrophilic head of the surfactant and the charged sites on the polymer. The emergence of small surfactant aggregates and the subsequent onset of polymer-surfactant interactions occur when the surfactant concentration exceeds a critical threshold, CAC. This process is unaffected by polymer concentration, emphasizing that it is primarily driven by hydrophobic forces. The higher value of CMC (pure surfactant) in comparison to CAC (polymer-surfactant system) is due to the strong hydrophobic forces arising from the exclusion of water molecules from the polymer's segments. As the surfactant concentration increases, it binds to the polymer sites until the polymer reaches its saturation concentration (C_S). Beyond this point, any further increase in surfactant concentration leads to a third breakpoint, at which free surfactant forms micelles, marking the onset of the extended critical micelle concentration (C_f). The interaction between surfactants and polymers is a complex process, yet distinct breakpoints become apparent when analysed through various techniques. The literature contains extensive studies investigating the interactions between polymers and surfactants

with opposing charges [120-123], as well as between polymers and surfactants sharing the same charge [124, 125]. Recently, surface-active ionic liquids (SAILs) have garnered significant attention from researchers for their ability to form intricate interactions with oppositely charged polyelectrolytes, facilitating the development of advanced functional colloidal systems [126-129].

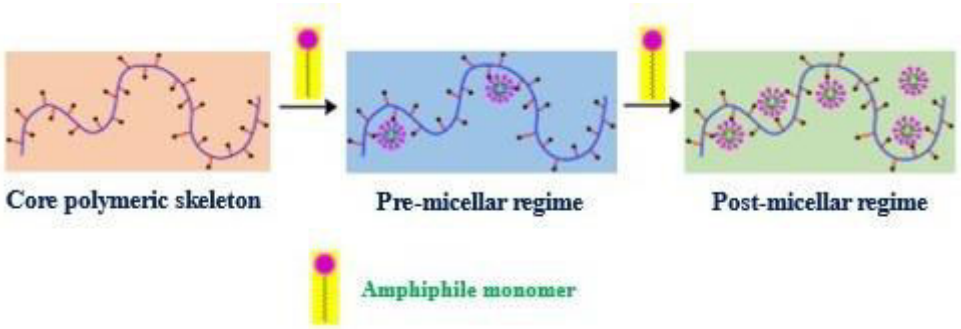

Figure 6. A visual guide to polymer and surfactant interaction.

Interactions between polymers and surfactants, like other surface-relevant phenomena, manifest a delicate interplay between supporting and obstructing linkage. The primary forces driving polymer-surfactant complex formation include electrostatic attractions and repulsions, hydrogen bonding, van der Waals interactions, and the hydrophobic effect. Although the electrical interactions are relatively simple, arising from the coupling of charged moieties on both the polymer and the surfactant, the other interactions are far more complex and challenging to evaluate. Polymers, specifically, introduce distinct complexities, as their secondary and tertiary structures in solution often require rearrangement to accommodate attached surfactant molecules. The association behaviour of the polymer-surfactant couple can have a significant effect on the overall thermodynamic stability of the system, often inducing substantial conformational changes in the polymer. Each of these changes brings about substantial modifications to both the large- and small-scale features of the system. Factors that hinder molecular association include internal energy, entropic effects, and electrostatic repulsion between similarly charged particles.

The behaviour of the polymer-surfactant interaction can vary depending on the specific features of the polymer and surfactant. Formation of the complex is less likely when the polymer has a stiff backbone, the surfactant features a bulky polar head, or when both the polymer and surfactant exhibit matching polarities. The interaction mechanism is not yet fully understood, although it is widely believed that the primary force governing the binding of surfactants to polymers in an aqueous medium is the hydrophobic effect. Uncharged polymers exhibit the capacity to interact with both cationic and anionic surfactants, but the nature of these interactions differs. Typically, anionic surfactants exhibit much more intense interactions than cationic surfactants of comparable chain length. Charged polymers are capable of interacting with surfactants carrying both opposite and like charges. Charged polymers, also known as polyelectrolytes, exhibit strong electrostatic interactions with surfactants of opposite charge in aqueous solutions. In contrast, when both the polymer and surfactant carry the same charge, interactions take place only under conditions where the polymer has significant hydrophobic traits.

When a polymer interacts with a surfactant carrying an opposite charge, the hydrophobicity of the resulting complex is enhanced, driving self-aggregation and the formation of coacervates. This process can lead to the appearance of turbidity in the solution and causes the complex to precipitate. The primary interaction is mediated by electrostatic forces, further strengthened by hydrophobic interactions occurring between the polymer's hydrophobic regions and the surfactant's nonpolar tail. As these interactions progress, the polymer’s net charge steadily diminishes, leading to an enhanced hydrophobicity of the resulting complexes.

In polymer-surfactant systems dominated by electrostatic interactions, surfactant monomers bind to oppositely charged polymer sites, driving the process of coacervation. This process reaches its peak at an optimal surfactant concentration, yielding maximum coacervate

precipitation. When the polymer binding sites reach saturation, the surfactant monomers initiate the formation of free micelles in the bulk medium. The redissolution mechanism is thought to take place as the coacervates are incorporated into the micellar hydrophobic cores. There is growing interest in coacervates because of their diverse potential applications across multiple fields, such as, smart materials, renewable energy, drug encapsulation, diagnostics, wastewater treatment, agriculture, bioplastics, and wound healing.

Salt significantly impacts the coacervation of oppositely charged polymer-surfactant binary systems by effectively shielding their electrostatic charges. Studies have shown that as salt concentration increases, these interactions are weakened, as evidenced by the corresponding rise in the CAC value at higher salt levels. Therefore, it can be concluded that the presence of salt will also affect the phase behaviour of these systems. Xiaoyong Wang [130] investigated the salt-enhancing effect on the complex formation between sodium carboxymethylcellulose (NaCMC) and dodecyltrimethylammonium bromide (DTAB) at different sodium bromide (NaBr) concentrations. This effect is attributed to the interplay between two opposing factors: the screening of the polyelectrolyte-surfactant interaction and the enhancement of this interaction due to micelle growth induced by the added salt. When the enhancement of the polyelectrolyte-surfactant interaction outweighs the screening effect, the formation of the complex is promoted. In a previous study, C. Wang [131] explored the interactions between cationic surfactant, DTAB and the anionic polymer, poly(acrylic acid) (PAA) at varying sodium chloride (NaCl) concentrations. The results revealed that increasing salt concentration weakens the electrostatic attraction between the oppositely charged polymer and surfactant, effectively suppressing polymer-induced micellization of the surfactant. These findings demonstrate that the addition of salt can either facilitate or hinder the complexation between the polymer and surfactant.

Surfactant attachment to the polymer's binding sites, whether in individual or clustered states, can induce polymer unfolding. This process occurs due to the increased pressure from rising surfactant concentrations. As the concentration increases, the added surfactant molecules are unable to access the hidden charged regions along the wrinkled polymer backbone because of the low polarity of the hydrophobic core. This process leads to an increased availability of charged regions, which first enhances the solubility of the amphiphile-bound polymer by improving its solvation. After this, the polymer undergoes a secondary phase of amphiphile binding. Once the CMC is exceeded, the excess surfactant molecules accumulate along the polymer chain, resulting in the formation of polymer-induced small surfactant aggregates. The second type of interaction between polymers and surfactants with opposite charges involves the attachment of both individual and aggregated surfactant particles onto the polymer.

The interaction between polymers and surfactants holds significant biological relevance, as proteins can exhibit biopolymer behaviours, which are regulated by the pH of the surrounding solution. At its isoelectric point (IEP), a protein carries no net charge. As the pH rises above the IEP, the protein progressively gains a negative charge, whereas at pH levels below the IEP, it adopts a net positive charge. Thus, the mechanism of bimodal interaction is fundamental in protein-surfactant interactions because of the protein's compact, globular conformation. The coacervation phenomenon in protein interactions with oppositely charged surfactants provides a highly efficient and effective approach for protein isolation. Chakraborty et al. [132] have conducted an in-depth study on the interaction of the bovine serum albumin (BSA) protein with three types of surfactants: cationic alkyltrimethylammonium bromide (ATAB), non-ionic pentaethylene glycol mono-n-dodecyl ether ($C_{12}E_5$), and anionic sodium dodecyl sulfate (SDS). The complexation of surfactants with DNA has garnered significant interest due to its potential to enable transfection and the

efficient delivery of genes into living cells. This process holds immense promise for advancing biotechnological applications. Recently, Zakharova et al. [133] explored the complexation of triphenylphosphonium surfactants (TPPB-n) with oligonucleotides (ONu) through a combination of experimental and theoretical approaches. Their findings highlighted the surfactants' ability to induce compaction and condensation of nucleotide multi anions. A polymer-surfactant system closely resembles the lipid-protein structure found in cell membranes, where lipids and proteins interact to form a complex arrangement. Surfactants are frequently utilized in experimental studies as analogues for lipids, providing crucial insights into the mechanisms underlying lipid transport within body fluids.

Coacervates

Coacervates are complex molecular assemblies with a broad spectrum of applications. In aqueous environments, ionic surfactants interact with oppositely charged polymers under varying conditions, giving rise to coacervates that segregate into a distinct phase within the solution. The solubilizing capacity of micelles is maintained in the micelle-polyelectrolyte complex (coacervate), and the protein structure stays intact in the polyelectrolyte-protein coacervate, as demonstrated by the sustained enzymatic activity and other supporting evidence. The gel-like nature of coacervates is significant in various applications, including food products, drug delivery systems, water purification, tissue engineering, and biodegradable plastics, among others [134-138].

The term "coacervate" was coined by Dutch chemist Bungenberg de Jong [139, 140], recognized as the pioneer of coacervate chemistry. While he acknowledged the biological significance of coacervates, it was Oparin [141, 142] who helped bring coacervates into the broader scientific spotlight, highlighting their importance beyond the realm of colloid science. Building on this foundation, Overbeek and Voorn [143, 144] formulated the first

theoretical model. For nearly a decade, coacervates were seen as one of the most fascinating colloidal systems. However, recent comprehensive reviews and key references [145-148] have now consolidated and advanced the body of research on coacervates. The term 'coacervate' originates from the Latin words "co," meaning "together," and "acerv," meaning "heap," suggesting the concept of particles or substances gathering together to form a concentrated cluster. This phenomenon refers to a process in which a colloidal solution undergoes phase separation into two immiscible aqueous layers: a coacervate phase, which is concentrated with colloidal particles, and an equilibrium liquid phase, which is generally poor in colloidal material. Therefore, two predominantly water-based layers do not easily combine, making the coacervate incompatible with the solvent it is in.

Kruyt [149, 150] classifies coacervation into two types: simple and complex coacervation. Simple coacervation is a phase separation process driven by (i) neutral groups in surfactants and (ii) the introduction of salts or alcohols into surfactant-water mixtures. The first type of coacervation is a form of phase separation, marked by a reduced water content in the entire system. Such a coacervate system dissolves upon dilution. Complex coacervates are dense, viscous liquids that arise from the association of oppositely charged macromolecules, leading to phase separation. This process is suppressed in the presence of salt. Complex coacervates can be formed through various interactions, including (i) the combination of surfactants with opposite charges (cationic) and dyes or (ii) the association of oppositely charged (bio)polymers with surfactants (lipids), charged polymer aggregates (such as pure or mixed micelles), or protein-polysaccharide complexes [151-153], particularly near the point of charge neutrality [154]. The interaction between oppositely charged polymers and surfactants

leads to the formation of neutral, soluble, or phase-separated coacervates, which are composed of an excess of either the polymer or the surfactant.

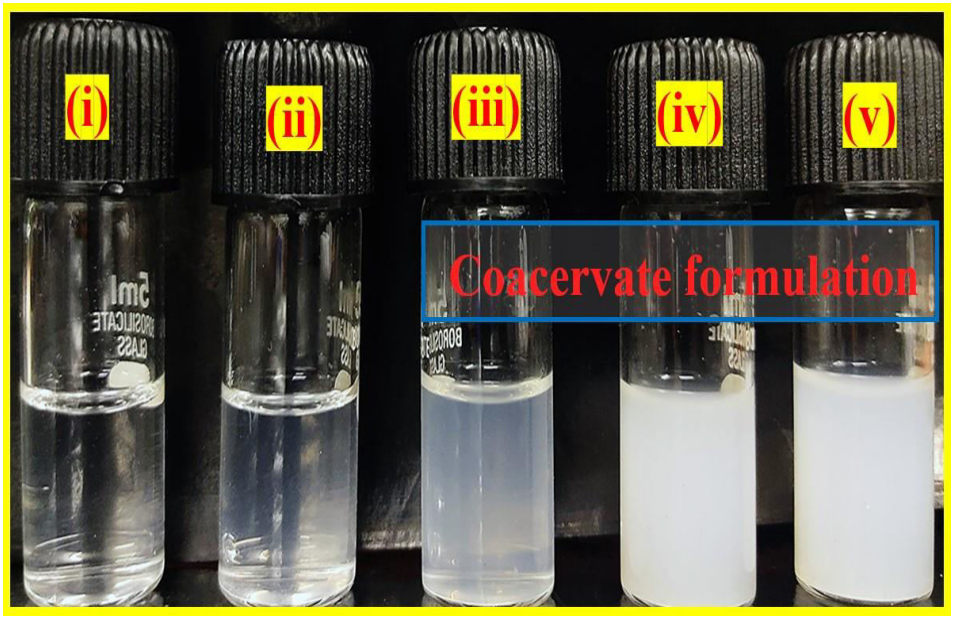

Figure 7. Formation of "coacervates".

The complexation between polyelectrolytes (such as polymers, biopolymers, and proteins) and surfactants carrying opposite charges has been a subject of considerable and ongoing research. Aqueous "complex salts" [155] consisting of ionic surfactants and polymeric counterions provide an ideal model system for exploring the fundamental poly-ion-mediated interactions in colloidal systems. In actual practice, systems featuring ionic surfactants and oppositely charged poly-ions are formed by dissolving two distinct salts in an aqueous medium: one being a surfactant salt, which includes a surfactant ion paired with its counterion, and the other a polyelectrolyte, consisting of a poly-ion with its associated counterion. Coacervation takes place in such mixtures through an ion exchange mechanism [156-158], where the concentrated phase holds the complex salt, and the dilute phase carries the simpler salt. Coacervation unfolds in two key stages: first, poly-ions experience charge neutralization driven by electrostatic interactions. This is followed by an increase in entropy,

stemming from the entropic distribution of poly-ions in the dense phase and the diffusion of counterions into the surrounding solvent. This phenomenon enables oppositely charged polymer-surfactant systems to be utilized in a wide variety of applications across materials science, biotechnology, drug development, and personal care sectors. In this context, an equilibrium is established between the bulk interactions of the polymer and surfactants and the surface interactions, which involve the interplay between the surface, the polymer, the surfactant, and the polymer/surfactant complexes. Pectin is highly regarded for its ability to form complex coacervates with a broad spectrum of molecules, including proteins (e.g., sodium caseinate [159], gelatin [160], lactoferrin [161], bovine serum albumin [162], β-lactoglobulin [163], wheat germ [164], whey protein isolate [165], and pea protein isolate [166]); polyelectrolytes such as chitosan [167]; and surfactants like lauric arginate [168].

Variables influencing the dynamics of the interaction

Several factors affect the micellization of surfactants when a polymer is present, showing similarities to the behaviour observed in the absence of a polymer. The key variables are outlined as follows:

Surfactant head group. The solution behaviour of a surfactant in the presence of a polymer is largely influenced by the surfactant's head group, as it dictates the nature of interactions (electrostatic, hydrophobic, or hydrogen bonding) occurring between the polymer and surfactant molecules. Ionic head groups, either cationic or anionic, interact strongly with oppositely charged polymers. In such cases, complex formation is driven by both electrostatic and hydrophobic interactions. Electrostatic interactions arise between the polar head groups of surfactants and the charged functional groups of the polymer, while hydrophobic interactions involve the alkyl chains of the surfactants and the nonpolar segments of the polymer chains. Although both forces are at play, electrostatic interactions typically prevail in

these systems. Non-ionic head groups, on the other hand, primarily interact through hydrophobic forces or hydrogen bonding.

The physicochemical interactions between oppositely charged polymers and surfactants are significantly more complex compared to those between ionic surfactants and non-ionic polymers [169]. Non-ionic polymers interact more readily with anionic surfactants compared to cationic surfactants, while their interaction with non-ionic surfactants is negligible and relatively weak [170].

The head size of the surfactant also plays a crucial role in the interaction process. The larger head groups, like cetyltrimethylpyridinium chloride (CPyC) [171], introduce steric hindrance that impedes interactions, whereas smaller head groups, such as alkyl sulfonates, enable more efficient binding.

Polymer concentration. The CAC value is generally unaffected by the polymer concentration or may only decrease slightly, while the C_f increases in direct proportion to the polymer concentration [172]. As the polymer concentration increases, the availability of binding sites also rises, which leads to a larger interaction zone. As a result, the attachment of small micellar aggregates to the polymer backbone takes place at increased surfactant concentrations. In accordance with the mass balance principle, both the threshold concentrations for the saturation of the polymer by surfactant monomers and the onset of polymer-induced micellization increase as the polymer concentration rises.

Surfactant alkyl chain length. The interaction between surfactants and polymers intensifies as the hydrophobic chain length of the surfactants increases. The hydrophobic nature of the amphiphile plays a crucial role in determining its association behaviour. The alkyl chain length of surfactants is a key determinant in shaping polymer-surfactant interactions by fine-tuning the balance between hydrophobic and hydrophilic forces. As the alkyl chain length

increases, the surfactant becomes more hydrophobic, leading to stronger interactions with the polymer's hydrophobic domains. Surfactants with longer alkyl chains typically exhibit a more negative free energy of binding with polymers, as stronger hydrophobic interactions enhance the thermodynamic favourability of the polymer-surfactant interaction. However, the electrostatic contribution to the polymer-surfactant interaction remains largely unaffected by the length of the alkyl chain. In a homologous series, the CAC value tends to decrease as the alkyl chain length of the surfactant binding to the polymer increases [173].

Salt. The introduction of inorganic salts typically facilitates polymer-surfactant complex formation, leading to a reduction in CAC values. The presence of salt enhances the surfactant-to-polymer binding ratio, causing a considerable broadening of the CAC/C_f profile. Murata and Arai [174] found that in the PVP-SDS system, the inclusion of 0.1 M NaCl elevated the SDS-to-PVP ratio to 0.9 mol per mole of PVP, significantly higher than the 0.3 mol SDS per mole of PVP observed in the salt-free solution. The presence of counterions modulates the water structure, where chaotropic [175] (structure-breaking) cations intensify the interaction between surfactant anions and polymers, while kosmotropic [176] (structure-making) cations weaken this interaction. Considering that some of the examined counterions are sizable organic ions, it is plausible that they may directly interact with and bind to the polymer.

Temperature. It is well-established that a slight increase in temperature leads to a rise in the CMC of charged surfactants. Similarly, higher temperatures generally weaken molecular association, resulting in a corresponding increase in the CAC [177].

Other key factors include the aggregation number and solubility of the surfactant, the conformation and molecular weight of the polymer [178-180], the dielectric constant [181], the pH [182, 183] of the medium, etc.

The impact of organic solvents on micelle formation and polymer-surfactant interaction

The interactions between polymers and surfactants have mostly been explored in aqueous environments, where hydrophobic forces are identified as the key factor. Moreover, examining the impact of organic solvents on these interactions offers valuable insights. Indeed, the effect of organic solvents on micellization has been the subject of extensive research.

Hydrophilic solvents, including methanol [184], ethanol [185], and acetone [186], tend to increase the CMC. The addition of an organic solvent alters the composition and behaviour of the aqueous solvent mixture, enhancing surfactant solubility and making the solution more hydrophobic. At the same time, the solvent's polarity decreases. These changes collectively lead to an increase in the CMC, a phenomenon known as the "cosolvent effect" [187, 188]. However, a different effect is observed with middle-chain alcohols (five or six carbons), where their solubilization into the micellar palisade reduces the CMC. This is because the alcohols lower the surface charge density and enhance hydrophobic interactions between the surfactants within the micelles. This phenomenon is referred to as the "cosurfactant effect" [189, 190]. Short-chain alcohols generally function as cosolvents, residing in the continuous phase and influencing the solvent structure near the headgroup. Medium-chain alcohols tend to distribute between the palisade layer and the aqueous phase, while long-chain alcohols are embedded within the hydrophobic interior of the micelle. In practice, particularly within the cosmetics and pharmaceutical industries, alcohols are widely utilized as additives to improve solubility, ensure better dispersion, and enhance product stability. 2,2,2-Trifluoroethanol (TFE) is environment friendly, non-toxic, and highly efficient as a co-solvent in biological research involving proteins and peptides [191, 192].

Therefore, it would be insightful to observe the effects of adding such organic solvents to polymer-surfactant systems [193, 194]. Specifically, it is important to thoroughly investigate the initiation of the interaction, its impact on polymer structure and aggregate dimensions, and how these dynamics are shaped by solvent composition. The complexation of polymers and surfactants is primarily driven by the incorporation of polymer chains into the micellar peripheral zone, ensuring effective isolation of the hydrophobic core from the surrounding aqueous environment. This scenario is more favourable because the polymer's natural hydrophobicity, which exceeds that of water, leads to a reduction in the CMC. Short-chain alcohols interact with the same site on the micelle, potentially leading to competitive effects akin to those observed in mixtures of polymers with anionic and non-ionic surfactants. Furthermore, changing the solvent polarity will modify the medium's dielectric properties, thereby significantly affecting the electrostatic forces acting on the bound micelles. The addition of alcohol imparts non-polar characteristics to the medium, promoting the smooth dispersion of polymer-surfactant complexes while effectively preventing the development of cloudiness and phase separation in the solution.

Research on polymer/surfactant systems in polar solvents apart from water is surprisingly limited. Naskar et al. [195] investigated the impact of isopropanol (IP) on the cooperative binding of the amphiphile CHAPS to the biopolymer inulin in aqueous solution. In a related study, Mukherjee et al. [196] carried out a comparative analysis of the interactions between the cationic polymer PDADMAC and various anionic surfactants (SDS, SDBS, and SDDS) in IP-water media. Mandal et al. [197] also studied the interactions between SDDS and modified cationic polymers, hydroxyethylcelluloses (JR 400 and LM 200), in IP solvent.

Experimental methods for studying the polymer-surfactant interaction process

A variety of experimental methods are commonly utilized to study polymer-surfactant interactions. Numerous experimental techniques have been utilized to explore the structure and behaviour of polymer-surfactant complexes in aqueous environments. Similarly, significant advancements have emerged from both the adoption of innovative experimental methods and the careful analysis of data derived from conventional physicochemical techniques. The following outlines are several widely used techniques for exploring these interactions and the key insights gained from studying such systems.

Tensiometry. This technique provides a distinctive and valuable approach for studying polymer-surfactant interactions. It can reveal a more profound understanding of the interaction between the polymer and the surfactant at the interface as well as within the bulk. Polymer-surfactant complexes exhibit remarkable surface activity, giving rise to various types of tensiometric profiles. Jones [198] was the first to make a significant contribution using this method, reporting the identification of two transition points (T_1 and T_3) in the PEO-SDS system. A distinct transition, T_2, was also detected, occurring between T_1 and T_3. It was shown that $T_1 < CMC < T_3$, where T_1 (CAC) marks the onset of PEO-SDS interactions, T_2 (C_S) corresponds to the saturation point at which the PEO chains are fully occupied by SDS aggregates, and T_3 (C_f) indicates the PEO-induced CMC of SDS. The fact that T_1 is much lower than the CMC suggests that the 'aggregated' state of SDS with PEO is energetically more stable for the surfactant molecules than the conventional micellar structure. It was noted that T_1 exhibited only a minimal dependence on polymer concentration, suggesting that the initial complexation was mainly governed by the surfactant concentration for a given polymer. In contrast, T_3 demonstrated a strong correlation with the polymer concentration. Other advanced techniques for characterizing surface complexation include ellipsometry [199], neutron reflectometry [200], dilational rheology [201], and others.

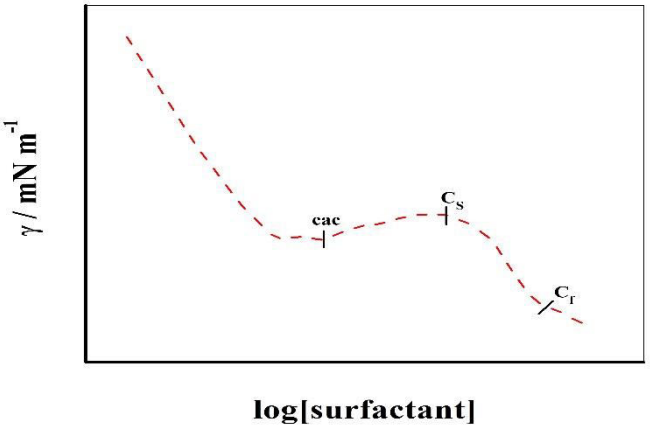

Figure 8. Tensiometric profile illustrating the interaction between oppositely charged polymer and surfactant.

Conductometry. Conductometry is an effective technique for exploring the bulk complexation between neutral or charged polymers and ionic surfactants. The presence of a polymer influences the specific conductance as a function of surfactant concentration, giving rise to a pre-micellar breakpoint, where the plot deviates from the behaviour of the surfactant alone, followed by a second breakpoint after micellar formation. The decrease in specific conductivity within the T_1-T_2 concentration range, compared to the polymer-free system, can be attributed to the loss of free surfactant ions in the solution, either through adsorption onto the polymer or through cluster formation with it. Schwager [202] reported similar findings for the PEO/SDS system. The presence of an initial interaction zone sparks curiosity about the underlying molecular mechanisms and is certain to stimulate further investigation in this field. It can be described as the surfactant binding with minimal aggregation at low polymer concentration, followed by more extensive aggregation at higher polymer concentration.

Microcalorimetry. Isothermal titration calorimetry (ITC) is an advanced and highly sensitive technique for accurately quantifying enthalpy changes as a function of surfactant concentration in the context of polymer-surfactant interactions. This technique is used for

identifying the different steps of molecular interactions and measuring their enthalpic contributions. This method can reveal the heat generated by various physicochemical processes within the bulk medium, many of which may not be detectable through other techniques. The analysis of ITC data can provide in-depth insights into the underlying mechanisms and characteristics of polymer-surfactant interactions, shedding light on the key factors that govern and influence these interactions. In an ITC experiment with a polymer-surfactant system, key transition points and enthalpy changes associated with interaction processes are extracted from a single measurement through the injection of one solution into the other. The binding enthalpies of both the surfactant monomers and micellar aggregates to the polymer backbone can also be calculated. The processes that result in observable enthalpy changes include (a) micelle dissociation, (b) the dilution effect of surfactant solutions, (c) structural alterations in polymers, and (d) binding interactions. Among these, binding interactions generally produce the most significant and measurable enthalpy change. Wagner et al. [203] employed ITC to study the interaction between Cat-HEC (JR-400) and SDS across a wide range of surfactant concentrations, including the precipitation region, where SDS was gradually titrated into the Cat-HEC (JR-400) solution. The results identified spinodal and binodal points within the precipitation region, along with unstable and metastable phases, where the precipitated complex diffused out of the bulk solution either instantaneously or gradually.

Light Scattering. Static light scattering is a powerful technique employed in polymer-surfactant systems to accurately measure the aggregate size and provide detailed insights into their structural properties. This method delivers valuable data on the formation of aggregates, such as micelles, explores the impact of surfactants on polymer conformation, and monitors changes in diffusion and viscosity. Furthermore, DLS can be used to examine the stability and size of surfactant micelles in the presence of polymers. Researchers have applied light

scattering techniques to explore polymer-surfactant systems with both similar and opposing charges. In a recent study, Bohidar et al. [204] used DLS measurements to compare the effects of various surfactants on the size of anionic pectin polymer. The results demonstrated that cationic surfactants (DTAB and CTAB) caused a decrease in polymer size, the anionic surfactant (SDS) showed no effect, and the non-ionic surfactant (TX-100) led to an increase in size.

Fluorimetry. Various steady-state and time-resolved fluorescence techniques have been used to study polymer-surfactant mixtures. Steady-state methods, such as fluorescence anisotropy measurements, provide insights into the local environments of the probes, molecular mobility, and the aggregation number of the structures. Time-resolved techniques, in particular, have proven to be highly effective, offering valuable information on surfactant aggregation numbers, distribution uniformity, and kinetic details. Both individual probe molecules and polymer-bound probes can be utilized. For pyrene, the most frequently used probe in such studies, the measurement is based on the ratio between the first (I_1) and third (I_3) fluorescence peaks [205]. Lin and coworkers [206] performed a comparative fluorescence study using two different probes, pyrene and Nile red, to examine the behaviour of oppositely charged carboxymethyl chitosan and alkyltrimethylammonium bromides in aqueous solution.

Viscosity. The viscosity method can be used to explore the bulk complexation process by analysing the structural changes within the polymer-surfactant system. Saito [207] observed a marked increase in the viscosity of methyl cellulose and PVP polymer solutions upon the addition of anionic SDS surfactant, likely resulting from the combined influence of electrostatic interactions and conformational alterations. A notable increase in viscosity was observed for PEO solutions at an SDS concentration around T_2, for PVP solutions at an SDS concentration near T_1, and for PVA solutions containing SDBS [208, 209]. This can be

attributed to the expansion of the polymer chain resulting from the interaction with the charged surfactant molecules.

UV-visible Spectroscopy. UV-VIS spectroscopy is primarily used to investigate polymer-surfactant interactions by observing shifts in the absorbance wavelengths of dyes that are solubilized within the hydrophobic regions of aggregates. Such studies are frequently conducted in conjunction with fluorescence measurements for a more comprehensive analysis. The aggregation of polymer-surfactant complexes causes the solution to become turbid. The electrophoretic mobility of these complexes diminishes to nearly zero around the peak of turbidity. As micelles progressively bind to the polymer, charge neutralization occurs. This charge neutralization promotes the formation of larger aggregates. These electrically neutral complexes combine into multipolymer structures that strongly scatter light. Once saturation is reached, the complexes develop a net charge, leading them to either dissociate due to repulsive forces or remain insoluble. Consequently, turbidity either decreases due to the dispersion of the larger aggregates or remains unaffected in the solution. Chang and coworkers [210-213] have extensively used turbidity measurements to explore the physicochemical interactions between oppositely charged polymers and surfactants, revealing insights into the resulting macrostructure, phase behaviour, and dynamic properties.

Microscopy. Visible microscopy is typically not effective for examining molecular-level aggregates in polymer-surfactant bulk systems. However, advanced techniques such as scanning electron microscopy (SEM), transmission electron microscopy (TEM), and atomic force microscopy (AFM) provide powerful tools for directly visualizing the aggregates at this scale. AFM is well-suited for examining surface coverage but not for analysing the internal structure or detailed morphology of the complexes. The changes in the composition and properties of the complex within the precipitation region imply a modification in its structure or morphology. It is essential to understand the interplay between morphological traits and

performance to optimize functionality. Somasundaran et al. [214] observed a spectacular mesh-like architecture of the cat-Guar/SDES complex through cryo-TEM imaging. Moulik et al. [196] investigated the morphological transformations of the PDADMAC/SDS mixture using SEM, exploring how varying concentrations of isopropanol solvent influenced the complex structure.

Besides the aforementioned techniques, researchers have utilized a wide spectrum of conventional and advanced technologies. These include CV [215] for particle size analysis and zeta potential [216] for surface charge assessment; FTIR [217], Raman [218], NMR [219], EPR [220], ESR [221], XRD [222], SANS [223], and SAXS [224] for in-depth structural characterization; CLSM [225] for detailed surface morphology visualization; and thermal analysis tools such as TGA-DTA [226] and DSC [227] to evaluate thermal stability.

Scope and Objective

The interaction of amphiphilic substances with polymeric materials has emerged as a key area of research in soft colloidal systems, driven by its crucial role in a diverse range of applications, including drug delivery systems, cosmetic formulations, food stabilization, cleaning agents, surface coatings, textile processing, and oil extraction technologies. Although this domain of research has a long-established history, there is still a limited depth of knowledge regarding the combinations of different types, particularly in terms of core concepts and practical use. Furthermore, research on polymer-surfactant binary systems in polar protic media apart from water is noticeably lacking. It is possible to explore the physicochemical dimensions of the issue more comprehensively by conducting detailed studies both in aqueous and aquo-organic environments with the aid of advanced experimental techniques.

The primary focus of this field is the self-assembly of amphiphilic molecules under various environmental conditions, either independently or in interaction with other similar, closely related, or distinct species. The formation of fundamental structural units and the subsequent changes in shape and arrangement within the resulting dispersed systems are crucial for advancing both practical applications and the core understanding of soft matter. Furthermore, their durability, flow behaviour, organization, and material properties significantly influence their functionality and performance.

Chapter I

This work explores the interaction between hydroxyethyl cellulose (HEC), a non-ionic, water-soluble biopolymer, and sodium N-dodecanoyl sarcosinate (SDDS), a novel, environmentally friendly, amino acid-based surfactant. HEC is widely used in various industries, including pharmaceuticals, wastewater treatment, drug delivery, and coatings. SDDS, known for its high biodegradability, biocompatibility, and low toxicity, is considered a sustainable, "green" surfactant. The interaction between HEC and SDDS is primarily hydrophobic, and the strength of this interaction increases at higher polymer concentrations.

Chapter II

This study discusses the impact of the cosurfactant 2,2,2-trifluoroethanol (TFE) on the self-aggregation of the anionic surfactant sodium N-dodecanoyl sarcosinate (SDDS) and its interaction with the non-ionic biopolymer hydroxyethyl cellulose (HEC). TFE, due to its excellent miscibility with water, serves as an effective cosolvent in biological research, particularly for proteins and peptides, as well as in various organic synthesis reactions. Hydrophobic interactions between HEC and SDDS are observed, with TFE further intensifying the hydrophobic environment, thereby reducing the CMC of SDDS.

Chapter III

This chapter investigates the colloidal behaviour of a series of cationic alkyl triphenylphosphonium bromide surfactants (C_nTPB, where n = 12, 14, and 16) in a pectin-based aqueous medium, with a particular focus on the formation of macroscopic complex coacervate phases. The study elucidates the mechanisms of pectin-C_nTPB complexation, highlighting the combined effects of electrostatic and hydrophobic interactions. Pectin was chosen due to its bioavailability, affordability, and widespread use in the food and pharmaceutical industries. The alkyl triphenylphosphonium bromides, a novel class of cationic surfactants, are emerging as promising alternatives to ammonium-based surfactants. The phosphonium cations (C_nTP^+) have garnered attention for their beneficial role in mitochondrial nucleic acid transport, making C_nTPB a subject of extensive biotechnological research, particularly in the context of DNA interactions.

Chapter IV

This study examines the interaction between the polyanion pectin and cationic alkyl trimethylammonium bromide (C_nTAB) surfactants, focusing on how polymer charge density and surfactant hydrophobicity (determined by the alkyl tail lengths: n = 12, 14, 16, and 18) affect their complexation behaviour. The research aims to understand these interactions, as cationic surfactants are increasingly important in applications, such as, enhanced oil recovery, emulsification, nanoparticle dispersion, corrosion inhibition, dye solubilization, and wetting. Given the versatile role of pectin in the food and pharmaceutical industries, this study is relevant, offering valuable insights for both academic and industrial applications.

Chapter V

This study investigates the interaction between the sodium salt of hyaluronic acid (HA), an anionic polyelectrolyte (PE), and 1-hexadecyl-3-methyl imidazolium chloride ($C_{16}MImCl$), a surface-active ionic liquid (SAIL), in an aqueous environment. The research focuses on

characterizing the resulting PE-SAIL colloidal complex, analysing its interfacial properties, electrical mobility, coacervation, size, and morphology. Surface-active ionic liquids (SAILs) have gained considerable attention in chemical, biological, and materials science research due to their unique amphiphilic properties. The primary advantage of PE-SAIL complexes is their ability to enhance the solubilization of hydrophobic substances, offering significant potentiality in pharmaceutical applications. The stability and physicochemical properties of these colloidal aggregates are predominantly influenced by the polyelectrolyte's charge and the functional properties of the alkyl chain in the SAIL.

The report begins with an introduction, followed by seven chapters presenting the experimental results, and ends with a comprehensive summary and final conclusions. The essential data for the study are provided in the appendix as well as PDF versions of the relevant published papers.

References:

1. M. Friedman, Chemistry, formulation, and performance of syndet and combo bars, Soap Manufacturing Technology, AOCS Press, 2016, pp. 73-106.

2. M. Marhamati, G. Ranjbar, M. Rezaie, Effects of emulsifiers on the physicochemical stability of Oil-in-water Nanoemulsions: A critical review, J. Mol. Liq. 340 (2021) 117218.

3. H. Zhu, L. Chen, J. Xu, Q. Han, Experimental study on performance improvement of anionic surfactant foaming agent by xanthan gum, Constr. Build. Mater. 230 (2020) 116993.

4. S. De, S. Malik, A. Ghosh, R. Saha, B. Saha, A review on natural surfactants, RSC Adv. 81 (2015) 65757-65767.

5. B. Petkova, S. Tcholakova, M. Chenkova, K. Golemanov, N. Denkov, D. Thorley, S. Stoyanov, Foamability of aqueous solutions: Role of surfactant type and concentration, Adv. Colloid Interface Sci. 276 (2020) 102084.

6. P. Raffa, D. A. Wever, F. Picchioni, A. A. Broekhuis, Polymeric surfactants: synthesis, properties, and links to applications, Chem. Rev. 115 (2015) 8504-8563.

7. N. M. Kovalchuk, M. J. Simmons, Review of the role of surfactant dynamics in drop microfluidics, Adv. Colloid Interface Sci. 312 (2023) 102844.

8. H. Lu, C. Zheng, M. Xue, Z. Huang, pH-regulated surface properties and pH-reversible micelle transition of a zwitterionic gemini surfactant in aqueous solution, Phys. Chem. Chem. Phys. 18 (2016) 32192-32197.

9. M. Mella, A. Tagliabue, L. Mollica, S. Vaghi, L. Izzo, Inducing pH control over the critical micelle concentration of zwitterionic surfactants via polyacids adsorption: Effect of chain length and structure, J. Colloid Interface Sci. 606 (2022) 1636-1651.

10. A. P. Gerola, P. F. Costa, F. Nome, F. Quina, Micellization and adsorption of zwitterionic surfactants at the air/water interface, Curr. Opin. Colloid Interface Sci. 32 (2017) 48-56.

11. M. S. Kamal, A review of gemini surfactants: potential application in enhanced oil recovery, J. Surfactants Deterg. 19 (2016) 223-236.

12. R. Sharma, A. Kamal, M. Abdinejad, R. K. Mahajan, H. B. Kraatz, Advances in the synthesis, molecular architectures and potential applications of gemini surfactants, Adv. Colloid Interface Sci. 248 (2017) 35-68.

13. Z. Lei, B. Chen, Y. M. Koo, D. R. MacFarlane, Introduction: ionic liquids, Chem. Rev. 117 (2017) 6633-6635.

14. C. S. Buettner, A. Cognigni, C. Schröder, K. Bica-Schröder, Surface-active ionic liquids: A review, J. Mol. Liq. 347 (2022) 118160.

15. Z. Lei, C. Dai, J. Hallett, M. Shiflett, Introduction: Ionic liquids for diverse applications, Chem. Rev. 124 (2024) 7533-7535.

16. D. R. Perinelli, M. Cespi, N. Lorusso, G. F. Palmieri, G. Bonacucina, P. Blasi, Surfactant self-assembling and critical micelle concentration: one approach fits all?, Langmuir 36 (2020) 5745-5753.

17. T. Chakraborty, I. Chakraborty, S. Ghosh, The methods of determination of critical micellar concentrations of the amphiphilic systems in aqueous medium, Arab. J. Chem. 4 (2011) 265-270.

18. M. Manaargadoo-Catin, A. Ali-Cherif, J. L. Pougnas, C. Perrin, Hemolysis by surfactants—A review. Adv. Colloid Interface Sci. 228 (2016) 1-6.

19. W. Al-Soufi, L. Piñeiro, M. Novo, A model for monomer and micellar concentrations in surfactant solutions: Application to conductivity, NMR, diffusion, and surface tension data, J. Colloid Interface Sci. 370 (2012) 102-110.

20. M. Karg, T. A. König, M. Retsch, C. Stelling, P. M. Reichstein, T. Honold, M. Thelakkat, A. Fery, Colloidal self-assembly concepts for light management in photovoltaics, Mater. Today 18 (2015) 185-205.

21. R. van Dommelen, P. Fanzio, L. Sasso, Surface self-assembly of colloidal crystals for micro-and nano-patterning, Adv. Colloid Interface Sci. 251 (2018) 97-114.

22. N. Scholz, T. Behnke, U. Resch-Genger, Determination of the critical micelle concentration of neutral and ionic surfactants with fluorometry, conductometry, and surface tension—a method comparison, J. Fluoresc. 28 (2018) 465-476.

23. B. Tanhaei, N. Saghatoleslami, M. P. Chenar, A. Ayati, M. Hesampour, M. Mänttäri, Experimental study of CMC evaluation in single and mixed surfactant systems, using the UV–Vis spectroscopic method, J. Surfactants Deterg. 16 (2013) 357-362.

24. H. Sifaoui, K. Ługowska, U. Domańska, A. Modaressi, M. Rogalski, Ammonium ionic liquid as modulator of the critical micelle concentration of ammonium surfactant at aqueous solution: conductometric and dynamic light scattering (DLS) studies, J. Colloid Interface Sci. 314 (2007) 643-650.

25. O. E. Smith, L. J. Waters, W. Small, S. Mellor, CMC determination using isothermal titration calorimetry for five industrially significant non-ionic surfactants, Colloids Surf. B 211 (2022) 112320.

26. T. Farías, L. C. de Ménorval, J. Zajac, A. Rivera, Solubilization of drugs by cationic surfactants micelles: Conductivity and ^{1}H NMR experiments, Colloids Surf. A: Physicochem. Eng. Asp. 345 (2009) 51-57.

27. S. I. Jenkins, C. M. Collins, M. G. Khaledi, Perfluorinated alcohols induce complex coacervation in mixed surfactants, Langmuir 32 (2016) 2321-2330.

28. W. Zhao, Y. Wang, Coacervation with surfactants: From single-chain surfactants to gemini surfactants, Adv. Colloid Interface Sci. 239 (2017) 199-212.

29. T. Geng, C. Zhang, Y. Jiang, H. Ju, Y. Wang, Synergistic effect of binary mixtures contained newly cationic surfactant: Interaction, aggregation behaviors and application properties, J. Mol. Liq. 232 (2017) 36-44.

30. A. Rehman, M. Usman, T. H. Bokhari, A. ul Haq, M. Saeed, H. M. Rahman, M. Siddiq, A. Rasheed, M. U. Nisa, The application of cationic-nonionic mixed micellar media for enhanced solubilization of direct Brown 2 dye, J. Mol. Liq. 301 (2020) 112408.

31. N. Azum, M. A. Rub, A. M. Asiri, Bile salt–bile salt interaction in mixed monolayer and mixed micelle formation, J. Chem. Thermodyn. 128 (2019) 406-414.

32. P. Y. Parekh, V. I. Patel, M. R. Khimani, P. Bahadur, Self-assembly of bile salts and their mixed aggregates as building blocks for smart aggregates, Adv. Colloid Interface Sci. 312 (2023) 102846.

33. F. Bot, D. Cossuta, J. A. O'Mahony, Inter-relationships between composition, physicochemical properties and functionality of lecithin ingredients, Trends Food Sci. Technol. 111 (2021) 261-270.

34. E. Kushan, C. Demir, E. Senses, Surfactant driven liquid to soft solid transition of cellulose nanocrystal suspensions, Langmuir 36 (2020) 9551-9561.

35. H. Lu, Q. Shi, B. Wang, Z. Huang, Spherical-to-wormlike micelle transition in a pseudogemini surfactant system with two types of effective pH-responsive groups, Colloids Surf. A: Physicochem. Eng. Asp. 494 (2016) 74-80.

36. B. Wen, B. Bai, R. G. Larson, Surfactant desorption and scission free energies for cylindrical and spherical micelles from umbrella-sampling molecular dynamics simulations, J. Colloid Interface Sci. 599 (2021) 773-784.

37. G. Garg, P. A. Hassan, S. K. Kulshreshtha, Dynamic light scattering studies of rod-like micelles in dilute and semi-dilute regime, Colloids Surf. A: Physicochem. Eng. Asp. 275 (2006) 161-167.

38. A. S. Poulos, M. Nania, P. Lapham, R. M. Miller, A. J. Smith, H. Tantawy, J. Caragay, J. Gummel, O. Ces, E. S. Robles, J. T. Cabral, Microfluidic SAXS study of lamellar and multilamellar vesicle phases of linear sodium alkylbenzenesulfonate surfactant with intrinsic isomeric distribution, Langmuir 32 (2016) 5852-5861.

39. N. Zoratto, I. Grillo, P. Matricardi, C. A. Dreiss, Supramolecular gels of cholesterol-modified gellan gum with disc-like and worm-like micelles, J. Colloid Interface Sci. 556 (2019) 301-312.

40. K. Vogtt, G. Beaucage, M. Weaver, H. Jiang, Thermodynamic stability of worm-like micelle solutions, Soft Matter 13 (2017) 6068-6078.

41. J. Iyer, D. Blankschtein, Are ellipsoids feasible micelle shapes? An answer based on a molecular-thermodynamic model of nonionic surfactant micelles, J. Phys. Chem. B 116 (2012) 6443-6454.

42. Y. Wei, F. Gao, H. Wang, G. Liu, Q. Xia, S. Yuan, A molecular dynamics study combining with entropy calculation on the packing state of hydrophobic chains in micelle interior, J. Mol. Liq. 283 (2019) 860-866.

43. K. Kondo, J. K. Klosterman, M. Yoshizawa, Aromatic micelles as a new class of aqueous molecular flasks, Chem.– Eur. J. 23 (2017) 16710-16721.

44. S. Fujii, J. H. Lee, K. Sakurai, Discovery of monodisperse micelles with discrete aggregation numbers, molecular assemblies: characterization and applications, American Chemical Society, 2020, pp. 1-13.

45. K. Khalid, M. A. Noh, S. M. Zain, M. N. Khan, Determination of relative counterion binding constant to cationic micelles, Top. Curr. Chem. 375 (2017) 1-8.

46. T. Morita, S. Yada, T. Yoshimura, Ellipsoidal micelle formation of quaternary ammonium salt-based gemini surfactants: structural analysis through small-angle X-ray scattering, Soft Matter 20 (2024) 7030-7037.

47. I. W. Hamley, V. Castelletto, Sodium Dodecyl Sulfate micelles: accurate analysis of Small-Angle X-ray Scattering data through form factor and Atomistic Molecular Dynamics modelling, Colloids Surf. A: Physicochem. Eng. Asp. (2024) 134394.

48. D. Morales, J. Miras, M. Homs, The spherical droplet model extended: The relation between surfactant packing and aggregate composition, Colloids Surf. A: Physicochem. Eng. Asp. 555 (2018) 111-120.

49. C. V. Kulkarni, Calculating the 'chain splay' of amphiphilic molecules: towards quantifying the molecular shapes, Chem. Phys. Lipids 218 (2019) 16-21.

50. F. M. Menger, H. Yoshinaga, K. S. Venkatasubban, A. R. Das, Solvolysis of a carbonate and a benzhydryl chloride inside micelles. Evidence for a porous cluster micelle, J. Org. Chem. 46 (1981) 415-419.

51. M. N. Khan, Effects of anionic micelles on the intramolecular general-base-catalysed hydrazinolysis and hydrolysis of phenyl salicylate. Evidence for a porous cluster micelle, J. Chem. Soc., Perkin Trans. 2 (1990) 445-457.

52. D. Danino, Cryo-TEM of soft molecular assemblies, Curr. Opin. Colloid Interface Sci. 17 (2012) 316-329.

53. D. Morales, J. Miras, M. Homs, The spherical droplet model extended: The relation between surfactant packing and aggregate composition, Colloids Surf. A: Physicochem. Eng. Asp. 555 (2018) 111-120.

54. Z. Hafidi, M. El Achouri, The effect of polar head and chain length on the physicochemical properties of micellization and adsorption of amino alcohol-based surfactants, J. Surfactants Deterg. 22 (2019) 663-672.

55. G. Trefalt, S. H. Behrens, M. Borkovec, Charge regulation in the electrical double layer: ion adsorption and surface interactions, Langmuir 32 (2016) 380-400.

56. A. Kundu, P. K. Verma, M. Cho, Water structure and dynamics in the stern layer of micelles: femtosecond mid-infrared pump-probe spectroscopy study, J. Phys. Chem. B 123 (2019) 5238-5245.

57. R. Pool, P. G. Bolhuis, The influence of micelle formation on the stability of colloid surfactant mixtures, Phys. Chem. Chem. Phys. 12 (2010) 14789-14797.

58. S. Javadian, J. Kakemam, Intermicellar interaction in surfactant solutions; a review study, J. Mol. Liq. 242 (2017) 115-128.

59. A. N. Semenov, A. V. Subbotin, Theory of self-assembling structures of model oligopeptides, Macromolecules 43 (2010) 3487-3501.

60. I. L. Topolnicki, P. A. FitzGerald, R. Atkin, G. G. Warr, Effect of protic ionic liquid and surfactant structure on partitioning of polyoxyethylene non-ionic surfactants, ChemPhysChem 15 (2014) 2485-2489.

61. H. Yang, J. Liang, C. Lin, Y. Zhu, J. Yan, W. Zhang, J. Pang, W. Yang, F. Yang, L. Wang, Effect of Dihydropyridine enrichment in the microstructure of the palisade layer on the stability of fat nano-emulsions, J. Pharm. Sci. 110 (2021) 3648-3658.

62. H. Akbaş, S. Kasapoğlu, M. Boz, Aggregation behavior and intermolecular interaction of binary surfactant mixtures based on cationic geminis and nonionic surfactants, Colloid Polym. Sci. 293 (2015) 3429-3437.

63. M. Velinova, D. Sengupta, A. V. Tadjer, S. J. Marrink, Sphere-to-rod transitions of nonionic surfactant micelles in aqueous solution modeled by molecular dynamics simulations, Langmuir 27 (2011) 14071-14077.

64. C. A. Gracia, S. Gómez-Barreiro, A. González-Pérez, J. Nimo, J. R. Rodrıguez, Static and dynamic light-scattering studies on micellar solutions of alkyldimethylbenzylammonium chlorides, J. Colloid Interface Sci. 276 (2004) 408-413.

65. M. Amann, L. Willner, J. Stellbrink, A. Radulescu, D. Richter, Studying the concentration dependence of the aggregation number of a micellar model system by SANS, Soft Matter 11 (2015) 4208-4217.

66. A. O. Ba-Salem, J. Duhamel, Determination of the aggregation number of pyrene-labeled gemini surfactant micelles by pyrene fluorescence quenching measurements, Langmuir 37 (2021) 6069-6079.

67. A. R. Tehrani-Bagha, J. Kärnbratt, J. E. Löfroth, K. Holmberg, Cationic ester-containing gemini surfactants: Determination of aggregation numbers by time-resolved fluorescence quenching, J. Colloid Interface Sci. 376 (2012) 126-132.

68. L. Piñeiro, M. Novo, W. Al-Soufi, Fluorescence emission of pyrene in surfactant solutions, Adv. Colloid Interface Sci. 215 (2015) 1-2.

69. J. K. Salem, I. M. El-Nahhal, S. F. Salama, Determination of the critical micelle concentration by absorbance and fluorescence techniques using fluorescein probe, Chem. Phys. Lett. 730 (2019) 445-450.

70. K. M. Glenn, R. M. Palepu, Fluorescence probing of aerosol OT based reverse micelles and microemulsions in n-alkanes (C6–C16) and quenching of Safranine-T in these systems, J. Photochem. Photobiol. A Chem. 179 (2006) 283-288.

71. S. Dhar, D. K. Rana, A. Sarkar, T. K. Mandal, S. Ghosh, S. C. Bhattacharya, Physicochemical characterization of reverse micelles of Triton X using 1-anthracene sulphonate as fluorescent probe: A spectroscopic study, Colloids Surf. A Physicochem. Eng. Asp. 349 (2009) 117-124.

72. A. K. Bordbar, A. Taheri-Kafrani, Binding and fluorescence study on interaction of human serum albumin (HSA) with cetylpyridinium chloride (CPC), Colloids Surf. B: Biointerfaces 55 (2007) 84-89.

73. A. G. Gilani, H. Dezhampanah, Z. Poormohammadi-Ahandani, A comparative spectroscopic study of thiourea effect on the photophysical and molecular association behavior of various phenothiazine dyes, Spectrochim. Acta A Mol. Biomol. Spectrosc. 179 (2017) 132-143.

74. S. S. Tan, S. J. Kim, E. T. Kool, Differentiating between fluorescence-quenching metal ions with polyfluorophore sensors built on a DNA backbone, J. Am. Chem. Soc. 133 (2011) 2664-2671.

75. S. Wu, M. Tachiya, Z. Yan, An improved procedure for determination of the mean aggregation number of micelles, Spectrochim. Acta A Mol. Biomol. Spectrosc. 138 (2015) 807-810.

76. S. S. Shah, N. U. Jamroz, Q. M. Sharif, Micellization parameters and electrostatic interactions in micellar solution of sodium dodecyl sulfate (SDS) at different temperatures, Colloids Surf. A: Physicochem. Eng. Asp. 178 (2001) 199-206.

77. K. S. Sharma, P. A. Hassan, A. K. Rakshit, Self aggregation of binary surfactant mixtures of a cationic dimeric (gemini) surfactant with nonionic surfactants in aqueous medium, Colloids Surf. A: Physicochem. Eng. Asp. 289 (2006) 17-24.

78. S. Ghosh, A. Das Burman, G. C. De, A. R. Das, Interfacial and self-aggregation of binary mixtures of anionic and nonionic amphiphiles in aqueous medium, J. Phys. Chem. B 115 (2011) 11098-11112.

79. S. E. Anachkov, K. D. Danov, E. S. Basheva, P. A. Kralchevsky, K. P. Ananthapadmanabhan, Determination of the aggregation number and charge of ionic surfactant micelles from the stepwise thinning of foam films, Adv. Colloid Interface Sci. 183 (2012) 55-67.

80. M. Poša, A. Sebenji, Determination of number-average aggregation numbers of bile salts micelles with a special emphasis on their oxo derivatives—The effect of the steroid skeleton Biochim. Biophys. Acta - Gen. Subj. 1840 (2014) 1072-1082.

81. D. Madenci, S. U. Egelhaaf, Self-assembly in aqueous bile salt solutions, Curr. Opin. Colloid Interface Sci. 15 (2010) 109-115.

82. J. Oremusová, Z. Vitková, A. Vitko, M. Tárník, E. Miklovičová, O. Ivánková, J. Murgaš, D. Krchňák, Effect of molecular composition of head group and temperature on micellar properties of ionic surfactants with C12 alkyl chain, Molecules 24 (2019) 651.

83. N. Patra, D. Ray, V. K. Aswal, S. Ghosh, Exploring physicochemical interactions of different salts with sodium N-dodecanoyl sarcosinate in aqueous solution, ACS Omega 3 (2018) 9256-9266.

84. B. Zehner, F. Schmidt, W. Korth, M. Cokoja, A. Jess, Determination of the critical micelle concentration of imidazolium ionic liquids in aqueous hydrogen peroxide, Langmuir 35 (2019) 16297-16303.

85. R. Zarganian, A. K. Bordbar, R. Amiri, M. Tamannaei, A. R. Khosropour, I. Mohammadpoor-Baltork, Micellization of pentanediyl-1, 5-bis (hydroxyethylmethyl hexadecylammonium bromide) as a cationic gemini surfactant in aqueous solutions: Investigation using conductometry and fluorescence techniques, J. Solution Chem. 40 (2011) 921-928.

86. R. Aggarwal, S. Singh, V. Saini, G. Kaur, Synthesis, characterization, and evaluation of surface and thermal properties and cytotoxicity of 2-hydroxy-3-phenoxypropyl imidazolium bola-type gemini amphiphiles, J. Surfactants Deterg. 22 (2019) 33-46.

87. G. A. Gainanova, G. I. Vagapova, V. V. Syakaev, A. R. Ibragimova, F. G. Valeeva, E. V. Tudriy, I. V. Galkina, O. N. Kataeva, L. Y. Zakharova, S. K. Latypov, A. I. Konovalov, Self-assembling systems based on amphiphilic alkyltriphenylphosphonium bromides: Elucidation of the role of head group, J. Colloid Interface Sci. 367 (2012) 327-336.

88. J. Dey, N. Sultana, K. Ismail, Counter ion binding in solutions of sodium dodecylsulfate in water–ethylene glycol mixtures and the Corrin–Harkins equation, J. Mol. Liq. 207 (2015) 107-111.

89. M. K. Banjare, R. Kurrey, T. Yadav, S. Sinha, M. L. Satnami, K. K. Ghosh, A comparative study on the effect of imidazolium-based ionic liquid on self-aggregation of cationic, anionic and nonionic surfactants studied by surface tension, conductivity, fluorescence and FTIR spectroscopy, J. Mol. Liq. 241 (2017) 622-632.

90. A. Ghasemi, A. Bagheri, Effects of alkyl chain length on synergetic interaction and micelle formation between a homologous series of n-alkyltrimethylammonium bromides and amphiphilic drug propranolol hydrochloride, J. Mol. Liq. 298 (2020) 111948.

91. B. Zhu, D. Belmessieri, J. F. Ontiveros, J. M. Aubry, G. R. Chen, N. Duguet, M. Lemaire, Trialkylamine-catalyzed aldolization of unprotected 1, 3-dihydroxyacetone (DHA) toward C–C bond-linked tetraol surfactants, ACS Sustain. Chem. Eng. 6 (2018) 2630-2640.

92. L. Zhou, Y. Li, S. Li, X. Shen, C. Wang, Cholic Acid-derived facial surfactants with long side-chain quaternary ammonium: synthesis and antimicrobial activity study, J. Surfactants Deterg. 19 (2016) 803-811.

93. U. Thapa, M. Kumar, R. Chaudhary, V. Singh, S. Singh, A. Srivastava, Binding behaviour of hydrophobic drug tetracaine hydrochloride used as organic counterion on ionic surfactants, J. Mol. Liq. 335 (2021) 116564.

94. S. I. Karakashev, S. K. Smoukov, CMC prediction for ionic surfactants in pure water and aqueous salt solutions based solely on tabulated molecular parameters, J. Colloid Interface Sci. 501 (2017) 142-149.

95. A. Rodríguez, M. D. Graciani, M. L. Moyá, Effects of addition of polar organic solvents on micellization, Langmuir 24 (2008) 12785-12792.

96. G. N. Smith, P. Brown, S. E. Rogers, J. Eastoe, Evidence for a critical micelle concentration of surfactants in hydrocarbon solvents, Langmuir 29 (2013) 3252-3258.

97. S. Chauhan, K. Sharma, Effect of temperature and additives on the critical micelle concentration and thermodynamics of micelle formation of sodium dodecyl benzene sulfonate and dodecyltrimethylammonium bromide in aqueous solution: A conductometric study, J. Chem. Thermodyn. 71 (2014) 205-211.

98. S. Chauhan, M. Kaur, K. Kumar, M. S. Chauhan, Study of the effect of electrolyte and temperature on the critical micelle concentration of dodecyltrimethylammonium bromide in aqueous medium, J. Chem. Thermodyn. 78 (2014) 175-181.

99. P. Kroll, J. Benke, S. Enders, C. Brandenbusch, G. Sadowski, Influence of temperature and concentration on the self-assembly of nonionic CiEj surfactants: A light scattering study, ACS Omega 7 (2022) 7057-7065.

100. M. Lesemann, K. Thirumoorthy, Y. J. Kim, J. Jonas, M. E. Paulaitis, Pressure dependence of the critical micelle concentration of a nonionic surfactant in water studied by 1H-NMR, Langmuir 14 (1998) 5339-5341.

101. K. Hara, H. Kuwabara, O. Kajimoto, K. Bhattacharyya, Effect of pressure on the critical micelle concentration of neutral surfactant using fluorescence probe method, J. Photochem. Photobiol. A Chem. 124 (1999) 159-162.

102. E. Mayoral, J. A. Arcos-Casarrubias, A. G. Goicochea, Self–assembly of model surfactants as reverse micelles in nonpolar solvents and their role as interfacial tension modifiers, Colloids Surf. A Physicochem. Eng. Asp. 615 (2021) 126244.

103. R. Urano, G. A. Pantelopulos, J. E. Straub, Aerosol-OT surfactant forms stable reverse micelles in apolar solvent in the absence of water, J. Phys. Chem. B 123 (2019) 2546-2557.

104. B. Kang, H. Tang, Z. Zhao, S. Song, Hofmeister series: Insights of ion specificity from amphiphilic assembly and interface property, ACS Omega 5 (2020) 6229-6239.

105. A. Jakubowska, Interactions of different counterions with cationic and anionic surfactants, J. Colloid Interface Sci. 346 (2010) 398-404.

106. B. Sarsenbekuly, W. Kang, H. Fan, H. Yang, C. Dai, B. Zhao, S. B. Aidarova, Study of salt tolerance and temperature resistance of a hydrophobically modified polyacrylamide based novel functional polymer for EOR, Colloids Surf. A: Physicochem. Eng. Asp. 514 (2017) 91-97.

107. A. Fanova, I. Davidovich, Y. Talmon, A. Skandalis, S. Pispas, M. Stepanek, Modification of the co-assembly behavior of double-hydrophilic block polyelectrolytes by hydrophobic terminal groups: ordered nanostructures with interpolyelectrolyte complex domains, ACS Appl. Polym. Mater. 3 (2021) 1956-1963.

108. P. Loganathan, M. Gradzielski, H. Bustamante, S. Vigneswaran, Progress, challenges, and opportunities in enhancing NOM flocculation using chemically modified chitosan: a review towards future development, Environ. Sci.: Water Res. Technol. 6 (2020) 45-61.

109. J. Wu, F. Xu, S. Li, P. Ma, X. Zhang, Q. Liu, R. Fu, D. Wu, Porous polymers as multifunctional material platforms toward task-specific applications, Adv. Mater. 31 (2019) 1802922.

110. A. Khan, M. Puttegowda, P. Jagadeesh, H. M. Marwani, A. M. Asiri, A. Manikandan, A. A. Khan, G. M. Ashraf, S. M. Rangappa, S. Siengchin, Review on nitride compounds and its polymer composites: a multifunctional material, J. Mater. Res. Technol. 18 (2022) 2175-2193.

111. Z. Shi, X. Gao, M. W. Ullah, S. Li, Q. Wang, G. Yang, Electroconductive natural polymer-based hydrogels, Biomaterials 111 (2016) 40-54.

112. J. A. Galbis, M. D. García-Martín, M. V. De Paz, E. Galbis, Synthetic polymers from sugar-based monomers, Chem. Rev. 116 (2016) 1600-1636.

113. I. Dmour, M. O. Taha, Natural and semisynthetic polymers in pharmaceutical nanotechnology, Organic materials as smart nanocarriers for drug delivery (2018) 35-100.

114. C. Duan, K. Gao, J. J. van Franeker, F. Liu, M. M. Wienk, R. A. Janssen, Toward practical useful polymers for highly efficient solar cells via a random copolymer approach, J. Am. Chem. Soc. 138 (2016) 10782-10785.

115. J. Huang, S. R. Turner, Recent advances in alternating copolymers: the synthesis, modification, and applications of precision polymers, Polymer 116 (2017) 572-586.

116. M. Karayianni, S. Pispas, Block copolymer solution self-assembly: Recent advances, emerging trends, and applications, J. Polym. Sci. 59 (2021) 1874-1898.

117. C. Cummins, R. Lundy, J. J. Walsh, V. Ponsinet, G. Fleury, M. A. Morris, Enabling future nanomanufacturing through block copolymer self-assembly: A review, Nano Today 35 (2020) 100936.

118. T. Nishimura, S. Fujii, K. Sakurai, Y. Sasaki, K. Akiyoshi, Manipulating the morphology of amphiphilic graft-copolymer assemblies by adjusting the flexibility of the main chain, Macromolecules 54 (2021) 54 7003-7009.

119. D. Kumar, S. Gihar, M. K. Shrivash, P. Kumar, P. P. Kundu, A review on the synthesis of graft copolymers of chitosan and their potential applications, Int. J. Biol. Macromol. 163 (2020) 2097-2112.

120. M. Gradzielski, I. Hoffmann, Polyelectrolyte-surfactant complexes (PESCs) composed of oppositely charged components, Curr. Opin. Colloid Interface Sci. 35 (2018) 124-141.

121. I. Varga, R. A. Campbell, General physical description of the behavior of oppositely charged polyelectrolyte/surfactant mixtures at the air/water interface, Langmuir 33 (2017) 5915-5924.

122. C. Brinatti, J. Huang, R. M. Berry, K. C. Tam, W. Loh, Structural and energetic studies on the interaction of cationic surfactants and cellulose nanocrystals, Langmuir 32 (2016) 689-698.

123. K. Kogej, Association and structure formation in oppositely charged polyelectrolyte–surfactant mixtures, Adv. Colloid Interface Sci. 158 (2010) 68-83.

124. S. Shrivastava, J. Dey, Interaction of anionic surfactant with polymeric nanoparticles of similar charge, J. Colloid Interface Sci. 350 (2010) 220-228.

125. M. Doiron, J. Moulins, R. Dean, R. M. Palepu, Interactions of alkyl triphenyl phosphonium bromides with aqueous solutions of LM200 and JR400 polymers, Phys. Chem. Liq. 46 (2008) 202-212.

126. A. Pal, S. Yadav, Effect of anionic polyelectrolyte sodium carboxymethylcellulose on the aggregation behavior of surface active ionic liquids in aqueous solution, J. Mol. Liq. 241 (2017) 584-594.

127. R. Sharma, A. Kamal, T. S. Kang, R. K. Mahajan, Interactional behavior of the polyelectrolyte poly sodium 4-styrene sulphonate (NaPSS) with imidazolium based surface active ionic liquids in an aqueous medium, Phys. Chem. Chem. Phys. 17 (2015) 23582-23594.

128. A. Pal, R. Maan, Investigations of interactions between surface active ionic liquid 1-butyl-3-methyl imidazolium dodecylbenzenesulfonate and cationic polyelectrolyte poly (diallyldimethylammonium chloride) in aqueous solution, J. Mol. Liq. 254 (2018) 304-311.

129. G. Singh, G. Singh, T. S. Kang, Colloidal systems of surface active ionic liquids and sodium carboxymethyl cellulose: physicochemical investigations and preparation of magnetic nano-composites, Phys. Chem. Chem. Phys. 20 (2018) 18528-18538.

130. X. Wang, Y. Li, J. Li, J. Wang, Y. Wang, Z. Guo, H. Yan, Salt effect on the complex formation between polyelectrolyte and oppositely charged surfactant in aqueous solution, J. Phys. Chem. B 109 (2005) 10807-10812.

131. C. Wang, K. C. Tam, New insights on the interaction mechanism within oppositely charged polymer/surfactant systems, Langmuir 18 (2002) 6484-6490.

132. T. Chakraborty, I. Chakraborty, S. P. Moulik, S. Ghosh, Physicochemical and conformational studies on BSA− surfactant interaction in aqueous medium, Langmuir 25 (2009) 3062-3074.

133. L. Y. Zakharova, G. I. Kaupova, D. R. Gabdrakhmanov, G. A. Gaynanova, E. A. Ermakova, A. R. Mukhitov, I. V. Galkina, S. V. Cheresiz, A. G. Pokrovsky, P. V. Skvortsova, Y. V. Gogolev, Alkyl triphenylphosphonium surfactants as nucleic acid carriers: complexation efficacy toward DNA decamers, interaction with lipid bilayers and cytotoxicity studies, Phys. Chem. Chem. Phys. 21 (2019) 16706-16717.

134. Y. P. Timilsena, T. O. Akanbi, N. Khalid, B. Adhikari, C. J. Barrow, Complex coacervation: Principles, mechanisms and applications in microencapsulation, Int. J. Biol. Macromol. 121 (2019) 1276-1286.

135. T. Moschakis, C. G. Biliaderis, Biopolymer-based coacervates: Structures, functionality and applications in food products, Curr. Opin. Colloid Interface Sci. 28 (2017) 96-109.

136. C. Schmitt, S. L. Turgeon, Protein/polysaccharide complexes and coacervates in food systems, Adv. Colloid Interface Sci. 167 (2011) 63-70.

137. W. C. Blocher, S. L. Perry, Complex coacervate-based materials for biomedicine, Wiley Interdiscip. Rev.: Nanomed. Nanobiotechnology 9 (2017) 1442.

138. C. Lim, W. C. Blocher McTigue, Form Equals Function: Influence of Coacervate Architecture on Drug Delivery Applications, ACS Biomater. Sci. Eng. 10 (2024) 6766-6789.

139. C. C. Schuurmans, A. Abbadessa, M. A. Bengtson, G. Pletikapic, H. B. Eral, G. Koenderink, R. Masereeuw, W. E. Hennink, T. Vermonden, Complex coacervation-based loading and tunable release of a cationic protein from monodisperse glycosaminoglycan microgels, Soft Matter 14 (2018) 6327-6341.

140. Y. Jho, H. Y. Yoo, Y. Lin, S. Han, D. S. Hwang, Molecular and structural basis of low interfacial energy of complex coacervates in water, Adv. Colloid Interface Sci. 239 (2017) 61-73.

141. B. Ghosh, R. Bose, T. D. Tang, Can coacervation unify disparate hypotheses in the origin of cellular life?, Curr. Opin. Colloid Interface Sci. 52 (2021) 101415.

142. T. Z. Jia, M. Caudan, I. Mamajanov, Origin of species before origin of life: the role of speciation in chemical evolution, Life 11 (2021) 154.

143. C. E. Sing, Development of the modern theory of polymeric complex coacervation, Adv. Colloid Interface Sci. 239 (2017) 2-16.

144. M. Radhakrishna, K. Basu, Y. Liu, R. Shamsi, S. L. Perry, C. E. Sing, Molecular connectivity and correlation effects on polymer coacervation, Macromolecules 50 (2017) 3030-3037.

145. C. E. Sing, S. L. Perry, Recent progress in the science of complex coacervation, Soft Matter 16 (2020) 2885-2914.

146. J. K. Tom, A. A. Deniz, Complex dynamics of multicomponent biological coacervates, Curr. Opin. Colloid Interface Sci. 56 (2021) 101488.

147. L. Zhou, H. Shi, Z. Li, C. He, Recent advances in complex coacervation design from macromolecular assemblies and emerging applications, Macromol. Rapid Commun. 41 (2020) 2000149.

148. A. M. Rumyantsev, N. E. Jackson, J. J. De Pablo, Polyelectrolyte complex coacervates: Recent developments and new frontiers, Annu. Rev. Condens. Matter Phys. 12 (2021) 155-176.

149. F. Comert, A. J. Malanowski, F. Azarikia, P. L. Dubin, Coacervation and precipitation in polysaccharide–protein systems, Soft Matter 12 (2016) 4154-4161.

150. Z. Lin, T. Beneyton, J. C. Baret, N. Martin, Coacervate droplets for synthetic cells, Small Methods 7 (2023) 2300496.

151. N. Devi, M. Sarmah, B. Khatun, T. K. Maji, Encapsulation of active ingredients in polysaccharide–protein complex coacervates, Adv. Colloid Interface Sci. 239 (2017) 136-145.

152. G. Y. Li, Q. H. Chen, C. R. Su, H. Wang, S. He, J. Liu, A. Nag, Y. Yuan, Soy protein-polysaccharide complex coacervate under physical treatment: Effects of pH, ionic strength and polysaccharide type, Innov. Food Sci. Emerg. Technol. 68 (2021) 102612.

153. L. Gentile, Protein–polysaccharide interactions and aggregates in food formulations, Curr. Opin. Colloid Interface Sci. 48 (2020) 18-27.

154. A. Napiórkowska, M. Kurek, Coacervation as a novel method of microencapsulation of essential oils—A review, Molecules 27 (2022) 5142.

155. G. A. Ferreira, W. Loh, Liquid crystalline nanoparticles formed by oppositely charged surfactant-polyelectrolyte complexes, Curr. Opin. Colloid Interface Sci. 32 (2017) 11-22.

156. U. Lappan, U. Scheler, Influence of the nature of the ion pairs on the segmental dynamics in polyelectrolyte complex coacervate phases, Macromolecules 50 (2017) 8631-8636.

157. S. P. Danielsen, S. Panyukov, M. Rubinstein, Ion pairing and the structure of gel coacervates, Macromolecules 53 (2020) 9420-9442.

158. J. Fu, H. M. Fares, J. B. Schlenoff, Ion-pairing strength in polyelectrolyte complexes, Macromolecules 50 (2017) 1066-1074.

159. F. Ardestani, A. Haghighi Asl, A. Rafe, Phase separation and formation of sodium caseinate/pectin complex coacervates: effects of pH on the complexation, Chem. Biol. Technol. Agric. 9 (2022) 83.

160. W. Xiong, Y. Li, C. Ren, J. Li, B. Li, F. Geng, Thermodynamic parameters of gelatin-pectin complex coacervation, Food Hydrocoll. 120 (2021) 106958.

161. J. K. Yan, W. Y. Qiu, Y. Y. Wang, J. Y. Wu, Biocompatible polyelectrolyte complex nanoparticles from lactoferrin and pectin as potential vehicles for antioxidative curcumin, J. Agric. Food Chem. 65 (2017) 5720-5730.

162. Q. Ru, Y. Wang, J. Lee, Y. Ding, Q. Huang, Turbidity and rheological properties of bovine serum albumin/pectin coacervates: Effect of salt concentration and initial protein/polysaccharide ratio, Carbohydr. Polym. 88 (2012) 838-846.

163. A. Y. Xu, L. D. Melton, T. M. Ryan, J. P. Mata, A. Rekas, M. A. Williams, D. J. McGillivray, Effects of polysaccharide charge pattern on the microstructures of β-lactoglobulin-pectin complex coacervates, studied by SAXS and SANS, Food Hydrocoll. 77 (2018) 952-963.

164. H. Jamshidian, A. Rafe, Complex coacervate of wheat germ protein/high methoxy pectin in encapsulation of d-limonene, Chem. Biol. Technol. Agric. 11 (2024) 60.

165. M. Raei, A. Rafe, F. Shahidi, Rheological and structural characteristics of whey protein-pectin complex coacervates, J. Food Eng. 228 (2018) 25-31.

166. Y. Lan, J. B. Ohm, B. Chen, J. Rao, Phase behavior and complex coacervation of concentrated pea protein isolate-beet pectin solution, Food Chem. 307 (2020) 125536.

167. V. B. Maciel, C. M. Yoshida, T. T. Franco, Chitosan/pectin polyelectrolyte complex as a pH indicator, Carbohydr. Polym. 132 (2015) 537-545.

168. D. Asker, J. Weiss, D. J. McClements, Analysis of the interactions of a cationic surfactant (lauric arginate) with an anionic biopolymer (pectin): isothermal titration calorimetry, light scattering, and microelectrophoresis, Langmuir 25 (2009) 116-122.

169. T. Chakraborty, I. Chakraborty, S. Ghosh, Sodium carboxymethylcellulose− CTAB interaction: a detailed thermodynamic study of polymer− surfactant interaction with opposite charges, Langmuir 22 (2006) 9905-9913.

170. S. E. Burke, R. M. Palepu, S. K. Hait, S. P. Moulik, Physicochemical investigations on the interaction of cationic cellulose ether derivatives with cationic amphiphiles in an aqueous environment, Progress in Colloid and Polymer Science, 122, 2003, pp. 47-55.

171. S. M. Shaban, J. Kang, D. H. Kim, Surfactants: Recent advances and their applications, Compos. Commun. 22 (2020) 100537.

172. S. Ghosh, A. Mal, T. Chakraborty, G. C. De, D. G. Marangoni, Interaction of a cationic surfactant with an oppositely charged polymer, J. Surface Sci. Technol. 32 (2016) 107-114.

173. A. A. Ansari, M. Kamil, Kabir-ud-Din, Polymer-surfactant interactions and the effect of tail size variation on micellization process of cationic ATAB surfactants in aqueous medium, J. Disper. Sci. Technol. 34 (2013) 722-730.

174. M. Murata, H. Arai, The interaction between polymer and surfactant: The effect of temperature and added salt on the interaction between polyvinylpyrrolidone and sodium dodecyl sulfate, J. Colloid Interface Sci. 44 (1973) 475-480.

175. M. C. Costa, S. M. Silva, F. E. Antunes, Adjusting the low critical solution temperature of poly (N-isopropyl acrylamide) solutions by salts, ionic surfactants and solvents: A rheological study, J. Mol. Liq. 210 (2015) 113-118.

176. S. F. van Nispen, J. P. Custers, L. J. van den Broeke, J. T. Keurentjes, Characterization of the binding of multivalent ions to modified pluronic micelles by isothermal titration calorimetry and modified conductometry, Colloids Surf. A: Physicochem. Eng. Asp. 361 (2010) 38-44.

177. M. Bali, O. Masalci, Interactions of cationic surfactants with polyvinylpyrrolidone (PVP): Effects of counter ions and temperature, J. Mol. Liq. 303 (2020) 112576.

178. I. S. Chronakis, P. Alexandridis, Rheological properties of oppositely charged polyelectrolyte−surfactant mixtures: effect of polymer molecular weight and surfactant architecture, Macromolecules 34 (2001) 5005-5018.

179. A. El Aferni, M. Guettari, M. Kamli, T. Tajouri, A. Ponton, A structural study of a polymer-surfactant system in dilute and entangled regime: Effect of high concentrations of surfactant and polymer molecular weight, J. Mol. Struct. 1199 (2020) 127052.

180. R. Mészáros, I. Varga, T. Gilányi, Effect of polymer molecular weight on the polymer/surfactant interaction, J. Phys. Chem. B 109 (2005) 13538-13544.

181. Y. Rao, A. Takahashi, C. P. Wong, Di-block copolymer surfactant study to optimize filler dispersion in high dielectric constant polymer-ceramic composite, Compos. - A: Appl. Sci. Manuf. 34 (2003) 1113-1116.

182. R. Petkova, S. Tcholakova, N. D. Denkov, Role of polymer–surfactant interactions in foams: Effects of pH and surfactant head group for cationic polyvinylamine and anionic surfactants, Colloids Surf. A: Physicochem. Eng. Asp. 438 (2013) 174-185.

183. S. S. Halacheva, J. Penfold, R. K. Thomas, J. R. Webster, Effect of polymer molecular weight and solution pH on the surface properties of sodium dodecylsulfate-poly (ethyleneimine) mixtures, Langmuir 28 (2012) 14909-14916.

184. A. Bhattarai, K. Pathak, B. Dev, Cationic and anionic surfactants interaction in water and methanol–water mixed solvent media, J. Mol. Liq. 229 (2017) 153-160.

185. S. K. Shah, S. K. Chatterjee, A. Bhattarai, Micellization of cationic surfactants in alcohol—water mixed solvent media, J. Mol. Liq. 222 (2016) 906-914.

186. Y. Ghimire, S. Amatya, S. K. Shah, A. Bhattarai, Thermodynamic properties and contact angles of CTAB and SDS in acetone–water mixtures at different temperatures, SN Appl. Sci. 2 (2020) 1-9.

187. S. A. Pillai, E. V. Lage, M. Casas, I. Sández-Macho, M. R. Wang, L. J. Chen, P. Bahadur, A comparative study on the effect of structural variations of co-solvent on the Tetronic® micelles with widely different hydrophobicity, J. Mol. Liq. 282 (2019) 282 97-104.

188. V. Sharma, O. Yañez, M. Alegría-Arcos, A. Kumar, R. C. Thakur, P. Cantero-López, A physicochemical and conformational study of co-solvent effect on the molecular interactions between similarly charged protein surfactant (BSA-SDBS) system, J. Chem. Thermodyn. 143 (2020) 106022.

189. R. Lunkad, A. Srivastava, A. Debnath, Influence of water concentrations on the phase transformation of a model surfactant/co-surfactant/water system, Chem. Phys. 483 (2017) 103-111.

190. A. Phukon, S. Ray, K. Sahu, Effect of cosurfactants on the interfacial hydration of CTAB quaternary reverse micelle probed using excited state proton transfer, Langmuir 32 (2016) 10659-10667.

191. D. Mohanta, M. Jana, Can 2, 2, 2-trifluoroethanol be an efficient protein denaturant than methanol and ethanol under thermal stress?, Phys. Chem. Chem. Phys. 20 (2018) 9886-9896.

192. J. Vymětal, L. Bednárová, J. Vondrášek, Effect of TFE on the helical content of AK17 and HAL-1 peptides: theoretical insights into the mechanism of helix stabilization, J. Phys. Chem. B 120 (2016) 1048-1059.

193. A. M. Percebom, W. Loh, Controlling the phase structures of polymer/surfactant complexes by changing macromolecular architecture and adding n-alcohols, J. Colloid Interface Sci. 466 (2016) 377-387.

194. B. Mandal, S. P. Moulik, S. Ghosh, Influence of aquo-organic solvent media on the self-aggregation of sodium dodecyl sulfate (SDS) and its interaction with polyvinylpyrrolidone (PVP), Colloid Polym. Sci. 292 (2014) 2485-2495.

195. B. Naskar, S. Ghosh, S. Nagadome, G. Sugihara, S. P. Moulik, Behavior of the amphiphile CHAPS alone and in combination with the biopolymer inulin in water and isopropanol–water media, Langmuir 27 (2011) 9148-9159.

196. S. Mukherjee, A. Dan, S. C. Bhattacharya, A. K. Panda, S. P. Moulik, Physicochemistry of interaction between the cationic polymer poly (diallyldimethylammonium chloride) and the anionic surfactants sodium dodecyl sulfate, sodium dodecylbenzenesulfonate, and sodium N-dodecanoylsarcosinate in water and isopropyl alcohol− water media, Langmuir 27 (2011) 5222-5233.

197. B. Mandal, S. Ghosh, S. P. Moulik, Interaction between a bio-tolerable amino-acid based amphiphile (N-dodecanoylsarcosinate, SDDS) and modified cationic polymers, hydroxyethylcelluloses (JR 400, and LM 200) in isopropanol-water medium, Colloids Surf. A Physicochem. Eng. Asp. 566 (2019) 156-165.

198. M. N. Jones, The interaction of sodium dodecyl sulfate with polyethylene oxide, J. Colloid Interface Sci. 23 (1967) 36-42.

199. F. Joabsson, K. Thuresson, B. Lindman, Interfacial interaction between cellulose derivatives and surfactants at solid surfaces. An ellipsometry study, Langmuir 17 (2001) 1499-1505.

200. R. A. Campbell, M. Yanez Arteta, A. Angus-Smyth, T. Nylander, I. Varga, Effects of bulk colloidal stability on adsorption layers of poly (diallyldimethylammonium chloride)/sodium dodecyl sulfate at the air–water interface studied by neutron reflectometry, J. Phys. Chem. B 115 (2011) 15202-15213.

201. H. Li, C. Cui, X. Cao, F. Yuan, Z. Xu, L. Zhang, L. Zhang, The Interfacial Dilational Rheology Properties of Betaine Solutions: Effect of Anionic Surfactant and Polymer, Molecules 28 (2023) 5436.

202. M. J. Schwuger, Mechanism of interaction between ionic surfactants and polyglycol ethers in water, J. Colloid Interface Sci. 43 (1973) 491-498.

203. D. Li, M. S. Kelkar, N. J. Wagner, Phase behavior and molecular thermodynamics of coacervation in oppositely charged polyelectrolyte/surfactant systems: A cationic polymer JR 400 and anionic surfactant SDS mixture, Langmuir 28 (2012) 10348-10362.

204. N. Joshi, K. Rawat, H. B. Bohidar, Influence of structure, charge, and concentration on the pectin–calcium–surfactant complexes, J. Phys. Chem. B 120 (2016) 4249-4257.

205. M. Akram, F. Ansari, F. A. Qais, Binding of cationic C_m-E_2O-C_m gemini surfactants with human serum albumin and the role of β-cyclodextrin, J. Mol. Liq. 312 (2020) 113365.

206. C. Lin, F. Fang, M. Lin, R. Jiang, Bulk properties of carboxymethylchitosan and cationic surfactant mixtures: fluorescence and surface tension studies, J. Disper. Sci. and Technol. 34 (2013) 1750-1757.

207. S. Saito, M. Yukawa, Interactions of polymers and cationic surfactants with thiocyanate as counterions, J. Colloid Interface Sci. 30 (1969) 211-218.

208. S. Shimabayashi, T. Uno, Y. Oouchi, E. Komatsu, Interaction between hydroxypropylcellulose and surfactant and its effect on dispersion stability of kaolinite suspension in an aqueous phase, Progress in Colloid and Polymer Science, 106(1997) 136-140.

209. B. Cabane, Structure of some polymer-detergent aggregates in water, J. Phys. Chem. 81 (1977) 1639-1645.

210. Y. Chang, L. McLandsborough, D. J. McClements, Interactions of a cationic antimicrobial (ε-polylysine) with an anionic biopolymer (pectin): An isothermal titration calorimetry, microelectrophoresis, and turbidity study, J. Agric. Food Chem. 59 (2011) 5579-5588.

211. Y. Chang, L. McLandsborough, D. J. McClements, Antimicrobial delivery systems based on electrostatic complexes of cationic ε-polylysine and anionic gum Arabic, Food Hydrocoll. 35 (2014) 137-143.

212. Y. Chang, L. McLandsborough, D. J. McClements, Interaction of cationic antimicrobial (ε-polylysine) with food-grade biopolymers: Dextran, chitosan, carrageenan, alginate, and pectin, Food Res. Int. 64 (2014) 396-401.

213. M. Loeffler, D. J. McClements, L. McLandsborough, N. Terjung, Y. Chang, J. Weiss, Electrostatic interactions of cationic lauric arginate with anionic polysaccharides affect antimicrobial activity against spoilage yeasts, J. Appl. Microbiol. 117 (2014) 28-39.

214. C. Totland, J. Martinez-Santiago, K. P. Ananthapadmanabhan, P. Somasundaran, Composition and structural transitions of polyelectrolyte–surfactant complexes in the presence of fatty acid studied by NMR and Cryo-SEM, Langmuir 31 (2015) 1623-1631.

215. R. Sharma, A. Kamal, T. S. Kang, R. K. Mahajan, Interactional behavior of the polyelectrolyte poly sodium 4-styrene sulphonate (NaPSS) with imidazolium based surface active ionic liquids in an aqueous medium, Phys. Chem. Chem. Phys. 17 (2015) 23582-23594.

216. W. Guan, W. Zhou, Q. Huang, C. Lu, Chemiluminescence as a novel indicator for interactions of surfactant–polymer mixtures at the surface of layered double hydroxides, J. Phys. Chem. C 118 (2014) 2792-2798.

217. V. Enev, P. Sedláček, S. Jarábková, T. Velcer, M. Pekař, ATR-FTIR spectroscopy and thermogravimetry characterization of water in polyelectrolyte-surfactant hydrogels, Colloids Surf. A Physicochem. Eng. Asp. 575 (2019) 1-9.

218. I. Estrela-Lopis, J. J. Iturri Ramos, E. Donath, S. E. Moya, Spectroscopic studies on the competitive interaction between polystyrene sodium sulfonate with polycations and the N-tetradecyl trimethyl ammonium bromide surfactant, J. Phys. Chem. B 114 (2010) 84-91.

219. L. Patel, O. Mansour, M. Crossman, P. Griffiths, Electrophoretic NMR characterization of charged side chain cationic polyelectrolytes and their interaction with the anionic surfactant, sodium dodecyl sulfate, Langmuir 35 (2019) 9233-9238.

220. A. M. Tedeschi, E. Busi, L. Paduano, R. Basosi, G. D'Errico, Influence of the headgroup molecular structure on the anionic surfactant–PVP interaction studied by electron paramagnetic resonance of a cationic nitroxide, Phys. Chem. Chem. Phys. 5 (2003) 5077-5083.

221. M. Cao, M. Hai, Investigation on the interaction between sodium dodecyl sulfate and polyethylene glycol by electron spin resonance, ultraviolet spectrum, and viscosity, J. Chem. Eng. Data 51 (2006) 1576-1581.

222. B. N. Jang, D. Wang, C. A. Wilkie, Relationship between the solubility parameter of polymers and the clay dispersion in polymer/clay nanocomposites and the role of the surfactant, Macromolecules 38 (2005) 6533-6543.

223. J. Xiao, F. Liu, V. M. Garamus, L. Almásy, U. A. Handge, R. Willumeit, B. Mu, A. Zou, Insights into the interactions among surfactin, betaines, and PAM: Surface tension, small-angle neutron scattering, and small-angle X-ray scattering study, Langmuir 30 (2014) 3363-3372.

224. T. Li, N. Shao, Y. Liu, J. Hu, Y. Wang, L. Zhang, H. Wang, D. Chen, Y. Cheng, Poly (amidoamine) and poly (propyleneimine) dendrimers show distinct binding behaviors with sodium dodecyl sulfate: insights from SAXS and NMR analysis, J. Phys. Chem. B 118 (2014) 3074-3084.

225. M. Vinceković, M. Ćurlin, D. Jurasin, Impact of cationic surfactant on the self-assembly of sodium caseinate, J. Agric. Food Chem. 62 (2014) 8543-8554.

226. C. Li, G. Li, S. Liu, Spherical hydroxyapatite with colloidal stability prepared in aqueous solutions containing polymer/surfactant pair, Colloids Surf. A Physicochem. Eng. Asp. 366 (2010) 27-33.

227. L. Li, E. Liu, C. H. Lim, Micro-DSC and rheological studies of interactions between methylcellulose and surfactants, J. Phys. Chem. B 111 (2007) 6410-6416.

CHAPTER-I

Detailed Physicochemical Study and Thermodynamic Aspects of the Interaction between Nonionic Cellulose Derivative Hydroxyethyl Cellulose and Anionic Surfactant Sodium N-Dodecanoyl Sarcosinate in Aqueous Media

Detailed Physicochemical Study and Thermodynamic Aspects of the Interaction between Nonionic Cellulose Derivative Hydroxyethyl Cellulose and Anionic Surfactant Sodium N-Dodecanoyl Sarcosinate in Aqueous Media

ABSTRACT

Scheme 1: Schematic Illustration of HEC/SDDS Interaction at Different [SDDS]

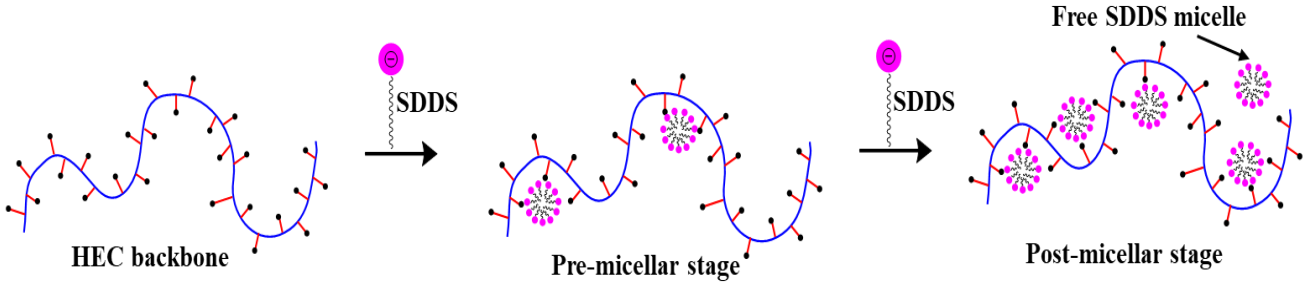

Journal of the Taiwan Institute of Chemical Engineers, 2023, 149, 104982.
(published)

Background

The scheme of this work was to study the interaction between hydroxyethyl cellulose (HEC), a non-ionic, water soluble biopolymer and sodium N-dodecanoyl sarcosinate (SDDS), a novel, environmentally friendly amino acid-based anionic surfactant in aqueous medium. The study of this type of interaction is relatively less complicated compared to that between a polymer and a surfactant with opposite charges.

Methods

The critical micelle concentration (CMC) of HEC-induced SDDS has been determined by various physicochemical methods such as tensiometry, conductometry, fluorimetry and microcalorimetry. Several thermodynamic and surface parameters related to the binding of SDDS with HEC have been assessed. The aggregation number (N_{agg}) of SDDS micelles in the presence of non-ionic HEC polymer has been measured by the steady-state fluorescence method. The hydrodynamic diameter (D_h) and zeta potential (ζ) of the polymer-surfactant aggregate have been measured by the dynamic light scattering method. The interaction study has further been amplified by detecting the change in the surface morphology of the polymer due to surfactant binding using Field Emission Scanning Electron Microscopy (FESEM) and high-resolution transmission electron microscopy (HR-TEM) imaging in solvent-free state, as well as visualization of the HEC-SDDS micelle in the solution phase using fluorescence microscopy technique.

Significant findings

From a physicochemical point of view, hydrophobic synergism seems to be important for understanding the interaction pattern of HEC-SDDS combination. In each scenario, the CMC

of SDDS decreases with an increase in weight percentage of HEC. The aggregation number (N_{agg}) of SDDS micelles is also found to decrease with an increase in weight percentage of HEC in the medium. The hydrodynamic diameter (D_h) and zeta potential (ζ) of the polymer-surfactant aggregate, these two parameters have been found to be strongly dependent on the amphiphile concentration. Finally, investigations of the surface morphologies by taking Field Emission Scanning Electron Microscopy (FESEM), high resolution transmission electron microscopy (HR-TEM) and fluorescence microscopy techniques assist the experimental data.

Keywords

Biopolymer; Anionic surfactant; Hydrophobic synergism; Aggregation number; Physicochemical methods

1. Introduction

Over the course of several decades, many research works have been studied with the polymer-surfactant interactions. The advancement of this course of investigation still continues to generate a great deal of interest due to the intricacy of the mechanisms for interpreting the nature of interactions involved and the divergence of applications in different fields, such as, pharmaceutical science **[1-3]**, enhanced oil recovery **[4-10]**, colloidal stability **[11,12]**, surface modification **[13]**, drug encapsulation **[14-17]**, paint formulation **[18]** etc. The polymer-surfactant interacted gels can be used as templates for nanomaterials synthesis **[19-22]**. Surfactant molecules can self-assemble to form micelles **[23-25]** both in aqueous medium as well as in aqueous polymer solution. The key factor of this study when choosing polymers and surfactants to various possible combinations is based on their physicochemical properties and the strength of interactions has been found to be highly dependent on the intrinsic properties of both polymers and surfactants, such as nature of charges, molecular compositions etc. The polymer-surfactant binding can be stabilized to a large extent by strong electrostatic force for oppositely charged pairs and weak hydrophobic force when one of them is uncharged. For non-ionic polymers, the more recommended combination for the investigation of interaction features has been found with anionic surfactants than other conventional surfactants **[26]**. The physicochemical interactions between them can either induce or prevent the binding of surfactant molecules at the polymer interface. Previous studies **[27,28]** suggest that the nature and charges of both polymers and surfactants have a significant impact on the nature of the interactions between them. There are strong hydrophobic interactions between non-ionic polymers and anionic surfactants **[29-31]**. In the case of polymer and surfactant with opposing charges **[32-34]**, both electrostatic and hydrophobic interactions have been established. Comparatively to oppositely charged polymer-surfactant systems, the former types of polymer-surfactant interactions are simpler to investigate. The hydrophobic synergism has been established experimentally in this work, operates between the anionic surfactant tail and the non-ionic polymeric lipophilic domain. According to a recent publication **[35]**, it has been reported that the enlargement of the surfactant tail using sodium dodecyl sulfate (SDS) and sodium tetradecyl sulfate (TSDS), two anionic surfactants, can induce polymer-surfactant binding with hydrophobically modified non-ionic hydroxypropyl cellulose (HPC) polymer.

Naturally occurring cellulose is the most abundant ‘biopolymer’. This polymer is prepared by the treatment of cellulose with ethylene oxide in the presence of sodium hydroxide in an esterification process **[36]**. Cellulose derivative, hydroxyethyl cellulose (HEC) is water

soluble and non-ionic carbohydrate-based polymer. Three hydroxyl groups (-OH) present in each unit of cellulose are esterified with hydroxyethyl groups (-CH_2CH_2OH) in the HEC skeleton, making it excellently soluble in water. The interaction of this polymer with amphiphilic molecules and its industrial applications on a large scale make it one of the most important materials for researchers. It has spacious uses in pharmaceutical fields **[37]**, waste water treatment **[38,39]**, drug delivery **[40]**, paint industry **[41]**, plasma expansion **[42]**, thickening **[43]**, dyeing **[44, 45]**, membrane preparation **[46-49],** etc. It is extensively used for grafting with other polymers **[50]**. The HEC grafted material is becoming an invaluable resource for researchers. Prior to the present study, several non-ionic cellulose polymers have been interacted with different amphiphiles **[51, 52]**.

Sodium N-dodecanoyl sarcosinate (SDDS) is the sodium salt of sarcosine (derivative of the amino acid glycine), a derivative of lauric acid. Thus, it belongs to one of the most significant naturally occurring amino acid-based surfactants **[53,54]**. Due to its high biodegradability **[55, 56]** and biocompatibility **[57],** extremely low toxicity **[58],** and environmental designation as a 'novel' **[59]** and 'green' surfactant **[60]**, modern research in the field of surface chemistry has been enormously interested in working with this surface-active substance **[61]**. Due to its ability to control dental decay in humans, SDDS is used as one of the ingredients of tooth paste **[62]**. In many cosmetic products, such as, shaving, shampoo, wash products etc., it is used as a foamy ingredient and a cleansing agent **[63]**. It has antimicrobial activity **[64]**, antibacterial **[65]** and anti-corrosive properties **[66]**. It is also used in anaerobic digestion of waste sludge **[67]** to remove organic matters (e.g., methane), wettability **[68]**, drug release **[69]** etc. Self-aggregation of anionic amphiphile SDDS in aqueous medium has already been reported **[70]**. The effect of different solvents **[71-73]**, salts **[74]** and mixed-micellization properties **[75]** of SDDS have been discussed. The interaction behaviour of anionic SDDS with various polymers **[76,77]**, proteins **[78,79]**, dyes **[80,81]** and drugs **[82]** has been investigated, but its interaction with the non-ionic polymer hydroxyethyl cellulose remains unexplored.

The majority of the previously reported pertinent works involve the study of hydrophobically modified non-ionic cellulose derivatives with anionic surfactants in order to identify the binding patterns between them using commonly used surface tension, fluorimetry, and viscosity methods. To understand the compositions and the mechanisms of polymer-surfactant binding as determined by physicochemical approaches, it is still imperative to develop a direct view of the polymer-surfactant complex using FESEM, HR-TEM, and fluorescence microscopy imaging. Furthermore, sodium dodecyl sulphate (SDS) has been used mostly as an anionic surfactant with non-ionic polymers **[83]**. Hence, using both of these materials, unmodified hydroxyethyl cellulose and SDDS, in the field of interaction study is quite unique as both have received significantly less attention with respect to earlier published reports. The focus of the present exertion is to explore the detailed reports on physicochemistry between HEC and an anionic surfactant, sodium N-dodecanoyl sarcosinate (SDDS) in aqueous medium using a number of technical methods, including tensiometry, conductometry, microcalorimetry, and fluorimetry at 298K. The zeta potential of the HEC-SDDS system is measured at varying concentrations of surfactant. The size and surface morphology of the polymer-surfactant aggregate has been illustrated by using DLS and FESEM instruments.

Ultimately, an attempt to correlate the physicochemistry and thermodynamics of the widely investigated polymer-surfactant interaction has been made.

2. Experimental section

2.1. Materials

Hydroxyethyl cellulose (Scheme 1) with molecular weight of 90,000 g mol^{-1} was purchased from Sigma. The average degree of substitution (α) of the polymer used was 1.5. The anionic surfactant, sodium N-dodecanoyl sarcosinate (SDDS, purity > 97%) (scheme1) was from Fluka, Germany. Pyrene, used as the fluorescence probe, was obtained from Sigma-Aldrich. All the experimental solutions were prepared in double distilled water. All these materials were used without any further purification. The polymer solutions were prepared in (w/v) percentage as the concentration unit. All these experiments were performed maintaining the constant temperature of 298 K.

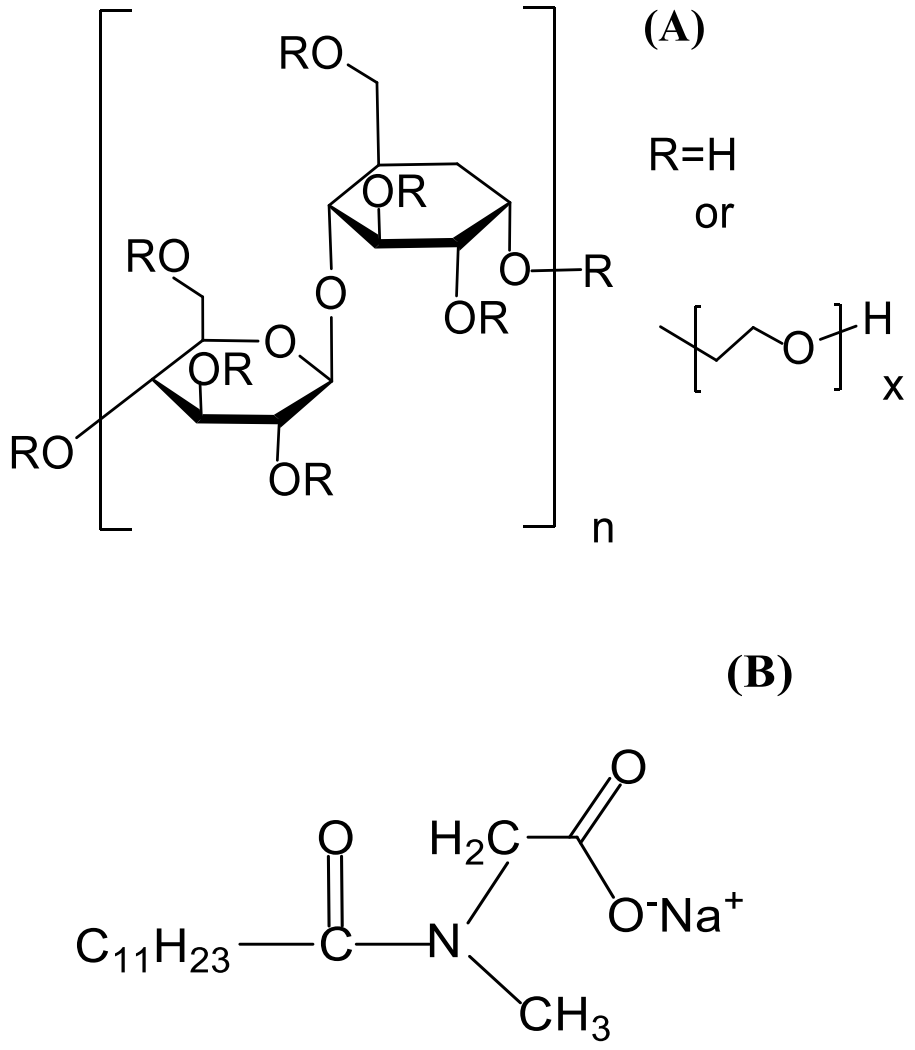

Scheme 2. Structures of (A) Hydroxyethyl cellulose, (B) Sodium N-dodecanoyl sarcosinate (SDDS).

2.2. Methods

2.2.1. Tensiometry

The surface tension (γ) values of the experimental solutions were taken by using a calibrated du Noüy tensiometer (Krüss, Germany). The values were measured by ring detachment method. A 5 mL initial volume of aqueous HEC solution of different concentrations were taken for the measurements to which aqueous concentrated SDDS solution was added in steps using Hamilton microsyringe. Thermal equilibration was done with 10-minute intervals between each measurement. The accuracy in the measurement was ±0.1mN m^{-1}.

2.2.2. Conductometry

A Jenway (UK) conductometer in a conductivity cell (cell constant 1.0 cm^{-1}) was used to measure the conductance values. A 7 mL initial volume of polymer solution of experimental concentration was taken in a thermostated container. Concentrated SDDS solution (~ 15 times that of CMC) was added step-by-step for the experiment. As the concentration used in the prepared aqueous solution of SDDS for conductometric titration was very high, the dilution impact was minimized. The measured values were accurate within ±0.5%.

2.2.3. Isothermal titration calorimetry (ITC)

An omega ITC micro calorimeter (Microcal, USA) was used for the thermometric studies. During measurements, temperature was maintained constant at 298K throughout the experimental process by using a Nesleb RTE 100 circulating water bath. A concentrated SDDS solution was added gradually into 0.2 mL of the polymer solution with time duration of 30 seconds in the calorimeter cell having equal time intervals of 210 seconds in multiple successive steps (20-30 additions) under constant stirring (300 rpm) conditions. The amount of heat involved during the micellization of SDDS in the absence and presence of HEC after each step of addition of SDDS was recorded, and the value of enthalpy change per mole of the injectant was calculated using ITC software. The reproducibility was verified by repeating the experiments.

2.2.4. Fluorimetry

The fluorimetric emissions were measured in a Perkin-Elmer fluorimeter (LS 55, USA) in a quartz cuvette having path length of 1cm. Pyrene was taken as the hydrophobic probe in fluorescence emission spectra to determine the CMC of SDDS in polymer solutions. The temperature was kept constant at 298 K with the help of a water flow thermostat. Concentrated aqueous solution of SDDS (225 mM) was used initially and added progressively in the sample cell containing polymer solution of three different concentrations. The excitation wavelength of the probe was 332 nm. The emission spectra were taken in the wavelength range of 350 to 450 nm. The slit widths for excitation and emission were taken at 14 nm and 2.5 nm respectively. The scan time was 250 nm / min. The CMC of the polymer-surfactant combinations were measured by plotting (I_1/I_3) vs. [SDDS], where, I_1 and I_3 are the intensities of first (373 nm) and third (383 nm) vibronic peaks of pyrene.

The aggregation numbers of both surfactant micelle and polymer- induced surfactant micelles were determined by the static fluorescence quenching (SFQ) study using tryptophan as the

probe. 1-hexadecylpyridinium chloride (CPC) was taken as the quencher. The concentration of the probe was maintained very low in the micelle assembly. Quencher, CPC was added stepwise into the experimental solution containing tryptophan probe using a Hamiltonian microsyringe and the intensity spectra were collected for data analysis. Hence, two different probes were used. Pyrene was used for the determination of CMC while tryptophan was used for the determination of aggregation number.

2.2.5. Dynamic light scattering (DLS)

Dynamic light scattering experiments were performed in a Malvern zetasizer Nano-zs (Malvern, UK) instrument at 173°scattering angle using He-Ne laser source of wavelength 632 nm at 298 K. All the experimental solutions were filtered 3-4 times through cellulose acetate paper of pore size 0.45 μm to remove unwanted extraneous particles. All the experiments were duplicated and the mean values were taken for analysis of the size of the polymer-surfactant aggregates in the aqueous solution.

2.2.6. Zeta potential

The same DLS instrument was used for zeta potential measurements using a gold coated copper electrode in the cell at 298 K. Before the experiment, the solutions were filtered as mentioned above. The experiments were performed twice and the mean values were reported.

2.2.7. Field emission scanning electron microscopy (FESEM)

High resolution field emission scanning electron microscope (FESEM, model FEI INSPECT F50, Japan) was used to study the surface morphology of the surfactant interacted polymer samples. The surface images were taken at two different surfactant concentrations (CMC and ≫CMC). 2 μL drops of the experimental solutions were taken by a 10 μL micro pipette on a glass slide for drying and spreading of the samples. The sputtering technique was introduced by supplying 5.5 mA current with 1 min time duration of these dried samples for gold plating.

2.2.8. High Resolution Transmission Electron Microscopy (HR-TEM)

TEM imaging of HEC and HEC-SDDS combination were carried out in JEOL JEM 2010 (Tokyo, Japan) high-resolution transmission electron microscope (HR-TEM) under 200 kV. Prior to measurements, the respective TEM samples were prepared by drop casting method of the desired solutions onto a copper grid (gold-coated) and the samples were kept overnight for drying (solvent removal).

2.2.9. Fluorescence microscopy

Olympus IX73 (one-deck system) inverted microscope was introduced for fluorescence imaging of the polymer-surfactant system. The experiment was carried out by taking DPH as the fluorophore. DPH was dissolved in absolute ethanol. A small drop of DPH solution was added to HEC-SDDS system prepared in 10% TFE solvent, surfactant concentration was taken much above CMC. In the final mixture, concentration of DPH was fixed at 0.1 mM. The experimental polymer-surfactant system containing DPH was well sonicated and kept overnight before the measurement. FITC filter included in the instrument was used for taking the required image.

3. Results and discussion

3.1. Tensiometry

The tensiometry is one of the most sophisticated methods and this method has the effectiveness to serve as an indicator in the polymer-surfactant interaction behaviour. The micellization of pure SDDS amphiphile in aqueous medium has been summarized in Fig. 1(A-D) providing tensiometry, conductometry, microcalorimetry and fluorimetry plots at 298 K. In each case, the location of CMC has been recognized. From microcalorimetry, the obtained value of CMC is slightly higher than other methods. The inconsistency in the magnitudes of CMCs in various methods is due to the fact that there are some systematic differences between these methods **[78]**. It should also be mentioned here that CMC does not study a particular concentration, rather it covers a small range of concentration, and different methods generate slightly different values. CMC represents the point of inflection meaning interfacial saturation of the amphiphile and in tensiometry, it is visualized by plotting surface tension (γ) vs. log [SDDS] (Fig. 1A).

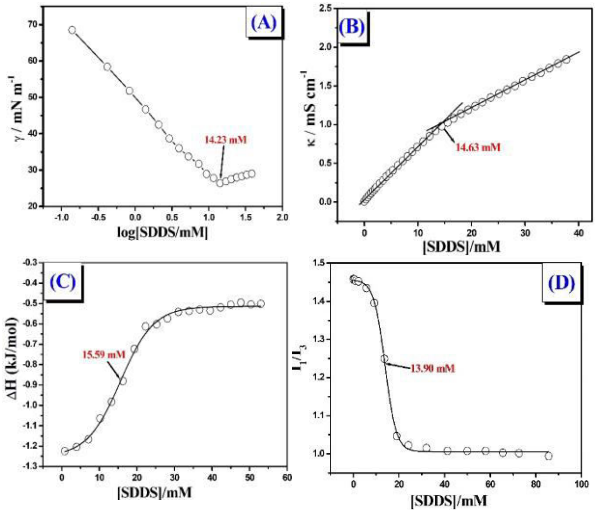

Fig. 1. Determination of CMC of pure SDDS surfactant in aqueous medium from (A) tensiometry, (B) conductometry, (C) microcalorimetry, (D) fluorimetry methods at 298 K.

In the tensiometric profile of pure SDDS, surface tension (γ) decreases with the stepwise addition of the aqueous solution of the surfactant into water. This decrease is due to the preferential adsorption of SDDS molecules on water surface which overcomes the strong intermolecular hydrogen bonding between water molecules that result in high surface tension value of water **[84]**. The decrease continues until 14.23 mM [SDDS] is reached. This specific concentration is termed as CMC showing minima in the plot. From this specific concentration, micelle formation is started. This phenomenon is related to interfacial saturation of the SDDS micelles in the aqueous medium. Beyond CMC, the surface tension of experimental solution slightly increases. This increase may be attributed to the higher affinity of the surfactant molecules to form micelle in the bulk at higher concentration that results more number of micelles in the bulk **[74]**. Other surfactants generally show almost constant nature of γ values beyond CMC in the tensiometric plots **[85]**. The determined CMC values

of pure amphiphile in these above-mentioned techniques are fairly satisfying the literature values (Table 1) **[71, 86]**. The nature of the interaction of the anionic amphiphile SDDS with non-ionic polymer HEC in terms of tensiometry plots has been attested in Fig. 2.

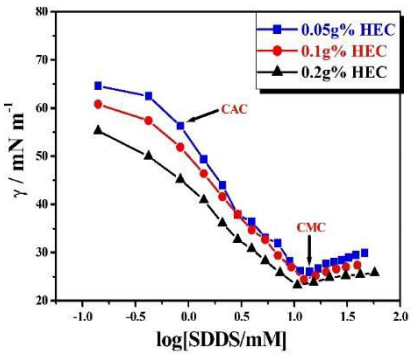

Fig. 2. Tensiometric profile for HEC-SDDS interaction with different polymer concentrations in aqueous medium at 298 K.

In general, the surfactant starts binding with the polymer at lower surfactant concentration called critical aggregation concentration (CAC) **[28,32]**. In this study, CAC is detected only at the lowest polymer concentration used in the experiment. It is not observed at higher polymer concentrations. With successive addition of the surfactant, surface tension (γ) of the polymer solution decreases linearly up to a transition point. This point is the CMC of the HEC-SDDS aggregate. The CMCs of the polymer-surfactant systems were found at lower surfactant concentration compared to pure SDDS. The measured values decrease noticeably with increasing weight percentage of polymer concentration. Few publications have documented such a decline in CMCs in the analysis of polymer-surfactant systems **[87, 88]**. In this study, concentration of saturation (C_s) is not detected suggesting only hydrophobic synergism and electrostatic interaction is absent. Hence, the presence of polymer enhances the surfactant monomer association ability by hydrophobic binding between the SDDS tails and the HEC lipophilic domain. As a result, micellization of surfactant monomer in the presence of polymer becomes more favourable and CMC decreases. Presence of HEC reduces the interfacial tension in the aqueous medium, and this reduction is enhanced with increasing HEC concentration. The reason behind this fact is that HEC polymer acts typically as long-chain alkane and tends to shift towards the surface of water from the bulk to lower the surface tension of aqueous HEC solution with respect to pure water **[89]**. Consequently, the surface tension of combined HEC-SDDS system also diminishes with increase in HEC concentration at the same SDDS concentration. It is observed that the tensiometric profiles of oppositely charged systems are much more complex to study due to the existence of strong electrostatic interaction **[90]**. The CMC values measured in different techniques of polymer-surfactant couple are slightly different due to the difference in sensitivity of different techniques. However, the trends of decreasing nature of CMCs are found in all methods. The initial surface tension readings for pure polymer solutions at various concentrations differ slightly. This suggests that HEC is feebly surface active **[91, 92]**.

3.2. Conductometry

Conductometry is another promising method for understanding the combination pattern and bulk property of the anionic amphiphile with the non-ionic polymer. The study of such

method is comparatively less sensitive to the presence of any impurity than the other conventional methods **[93]**. However, presence of ionic impurities may cause difficulty in CMC measurement by this method as the conductivity produced by ionic amphiphile is low compared to the ionic impurities **[94]**. All the materials taken for this conductometric titration are pure and double distilled water has been used to make the required solutions (section 2.1.), hence, the interference from ionic contaminants has been minimized in this study. The conductometric titrations of the polymer-surfactant system are presented in Fig. 3.

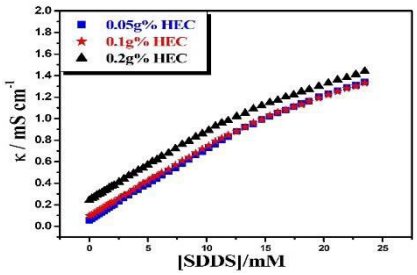

Fig. 3. Conductometic plots for HEC-SDDS interaction with different [HEC] in aqueous medium at 298 K.

The CMCs of SDDS amphiphile in the absence and presence of polymer are determined from the inflection point of the conductometric plots of specific conductance vs. [SDDS] (Table 2). In both cases, the specific conductance (κ) increases linearly upon stepwise addition of SDDS. Two zones, known as the pre-micellar and the post-micellar regions, can be found on the conductometric plots before and after the inflection point. The slope of the former is greater than that of the latter indicating that after the micellization of the surfactant, the rate of increase of specific conductance decreases. The ratio of these two slopes (S_2/S_1) can give the nature of the counter-ion binding (β). This parameter is useful for the determination of the energetics of micellization. This conductometric method can also find single major break point termed as CMC of the polymer-surfactant couple as it is found in the previous mentioned method. It is observed from Figure 3, the slopes are almost equal for 0.05 and 0.1 (w/v) % of HEC. This implies the same specific conductivity for non-ionic polymer at lower concentration. Although HEC is a non-ionic polymer, it exhibits changes in conductivity at higher concentration. The hydroxyl groups present in HEC have a strong propensity to form hydrogen bonds with water, which boosts its capacity as a proton donor **[95]** in aqueous media and thus HEC exhibits better conductivity at higher concentration. Now, comparing the conductometric results for pure SDDS (Fig. 1B) and HEC-SDDS systems (Fig. 3), it is seen that solutions of HEC-SDDS systems display higher conductivity than pure SDDS solution. The increase in conductivity of the SDDS solution in presence of HEC can be justified on the basis of the higher mobility of the counter ion Na^+ of the amphiphile in the solution **[96]**. In HEC-SDDS systems, DDS^- can bind hydrophobically with HEC backbone allowing Na^+ to be more free than the solution containing only SDDS. As a result, Na^+ ion gets higher mobility in combined HEC-SDDS systems, whereas its mobility gets lowered in pure SDDS solution by pairing strongly with anionic DDS^- through charge attraction. The characteristic results observed in the conductometric plots is the indirect evidence of the interaction between HEC and SDDS and also the micellization of SDDS in presence of HEC. The value of CMC of the interacted polymer-surfactant system decreases as the weight percentage of polymer increases. Upon stepwise addition of anionic surfactant into non-ionic

polymer in aqueous medium, the shape of the resultant conductometric curve is nearly identical to that of the pure SDDS. This similarity causes only for hydrophobic interaction between the polymer and the surfactant in terms of physicochemistry in the bulk. Two linear regions with inconsistent slopes can be attributed to the monomeric and micellar aggregates of SDDS in aqueous polymeric medium. This clearly evidences the change in the nature of the charge carriers or ionic mobility from pre-CMC region to post-CMC region. The first region can be ascribed to the existence of SDDS monomers in the bulk whereas the second region corresponds to the formed free SDDS micelles in the aqueous polymeric solution. The Na^+ counter-ion is concentrated in the ionic atmosphere termed as electrical double layer of micellar aggregates which cause a reduction of the ionic mobility in the post-micellar state **[84]**.

3.3. Discussion of interfacial and thermodynamic parameters

For the calculation of Gibbs surface excess (Γ_{max}), minimum amphiphile head group area (A_{min}), standard Gibbs free energy change of micellization (ΔG^0_{mic}), counter ion binding (β), standard free energy change of adsorption (ΔG^0_{Ads}) for both pure SDDS and HEC-SDDS systems, the following five equations have been introduced [Eq. (1)- (5)]

$$\Gamma_{max} = -\frac{1}{2.303iRT}\lim_{[SDDS]\to cmc}\frac{d\gamma}{dlogC} \quad (1)$$

where, 'i' is designated as the no. of ionic species per SDDS molecule (n = 2) in solution. Γ_{max} gives the information about the relative amount of SDDS adsorption at the interface compared to the bulk in the solution.

$$A_{min} = \frac{10^{18}}{N_A\Gamma_{max}} \quad (2)$$

'N_A' is the Avogadro's number and A_{min} represents the area of excursion per monomeric SDDS.

$$\Delta G_{mic} = (1+\beta)\mathrm{RT}lnX_{CMC} \quad (3)$$

'T' is absolute temperature (in Kelvin scale) and 'R' is universal gas constant (in $Jmol^{-1}K^{-1}$). X_{CMC} is (the mole-fraction of the amphiphile at CMC) calculated from tensiometry method.

$$\beta = 1 - \frac{S_2}{S_1} \quad (4)$$

The fraction of counter ion that is bound to the micellar aggregate is expressed in terms of β. It is determined by conductometric slope ratio method, where, S_1 and S_2 are the slopes in the pre- and post-cmc regions. The equation related to the change in standard Gibbs free energy of adsorption (ΔG^0_{Ads}) is:

$$\Delta G^0_{Ads} = \Delta G^0_{mic} - \frac{\pi_{CMC}}{\Gamma_{max}} \quad (5)$$

where, π_{CMC} is the surface pressure at CMC calculated by the following equation:

$$\pi_{CMC} = \gamma_{inital} - \gamma_{CMC} \quad (6)$$

Hence, π_{CMC} is measured by taking difference of the surface tension (γ) values of the initial aqueous polymer solution and the polymer-surfactant system at CMC.

Γ_{max}, A_{min}, ΔG^0_{mic}, and ΔG^0_{Ads} are expressed in mol m^{-2}, $nm^2\ molecule^{-1}$, kJ mol^{-1} and kJ mol^{-1} repectively. The negative values of free energy change indicate the spontaneity of both micellization and adsorption of surfactant molecules on the polymeric interface.

All the calculated values are arranged in Table 1.

Table 1 Determination of CMC by tensiometric method, interfacial parameters and thermodynamics of micellization of SDDS interacting with different HEC concentrations in aqueous medium at 298 K.

[HEC]/g %	CMC (mM)	γ_{CMC} (mN m^{-1})	$\Gamma_{max} \times 10^6$ (mol/m^{-2})	A_{min} (nm^2/molecule)	β	$-\Delta G^0_{mic}$ (KJ/mol)	$-\Delta G^0_{Ads}$ (KJ/mol)
0	14.23	26.4	1.66	1.00	0.465	40.98	68.51
0.05	13.91	26	1.68	0.99	0.377	40.89	64.58
0.1	12.29	24.4	1.73	0.96	0.385	40.87	62.02
0.2	10.65	23.2	1.64	1.01	0.400	42.62	63.90

Standard deviations: CMC (6%), Γ_{max} (8%), A_{min} (6%), ΔG^0_{mic} (7%), ΔG^0_{Ads} (3%).

3.4. Isothermal Titration Calorimetry

Calorimetry is another potential method for demonstrating the thermodynamic aspects of the polymer-surfactant binding process. The titrations are carried out by the stepwise injection of concentrated SDDS solution into aqueous solution of HEC in a cell at constant temperature (298K). The isothermal titration calorimetry (ITC) results for the pure SDDS and the interaction of SDDS with HEC of different weight percentage are shown in Fig. 1C and 4 respectively. The measured net standard enthalpy change depends on heat from several factors including the dissociation of SDDS micelles to monomers, the binding of SDDS onto HEC. However, enthalpy change from the dilution effect is negligible in this experiment as the other enthalpy changes are too high. In each case, the plots of standard enthalpy change vs. concentration of the surfactant are fitted as sigmoidal curve **[97]**. The CMCs of the pure surfactant and the polymer-interacted surfactant solutions are determined (Table 2) from sigmoidal Boltzmann equation **[28]**. An abrupt increase at an inflection point in the intermediate region provides the quantitative measurement of CMC. The resulting sigmoidal ITC curves exhibit three distinct concentration zones **[98]** in the endothermic enthalpograms as SDDS micellizes both with and without HEC. The enthalpy changes in the pre- and post-micellar regimes are nearly constant and virtually plateau-like, whereas the intermediate micellization zone between two shows a sharp increase. Initially in the pre-micellar condition, when adding concentrated SDDS micellar solution to the medium induces micellar breakdown into monomers with subsequent dilution of the monomers. Dilution of both free micelles and monomers occurs in the post-micellar stage at high SDDS concentration **[99]**. The heat change when CMC is achieved in the transition region essentially corresponds to a fractional dissociation of micelles into monomers. There is a sharp upward line in this

micellization zone and from the inflection point, CMC is measured. Again, the quantitative information about the standard net enthalpy change of micellization (ΔH^0_{mic}) is the integrated enthalpy change for each step of injection per mole of the surfactant. In the sigmoidal curve, it is obtained by measuring the difference of enthalpy in the pre- and post-micellar regions as identified by two horizontal parts **[100]**. The micellization process of pure SDDS in aqueous solution and the binding process of SDDS with HEC both are found to be endothermic in nature. Different polymer-surfactant systems are investigated on the basis of microcalorimetric study.

Scheme 3: Schematic Presentation of Mechanism of Micellization in ITC experiment

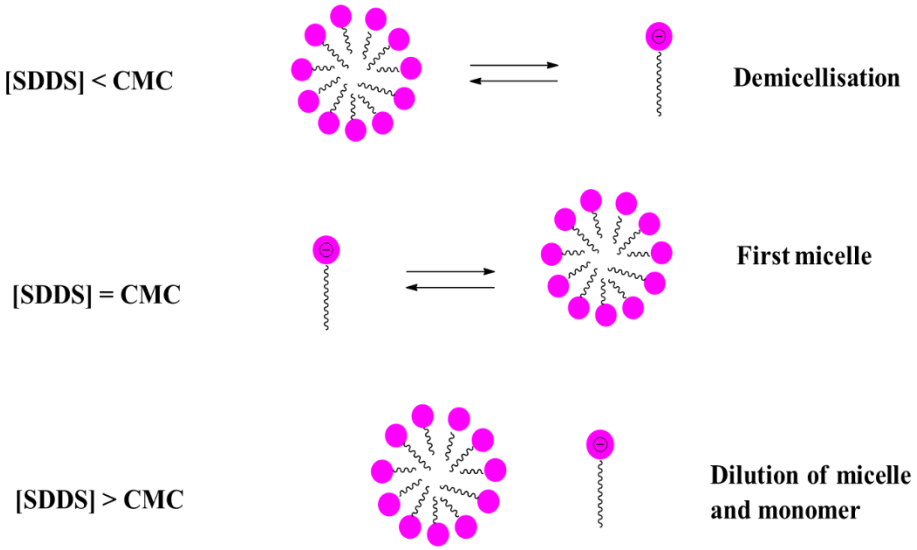

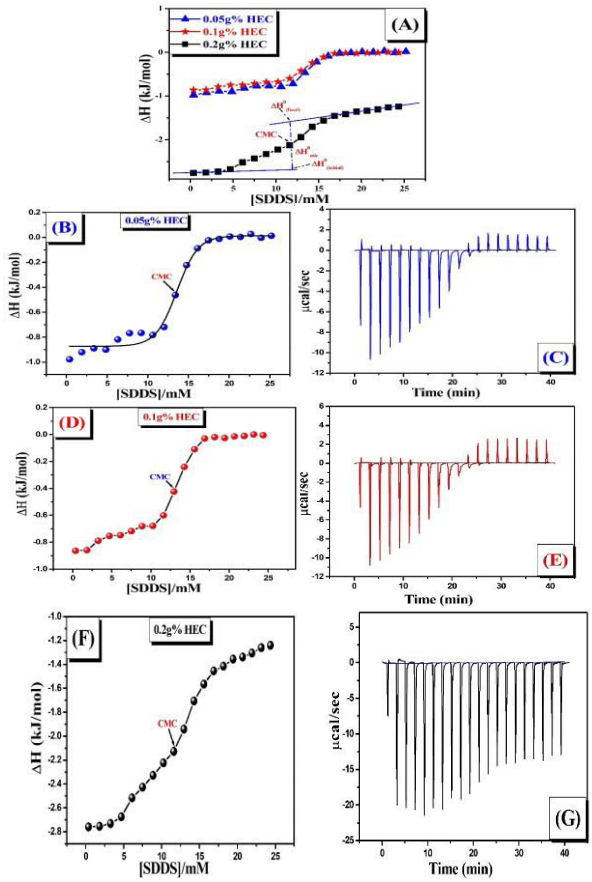

Fig. 4. (A), (B), (D) and (F) Enthalpy profiles of interaction of HEC with SDDS at different HEC concentrations at 298 K. (C), (E) and (G) represent enthalpograms for 0.05, 0.1 and 0.2 (w/v) % HEC interacting with aqueous SDDS solution respectively.

3.5. Micropolarity

The study of interaction of HEC-SDDS system has become more diverse through further exploration of the micro environment of the micellar behaviour in the bulk medium by efficient fluorescence probe method. Here, pyrene is preferentially used as spectroscopic probe as its molecules can easily bind to the hydrophobic environment of the molecular assembly **[101]**. Pyrene molecule has thus, photophysical property, as it is highly sensitive to the polarity of the investigated system **[102,103]**. Pyrene is an aromatic compound containing four extensively conjugated planar aromatic rings. The emission spectrum of pyrene in the vibrational pattern consists of five peaks (viz. I_1, I_2, I_3, I_4, and I_5). Among these five fine emission peaks, intensities of I_1 and I_3 were used in the present study (where I_1 and I_3 are the intensity values of first and third vibronic peaks) as I_1 increased with medium polarity but I_3 was polarity insensitive. The intensity ratio (I_1/I_3), known as micro polarity index, of hydrophobic pyrene was used for qualitative analysis of micro polarity sensed by probe molecules in the environment of the investigated system **[104]**. This micro polarity index (I_1/I_3) is an important parameter as it is highly sensitive to any change in the micro polarity of the medium relating to the change in micellar aggregation behaviour. This intensity ratio (I_1/I_3) is highly dependent on surfactant concentration confirming the change in polarity of the medium with surfactant addition. The ratio (I_1/I_3) having values less than unity and

greater than unity reveals the non-polar and polar environment surrounding the probe respectively. By using this method, CMC values of both pure SDDS and HEC-SDDS system (Table 2) in aqueous medium are determined. The values of CMC are calculated by sigmoidal fitting of the plot (I_1/I_3) vs. [SDDS] for both the systems **[105]** (Fig. 1D and 5), which are comparable with those determined by other methods.

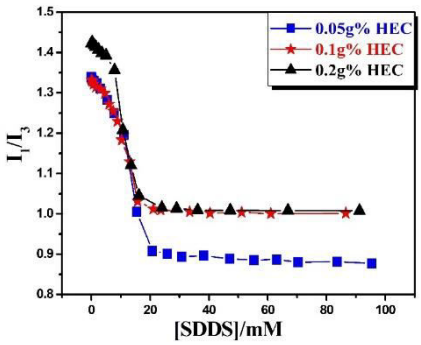

Fig. 5. Fluorimetric profiles for HEC-SDDS interaction at different HEC concentrations in aqueous medium at 298 K.

The identical orientation of decreasing trend of CMC of SDDS with increasing weight percentage of HEC in aqueous medium is also followed here similar to the other methods. In case of pure SDDS, an initial plateau is observed. This plateau region signifies unchanged nature of polarity of medium with increasing surfactant concentration. The value of (I_1/I_3) decreases sharply indicating the micellization of the surfactant molecules. Slight different types of plateau are observed in case of polymer-surfactant systems. HEC-SDDS systems experience a sudden drop in polarity which proves strong hydrophobic interaction between them and after that, the polarity of the medium practically remains unchanged with respect to surfactant concentration.

Table 2 Determination of CMC (mM**)** of SDDS with different (w/v) % of HEC in aqueous medium from tensiometry, conductometry, microcalorimetry, and fluorimetric methods at 298 K.

[HEC]/ g %	**Tensiometry**	**Conductometry**	**Fluorimetry**	**Microcalorimetry**
0	14.23	14.63	13.90	15.59
0.05	13.91	13.54	12.75	13.57
0.1	12.29	12.83	10.75	13.05
0.2	10.65	11.15	10.90	11.94

Standard deviation in CMC measurement: 6%

3.6. Aggregation Number

Comparative measurement of aggregation number of polymer bound surfactant micelle is another useful parameter for the conception of interaction between polymer and surfactant. This parameter can give an idea about micellar size. There are many methods available to determine the aggregation number. Here, the effect of polymer on SDDS micellar structure is

determined by calculating the aggregation number by SFQ method using the following eq. **[106,107]**:

$$\ln\left(\frac{I_0}{I}\right) = \frac{n_{agg}\,[CPC]}{[SDDS]-CMC}$$

Where, I and I_0 are the quenched and non-quenched fluorescence intensities respectively. [SDDS] and [CPC] are the concentrations of the surfactant SDDS and the quencher (Q) used CPC respectively. The slope of the plot of ln $(\frac{I_0}{I})$ vs [CPC] is used to calculate N_{agg} (Fig. 6) by linear fitting of the plot. In all measurements, [SDDS] is taken much higher than the corresponding CMC values. The $N_{agg}$of pure SDDS micelles is found as 51 in aqueous medium **[53]**. The aggregation number of HEC-bound micelles of SDDS is found to decrease with increasing HEC concentration. The calculated N_{agg} values are 45, 39 and 35 with changed [HEC] of 0.05, 0.1 and 0.2 g% respectively. Hence, more is the hydrophobicity, less is the number of SDDS monomers associated with the micelle in the system. Many authors have previously claimed the decreasing trend of aggregation number of the ionic amphiphilic micelle in the presence of non-ionic polymer systems **[108,109]**.

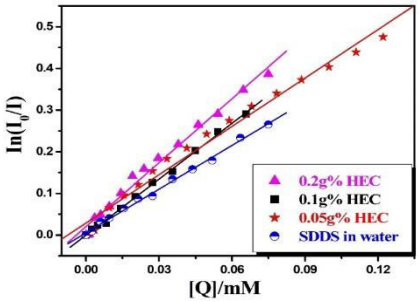

Fig. 6. Plot of In (I_0/I) vs. [Q] for pure SDDS and in presence of different [HEC] in aqueous medium at 298 K.

3.7. DLS size measurement

DLS study for 0.1 g% HEC and its interaction with SDDS in aqueous medium at different [SDDS] involves the measurement of both the hydrodynamic diameter (D_h) and polydispersity index (PDI). The diffusion of colloidal particles in the polymer-surfactant system is measured by hydrodynamic radius. Such size distributions are shown in Fig. 7. The presentation of measured values is shown in Table 3. Two discrete hydrodynamic diameters (D_h^I) and (D_h^{II}) are observed in each case ($D_h^{II} \gg D_h^I$). The DLS study of 0.1 g% pure HEC in water shows distinct bimodal distribution. The resulting two peaks correspond to the behaviour of monomeric or unassociated and aggregated states of HEC polymer in aqueous medium. The tendency of carbohydrate based neutral polymer to form aggregates in aqueous medium has been reported earlier **[110]**. It is found that both diameters are highly dependent on [SDDS] and increased with increasing concentration of SDDS (except at CMC and less than CMC, D_h^I values are found equal) due to aggregation of the surfactant molecules in the aqueous polymer system. The noticeable changes in the hydrodynamic diameters of the polymer-surfactant aggregates with respect to surfactant concentration are the result of surfactant aggregation assisted by non-ionic polymer. Hence, the presence of the amphiphile can change the configuration of the polymer. The measured PDI values are quite high (larger than 0.30), suggesting multidispersity of the studied systems **[111]**. The polydispersity of

non-ionic HEC is essentially due to the polymer aggregation at the concentration of 0.1 g% (w/v) in aqueous medium. The PDI value at this concentration has been found 0.470. The development of the polymer aggregation is relevant to the TEM morphographs (section 3.10.) of pure HEC polymer **[112]**.

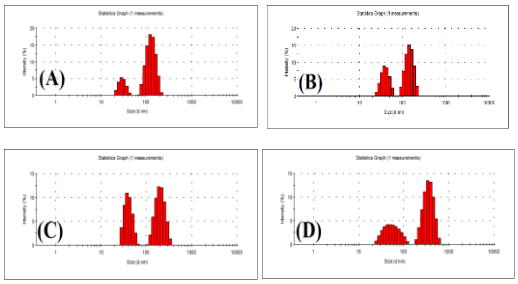

Fig. 7. DLS size distribution curves of (A) pure 0.1g% HEC; (B) with [SDDS]<CMC; (C) with [SDDS] at CMC; (D) with [SDDS]>>CMC in aqueous medium at 298K.

3.8. Zeta Potential

Measurement of zeta potential (ζ) is a significant parameter associated with the surface charge of the colloidal system. Its magnitude depends on the stability of the colloidal particles within the polymer-surfactant system. The zeta potential is measured as the electrostatic potential of the interfacial electrical double layer of the colloidal system. In general, the physical stability of colloid is considered to have zeta potential magnitude $|\zeta| > 30$ **[113]**. In the present study, both the zeta potential and the electrophoretic mobility of the HEC- SDDS system have been measured at four different [SDDS] (Fig. 8). The measured values are presented in Table 4. In each case, the negative zeta potential is attributed to the negative surface charge of the colloidal particles in the system. The magnitudes of zeta potential sharply become more and more negative with increasing [SDDS] until the system reaches up to critical micelle concentration of HEC-SDDS system. At CMC, maximum charge accumulation is expected **[114]** and thereafter, in between CMC and 2 CMC, there occurs very slow rate of increasing in negative value of the zeta potential. Study of zeta potential measurement of polymer-surfactant systems has been reported earlier **[115]**.

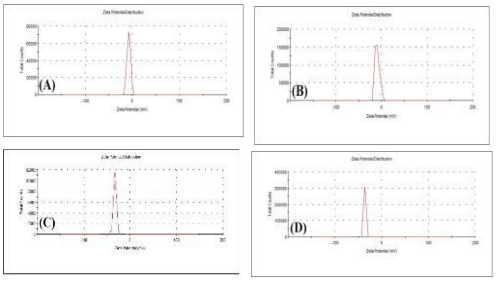

Fig. 8. Zeta potential distribution curves of HEC-SDDS interaction measured at [SDDS] (A) ¼ CMC; (B) ½ CMC; (C) CMC; (D) 2 CMC in aqueous medium at 298K.

Table 3 Hydrodynamic diameter (D_h) and polydispersity index (PDI) for 0.1(w/v) % of HEC interacting with various SDDS concentrations at 298 K.

0.1 g % HEC+ SDDS system

[SDDS]	Hydrodynamic diameter($D_h^{I,II}$)/nm	Polydispersity Index(PDI)
0	28.2, 122.4	0.470
<CMC	37.8, 141.8	0.382
CMC	37.8, 190.1	0.389
>>CMC	43.8, 342.0	0.671

The errors in measuring D_h and PDI are within 7% and 9% respectively.

Table 4 Zeta potential (ζ) and electrophoretic mobility (μ) for 0.1 (w/v) % of HEC-SDDS system using various SDDS concentrations at 298 K.

0.1 g % HEC+ SDDS system		
[SDDS]	ζ /mv	$10^8\mu/m^{-2}V^{-1}s^{-1}$
¼ CMC	-7.31	-0.57
½ CMC	-9.34	-0.73
CMC	-33.7	-2.63
2CMC	-38.3	-3.04

The error is within $\pm 10\%$ in measuring zeta potential (ζ).

3.9. Field Emission Scanning Electron Microscopy (FESEM)

In order to characterise the scientific eye-catching change in the surface morphology and topography of the polymer-surfactant aggregates from the pure polymer material via complexation with anionic surfactant and the analysis of microstructure of the aggregates, FESEM images have been displayed in Fig. 9 (A-C). The FESEM images of 0.1% (w/v) pure HEC polymer and its complexes with anionic SDDS surfactant (at CMC and >> CMC) have been reported in this study. All these taken images (in the solvent-free states) having own distinguished entities are different in shapes and sizes from each other. It is clearly observed that the particles of pure HEC polymer (Fig. 9A) have been aggregated on the surface. The aggregated particles are arranged to form branched fern tree-like structures. Similar type of FESEM findings have been noticed during investigation of the microstructure imaging of pure hydroxypropyl cellulose (HPC) polymer **[35]**. A striking surface morphological change is detected when HEC polymer is subjected to interact with anionic SDDS surfactant at two different 5concentrations. The wrecking of the branched fern tree-like structures is observed in both occasions due to the very strong binding of the surfactant molecules on the surface of the polymer. The two polymer-surfactant aggregated structures have different patterns of coating of the surfactant molecules on the polymeric interface. Consequently, such interactions are strongly dependent on the concentration of surfactant. At CMC, porosity is developed and the particles of the polymer are distributed with the surfactant molecules reconstructing a new patterned morphology (Fig. 9B). The aggregates are looking like perforated non-uniform spherical bodies. Further, at higher concentration of SDDS (>> CMC), more surfactant molecules are held back strongly by the polymer backbone and it forms homogeneous like aggregates (Fig. 9C). Different types of surface morphologies due to interaction between cationic gemini surfactant (14-4-14) with anionic polymer NaCMC in

aqueous and aquo-isopropanol media can also be cited for our study **[116]**. Hence, the strong association of the polymer-surfactant is highly recommended by such surface morphological change via FESEM imaging.

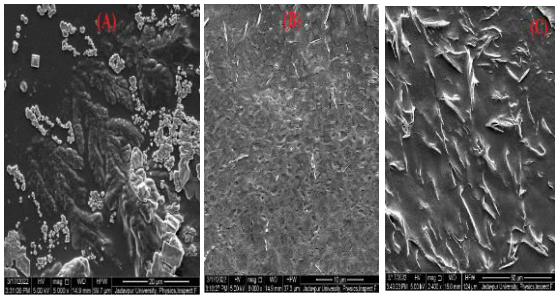

Fig. 9. FESEM images of (A) pure 0.1g% HEC; in presence of (B) [SDDS] at CMC; (C) [SDDS] > CMC.

3.10. High Resolution Transmission Electron Microscopy (HR-TEM)

The surface morphological analysis in this interaction study has been further elaborated by HRTEM measurements. The resulting HRTEM morphographs of pure HEC (0.1 g%) and HEC-SDDS binding at sufficiently high [SDDS] (≫ CMC) have been illustrated in Fig. 10(A-D). Pure HEC shows similar branched fern tree-like morphology as found in FESEM characterization. But, the morphology has been completely changed in case of HEC-SDDS aggregation. It looks as some accumulation of stones like appearance of varied shapes and sizes. The multidispersity of the HEC-SDDS binding beyond CMC from DLS results can be verified in HRTEM detection. The HRTEM analysis thus can be supportive in conjunction with FESEM findings as it imparts competence to distinguish between the morphologies of HEC and SDDS micellized HEC.

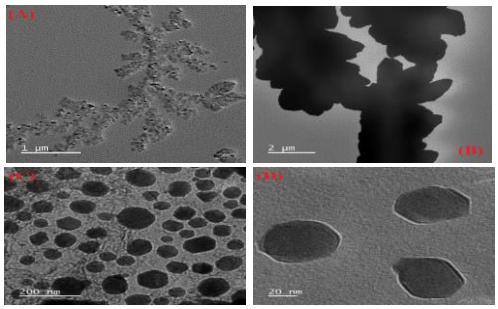

Fig. 10. HRTEM images of (A-B) pure 0.1g% HEC; (C-D) with [SDDS] > CMC.

3.11. Fluorescence microscopy

The binding pattern of anionic SDDS with non-ionic HEC has been supported by fluorescence technique. Such images are solid visual evidences for HEC-SDDS interaction. In this manuscript, FESEM (section 3.10.) and HR-TEM (section 3.11.) images have already been proved to be immensely effectual for the visualization of SDDS micelles that aggregate in presence of HEC. In the present fluorescence microscopy investigation, it is only reported the image of HEC-SDDS binding beyond critical micelle concentration (CMC) of the experimental system. The micellar aggregates are showed (Fig. 11) by observing fluorescence

intensity as bright green coloured fluorescent dots (10 μm) probed by DPH dye. In this case, the fluorescence microscopy images of HEC-SDDS system have been studied at different stages of polymer-surfactant binding including free HEC. But, fluorescence probe DPH cannot visualize effective micelle-like aggregates at low or moderate SDDS concentration. It is obvious that at pre-CMC stage, DPH molecules are not able to enter into the core of the micellar aggregates in such insufficient SDDS concentration. Beyond CMC, when SDDS concentration is large enough, HEC-SDDS micelles (i.e. aggregated SDDS micelles wrapped by HEC polymer chains) can be easily trapped by DPH probe **[117]**. Hence, the fluorescence microscopy images of free HEC and HEC-SDDS micelles at lower SDDS concentration are not reported in the present study.

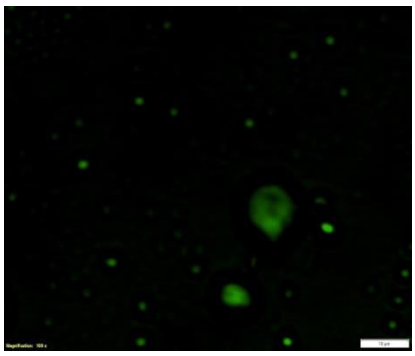

Fig. 11. Fluorescence microscopy image of 0.1g% HEC – SDDS binding ([SDDS] > CMC). Scale bar = 10 μm.

4. Conclusions

Owing to versatile applications in multidimensional fields as mentioned above, polymer-surfactant interaction study is still taking a significant place in modern research. Due to the complexity of the types of interactions existing between them, such area of research is still quite intriguing. The current research plan that led to the selection of this particular field is to break the complicity of the interaction behaviour between the non-ionic polymer and the anionic surfactant in aqueous medium through clear understanding via usage of multi technical approaches. Several works have been reported prior to this study to investigate the interaction characteristics of non-ionic cellulose derivatives with anionic amphiphilic molecules. Most often, non-ionic cellulose ethers, e.g., hydroxypropyl cellulose (HPC) and methyl cellulose (MC) and their derivatives; ethyl derivative and hydrophobically modified form (both cationic and anionic) of hydroxyethyl cellulose (HEC) etc. have been studied for understanding the interaction behaviour with anionic surfactants. These reports on pure HEC are, however, largely unexplored. At the same time, anionic SDDS has been only rarely studied with non-ionic polymer.

Anionic sodium dodecyl sulphate (SDS) has typically been reported with non-ionic polymer in this kind of study. In this paper, it has been tried to investigate the interaction by using multimethods such as tensiometry, conductometry, microcalorimetry and fluorimetry. The change in aggregation number of SDDS micelles in the presence of HEC has been determined. Both size and zeta potential of HEC-SDDS systems has been measured by dynamic light scattering method. FESEM, HR-TEM, and fluorescence microscopy images

are taken to analyse the surface morphology. Finally, the key observations can be summarised as:

The nature of the interaction found between them is purely hydrophobic and the tenacity of such interaction leads in higher polymer concentration. The CMC values of SDDS are found to decrease with increase in HEC concentration denoting quick aggregation. This is extremely rare in literature. The negative value of ΔG^0_{mic} confirms the spontaneity of the micellization process of the surfactant in the presence of polymer and the feasibility of interaction between them. Endothermic enthalpy change (ΔH^0_{mic}) during micellization process is supported by ITC plots. The values of N_{agg} of SDDS micelles are lowered in the presence of polymer and it decreases with increasing hydrophobicity of the medium. The hydrodynamic diameter (D_h) of the HEC-SDDS system is found to increase with [SDDS] in aqueous medium. Zeta potential (ζ) of HEC-SDDS system acquires fairly negative charge value. After reaching CMC, the zeta potential of the system only slightly increases with [SDDS]. Both FESEM and HR-TEM analysis produces significant changes in surface morphology and affirms their interactive behaviour. Development of HEC-SDDS micelle structure in fluorescence microscopy imaging provides fundamental concepts of SDDS micellization induced by HEC. All of these experimental findings are consistent with the existence of hydrophobic forces that act significantly between the SDDS tails and the lipophilic region of HEC, which lead to HEC-SDDS binding and micelle formation at lower SDDS concentration in non-ionic HEC compared to free SDDS micellization.

The interaction between HEC and SDDS leads to the development of a typical polymer-surfactant complex with a distinct composition and morphology. We can get the conclusion that studying such systems is a challenging issue. A variety of interaction phenomenon traits have been shown, discussed, and some interpretations have been made. A mixed HEC/SDDS system may give rise to a variety of beneficial features. In addition to the potential applications of both HEC and SDDS in drug delivery and cosmetic formulations, we believe that the environment-friendly HEC-SDDS complexes are potential candidates for enhanced oil recovery as well as templates for nanomaterials synthesis.

Optimistically, our little effort can be innovating and encouraging for the upcoming researchers to expand the practical applications of this prominent field by formulating new and more advanced ideas in diverse directions.

References

[1] Deshpande TM, Shi H, Pietryka J, Hoag SW, Medek A. Investigation of polymer/surfactant interactions and their impact on itraconazole solubility and precipitation kinetics for developing spray-dried amorphous solid dispersions. Mol Pharm 2018;15(3):962-74.

[2] Zhang W, Hate SS, Russell DJ, Hou HH, Nagapudi K. Impact of surfactant and surfactant-polymer interaction on desupersaturation of clotrimazole. J Pharm Sci 2019; 108(10):3262-71.

[3] Mdlovu NV, Lin KS, Chen Y, Juang RS, Chang TW, Mdlovu NB. Formulation and characterization of multifunctional polymer modified-iron oxide magnetic nanocarrier for doxorubicin delivery. J. Taiwan Inst. Chem. Eng. 2019;104:260-72.

[4] Zhao G, Li J, Gu C, Li L, Sun Y, Dai C. Dispersed particle gel-strengthened polymer/surfactant as a novel combination flooding system for enhanced oil recovery. Energy Fuels 2018;32(11):11317-27.
[5] Raffa P, Broekhuis AA, Picchioni F. Polymeric surfactants for enhanced oil recovery: A review. J Pet Sci Eng 2016;145:723-33.
[6] Saleem SM, Hernandez A. Enhanced oil recovery of acidic crudes by caustic cosurfactant-polymer flooding. J Surface Sci Technol 1987;3(1):1-10.
[7] Maurya NK, Kushwaha P, Mandal A. Studies on interfacial and rheological properties of water soluble polymer grafted nanoparticle for application in enhanced oil recovery. J. Taiwan Inst. Chem. Eng. 2017;70:319-30.
[8] Pal N, Vajpayee M, Mandal A. Cationic/nonionic mixed surfactants as enhanced oil recovery fluids: Influence of mixed micellization and polymer association on interfacial, rheological, and rock-wetting characteristics. Energy & Fuels. 2019;33(7):6048-59.
[9] Pal N, Mandal A. Enhanced oil recovery performance of gemini surfactant-stabilized nanoemulsions functionalized with partially hydrolyzed polymer/silica nanoparticles. Chemical Engineering Science. 2020;226:115887.
[10] Pal N, Babu K, Mandal A. Surface tension, dynamic light scattering and rheological studies of a new polymeric surfactant for application in enhanced oil recovery. Journal of Petroleum Science and Engineering. 2016 Oct 1;146:591-600.
[11] Li C, Li G, Liu S, bai J, zhang A. Spherical hydroxyapatite with colloidal stability prepared in aqueous solutions containing polymer/surfactant pair. Colloids Surf A 2010;366(1-3):27-33.
[12] Sakai T, Oishi T. Colloidal stabilization of surfactant-free emulsion by control of molecular diffusion among droplets. J. Taiwan Inst. Chem. Eng. 2018;92:123-8.
[13] Michael FM, Khalid M, Walvekar R, Siddiqui H, Balaji AB. Surface modification techniques of biodegradable and biocompatible polymers. Biodegradable and Biocompatible Polymer Composites: Processing, Properties and Applications. Shimpi NG Ed 2018;33-54.
[14] Qi S, Roser S, Edler KJ, Pigliacelli C, Rogerson M, Weuts I, Dycke FV, Stokbroekx S. Insights into the role of polymer-surfactant complexes in drug solubilisation/stabilisation during drug release from solid dispersions. Pharm Res 2013;30(1):290-302.
[15] Pokharkar V, Patil V, Mandpe L. Engineering of polymer–surfactant nanoparticles of doxycycline hydrochloride for ocular drug delivery. Drug Deliv 2015;22(7):955-68.
[16] Shagholani H, Ghorbani M, Nikpay A, Soltani M. Chitosan nanocapsule-mounted cellulose nanofibrils as nanoships for smart drug delivery systems and treatment of avian trichomoniasis. J. Taiwan Inst. Chem. Eng. 2019;95:290-9.
[17] Nachari Y, Jabbari M. A case study on the partitioning of pharmaceutical compound naproxen in edible oil-water system in the presence of ionic and non-ionic surfactants. J. Taiwan Inst. Chem. Eng. 2021;119:1-5.
[18] Tam KC, Wyn-Jones E. Insights on polymer surfactant complex structures during the binding of surfactants to polymers as measured by equilibrium and structural techniques. Chem Soc Rev 2006;35(8):693-709.
[19] Capek I. Preparation and functionalization of gold nanoparticles. J Surface Sci Technol 2013;29(3-4):1-18.
[20] Yu M, Liang C, Liu M, Liu X, Yuan K, Cao H, Che R. Yolk–shell Fe 3 O 4@ ZrO 2 prepared by a tunable polymer surfactant assisted sol–gel method for high temperature stable microwave absorption. J Mater Chem C 2014;2(35):7275-83.

[21] Duan P, Su R, Xu X, Li Q, Gao B. Preparation of Cu2O-Fe3O4@ carbon nanocomposites derived from natural polymer hydrogel template for organic pollutants degradation. J. Taiwan Inst. Chem. Eng. 2019;102:456-64.
[22] Pal N, Mandal A. Compositional simulation model and history-matching analysis of surfactant-polymer-nanoparticle (SPN) nanoemulsion assisted enhanced oil recovery. J. Taiwan Inst. Chem. Eng. 2021;122:1-3.
[23] Chakraborty T, Ghosh S. A unique survey of applicability of theories of mixed adsorbed film and mixed micellization. J Surfactants Detergents 2008;11:323-34.
[24] Perinelli DR, Cespi M, Lorusso N, Palmieri GF, Bonacucina G, Blasi P. Surfactant self-assembling and critical micelle concentration: one approach fits all?. Langmuir 2020;36(21):5745-53.
[25] Zhou M, Li S, Zhang Z, Luo G, Zhao J. Synthesis of oligomer betaine surfactant (DDTPA) and rheological properties of wormlike micellar solution system. J. Taiwan Inst. Chem. Eng. 2016;66:1-1.
[26] Khan MY, Samanta A, Ojha K, Mandal A. Interaction between aqueous solutions of polymer and surfactant and its effect on physicochemical properties. Asia-Pacific Journal of Chemical Engineering. 2008;3(5):579-85.
[27] Ghosh S, Mal A, Chakraborty T, De GC, Marangoni DG. Interaction of a cationic surfactant with an oppositely charged polymer. J Surface Sci Technol 2016;32(3-4):107-14.
[28] Das S, Ghosh S. A detailed assessment on the interaction of sodium alginate with a surface-active ionic liquid and a conventional surfactant: a multitechnique approach. Phys Chem Chem Phys 2022;24:13738–62.
[29] Rangaraj A, Rakshit AK. Solution properties of mixed nonionic surfactant-polymer systems. J Surface Sci Technol 2000;16(1-4):246-65.
[30] Chauhan S, Singh R, Sharma K, Kumar K. Interaction study of anionic surfactant with aqueous non-ionic polymers from conductivity, density and speed of sound measurements. J Surfactants Deterg 2015;18(2):225-32.
[31] Burman AD, Ghosh S, Das AR. Behavior of Cationic and Anionic Surfactants including Bile Salts in presence of Hydroxy propyl cellulose (HPC). J Nanofluids 2014;3:140-53.
[32] Chakraborty T, Chakraborty I, Ghosh S. Sodium carboxymethylcellulose−CTAB interaction: a detailed thermodynamic study of polymer− surfactant interaction with opposite charges. Langmuir 2006;22(24):9905-13.
[33] Asker D, Weiss J, McClements DJ. Analysis of the interactions of a cationic surfactant (lauric arginate) with an anionic biopolymer (pectin): isothermal titration calorimetry, light scattering, and microelectrophoresis. Langmuir 2009;25(1):116-22.
[34] Tseng HW, Chen PC, Tsui HW, Wang CH, Hu TY, Chen LJ. Effect of molecular weight of poly (acrylic acid) on the interaction of oppositely charged ionic surfactant–polyelectrolyte mixtures. J. Taiwan Inst. Chem. Eng. 2018;92:50-7.
[35] Mondal S, Pyne P, Patra A, Mitra RK, Ghosh S. Effect of Surfactant Tail Length on the Hydroxypropyl Cellulose-Mediated Premicellar Aggregation of Sodium n-Alkyl Sulfate Surfactants. Langmuir 2021;37(20):6168-77.
[36] Giudice FD, Tassieri M, Oelschlaeger C, Shen AQ. When microrheology, bulk rheology, and microfluidics meet: Broadband rheology of hydroxyethyl cellulose water solutions. Macromolecules 2017;50(7):2951-63.
[37] Sehaqui H, Morimune S, Nishino T, Berglund LA. Stretchable and strong cellulose nanopaper structures based on polymer-coated nanofiber networks: An alternative to

nonwoven porous membranes from electrospinning. Biomacromolecules 2012;13(11): 3661-67.
[38] Mukerabigwi JF, Lei S, Fan L, Wang H, Luo S, Ma X, Qin J, Huang X, Cao Y. Eco-friendly nano-hybrid superabsorbent composite from hydroxyethyl cellulose and diatomite. RSC Adv 2016;6(38):31607-18.
[39] Mdlovu NV, Lin KS, Chen ZW, Liu YJ, Mdlovu NB. Treatment of simulated chromium-contaminated wastewater using polyethylenimine-modified zero-valent iron nanoparticles. J. Taiwan Inst. Chem. Eng. 2020;108:92-101.
[40] Angadi SC, Manjeshwar LS, Aminabhavi TM. Interpenetrating polymer network blend microspheres of chitosan and hydroxyethyl cellulose for controlled release of isoniazid. Int J Biol Macromol 2010;47(2):171-9.
[41] Maestro A, González C, Gutiérrez JM. Interaction of surfactants with thickeners used in waterborne paints: A rheological study. J Colloid Interface Sci 2005;288(2):597-605.
[42] Mahmoud KH. Optical properties of hydroxyethyl cellulose film treated with nitrogen plasma. Spectrochim Acta Part A 2016;157:153-7.
[43] Li MX, Wang XW, Yang YQ, Chang Z, Wu YP, Holze R. A dense cellulose-based membrane as a renewable host for gel polymer electrolyte of lithium ion batteries. J Membr Sci 2015;476:112-8.
[44] Chen P, Liu X, Jin R, Nie W, Zhou Y. Dye adsorption and photo-induced recycling of hydroxypropyl cellulose/molybdenum disulfide composite hydrogels. Carbohydrate polymers. 2017;167:36-43
[45] Liang Y, Liu X, Fang K, An F, Li C, Liu H, Qiao X, Zhang S. Construction of new surface on linen fabric by hydroxyethyl cellulose for improving inkjet printing performance of reactive dyes. Prog Org Coat 2021;154:106179.
[46] Chanachai A, Jiraratananon R, Uttapap D, Moon GY, Anderson WA, Huang RY. Pervaporation with chitosan/hydroxyethylcellulose (CS/HEC) blended membranes. J Membr Sci 2000;166(2):271-80.
[47] Gu J, Xu S, Lu X, Ma R, Zhang S, Zheng S, Wang H, Shen H. Study on the membrane formation mechanism of PVDF/PVDF-CTFE blends. J. Taiwan Inst. Chem. Eng. 2023:104655.
[48] Dirin AChen P,M, Saljoughi E, Mousavi SM, Kiani S. Pervaporation separation of isopropylbenzene from water using four different polymeric membranes: Membrane preparation, modification, characterization, and performance evaluation. J. Taiwan Inst. Chem. Eng. 2020;114:67-80.
[49] da Rocha HD, Reis ES, Ratkovski GP, da Silva RJ, Gorza FD, Pedro GC, de Melo CP. Use of PMMA/(rice husk ash)/polypyrrole membranes for the removal of dyes and heavy metal ions. J. Taiwan Inst. Chem. Eng. 2020;110:8-20.
[50] Noreen A, Zia KM, Tabasum S, Khalid S, Shareef R. A review on grafting of hydroxyethylcellulose for versatile applications. Int J Biol Macromol 2020;150:289-303.
[51] Lo JT, Yen HT, Tsai CC, Chen BH, Hou SS. Interaction between hydrophobically modified 2-hydroxyethyl cellulose and sodium dodecyl sulfate studied by viscometry and two-dimensional NOE NMR spectroscopy. J Phys Chem B 2014;118(24):6922-30.
[52] Villegas-Pañeda X, Pérez-Casas S, Hernández-Baltazar E, Chávez-Castellanos AE. Study of interactions between octyl-β-D-glucopyranoside and the hydroxyethyl-cellulose biopolymer in aqueous solution. J Chem Thermodyn 2014;79:69-75.

[53] Tripathy DB, Mishra A, Clark J, Farmer T. Synthesis, chemistry, physicochemical properties and industrial applications of amino acid surfactants: A review. C. R. Chim. 2018;21(2):112-30.
[54] Bordes R, Holmberg K. Amino acid-based surfactants–do they deserve more attention?. Adv Colloid Interface Sci 2015;222:79-91.
[55] Bourkaib MC, Delaunay S, Framboisier X, Hôtel L, Aigle B, Humeau C, Guiavarc'h Y, Chevalot I. N-acylation of L-amino acids in aqueous media: Evaluation of the catalytic performances of Streptomyces ambofaciens aminoacylases. Enzyme Microb Technol 2020;137:109536.
[56] Akter N, Radiman S, Mohamed F, Rahman IA, Reza MI. Ternary phase behaviour and vesicle formation of a sodium N-lauroylsarcosinate hydrate/1-decanol/water system. Sci Rep 2011;1(1):71.
[57] Pinazo A, Pons R, Pérez L, Infante MR. Amino acids as raw material for biocompatible surfactants. Ind Eng Chem Res 2011;50(9):4805-17.
[58] Katiyar SS, Kushwah V, Dora CP, Patil RY, Jain S. Design and toxicity evaluation of novel fatty acid-amino acid-based biocompatible surfactants. AAPS PharmSciTech 2019;20(5):186.
[59] Brito RO, Silva SG, Fernandes RM, Marques EF, Enrique-Borges J. do Vale ML. Enhanced interfacial properties of novel amino acid-derived surfactants: Effects of headgroup chemistry and of alkyl chain length and unsaturation. Colloids Surf B 2011; 86(1):65-70.
[60] Morán MC, Pinazo A, Pérez L, Clapés P, Angelet M, García MT, Vinardell MP, Infante MR. "Green" amino acid-based surfactants. Green Chem 2004;6(5):233-40.
[61] Zhou M, Zhang Z, Xu D, Hou L, Zhao W, Nie X, Zhou L, Zhao J. Synthesis of three gemini betaine surfactants and their surface active properties. J. Taiwan Inst. Chem. Eng. 2017;74:7-13.
[62] Rajstein J, Fuks M, Markitziu A, Gedalia I. Solubility of enamel powder following treatment with a sodium-n-lauroyl sarcosinate containing toothpaste in the presence and absence of fluoride. J Oral Rehabil 1983;10(6):469-71.
[63] Ananthapadmanabhan KP. Amino-acid surfactants in personal cleansing. Tenside Surfactants Deterg 2019;56(5):378-86.
[64] Pinazo A, Manresa MA, Marques AM, Bustelo M, Espuny MJ, Pérez L. Amino acid–based surfactants: New antimicrobial agents. Adv Colloid Interface Sci 2016;228:17-39.
[65] Yapar S, Ateş M, Özdemir G. Preparation and characterization of sodium lauroyl sarcosinate adsorbed on cetylpyridinium-montmorillonite as a possible antibacterial agent. Appl Clay Sci 2017;150:16-22.
[66] Yu Y, Zhang D, Zeng H, Xie B, Gao L, Lin T. Synergistic effects of sodium lauroyl sarcosinate and glutamic acid in inhibition assembly against copper corrosion in acidic solution. Appl Surf Sci 2015;355:1229-37.
[67] Du W, Huang X, Zhang J, Wang D, Yang Q, Li X. Enhancing methane production from anaerobic digestion of waste activated sludge with addition of sodium lauroyl sarcosinate. Bioresour Technol 2021;336:125321.
[68] Xu C, Wang D, Wang H, Ma L, Zhu X, Zhu Y, Zhang Y, Liu F. Experimental investigation of coal dust wetting ability of anionic surfactants with different structures. Process Saf Environ Prot 2019;121:69-76.
[69] Zhang M, Zhao SX, Ding B, Zhang YQ. Sodium N-lauryl amino acids derived from silk protein can form catanionic aggregates with cytarabine as novel anti-tumor drug delivery systems. Drug Deliv 2020;27(1)482-90.

[70] Ray GB, Ghosh S, Moulik SP. Physicochemical studies on the interfacial and bulk behaviors of sodium N-dodecanoyl sarcosinate (SDDS). J Surfactants Deterg 2009; 12(2):131-43.
[71] Das S, Mondal S, Ghosh S. Physicochemical studies on the micellization of cationic, anionic, and nonionic surfactants in water–polar organic solvent mixtures. J Chem Eng Data 2013;58(9):2586-95.
[72] Shah RA, Chat OA, Rather GM, Dar AA. Volumetric properties of sodium lauroylsarcosinate in aqueous alcohol solutions of methanol, ethanol, and 1-propanol. J Chem Eng Data 2017;62(10):3015-24.
[73] Ren ZH, Huang J, Luo Y, Zheng YC, Mei P, Yu WC, Lai L, Chang YL, Li FX. Effect of isopropanol on the micellization of binary mixture containing amino sulfonate amphoteric surfactant in aqueous solution: mixing with sodium dodecylbenzene sulfonate. Journal of the Taiwan Institute of Chemical Engineers. 2016;65:482-7.
[74] Patra N, Ray D, Aswal VK, Ghosh S. Exploring physicochemical interactions of different salts with sodium N-dodecanoyl sarcosinate in aqueous solution. ACS Omega 2018;3(8): 9256-66.
[75] Bagheri A, Jafari-Chashmi P. Study of aggregation behavior between N-lauryl sarcosine sodium and dodecyltrimethylammonium bromide in aqueous solution, using conductometric and spectrophotometric techniques. J Mol Liq 2019;282:466-73.
[76] Dan A, Ghosh S, Moulik SP. Interaction of cationic hydroxyethylcellulose (JR400) and cationic hydrophobically modified hydroxyethylcellulose (LM200) with the amino-acid based anionic amphiphile Sodium N-Dodecanoyl Sarcosinate (SDDS) in aqueous medium. Carbohydr Polym 2010;80(1):44-52.
[77] Naskar B, Ghosh S, Moulik SP. Interaction of normal and reverse pluronics (L44 and 10R5) and their mixtures with anionic surfactant sodium N-dodecanoylsarcosinate. J Colloid Interface Sci 2014;414:82-89.
[78] Rudra S, Dasmandal S, Mahapatra A. Binding interaction of sodium-N-dodecanoyl sarcosinate with hemoglobin and myoglobin: Physicochemical and spectroscopic studies with molecular docking analysis. J Colloid Interface Sci 2017;496:267-77.
[79] Mandal B, Ghosh S, Moulik SP. Detailed characterization of lysozyme (Lyz)–surfactant (SDDS) interaction and the structural transitions. New J Chem 2016;40(5):4617-24.
[80] Owoyomi O, Junaid OZ, Olaoye OE. Spectroscopic investigation of the interaction between crystal-violet and sodium dodecanoylsarcosinate. Phys Chem Liq 2022;60(1): 129-40.
[81] Mondal S, Doloi B, Ghosh S. Spectroscopic studies of interaction of safranine T with ionic surfactants. Fluid Phase Equilib 2013;360:180-7.
[82] Azum N, Rub MA, Khan A, Alotaibi MM, Asiri AM. Synergistic Interaction and Binding Efficiency of Tetracaine Hydrochloride (Anesthetic Drug) with Anionic Surfactants in the Presence of NaCl Solution Using Surface Tension and UV–Visible Spectroscopic Methods. Gels 2022;8(4):234.
[83] Banerjee T, Samanta A, Mandal A. Mathematical regression models for rheological behavior of interaction between polymer-surfactant binary mixtures and electrolytes. Journal of Dispersion Science and Technology. 2022;43(9):1333-45.
[84] Chakraborty T, Chakraborty I, Ghosh S. The methods of determination of critical micellar concentrations of the amphiphilic systems in aqueous medium. Arab J Chem 2011;4(3):265-70.
[85] Elarbi FM, Janger AA, Abu-sen LM, Ettarhouni ZO. Determination of CMC and interfacial properties of anionic (SDS) and cationic (CPB) surfactants in aqueous solutions. Am J Eng Res 2020;9:118-26.

[86] Mandal B, Ghosh S, Moulik SP. Interaction between a bio-tolerable amino-acid based amphiphile (N-dodecanoylsarcosinate, SDDS) and modified cationic polymers, hydroxyethylcelluloses (JR 400, and LM 200) in isopropanol-water medium. Colloids Surf A 2019;566:156-65.
[87] Niranjan PS, Upadhyay SK. Interaction of polyacrylamide with conventional anionic and gemini anionic surfactants. J Dispersion Sci Technol 2010;32(1):109-13.
[88] Besra L, Sengupta DK, Roy SK, Ay P. Flocculation and dewatering of kaolin suspensions in the presence of polyacrylamide and surfactants. Int J Miner Process 2002; 66(1-4):203-32.
[89] Li Q, Ye L, Cai Y, Huang R. Study of rheological behavior of hydrophobically modified hydroxyethyl cellulose. Journal of applied polymer science. 2006 May 15;100(4):3346-52.
[90] Mal A, Saha A, Dinda G, Ghosh S. Effect of carbohydrate based polymers on worm-like micelles of cetyltrimethylammonium p-toluenesulfonate in aqueous media: Detail physicochemical and antimicrobial properties survey. J Mol Liq 2020;299:112153.
[91] McNally EJ, Gau CS, Zografi G. Effects of hydroxypropyl cellulose and hydroxyethyl cellulose adsorption on the wetting of low energy solid surfaces. J Adhes Sci Technol 1992;6(4):445-54.
[92] Božič M, Elschner T, Tkaučič D, Bračič M, Hribernik S, Kleinschek KS, Kargl R. Effect of different surface active polysaccharide derivatives on the formation of ethyl cellulose particles by the emulsion-solvent evaporation method. Cellulose 2018;25(12):6901-22.
[93] Petrović LB, Sovilj VJ, Milanović JL, Katona JM. A conductometric investigation of hydroxypropylmethyl cellulose/sodium dodecyl sulfate/nonionic surfactant systems. J Serb Chem Soc 2014;79(11):1421-32.
[94] Carey E, Patil SR, Stubenrauch C. Conductivity measurements as a method for studying ionic technical grade surfactants. Tenside Surfactants Detergents. 2008;45(3):120-5.
[95] Zhang P, Zhang J, Wang D, Zhang F, Zhao Y, Yan M, Zheng C, Wang Q, Long M, Chen C. Modification of g-C3N4 with hydroxyethyl cellulose as solid proton donor via hydrogen bond to enhance H2O2 production. Applied Catalysis B: Environmental. 2022;318:121749.
[96] Winnik MA, Bystryak SM, Chassenieux C, Strashko V, Macdonald PM, Siddiqui J. Study of interaction of poly (ethylene imine) with sodium dodecyl sulfate in aqueous solution by light scattering, conductometry, NMR, and microcalorimetry. Langmuir. 2000;16(10):4495-510.
[97] Loh W, Brinatti C, Tam KC. Use of isothermal titration calorimetry to study surfactant aggregation in colloidal systems. Biochim. Biophys Acta 2016;1860(5):999-1016.
[98] Majhi PR, Moulik SP. Energetics of micellization: reassessment by a high-sensitivity titration microcalorimeter. Langmuir 1998;14(15):3986-90.
[99] Bouchemal K, Agnely F, Koffi A, Djabourov M, Ponchel G. What can isothermal titration microcalorimetry experiments tell us about the self-organization of surfactants into micelles?. Journal of molecular recognition 2010;23(4):335-42.
[100] Das S, Patra N, Banerjee A, Das B, Ghosh S. Studies on the self-aggregation, interfacial and thermodynamic properties of a surface active imidazolium-based ionic liquid in aqueous solution: Effects of salt and temperature. J Mol Liq 2020;320:114497.
[101] Piñeiro L, Novo M, Al-Soufi W. Fluorescence emission of pyrene in surfactant solutions. Adv Colloid Interface Sci 2015;215:1-12.

[102] Howarth AJ, Majewski MB, Wolf MO. Photophysical properties and applications of coordination complexes incorporating pyrene. Coord Chem Rev 2015;282-283:139-49.
[103] Ottonelli M, Piccardo M, Duce D, Thea S, Dellepiane G. Tuning the photophysical properties of pyrene-based systems: A theoretical study. J Phys Chem A 2012;116(1): 611-30.
[104] Dar AA, Garai A, Das AR, Ghosh S. Rheological and fluorescence investigation of interaction between hexadecyltrimethylammonium bromide and methylcellulose in the presence of hydrophobic salts. J Phys Chem A 2010;114(15):5083-91.
[105] Halasová T, Krouská J, Mravec F, Pekař M. Hyaluronan-surfactant interactions in physiological solution studied by tensiometry and fluorescence probe techniques. Colloids Surf A 2011;391(1):25-31.
[106] Ghosh S, Mondal S. Spectroscopic Study on the Interaction of Medicinal Pigment, Curcumin with Various Surfactants: An Overview. J Surface Sci Technol 2012;28(3-4): 179-95.
[107] Alargova RG, Kochijashky II, Sierra MR, Zana R. Micelle aggregation numbers of surfactants in aqueous solutions: A comparison between the results from steady-state and time-resolved fluorescence quenching. Langmuir 1998;14(19):5412-8.
[108] Turro NJ, Baretz BH, Kuo PL. Photoluminescence probes for the investigation of interactions between sodium dodecylsulfate and water-soluble polymers. Macromolecules 1984;17(7):1321-4.
[109] Mylonas Y, Staikos G, Lianos P. Investigation of the poly (N-isopropylacrylamide)-sodium dodecyl sulfate complexation with viscosity, dialysis, and time-resolved fluorescence-quenching measurements. Langmuir 1999;15(21):7172-5.
[110] Dan A, Ghosh S, Moulik SP. Physicochemical studies on the biopolymer inulin: A critical evaluation of its self-aggregation, aggregate-morphology, interaction with water, and thermal stability. Biopolymers: Original Research on Biomolecules 2009;91(9):687-99.
[111] Mandal B, Moulik SP, Ghosh S. Influence of aquo-organic solvent media on the self-aggregation of sodium dodecyl sulfate (SDS) and its interaction with polyvinylpyrrolidone (PVP). Colloid Polym Sci 2014;292(10):2485-95.
[112] Naskar B, Dan A, Ghosh S, Moulik SP. Characteristic physicochemical features of the 9biopolymer inulin in solvent added and depleted states. Carbohydrate Polymers. 2010;81(3):700-6.
[113] Honary S, Zahir F. Effect of zeta potential on the properties of nano-drug delivery systems-a review (Part 2). Trop J Pharm Res 2013;12(2):265-73.
[114] Nizri G, Lagerge S, Kamyshny A, Major DT, Magdassi S. Polymer–surfactant interactions: Binding mechanism of sodium dodecyl sulfate to poly (diallyldimethylammonium chloride). J Colloid Interface Sci 2008;320(1):74-81.
[115] Nambam JS, Philip J. Effects of interaction of ionic and nonionic surfactants on self-assembly of PEO–PPO–PEO triblock copolymer in aqueous solution. J Phys Chem B 2012;116(5):1499-1507.
[116] Das S, Mondal S, Ghosh S. Interaction of cationic gemini surfactant tetramethylene-1, 4-bis (dimethyltetradecylammonium bromide) with anionic polyelectrolyte sodium carboxymethyl cellulose, with two different molar masses, in aqueous and aquo-organic (isopropanol) media. RSC Adv 2016;6(37):30795-803.
[117] Jiao L, Zhang L, Guan W, Lu C. Fluorescence visualization of interactions between surfactants and polymers. RSC Adv 2016;6(92):88954-58.

CHAPTER-II

Impact of 2,2,2-trifluoroethanol (TFE) on hydrophobicity enhancement in the aggregation of Sodium N-Dodecanoyl Sarcosinate (SDDS) with nonionic Hydroxyethyl Cellulose

Impact of 2,2,2-trifluoroethanol (TFE) on hydrophobicity enhancement in the aggregation of Sodium N-Dodecanoyl Sarcosinate (SDDS) with nonionic Hydroxyethyl Cellulose

Colloids and Surfaces A: Physicochemical and Engineering Aspects, 2024 681, 132781.

(published)

ABSTRACT

An organic solvent has the ability to improve the extent of hydrophobicity in a mixed polymer-surfactant system. The carbohydrate-based polymers, having spacious applications in food and pharmaceutical industries, can interact effectively with anionic surfactants in a hydrophobic fashion. This article has been highlighted to gain perception about the effect of 'cosurfactant' like organic solvent 2,2,2-trifluoroethanol (TFE) on the self-aggregation of anionic surfactant Sodium N-dodecanoyl sarcosinate (SDDS), and its interaction with non-ionic biopolymer hydroxyethyl cellulose (HEC). In this work, the interaction behaviour has been detailed by the use of some conventional methods, such as, tensiometry, conductometry, fluorimetry and microcalorimetry in mixed aquo-alcohol solution. Understanding the binding pattern of the HEC-SDDS system, it appears to be dependent on hydrophobic interaction. From tensiometry, TFE exhibits a fair extent of surface activity and thus, it further enhances the hydrophobicity of the medium. An increased alcohol percentage in the water medium has resulted in a significant reduction in the critical micelle concentration (CMC). TFE promotes micellization of the ionic surfactants at a lower concentration by lowering the charge intensity on the polar head groups of the micelles. Thus, the micellization becomes favoured in TFE solvent. The related thermodynamic and surface parameters have been estimated to get an insight into the bulk and interfacial properties of the anionic amphiphile on the polymeric interface in mixed aquo-alcohol solution. The decreasing trend of aggregation number (N_{Agg}) in TFE solvent has been discussed with the aid of steady state fluorescence spectroscopic technique. Dynamic light scattering (DLS) study has been used for the measurement of hydrodynamic size (D_h) and polydispersity index (PDI) of HEC polymer in the presence of varying percentage of TFE. All these observations have been displayed and explored conceptually and in stepwise fashion. Further, HEC-SDDS aggregate has been visualized from Field Emission Scanning Electron Microscopy (FESEM) imaging A striking change in the morphology has been seen in the TFE environment. As an additive, TFE is opted because of its unique properties as a solvent and also vast applications in the field of biological and pharmaceutical industry. The system chosen in this study is completely new in the field of surface chemistry and each of the experimental results provided below is distinct. At higher TFE contents, the micellization of SDDS is not feasible.

Keywords

Cosurfactant; Anionic surfactant; Biopolymer; Conventional methods; Aggregation number.

1. Introduction

The study of quaternary interacting systems containing polymer-surfactant-water-additive are rarely found in literatures. This topic has been extremely fascinated for continuously growing research interest to understand the fundamental mechanisms of interactions among them. The

researchers are being able to take advantages of such interacted systems in diverse fields of modern science such as pharmaceutics **[1]**, drug encapsulation **[2,3]**, cosmetics **[4]** and many other industrial applications **[5,6]**. An amphiphile can undergo micellization not only in aqueous medium **[7]**, but also in the presence of additives such as salts **[8,9]**, non-aqueous solvents **[10,11]** etc. Depending upon the chemical nature of such additives, physicochemical modification of micellization process can be possible by introducing further complexity in such systems. Among different additives, use of alcohols are most frequently reported in literatures. The alcohol solvents are characterized by their hydrogen bonding abilities, solubilisation, dielectric constant values etc **[12]**. The mixtures of certain surfactants and alcohols have the potential to display synergism and improve the individual qualities, e.g., surface activity, foaming, wetting, and many others **[13]**. It is that both the nature and concentration of the alcohol modify the features of the surfactant formulations. Among all the surfactants, anionic sodium dodecyl sulphate (SDS) is the most widely studied in mixed aquo-alcohol solvents by different research groups **[14-18]**. Fatima et al. **[19]** has recently conducted a comparative study between TFE and ethanol, while studying their effects on the thermophysical properties of an ionic liquid (1-ethyl-3-methylimidazolium dicyanamide) in binary alcohol mixture. In an another study, Patidar et al. **[20]** has compared the effects of TFE with various alcohols (ethanol, 1-butanol, 1-hexanol, 1-octanol, etc.) on the clouding behaviour of two block copolymers, finding a decreasing trend of clouding points with [TFE]. The most interesting aspects about the alcohols is that they can act either as ‘cosurfactants’ **[21,22]** or ‘cosolvents’ **[23]** depending on their concentration in the mixture to decrease or increase the critical micelle concentration (CMC) of the surfactant respectively during the micelle formation. The widely used alcohol, ethanol, works as a ‘cosurfactant’ at lower concentration but as a ‘cosolvent’ at higher concentration **[24]**. Dan et al. **[17]** has claimed that isopropanol (IP) functions as a cosurfactant below 6.62% to lower the CMC of sodium dodecylsulfate (SDS), and as a cosolvent above that. Instead, TFE serves only as a ‘cosurfactant’ in the present study by lowering the CMC of SDDS at the studied concentration ranges. The TFE solvent molecules can easily enter into the micellar palisade layer, and undergo co-aggregation with SDDS micelles. The micellization behaviour of surfactants also gets affected by the hydrocarbon chain length of the alcohol being used. When the chain length is larger, the alcohol becomes more hydrophobic and its hydrophobicity causes the CMC to fall more rapidly **[25]**. The appearance of alcohols in the field of colloid chemistry has immense impact for their properties of structure making or breaking **[26,27]** of water in water-alcohol mixture. The micellization of surfactant can also be modified in a polymer/surfactant mixture, resulting in either increase or decrease in the CMC value. Using polymer or surfactant alone is insufficient for the development of several beneficial features but their mixture does **[28,29]**. For instance, rheological control and colloidal stability are provided by the polymer, whereas the surfactant aids in emulsification and interfacial tension control. The surfactants are commonly known to bind with polymers through either electrostatic or hydrophobic interactions or both depending upon their nature and charges. The interaction between anionic surfactant (SDDS) and neutral polymer (HEC) is hydrophobic in nature. The driving force responsible for their interaction is to minimize the interfacial territory that exists between the non-polar segments of the polymer and the hydrophobic parts of the surfactant in the solvent medium. For interactions to be effective, the non-ionic polymer and the anionic surfactant must have different chemical affinities. Further, the interaction behavior can be controlled by several factors, such as, presence of

additives (solvent, salt, etc.), hydrophobic chain of the surfactant, and the rigidity of the polymer backbone. The presence of additive is very much effective to induce their mutual interactions as well as their individual fundamental properties. Because of this, the interaction study appears to still be developing.

Cellulose is known as the most abundant natural biopolymer. Non-ionic hydroxyethyl cellulose (HEC) is carbohydrate based, cellulose derivative with high molecular weight. Industrially, this polymer is synthesized **[30]** using cellulose in sodium hydroxide and ethylene oxide. High water solubility of HEC makes this polymer as an important material both in industry and academic research. The biodegradability, biocompatibility, and low immunogenicity of the carbohydrate-based polymers make them particularly attractive **[31-33]**. In recent times, the cellulose polymers have been turned into excellent research materials as they are widely used in grafting **[34,35]** with different polymers and also their physicochemical changes in presence of various surface-active agents **[36,37]**. In a recent publication, Mondal et al. **[38]** has examined the aggregation of two different anionic surfactants in the presence of a cellulose polymer (HPC) as well as the effect of their tail length on the formation premicellar polymer-surfactant complexes (PS). The biomedical and industrial importance of hydroxyethyl cellulose has already been reported in a variety of areas, including treatment of waste water **[39,40]**, paint formulation **[41,42]**, plasma expansion **[43]**, drug delivery **[44]**, membrane preparation **[45],** etc.

Sodium N-dodecanoyl sarcosinate (SDDS) is one of the most important amino acid surfactants. Now-a- days, novel amino acid surfactants **[46]** have immense impact on modern surface chemistry research over a large scale due to their biocompatible **[47]** and biodegradable **[48]** nature. Furthermore, attention has been drawn to this naturally occurring anionic surface-active agent due to its antimicrobial **[49]** and antibacterial **[50]** properties. It is a derivative of lauric acid. In human dental system, it is used in tooth paste production to regulate dental caries **[51]**. In cosmetics industry (e.g. shampoo, shaving cream, wash products etc.), it is largely used for its foaming and cleansing actions **[52]**. A number of detailed physicochemical studies have been reported on the micellization of this amphiphile **[53]**. The amphiphilic behaviour of SDDS in presence of salts **[54]**, solvents **[55]**, polymers **[56,57]**, proteins **[58,59]**, drugs **[60],** etc. has also been the subject of numerous earlier research. The study of biopolymer with surfactant is important because it resembles the protein-surfactant interaction, in which the surfactant can induce protein denaturation. Recently, Mandal et al. **[61]** has explored the impact of IP solvent on the SDDS-modified HEC system (cationic JR 400, and LM 200). In a related work, Mukherhee et al. **[62]** has made a comparative study on the interaction between cationic polymer PDADMAC with various anionic surfactants (SDS, SDBS, and SDDS) in water and IP-water media. However, there is no such reported work involving SDDS and non-ionic polymer in aqueous organic media.

2,2,2-Trifluoroethanol (TFE), a classical fluorinated alcohol **[63,64]**, has a large-scale demand for the researchers both in academic and biophysical fields **[65]** for its unique physicochemical properties. Owing to its excellent water miscibility **[66]**, TFE can act as an efficient cosolvent with water for the biological research studies of proteins and peptides **[67-69]** and also as a solvent medium in many organic synthesis reactions **[70-73]**. It is prepared commercially from acid chloride derivative of trifluoroacetic acid by catalytic hydrogenation **[74]**. The trifluoromethyl group (-CF_3), due to its strong electron withdrawing nature, makes

TFE a superior proton donor [α(TFE) = 1.51] **[75]** compared to proton acceptor in the formation of hydrogen bonds with water molecules. It also makes TFE significantly more acidic (p^{Ka} = 12.4) **[76]** than other commonly used conventional alcohols. The lower dielectric constant value (ϵ = 27) **[66]** of TFE in comparison to water may be responsible for the reduced polarity in TFE-water mixture. At the same time, hydrophobic part of TFE molecule, i.e., trifluoromethyl group definitely may impart some hydrophobicity in the medium and also increases the hydrogen bonding ability **[77, 78]** with water in the duo solvent mixture. Owing to this interesting behaviour, there is a great deal of curiosity to study the micellar properties of amphiphiles and ionic liquids taking TFE as an additive in water medium and only a few research works **[79-81]** have been done in this motive.

Hence, TFE has been chosen as an additive for its interesting solvent character **[82]** in the present survey to investigate the amphiphilic behaviour of SDDS alone and in HEC-SDDS systems. The micellization of anionic surfactants in solution and their interaction with non-ionic polymers are both significantly influenced by the short chain alcohols **[17]**. Depth analysis for understanding the enhancement in hydrophobicity in presence of TFE has been explained. A multi physicochemical techniques (tensiometry, conductometry, fluorimetry and microcalorimetry) have been applied for designing the focus of this work. The influence of TFE solvent on polymer size has been revealed by dynamic light scattering (DLS) method. Development of FESEM imaging helps us to elucidate the composition and surface morphology of HEC-SDDS complex in TFE-water solvent mixture.

2. Experimental section

2.1. Materials

Hydroxyethyl cellulose (HEC) (molar mass = 90,000 $g\ mol^{-1}$, degree of substitution (α) = 1.5), a carbohydrate-based polymer, has been purchased from Sigma Aldrich (USA). The anionic surfactant, Sodium N-dodecanoyl sarcosinate (SDDS) (AR-grade quality, purity> 97%), has been obtained from Fluka, Germany. Pyrene (fluorescence probe for polarity index (I_1/I_3) determination), cetylpyridinium chloride (CPC, fluorescence quencher) and 1,6-diphenyl-1,3,5-triene (DPH, fluorescence probe for the determination of micellar aggregation number) are the products of Sigma Aldrich (USA). All these materials are used in the experiment without any further purification. The solvent 2,2,2-trifluoroethanol (TFE) (purity 99%), an AR-grade product, has been received from SRL, India. Double-distilled water (specific conductance (κ)~1.0 $\mu S\ cm^{-1}$) has been used to prepare all the experimental solutions. A constant temperature of 298 K has been strictly maintained throughout all the measurements. HEC having 0.01 g% (w/v) concentration has been taken in this investigation. The concentration of TFE has been expressed in % (v/v). In this study, 5%, 10% and 15% (v/v) TFE solutions were prepared in double-distilled water. The structures of HEC, SDDS and TFE are presented in Scheme 1.

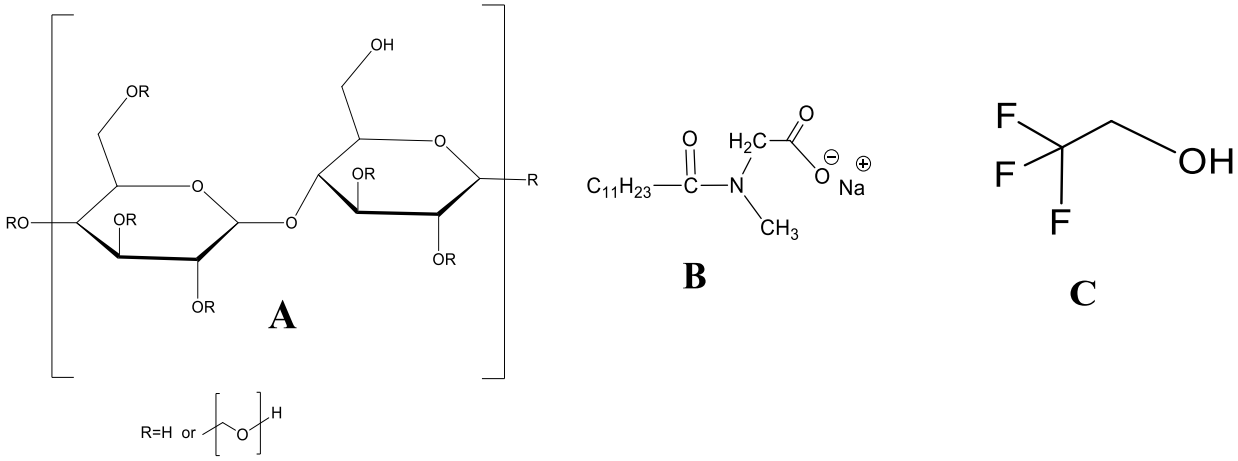

Scheme 1. Structures of (A) Hydroxyethyl Cellulose (HEC), (B) Sodium N-Dodecanoyl Sarcosinate (SDDS), (C) 2,2,2-Trifluoroethanol (TFE).

2.2. Methods

2.2.1. Tensiometry

The surface tension data were collected from calibrated Krüss du Noüy tensiometer (Germany) using platinum ring detachment technique at 298 K. A 5 mL of the experimental solution was taken in a double-walled container to which surfactant solution was added stepwise. Hamilton microsyringe was used for the addition process. All the equipment required for the experiment were properly cleaned using double distilled water and dried with acetone before each experiment. The platinum ring was further burned in ethanol flame. The concentration of the stock surfactant solution was taken as 225 mM (15 times of CMC). The temperature of the system was kept constant (accuracy of ± 0.1 K) throughout the experiment using a thermostatic water bath. Each data was collected by allowing time interval of 10 min for equilibration. In all experiments, the accuracy was maintained as ± 0.1 mN m^{-1}.

2.2.2. Conductometry

The specific conductance values were collected by using Jenway (UK) conductometer (cell constant 1.0 cm^{-1}). The experiment was initiated by taking 7 mL of experimental solution in a double-walled glass container. The whole system was kept in a thermostatic water bath to maintain temperature accuracy of ± 0.1 K. The surfactant solution (225 mM) was added into the experimental solution using a Hamilton microsyringe. The error in the specific conductance measurement was maintained within ± 0.5%.

2.2.3. Isothermal Titration Calorimetry (ITC)

An Omega ITC-200 microcalorimeter (Microcal, USA) instrument was used for carrying ITC measurements. The experimental system was kept in a Neslab RTE 100 circulating water bath for the maintenance of constant temperature at 298 K. The titration was carried out by adding

surfactant solution (10-15 times of CMC) with the help of a micro syringe in 20-30 successive additions taking a time interval of 210 seconds for each addition with constant stirring (300 rpm). The heat change involved in each step of the surfactant addition was recorded in ITC software.

2.2.4. Fluorimetry

Steady state fluorimetric emission measurements were performed in a Perkin Elmer LS 55 (USA) spectrofluorimeter. The CMC of both surfactant and polymer-surfactant systems were determined using pyrene as a hydrophobic probe. For maintaining constant temperature of the experimental system at 298 K, a water flow thermostat was applied. The hydrophobic pyrene was excited at 332 nm. The wavelength range was 350-450 nm for measuring emission spectra. The slit widths were fitted at 14 and 2.5 nm for excitation and emission respectively. The scan rate was maintained 250 nm/min for each experiment. The polymer solutions prepared in both aqueous medium and in presence of different (v/v) % of TFE were taken in quartz cuvette having path length of 10 mm. The surfactant concentration was 225 mM. During fluorimetric measurement, surfactant solution (prepared in both aqueous and aquo-organic media) was added stepwise by a Hamilton micro syringe and the consequent change in intensity ratio of the first (I_1) and third (I_3) vibrational peak of the probe was taken for the determination of CMC.

On the other hand, aggregation number (n_A) of the same systems were calculated by static fluorescence quenching (SFQ) method. Here, tryptophan and 1-hexadecylpyridinium chloride (CPC) were used as the probe and quencher respectively, and quencher CPC was added with Hamilton micro syringe to the system to measure fluorescence intensity. The concentration of the surfactant used in the experiment was much above their measured CMC and that of tryptophan was used in very low amount.

2.2.5. Dynamic Light Scattering

DLS size measurements of HEC polymer in aqueous solution and water-TFE medium were taken using Malvern Nano ZS Zetasizer (United Kingdom) instrument at 173° angle in He-Ne laser source (wavelength 632.8 nm) at 298 K. All these solutions before experiment were filtered through cellulose acetate paper for 3-4 times to remove unwanted dust particles. Each measurement was duplicated for reproducibility and then the mean values were reported for analysis.

2.2.6. Field Emission Scanning Electron Microscopy (FESEM)

The images of surface morphology of experimental systems were taken from high resolution field emission scanning electron microscope (FEI INSPECT F50, Japan). A 2 μL drop of the investigated systems was placed on a tiny square glass slide followed by overnight drying (solvent removal) and spreading of the samples. The samples were then processed for gold coating via sputtering method with time duration of 1 min and applied 5.5 mA current.

3. Results and discussion

3.1. Effect of TFE on self-aggregation of SDDS

The amphiphilic nature of SDDS in TFE-water medium has been investigated via tensiometry, conductometry, microcalorimetry and fluorimetric measurements. The resultant plots are displayed in Fig. 1(A-E). The CMC values, and the related interfacial and thermodynamic parameters have been represented in Tables 1 and 2 respectively. The appearance of CMC evidences the self-aggregation of SDDS in TFE solvent. Using the concept of CMC, it is feasible to measure several thermodynamic parameters that can be used to ascribe the thermodynamic stability of the micelles.

It is found that the CMC of anionic SDDS surfactant has been decreased markedly with increasing (v/v) % of TFE solvent. At 15% TFE, the value of CMC has been decreased by about 43%. Hence, TFE acts as the 'co-surfactant' **[21]** in the aqueous environment. When TFE molecules interact with ionic surfactants, they are more likely to get into the micellar surface layer, which reduces the micellar charge density by lengthening the average distance between the polar head groups **[83]**. At higher TFE percentage, due to higher solubilization of TFE molecules in the micellar surface, the CMC decreases. Addition of TFE solvent to water medium can act in two different ways. In one hand, TFE serves for making water structure to decrease CMC of SDDS amphiphile. At the same time, TFE decreases the medium polarity (ϵ_{TFE} = 27) **[66]** to increase CMC. The decrease in medium polarity is opposed by the way of making water structure. The overall result tends to decrease in CMC. For non-ionic TX-100, an exception is observed. García-Blanco et al. **[81]** has outlined a tendency towards increase in the CMC value with the increase in [TFE], and at 0.83 M TFE, the CMC has reached only 30% higher, which is compatible with a slight rise in solubility of TX-100 micelles in higher [TFE]. In another investigation, Civera et al. **[80]** has examined the effect of TFE on CMC and CP of non-ionic TX-165 micelles, both are found to decrease with an increase in [TFE] because of an enhancement in hydrophobicity. Beyond 15% TFE, SDDS surfactant shows difficulty in micelle formation and no inflection point is found in either tensiometric or conductometric plot. When TFE exceeds 15%, either the tensiometric plots scatter too much or the conductometric plots are insensitive to detect the observable slope change before and after the micellization. In fact, the micellization of amphiphiles cannot be defined above a certain alkanol percentage, which is also seen in the present system. Therefore, the highest concentration of TFE is taken to be 15% (v/v) to accurately present and compare data in this study. Mandal et al. **[61]** has observed that above 20% IP, micellization of SDDS becomes non-existent. In another investigation, Naskar at el. **[84]** has reported the same about the micellization of CHAPS amphiphile above 10% IP. According to Das et al., **[85]** in case of cationic gemini surfactant (14-4-14), micelle formation is not possible above 15% IP.

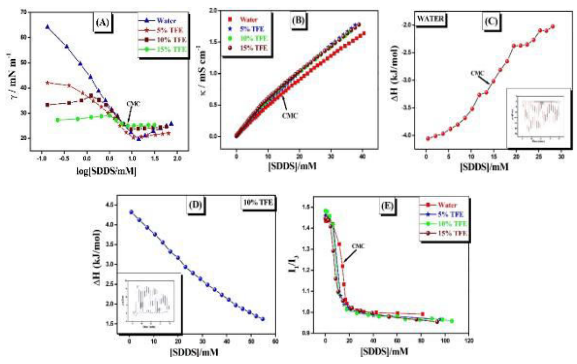

Fig. 1. Determination of CMC of SDDS in water and TFE-water media from (A) Tensiometry, (B) Conductometry; (C), (D) Microcalorimetry in water and 10% TFE-water media respectively (Inset: enthalpograms), (E) Fluorimetry methods at 298 K.

Gibbs adsorption equation represents the surface excess of SDDS surfactant at CMC in eq 1.

$$\Gamma_{max} = -\frac{1}{2.303iRT}\lim_{[S]\to CMC}\frac{d\gamma}{dlogC} \quad (1)$$

where, i represents the number of dissociated species per amphiphile molecule in solution. For SDDS molecule, i=2. T is the temperature in Kelvin scale and R is the molar gas constant ($Joule\ mol^{-1}\ K^{-1}$).

The following equation (eq 2) represents the expression ofA_{min}, i.e., minimum surface area per SDDS molecule.

$$A_{min} = \frac{10^{18}}{N_A\Gamma_{max}} \quad (2)$$

N_A is called Avogadro's constant.

The changes in standard Gibbs free energy of both micellization (ΔG^0_{mic}) and adsorption (ΔG^0_{Ads}) are represented in eqs 3 and 4 respectively.

$$\Delta G_{mic} = (1+\beta)\ \mathrm{RT}lnX_{CMC} \quad (3)$$

$$\Delta G^0_{Ads} = \Delta G^0_{mic} - \frac{\pi_{CMC}}{\Gamma_{max}} \quad (4)$$

The units used for Γ_{max}, A_{min}, ΔG^0_{mic} and ΔG^0_{Ads} are $mol\ m^{-2}$, $nm^2 molecule^{-1}$, $kJ\ mol^{-1}$ and $kJ\ mol^{-1}$ respectively.

where, β is known as counter ion binding calculated from the ratio of post- and pre-micellar regions in the conductometric plots subtracted from unity. The value of slope in pre-CMC region (S_1) is higher than that found in post-CMC region (S_2). Consequently, the numerical value of β is found lower than unity (eq 5).

$$\beta = 1 - \frac{S_2}{S_1} \quad (5)$$

The term X_{CMC} denotes the fraction of moles of SDDS at CMC in tensiometric profiles.

π_{CMC} is calculated from the following equation. It is the surface excess pressure measured at CMC.

$$\pi_{CMC} = \gamma_{iniial} - \gamma_{CMC} \quad (6)$$

The surfactants are recognized for surface activity properties. When surface active agents are added to aqueous medium, the surface tension value is reduced due to the adsorption of the surfactant molecules at the air-water interface. The surfactants are aggregated to form micelles beyond a threshold concentration. This particular concentration is known as the critical micelle concentration (CMC) **[86]**. The term γ_{CMC} is the numerical value of surface tension at the CMC. In this experiment, the values of γ_{CMC} are found considerably low. The values are 19.6, 20.3, 23.6 and 25 mN m^{-2} for SDDS at 0%, 5%, 10% and 15% TFE-water media respectively. Mandal at el. **[61]** has also found quite low values of γ_{CMC} in the

micellization of SDDS in IP/water media. The reported values are 17.4, 22.8, 25.8, 26.1, 28.3 and 30.9 mN m^{-2} at 0%, 2%, 5%, 7%, 10% and 15% IP-water media respectively. The γ_{CMC} values in each instance increase with solvent concentration, which is another similarity.

The value of Γ_{max} decreases with increasing percentage of TFE solvent, as a result A_{min} increases. The increase in A_{min} indicates the presence of surface active TFE solvent which enhances the minimum head group area of SDDS amphiphile at CMC. Maximum increase of A_{min} per SDDS molecule is observed in presence of 15% TFE (Table 2) where CMC is minimum (Table 1). The value of A_{min} increases with TFE percentage due to lesser tendency of SDDS molecules to populate at the air-water interface at higher TFE concentration. The value of β, i.e., the part of the counter-ions that are bound to micelle increases with volume % of TFE (except at 5% TFE, β slightly decreases). At higher TFE percentage, due to greater solubilization of TFE solvent at the micellar surface, the micellar surface charge density decreases. As a result, the value of β increases at higher TFE contents **[85]**. The negative change in both ΔG^0_{mic} and ΔG^0_{Ads} confirms about the spontaneity of SDDS micellization and interfacial adsorption in the presence of TFE solvent. The higher negative value of ΔG^0_{Ads} than ΔG^0_{mic} means greater spontaneity of interfacial adsorption than micellization process.

Table 1

Determination of the CMC of SDDS in Water and Different % TFE-Water Media from Tensiometry, Conductometry, Microcalorimetry, and Fluorimetric Methods at 298 K.

% ***TFE*** (v/v)	***CMC*** (mM)			
	Tensiometry	***Conductometry***	***Fluorimetry***	***ITC***
0	13.97	14.51	13.96	14.32
5	10.71	11.32	10.25	–
10	9.48	9.53	9.08	9.58
15	7.98	8.38	7.73	–

Table 2

Determination of Interfacial Parameters, and Thermodynamics of Micellization of SDDS in Water and Different % TFE-Water Media at 298 K.

% ***TFE*** (v/v)	γ_{CMC} $(mN\ m^{-2})$	$\Gamma_{max} \times 10^6$ (mol/m^{-2})	A_{min} $(nm^2$/molecule)	β	$-\Delta G^0_{mic}$ (kJ/mol)	$-\Delta G^0_{Ads}$ (kJ/mol)
0	19.6	1.79	0.92	0.21	24.85	53.73
5	20.3	1.64	1.01	0.20	25.44	38.42
10	23.6	1.44	1.15	0.29	27.74	33.92

15	25	0.52	3.19	0.36	29.82	31.12

3.2. Interaction of SDDS with HEC in TFE-Water Medium

Further, the solvent effect of TFE on the physicochemical interaction between SDDS and non-ionic HEC has been assessed. In this experiment, [HEC] is taken as 0.01 g%. The details of the results are provided below.

3.2.1. Tensiometry

In case of polymer-surfactant systems, tensiometric measurements are very much fruitful for the determination of both bulk and interfacial parameters. The tensiometric profiles for 0.01 g% HEC-SDDS interaction in both aqueous and TFE-water media have been illustrated in Fig. 2. The values of CMC for each of these have been calculated from surface tension (γ) vs log [SDDS] plot by visualizing the sharp break point. From this inflection point, SDDS molecules started micellization. Several combinations are feasible between polymers and surfactants in their interaction study, viz., non-ionic polymer/non-ionic surfactant **[87,88]**, non-ionic polymer/cationic or anionic surfactant **[89-92]**, and polymer and surfactant of opposite or similar charges **[93-95]**. The relative charge and hydrophobicity of the polymer-surfactant pairs have a significant impact on their interaction aspects. For oppositely charged polymer-surfactant systems, both electrostatic attraction and hydrophobic effect work in collaboration to strengthen their interactions **[96]**. In other cases, only hydrophobic effect operates. Joshi et al. **[97]** has made a comparative study of the strength of interaction of an anionic polymer (pectin) with different charged surfactants, and the sequence has been found as: cationic (CTAB, DTAB) > non-ionic (TX-100) > anionic (SDS). According to Chakraborty at el., **[98]** polymer-surfactant system of opposite charges is much more complicated to study than non-ionic polymer/ionic surfactant system in terms of physicochemical interaction. Following several investigations, the non-ionic polymers are found to have a much stronger interaction with anionic surfactants than cationic or non-ionic surfactants **[99]**. In aqueous non-ionic polymer medium, the hydrophobic interaction causes reduction in the CMC of SDDS micelles. In HEC-SDDS system, the association ability of SDDS monomers is enhanced owing to the hydrophobic interaction between the hydrophobic tails of SDDS and the lipophilic domain of non-ionic HEC **[100]**. As a result, the micellization of SDDS occurs at a lower [SDDS] and the CMC is decreased. Beyond CMC, the free SDDS micelles can coexist with the HEC-SDDS aggregates supported on HEC backbone. When surface active TFE **[101]** is added, the tensiometric plots become slightly different than that found in aqueous medium. In the presence of TFE, the surface tension values have been lowered (fig. 1A and 2), that corresponds to the water structure making ability of TFE solvent **[80]**. Here, with increasing TFE percentage in the medium, adsorption of TFE molecules also increases significantly at the water-air interface. This tends to diminution of surface tension at higher TFE concentration. A similar propensity is shown by other alcohols such as methanol, ethanol and propanol **[13]**. In case of 10% and 15% TFE, with stepwise addition of SDDS, the surface tension values first increase slightly, then decrease sharply until CMC is reached. However, in 2% and 5% TFE, the tensiometry plots look as in the aqueous medium. In this investigation, TFE further promotes micellization of SDDS at a lower surfactant concentration in presence of non-ionic polymer solution. Hence, CMC of HEC-SDDS system has been reduced with increasing TFE percentage in water. At

15% TFE, the CMC value of HEC-SDDS system in aqueous medium is reduced by about 25%. Previously, it has been mentioned (section 3.1.) that exceeding a certain alkanol percentage as a solvent in the medium, micellization of amphiphile becomes difficult **[84]**. In this study, it has been observed that above 15% TFE, micellization of SDDS becomes non-existent and the measured surface tension values are so scattered to find a definite break point needed for CMC detection.

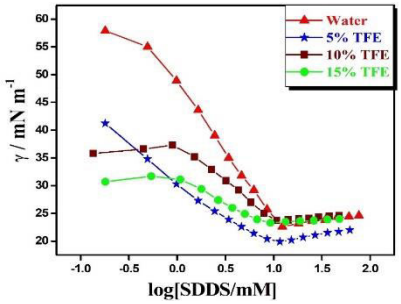

Fig. 2. Tensiometric profile for 0.01 g% HEC-SDDS interaction in water and different % TFE-water media at 298 K.

3.2.2. Conductometry

Conductometry is another significant conventional method which can be useful for the investigation of non-ionic polymer and anionic surfactant aggregation. This method is dependent on the transport capacity of charged species present in the bulk. The conductometric titration in this study is correlated to the linear change of specific conductance (κ) of the investigated system with the concentration of anionic surfactant. During stepwise addition of SDDS in the HEC solution, DDS^- ions progressively bind with HEC backbone hydrophobically that allows Na^+ counter ions to be free in the medium. As a result, conductivity steeply increases. Now, CMC of HEC-SDDS system is ascertained from the intersection point lying between two straight lines both in aqueous and aquo-TFE media (Fig. 3). Hence, in such conductometric plots, two regions before and after CMC with different slopes have been found, viz., pre-micellar and post-micellar regions. In the pre-micellar region, only SDDS monomers present in the bulk move freely and the specific conductance increases more rapidly with SDDS concentration. In the post-micellar region, SDDS monomers spontaneously aggregate to form micelles resulting in lesser rate of increase in ion conductivity. Hence, post-micellar part has comparatively smaller value of slope than pre-micellar one. The term counter-ion binding (β) **[102, 103]** measures the strength of micelle ionization following eq 5 (Table 4). When binding with non-ionic HEC in aqueous environment, less SDDS monomers are needed for micellization, i.e., CMC is decreased. Therefore, the presence of polymer reduces CMC similar to tensiometric results. In this case, above 15% TFE, the conductometric plots are going up steeply showing no change in the slope and detection of CMC becomes not possible (no break point is observed).

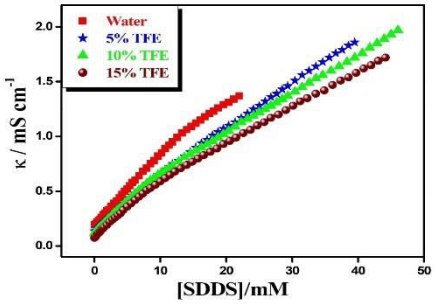

Fig. 3. Conductometric plots for 0.01 g% HEC-SDDS interaction in water and different % TFE-water media at 298 K.

Table 3

Determination of Interfacial Parameters, and Thermodynamics of Micellization of HEC-SDDS Interaction in Water and Different % TFE-Water Media at 298 K.

% TFE (v/v)	γ_{CMC} $(mN\,m^{-1})$	$\Gamma_{max} \times 10^6 (mol/m^{-2})$	A_{min} $(nm^2/molecule)$	β	$-\Delta G^0_{mic}$ (kJ/mol)	$-\Delta G^0_{Ads}$ (kJ/mol)
0	22.6	1.89	0.87	0.40	29.19	48.66
5	19.9	0.47	3.53	0.23	25.83	72.21
10	23.7	1.22	1.36	0.34	28.39	36.91
15	23.3	0.41	4.05	0.38	29.75	44.38

3.2.3. Isothermal Titration Calorimetry.

Isothermal titration calorimetry (ITC) provides basic thermodynamics of micellar aggregation of amphiphile. This method is highly sensitive to heat changes during micellization of the amphiphile alone or in presence of polymer. The gradual binding of SDDS with HEC corresponds to different rates of enthalpy change in the enthalpograms. Both the values of CMC and net heat change of micellization measurements are possible from the resulting ITC plots. Interaction of SDDS with HEC are studied in aqueous and 10% TFE medium and the plots are showed in Fig. 4(A-D). The determined CMC values are displayed in Table 4. In each case, the plots are found to be sigmoidal **[104]** and the CMCs are calculated from the inflection point in the intermediate zone of the respective enthalpograms **[105,106]** using Boltzmann-sigmoidal fitting **[107]**. The calorimetric profile can be assumed to have three separate zones: (i) premicellar zone, where the concentrated surfactant solution is diluted, (ii) intermediate zone, where a sudden change in the enthalpy value (either a drop or an increase) is seen as a result of a portion of micelles dissolving into free monomers, (iii) post micellar zone, where the micelles are diluted. The initial enthalpy of dilution $\Delta H^0_{dil}(initial)$ is found at the point where the vertical line across the CMC intersects the premicellar line, and the final enthalpy of dilution $\Delta H^0_{dil}(final)$ is determined at the point where this vertical line intersects the post micellar line. The net enthalpy change during the micellization ΔH^0_{obs} is obtained from the difference between $\Delta H^0_{dil}(final)$ and $\Delta H^0_{dil}(initial)$

values **[108]**. The calculated values of both CMC and are shown in Fig. 1(C)(i), 1(D)(i), 4(A) and 4(C) for the relevant systems. In aqueous medium, in the micellization of SDDS alone and its binding with HEC are found endothermic, i.e., net positive enthalpy change. In 10% TFE, both SDDS micellization and HEC-SDDS binding becomes exothermic. The micellization of SDDS in IP/water media has been observed to follow a similar trend **[61]**. The resulting CMC values from microcalorimetry are compatible with the tensiometric and conductometric data.

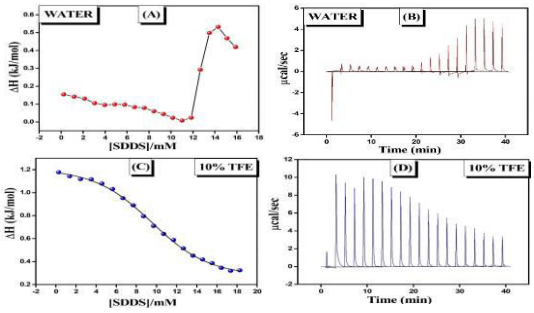

Fig. 4. ITC plots of 0.01 g% HEC-SDDS interaction in (A) water, (C) 10% TFE at 298 K. (B) and (D) represent corresponding enthalpograms.

3.2.4. Fluorescence Study

The solvent effect of TFE on the micellization behaviour of SDDS in absence and presence of non-ionic HEC has been described by steady-state fluorescence measurement. The value of CMC of anionic surfactant has been determined by varying TFE percentage without and with 0.01 g% HEC by this method. The values of CMC obtained from fluorescence intensity measurements are found close to those obtained from tensiometric and conductometric results. The difference in sensitivity of the experimental techniques used can be a justification for the slight difference in measured CMC values. To succeed this procedure, it is essential to select an efficient fluorescent probe to obtain invaluable information about the polarity change of the experimental system as a consequence of surfactant addition. Pyrene, already well established in literatures as a spectroscopic probe **[109, 110]**, is employed in our study to detect the micellization of SDDS alone as well as its aggregation behaviour with HEC in TFE solvent. In spite of its low water solubility, the pyrene molecules can introduce adequate fluorescence signal to identify the medium polarity. The fluorescence spectrum of pyrene can emit with five vibrational peaks **[111]**. Among these five emission bands, the relative intensity ratio (I_1/I_3) or 'micropolarity index' **[112]** (where, I_1 and I_3 are the fluorescence intensities of pyrene emission spectra), an important parameter providing details of the change in microstructural properties during the assembly of micelles, has been used for qualitative measurement of micropolarity experienced by the probe molecules surrounding it. During the experiment, hydrophobic pyrene molecules bind themselves to the hydrophobic region of gradually added surfactant molecules. Thus, the surfactant concentration has an extensive effect on the polarity of the system as well as on the intensity ratio(I_1/I_3). The micropolarity index(I_1/I_3) having values greater and less than unity accounts for the polar and non-polar environments respectively surrounding pyrene molecules **[113]**. The medium becomes more non-polar as TFE concentration is increased, and as a result, pyrene molecules perceive more non-polar environments, as evidenced by the decline in the CMC value. The early plateau region in the plot at very low [SDDS] is an indication of nearly constant value

of(I_1/I_3) and non-micellization of SDDS molecules on HEC chains. Thereafter, the abrupt decrease in micropolarity is a consequence of the feasibility in the micellization process at intermediate [SDDS]. The saturation of SDDS micelles on HEC chain gives rise to further constant nature of micropolarity at higher amphiphile concentration. The values of CMC of the experimental systems have been detected from(I_1/I_3) vs [SDDS] plots. The resultant plots have been fitted as sigmoidal to quantify the single prominent break point.

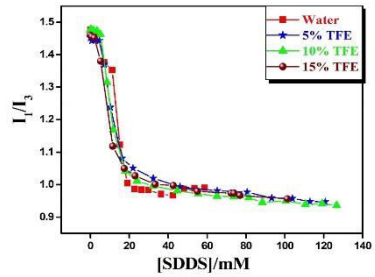

Fig. 5. Fluorimetric profile for 0.01 g% HEC-SDDS interaction in water and different % TFE-water media at 298 K.

Table 4

Interaction Characteristic of HEC-SDDS Interaction in Water and Different % TFE-Water Media from Tensiometry, Conductometry, Microcalorimetry, and Fluorimetric Methods at 298 K.

% TFE	***CMC* (*mM*)**			
(v/v)	***Tensiometry***	***Conductometry***	***Fluorimetry***	***ITC***
0	12.29	13.07	13.31	12.61
5	11.56	11.94	11.23	–
10	10.75	10.82	10.62	9.50
15	9.23	10.31	8.56	–

3.2.5. Aggregation Number (n_{Agg}).

Comparative study of mean aggregation number (n_{Agg}) determination of amphiphile is a useful method which gives an idea about the size of the micelle **[114]** formed. In this work, the effect of TFE solvent has been performed on the aggregation number of pure SDDS and HEC-SDDS systems. Here, static fluorescence quenching technique has been applied. The quenching of tryptophan (an efficient fluorescence probe) has been measured with the help of CPC, used as a quencher, throughout the experiment **[115]**. The following eq. 7 has been utilised to calculate the aggregation number (n_{Agg}) **[116]**.

$$\ln\left(\frac{I_0}{I_1}\right) = \frac{n_{Agg}\,[CPC]}{[SDDS]-CMC} \quad (7)$$

where, I_0 and I_1 are the measured fluorescence intensities of tryptophan probe in the absence and presence of CPC quencher respectively. [SDDS] is taken as much higher than the corresponding CMC values in each experiment. [CPC] is the concentration of the quencher (3 mM). In this titrimetric method, the slope has been evaluated by linear fitting of ln $(\frac{I_0}{I_1})$ vs [CPC] plot to quantify the aggregation number. The aggregation number of SDDS has been found 52 in water medium **[55]**. The added TFE causes a reduction in the polarity of the medium. In aquo-TFE media, the value of n_{Agg} has been lowered and decreases with increasing percentage of TFE. The calculated values of n_{Agg} are found as 47, 44 and 37 in 5%, 10% and 15% TFE in water respectively. At 15% TFE, the n_{Agg} value of SDDS found in the aqueous medium is reduced by about 29%. The decreasing order of aggregation number of amphiphile by non- aqueous alcoholic solvent in water has been affirmed by many authors **[80, 81]** previously. In the presence of TFE, lowering of n_{Agg} of SDDS is caused by the cosurfactant nature of TFE in the medium. Further, in the presence of non-ionic polymer HEC, hydrophobicity of the system is increased. Hence, n_{Agg} of HEC-bound SDDS micelle is lower than pure SDDS. The values of n_{Agg} of 0.01 g% HEC-SDDS system are 51, 46, 31 and 19 in 0%, 5%, 10% and 15% TFE respectively. At 15% TFE, the n_{Agg} value of HEC-SDDS system in the aqueous medium has been reduced by about 63%. According to literature **[117]**, the aggregation number of anionic surfactant has been reduced during binding with non-ionic polymer.

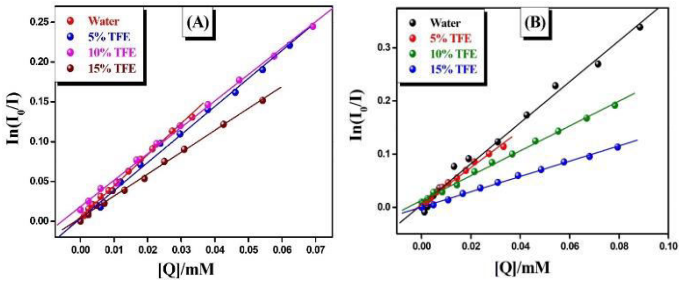

Fig. 6. Plot of In(I_0/I) vs [Q] for (A) SDDS, (B) 0.01 g% HEC-SDDS interaction in water and different % TFE-water media at 298 K.

3.2.6. Dynamic Light Scattering

DLS is the most effective technique for the analysis of particle size (in solution state) in the nanometer (nm) range. DLS measurements of HEC (0.01 g %) in aqueous solution as well as in TFE-water solvent media have been performed. Both hydrodynamic diameter (D_h) and polydispersity index (PDI) are studied. The calculated values of both D_h and PDI are presented in Table 6. In case of water and 5% TFE media, two hydrodynamic diameters (D_h^I, D_h^{II}) are observed. But three discrete diameters (D_h^I, D_h^{II} andD_h^{III}) are found in 10% and 15% TFE solutions. In general, the DLS distribution of polymers shows one or two peaks **[118]**. Here, the D_h values depend on TFE percentage. For each distribution, first one is assumed to be in monomeric state and the others are in aggregated states. The aggregated form is definitely larger than the monomeric form ($D_h^{III} > D_h^{II} > D_h^I$). The PDI values follow an

irregular trend with TFE composition. Each measurement shows that PDI values are much larger than 0.30. Hence, the distributions are multidisperse.

Table 5

Hydrodynamic Diameter (D_h) and Polydispersity Index (PDI) for 0.01 g% HEC in Water and Different % TFE-Water Media at 298 K.

% ***TFE*** **(v/v)**	D_h/nm	***PDI***
0	32.6, 190.1	0.621
5	58.7, 396.1	0.722
10	7.5, 50.7, 255	0.544
15	28.2, 105.7, 615.1	0.666

3.2.7. FESEM Imaging

Surface morphology images of 0.01 g% HEC without and with SDDS are taken by FESEM technique. The images are depicted in Fig. 7(A-D). The experimental sample solutions are prepared in water and 10% TFE-water. To observe the morphological change of HEC in the presence of SDDS, concentration of SDDS has been taken much higher than CMC. In water, HEC forms fern-tree like clusters **[119]** with wide branching (Fig. 7A). In 10% TFE, HEC shows relatively smaller cluster with somewhat elongated branching (Fig. 7B), but the main structure remains same. In the presence of SDDS, the fern-like pattern of HEC has been destroyed and SDDS micelles are aggregated on the surface of HEC polymer (Fig. 7C). The morphology looks like flower like cluster. On the other hand, in 10% TFE, on further addition of SDDS, HEC polymer cluster turns into leafy canopy like morphology (Fig. 7D).

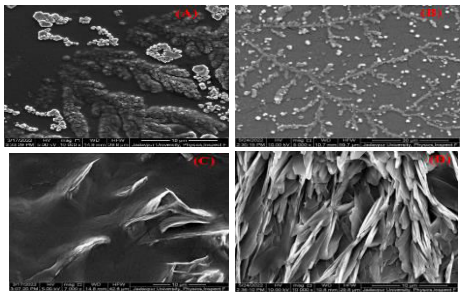

Fig. 7. FESEM images of pure 0.01 g% HEC in (A) water, (B) 10% TFE, (C) 0.01 g% HEC-SDDS in water, and (D) 10% TFE at [SDDS] > CMC.

4. Conclusion

Reports on polymer-surfactant interactions are noteworthy and therefore valuable research materials with potential applications in the aforementioned areas of modern science. Thus, a research strategy in this discipline needs an overview of previous and related investigations

as well as an amplification of the observed findings. In order to develop distinct analogy, it is important to choose newer systems, and investigate their interactions using a variety of measurement approaches. In this manuscript, an effort has been made to coordinate between polymer and surfactant in presence of an alcoholic solvent. The quaternary combination discussed here belongs to a completely new category in this field, where the solvency effect of aquo-alcohol mixture on the polymer-surfactant system has been reported. The complexity of studying such quaternary systems deserves greater emphasis. It has become more intriguing in the presence of TFE because of its unique solvent properties as compared to other ordinary alcohols, as well as the fact that it has never been studied as an additive in the polymer-surfactant aggregation process. Furthermore, the effect of TFE on the self-aggregation of surfactants has gained scant attention in the literature. The non-ionic cellulose derivatives are most often used in the hydrophobically modified form in terms of interaction with anionic surfactant, while using it in the form of pure HEC is rather uncommon. Similarly, the amino acid-based green surfactant SDDS has also received limited attention relevant to such studies. In most instances, Sodium dodecyl sulfate (SDS) as the anionic surfactant has conventionally been interacted with a non-ionic polymer. This article has comprehensively discussed the aggregation of SDDS with HEC in water and TFE-water media through a comparative study. It has been attempted to interpret the interaction features using some assumptions. Further investigation in this field employing a variety of experimental approaches would be beneficial. A step-by-step presentation of the summary of this manuscript has been made:

(1) Typical hydrophobic interactions have been established between non-ionic HEC and anionic SDDS. The 'cosurfactant' nature of TFE solvent further reinforces the hydrophobicity in the medium to reduce the CMC, observed experimentally using tensiometry, conductometry, fluorimetry and ITC techniques. The decrease in micellar charge density of the polar head groups can be used to explain the phenomenon of lowering CMC in the presence of TFE. At 15% TFE, the CMC value of pure SDDS has been reduced by about 43%, but when SDDS is bound with HEC, it is reduced by about 25% (tensiometry).

(2) Endothermic heat change during micellization of SDDS has been switched to exothermic nature both in the absence and presence of HEC in 10% TFE solvent.

(3) TFE causes a decline in micellar aggregation number (n_{Agg}) as a consequence of decreasing polarity in the medium. At 15% TFE, this decrease is about 29% for pure SDDS; but for HEC-SDDS system, it is decreased by about 63%.

(4) The change in HEC polymer configuration in TFE solvent has been justified in dynamic light scattering (DLS) method.

(5) The spontaneity of SDDS micellization has been affirmed by negative ΔG^0_{mic} values in each measurement.

(6) Finally, the changes in surface morphologies of pure HEC and HEC-SDDS binding have been recognized in 10% TFE from FESEM images.

The literature survey finds that the structures of proteins and peptides are much more complex to study. Analogous to biological aggregates, surfactant-induced micelles feature a hydrophilic part that remains exposed while the hydrophobic part stays away from the

aqueous environment. Keeping in mind the importance of TFE in the conformational analysis of proteins and peptides, the present work is relevant, and thus it merits attention.

References

[1] Chavanpatil MD, Khdair A, Patil Y, Handa H, Mao G Panyam J. Polymer-surfactant nanoparticles for sustained release of water-soluble drugs. Journal of pharmaceutical sciences 2007; 96(12):79-3389.

[2] Decato S, Bemis T, Madsen E, Mecozzi S. Synthesis and characterization of perfluoro-tert-butyl semifluorinated amphiphilic polymers and their potential application in hydrophobic drug delivery. Polymer chemistry 2014;5(22):6461-71.

[3] Torchilin VP. Structure and design of polymeric surfactant-based drug delivery systems. Journal of controlled release 2001;73(2-3):137-72.

[4] Somasundaran P, Chakraborty S, Qiang Q, Deo P, Wang J, Zhang R. Surfactants, polymers and their nanoparticles for personal care applications. Journal of cosmetic science 2004; 55:S1.

[5] Villetti MA, Bica CI, Garcia IT, Pereira FV, Ziembowicz FI, Kloster CL, Giacomelli C. Physicochemical properties of methylcellulose and dodecyltrimethylammonium bromide in aqueous medium. The Journal of Physical Chemistry B 2011;115(19):5868-76.

[6] Raffa P, Wever DA, Picchioni F , Broekhuis AA. Polymeric surfactants: synthesis, properties, and links to applications. Chemical reviews 2015;115(16):8504-63.

[7] Moulik S P, Ghosh S. Surface chemical and micellization behaviours of binary and ternary mixtures of amphiphiles (Triton X-100, Tween-80 and CTAB) in aqueous medium. Journal of Molecular Liquids 1997;72:145-61.

[8] Šarac B, Bešter-Rogač M. Temperature and salt-induced micellization of dodecyltrimethylammonium chloride in aqueous solution: A thermodynamic study. Journal of colloid and interface science 2009;338(1):216-21.

[9] Ren ZH. Mechanism of the salt effect on micellization of an aminosulfonate amphoteric surfactant. Industrial & Engineering Chemistry Research 2015; 54(40):9683-8.

[10] Saha A, Mal A , Ghosh S. An elaborate investigation on the transition of rod-like micelle of cetyltrimethylammonium p-toluenesulfonate in presence of different additives. Journal of Molecular Liquids 2020; 309:113084.

[11] Dey A, Patra N, Mal A, Ghosh S. Impact of organic polar solvents (DMSO and DMF) on the micellization and related behavior of an anionic (AOT), cationic (CEM2AB) and cationic gemini surfactant (16-5-16). Journal of Molecular Liquids 2017; 244:85-96.

[12] Aslanzadeh S, Yousefi A. The effect of ethanol on nanostructures of mixed cationic and anionic surfactants. Journal of Surfactants and Detergents. 2014;17:709-16.

[13] Zdziennicka A. Surface behavior of Triton X-165 and short chain alcohol mixtures. Langmuir. 2010;26(3):1860-9.

[14] Pan A, Naskar B, Prameela GK, Kumar BP, Mandal AB, Bhattacharya SC, Moulik SP. Amphiphile behavior in mixed solvent media I: self-aggregation and ion association of sodium dodecylsulfate in 1, 4-dioxane–water and methanol–water media. Langmuir. 2012;28(39):13830-43.

[15] Dubey N. Micellar properties and related thermodynamic parameters of aqueous anionic surfactants in the presence of monohydric alcohols. Journal of Chemical & Engineering Data. 2011;56(8):3291-300.

[16] Rodríguez A, Graciani MD, Moyá ML. Effects of addition of polar organic solvents on micellization. Langmuir. 2008;24(22):12785-92.

[17] Dan A, Chakraborty I, Ghosh S, Moulik SP. Interfacial and bulk behavior of sodium dodecyl sulfate in isopropanol− water and in isopropanol− poly (vinylpyrrolidone)− water media. Langmuir. 2007;23(14):7531-8.

[18] Totland C, Blokhus AM. Swollen micelles and alcohol–surfactant co-adsorption: structures and mechanisms from liquid-and solid-state 1 H–1 H NMR spectroscopy. Physical Chemistry Chemical Physics. 2017;19(11):7708-13.

[19] Fatima U, Riyazuddeen, Dhakal P, Shah JK. Comparative study of influence of ethanol and 2, 2, 2-trifluoroethanol on thermophysical properties of 1-ethyl-3-methylimidazolium dicyanamide in binary mixtures: experimental and MD simulations. Journal of Chemical & Engineering Data. 2020;66(1):101-15.

[20] Patidar P, Bahadur A. Modulating effect of different biomolecules and other additives on cloud point and aggregation of amphiphilic linear and starblock copolymer. Journal of Molecular Liquids. 2018;249:219-26.

[21] Handa M, Ujjwal RR, Vasdev N, Flora SJ, Shukla R. Optimization of surfactant-and cosurfactant-aided pine oil nanoemulsions by isothermal low-energy methods for anticholinesterase activity. ACS omega 2020;6(1):559-68.

[22] Santhanalakshmi J, Parameswari A. Studies on the effect of cosurfactant on the phase behaviour of water in oil (CCl_4/water/Triton X – 100/n-alkanol) microemulsions. Journal of Surface Science and Technology 1997;13(2-4):113-29.

[23] Jiang H, Beaucage G, Vogtt K, Weaver M. The effect of solvent polarity on wormlike micelles using dipropylene glycol (DPG) as a cosolvent in an anionic/zwitterionic mixed surfactant system. Journal of colloid and interface science 2018; 509:25-31.

[24] Shah SK, Chatterjee SK, Bhattarai A. Micellization of cationic surfactants in alcohol—water mixed solvent media. Journal of Molecular Liquids. 2016;222:906-14.

[25] Sidim T, Acar G. Alcohols effect on critic micelle concentration of polysorbate 20 and cetyl trimethyl ammonium bromine mixed solutions. Journal of surfactants and detergents. 2013;16:601-7.

[26] Parekh P, Singh K, Marangoni DG, Bahadur P. Effect of alcohols on aqueous micellar solutions of PEO–PPO–PEO copolymers: a dynamic light scattering and ^{1}H NMR study. Journal of Molecular Liquids 2012;165:49-54.

[27] MacLennan S, Marangoni DG. Thermodynamics of glyme-sodium dodecyl sulfate (SDS) mixed micelle formation via isoperibol solution calorimetry: Temperature, and concentration effects. Journal of the Indian Chemical Society 2023;100(5):100980-90.

[28] Gradzielski M. Polymer-Surfactant Interaction for Controlling the Rheological Properties of Aqueous Surfactant Solutions. Current Opinion in Colloid & Interface Science. 2022:101662.

[29] Bureiko A, Trybala A, Kovalchuk N, Starov V. Current applications of foams formed from mixed surfactant–polymer solutions. Advances in colloid and interface science. 2015;222:670-7.

[30] Del Giudice F, Tassieri M, Oelschlaeger C, Shen AQ. When microrheology, bulk rheology, and microfluidics meet: Broadband rheology of hydroxyethyl cellulose water solutions. Macromolecules 2017;50(7):2951-63.

[31] Jiang T, Duan Q, Zhu J, Liu H, Yu L. Starch-based biodegradable materials: Challenges and opportunities. Advanced Industrial and Engineering Polymer Research. 2020;3(1):8-18.

[32] Dabholkar N, Gorantla S, Waghule T, Rapalli VK, Kothuru A, Goel S, Singhvi G. Biodegradable microneedles fabricated with carbohydrates and proteins: Revolutionary approach for transdermal drug delivery. International Journal of Biological Macromolecules. 2021;170:602-21.

[33] Liu K, Jiang X, Hunziker P. Carbohydrate-based amphiphilic nano delivery systems for cancer therapy. Nanoscale. 2016;8(36):16091-156.

[34] Noreen A, Zia KM, Tabasum S, Khalid S, Shareef R. A review on grafting of hydroxyethylcellulose for versatile applications. International journal of biological macromolecules 2020;150:289-303.

[35] Oprea M, Voicu SI. Recent advances in composites based on cellulose derivatives for biomedical applications. Carbohydrate polymers 2020;247:116683.

[36] Lo JT, Yen HT, Tsai CC, Chen BH, Hou SS. Interaction between hydrophobically modified 2-hydroxyethyl cellulose and sodium dodecyl sulfate studied by viscometry and two-dimensional NOE NMR spectroscopy. The Journal of Physical Chemistry B 2014; 118(24):6922-30.

[37] Kästner U, Hoffmann H, Dönges R, Ehrler R. Interactions between modified hydroxyethyl cellulose (HEC) and surfactants. Colloids and Surfaces A: Physicochemical and Engineering Aspects 1996;112(2-3):209-25.

[38] Mondal S, Pyne P, Patra A, Mitra RK, Ghosh S. Effect of surfactant tail length on the hydroxypropyl cellulose-mediated premicellar aggregation of sodium n-alkyl sulfate surfactants. Langmuir. 2021;37(20):6168-77.

[39] Peng B, Yao Z, Wang X, Crombeen M, Sweeney DG, Tam KC. Cellulose-based materials in wastewater treatment of petroleum industry. Green Energy & Environment 2020;5(1):37-49.

[40] Akter M, Bhattacharjee M, Dhar AK, Rahman FB, Haque S, Rashid TU, Kabir SF. Cellulose-based hydrogels for wastewater treatment: A concise review. Gels 2021;7(1): 30.

[41] Gwebu SS, Chiririwa H. The effect of hydroxyl ethyl cellulose (HEC) and hydrophobically–modified alkali soluble emulsions (HASE) on the properties and quality of water based paints. Int J App Chem 2017;13:1-3.

[42] Maestro A, González C, Gutiérrez JM. Interaction of surfactants with thickeners used in waterborne paints: A rheological study. Journal of colloid and interface science 2005; 288(2):597-605.

[43] Mahmoud KH. Optical properties of hydroxyethyl cellulose film treated with nitrogen plasma. Spectrochimica Acta Part A: Molecular and Biomolecular Spectroscopy. 2016;157:153-7.

[44] Angadi SC, Manjeshwar LS, Aminabhavi TM. Interpenetrating polymer network blend microspheres of chitosan and hydroxyethyl cellulose for controlled release of isoniazid. International journal of biological macromolecules. 2010;47(2):171-9.

[45] Choudhury PR, Majumdar S, Sahoo GC, Saha S, Mondal P. High pressure ultrafiltration CuO/hydroxyethyl cellulose composite ceramic membrane for separation of Cr (VI) and Pb (II) from contaminated water. Chemical Engineering Journal 2018;336:570-8.

[46] Brito RO, Silva SG, Fernandes RM, Marques EF, Enrique-Borges J, do Vale ML. Enhanced interfacial properties of novel amino acid-derived surfactants: Effects of headgroup chemistry and of alkyl chain length and unsaturation. Colloids and Surfaces B: Biointerfaces 2011;86(1):65-70.

[47] Pinazo A, Pons R, Pérez L, Infante MR. Amino acids as raw material for biocompatible surfactants. Industrial & Engineering Chemistry Research 2011;50(9):4805-17.

[48] Bourkaib MC, Delaunay S, Framboisier X, Hôtel L, Aigle B, Humeau C, Guiavarc'h Y, Chevalot I. N-acylation of L-amino acids in aqueous media: Evaluation of the catalytic performances of Streptomyces ambofaciens aminoacylases. Enzyme and Microbial Technology 2020; 137:109536.

[49] Pinazo A, Manresa MA, Marques AM, Bustelo M, Espuny MJ and Pérez L, Amino acid–based surfactants: New antimicrobial agents. Advances in colloid and interface science 2016;228:17-39.

[50] Lee CM, Kim SY, Yoon SH, Kim JB, Yeo YS, Sim JS, Hahn BS, Kim DG. Characterization of a novel antibacterial N-acyl amino acid synthase from soil metagenome. Journal of biotechnology 2019;294:19-25.

[51] Rajstein J, Fuks M, Markitziu A, Gedalia I. Solubility of enamel powder following treatment with a sodium-n-lauroyl sarcosinate containing toothpaste in the presence and absence of fluoride. Journal of Oral Rehabilitation 1983;10(6):469-71.

[52] Ananthapadmanabhan KP. Amino-acid surfactants in personal cleansing. Tenside Surfactants Detergents 2019;56(5):378-86.

[53] Ray GB, Ghosh S, Moulik SP. Physicochemical studies on the interfacial and bulk behaviors of sodium N-dodecanoyl sarcosinate (SDDS). Journal of Surfactants and Detergents 2009; 12(2):131-43.

[54] Patra N, Ray D, Aswal VK, Ghosh S. Exploring physicochemical interactions of different salts with sodium N-dodecanoyl sarcosinate in aqueous solution. ACS omega 2018;3(8):9256-66.

[55] Das S, Mondal S, Ghosh S. Physicochemical studies on the micellization of cationic, anionic, and nonionic surfactants in water–polar organic solvent mixtures. Journal of Chemical & Engineering Data 2013;58(9):2586-95.

[56] Dan A, Ghosh S, Moulik SP. Interaction of cationic hydroxyethylcellulose (JR400) and cationic hydrophobically modified hydroxyethylcellulose (LM200) with the amino-acid based anionic amphiphile Sodium N-Dodecanoyl Sarcosinate (SDDS) in aqueous medium. Carbohydrate polymers 2010;80(1):44-52.

[57] Naskar B, Ghosh S, Moulik SP. Interaction of normal and reverse pluronics (L44 and 10R5) and their mixtures with anionic surfactant sodium N-dodecanoylsarcosinate. Journal of colloid and interface science 2014;414:82-9.

[58] Alsenaidy MA. Biophysical evaluation of amyloid fibril formation in bovine cytochrome c by sodium lauroyl sarcosinate (sarkosyl) in acidic conditions. Journal of Molecular Liquids 2017;241:722-9.

[59] Mondal S, Raposo ML, Ghosh A, Prieto G, Ghosh S. Physicochemical and conformational studies on interaction of myoglobin with an amino-acid based anionic surfactant, sodium N-dodecanoyl sarcosinate (SDDS). Colloids and Surfaces A Physicochemical and Engineering Aspects 2019;577:167-74.

[60] Azum N, Rub MA, Khan A, Alotaibi MM, Asiri AM. Synergistic Interaction and Binding Efficiency of Tetracaine Hydrochloride (Anesthetic Drug) with Anionic Surfactants in the Presence of NaCl Solution Using Surface Tension and UV–Visible Spectroscopic Methods. Gels 2022;8(4):234.

[61] Mandal B, Ghosh S, Moulik SP. Interaction between a bio-tolerable amino-acid based amphiphile (N-dodecanoylsarcosinate, SDDS) and modified cationic polymers, hydroxyethylcelluloses (JR 400, and LM 200) in isopropanol-water medium. Colloids and Surfaces A Physicochemical and Engineering Aspects 2019;566:156-65.

[62] Mukherjee S, Dan A, Bhattacharya SC, Panda AK, Moulik SP. Physicochemistry of interaction between the cationic polymer poly (diallyldimethylammonium chloride) and the anionic surfactants sodium dodecyl sulfate, sodium dodecylbenzenesulfonate, and sodium N-dodecanoylsarcosinate in water and isopropyl alcohol− water media. Langmuir. 2011;27(9):5222-33.

[63] Berkessel A, Adrio JA, Hüttenhain D, Neudörfl JM. Unveiling the “booster effect” of fluorinated alcohol solvents: aggregation-induced conformational changes and cooperatively enhanced H-bonding. Journal of the American Chemical Society 2006;128(26):8421-6.

[64] Khaksar S. Fluorinated alcohols: A magic medium for the synthesis of heterocyclic compounds. Journal of Fluorine Chemistry 2015;172:51-61.

[65] Hong DP, Hoshino M, Kuboi R, Goto Y. Clustering of fluorine-substituted alcohols as a factor responsible for their marked effects on proteins and peptides. Journal of the American Chemical Society 1999;121(37):8427-33.

[66] Chitra R, Smith PE. Properties of 2, 2, 2-trifluoroethanol and water mixtures. The Journal of Chemical Physics 2001;114(1):426-35.

[67] Chaubey B, Dey A, Banerjee A, Chandrakumar N, Pal S. Assessment of the Role of 2, 2, 2-Trifluoroethanol Solvent Dynamics in Inducing Conformational Transitions in Melittin: An Approach with Solvent 19F Low-Field NMR Relaxation and Overhauser Dynamic Nuclear Polarization Studies. The Journal of Physical Chemistry B 2020;124(28):5993-6003.

[68] Mohanta D, Jana M. Can 2, 2, 2-trifluoroethanol be an efficient protein denaturant than methanol and ethanol under thermal stress?. Physical Chemistry Chemical Physics 2018; 20(15):9886-96.

[69] Anderson VL, Webb WW. A desolvation model for trifluoroethanol-induced aggregation of enhanced green fluorescent protein. Biophysical journal 2012;102(4):897-906.

[70] Yu C, Sanjosé-Orduna J, Patureau FW, Pérez-Temprano MH. Emerging unconventional organic solvents for C–H bond and related functionalization reactions. Chemical Society Reviews. 2020;49(6):1643-52.

[71] Gimenez D, Dose A, Robson NL, Sandford G, Cobb SL, Coxon CR. 2, 2, 2-Trifluoroethanol as a solvent to control nucleophilic peptide arylation. Organic & Biomolecular Chemistry 2017;15(19):4081-5.

[72] Lu S, Chen W, Shen Q. Friedel-Crafts trifluoromethylthiolation of electron-rich (hetero) arenes with trifluoromethylthio-saccharin in 2, 2, 2-trifluoroethanol (TFE). Chinese Chemical Letters 2019;30(12):2279-81.

[73] Abe H, Amii H, Uneyama K. Pd-catalyzed asymmetric hydrogenation of α-fluorinated iminoesters in fluorinated alcohol: a new and catalytic enantioselective synthesis of fluoro α-amino acid derivatives. Organic letters 2001;3(3):313-5.

[74] Siegemund G, Schwertfeger W, Feiring A, Smart B, Behr F, Vogel H, McKusick B, Kirsch P. Fluorine compounds, organic. Ullmann's encyclopedia of industrial chemistry 2016; 11:361.

[75] Begue JP, Bonnet-Delpon D, Crousse B. Fluorinated alcohols: A new medium for selective and clean reaction. Synlett 2004;2004(01):18-29.

[76] Shuklov IA, Dubrovina NV, Boerner A. Fluorinated alcohols as solvents, cosolvents and additives in homogeneous catalysis. Synthesis 2007;2007(19):2925-43.

[77] Matsugami M, Yamamoto R, Kumai T, Tanaka M, Umecky T, Takamuku T. Hydrogen bonding in ethanol–water and trifluoroethanol–water mixtures studied by NMR and molecular dynamics simulation. Journal of Molecular Liquids 2016;217:3-11.

[78] Mondal S, Biswas B, Nandy T, Singh PC. Understanding the role of hydrophobic terminal in the hydrogen bond network of the aqueous mixture of 2, 2, 2-

trifluoroethanol: IR, molecular dynamics, quantum chemical as well as atoms in molecules studies. The Journal of Physical Chemistry B 2018;122(25):6616-26.

[79] Islam MR, Warsi F, Khan AB, Kausar T, Khan I, Ali M. Solvatochromism of binary mixtures of 2, 2, 2-trifluoroethanol+ ionic liquid [bmim][Tf2N]: a comparative study with molecular solvents. Journal of Chemical & Engineering Data 2019;64(3):1140-54.

[80] Civera C, Arias C, Elorza MA, Elorza B, García-Blanco F, Galera-Gómez PA. Hydrophobicity enhancement in micelles of Triton X-165 by the presence of the cosolvent 2, 2, 2 trifluoroethanol (TFE). Journal of Molecular Liquids 2014;199:29-34.

[81] García-Blanco F, Elorza MA, Arias C, Elorza B, Gómez-Escalonilla I, Civera C, Galera-Gómez PA. Interactions of 2, 2, 2-trifluoroethanol with aqueous micelles of Triton X-100. Journal of colloid and interface science 2009;330(1):163-9.

[82] Burakowski A, Gliński J, Czarnik-Matusewicz B, Kwoka P, Baranowski A, Jerie K, Pfeiffer H, Chatziathanasiou N. Peculiarity of aqueous solutions of 2, 2, 2-trifluoroethanol. The Journal of Physical Chemistry B 2012;116(1):705-10.

[83] Rao IV, Ruckenstein E. Micellization behavior in the presence of alcohols. Journal of colloid and interface science. 1986;113(2):375-87.

[84] Naskar B, Ghosh S, Nagadome S, Sugihara G, Moulik SP. Behavior of the amphiphile CHAPS alone and in combination with the biopolymer inulin in water and isopropanol–water media. Langmuir 2011;27(15):9148-59.

[85] Das S, Naskar B, Ghosh S. Influence of temperature and organic solvents (isopropanol and 1, 4-dioxane) on the micellization of cationic gemini surfactant (14-4-14). Soft Matter. 2014;10(16):2863-75.

[86] Perinelli DR, Cespi M, Lorusso N, Palmieri GF, Bonacucina G, Blasi P. Surfactant self-assembling and critical micelle concentration: one approach fits all?. Langmuir. 2020;36(21):5745-53.

[87] Fijan R, Šostar-Turk S, Lapasin R. Rheological study of interactions between non-ionic surfactants and polysaccharide thickeners used in textile printing. Carbohydrate Polymers. 2007;68(4):708-17.

[88] Ortona O, D'Errico G, Paduano L, Vitagliano V. Interaction between cationic, anionic, and non-ionic surfactants with ABA block copolymer Pluronic PE6200 and with BAB reverse block copolymer Pluronic 25R4. Journal of colloid and interface science. 2006;301(1):63-77.

[89] Dan A, Ghosh S, Moulik SP. Physicochemistry of the interaction between inulin and alkyltrimethylammonium bromides in aqueous medium and the formed coacervates. The Journal of Physical Chemistry B. 2009;113(25):8505-13.

[90] Patra N, Mal A, Das S, Ghosh S. Detailed physicochemical interaction of inulin with some conventional surfactants and surface active ionic liquid. Journal of Molecular Liquids. 2021;340:116849.

[91] Sardar N, Kamil M. Interaction between nonionic polymer hydroxypropyl methyl cellulose (HPMC) and cationic gemini/conventional surfactants. Industrial & engineering chemistry research. 2012;51(3):1227-35.

[92] Altman RM, Richmond GL. Coming to order: adsorption and structure of nonionic polymer at the oil/water interface as influenced by cationic and anionic surfactants. Langmuir. 2020;36(8):1975-84.

[93] Miyake M. Recent progress of the characterization of oppositely charged polymer/surfactant complex in dilution deposition system. Advances in Colloid and Interface Science. 2017;239:146-57.

[94] Asker D, Weiss J, McClements DJ. Analysis of the interactions of a cationic surfactant (lauric arginate) with an anionic biopolymer (pectin): isothermal titration calorimetry, light scattering, and microelectrophoresis. Langmuir. 2009;25(1):116-22.

[95] Shrivastava S, Dey J. Interaction of anionic surfactant with polymeric nanoparticles of similar charge. Journal of colloid and interface science. 2010;350(1):220-8.

[96] Burrows HD, Tapia MJ, Silva CL, Pais AA, Fonseca SM, Pina J, Seixas de Melo J, Wang Y, Marques EF, Knaapila M, Monkman AP. Interplay of electrostatic and hydrophobic effects with binding of cationic gemini surfactants and a conjugated polyanion: Experimental and molecular modeling studies. The Journal of Physical Chemistry B. 2007;111(17):4401-10.

[97] Joshi N, Rawat K, Bohidar HB. Influence of structure, charge, and concentration on the pectin–calcium–surfactant complexes. The Journal of Physical Chemistry B. 2016;120(18):4249-57.

[98] Chakraborty T, Chakraborty I, Ghosh S. Sodium carboxymethylcellulose− CTAB interaction: a detailed thermodynamic study of polymer− surfactant interaction with opposite charges. Langmuir. 2006;22(24):9905-13.

[99] Khan MY, Samanta A, Ojha K, Mandal A. Interaction between aqueous solutions of polymer and surfactant and its effect on physicochemical properties. Asia-Pacific Journal of Chemical Engineering. 2008;3(5):579-85.

[100] Mondal BB, Banik R, Ghosh S. Detailed physicochemical study and thermodynamic aspects of the interaction between nonionic cellulose derivative hydroxyethyl cellulose and anionic surfactant sodium N-dodecanoyl sarcosinate in aqueous media. Journal of the Taiwan Institute of Chemical Engineers. 2023;149:104982.

[101] Gente G, La Mesa C. Water—Trifluoroethanol Mixtures: Some Physicochemical Properties. Journal of solution chemistry 2000;29(11):1159-72.

[102] Chakraborty T, Chakraborty I, Ghosh S. The methods of determination of critical micellar concentrations of the amphiphilic systems in aqueous medium. Arabian Journal of Chemistry 2011;4(3):265-70.

[103] Sugihara G and Hisatomi M, Roles of counterion binding in the micelle formation of ionic surfactants in water. Journal of Japan Oil Chemists' Society 1998;47(7):661-83.

[104] Piekarski H, Łudzik K. A microcalorimetric titration study on the micelle formation of alkanediyl-α, ω-bis (dimethylalkylammonium bromide) surfactants at a 283.15–

343.15 K temperature range. Journal of thermal analysis and calorimetry 2012;110(1):263-71.

[105] Loh W, Brinatti C, Tam KC. Use of isothermal titration calorimetry to study surfactant aggregation in colloidal systems. Biochimica et Biophysica Acta (BBA)-General Subjects. 2016;1860(5):999-1016.

[106] Beyer K, Leine D, Blume A. The demicellization of alkyltrimethylammonium bromides in 0.1 M sodium chloride solution studied by isothermal titration calorimetry. Colloids and Surfaces B: Biointerfaces. 2006;49(1):31-9.

[107] Brinatti C, Mello LB, Loh W. Thermodynamic study of the micellization of zwitterionic surfactants and their interaction with polymers in water by isothermal titration calorimetry. Langmuir 2014;30(21):6002-10.

[108] Das S, Patra N, Banerjee A, Das B, Ghosh S. Studies on the self-aggregation, interfacial and thermodynamic properties of a surface active imidazolium-based ionic liquid in aqueous solution: effects of salt and temperature. Journal of Molecular Liquids. 2020;320:114497.

[109] Osa M, Itoda Y, Suzuki Y, Yumoto T, Yoshida A. A fluorescence probe study on the effects of surfactants on cloud points in aqueous poly (N-isopropylacrylamide) solutions. Polymer journal 2015;47(1):59-65.

[110] Barry NP, Therrien B. Pyrene: The guest of honor. Inorganic Nanoreactors 2016;421-461: Academic Press.

[111] Ritter JR, Caldas MJ, da Silva TJ, Calzolari A, McCluskey MD. Surface effects on pyrene luminescence excitation. ACS Applied Electronic Materials. 2020;2(9):2806-12.

[112] Băran A, Stîngă G, Anghel DF, Iovescu A, Tudose M. Comparing the spectral properties of pyrene as free molecule, label and derivative in some colloidal systems. Sensors and Actuators B Chemical 2014;197:193-9.

[113] Wu T, Oake J, Liu Z, Bohne C, Branda NR. Probing the Microenvironments in a Polymer-Wrapped Core–Shell Nanoassembly Using Pyrene Chromophores. ACS Omega 2018;3(7):7673-80.

[114] Kralchevsky PA, Danov KD, Anachkov SE, Georgieva GS, Ananthapadmanabhan KP. Extension of the ladder model of self-assembly from cylindrical to disclike surfactant micelles. Current opinion in colloid & interface science 2013;18(6):524-31.

[115] Wu S, Tachiya M, Yan Z. An improved procedure for determination of the mean aggregation number of micelles. Spectrochimica Acta Part A Molecular and Biomolecular Spectroscopy 2015;138:807-10.

[116] Alargova RG, Kochijashky II, Sierra ML, Zana R. Micelle aggregation numbers of surfactants in aqueous solutions: A comparison between the results from steady-state and time-resolved fluorescence quenching. Langmuir. 1998;14(19):5412-8.

[117] Turro NJ, Baretz BH, Kuo PL. Photoluminescence probes for the investigation of interactions between sodium dodecylsulfate and water-soluble polymers. Macromolecules 1984;17(7):1321-4.

[118] Mandal B, Moulik SP, Ghosh S. Influence of aquo-organic solvent media on the self-aggregation of sodium dodecyl sulfate (SDS) and its interaction with polyvinylpyrrolidone (PVP). Colloid and Polymer Science 2014;292(10):2485-95.

[119] Das S, Mondal S, Ghosh S. Interaction of cationic gemini surfactant tetramethylene-1, 4-bis (dimethyltetradecylammonium bromide) with anionic polyelectrolyte sodium carboxymethyl cellulose, with two different molar masses, in aqueous and aquo-organic (isopropanol) media. RSC advances 2016;6(37):30795-803.

CHAPTER-III

Thermodynamic and Structural Insights into Pectin-Phosphonium Surfactant Coacervation: Bridging Electrostatics and Hydrophobicity

Thermodynamic and Structural Insights into Pectin-Phosphonium Surfactant Coacervation: Bridging Electrostatics and Hydrophobicity

ABSTRACT

In recent times, the robust complexation efficacy of oppositely charged polyelectrolyte-surfactant systems has prompted significant advancements in both academic research and industrial applications. The ongoing study focuses on exploring the synergistic effects of combining a polyanion with cationic surfactants of varying alkyl chain lengths, aiming to optimize overall performance characteristics. It is reasonable to anticipate that an intense coulombic force of attraction will compel negatively charged polymeric surfaces to interact with cationic components, and vice versa. Pectin, a bio-polyanion, has large-scale demand in both the food and pharmaceutical industries. Cationic phosphonium surfactants are indispensable in transporting nucleic acids, thanks to their strong affinity for the negatively charged DNA backbones. This article delves deeply into the colloidal behavior of a homologous set of cationic alkyltriphenylphosphonium bromide surfactants (C_nTPBs: n = 12, 14, and 16) in pectin-based aqueous medium, with a specific emphasis on the formation of macroscopic complex coacervate phases. The mechanisms underlying the pectin-C_nTPB complexation can be figured out on the basis of the cumulative effects of electrostatic and hydrophobic interactions. A variety of technical methods, including tensiometry, conductometry, turbidimetry, fluorimetry (steady-state and time-resolved), and viscometry, have been used to comprehend the physiochemical aspects of interaction phenomena. The size and electrokinetic properties of the colloidal aggregates have been investigated using the dynamic light scattering (DLS) method. Further, FESEM, HR-TEM, and fluorescence microscopy have been employed to visualize the complex aggregates. The dynamic interactions between the polymer and surfactant, as well as their respective molecular structures, determine the interfacial architectures of the complex assembly. For structural analysis, FTIR-ATR, and XRD have been employed as supporting tools.

Keywords: Complexation efficacy; Synergistic effects; Pectin; Alkyltriphenylphosphonium bromide; Complex coacervate; Colloidal aggregates.

1. Introduction

The interplay between theoretical frameworks and experimental investigations on ‘complex coacervation’ **[1-3]** has been a source of enduring fascination across scientific disciplines. This phenomenon is not only of significant academic interest but also holds a myriad of practical implications, including cosmetic formulations **[4]**, food products **[5]**, drug delivery **[6]**, encapsulation of proteins **[7]** and viruses **[8]**, enhanced oil recovery **[9]**, and waste water treatment **[10]**. In numerous scenarios, the attractive forces between the oppositely charged components in binary mixtures, such as polyelectrolytes **[11]**, surfactants **[12,13]**, colloids **[14,15]**, or proteins **[16-18]**, spontaneously induce the formation of coacervates. Ionic interactions between oppositely charged segments can lead to the emergence of either associative liquid/liquid (coacervation) or solid/liquid (precipitation) phase separation, resulting in the formation of less soluble complexes within the bulk solution. As these charge-driven complexes approach electrical neutrality, coacervation becomes apparent **[19]**. One of the key factors influencing the complex coacervation is polyelectrolyte charge density, among other contributing elements **[20–22]**. In polyelectrolyte-absent amphiphilic systems,

micellization of surfactant is driven solely by the hydrophobicity **[23]** of the medium above a certain concentration, termed the critical micelle concentration (CMC) **[24]**. However, in polyelectrolyte-surfactant systems, complexation arises from the collaborative participation of different chemical forces, primarily electrostatic and hydrophobic interactions **[25]**. Another characteristic feature is the premature formation of tiny micelle-like clusters along the polyelectrolyte chain at a concentration well below the micellization concentration, defined as critical aggregation concentration (cac) **[26]**. This underscores the pivotal role of polyelectrolytes in promoting surfactant aggregation. Thus, the choice of studying oppositely charged polyelectrolyte-surfactant systems is highly relevant in the context of complex coacervation.

Among polysaccharides, the naturally occurring biomolecule pectin is extensively highlighted in the scientific literature for its exceptional qualities of biocompatibility, biodegradability, and non-toxicity **[27]**. The biopolymer "pectin" refers to a family of structurally and functionally complex molecules with similar molecular characteristics and natural origins. Chemically, it consists of D-galacturonic acid (GalA) units along with other natural sugars, forming a complex heteropolysaccharide structure **[28]**. A distinctive feature of pectin is the degree of methylation (DM) of its GalA residues (COOH), which significantly influences its physicochemical properties and functional activities **[29, 30]**. Pectin has been selected for this study based on the evidence of its bioavailability, affordability, and widespread applications in the food and pharmaceutical industries **[31]**. Researchers have designed a variety of pectin-based formulations in biomedical science **[32]**, including hydrogels **[33-35]**, nanocomposite films **[36,37]**, microspheres **[38,39]**, etc. For instance, pectin has been valued since long time as a promising material for colon-targeted drug delivery protocols **[40,41]**. The gelling ability of pectin has found immense importance in various food products **[42]**. Intermolecular cross-linking with divalent metal ions, specifically Ca^{2+} ion **[43-45]**, stimulates pectin-gelation. The hypothesis behind the binding mechanism of pectin-Ca^{2+} network has been proposed by the conventional ‘egg-box’ model **[46, 47]**. Hence, the beneficial attributes of pectin in diverse fields can be improved through cationic modifications [48]. Anionic pectin, as observed in prior studies, forms complex coacervates with oppositely charged biopolymers (such as polylysine **[49]**) and proteins (such as gelatin **[50]**, lysozyme **[51]**, bovine serum albumin **[52]**, ovalbumin **[53]**, pea protein **[54]**, whey protein **[55]**, beta-lactoglobulin **[56]**, sodium caseinate **[57]**, lactoferrin **[58]**, etc.). Despite this, we still lack the fundamentals necessary to grasp the complex coacervation of pectin with an oppositely charged surfactant.

The inherent ability of surfactants to form micelles, facilitated by their unique combination of hydrophilic and lipophilic moieties functioning in tandem, is the principal driving force behind the recent spectacular developments in applied colloid and surface chemistry. Cationic surfactants **[59]** are of special interest in the development of nanomaterials for gene and drug delivery applications **[60, 61]**, known for their exceptional effectiveness against bacteria **[62]**, capacity to combat fungi **[63]**, and beneficial antiseptic properties **[64]**. The electrostatic linkage between the hydrophobic head of cationic surfactants and the phosphate backbone aids the DNA condensation process to a great extent **[65, 66]**. The aforementioned contemplations emphasize the fundamental study of cationic surfactants, specifically focusing on alkyltrimethylammonium bromides (C_nTABs) **[67]**. Meanwhile, shifting the cationic center from nitrogen to phosphorus significantly alters the binding dynamics of surfactants

with DNA and lipids. Alkyltriphenylphosphonium bromides (C_nTPBs), a novel class of cationic surfactants, show promise as viable alternatives to their ammonium analogues **[68]**. The presence of sterically hindered quaternary phosphonium groups (Ph_3P^+) **[69]** profoundly shapes the performance level of C_nTPB in solution, exerting significant influence over solubilizing capacity, aggregation behaviour **[70,71]**, and various other key properties. So far, surface chemists have largely overlooked studying the solution behaviours of C_nTPB **[72, 73]**, in contrast to the considerable attention devoted to C_nTAB **[74]**. Phosphonium cations (C_nTP^+) have been noted for their beneficial role in the mitochondrial nucleic acid transport process, prompting extensive biotechnological research into C_nTPB-DNA interactions **[75, 76]**. Currently, there is growing interest in exploring the mechanistic pathways underlying the micellar catalytic activity **[77]** of phosphonium surfactants in diverse reactions. Thereby, cationic phosphonium surfactants can form different colloidal frameworks with biomolecules, which get stabilized through electrostatic, hydrophobic, or hydrogen bonding interactions. This treatment incorporates the contributions of both the hydrophobicity of the alkyl tail and the electrostatic nature of the cationic head. Such insights underline the potential of phosphonium surfactants for efficiently complexing with bio-polyanions **[78]**, stimulating further exploration in this field.

Despite continual exposure and development in this field, fully comprehending the fundamental mechanisms and successfully implementing them in practical scenarios remains an enduring challenge. Drawing inspiration from previous surveys, our investigation provides a detailed overview of the complexation process between the bio-polyanion pectin and the cationic alkyltriphenylphosphonium bromide surfactants. The experimental findings from various methods exhibit a strong correlation with each other, which has been well-clarified through citations of earlier research reports.

The structure of the paper is organized as follows: Section 2 outlines the experimental procedures undertaken. In Section 3, we present our findings and provide a discussion. Finally, Section 4 summarizes the key conclusions and proposes potential avenues for future research.

2. **Experimental section**

2.1. Materials

The polyanion, pectin (poly-D-galacturonic acid methyl ester), was supplied by Thomas Baker Chemicals (India). The cationic surfactants (C_nTPBs): (1-dodecyl)triphenylphosphonium bromide (C_{12}TPB, purity >98%), (1-tetradecyl)triphenylphosphonium bromide (C_{14}TPB, 97% purity), and (1-hexadecyl)triphenylphophonium bromide (C_{16}TPB, 98% purity) were sourced from Alfa Aesar (Thermo Fisher Scientific, India). None of the above samples were subjected to further purification procedures. Scheme 1 represents the structures of pectin and the surfactants. AR-grade pyrene, coumarin 153, and 1,6-diphenyl-1,3,5-hexatriene (DPH) were ordered and collected from Sigma Aldrich (USA). These materials were used directly out of the package.

Table 1: Chemical Name, Chemical Formula, Symbol, Tail Group, and Molecular Weight (MW) of the C_nTPB Surfactants used in the Present Study.

Chemical Name	Chemical Formula	Symbol	Tail Group	MW (g/mol)
(1-dodecyl)triphenylphosphonium bromide	$C_{30}H_{40}P^{+}$ Br^{-}	C_{12}TPB	$-C_{12}H_{25}$	511.54
(1-tetradecyl)triphenylphosphonium bromide	$C_{32}H_{44}P^{+}$ Br^{-}	C_{14}TPB	$-C_{14}H_{29}$	539.59
(1-hexadecyl)triphenylphophonium bromide	$C_{34}H_{48}P^{+}$ Br^{-}	C_{16}TPB	$-C_{16}H_{33}$	567.62

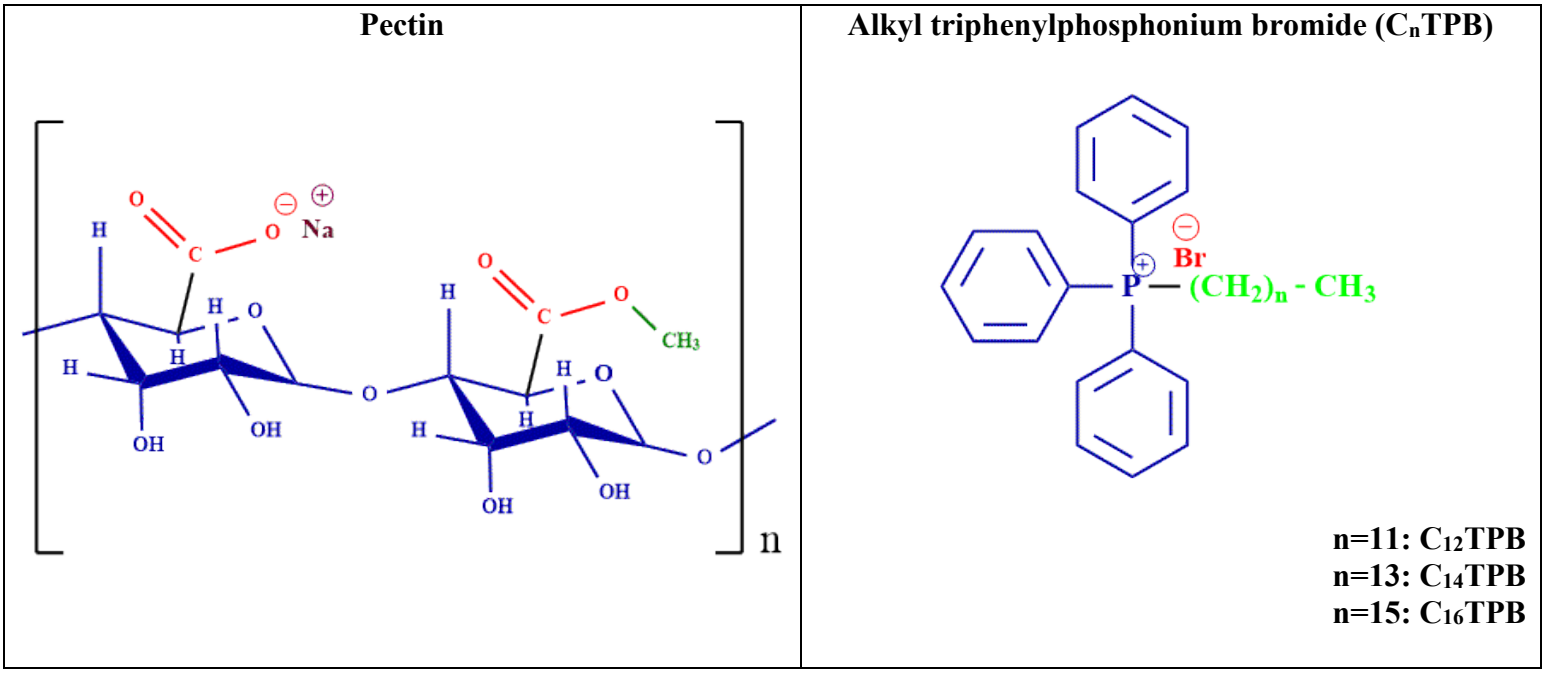

Scheme 1. Chemical structures of pectin (left) and alkyltriphenylphosphonium bromides (right).

2.2. Solution Preparation

The stock polymer solution (0.2% w/v) was prepared by dissolving the appropriate amount of powdered pectin in double-distilled water, stirred continuously for at least 3 hours at room temperature to ensure complete dissolution and uniform dispersion. The solution was then stored in a refrigerator until use. For this study, polymer concentrations of 0.001%, 0.005%, and 0.01% (w/v) were selected. The stock solution was diluted as required to achieve target concentrations of 0.05% and 0.1% (w/v). Although pH was not monitored, the physicochemical properties of the aqueous pectin solutions remained stable for a minimum of a week. Fresh surfactant solutions were prepared just before each experiment to prevent surface precipitation, and all experiments were carried out at a controlled temperature of 298 K.

2.3. Methods

2.3.1. Tensiometry

Tensiometric study involved the measurement of surface tension (γ) values based on the ring detachment technique at the air/solution interface. Tensiometric analysis not only unveils interfacial properties but also serves as an essential tool for comprehending bulk behavior. In this study, each experiment was conducted using a calibrated du Noüy tensiometer instrument crafted by Krüss (Hamburg, Germany). The experimental procedure initiated with smooth cleaning of a platinum ring, a double-walled container, and a magnetic stirrer. This was done by sequentially washing them with double-distilled water, followed by acetone. The platinum ring was carefully exposed to a pure ethanol flame, effectively purging it of any volatile impurities. In a double-walled container, precisely measured 5 ml volumes of aqueous pectin solutions at the investigated concentration range were placed. Subsequently, highly concentrated surfactant solutions (≈ 15-fold of CMC), were injected into the container using a Hamiltonian microsyringe in a series of calibrated steps, expertly adjusted to meet the specific demands of the experiment. The magnetic stirrer was employed to ensure uniform dispersion of the surfactant throughout the polymer solution after each addition. Following thorough mixing, a 10-minute stabilization period was allowed for the system before taking readings. The mean data were obtained through a dual-measurement approach, ensuring the utmost precision and reliability of the results. The entire setup was integrated with a thermostatic water bath to control the temperature at a constant 298 K. In an aqueous medium, the stock solutions of surfactants C_{12}TPB, C_{14}TPB, and C_{16}TPB were respectively prepared at 27, 8.4, and 3 mM. The technical protocols were replicated for both polymer-surfactant systems and pure surfactants to maintain uniformity in execution. The surface tension measurements were consistently accurate, staying within a narrow range of ± 0.1 $mN\ m^{-1}$.

2.3.2. Conductometry

The conductometric titrations were carried out using a Jenway (UK) conductometer, featuring a cell constant of 1.0 cm^{-1}, to measure the specific conductance (κ) values. Initially, 7 ml of various w/v % pectin solutions were placed in a double-walled glass container. Surfactant solutions were incrementally introduced using a Hamiltonian microsyringe, ensuring thorough mixing and providing ample time for temperature equilibration thereafter. The surfactant solutions were meticulously adjusted to precisely match the concentrations outlined in the tensiometric measurements. The experimental setup was immersed in a thermostatic water bath to maintain a constant temperature of 298 K. The error margin in specific conductivity measurements was rigorously monitored to remain within ± 0.1%.

2.3.3. Turbidimetry

A dual-beam Shimadzu 1601 (Japan) UV-VIS spectrophotometer, thermostated at 298 K, was used to measure the turbidity arising from the interactions between oppositely charged pectin and CnTPB. Two identical quartz cuvettes, each with a 1 cm path length, were utilized. Prior to conducting turbidity measurements, a baseline correction was made with double-distilled water in both cuvettes. During the experiment, 2.5 ml of different (w/v) % pectin solutions were contained within a quartz cuvette, followed by the progressive addition of the

concentrated surfactant solution with a Hamiltonian microsyringe. After introducing each dose of surfactant, the resultant solution was cautiously mixed using a magnetic stirrer to ensure homogeneity, allowing it to stabilize for 2-3 minutes before absorbance readings were recorded. The absorbance spectra were studied using the transmittance (% T) mode across the UV-visible wavelength range, spanning from 200 to 800 nm. The data were documented at 500 nm, marking the midpoint of the operational wavelength range (200–800 nm). The turbidity index (100–%T) was computed and graphed against the surfactant concentration.

2.3.4. DLS size measurement

The size of the polymer and polymer-surfactant aggregates in an aqueous medium was determined using dynamic light scattering with a Malvern Nano-ZS Zetasizer (Malvern, United Kingdom) instrument. The data were collected by directing a He-Ne laser beam, with a wavelength (λ) of 632 nm, at a scattering angle of 90 degrees. During the measurements, stringent temperature regulation was enforced to ensure that the experimental sample, confined within a fluorescence cell, remained at a stable 298 K. The freshly prepared sample solutions were subjected to thorough sonication to ensure uniformity before being filtered using cellulose acetate paper with a 0.45 μm porosity, effectively removing any unwanted dust particles. In each scenario, size analysis presented the mean value of duplicated measurements.

2.3.5 Zeta potential

The ζ-potential measurements, using the same DLS apparatus detailed in Section 2.2.4., were performed to probe the electrophoretic mobility and surface charge of colloidal particles within the oppositely charged binary system. The dynamic light scattering (DLS) method excelled in providing exceptional resolution and precise evaluation of electrokinetic potential, surpassing other techniques in both accuracy and reliability, thereby becoming the preferred choice. The instrument was equipped with a cell containing a copper (Cu) electrode coated in gold (Au). Following the protocols outlined in Section 2.2.4, the sample solutions underwent multiple filtration cycles prior to measurement, typically three or four times. The outcomes were reported as the average of two successive readings.

2.3.6. Fluorescence emission studies

The Perkin-Elmer LS 55 fluorimeter, manufactured in the USA, was employed for accurate measurement of fluorescence emission spectra intensity. Optimal fluorescence-based characterization of polymer-surfactant aggregate formation necessitates careful selection of the probe. This study utilized Pyrene (0.1 μM), a fluorescence probe well-known for its superior performance and extensive research background. The experimental temperature was maintained at 298 K, regulated by a water flow thermostat. The hydrophobic probe was excited specifically at 332 nm, while its emission spectra were finely tuned within the range of 350 to 450 nm. The experimental configuration calibrated slit widths to 14 nm for excitation and a narrower 2.5 nm for emission. The spectra were swiftly scanned at a rate of 250 nm per minute. Using a Hamiltonian microsyringe, a concentrated surfactant solution was added in multiple steps to a quartz cuvette (path length 1 cm) containing either an aqueous medium or an aqueous polymer solution. Throughout the experiment, a tiny magnetic bar was continuously spun inside the cuvette. A key outcome was the development

of the plot illustrating the correlation between the ratio (I_1/I_3) and the concentration of surfactant. Here, I_1 and I_3 denote the intensities of pyrene emission at 373 nm and 383 nm, respectively.

2.3.7. Time-resolved fluorescence

The fluorimetric strategy has been further extended to gain deep insights into the complexation dynamics of the polymer-surfactant system based on advanced time-resolved fluorescence spectroscopy (TRFS). The fluorescence decay curve, recorded by a HORIBA-Jobin-Yvon TCSPC instrument, was examined to precisely measure the fluorescence lifetime of C_{14}TPB under two conditions: with and without the presence of pectin, both at a temperature of 298 K. In this context, coumarin 153 dye was identified as the optimal choice for probing and monitoring fluorimetric detection. The probe was stimulated at 450 nm with a NanoLED light source (IBH, UK), and the emission decay was finely tuned at 544 nm using a TBX photon detection module. The decay profiles of each individual were fitted and analyzed with the support of the IBH DAS-6 software program. The titration procedure was executed to emulate the parameters of the steady-state fluorescence experiment (detailed in Section 2.2.6.). The lamp profile was collected by substituting the sample with an aqueous micellar solution of sodium dodecyl sulfate (SDS) as the scattering medium. In order to have proper instrumental fittings, the χ^2 values were manipulated in close proximity to unity. Using bi-exponential fitting, the average lifetime (τ_{av}) was calculated through the incorporation of the pre-exponential components (a_1, a_2) and corresponding decay periods (τ_1,τ_2) in the following equation:

$$\tau_{av} = a_1\tau_1 + a_2\tau_2 \quad (1)$$

2.3.8. Viscometry

The viscometric titration of the pectin-C_{14}TPB system was carried out in a conventional double-limbed glass Ostwald viscometer, immersed in a thermo-controlled water bath set to 298 K. The viscometer measured a flow time of 84.8 s for 10 ml of double-distilled water. The experiment started with measuring the flow time of a 10 ml solution containing 0.1 g% pectin using the same viscometer. Then, 16.8 mM C_{14}TPB solution was injected with a Hamiltonian microsyringe in a titrimetric fashion. Following each stage of surfactant addition, the resulting solution was well mixed and allowed to equilibrate before recording the flow time. Each measurement underwent repetition, and the mean data was noted. Relative viscosity (η_{rel}) is calculated using the formula $\eta_{rel} = {}^{t}/_{t_0}$, where t and t_0 represent the flow times of the solution and pure water, respectively, measured under the same experimental conditions. The correlation between η_{rel} and [C_{14}TPB] was analyzed to investigate the complexation dynamics within the pectin-C_{14}TPB system. The viscosity data were precise, with an accuracy tolerance of $\pm$ 5%.

2.3.9. FTIR spectroscopy

The infra-red spectral analysis was performed using a Perkin Elmer (USA) FTIR spectrophotometer. Attenuated total reflectance (ATR) was utilized as a sampling technique in conjunction with a LiTaO3 detector. The spectra were recorded over the wavelength range of 450 to 4000 cm^{-1}. For the characterization of pure pectin and C_{14}TPB surfactant, solid

samples were introduced. The complex formulation was prepared with pectin (0.1 g%) and C_{14}TPB at C_f, where [C_{14}TPB] = 2.12 mM. Following hours of sonication, the mixture was left undisturbed until the complex coacervate settled to the bottom. It was filtered and then dried under vacuum conditions. The solid material (pectin-surfactant complex) was subjected to FTIR analysis.

2.3.10. X-Ray Diffraction (XRD)

The samples subjected to FTIR analysis were further characterized by X-ray diffraction (XRD) using a Philips XRD-PW 1700 system (USA). The measurements were conducted with Cu Kα radiation operating at 40 kV and 40 mA, over a 2θ diffraction angle range of 4° to 70°.

2.3.11. Field Emission Scanning Electron Microscopy (FESEM)

Surface textures of the polymer and polymer-bound surfactant (cac, C_S, C_f and $\gg C_f$) were collected via imaging with a FEI INSPECT F50 (Japan) high resolution field emission scanning electron microscope (FESEM). Two microliters of the experimental sample solutions were delicately applied onto tiny glass slides and left overnight to naturally spread, facilitating the gradual evaporation of the solvent. The sputtering method was utilized to gold-coat the dried sample, with a current of 5.5 mA passing for a duration of one minute. FESEM imaging is adept at revealing the surface coverage of complexes, yet its scope is limited regarding internal architecture visualization.

2.3.12. High Resolution Transmission Electron Microscopy (HR-TEM)

For microanalysis of aggregated formulations, HRTEM imaging indisputably emerges as the most efficient and convenient approach available. TEM images of pure pectin and pectin-C_{14}TPB complexes were captured using a JEOL JEM-2100 Plus (Tokyo, Japan) 200 kV High-Resolution Transmission Electron Microscope. Before conducting measurements, a single droplet of the liquid sample was cast onto a tiny Cu-grid (gold-coated) and allowed to dry overnight within a desiccator containing silica gel. Only images with discernibly observable particles were selected for TEM analysis.

2.3.13. Fluorescence microscopy

Fluorescence microscopy was employed to image the microscopic distribution of aggregated particles with an Olympus IX73 inverted microscope (one-deck system: IX73P1F configuration). DPH (0.1 mM), dissolved in absolute ETOH, was used as a fluorophore to probe the sample solutions under investigation. After two hours of sonication to ensure proper mixture homogeneity, the resultant solutions were kept overnight to equilibrate. Before conducting spectral observations, a 10 μl droplet of the solution was gently spread on a glass microscope slide and shielded with a thin glass coverslip to prevent evaporation. A thin layer of immersion oil was applied to the upper surface of the coverslip to markedly improve the resolution and visibility of the microscopic images. Each individual optical image was characterized using the Olympus cellSens Imaging Software. The images inspected under the microscope were selected for analysis simply on the basis of visual perception with the naked eye. The magnification of the images was performed using the FITC filter.

3. Results and discussions

3.1. Amphiphilic Behavior of Pure C_nTPBs in Aqueous Medium

To better illustrate the progression of complexation in pectin-C_nTPB systems, it is essential to provide a concise statistical overview of the self-aggregation behaviour of pure amphiphiles in an aqueous medium for an insightful comparison. The magnitude of critical micelle concentration (cmc) of a surfactant reflects the relative stability of its micellar form compared to the monomers, with a lower cmc indicating higher stability. Increasing the number of non-polar alkyl groups along the long hydrocarbon chain of the surfactant tail is expected to lower the cmc in the aqueous medium **[79]**. The micellization and related interfacial and bulk properties have been investigated through tensiometry, conductometry, and fluorimetry techniques. The identification of cmc using these methods is depicted in Figure 1A, and 1B respectively. The measured cmc values are in good concordance with those reported in the literature **[80]**.

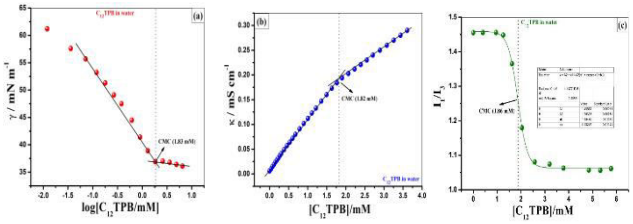

Figure 1A. CMC determination of C_{12}TPB in aqueous solution at 298 K using (a) tensiometry, (b) conductometry, and (c) spectrofluorimetry techniques. In (a) and (b), CMC is obtained from the intersection of two black solid lines, and in (c), from Boltzmann curve fitting (indicated as green solid curve).

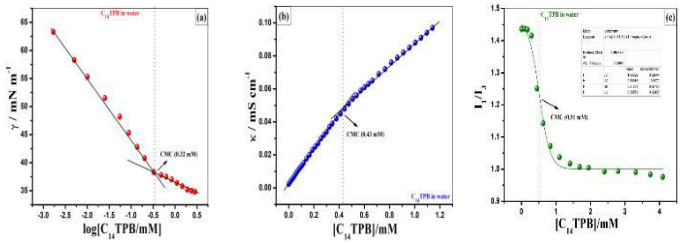

Figure 1B. CMC determination of C_{14}TPB in aqueous solution at 298 K using (a) tensiometry, (b) conductometry, and (c) spectrofluorimetry techniques. In (a) and (b), CMC is obtained from the intersection of two black solid lines, and in (c), from Boltzmann curve fitting (indicated as green solid curve).

Table 2. Determination of Critical Micelle Concentration (CMC) values using Surface Tension (ST), Conductometry (Cond), and Steady-State Fluorescence (Flr) techniques, including the relevant interfacial and bulk properties of pure C_nTPB in aqueous solution at 298 K.

	CMC			γ_{CMC} $(mN\ m^{-1})$	π_{CMC} $(mN\ m^{-1})$	$-(\frac{d\gamma}{dlogC} \times 10^3)$	$\Gamma_{max} \times 10^6$ (mol/m^2)	A_{min} $(nm^2/molecule)$	G_{min} (KJ/mol)	β	$-\Delta G^0_{mic}$ (KJ/mol)	$-\Delta G^0_{Ads}$ (KJ/mol)	$\frac{\Delta G^0_{Ads}}{\Delta G^0_{mic}}$	$-\Delta G^0_{eff}$ (KJ/mol)	$p^{C_{20}}$	P
	ST	cond	Flr													
C_{12}TPB	1.83	1.82	1.86	36.9	33.7	17.11	1.50	1.10	24.44	0.44	36.82	59.28	1.60	22.46	0.69	0.190
C_{14}TPB	0.32	0.43	0.51	38.3	32.5	13.46	1.18	1.40	32.29	0.34	40.05	67.59	1.68	27.54	1.52	0.149
C_{16}TPB	0.16	0.20	0.21	42.3	28.3	9.12	0.80	2.07	52.74	0.29	41.20	76.57	1.85	35.37	1.91	0.101

3.2. Interactional Behavior of C_nTPBs in Aqueous Pectin Environment

3.2.1. Tensiometry

Surface tension measurements are fundamental for exploring the interactions between polyelectrolytes and amphiphiles, providing in-depth insights into their complex behavior both at the interface and within the bulk phase. While surface tension is primarily an interfacial property, tensiometric titration bridges the gap between the bulk solution and the interface through steady measurements, enabling the assessment of key bulk characteristics. In the case of pure amphiphiles, the surface tension curve typically shows a sharp change in slope, with a clear transition point corresponding to the cmc. At the water-air interface, surfactant molecules align such that the hydrophilic (water-attracting) parts extend into the bulk phase, while the hydrophobic (water-repelling) segments are oriented toward the interface. The delicate balance between these hydrophilic and hydrophobic components is key to effectively reducing the surface tension and achieving interfacial saturation. In comparison, the nature of γ-log C plots for pectin-C_nTPB systems, as illustrated in Figure 2A (a) (b) and (c), displays a much greater complexity than those for individual amphiphiles. The emergence of multiple surface-active regions (Figure 2B) indicates the likelihood of strong interactions between pectin and C_nTPB. Three major break points (cac, C_S, and C_f) have been identified at the tangential intersections, akin to other strongly interacting polymer-surfactant systems **[81]**. Each point delineates the transition to a distinct mode of amphiphile aggregation at the polymeric surface. A striking observation has been made by A. Pal **[82]** during tensiometric analysis of the oppositely charged PE-SAIL system, detecting four distinct break points. In contrast, non-ionic polymers exhibit much less complex surface interactions with ionic surfactants. In our first publication, we find a single break point in the ST curve for the HEC-SDDS system **[83]**, with no evidence of electrostatic participation. The γ profiles of the systems under investigation are qualitatively similar but show notable quantitative differences at the inflection points. Pectin (0.05-0.2%) itself does not exhibit surface-active behavior **[84]** and lowers the γ value of water only marginally by 2-3 units. Consequently, pectin remains confined to the bulk phase without affecting the surface. The gradual adsorption of C_nTPB monomers at the pectin-water interface leads to a steep decline in γ, making the first major inflection point (cac) becomes evident (zone I). This suggests that

even a small amount of surfactant can produce substantial changes at the surfaces only. The cationic headgroup strongly directs the orientation of pectin COO^- groups, which results in the early formation of smaller premicellar assemblies of C_nTPB. The 'cac' point signifies the threshold concentration at which cooperative binding between polymer and surfactant starts to occur. In surfactants bearing identical head groups, longer alkyl chain lengths induce greater hydrophobicity to expedite the initiation of the complexation process, leading to a reduction in cac values from $C_{12}TPB$ to $C_{16}TPB$. J. Xiao **[85]** has primarily attributed such observation to the hydrophobic interactions between the polymer and the surfactant. The trend in cac shows different responses to increasing [pectin]: for $C_{14}TPB$ and $C_{16}TPB$, cac consistently decreases, whereas for $C_{12}TPB$, cac initially drops and then rises. The reason behind the observed decrease in cac at higher polymer concentrations remains unclear from a physicochemical standpoint. It is proposed that increased polymer charge density strengthens electrostatic interactions, making cooperative aggregation of surfactant monomers on the polymer segments more favorable, thus lowering cac **[86]**. According to the thermodynamic model proposed by P. Hansson **[87]**, cac is found to be a linear function of PE concentration when plotted on a log-log scale. As [C_nTPB] exceeds the cac point, there is an observed rise in γ due to the transfer of complex formulation from the interface to the bulk phase (zone II), which frees up the interface. During this process, the surfactant ion (C_nTP^+) progressively displaces the counter ion (Na^+) of pectin, leading to the formation of neutral ion pairs (pectin$^{(-)}$-$C_nTP^{(+)}$ complex) within the bulk solution. The interaction reaches its peak at C_S (second inflection point), where the polymer binding sites become fully occupied. In this zone, the interactions are governed by a combination of electrostatic and hydrophobic forces. The shape of the cac-C_S region is significantly affected by the surfactant alkyl chain length. For instance, the tensiograph shows a prominent hump (Figure 2B) for $C_{12}TPB$, while $C_{14}TPB$ and $C_{16}TPB$ exhibit a well-defined plateau (Figure 2B), which is considerably broader for $C_{16}TPB$. In such scenarios, the peak of the hump or the terminal point of the plateau is marked as the C_S. As polymer concentration increases, the hump height rises, and the plateau widths expand. A. Bahramian **[88]** and co-workers have derived an ST model based on the Butler concept to explain such surface phase behavior for strongly interacting PE-surfactant systems. The model excels in accurately depicting the origins of both the plateau and peak in the ST curve of oppositely charged systems, as exemplified by PDMDAAC-SDS **[89]** and NaPSS-C_nTAB **[90]**. Thomas and Penfold **[91]** have introduced the concept of non-surface activity in complexes to account for the occurrence of plateau regions. In another study, R. A. Campbell **[92]** defines this peak as the point at which charge neutrality is established. The increase in C_S values with higher pectin concentrations follows mass balance principles, indicating that more C_nTPB is required to achieve polymer saturation, a trend is also found in previously investigated systems **[93]**. Additionally, the manifestation of a turbid dispersion or coacervate phase (complex ensembles) near C_S is a significant visual indicator (Figure 2C), as briefly covered in Section 3.2.4. Beyond C_S, free C_nTPB monomers start to repopulate at the interface, further reducing γ (zone III). This amphiphilic behavior continues until the interface reaches fully saturation, marked by the appearance of a third and final inflection point. This point, so-called the extended critical micelle concentration (C_f), signals the start of polymer-induced micelle formation, occurring at a concentration much higher than that of pure amphiphiles. The reduction in γ is driven by the enhanced hydrophobic interactions at sufficiently high amohiphile concentrations. However, once zone IV is reached, the γ value stabilizes, unaffected by the addition of more amphiphile molecules. The explanation is that

the incoming surfactant molecules form micelles within the bulk solution without causing any perturbance to the absorbed complexes at the interface. It is relevant to mention that the cac and C_S correspond to the specific concentrations at which the initiation and termination of the complexation process occur, respectively. The observed increment in C_f values with [pectin] can be understood through the concept of polymer saturation effect. Higher pectin content provides more charged groups or binding sites available for surfactants, necessitating a higher surfactant concentration to reach a saturation point (C_S), which consequently delays entering the micellization process (C_f). Comparing with and without pectin, the micellization concentration increases by ~2.5, ~8.4, and ~10.9 folds for C_{12}TPB, C_{14}TPB, and C_{16}TPB, respectively, in 0.2% pectin medium. The values of cac, C_S, and C_f, as measured by tensiometry, are detailed in Tables 3, 4, and 5 for C_{12}TPB, C_{14}TPB, and C_{16}TPB, respectively.

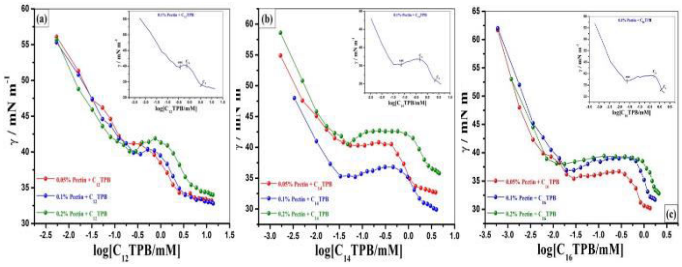

Figure 2A. Tensiometric profiles of pectin-C_nTPB systems at varying pectin concentrations (% w/v) in aqueous solution at 298 K: (a) C_{12}TPB, (b) C_{14}TPB, and (c) C_{16}TPB. Inset: Transition points (cac, C_S, and C_f) shown for the 0.1% pectin solution.

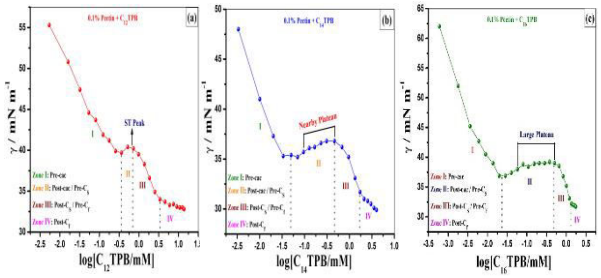

Figure 2B. Comparison of zone II (post-cac) for (a) C_{12}TPB (peak), (b) C_{14}TPB (nearly plateau), and (c) C_{16}TPB (large plateau) in the presence of a 0.1% pectin solution, showing the effect of surfactant alkyl chain length on ST behaviour. The ST curves for the binary pectin-C_nTPB systems can be categorized into four zones (I, II, III, and IV), as marked by the black dotted lines.

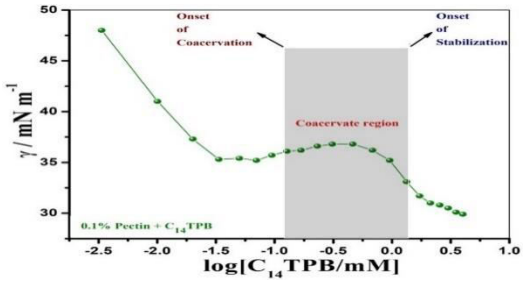

Figure 2C. The coacervate region of the pectin-C_{14}TPB complex, highlighted by the gray shaded area, where [pectin] = 0.1% (w/v).

Figure 2D. Visual appearance of as-prepared 0.1% (w/v) pectin/C_{14}TPB samples at key transition points of [C_{14}TPB] obtained from tensiometry: (i) 0 mM, (ii) cac (0.069 mM), (iii) C_S (0.46 mM), (iv) C_f (2.12 mM), (v) above C_f (3 mM).

3.2.2. Conductometry

Electrical conductivity measurements are employed to study the bulk complexation behavior of oppositely charged polyelectrolyte-amphiphile systems, with a specific focus on characterizing the ionic transport properties of charged colloidal particles in this context. The conductometric titrations (Figure 3A, 3B, and 3C) are characterized by changes in specific conductance (κ) with respect to amphiphile concentration ([C_nTPB]). As per the expectation for pure C_nTPB, the conductivity-concentration curve exhibits a sudden shift at the breakpoint. For each instance, the cmc is identified at the intersection of two well-fitted straight lines with different slopes. Thus, the conductometric plot displays a couple of distinct phases prior to and subsequent to the point of intersection, known as the pre- and post-micellar zones, respectively. The more pronounced slope in the former zone indicates a reduction in the rate of conductivity rise following micellization. As strong electrolytes, the C_nTPB monomers fully dissociate in water, releasing the respective constituent ions (C_nTP^+ and Br^-) into the aqueous medium. The combined ion transport activities of the counterions (Br^-) and surfactant ions (C_nTP^+) likely contribute to a more rapid rise in conductivity prior to entering the micellar phase. The point of transition establishes an equilibrium atmosphere, allowing free micelles, counterions, and individual monomers to coexist independently. However, the relatively larger size of the micelles (self-aggregates of monomers) and the accumulated state of the counterions on the micellar surface impede the free mobility of the charge carriers beyond the micellization point. Therefore, the reduced presence of active charge carriers in the bulk restricts the conductivity increase during the post-micellization period, even when surfactant concentrations are higher. The introduction of C_nTPB into aqueous pectin media reveals three distinctive interactional regions, i.e., two break points identified as C_S and C_f. This stands in contrast to the conductometric profile of pure amphiphiles in aqueous media, which displays a single breakpoint (cmc). Due to the closely aligned conductivity slopes in the lower concentration range, conductometry fails to accurately detect a break point near the cac, unlike tensiometry, which excels in this regard. The literature has already articulated strong arguments highlighting the insensitivity of the conductrometry approach to detecting cac **[94]**. The disparity stems from the fact that the tensiometric method promptly identifies the onset of the surface-active pectin-$C_{14}TP^+$ complex, whereas the conductometric approach registers a notable shift only after the

occurrence of coacervation in the bulk. The absence of cac in conductometry suggests that the interactions between pectin and C_nTPB at the earlier stage are concentrated at the interface rather than dispersed throughout the bulk medium. Interestingly, in a rare anomaly, the oppositely charged NaCMC-CTAB **[95]** combination displays all three documented conductometric breakpoints (cac, C_S, and C_f) in satisfactory agreement with tensiometric observations. The first mild break point, C_S, has been realized due to the continual adsorption of small C_nTPB aggregates onto the anionic pectin backbone during the formulation of completely saturated pectin-C_nTPB complexes. The concept of slope in different regions of the conductivity curve can be used to interpret the extent of interactions. For instance, a lower slope in the pre-C_S region predicts a stronger association with a minor influence on the solution conductivity. The post-C_S region (where further polymer-surfactant binding is absent) experiences a higher slope in conductivity as the incoming C_nTPB monomers remain unattached to the polymer, allowing them to persist in their dissociated form (as efficient charge carriers) up to the second prominent break point (C_f). The transition at C_f involves the pectin-assisted formation of C_nTPB micelles, concurrent with the migration of counterions (Br^-) from the bulk phase to the electrical double layer within the ionic micellar environment. Therefore, the post-micellization state can be distinguished by having the least steep gradient amongst the three interactional regions. A higher concentration of polymer extends the availability of saturation sites for surfactant molecules, thereby effectively delaying the polymer-mediated self-aggregation process. The transition points (C_S and C_f values) exhibit a consistent trend analogous to tensiometry with variation in pectin concentration, as shown in Tables 3, 4, and 5 for $C_{12}TPB$, $C_{14}TPB$, and $C_{16}TPB$, respectively. In this study, pectin shows a significant enhancement in ionic conductivity with increasing surfactant content, following the sequence: $C_{12}TPB < C_{14}TPB < C_{16}TPB$.

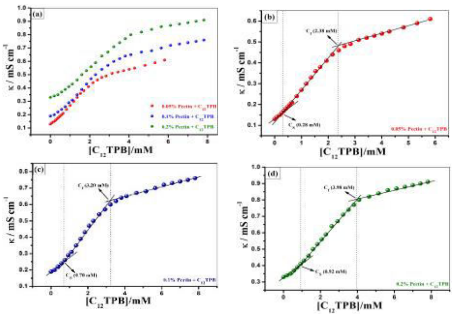

Figure 3A. Plots of specific conductance (κ) vs. [$C_{12}TPB$] in aqueous solution at 298 K. (a) The combined plot shows the influence of pectin weight percentage on the electrical conductivity of pectin-$C_{12}TPB$ systems; (b), (c), and (d) display individual plots for pectin concentrations of 0.05%, 0.1%, and 0.2%, respectively, marking the breakpoints (C_S and C_f).

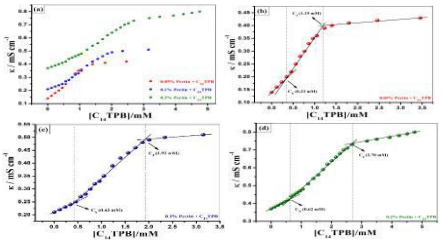

Figure 3B. Plots of specific conductance (κ) vs. [C_{14}TPB] in aqueous solution at 298 K. (a) The combined plot shows the influence of pectin weight percentage on the electrical conductivity of pectin-C_{14}TPB systems; (b), (c), and (d) display individual plots for pectin concentrations of 0.05%, 0.1%, and 0.2%, respectively, marking the breakpoints (C_S and C_f).

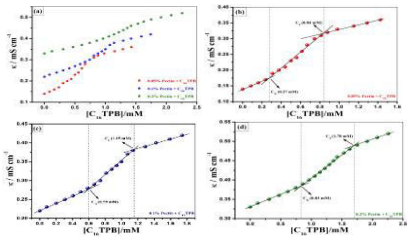

Figure 3C. Plots of specific conductance (κ) vs. [C_{16}TPB] in aqueous solution at 298 K. (a) The combined plot shows the influence of pectin weight percentage on the electrical conductivity of pectin-C_{16}TPB systems; (b), (c), and (d) display individual plots for pectin concentrations of 0.05%, 0.1%, and 0.2%, respectively, marking the breakpoints (C_S and C_f)

Table 3. Critical Concentrations Corresponding to Various Transitions (cac, C_S, and C_f) obtained from Different Techniques (Surface Tension, Conductometry, and Turbidimetry) during the Complexation of Pectin-C_{12}TPB Systems in Aqueous Solution at 298 K.

	Tensiometry			*Conductometry*		*Turbidimetry*		
[Pectin]/% (w/v)	cac	C_S	C_f	C_S	C_f	T_1	T_2	T_3
0.05	0.17	0.36	2.53	0.28	2.38	0.15	0.59	1.60
0.1	0.36	0.72	3.39	0.70	3.20	0.24	0.82	2.03
0.2	0.28	0.75	4.58	0.92	3.98	0.16	1.05	2.54

Table 4. Critical Concentrations Corresponding to Various Transitions (cac, C_S, and C_f) obtained from Different Techniques (Surface Tension, Conductometry, and Turbidimetry) during the Complexation of Pectin-C_{14}TPB Systems in Aqueous Solution at 298 K.

	Tensiometry			*Conductometry*		*Turbidimetry*		
[Pectin]/% (w/v)	cac	C_S	C_f	C_S	C_f	T_1	T_2	T_3
0.05	0.079	0.42	1.42	0.33	1.19	0.093	0.33	0.79
0.1	0.069	0.46	2.12	0.43	1.92	0.046	0.39	0.98
0.2	0.048	0.58	2.70	0.62	2.70	0.030	0.62	1.47

Table 5. Critical Concentrations Corresponding to Various Transitions (cac, C_S, and C_f) obtained from Different Techniques (Surface Tension, Conductometry, and Turbidimetry) during the Complexation of Pectin-C_{16}TPB Systems in Aqueous Solution at 298 K.

	Tensiometry			*Conductometry*		*Turbidimetry*		
[Pectin]/% (w/v)	cac	C_S	C_f	C_S	C_f	T_1	T_2	T_3
0.05	0.028	0.28	0.83	0.27	0.84	0.107	0.43	0.67
0.1	0.024	0.50	1.19	0.59	1.15	0.089	0.64	1.19
0.2	0.017	0.73	1.75	0.83	1.70	0.045	0.84	1.50

3.2.3. Thermodynamics of Micellization and Complexation Behaviour

Tensiometric and conductometric data have been used to quantify several key interfacial and bulk parameters relevant to this study, providing insightful perspectives on the complexation process. Tables 2, 6, 7, and 8 present a summary of the calculated parameter values for both the pure C_nTPB and pectin-C_nTPB systems, enabling a comprehensive comparative analysis.

Due to the substantial uncertainty and inaccuracies in experimental data, it is crucial to rigorously scrutinize all aspects of chemical data collection. In the ensuing discussion, we delve into the requisite fundamental equations, highlight the importance of the parameters within this specific context, and furnish a detailed interpretation of the observed findings.

(a) Interfacial tension at cmc (γ_{CMC})

In phenomenological terms, the cmc defines the threshold concentration on the tensiometric curve where interfacial saturation occurs, causing the surface tension (γ) to stabilize without significant further decrease. The parameter γ_{CMC} (measured in $mN\,m^{-1}$) stands for the specific surface tension value at cmc, reflecting the propensity of the amphiphilic monomers to accumulate at the air/solution interface prior to micellization in the bulk. A higher γ_{CMC} value suggests reduced surface activity of the experimental solution. Increasing the alkyl chain length usually enhances the hydrophobicity of surfactants, leading to a decrease in γ_{CMC}. However, the observed trend does not align with the expectation in this instance. For C_nTPB amphiphiles, the longer alkyl chain causes the bulky triphenylphosphonium head groups to experience greater steric repulsion, resulting in a less compact interfacial layer and higher γ_{CMC}. The lower γ_{CMC} observed with pectin, compared to surfactants alone, suggests that pectin improves the ability of surfactants to accumulate at the interface. Thus, the complex interactions between the polymer and surfactant can modify the interfacial behaviour, leading to a more favorable arrangement of surfactant molecules at the air-solution interface.

(b) Surface pressure (π_{CMC})

Surface tension and surface pressure are interconnected aspects, exerting a profound influence on one another. Thus, the concept of surface pressure illuminates the precise interfacial characteristics of the amphiphile molecules. The formula for calculating π_{CMC} utilizes surface tension data at two specific points, as follows **[96]**:

$$\pi_{CMC} = \gamma_{iniial} - \gamma_{CMC/Cf} \quad (2)$$

Here, π_{CMC} is assigned as the surface pressure at the interfacial saturation (cmc), γ_{iniial} is the surface tension of the amphiphile-free surface (double-distilled water or aqueous pectin medium), and $\gamma_{CMC/Cf}$ is the surface tension in the presence of C_nTPB at cmc or C_f. Here, γ_{CMC} is applicable for the micellization of pure amphiphile, whereas, γ_{Cf} is measured for mixed systems at different (w/v) % pectin. With the addition of amphiphile, the surface tension of the respective systems reaches its minimum possible value at cmc or C_f. The π_{CMC} value actually signifies the maximum surface tension reduction measured in the experimental solution. The efficacy of this surface tension reduction (π_{CMC}), as estimated, follows a reverse trend with $\gamma_{CMC/Cf}$. This parameter is valuable in the comparison of the surface-active nature of C_nTPB in both aqueous and pectin media. The measurement of surface π_{CMC} can also reveal the behavior of polymer-surfactant systems at interfaces. In particular, it can differentiate whether the interaction is synergistic (higher π_{CMC}) or antagonistic (lower π_{CMC}). Another important aspect of this parameter is its utilization in the equation concerning ΔG^0_{Ads} (discussed later).

(c) Counterion binding (β):

The conductometric slope ratio method is applied to determine the degree of counterion adsorption on charged micellar surfaces. This approach is highly valued for its ease of calculation and broad acceptance in the scientific literature **[97]**. In this context, the degree of counterion binding (β) quantifies the fraction of counterions bound to the micellar surface. Mathematically, β can be expressed as **[98]**:

$$\beta = 1-\alpha \quad (3)$$

Here, α represents the degree of dissociation, measured by comparing the slopes of the post-micellar (S_2) and pre-micellar (S_1) phases. Thus, the following equation offers an alternative formulation of β using the slope ratio method **[99]**:

$$\beta = 1 - \frac{S_2}{S_1} \quad (4)$$

Since S_2 is lower than S_1, β typically ranges between 0 and 1 ($0 < \beta < 1$) in experimental observations. Pure C_nTPB exhibits a single breakpoint (cmc) with two distinct slopes, while its introduction into pectin medium produces two breakpoints (C_S and C_f) with three distinct slopes of reducing magnitude. In the mixed system, the pre-micellization phase is therefore identified as occurring between the C_S and C_f regions. This parameter is fundamental for understanding the dynamics of micelle-counterion interactions, shedding light on the equilibrium between free and bound states of counterions at the micellar surface. Increasing the chain length of C_nTPB amphiphiles lowers the β value. It is also noteworthy that β decreases concurrently with the reduction in cmc values. In certain instances, evidence suggests that the cmc and β values may not necessarily be directly correlated. The expansion of the micellar surface area reduces the surface charge density, thereby diminishing the electrostatic repulsion between the micelles. The β values indicate that 29–44% of Br^- ions are bound to the micelles. In the presence of pectin, the higher β values for all surfactants reflect a more intense interaction between Br^- ions and the micelles.

(d) Maximum surface excess (Γ_{max}):

Surfactants exhibit an inherent tendency to minimize surface energy, which drives molecules to preferentially gather at interfaces. The parameter, Γ_{max}, gives a quantitative estimate of the enriched interfacial populations of amphiphilic monomers relative to the bulk phase, under the assumption of negligible interfacial thickness. It is also referred to as Gibbs surface excess, derived from the Gibbs adsorption isotherm equation **[100]** outlined below:

$$\Gamma_{max} = -\left(\frac{1}{2.303nRT}\right) \lim_{[C_nTPB]\to cmc} \frac{d\gamma}{dlogC} \quad (5)$$

The term 'i' symbolizes the effective number of dissociated ionic species per amphiphile monomer adsorbed at the air/solution interface. For the investigated CnTPBs, i = 2 (C_nTP^+ and Br^-) in both pure and mixed environments. The other terms, 'R' and 'T', stand for the universal gas constant (8.314 joule $mol^{-1}K^{-1}$) and absolute temperature (298 K), respectively. The differential part $\left(\frac{d\gamma}{dlogC}\right)$ indicates the premicellar slope near interfacial saturation, obtained by fitting a second-order polynomial to the tensiometric plot of γ vs. log [C_nTPB]. In the mixed system, the pre-micellar region is defined as the segment extending from C_S to C_f, marking the transitional phase prior to micelle formation. As the alkyl chain

length extends, the bulkiness of C_nTPB molecules also increases, leading to less efficient packing of surfactant molecules at the interface. Consequently, Γ_{max} decreases with increasing chain length. In aqueous pectin medium, Γ_{max} of C_{12}TPB and C_{14}TPB decreases as the formation of bulk complexes lowers the availability of free surfactant molecules for interfacial adsorption. The higher Γ_{max} value in pectin-C_{16}TPB mixed systems, compared to pectin-free C_{16}TPB, may result from the preferential adsorption of $C_{16}TP^+$ monomers at the interface after pectin becomes completely saturated with C_{16}TPB during the post-C_S stage.

(e) Minimum headgroup area (A_{min}):

The minimum area occupied by the surfactant head group at a fully saturated interface is given by **[101]**:

$$A_{min} = \frac{10^{18}}{N_A \Gamma_{max}} \quad (6)$$

Here, 'N_A' is the Avogadro's constant and the exponential term 10^{18} results from converting transformation of square meters (m^2) to square nanometers (nm^2) (since 1nm = 10^{-9} m). knowing A_{min} is essential for understanding the distribution of amphiphiles, describing whether the molecules are loosely or tightly packed at the interface. There is an inverse relationship between Γ_{max} and A_{min}, with each varying in opposition to the other. This means that as the surface area of a surfactant molecule increases, there is a decline in the surface coverage. As expected, A_{min} values for pure amphiphiles increase with chain length. This is because longer hydrophobic tails create more steric hindrance around the head groups, increasing head-to-head repulsion and causing the head groups to occupy a larger area to reduce this repulsion. With pectin present, A_{min} increases for C_{12}TPB and C_{14}TPB but decreases for C_{16}TPB compared to pectin-free systems. In the mixed monolayers, the average A_{min} values for C_{12}TPB, C_{14}TPB, and C_{16}TPB are 1.83, 1.61, and 0.81 $nm^2/molecule$, respectively. This indicates that when complexed with pectin, the packing density of C_nTPB monomers at the air-solution interface follows a reverse trend. The arrangement of counter-ions at the air-solution interface is an ongoing research topic and will be further explored in future reports.

(f) Minimum free energy of adsorption (G_{min})
Sugihara has introduced a thermodynamic parameter called the minimum free energy of adsorption to measure synergistic effects in mixed systems. This parameter is calculated using a specific equation **[102]:**

$$G_{min} = \gamma_{CMC}. A_{min}. N_A \quad (7)$$

The meaning of each term in the equation has already been explained. It quantifies the change in free energy associated with the phase transition of the solution elements from the bulk to the interface. A lower value of G_{min} reflects enhanced thermodynamic stability of the surface or improved surface activity, highlighting more substantial synergistic interaction. The calculated G_{min} values for the three surfactants in aqueous pectin solution exhibit different trends: C_{12}TPB shows slightly higher values, C_{14}TPB almost same, and C_{16}TPB much lower. Accordingly, C_{16}TPB demonstrates the most favourable synergistic interactions with pectin.

(g) Standard Gibbs free energy of micellization (ΔG^0_{mic})

The Gibbs free energy contribution to micelle formation and stability (ΔG^0_{mic}) can be determined using the pseudophase model equation **[103]**:

$$\Delta G^0_{mic}=(1+\beta)\mathrm{RT}lnX_{CMC} \quad (8)$$

In this formula, X_{CMC} represents the micellization concentration (cmc or C_f) on the mole-fraction scale, while the β factor accounts for the portion of free energy required to bind counterions to the aggregates during micellization, minimizing repulsion between the monomer head groups. More negative ΔG^0_{mic} values for pure amphiphiles (Table 1) with enhanced hydrophobic character suggest that micellization is primarily driven by the hydrophobic effect. In 0.05% pectin medium, the ΔG^0_{mic} values for all surfactants initially become more negative but then gradually increase at higher pectin concentrations. This statistic enlightens that micellization in mixed systems turns out to be more convenient at lower pectin concentrations.

(h) Standard Gibbs free energy of adsorption (ΔG^0_{Ads})

Rosen and Aronson **[104]** have derived an equation that directly relates ΔG^0_{mic} to ΔG^0_{Ads} as follows:

$$\Delta G^0_{Ads} = \Delta G^0_{mic} - \frac{\pi_{CMC}}{\Gamma_{max}} \quad (9)$$

In this equation, the ratio $\frac{\pi_{CMC}}{\Gamma_{max}}$ quantifies the work required to transfer an amphiphile molecule from the surface layer (where $\pi_{CMC} = 0$) into the micelle. The ΔG^0_{Ads} values hold a similar trend as ΔG^0_{mic} in the cases of pure amphiphiles and pectin-C_{14}TPB systems. In contrast, for pectin-C_{12}TPB and pectin-C_{12}TPB systems, the negative ΔG^0_{Ads} values show a consistent increase and decrease, respectively, at higher pectin concentrations. The negative values of both free energy parameters indicate that the formation of micelles and the adsorption of amphiphile molecules at the air/water interface are energetically favorable processes. However, higher ΔG^0_{Ads} values relative to ΔG^0_{mic} suggest that amphiphiles are more efficient at interfacial adsorption than at bulk micellization.

(i) Effective Gibbs free energy (ΔG^0_{eff}):

The predominance of ΔG^0_{Ads} over ΔG^0_{mic} indicates that amphiphile molecules have a greater propensity to adsorb at the interface rather than to aggregate into micelles within the bulk solution. Thus, after the completion of interfacial saturation, micellization can take place as the secondary process. In both pure C_nTPB and mixed pectin-C_nTPB systems, ΔG^0_{Ads} values are consistently higher than ΔG^0_{mic} values, with an average ratio ($\frac{\Delta G^0_{Ads}}{\Delta G^0_{mic}}$) of about 1.3 to 2, assuring that adsorption is more energetically favorable than micellization. The term "effective Gibbs free energy" **[105]** refers to the difference between ΔG^0_{Ads} and ΔG^0_{mic}:

$$\Delta G^0_{eff} = \Delta G^0_{Ads} - \Delta G^0_{mic} \quad (10)$$

The experimental results show that the ΔG^0_{eff} values for the mixed systems are higher than their pure amphiphile systems, with the exception of C_{16}TPB. Therefore, the micellization of C_{16}TPB becomes more favorable when pectin is present.

(j) Gibbs energy difference (ΔG_{ps}^{0}):

The ratio of cac to cmc is a key indicator for evaluating the binding affinity of a surfactant to a polymer chain. The quantification of the interaction parameter, the Gibbs energy difference (ΔG_{ps}^{0}), utilizes the value of this ratio. The excess Gibbs energy that contributes to the stabilization of polymer-bound surfactant aggregates over free surfactant micelles can be determined from the following equation **[106]**:

$$\Delta G_{ps}^{0} = RT\ ln\frac{cac}{cmc} \tag{11}$$

The apparent variation in the cac/cmc value arises not only from the self-aggregation behavior of the surfactants but also from the strength of their binding interactions with polymers. A lower (cac/cmc) ratio reflects a more negative value of ΔG_{ps}^{0}, suggesting significantly stronger and thermodynamically favorable interactions. The average values of ΔG_{ps}^{0} for C_{12}TPB, C_{14}TPB, and C_{16}TPB are found to be - 4.85, - 3.98, and - 4.85 $kJ\ mol^{-1}$, respectively. These values indicate that C_{12}TPB and C_{16}TPB have equal binding strength, both exceeding that of C_{14}TPB.

(k) Efficiency of adsorption ($p^{C_{20}}$):

Rosen **[107]** has proposed an innovative measure, termed $p^{C_{20}}$, for comparing the interfacial adsorption efficiency of different surfactants. Defined as the negative logarithm of the surfactant concentration (C_{20}) required to lower the surface tension of the pure solvent by 20 mN m^{-1}, this physical quantity provides a precise and standardized approach for evaluating surfactant performance in mixed polymer-surfactant systems. It is quantitatively measured using the following equation:

$$p^{C_{20}} = -\log_{10} C_{20} \tag{12}$$

The C_{20} values are directly obtained from the tensiometric plots of gamma vs. log [surfactant]. According to the equation, a higher value of $p^{C_{20}}$ signifies enhanced surfactant adsorption at the air-solution interface, resulting in a more substantial reduction in surface tension. M. Ben-Moshe **[108]** has noted that in homologous ionic surfactants, the $p^{C_{20}}$ tends to increase by around 0.3 units for each additional methylene group in the alkyl tail chain. This trend suggests that $p^{C_{20}}$ is fundamentally associated with the adsorption-free energy, which governs the spontaneous movement of surfactant molecules from the bulk phase to the interface region. As presented in Table 1, for C_nTPB surfactants, the $\Delta p^{C_{20}}$ per methylene group is found somewhat higher than the reported data (n= (12 to 14): $\Delta p^{C_{20}}$ = (1.52-0.69) = 0.83 and n= (14 to 16): $\Delta p^{C_{20}}$ = (1.91-1.52) = 0.39). In the presence of pectin, the mixed system exhibits higher $p^{C_{20}}$ values compared to the pure systems, indicating improved adsorption efficiency. However, $p^{C_{20}}$ does not follow any consistent trend with increasing pectin content.

(l) Packing parameter (P):

The packing parameter (P), formulated by Israelachvili **[109]**, provides a means to predict the geometrical arrangement of micelles. For example, the micellar shape can vary depending on the magnitude of P: (a) $0 < P \leq 0.33$ for spherical shape, (b) $0.33 < P \leq 0.5$ for cylindrical or rod-like shape, (c) $0.5 < P \leq 1$ for lamellar or bilayer phases, and (d) $P > 1$ for inverted structures. It is calculated using the following equation:

$$P = \frac{V}{l\,A0} \quad (13)$$

Thus, the geometric packing of micelles is governed by three critical physical quantities: (i) volume of the hydrophobic segment (v), (ii) hydrophobic chain length (l), and (iii) surface area of the hydrophilic head (A_0). The values of l and v were computed based on Tanford's formulae **[110]**, as outlined below:

$$l = (0.154 + 0.1265\ N_c)\ nm \quad (14)$$

$$v = (0.0274 + 0.0269\ N_c)\ nm^3 \quad (15)$$

N_c counts the number of carbon atoms in the alkyl saturated hydrocarbon chain for C_nTPB surfactants, where N_c equals 12, 14, or 16, for $C_{12}TPB$, $C_{14}TPB$, and $C_{16}TPB$, respectively. Due to the difficulty in accurately quantifying A_0, the literature recommends using A_{min} as a substitute in the equation. For a particular surfactant, the ratio ($^{v}/_{l}$) remains constant since both v and l are intrinsic molecular properties. However, the quantity A_0 can be modified by adjusting the solution conditions, such as by adding polymers, which directly affect the spatial distribution of the surfactant's polar head groups. It is reasonable to anticipate the formation of spherical micelles ($P < 0.33$) for all three surfactants, both with and without varying concentrations of pectin. Hence, the addition of pectin does not substantially affect the core shape of micelles. In fact, P values fall well below 0.2, with the exception of the pectin-$C_{16}TPB$ mixed systems (relatively lower value of A_{min}).

Table 6. Interfacial and Thermodynamic Parameters of $C_{12}TPB$ Micellization at Different Pectin Concentrations (0.05%, 0.1%, and 0.2% w/v) at 298 K.

[Pectin]/% (w/v)	γ_{CMC} $(mN\ m^{-1})$	π_{CMC} $(mN\ m^{-1})$	$-(\frac{d\gamma}{dlogC} \times 10^3)$	$\Gamma_{max} \times 10^6$ (mol/m^2)	A_{min} $(nm^2/molecule)$	G_{min} (KJ/mol)	β	$-\Delta G^0_{mic}$ (KJ/mol)	$-\Delta G^0_{Ads}$ (KJ/mol)	$\frac{\Delta G^0_{Ads}}{\Delta G^0_{mic}}$	$-\Delta G^0_{eff}$ (KJ/mol)	ΔG^0_{ps} (KJ/mol)	$p^{C_{20}}$	P
0	**36.9**	**33.7**	**17.11**	**1.50**	**1.10**	**24.44**	**0.44**	**36.82**	**59.28**	**1.60**	**22.46**	**-**	**0.69**	**0.190**
0.05	**34.3**	**34.1**	**11.98**	**1.05**	**1.58**	**32.64**	**0.72**	**42.60**	**75.07**	**1.76**	**32.47**	**5.88**	**1.57**	**0.132**
0.1	**34**	**32.7**	**10.38**	**0.91**	**1.82**	**37.27**	**0.77**	**42.56**	**78.49**	**1.84**	**35.93**	**4.02**	**1.43**	**0.115**
0.2	**35.4**	**31.4**	**9.01**	**0.79**	**2.10**	**44.77**	**0.75**	**40.77**	**80.51**	**1.97**	**39.74**	**4.65**	**1.58**	**0.099**

Table 7. Interfacial and Thermodynamic Parameters of $C_{14}TPB$ Micellization at Different Pectin Concentrations (0.05%, 0.1%, and 0.2% w/v) at 298 K.

[Pectin]/ % (w/v)	γ_{CMC} $(mN\ m^{-1})$	π_{CMC} $(mN\ m^{-1})$	$-(\frac{d\gamma}{dlogC} \times 10^3)$	$\Gamma_{max} \times 10^6$ (mol/m^2)	A_{min} $(nm^2/molecule)$	G_{min} $(KJ/mol$	β	$-\Delta G^0_{mic}$ (KJ/mol)	$-\Delta G^0_{Ads}$ (KJ/mol)	$\frac{\Delta G^0_{Ads}}{\Delta G^0_{mic}}$	$-\Delta G^0_{eff}$ (KJ/mol)	ΔG^0_{ps} (KJ/mol)	$p^{C_{20}}$	P
0	38.3	32.5	13.46	1.18	1.40	32.29	0.34	40.05	67.59	1.68	27.54	-	1.52	0.149
0.05	33.7	35	11.06	0.97	1.71	34.70	0.93	50.56	86.64	1.71	36.08	3.46	2.37	0.122
0.1	31	36.8	11.52	1.01	1.64	30.62	0.90	47.89	84.32	1.76	36.43	3.80	2.45	0.127
0.2	37	31.4	12.66	1.11	1.49	33.20	0.79	44.05	72.33	1.64	28.28	4.70	2.14	0.140

Table 8. Interfacial and Thermodynamic Parameters of C_{16}TPB Micellization at Different Pectin Concentrations (0.05%, 0.1%, and 0.2% w/v) at 298 K.

[Pectin]/% (w/v)	γ_{CMC} $(mN\ m^{-1})$	π_{CMC} $(mN\ m^{-1})$	$-(\frac{d\gamma}{dlogC} \times 10^3)$	$\Gamma_{max} \times 10^6$ (mol/m^2)	A_{min} $(nm^2/molecule)$	G_{min} (KJ/mol)	β	$-\Delta G^0_{mic}$ (KJ/mol)	$-\Delta G^0_{Ads}$ (KJ/mol)	$\frac{\Delta G^0_{Ads}}{\Delta G^0_{mic}}$	$-\Delta G^0_{eff}$ (KJ/mol)	ΔG^0_{ps} (KJ/mol)	$p^{C_{20}}$	P
0	42.3	28.3	9.12	0.80	2.07	52.74	0.29	41.20	76.57	1.85	35.37	-	1.91	0.101
0.05	31.2	36.7	25.10	2.20	0.75	14.09	0.72	47.36	64.04	1.35	16.68	4.31	2.75	0.280
0.1	33.1	34.4	24.87	2.18	0.76	15.15	0.66	43.69	59.46	1.36	15.77	4.70	2.54	0.276
0.2	33.4	33.8	20.42	1.79	0.92	18.50	0.53	39.29	58.17	1.48	18.88	5.55	2.60	0.228

3.2.4. Turbidimetry

A turbidimetric survey has been undertaken to evaluate the stability of oppositely charged colloidal systems as well as to monitor the continuous formation of intermolecular complexes within the bulk medium. The turbidity profiles of pectin-C_nTPB systems (Figure 4A, 4B, and 4C) depict changes in optical density (measured as 100–%T) as a function of surfactant concentration. Key inflection points, marked as T_1, T_2, and T_3 are listed in Tables 3, 4, and 5 for C_{12}TPB, C_{14}TPB, and C_{16}TPB, respectively. For all pectin concentrations, the aggregation behaviour of C_{14}TPB and C_{16}TPB follow a similar qualitative pattern, while C_{12}TPB shows a slight deviation in the early stages. Up to T_1, surfactants do not cause any cloudiness in the system, allowing soluble complexes to form in a homogeneous solution. In this small-scale region, the [surfactant] is insufficient to neutralize the intense charge density of pectin. Consequently, the complexes maintain a high negative charge, preventing the formation of larger aggregates due to electrostatic repulsion. The first visual indication of turbidity has been spotted above T_1, followed by a steep increase through two consecutive regions (T_1-T_2 and T_2-T_3), reaching its peak height at T_3. The initial rapid rise in turbidity (post-T_1 region) is driven by enhanced electrostatic adsorption affinity of C_nTP^+ ions at the pectin surface. Between T_2 and T_3, the inclusion of hydrophobic factors slows down the growth of aggregates. In fact, at higher [C_nTPB], hydrophobic forces strengthen while electrostatic forces weaken, as charge neutralization reduces the overall negative charge of the complexes. The significance of T_2 lies in the fact that it marks the point of maximum adsorption of C_nTPB monomers onto the pectin chain. T_3, on the other hand, refers to the point of maximum liquid-solid phase separation, leading to the accumulation of the largest amount of insoluble complex. The turbidity maximum maintains a just-about constant height ($\sim 98-99\%$) under different conditions, suggesting that variations in pectin concentration and surfactant chain length do not impact the population of the complex aggregates at T_3. The rationale behind the post-T_3 nearly plateau region is likely due to the minimal solubilization of the complex coacervates within the micellar medium. Therefore, the turbidity readings remain relatively invariant, even with the addition of excess surfactant **[111]**. At this stage, after prolonged standing, the turbid solution undergoes slow and partial separation, with the larger particles settling down to a minor deposition of precipitate at the bottom of the cuvette. There are also reports of the dissolution of the larger coacervate particles in the micellar solution, showing a clear downward trend in the turbidity plot **[112, 113]**. The T_1 and T_2 values closely match cac and C_S respectively, when comparing this visual approach to

tensiometry. Interestingly, the T_3 values for both C_{12}TPB and C_{14}TPB are much lower than C_f. This inconsistency is quite understandable, as the measurements of turbidity and surface tension pertain to bulk and surface phenomena, respectively. The transition at T_3 maximizes turbidity, while C_f signals the initiation of pectin-induced surfactant micellization. The distinct interaction mechanisms of each technique can significantly influence the outcomes.

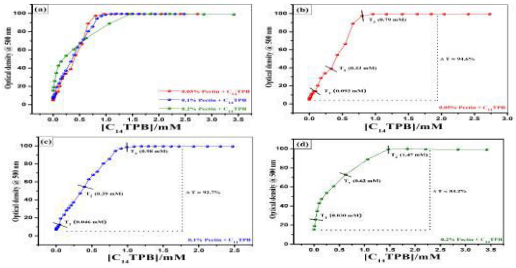

Figure 4A. (a) Variation in turbidity (100 - %T) of pectin-C_{12}TPB mixtures at different pectin concentrations; (b), (c), and (d) present the turbidity profiles for pectin concentrations of 0.05%, 0.1%, and 0.2%, respectively, marking the transition points (T_1, T_2, and T_3). "ΔT" stands for turbidity rise.

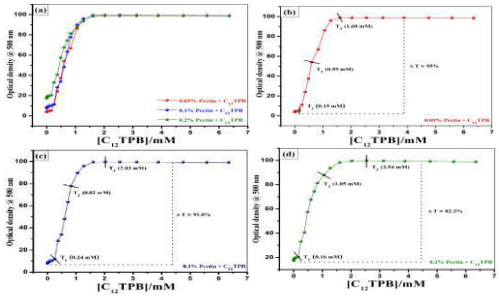

Figure 4B. (a) Variation in turbidity (100 - %T) of pectin-C_{14}TPB mixtures at different pectin concentrations; (b), (c), and (d) present the turbidity profiles for pectin concentrations of 0.05%, 0.1%, and 0.2%, respectively, marking the transition points (T_1, T_2, and T_3). "ΔT" stands for turbidity rise.

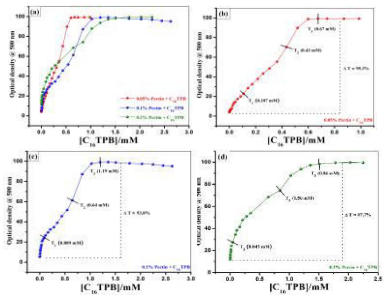

Figure 4C. (a) Variation in turbidity (100 - %T) of pectin-C_{16}TPB mixtures at different pectin concentrations; (b), (c), and (d) present the turbidity profiles for pectin concentrations of 0.05%, 0.1%, and 0.2%, respectively, marking the transition points (T_1, T_2, and T_3). "ΔT" stands for turbidity rise.

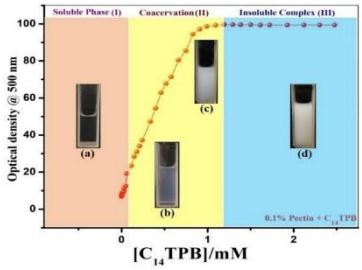

Figure 4D. Observed visual transition of pectin-C_{14}TPB complexes at different turbid phases: (a) soluble, (b) coacervation, and (c) insoluble. Complex coacervation is maximized at the plateau region. The pictures of 1 cm quartz cuvettes containing samples with C_{14}TPB concentrations of (a) 0.063 mM, (b) 0.14 mM, (c) 0.98 mM, and (d) 2.47 mM, at a fixed pectin concentration of 0.1% (w/v).

3.3. Characterization of Pectin-C_{14}TPB Colloidal System

3.3.1. Zeta potential

The role of surface charge on the colloidal physical stability of mixed polymer-surfactant systems can be analyzed by quantifying the zeta potential values. According to Smoluchowski's equation **[114]**, there is a well-established correlation between the zeta potential and the surface charge of the colloidal particles within polymer-surfactant composites. In these systems, molecular associations can be explained on the basis of classical ion-exchange mechanisms **[115]**, wherein the electrostatic interactions favour the entrapment of surfactant ions around the macroions. Moreover, ion-pair formation can be realized in accordance with the associative network of functional groups within the binary system (briefly discussed in Section 3.3.6). Within the zeta potential range of -30 to +30 mV **[116]**, the coacervate particles experience charge stabilization, where coagulation is largely inhibited by the repulsion effect. Precipitation or turbidity may arise in the solution if the net charges of the complexes are not very high (either positive or negative). In fact, electrostatic repulsion between charged particles is the key factor in prolonging the stability of the complex coacervate system. As expected, 0.1% (w/v) pectin in its native state has a highly negative zeta potential (-35.7 mV) under the experimental conditions, attributed to partially ionized carboxylic acid groups (COO^-) along the polysaccharide chain **[117]**. The lower the percentage of methylated carboxyl acid groups (-$COOCH_3$) on the anionic pectin backbone, the higher its negative charge density. Earlier, zeta potential measurements by Chang **[118]** in 0.1 w/v% samples of low (DM 42%), medium (DM 51%), and high (DM 61%) methoxy pectin (pH 3.5) reported values of -32, -28, and -25 mV, respectively. The stoichiometric binding (approximately 1:1 molar ratio) of C_{14}TPB cationic head with anionic pectin segments promotes the continual formation of complex salts in the medium, which carry variable surface charges depending on the polymer-to-surfactant bulk composition ratio.

During charge titration, the adsorption of $C_{14}TP^+$ ions onto the pectin backbone gradually decreases its net negative charge until reaching the charge-neutralization point (CNP) **[119]** (zero charge) at [C_{14}TPB] ≈ 1.52 mM, beyond which excess surfactant imparts a high positive charge (charge reversal) to the system. Thus, the complexes retain the negative charge of pectin at low C_{14}TPB-to-pectin ratios, while higher ratios result in a positive charge. The phenomenon of charge reversal is not a rare finding; rather, it has been encountered in similar systems **[120]**. The development of a positive charge on the composite surface cannot be solely explained by polyanion-mediated pure electrostatic interactions; the hydrophobic nature of the interactions must also be taken into account as a significant contributor to the molecular binding process. Thus, the primary driving force in cooperative binding is the polymer charge density, with surfactant hydrophobicity being a secondary factor. At charge neutralization, the complex composition shows a lower pectin content compared to the surfactant, reflecting their different charge intensities. The observed zeta potential curve (Figure 5) as a function of [C_{14}TPB] exhibits four distinct regions with inflection points ϕ_1, ϕ_2 and ϕ_3 closely correlating with tensiometric results. At very low concentrations, C_{14}TPB monomers induce a rapid decline in the negative charge up to ϕ_1 (0.067 mM), followed by saturation of the polymeric surface within the bulk region. The large triphenyl rings attached to the surfactant head group restrict $C_{14}TP^+$ ions from easy access to the anionic carboxyl groups of pectin, thereby decelerating the neutralization rate. However, upon completion of polymer saturation at ϕ_2 (0.71 mM), the interfacial re-accumulation of incoming surfactant molecules quickens the neutralization process. More importantly, the growth of positive zeta potential beyond the charge equivalence signals the active participation of hydrophobic interactions to take control over the complexation behavior. In the post-ϕ_3 regime (> 2.12 mM), the positive surface charge of the "pectin-stabilized" micellar aggregates causes the electrostatic adsorption of the excess free counterions, therefore scarcely affecting the electrical properties of the system. As can be seen, the overall hierarchy of the rate of zeta potential amplification is as follows: pre-ϕ_1>>ϕ_2 -ϕ_3>$\phi_1 - \phi_2$ >post-ϕ_3. Here, it is noteworthy that after reaching a certain [C_{14}TPB], particle charge becomes less important in sustaining colloidal stability in the long term, leading to a steady transition of the coacervate phase into a precipitate form.

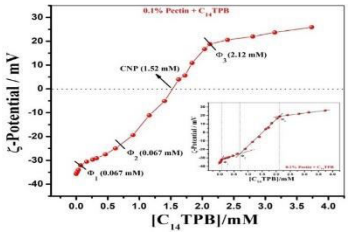

Figure 5. Variation in the ζ-potential (electrical charge) of aqueous pectin-C_{14}TPB solution as a function of C_{14}TPB concentration at 298 K. Charge neutralization of pectin (0.1 wt%) occurs at a C_{14}TPB concentration of 1.52 mM (CNP). Inset: Arrows indicate the corresponding transition points (ϕ_1, ϕ_2, and ϕ_3).

3.3.2. DLS size measurements

Dynamic light scattering (also known as quasi-elastic light scattering) is the most prevalent method for measuring particle sizes at the nanoscale level. The dimensions of the aggregated structures can provide valuable insights into the strength of the polymer-surfactant interactions. During the course of the study, the size parameters, viz., hydrodynamic radius (D_h) and polydispersity index (PDI), for both pectin and pectin-C_{14}TPB complexes with varying pectin concentrations (0.05, 0.1, and 0.2 g%) have been measured and summarized in Table 10. The particle size distribution (PSD) patterns are unimodal, each exhibiting a single distinct peak, as depicted in Figure 6. The DLS data for pectin-C_{14}TPB systems have been conducted only at the cac point. As the coacervate phase develops between the cac and C_S points and remains stable even beyond C_f, accurately interpreting DLS findings becomes increasingly impractical at higher cac concentrations. The DLS data for pure pectin reveals an expected trend in D_h values, with approximately 34% and 29% increases as the pectin concentration shifts from 0.05% to 0.1% g and 0.1% to 0.2% g, respectively. However, in the presence of C_{14}TPB, the charge neutralization effect enforces pectin chains to undergo shrinkage. Upon treatment with the oppositely charged surfactant, the electrostatic movement of $C_{14}TP^+$ ions towards the polymeric surfaces minimizes the interparticle repulsion arising from anionic carboxyl groups along the pectin backbone, resulting in a reduced particle size within the pectin-C_{14}TPB system. The data comparison shows that for each pectin concentration, the D_h values consistently reduce by the same percentage (≈13.6%). These observed findings conclusively establish a strong association between pectin and C_{14}TPB, even at very low surfactant concentrations. According to literature sources **[121]**, complex particles with a D_h parameter ranging from 30 to 500 nm find diverse applications in nanomedicine, particularly in the development of bio-based delivery systems (such as drugs, DNA, RNA, etc.). Both systems have low PDI values (<0.7), indicating high monodispersity **[83]**. However, the pure systems, with relatively higher PDI values, are less monodisperse compared to their mixed counterparts.

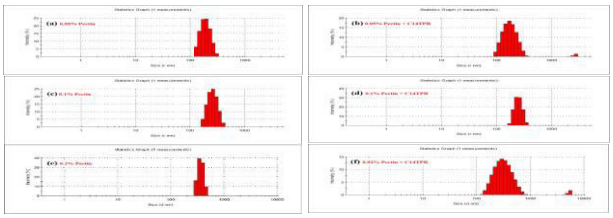

Figure 6. Particle Size Distribution (PSD) profiles (unimodal) for pectin-C_{14}TPB systems in aqueous medium at 298 K: (a) 0.05% pectin, (b) 0.05% pectin + 0.079 mM C_{14}TPB, (c) 0.1% pectin, (d) 0.1% pectin + 0.069 mM C_{14}TPB, (e) 0.2% pectin, (f) 0.2% pectin + 0.048 mM C_{14}TPB; In each instance, [C_{14}TPB] = cac.

3.3.3. Viscometry

Mixed polymer-surfactant systems provide superior features as compared to free polymers, significantly improving polymer functionality. The binding of surfactant molecules along the polymer chains can also give rise to substantial modifications in the conformational structure of polymer in solution. The study of solution viscosity **[122,123]** can probe the polymer

conformations at different stages of bulk complexation. The inherent viscous nature of pure polymer can be understood by considering the entanglement effect throughout the polymer chains. The relative viscosities (η_{rel}) of 0.1 % (w/v) pectin solution have been measured with the progressive addition of $C_{14}TPB$, illustrating the correlation between η_{rel} vs log[$C_{14}TPB$] in Figure 7. The surfactant concentration-dependent viscosity variations in the pectin solution unambiguously point to the polymer-surfactant association. The viscosity-derived curve displays four distinct regions, where the intersection points between each pair of adjacent segments sequentially represent cac (0.12 mM), C_S (0.81 mM), and C_f (1.72 mM), respectively. Below the cac point, adding a small amount of $C_{14}TPB$ has only a little effect on the viscosity of pectin solution. At this stage, the electrostatic induction of $C_{14}TP^+$ ions in close proximity to the anionic sites of pectin leads to a certain degree of compactness in the polymer structure. Thereby, the viscosity of the solution slightly drops until [$C_{14}TPB$] approaches cac. As [$C_{14}TPB$] rises, the viscosity continues to decline more sharply, attaining the minimum value at the binding saturation point (C_S). The electrostatic binding of tiny $C_{14}TPB$ aggregates to the pectin backbone tends to neutralize the polymer charge density, resulting in a highly compact pectin structure. As discussed in Section 3.2.1., at the C_S, all available binding sites on the pectin chains become fully saturated through the adsorption of oppositely charged $C_{14}TPB$ aggregates. Thus, at lower surfactant concentrations, both regions experience a shrinkage in the pectin structure. Initially, there is a gradual decrease in $\eta_{rel,}$ followed by a sharp drop to its minima. The excess $C_{14}TPB$ does not stick to the polymer surface but disperses independently in a monomeric state beyond Cs. Consequently, it exerts negligible influence on the saturated polymer-surfactant complexes. A striking observational feature is the appearance of a dense "coacervate" phase between the cac and C_S regions, expanding into large-scale assemblies through self-association within the C_S and C_f regions. As the colloidal phase transition occurs, the complex solution encounters heightened fluid resistance, causing viscosity to sharply increase until [$C_{14}TPB$] reaches C_f. Following the micellization process, the ion-substitution interactions of free $C_{14}TP^+$ micelles with surfactant-saturated pectin complexes induce the formation of a condensed phase known as "pectin-decorated" micelles. The elongated pectin chain increases viscosity within the micellar solution, but at a slower rate than the preceding stage. However, the final mixture is considerably less viscous than the pure pectin solution, as the complexed pectin still retains some degree of compactness in its structure. In this context, various pectin-based admixtures have been formulated with viscosity-modifying agents, such as amphiphiles, to maximize the beneficial effects of their individual use in the food processing and pharmaceutical industries. More importantly, it is within the realm of feasibility to control the viscosity behaviour of polymer-surfactant blends by fine-tuning both the nature and strength of their interactions as well as the composition concentrations, as deemed necessary.

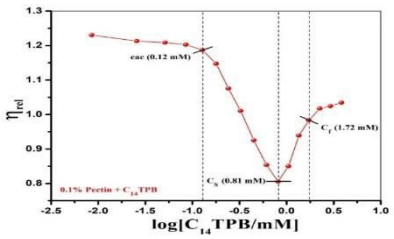

Figure 7. Relative viscosity (η_{rel}) of 0.1% (w/v) pectin solution as a function of added C_{14}TPB concentration at 298 K.

3.2.4. Fluorescence emission studies

Fluorescence quenching spectroscopy is extensively employed to probe the interactions within oppositely charged polymer-surfactant complexes in terms of the relative dynamics between hydrophobic and hydrophilic components. The choice of an appropriate external probe is crucial for sensitively detecting minor polarity shifts during fluorimetric titration. Pyrene, a hydrophobic probe, is particularly suited for this purpose due to its unique photophysical properties **[124]**. Despite its limited water solubility **[125]**, pyrene emits intense fluorescence signals, making it ideal for accurately characterizing medium polarity. The emission spectrum of pyrene features five well-defined peaks (I_1 through I_5), each corresponding to a distinct vibrational transition. As per literature reports **[126, 127]**, fluorescence spectral analysis typically focuses on the intensities of the first and third vibrational peaks, with the other three often overlooked. The micropolarity index, defined as the ratio (I_1/I_3), is a key metric for monitoring complex formation progression with respect to amphiphile concentration (Figure 8). This ratio reveals details about the microenvironment of the probe molecules, with values < and > 1 indicating nonpolar and polar ones, respectively **[23]**. The (I_1/I_3) values of pyrene in 0.05%, 0.1%, and 0.2% aqueous pectin solutions are 1.45, 1.46, and 1.39, respectively, comparable to the value of 1.43 observed in double-distilled water. Pectin is primarily hydrophilic due to its polysaccharide structure, rich in polar hydroxyl (-OH) and carboxyl (-COOH) groups, resulting in minimal impact of pectin concentration on medium polarity. Consequently, pyrene encounters a similar microenvironment in both pectin solutions and double-distilled water. The micellization concentration (cmc) of pure C_{14}TPB is determined by using a sigmoidal curve fitting **[128]** approach to the relevant data plot (Figure 1A (c)). At very low surfactant concentrations, pyrene molecules cannot effectively bind with the limited number of surfactant monomers available in the medium, resulting in an early-stage plateau that indicates steady polarity within the premicellar zone. However, as the system transitions into the micellar phase, the steady state is abruptly disrupted by a sudden drop in polarity. During micellization, pyrene selectively incorporates into the hydrophobic regions of micelles, leading to a reduction in polarity. As the number of free micelles increases, pyrene molecules redistribute within the micellar system. Nevertheless, the overall polarity remains largely unchanged, allowing the system to reach equilibrium, represented by the final plateau. In contrast, the pectin-C_{14}TPB complex systems exhibit a distinctive fluorimetric profile, with the resulting plots deviating from the conventional sigmoidal pattern. The fluorescence intensity curve illustrates a continuous variation in medium hydrophobicity as the assembled complexes undergo structural changes with increasing surfactant concentrations. At lower [C_{14}TPB], the (I_1/I_3) values decrease sharply, passing through the C_1 (cac) point (considered as the midpoint of the nearly vertical segment) without the appearance of an initial plateau and continuing to decline up to C_2 (C_S). Initially, charge interactions on the pectin backbone, wrapped with an increasing number of C_{14}TPB monomers, create hydrophobic domains within the pectin-C_{14}TPB complexes. This results in reduced polarity around pyrene, as evidenced by the marked decrease in (I_1/I_3) values up to the first observed break point, C_1. As coacervates start to accumulate after C_1 (as detailed in Section 3.2.1.), these dense particles effectively shield the probe molecules from the surrounding environment. Consequently, the hydrophobicity of

the complexes increases gradually, further reducing polarity until the pectin chain is fully saturated at C_2. Beyond the saturation point, the polarity (I_1/I_3) exhibits only a slight increase, likely due to turbidity effects, unless a weak hump or C_3 (C_f) is detected. At this stage, pyrene molecules are distributed between free micelles and the saturated pectin surface. The internal structure of the complexes remains fundamentally unaltered after micellization, as evidenced by the steady intrinsic polarity of the system. These observations are further supported by complementary tensiometric data, confirming the reliability of the results.

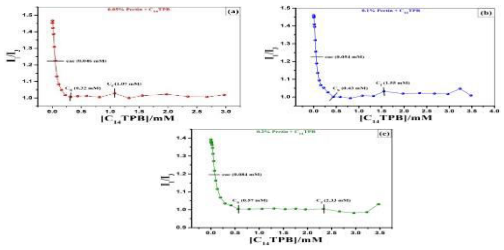

Figure 8. Plots of pyrene fluorescence intensity ratio (I_1/I_3) as a function of [C_{14}TPB] at varying pectin concentrations: (a) 0.05%, (b) 0.1%, and (c) 0.2%.

3.3.5. Time-resolved fluorescence

The time-resolved fluorescence quenching (TRFQ) method **[129, 130]** is used as an alternative approach to validate the transitions involved in polymer-surfactant interaction behavior. Titrimetric analysis compares the lifetime of the probe, coumarin 153 dye **[131]**, in both aqueous and pectin (0.1%) solutions. The relative stability of the dye molecule in the electronically excited state depends on the molecular dynamics of nearby entities. Environmental molecular interactions can favour quenching, leading to a shorter fluorescence lifetime, while the lifetime remains constant in stable conditions and increases with the removal of quenchers. An increase in [C_{14}TPB], extends the average life time (τ_{av}) of dye in both media, but the resulting graph patterns differ significantly. A breakpoint is observed at 0.32 mM (cmc) for pure C_{14}TPB (Figure 9(a)), as determined through sigmoidal fitting analysis **[132]**. In contrast, the pectin-C_{14}TPB system (Figure 9(b)) produces different nanoscale environments that are detected by the dye molecules. Initially, τ_{av} increases gradually from 1.65 ns to 1.77 ns until [C_{14}TPB] reaches 0.12 mM, which is comparable to cac. Afterward, it rises steeply, reaching a maximum at 0.68 M (C_S). The complexation of oppositely charged polymer and surfactant occurs between the cac and C_S regions, where the dye becomes encapsulated in an increasingly less polar environment. This reduced polarity (also supported by steady-state fluorescence) stabilizes its excited state and prolongs the duration of τ_{av}. Subsequently, the τ_{av} suddenly declines to a minimum at 1.27 mM (C_f). Between C_S and C_f, the additional surfactant molecules start to self-aggregate instead of

binding to the polymer. Thus, the surfactant molecules are not fully organized into micelles, which means the dye might not be as effectively protected within the polymer matrix, leading to a shorter fluorescence lifetime. Once the surfactant concentration exceeds C_f, the dye molecules are evenly distributed within the micellar core and saturated polymer components, establishing a relatively uniform and stable environment. This contributes to a steady fluorescence lifetime. In the overall scenario, the τ_{av} versus [C_{14}TPB] profile reveals three break points, which correspond closely to those observed with the steady-state fluorescence method.

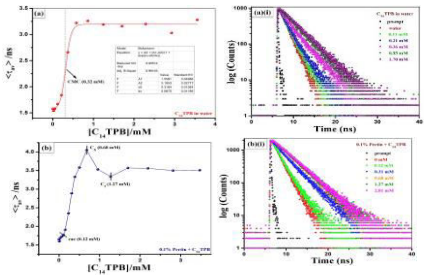

Figure 9. Time-resolved fluorescence lifetime curves of C_{14}TPB in (a) water and (b) 0.1% (w/v) pectin, using coumarin 153 as a probe. The respective decay profiles are presented in (a)(i) and (b)(i), respectively.

3.3.6. FTIR analysis

The chemical structure of the complex coacervate is analysed using FTIR spectroscopy. Key spectral changes, such as band shifts, the appearance of new bands, or the disappearance of existing ones, confirm the complexation between pectin and C_{14}TPB. Figure 10 illustrates the FTIR spectra of pectin, C_{14}TPB, and their complex, whereas Table 12 lists the characteristic vibration peaks observed. The complexation between pectin and C_{14}TPB is most evident in the wavenumber range of 3400–1000 cm^{-1}, with only insignificant or negligible peaks detected outside this region. The strong absorption band of pure pectin at 3383 cm^{-1}, attributed to O-H stretching **[133]**, shows a notable shift and difference in peak shape when compared to the corresponding band at 3361 cm^{-1} in the pectin-C_{14}TPB complex, indicating the involvement of -OH functionality in the interaction process. The weak band at 2936 cm^{-1} (C-H stretching) **[134]**, observed in pectin, is no longer present in the complex. The prominent peaks at 1732 cm^{-1} and 1627 cm^{-1}, corresponding to the carbonyl stretching of esterified carboxylic groups ($COOCH_3$) and free carboxylic groups (-COOH) **[135]**, respectively, exhibit an up-shift in the complex. This can be explained by the variations in the chemical environments surrounding the carbonyl groups. Not surprisingly, the electrostatic interactions between carboxylate groups (COO^-) of pectin and triphenyl phosphonium groups ($-Ph_3P^+$) of C_{14}TPB, which induce a shift of the carbonyl stretching vibrations to a higher wavenumber, now observed at 1638 cm^{-1}. Furthermore, the peaks at 1230 cm^{-1} (C-O stretching of $COOCH_3$) **[136]** and 1012 cm^{-1} (-CH-O-CH stretching) **[134]** show a down-shift and an up-shift, respectively, when compared to the spectrum of the complex. The

characteristic bands at 2917 cm^{-1} and 2848 cm^{-1}, corresponding to the methylene group (-CH_2) vibrations **[137]** in C_{14}TPB, shift to 2924 cm^{-1} and 2853 cm^{-1}, respectively, due to hydrophobic interactions between pectin and the hydrocarbon chains of C_{14}TPB. Moreover, the bands associated with C-H and C=C vibrations **[138]** at 3056 cm^{-1} and 1587 cm^{-1}, respectively, disappear in the complex. So, there is a possibility that the aromatic rings within the pectin-C_{14}TPB complex may undergo disruption. The other less prominent peaks, associated with -CH_2 bending (1436 cm^{-1}) and P-C stretching of phosphonium (1110 cm^{-1}) **[139]**, experience an upward (1440 cm^{-1}) and downward (1105 cm^{-1}) shift, respectively, upon complexation. In conclusion, the comparative FTIR profiles show that the complex retains the characteristics of the pectin backbone, while C_{14}TPB appears to lose its distinct identity within the complex.

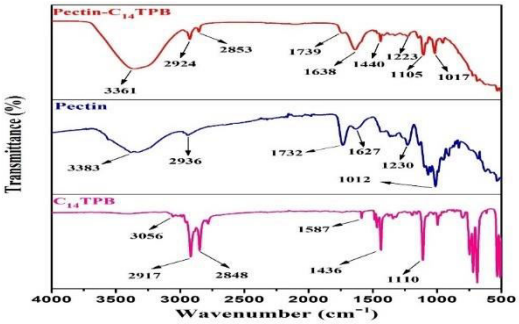

Figure 10. FTIR spectra of pectin, C_{14}TPB, and pectin-C_{14}TPB complex.

3.3.7. X-Ray Diffraction (XRD) characterization

XRD data provides valuable structural insights, particularly in differentiating crystalline and amorphous materials. Sharp diffraction peaks are indicative of a well-ordered crystalline structure, while broadened peaks suggest the presence of an amorphous arrangement. Figure 11 presents the X-ray diffraction patterns of pectin, C_{14}TPB, and the formulated coacervate. The diffractogram of pure pectin shows sharp crystalline peaks at 2θ values of 13.51°, 21.11°, 25.67°, 28.98°, and 40.24°, indicating its well-defined crystalline structure **[140]**. For pure C_{14}TPB, distinct diffraction peaks at 2θ values of 11.52° and 23.33° are observed, reflecting its characteristic crystal arrangement. However, in the complex coacervate, these sharp peaks disappear, yielding a smooth XRD curve characterized by a broad peak at around 19.4^0. This finding confirms that pectin chains are entirely encapsulated by C_{14}TPB molecules, leading to the formation of an amorphous complex driven by a synergy of electrostatic and hydrophobic interactions.

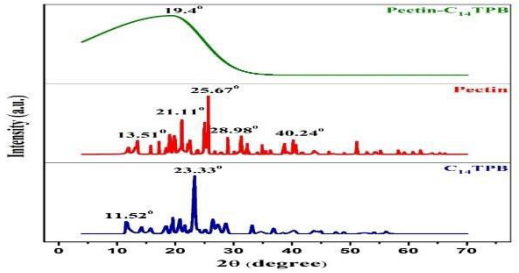

Figure 11. XRD curves of pectin, C_{14}TPB, and pectin-C_{14}TPB complex.

3.3.8. Field Emission Scanning Electron Microscopy (FESEM)

Studying the morphology of polymer-surfactant aggregates uncovers key insights into their complex physicochemical interactions. The complexation ability of surfactants to induce structural changes in polymers predicts that their simultaneous presence is likely to have a substantial effect on the interfacial and solution properties of the surfactant system as well. Using FESEM imaging (Figure 12), the surface micrographs of pectin-C_{14}TPB complexes at various C_{14}TPB concentrations (cac, C_S, C_f, and >>C_f) are characterized. The pectin-C_{14}TPB system exhibits strong associative behaviour, as clearly evidenced by the detailed analysis of surface morphologies observed at different complexation stages. The surface of non-complexed pectin can be seen as the dispersion of several irregular-shaped granular particles. A striking morphological transformation takes place as pectin is associated with cationic C_{14}TPB. The premicellar aggregation of C_{14}TPB monomers, driven by the pectin charge density, commences at the critical aggregation concentration (cac). The induced electrostaticity in the mixed system enhances the compactness of the pectin backbone by suppressing its negative surface charge. It is, of course, salient to correlate the FESEM observations with the DLS data (Section 3.2.2.) obtained at cac, as both reveal a parallel reduction in particle size. After exceeding cac, the enhanced electrostatic interactions enable the complex aggregates to grow larger but more compact at the same time. The condensed, cloudy appearance of the aggregated solution, observed through optical inspection, ensures the already-growing coacervate phase at the saturation point (C_S). However, the surface structure at C_f displays a distinctly unique morphology, as the micelles seem to be implanted on the exterior portions of globular-type polymer clusters. Excess surfactant ([C_{14}TPB] >> C_f) in the micellar solution fragments the larger coacervates into dispersions of smaller entities, fundamentally reconstructing the surface morphology. The coacervation dissolution within the micellar solution also corroborates with the viscosity increment (Section 3.3.3.). In contrast, this phenomenon does not align with the turbidimetry data (Section 3.2.4.), where changes beyond C_f are insignificant. In future endeavours, further research on the interior structural features of coacervates needs to be conducted.

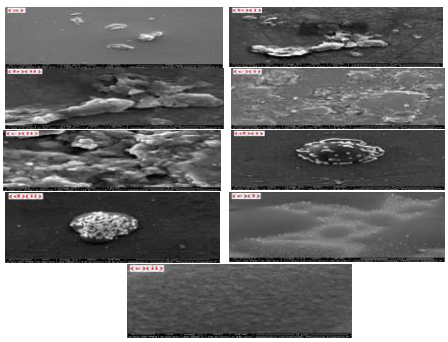

Figure 12. FESEM morphographs of (a) 0.1% pectin as a control; pectin-C_{14}TPB samples at different transitions: (b) (i, ii) cac at 0.069 mM; (c) (i, ii) C_S at 0.46 mM; (d) (i, ii) C_f at 2.12 mM; (e) (i, ii) above C_f at 3.50 mM.

3.3.9. High Resolution Transmission Electron Microscopy (HR-TEM)

TEM analysis of surfactant-complexed polymer structures imparts a physical approach to probing morphological parameters, such as geometric shape and size. A comparison of the surface morphologies of pectin-C_{14}TPB complexes at various C_{14}TPB concentrations (same as FESEM measurements) has been made based on the careful selection of the TEM images. Figures 13 (a-e) present a detailed schematic overview of the respective morphological structures. As shown in Figure 13 (a), the pure pectin in its desolvated state agglomerates into an oval-shaped cluster, composed of spherical particles of varying sizes with radii (Dh) ranging from 180 to 190 nm. During complexation, the high-affinity cation binding sites on pectin, surrounded by $C_{14}TP^+$ ions, become sufficiently activated to establish intermolecular bridge networks with C_{14}TPB molecules. The co-operative binding, primarily controlled by electrostatic attractive forces, gets further reinforced by hydrophobic interactions at higher surfactant concentrations, thereby maximizing their synergistic effect. Accordingly, the surfactant concentration significantly shapes the extent of complexation, as also demonstrated through TEM measurements. At the critical aggregation concentration (cac), monomeric $C_{14}TP^+$ ions bind to the pectin chain, resulting in the formation of small spherical aggregates that measure between 120 and 140 nm in radius. As per expectation, the electrostatic dominance in the lower concentration range of surfactant induces compactness in the spherical surface structure, which is congruent with the DLS analysis. The transition of [C_{14}TPB] from cac to C_S causes the complexes to enlarge in size (≈ 250 nm), yet their spherical architecture remains unchanged. At C_f, near-spherical micellar aggregates with slightly greater dimensions (≈ 280 nm) have been detected, creaming at the top of the pectin surface. This scenario is also well supported by FESEM characterization (Figure 12 (d) (i, ii)). TEM observations have led us to the conclusion that the presence of C_{14}TPB forces the pectin chains to shrink initially, followed by enlargement at higher surfactant concentrations. However, in the higher micellar environment ([C_{14}TPB] > C_f), the spherical arrangements collapse, causing the complex coacervate to disintegrate into a large number of tiny granular dispersions. This finding is particularly significant in light of the viscosity increment following the micellization concentration. In such a colloidal system, the integral role of surfactant concentration in modulating the inherent structure of the complexes as well as in understanding the relative interaction strength cannot be overlooked.

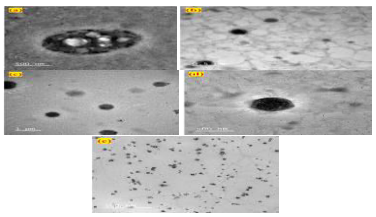

Figure 13. (a), (b), (c), (d), and (e) display corresponding HR-TEM images of the same samples analyzed with FESEM.

3.3.10. Fluorescence microscopy

Fluorescence microscopy **[141, 142]** photographs have significantly amplified the visualization of microstructural features in polymer-surfactant aggregates, providing strong support for the findings from FESEM and HR-TEM analyses. Pectin, a carboxylate-rich

multivalent electrolyte, potently distributes charges throughout the medium, utilizing multiple high-affinity cation-binding sites along its molecular chain. Pectin and the cationic surfactant C_{14}TPB interact via ion-exchange, leading to a coacervate system that vividly illustrates their electrostatic association. During the imaging study, pectin-C_{14}TPB complex solutions are examined over a wide range of [C_{14}TPB]. Microscopy images (Figure 14 (a), (b)) displaying intense fluorescent spots labeled with DPH dye are selected for the analysis of coacervation phenomena. Below the C_S of the pectin-C_{14}TPB system, the dye molecules are not so effective in visualizing the complex coacervates. This is due to the formation of minor aggregates that elude detection by the fluorescent probe. In fact, at the pre-C_S stage, the coacervate particles do not have enough interior space to effectively confine dye molecules, rendering smaller aggregates undetectable **[143]**. At sufficiently high concentrations of C_{14}TPB, particularly above C_S, DPH molecules can readily penetrate deep into the larger aggregates, leading to the development of distinct and observable fluorescent spots. Microscope images at higher micellization concentrations (above C_f) are not taken to avoid any interference from the precipitation effect. Hence, the images are reported only at C_S and C_f, but neither below C_S nor above C_f. It can be seen that the aggregates are non-uniformly dispersed throughout the sample solution, with no observable structure. Interestingly, the complex aggregates appear significantly larger and denser at C_f compared to C_S, manifesting varying binding affinities between pectin and C_{14}TPB depending on the concentration of C_{14}TPB. Indeed, the micellar population surrounding the saturated pectin chains plays a pivotal role in driving the evolution of small aggregates into larger entities. Therefore, it follows that the polymer-to-surfactant ratio in the mixture will certainly have an influence on the complexation process and, in turn, the coacervate structure. The coacervate particles dragging microscopic micelles create highly stable colloidal formulations, with superior encapsulation efficiencies for bioactive molecules (such as drugs) compared to other delivery systems.

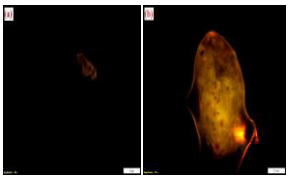

Figure 14. Microscopic images of pectin-C_{14}TPB complex coacervates taken at (a) C_S (0.46 mM), (b) C_f (2.12 mM); [pectin] = 0.1% (w/v), Scale bar = 10 µm.

3.3.11. The compositional phase transitions of the complex coacervate

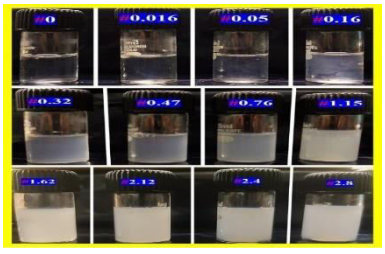

Figure 15. Phase behaviour of 0.1% (w/v) pectin/C_{14}TPB mixtures, with C_{14}TPB concentrations labeled above each bottle, showcasing the effects of increasing surfactant levels on the system.

4. Conclusions and Future Perspectives

Herein, we have performed experimental and visual investigation into the formation of complex coacervates between pectin and alkyltriphenylphosphonium bromides (C_nTPB), utilizing a wide range of interface and bulk techniques, including tensiometry, conductometry, turbidimetry, zeta potential, DLS, viscometry, fluorimetry (steady-state and time-resolved), FTIR, XRD, FESEM, HR-TEM, and fluorescence microscopy. The key findings are summarized as follows:

(i) The complexation between anionic pectin and cationic C_nTPB surfactants is largely controlled by the combined interplay of two fundamental molecular forces: concentration-dependent electrostatic and hydrophobic interactions. The initial phase of complexation is driven by an electrostatic mechanism, wherein C_nTP^+ ions are effectively immobilized on the negatively charged pectin surface. This is subsequently followed by hydrophobic-induced growth and stabilization of the complexes.

(ii) The strength and efficiency of this molecular association are strongly influenced by the surfactant hydrophobicity and the polymer charge density. Stronger binding affinities are observed with higher pectin concentrations and longer hydrocarbon chains in the surfactant tail, emphasizing the importance of these factors in determining complex stability.

(iii) The complexes formed at different stages exhibit behavioral changes in various physicochemical properties, including surface activity, ionic mobility, cloudiness, bulk polarity, fluidity, surface charge, and structural morphology. These variations reflect the dynamic nature of the interaction process between pectin and C_nTPB.

(iv) At the outset, pectin chains undergo shrinkage due to rapid charge neutralization, resulting in a more compact structure. However, as surfactant concentration increases, there is a noticeable growth in particle size, indicating a transition to a more extended and possibly more organized structure.

(v) The onset of the coacervate phase occurs within a specific concentration range, between the critical aggregation concentration (cac) and the polymer saturation concentration (C_S). This observation aligns with established literature, confirming that coacervation appears within this well-defined concentration window, where optimal conditions are achieved.

This investigation provides valuable experimental data and detailed explanations of observed behaviors, which may potentially improve the predictive accuracy of colloid chemists in formulating new colloidal systems. We look forward to advanced surface-sensitive spectroscopic techniques, such as neutron reflectivity (NR) and small-angle neutron scattering (SANS), enabling us to uncover more precise details about complex surfaces in the future. The distinct combination of a hydrophilic surface and a hydrophobic core in coacervate structures makes these systems exceptionally well-suited for delivery applications, particularly in cellular biology. The growing fascination with pectin-based complex

coacervates holds great promise for advancements in the food industry, which may uncover the substantial practical importance of this work. Despite the extensive efforts undertaken, establishing a correlation between experimental findings and theoretical frameworks remains challenging. A collaborative approach that merges experimental and theoretical research is essential for unlocking the potential to design a broad spectrum of novel bio-based materials.

References

(1) Sing CE, Perry SL. Recent progress in the science of complex coacervation. Soft Matter. 2020;16(12):2885-914.

(2) Timilsena YP, Akanbi TO, Khalid N, Adhikari B, Barrow CJ. Complex coacervation: Principles, mechanisms and applications in microencapsulation. International journal of biological macromolecules. 2019 Jan 1;121:1276-86.

(3) Sing CE. Development of the modern theory of polymeric complex coacervation. Advances in colloid and interface science. 2017 Jan 1;239:2-16.

(4) Llamas S, Guzman E, Ortega F, Baghdadli N, Cazeneuve C, Rubio RG, Luengo GS. Adsorption of polyelectrolytes and polyelectrolytes-surfactant mixtures at surfaces: A physico-chemical approach to a cosmetic challenge. Advances in colloid and interface science. 2015 Aug 1;222:461-87.

(5) Moschakis T, Biliaderis CG. Biopolymer-based coacervates: Structures, functionality and applications in food products. Current Opinion in Colloid & Interface Science. 2017 Mar 1;28:96-109.

(6) Saravanan M, Rao KP. Pectin–gelatin and alginate–gelatin complex coacervation for controlled drug delivery: Influence of anionic polysaccharides and drugs being encapsulated on physicochemical properties of microcapsules. Carbohydrate Polymers. 2010 May 5;80(3):808-16.

(7) Black KA, Priftis D, Perry SL, Yip J, Byun WY, Tirrell M. Protein encapsulation via polypeptide complex coacervation. ACS Macro Letters. 2014 Oct 21;3(10):1088-91.

(8) Mi X, McTigue WC, Joshi PU, Bunker MK, Heldt CL, Perry SL. Thermostabilization of viruses via complex coacervation. Biomaterials science. 2020;8(24):7082-92.

(9) Hamouma M, Delbos A, Dalmazzone C, Colin A. Polymer surfactant interactions in oil enhanced recovery processes. Energy & Fuels. 2021 May 13;35(11):9312-21.

(10) Valley B, Jing B, Ferreira M, Zhu Y. Rapid and efficient coacervate extraction of cationic industrial dyes from wastewater. ACS applied materials & interfaces. 2019 Jan 28;11(7):7472-8.

(11) Kayitmazer AB, Koksal AF, Iyilik EK. Complex coacervation of hyaluronic acid and chitosan: effects of pH, ionic strength, charge density, chain length and the charge ratio. Soft Matter. 2015;11(44):8605-12.

(12) Seyrig C, Kignelman G, Thielemans W, Le Griel P, Cowieson N, Perez J, Baccile N. Stimuli-induced nonequilibrium phase transitions in polyelectrolyte–surfactant complex coacervates. Langmuir. 2020 Jul 23;36(30):8839-57.

(13) Gradzielski M, Hoffmann I. Polyelectrolyte-surfactant complexes (PESCs) composed of oppositely charged components. Current Opinion in Colloid & Interface Science. 2018 May 1;35:124-41.

(14) Rumyantsev AM, Borisov OV, de Pablo JJ. Structure and Dynamics of Hybrid Colloid–Polyelectrolyte Coacervates. Macromolecules. 2023 Feb 14;56(4):1713-30.

(15) Kizilay E, Kayitmazer AB, Dubin PL. Complexation and coacervation of polyelectrolytes with oppositely charged colloids. Advances in colloid and interface science. 2011 Sep 14;167(1-2):24-37.

(16) Devi N, Sarmah M, Khatun B, Maji TK. Encapsulation of active ingredients in polysaccharide–protein complex coacervates. Advances in colloid and interface science. 2017 Jan 1;239:136-45.

(17) Zhou J, Wan Y, Cohen Stuart MA, Wang M, Wang J. Effects of Control Factors on Protein–Polyelectrolyte Complex Coacervation. Biomacromolecules. 2023 Nov 13.

(18) Zheng J, Van der Meeren P, Sun W. New insights into protein–polysaccharide complex coacervation: Dynamics, molecular parameters, and applications. Aggregate. 2023:e449.

(19) Kayitmazer AB. Thermodynamics of complex coacervation. Advances in colloid and interface science. 2017 Jan 1;239:169-77.

(20) Madinya JJ, Tjo H, Meng X, Ramírez Marrero IA, Sing CE, Perry SL. Surface Charge Density and Steric Repulsion in Polyelectrolyte–Surfactant Coacervation. Macromolecules. 2023.

(21) Li D, Kelkar MS, Wagner NJ. Phase behavior and molecular thermodynamics of coacervation in oppositely charged polyelectrolyte/surfactant systems: A cationic polymer JR 400 and anionic surfactant SDS mixture. Langmuir. 2012 Jul 17;28(28):10348-62.

(22) Liu Z, Shang Y, Feng J, Peng C, Liu H, Hu Y. Effect of hydrophilicity or hydrophobicity of polyelectrolyte on the interaction between polyelectrolyte and surfactants: molecular dynamics simulations. The Journal of Physical Chemistry B. 2012 May 10;116(18):5516-26.

(23) Mondal BB, Banik R, Ghosh S. Impact of 2, 2, 2-trifluoroethanol (TFE) on hydrophobicity enhancement in the aggregation of Sodium N-Dodecanoyl Sarcosinate (SDDS) with nonionic Hydroxyethyl Cellulose. Colloids and Surfaces A: Physicochemical and Engineering Aspects. 2023 Nov 15:132781.

(24) Tiwari S, Mall C, Solanki PP. CMC studies of CTAB, SLS & tween 80 by spectral and conductivity methodology to explore its potential in photogalvanic cell. Surfaces and Interfaces. 2020 Mar 1;18:100427.

(25) Seres L, Varga N, Juhász Á, Csapó E. Novel approaches to monitoring the formation of self-assembled colloids composed of cationic surfactants and alginate polysaccharide. Surfaces and Interfaces. 2024 Jun 1;49:104430.

(26) Uehara N, Ogawa M. Interaction of poly (N-isopropylacrylamide) with sodium dodecyl sulfate below the critical aggregation concentration. Langmuir. 2014 Jun 10;30(22):6367-72.

(27) Noreen A, Akram J, Rasul I, Mansha A, Yaqoob N, Iqbal R, Tabasum S, Zuber M, Zia KM. Pectins functionalized biomaterials; a new viable approach for biomedical applications: A review. International journal of biological macromolecules. 2017 Aug 1;101:254-72.

(28) Joshi N, Rawat K, Bohidar HB. Influence of structure, charge, and concentration on the pectin–calcium–surfactant complexes. The Journal of Physical Chemistry B. 2016 May 12;120(18):4249-57.

(29) Watrelot AA, Le Bourvellec C, Imberty A, Renard CM. Interactions between pectic compounds and procyanidins are influenced by methylation degree and chain length. Biomacromolecules. 2013 Mar 11;14(3):709-18.

(30) Alba K, Bingham RJ, Gunning PA, Wilde PJ, Kontogiorgos V. Pectin conformation in solution. The Journal of Physical Chemistry B. 2018 Jul 2;122(29):7286-94.

(31) Martău GA, Mihai M, Vodnar DC. The use of chitosan, alginate, and pectin in the biomedical and food sector—biocompatibility, bioadhesiveness, and biodegradability. Polymers. 2019 Nov 8;11(11):1837.

(32) Eivazzadeh-Keihan R, Noruzi EB, Aliabadi HA, Sheikhaleslami S, Akbarzadeh AR, Hashemi SM, Gorab MG, Maleki A, Cohan RA, Mahdavi M, Poodat R. Recent advances on biomedical applications of pectin-containing biomaterials. International Journal of Biological Macromolecules. 2022 Jul 6.

(33) Wu X, Sun H, Qin Z, Che P, Yi X, Yu Q, Zhang H, Sun X, Yao F, Li J. Fully physically crosslinked pectin-based hydrogel with high stretchability and toughness for biomedical application. International journal of biological macromolecules. 2020 Apr 15;149:707-16.

(34) Tortorella S, Inzalaco G, Dapporto F, Maturi M, Sambri L, Buratti VV, Chiariello M, Franchini MC, Locatelli E. Biocompatible pectin-based hybrid hydrogels for tissue engineering applications. New Journal of Chemistry. 2021;45(47):22386-95.

(35) Dziadek M, Dziadek K, Salagierski S, Drozdowska M, Serafim A, Stancu IC, Szatkowski P, Kopec A, Rajzer I, Douglas TE, Cholewa-Kowalska K. Newly crosslinked chitosan-and chitosan-pectin-based hydrogels with high antioxidant and potential anticancer activity. Carbohydrate Polymers. 2022 Aug 15;290:119486.

(36) Eivazzadeh-Keihan R, Ahmadpour F, Aliabadi HA, Radinekiyan F, Maleki A, Madanchi H, Mahdavi M, Shalan AE, Lanceros-Méndez S. Pectin-cellulose hydrogel, silk fibroin and magnesium hydroxide nanoparticles hybrid nanocomposites for biomedical applications. International Journal of Biological Macromolecules. 2021 Dec 1;192:7-15.

(37) Kodoth AK, Ghate VM, Lewis SA, Prakash B, Badalamoole V. Pectin-based silver nanocomposite film for transdermal delivery of Donepezil. International journal of biological macromolecules. 2019 Aug 1;134:269-79.

(38) Lemos TS, de Souza JF, Fajardo AR. Magnetic microspheres based on pectin coated by chitosan towards smart drug release. Carbohydrate Polymers. 2021 Aug 1;265:118013.

(39) Nižić L, Potaś J, Winnicka K, Szekalska M, Erak I, Gretić M, Jug M, Hafner A. Development, characterisation and nasal deposition of melatonin-loaded pectin/hypromellose microspheres. European Journal of Pharmaceutical Sciences. 2020 Jan 1;141:105115.

(40) Khotimchenko M. Pectin polymers for colon-targeted antitumor drug delivery. International journal of biological macromolecules. 2020 Sep 1;158:1110-24.

(41) Zhu J, Zhong L, Chen W, Song Y, Qian Z, Cao X, Huang Q, Zhang B, Chen H, Chen W. Preparation and characterization of pectin/chitosan beads containing porous starch embedded with doxorubicin hydrochloride: A novel and simple colon targeted drug delivery system. Food Hydrocolloids. 2019 Oct 1;95:562-70.

(42) Freitas CM, Coimbra JS, Souza VG, Sousa RC. Structure and applications of pectin in food, biomedical, and pharmaceutical industry: A review. Coatings. 2021 Aug 1;11(8):922.

(43) Assifaoui A, Lerbret A, Uyen HT, Neiers F, Chambin O, Loupiac C, Cousin F. Structural behaviour differences in low methoxy pectin solutions in the presence of divalent cations (Ca 2+ and Zn 2+): A process driven by the binding mechanism of the cation with the galacturonate unit. Soft Matter. 2015;11(3):551-60.

(44) Celus M, Kyomugasho C, Van Loey AM, Grauwet T, Hendrickx ME. Influence of pectin structural properties on interactions with divalent cations and its associated functionalities. Comprehensive Reviews in Food Science and Food Safety. 2018 Nov;17(6):1576-94.

(45) Kyomugasho C, Gwala S, Christiaens S, Kermani ZJ, Van Loey AM, Grauwet T, Hendrickx ME. Pectin nanostructure influences pectin-cation interactions and in vitro-bioaccessibility of Ca2+, Zn2+, Fe2+ and Mg2+-ions in model systems. Food Hydrocolloids. 2017 Jan 1;62:299-310.

(46) Huang ST, Yang CH, Lin PJ, Su CY, Hua CC. Multiscale structural and rheological features of colloidal low-methoxyl pectin solutions and calcium-induced sol–gel transition. Physical Chemistry Chemical Physics. 2021;23(35):19269-79.

(47) John J, Ray D, Aswal VK, Deshpande AP, Varughese S. Dissipation and strain-stiffening behavior of pectin–Ca gels under LAOS. Soft Matter. 2019;15(34):6852-66.

(48) Bonnaud M, Weiss J, McClements DJ. Interaction of a food-grade cationic surfactant (lauric arginate) with food-grade biopolymers (pectin, carrageenan, xanthan, alginate, dextran, and chitosan). Journal of agricultural and food chemistry. 2010 Sep 8;58(17):9770-7.

(49) Chang Y, McLandsborough L, McClements DJ. Physicochemical properties and antimicrobial efficacy of electrostatic complexes based on cationic ε-polylysine and anionic pectin. Journal of agricultural and food chemistry. 2011 Jun 22;59(12):6776-82.

(50) Xiong W, Li Y, Ren C, Li J, Li B, Geng F. Thermodynamic parameters of gelatin-pectin complex coacervation. Food Hydrocolloids. 2021 Nov 1;120:106958.

(51) Souza CJ, da Costa AR, Souza CF, Tosin FF, Garcia-Rojas EE. Complex coacervation between lysozyme and pectin: Effect of pH, salt, and biopolymer ratio. International journal of biological macromolecules. 2018 Feb 1;107:1253-60.

(52) Li Y, Zhao Q, Huang Q. Understanding complex coacervation in serum albumin and pectin mixtures using a combination of the Boltzmann equation and Monte Carlo simulation. Carbohydrate polymers. 2014 Jan 30;101:544-53.

(53) Zhang HH, Huang GQ, Geng X, Teng J, Xiao JX. Interaction between ovalbumin and pectin and coacervate characterization. Colloid and Polymer Science. 2021 Jun;299:943-53.

(54) Archut A, Klost M, Drusch S, Kastner H. Complex coacervation of pea protein and pectin: Contribution of different protein fractions to turbidity. Food Hydrocolloids. 2023 Jan 1;134:108032.

(55) Du Q, Zhou L, Lyu F, Liu J, Ding Y. The complex of whey protein and pectin: Interactions, functional properties and applications in food colloidal systems–A review. Colloids and Surfaces B: Biointerfaces. 2022 Feb 1;210:112253.

(56) Xu AY, Melton LD, Ryan TM, Mata JP, Rekas A, Williams MA, McGillivray DJ. Effects of polysaccharide charge pattern on the microstructures of β-lactoglobulin-pectin complex coacervates, studied by SAXS and SANS. Food Hydrocolloids. 2018 Apr 1;77:952-63.

(57) Ke J, Chang Y, Nie C, Yang R, Ma J, Zhao T, Deng X, Zhang Z. Formation mechanism of complex coacervation of chayote (Sechium edule) pectin-sodium caseinate in aqueous solution. Food Hydrocolloids. 2023 Oct 1;143:108902.

(58) Bengoechea C, Jones OG, Guerrero A, McClements DJ. Formation and characterization of lactoferrin/pectin electrostatic complexes: Impact of composition, pH and thermal treatment. Food Hydrocolloids. 2011 Jul 1;25(5):1227-32.

(59) Gonçalves RA, Holmberg K, Lindman B. Cationic surfactants: A review. Journal of Molecular Liquids. 2023 Feb 1:121335.

(60) Damen M, Groenen AJ, Van Dongen SF, Nolte RJ, Scholte BJ, Feiters MC. Transfection by cationic gemini lipids and surfactants. MedChemComm. 2018;9(9):1404-25.

(61) Kuznetsova DA, Gaynanova GA, Vasileva LA, Sibgatullina GV, Samigullin DV, Sapunova AS, Voloshina AD, Galkina IV, Petrov KA, Zakharova LY. Mitochondria-targeted cationic liposomes modified with alkyltriphenylphosphonium bromides loaded with hydrophilic drugs: Preparation, cytotoxicity and colocalization assay. Journal of materials chemistry B. 2019;7(46):7351-62.

(62) Hao N, Chen X, Jayawardana KW, Wu B, Sundhoro M, Yan M. Shape control of mesoporous silica nanomaterials templated with dual cationic surfactants and their antibacterial activities. Biomaterials science. 2016;4(1):87-91.

(63) Yarza F, Morantes CF, Montes ML, Bellotti N, Salduondo J, Yapar S, Cravero F, Sánchez RM. Quantification of the distribution of cetylpyridinium chloride on the external and internal surfaces of montmorillonite: Relevance in antifungal activity assessment. Materials Chemistry and Physics. 2020 Oct 1;253:123390.

(64) Zhou C, Wang Y. Structure–activity relationship of cationic surfactants as antimicrobial agents. Current Opinion in Colloid & Interface Science. 2020 Feb 1;45:28-43.

(65) Liu K, Zheng L, Ma C, Göstl R, Herrmann A. DNA–surfactant complexes: self-assembly properties and applications. Chemical Society Reviews. 2017;46(16):5147-72.

(66) Akram M, Lal H. Exploring the binding mode of ester-based cationic gemini surfactants with calf thymus DNA: A detailed physicochemical, spectroscopic and theoretical study. Bioorganic Chemistry. 2022 Feb 1;119:105555.

(67) Xu L, Chen J, Feng L, Dong S, Hao J. Loading capacity and interaction of DNA binding on catanionic vesicles with different cationic surfactants. Soft Matter. 2014;10(45):9143-52.

(68) Madejová J, Barlog M, Jankovič Ľ, Slaný M, Pálková H. Comparative study of alkylammonium-and alkylphosphonium-based analogues of organo-montmorillonites. Applied Clay Science. 2021 Jan 1;200:105894.

(69) Arkhipova DM, Ermolaev VV, Milyukov VA, Valeeva FG, Gaynanova GA, Zakharova LY. Micellar nanocontainers based on sterically hindered cationic phosphonium amphiphiles. Russian Chemical Bulletin. 2022 Apr;71(4):804-11.

(70) Gainanova GA, Vagapova GI, Syakaev VV, Ibragimova AR, Valeeva FG, Tudriy EV, Galkina IV, Kataeva ON, Zakharova LY, Latypov SK, Konovalov AI. Self-assembling systems based on amphiphilic alkyltriphenylphosphonium bromides: Elucidation of the role of head group. Journal of colloid and interface science. 2012 Feb 1;367(1):327-36.

(71) Vagapova G, Ibragimova A, Zakharov A, Dobrynin A, Galkina I, Zakharova L, Konovalov A. Novel biomimetic systems based on polyethylene glycols and amphiphilic phosphonium salt. Self-organization and solubilization of hydrophobic guest. European polymer journal. 2013 May 1;49(5):1031-9.

(72) Vagapova GI, Valeeva FG, Gainanova GA, Syakaev VV, Galkina IV, Zakharova LY, Latypov SK, Konovalov AI. Novel self-assembling systems based on amphiphilic phosphonium salt and polyethylene glycol. Kinetic arguments for synergetic aggregation behavior. Colloids and Surfaces A: Physicochemical and Engineering Aspects. 2013 Feb 20;419:186-93.

(73) Thakkar K, Bharatiya B, Shah DO, Ray D, Aswal VK, Bahadur P. Interaction of ionic liquid type cationic surfactants with triton X-100 nonionic micelles. Colloids and Surfaces A: Physicochemical and Engineering Aspects. 2015 Nov 5;484:547-57.

(74) Patil RS, Shaikh VR, Patil PD, Borse AU, Patil KJ. Volumetric properties of alkyltrimethylammonium bromides in aqueous solutions. Journal of Chemical & Engineering Data. 2016 Jan 14;61(1):195-206.

(75) Zakharova LY, Kaupova GI, Gabdrakhmanov DR, Gaynanova GA, Ermakova EA, Mukhitov AR, Galkina IV, Cheresiz SV, Pokrovsky AG, Skvortsova PV, Gogolev YV. Alkyl triphenylphosphonium surfactants as nucleic acid carriers: complexation efficacy toward DNA decamers, interaction with lipid bilayers and cytotoxicity studies. Physical Chemistry Chemical Physics. 2019;21(30):16706-17.

(76) Ibragimova AR, Gabdrakhmanov DR, Valeeva FG, Vasileva LA, Sapunova AS, Voloshina AD, Saifina AF, Gubaidullin AT, Danilaev MP, Egorova SR, Tyryshkina AA. Mitochondria-targeted mesoporous silica nanoparticles noncovalently modified with triphenylphosphonium cation: Physicochemical characteristics, cytotoxicity and intracellular uptake. International Journal of Pharmaceutics. 2021 Jul 15;604:120776.

(77) Gaynanova GA, Vagapova GI, Valeeva FG, Vasilieva EA, Galkina IV, Zakharova LY, Sinyashin OG. A novel supramolecular catalytic system based on amphiphilic triphenylphosphonium bromide for the hydrolysis of phosphorus acid esters. Colloids and Surfaces A: Physicochemical and Engineering Aspects. 2016 Jan 20;489:95-102.

(78) Vasilieva EA, Samarkina DA, Gaynanova GA, Lukashenko SS, Gabdrakhmanov DR, Zakharov VM, Vasileva LA, Zakharova LY. Self-assembly of the mixed systems based on cationic surfactants and different types of polyanions: The influence of structural and concentration factors. Journal of Molecular Liquids. 2018 Dec 15;272:892-901.

(79) Smith GN, Brown P, James C, Rogers SE, Eastoe J. The effect of solvent and counterion variation on inverse micelle CMCs in hydrocarbon solvents. Colloids and Surfaces A: Physicochemical and Engineering Aspects. 2016 Apr 5;494:194-200.

(80) Owoyomi O, Ige J, Soriyan O. Mixed micelles of tetradecyltrimethylammonium and n-alkyltriphenylphosphonium bromides. Journal of dispersion science and technology. 2014 Jun 3;35(6):826-31.

(81) Goswami A, Hassan PA, Bhagwat SS. Static and dynamic surface tension behaviour of a triblock copolymer and a non ionic surfactant mixture. Colloids and Surfaces A: Physicochemical and Engineering Aspects. 2015 Nov 5;484:190-6.

(82) Pal A, Maan R. Interactional behavior of surface active ionic liquid lauryl isoquinolinium bromide and anionic polyelectrolyte poly (4-styrenesulfonic acid-co-maleic acid) sodium salt in aqueous solution. Colloid and Polymer Science. 2018 Mar;296:483-94.

(83) Mondal BB, Banik R, Ghosh S. Detailed physicochemical study and thermodynamic aspects of the interaction between nonionic cellulose derivative hydroxyethyl cellulose and anionic surfactant sodium N-dodecanoyl sarcosinate in aqueous media. Journal of the Taiwan Institute of Chemical Engineers. 2023 Aug 1;149:104982.

(84) Tamm F, Drusch S. Impact of enzymatic hydrolysis on the interfacial rheology of whey protein/pectin interfacial layers at the oil/water-interface. Food Hydrocolloids. 2017 Feb 1;63:8-18.

(85) Xiao J, Liu F, Garamus VM, Almásy L, Handge UA, Willumeit R, Mu B, Zou A. Insights into the interactions among surfactin, betaines, and PAM: Surface tension, small-angle neutron scattering, and small-angle X-ray scattering study. Langmuir. 2014 Apr 1;30(12):3363-72.

(86) Raffa P. Interactions between an associative amphiphilic block polyelectrolyte and surfactants in water: Effect of charge type on solution properties and aggregation. Polymers. 2021 May 25;13(11):1729.

(87) Hansson P. Self-assembly of ionic surfactants in polyelectrolyte solutions: a model for mixtures of opposite charge. Langmuir. 2001 Jul 10;17(14):4167-80.

(88) Bahramian A, Thomas RK, Penfold J. The adsorption behavior of ionic surfactants and their mixtures with nonionic polymers and with polyelectrolytes of opposite charge at the air–water interface. The Journal of Physical Chemistry B. 2014 Mar 13;118(10):2769-83.

(89) Staples E, Tucker I, Penfold J, Warren N, Thomas RK, Taylor DJ. Organization of polymer− surfactant mixtures at the air− water interface: sodium dodecyl sulfate and poly (dimethyldiallylammonium chloride). Langmuir. 2002 Jun 25;18(13):5147-53.

(90) Taylor DJ, Thomas RK, Penfold J. The adsorption of oppositely charged polyelectrolyte/surfactant mixtures: neutron reflection from dodecyl trimethylammonium bromide and sodium poly (styrene sulfonate) at the air/water interface. Langmuir. 2002 Jun 11;18(12):4748-57.

(91) Thomas RK, Penfold J. Thermodynamics of the air–water interface of mixtures of surfactants with polyelectrolytes, oligoelectrolytes, and multivalent metal electrolytes. The Journal of Physical Chemistry B. 2018 Dec 4;122(51):12411-27.

(92) Campbell RA, Yanez Arteta M, Angus-Smyth A, Nylander T, Varga I. Effects of bulk colloidal stability on adsorption layers of poly (diallyldimethylammonium chloride)/sodium dodecyl sulfate at the air–water interface studied by neutron reflectometry. The Journal of Physical Chemistry B. 2011 Dec 29;115(51):15202-13.

(93) Ansari AA, Kamil M, Kabir-ud-Din. Polymer-surfactant interactions and the effect of tail size variation on micellization process of cationic ATAB surfactants in aqueous medium. Journal of dispersion science and technology. 2013 May 1;34(5):722-30.

(94) Mitra D, Bhattacharya SC, Moulik SP. Physicochemical studies on the interaction of gelatin with cationic surfactants alkyltrimethylammonium bromides (ATABs) with special focus on the behavior of the hexadecyl homologue. The Journal of Physical Chemistry B. 2008 May 29;112(21):6609-19.

(95) Chakraborty T, Chakraborty I, Ghosh S. Sodium carboxymethylcellulose− CTAB interaction: a detailed thermodynamic study of polymer−surfactant interaction with opposite charges. Langmuir. 2006 Nov 21;22(24):9905-13.

(96) Zheng Y, Lu X, Lai L, Yu L, Zheng H, Dai C. The micelle thermodynamics and mixed properties of sulfobetaine-type zwitterionic Gemini surfactant with nonionic and anionic surfactants. Journal of Molecular Liquids. 2020 Feb 1;299:112108.

(97) Kumar M, Bhardwaj A, Elahi D, Singh OG, Singh SK, Gatasheh MK, Irfan M, Singh N, Srivastava A. Counterion association of ionic drugs with sodium tetradecyl sulfate in the aqueous medium. ACS omega. 2023 Nov 20;8(48):45942-51.

(98) Mahbub S, Mia ML, Roy T, Akter P, Uddin AR, Rub MA, Hoque MA, Asiri AM. Influence of ammonium salts on the interaction of fluoroquinolone antibiotic drug with sodium dodecyl sulfate at different temperatures and compositions. Journal of Molecular Liquids. 2020 Jan 1;297:111583.

(99) Sultana N, Dey J, Ismail K. Effect of added counterions on the micellization of cetylpyridinium chloride in the presence of acetonitrile–water mixture. Journal of Chemical & Engineering Data. 2019 Sep 20;64(10):4193-205.

(100) Sheng R, Ding QY, Ren ZH, Li DN, Fan SC, Quan XF, Wang Y, Yi MT, Zhang YX, Cao YX, Wang H. Interfacial and micellization behavior of binary mixture of amino sulfonate amphoteric surfactant and octadecyltrimethyl ammonium bromide: Effect of short chain alcohol and its chain length. Journal of Molecular Liquids. 2021 Jul 15;334:116064.

(101) Bhadani A, Shrestha RG, Koura S, Endo T, Sakai K, Abe M, Sakai H. Self-aggregation properties of new ester-based gemini surfactants and their rheological behavior in the presence of cosurfactant—monolaurin. Colloids and Surfaces A: Physicochemical and Engineering Aspects. 2014 Nov 5;461:258-66.

(102) Rub MA, Azum N, Asiri AM. Interaction of cationic amphiphilic drug nortriptyline hydrochloride with TX-100 in aqueous and urea solutions and the studies of physicochemical parameters of the mixed micelles. Journal of Molecular Liquids. 2016 Jun 1;218:595-603.

(103) Kwaśniewska D, Kiewlicz J. Study of interaction between cationic surfactant (CTAB) and ascorbic acid/ascorbic acids derivatives by tensiometric and spectroscopic methods. Journal of Molecular Liquids. 2022 May 15;354:118917.

(104) Mańko DI, Zdziennicka AN, Jańczuk BR. Thermodynamic properties of rhamnolipid micellization and adsorption. Colloids and Surfaces B: Biointerfaces. 2014 Jul 1;119:22-9.

(105) Shah SK, Bhattarai A. Interfacial and micellization behavior of cetyltrimethylammonium bromide (CTAB) in water and methanol-water mixture at 298.15 to 323.15 K. Journal of Chemistry. 2020;2020(1):4653092.

(106) Bhattarai A. Studies of aggregation properties of surfactant with and without polyelectrolyte in water and binary mixture of methanol-water from the surface tension measurements. Journal of Molecular Liquids. 2020 Aug 15;312:113438.

(107) Gaudin T, Lu H, Fayet G, Berthauld-Drelich A, Rotureau P, Pourceau G, Wadouachi A, Van Hecke E, Nesterenko A, Pezron I. Impact of the chemical structure on amphiphilic properties of sugar-based surfactants: A literature overview. Advances in Colloid and Interface Science. 2019 Aug 1;270:87-100.

(108) Ben-Moshe M, Magdassi S. Surface activity and micellar properties of anionic gemini surfactants and their analogues. Colloids and Surfaces A: Physicochemical and Engineering Aspects. 2004 Dec 10;250(1-3):403-8.

(109) Kumar D, Rub MA, Azum N, Asiri AM. Mixed micellization study of ibuprofen (sodium salt) and cationic surfactant (conventional as well as gemini). Journal of Physical Organic Chemistry. 2018 Jan;31(1):e3730.

(110) Parekh P, Varade D, Parikh J, Bahadur P. Anionic–cationic mixed surfactant systems: micellar interaction of sodium dodecyl trioxyethylene sulfate with cationic gemini surfactants. Colloids and Surfaces A: Physicochemical and Engineering Aspects. 2011 Jul 20;385(1-3):111-20.

(111) Pan H, Bu YN, Lian WJ, Zhang SL, Sun SH, Han J. Solution and rheological properties of cationic cellulose/gemini surfactant: Effect of the alkyl chain and spacer length. Carbohydrate polymers. 2020 Jun 15;238:116200.

(112) Lundin M, Macakova L, Dedinaite A, Claesson P. Interactions between chitosan and SDS at a low-charged silica substrate compared to interactions in the bulk the effect of ionic strength. Langmuir. 2008 Apr 15;24(8):3814-27.

(113) Bu H, Kjøniksen AL, Elgsaeter A, Nyström B. Interaction of unmodified and hydrophobically modified alginate with sodium dodecyl sulfate in dilute aqueous solution: Calorimetric, rheological, and turbidity studies. Colloids and Surfaces A: Physicochemical and Engineering Aspects. 2006 Apr 20;278(1-3):166-74.

(114) Yang A, McKenzie BE, Yi Y, Khair AS, Garoff S, Tilton RD. Effect of polymer/surfactant complexation on diffusiophoresis of colloids in surfactant concentration gradients. Journal of Colloid and Interface Science. 2023 Jul 15;642:169-81.

(115) Tonigold K, Varga I, Nylander T, Campbell RA. Effects of aggregates on mixed adsorption layers of poly (ethylene imine) and sodium dodecyl sulfate at the air/liquid interface. Langmuir. 2009 Apr 7;25(7):4036-46.

(116) Lowry GV, Hill RJ, Harper S, Rawle AF, Hendren CO, Klaessig F, Nobbmann U, Sayre P, Rumble J. Guidance to improve the scientific value of zeta-potential measurements in nanoEHS. Environmental Science: Nano. 2016;3(5):953-65.

(117) Chang Y, McLandsborough L, McClements DJ. Interactions of a cationic antimicrobial (ε-polylysine) with an anionic biopolymer (pectin): An isothermal titration calorimetry, microelectrophoresis, and turbidity study. Journal of agricultural and food chemistry. 2011 May 25;59(10):5579-88.

(118) Chang Y, McLandsborough L, McClements DJ. Cationic antimicrobial (ε-polylysine)–anionic polysaccharide (pectin) interactions: influence of polymer charge on physical stability and antimicrobial efficacy. Journal of agricultural and food chemistry. 2012 Feb 22;60(7):1837-44.

(119) Khan N, Brettmann B. Intermolecular interactions in polyelectrolyte and surfactant complexes in solution. Polymers. 2018 Dec 31;11(1):51.

(120) Nizri G, Lagerge S, Kamyshny A, Major DT, Magdassi S. Polymer–surfactant interactions: Binding mechanism of sodium dodecyl sulfate to poly (diallyldimethylammonium chloride). Journal of Colloid and Interface Science. 2008 Apr 1;320(1):74-81.

(121) Fischer K, Schmidt M. Pitfalls and novel applications of particle sizing by dynamic light scattering. Biomaterials. 2016 Aug 1;98:79-91.

(122) Ramos GA, Akanji LT, Afzal W. A novel surfactant–polymer/alkaline–surfactant–polymer formulation for enhanced oil recovery (eor) processes. Energy & Fuels. 2020 Jan 10;34(2):1230-9.

(123) El Aferni A, Guettari M, Kamli M, Tajouri T, Ponton A. A structural study of a polymer-surfactant system in dilute and entangled regime: Effect of high concentrations of surfactant and polymer molecular weight. Journal of Molecular Structure. 2020 Jan 5;1199:127052.

(124) Song X, Guo H, Yu S, Huang L, Redshaw C, Zhang Q, Ye R, Feng X. Experimental and theoretical studies of the effect of molecular conformation on the photophysical properties in the pyrene system. Dyes and Pigments. 2023 Feb 1;210:111036.

(125) Piñeiro L, Novo M, Al-Soufi W. Fluorescence emission of pyrene in surfactant solutions. Advances in colloid and interface science. 2015 Jan 1;215:1-2.

(126) Singh G, Singh G, Kancharla S, Kang TS. Complexation behavior of β-lactoglobulin with surface active ionic liquids in aqueous solutions: An experimental and computational approach. The Journal of Physical Chemistry B. 2019 Feb 14;123(9):2169-81.

(127) Singh G, Kaur M, Aswal VK, Kang TS. Aqueous colloidal systems of bovine serum albumin and functionalized surface active ionic liquids for material transport. RSC advances. 2020;10(12):7073-82.

(128) Halasová T, Krouská J, Mravec F, Pekař M. Hyaluronan-surfactant interactions in physiological solution studied by tensiometry and fluorescence probe techniques. Colloids and Surfaces A: Physicochemical and Engineering Aspects. 2011 Nov 5;391(1-3):25-31.

(129) Mora AK, Singh PK, Nath S. Controlled sequestration of DNA intercalated drug by polymer–surfactant supramolecular assemblies. The Journal of Physical Chemistry B. 2016 May 5;120(17):4143-51.

(130) Mondek J, Mravec F, Halasová T, Hnyluchová Z, Pekař M. Formation and dissociation of the acridine orange dimer as a tool for studying polyelectrolyte–surfactant interactions. Langmuir. 2014 Jul 29;30(29):8726-34.

(131) Li S, Yu A, Lu R. Fluorescence quenching of coumarin 153 by hydroxyl-functionalized room temperature ionic liquids. Spectrochimica Acta Part A: Molecular and Biomolecular Spectroscopy. 2016 Aug 5;165:161-6.

(132) Biswas B, Shah D, Cox-Vázquez SJ, Vázquez RJ. Sensing cholesterol-induced rigidity in model membranes with time-resolved fluorescence spectroscopy and microscopy. Journal of Materials Chemistry B. 2024;12(27):6570-6.

(133) Hassan EA, Abou Elseoud WS, Abo-Elfadl MT, Hassan ML. New pectin derivatives with antimicrobial and emulsification properties via complexation with metal-terpyridines. Carbohydrate Polymers. 2021 Sep 15;268:118230.

(134) Perumal P, Christopher Selvin P, Selvasekarapandian S. Characterization of biopolymer pectin with lithium chloride and its applications to electrochemical devices. Ionics. 2018 Oct;24:3259-70.

(135) Ma X, Jing J, Yu J, Wang J, Zhu H, Hu Z. Synthesis and characterization of a novel apple pectin–Fe (III) complex. ACS omega. 2021 Jan 7;6(2):1391-9.

(136) Bichara LC, Alvarez PE, Bimbi MV, Vaca H, Gervasi C, Brandán SA. Structural and spectroscopic study of a pectin isolated from citrus peel by using FTIR and FT-Raman spectra and DFT calculations. Infrared Physics & Technology. 2016 May 1;76:315-27.

(137) Li S, Xing P, Hou Y, Yang J, Yang X, Wang B, Hao A. Formation of a sheet-like hydrogel from vesicles via precipitates based on an ionic liquid-based surfactant and β-cyclodextrin. Journal of Molecular Liquids. 2013 Dec 1;188:74-80.

(138) Lu F, Zhang S, Zheng L. Dispersion of multi-walled carbon nanotubes (MWCNTs) by ionic liquid-based phosphonium surfactants in aqueous solution. Journal of Molecular Liquids. 2012 Sep 1;173:42-6.

(139) Cai Y, Hu Y, Xiao J, Song L, Fan W, Deng H, Gong X, Chen Z. Morphology, thermal and mechanical properties of poly (styrene-acrylonitrile)(SAN)/clay nanocomposites from organic-modified montmorillonite. Polymer-Plastics Technology and Engineering. 2007 May 9;46(5):541-8.

(140) Namratha S, Sreejit V, Preetha R. Fabrication and evaluation of physicochemical properties of probiotic edible film based on pectin–alginate–casein composite. International Journal of Food Science & Technology. 2020 Apr;55(4):1497-505.

(141) Najafi H, Jerri HA, Valmacco V, Petroff MG, Hansen C, Benczedi D, Bevan MA. Synergistic polymer–surfactant-complex mediated colloidal interactions and deposition. ACS applied materials & interfaces. 2020 Mar 3;12(12):14518-30.

(142) Chatterjee S, Prajapati R, Bhattacharya A, Mukherjee TK. Microscopic evidence of “necklace and bead”-like morphology of polymer–surfactant complexes: a comparative study on poly (vinylpyrrolidone)–sodium dodecyl sulfate and poly (diallyldimethylammonium chloride)–sodium dodecyl sulfate systems. Langmuir. 2014 Aug 19;30(32):9859-65.

(143) Jiao L, Zhang L, Guan W, Lu C. Fluorescence visualization of interactions between surfactants and polymers. RSC advances. 2016;6(92):88954-8.

CHAPTER-IV

Influence of Surfactant Alkyl Tail Length and Polymer Concentration on the Interfacial and Bulk Behavior in Electrostatic Assemblies of Cationic Alkyltrimethylammonium Bromides and Anionic Pectin

Influence of Surfactant Alkyl Tail Length and Polymer Concentration on the Interfacial and Bulk Behavior in Electrostatic Assemblies of Cationic Alkyltrimethylammonium Bromides and Anionic Pectin

ABSTRACT

The study of mixed polymer-surfactant complexes stands at the forefront of colloid and interface science, making significant contributions to a broad spectrum of industrial formulations. The association between polymers and surfactants of opposite charge leads to phase separation, which can manifest as either coacervation (liquid-liquid) or precipitation (solid-liquid). Spontaneous complex formation can induce profound physicochemical modifications in polymers to achieve the desired features both in the bulk and at the air-water interface. The primary focus of the present research endeavour is to elucidate the effects of polymer charge density and surfactant hydrophobicity on their complexation behaviour. Herein, we provide a concise overview of the interaction between the polyanion pectin and cationic alkyltrimethylammonium bromide (C_nTAB) surfactants, which are characterized by their varying alkyl tail lengths (n values of 12, 14, 16, and 18). A comprehensive dataset from tensiometry, conductometry, and turbidimetry measurements has been systematically analysed to explore the fundamental physicochemical behaviour of the interaction. Experimental findings confirm that each of the surfactants (i.e., CTAB, TTAB, DTAB, and OTAB) exhibits strong molecular interactions with pectin. The bulk complexation originates from electrostatic binding between oppositely charged groups, while the hydrophobicity of the surfactant tails provides further stabilization. The thermodynamic parameters of interest for the investigated systems have been calculated on the basis of the tensiometric and conductometric data. To provide visual support for the structural changes, high-resolution scanning electron microscopy (HR-SEM) and high-resolution transmission electron microscopy (HR-TEM) imaging techniques have been employed. Fluorescence microscopy analysis of the pectin-DTAB system has further validated the evidence of electrostatic coupling between the oppositely charged polymer and surfactant. Taking into account the versatile applications of pectin specifically in the food and pharmaceutical industries, this study is highly relevant and impactful.

1. Introduction

The study of polymer-surfactant complexes has been the topic of continual research for many years, focusing on understanding the thermodynamic and mechanistic aspects of the interactions while also assessing their suitability for the improvement of human quality of life. The synergistic combination of polymers and surfactants delivers a multitude of beneficial features across multiple sectors, including pharmaceutical science **[1]**, oil recovery **[2-4]**, drug encapsulation **[5,6]**, paints and coatings **[7]**, personal care products **[8,9]**, and surface modification **[10]**. Polymer-surfactant mixtures typically display superior performance and functionality compared to their individual components. In these formulations, polymers contribute to rheological control **[11,12]** and colloidal stability **[13]**, while surfactants facilitate emulsification **[14]** and modulate the interfacial properties **[15]** through micelle formation. To date, researchers have successfully developed a wide variety of

feasible combinations, such as neutral polymers with ionic **[16,17]** or non-ionic surfactants **[18]**, polyelectrolytes with surfactants carrying either like **[19,20]** or opposite charges **[21,22]**, and more. Based on the evaluation of previously published papers, Burke et al. **[23]** stated that the non-ionic polymers exhibit very little interaction with cationic surfactants, but interact considerably with anionic surfactants. In contrast, polyelectrolytes containing charged functional groups demonstrate exceptional complexation behaviour with oppositely charged surfactants, enabling more significant modifications to the features of a given system. Recent advancements in the polymer industry have gifted colloid chemists with various synthetic polyelectrolytes, unlocking new avenues for the design of novel polyelectrolyte-surfactant systems and creating promising opportunities to investigate their behaviours in future research. Polymer-surfactant binding is largely controlled by two key molecular forces: electrostatic and hydrophobic interactions, or a combination of both. In the case of an ionic surfactant binding to an uncharged polymer, the interaction is solely driven by hydrophobic forces. In contrast, systems involving oppositely charged polyelectrolytes and surfactants, termed "strongly interacting systems," exhibit much more complex dynamics from a physicochemical standpoint, as observed by Petkova et al. **[24]**. Moreover, it is possible to amplify the interactions between the two components by manipulating a number of variables, including the molecular weight and composition of the polymer, the micellar size and tail length of the surfactant, the charge density of both, as well as the introduction of specific additives (salt, solvent, etc.) **[25]**. Researchers have already made use of a wide range of relevant conventional and advanced technologies: tensiometry, conductometry, ITC **[26]**, turbidimetry **[27]**, fluorimetry **[17]**, rheology **[28]**, etc. for understanding interaction mechanisms; DLS **[29]**, CV **[30]** for particle size measurement, and zeta potential **[31]** for surface charge estimation; FTIR **[32]**, Raman **[33]**, NMR, EPR **[34]**, ESR **[35]**, XRD **[36]**, SANS **[34]**, SAXS **[37]**, neutron reflectometry **[38],** etc. for complex structure characterization; FESEM, HRTEM **[17]**, AFM **[39]**, CLSM **[40],** etc. for surface morphology visualization; TGA-DTA, DSC, **[41]** etc. for thermal stability analysis, and so on. However, there are still a lot of controversies and unresolved issues concerning this scientific discipline.

Pectin is a naturally occurring, water-soluble polyelectrolyte commercially extracted from apple and citrus fruits. The chemical structure of the complex heteropolysaccharide primarily consists of partially methylated D-galacturonic acid (GalA) units, along with various natural sugar side chains **[42]**. Thus, the polyanionic nature of pectin is inherently associated with the presence of non-methylated GalA residues. The degree of esterification (DE) or methylation (DM) of pectin is determined by calculating the ratio of methylated carboxyl groups ($COOCH_3$) to total carboxyl groups in GalA units. This characteristic influences the physicochemical properties and functionality of pectin, classifying it into two categories: high methoxy pectin (HMP, DE > 74%) and low methoxy pectin (LMP, DE < 34%) **[43]**. Pectin, considered as one of the finest natural polymers, has attracted a lot of attention due to its several beneficial approaches in diverse fields. Biocompatibility, biodegradability, bioavailability, and non-toxicity **[44]** are all excellent biological features of pectin, which enhance its utility as a pharmaceutical ingredient, particularly in drug delivery systems (DDSs) **[45]**. In the food industry, the multifunctional role of pectin is unparalleled, acting as an emulsifier, stabilizer, thickener, and gelling agent **[46]** to improve the overall product

quality. So far, researchers have accepted pectin as one of the promising candidates for the development of numerous polymer-based materials, including hydrogels **[47]**, solid polymer electrolytes **[48]**, biocomposite films **[49]**, and nanoparticles **[50]** in the electrochemical and biomedical fields. The anionic backbone of this biopolymer imparts a strong binding affinity for divalent and trivalent cations (such as Ca^{2+}, Zn^{2+}, Fe^{2+}, Pb^{2+}, Fe^{3+}, Al^{3+} etc.) **[51-54]** as well as cationic surfactants **[55]**, which substantially modifies its gelation properties. Moreover, the literature extensively documents the complex interactions of pectin with various biochemical entities, including biopolymers **[56]**, proteins **[57]**, drugs **[58]**, lipids **[59]**, bile salts **[60]**, lipases **[61]**, fatty acids **[62]**, and others. McClements et al. **[63]** investigated the interaction between pectin and two different surfactants, namely, DTAB and SDS, using ITC measurements. Joshi et al. **[44]** conducted a study on the role of the cross-linker Ca^{2+} ion in the pectin-surfactant complexation with cationic (DTAB, CTAB), anionic (SDS), and non-ionic (TX-100) surfactants. However, a comparative study on the interaction behaviour of pectin with a homologous series of cationic surfactants has not yet been addressed in the literature.

Surfactants or surface-active agents are well-known for their tendency to form various-shaped micellar-like aggregates (typically spherical), owing to self-assembly, and reduce the interfacial tension of the liquid significantly (both in aqueous and non-aqueous media) at and above a specific concentration, known as the critical micelle concentration (cmc) **[64]**. A key feature of the amphiphilic systems is the simultaneous location of both hydrophilic and hydrophobic moieties within the same molecule. This dual nature gives rise to their unique qualities in solution. The classification of cationic surfactants is based on the positively charged hydrophilic part of their structure. The importance of cationic surfactants is projected to expand significantly in the coming years, driven by their extensive applications in enhanced oil recovery **[65]**, emulsification **[66]**, dispersion of nanoparticles **[67]**, corrosion inhibition **[68]**, dye solubilization **[69]**, and wetting processes **[70]** across various industries. Mastering the art of surfactant formulations maximizes the aforementioned benefits, especially when synergistically combined with a variety of additives. In this context, alkyltrimehylammonium bromides (C_nTAB) are repeatedly complexed with different types of charged or non-charged polymers. In a recent study, Brinatti et al. **[71]** reported on the interactions between C_nTAB and anionic cellulose nanocrystals (CNCs). In another study, Schulze-Zachau and Braunschweig **[72]** investigated the binding interactions between the oppositely charged polyanion (NaPSS) and cationic C_nTAB surfactants, with alkyl chain lengths of n = 12, 14, and 16.

Over the past decade, growing interest in this field has led to the publication of some excellent review articles **[73-76]** that discuss everything from foundational concepts to recent advancements while also offering valuable perspectives for future research directions. Lately, Chatterjee et al. **[77]** have proposed the most conventional “necklace and bead” model to shed light on the binding mechanisms in PVP-SDS and PDADMAC-SDS systems. Building on key outcomes from prior studies, the current research plan aims to conduct a comprehensive investigation into the interactions between anionic pectin and homologous cationic surfactants (C_nTAB). Hopefully, the experimental observations will provide valuable

insights into the fundamental mechanisms of the interaction behaviour, as well as the various components influencing the complex stability.

2. **Experimental section**

2.1. Materials

The carbohydrate polymer, pectin (poly-D-galacturonic acid methyl ester) was obtained from Thomas Baker Chemicals (India). All the cationic surfactants used, (1-dodecyl)trimethylammonium bromide (DTAB, 99% purity), tetradecyltrimethylammonium bromide (TTAB, 99% purity), (1-hexadecyl)trimethylammonium bromide (CTAB, 98% purity), and octadecyltrimethylammonium bromide (OTAB, 99% purity) were purchased from Alfa Aesar (A Johnson Matthey Company, UK). There was no further purification done with any of the samples. The structures of pectin and surfactants are shown in Scheme 1. AR-grade pyrene, coumarin 153, and 1,6-diphenyl-1,3,5-hexatriene (DPH) were procured from Sigma Aldrich (USA). These materials were utilized straight out of the package. Double-distilled water was used to prepare all of the experimental solutions. In this study, the concentration of pectin solution was taken as 0.05, 0.1 and 0.2% (w/v). All of the experiments were carried out at a steady temperature of 298 K.

Table 1: Chemical Name, Molecular Formula, Symbol, Tail Group, and Molecular Weight (MW) of the C_nTAB Surfactants used in this work.

Chemical Name	Molecular Formula	Symbol	Tail Group	MW (g/mol)
(1-dodecyl)trimethylammonium bromide	$C_{15}H_{34}N^+ Br^-$	DTAB	$-C_{12}H_{25}$	308.34
Tetradecyltrimethylammonium bromide	$C_{17}H_{38}N^+ Br^-$	TTAB	$-C_{14}H_{29}$	336.40
(1-hexadecyl)trimethylammonium bromide	$C_{19}H_{42}N^+ Br^-$	CTAB	$-C_{16}H_{33}$	364.46
Octadecyltrimethylammonium bromide	$C_{21}H_{46}N^+ Br^-$	OTAB	$-C_{18}H_{37}$	392.52

Pectin	Alkyl trimethylammonium bromide (C_nTAB)
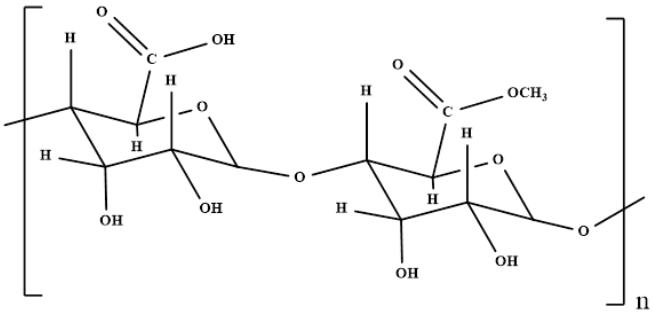	**DTAB**  **TTAB**  **CTAB**  **OTAB** 

Scheme 1. Molecular structures of pectin (left) and alkyltrimethylammonium bromide (C_nTAB) surfactants (right).

2.2. Methods

2.2.1. Tensiometry

For the analysis of surface activity of the pectin-C_nTABs interacting systems at the air/solution interface, a calibrated tensiometer (Krüss, Germany) instrument was used. The resultant data were collected by making the use of a platinum ring (du Noüy) detachment technique. Before each experiment, the platinum ring was thoroughly cleaned with double-distilled water and acetone consecutively and after that, it was burned in ethanol flame sufficiently until glowing. 5 mL of the aqueous pectin solutions (0.05, 0.1 and 0.2% w/v) were taken in a properly cleaned double-distilled glass container to initiate the experiment. A concentrated aqueous solution of C_nTABs were then quantitatively added by a Hamilton microsyringe to the pectin sample in several steps as per requirements of the experiment. After each step of amphiphile addition, the pectin-C_nTABs systems were thoroughly mixed with the help of a magnetic stirrer and a time-gap of 10 min was maintained before taking each tensiometric data. The whole system was connected to a thermostatic water bath to maintain the desired constant temperature at 298 K. The accuracy of the collected data was ± 0.1 mN m^{-1} for each measurement. The developed break points (cac, C_s and C_f) for the experimental systems were detected form the relevant surface tension (γ) vs log [surfactant]

plots. For the pure amphiphiles, the same procedure was applied to estimate the CMC values in aqueous medium by observing the single sharp break point from the tensiometric plots.

2.2.2. Conductometry

To get information about the ionic mobility of the above interacted systems, a conductometer (Jenway, UK) of 1 cm^{-1} cell constant value was used for the specific conductance (κ) measurements with an accuracy of ± 0.5%. Initially, a thermostated glass container was taken to place 7 mL of different (% w/v) pectin solutions, in which the surfactant solutions were added dropwise in same fashion as described in section 2.2.1. The identification of the inflection points for both systems was performed by plotting the specific conductance (μS) with [surfactant] (mM).

2.2.3. Fluorescence emission study

Fluorescence emission spectra of pyrene as a hydrophobic probe were recorded in a Perkin-Elmer LS 55 spectrofluorimeter (USA) taking the solution in a transparent quartz cuvette (path length 1 cm) at a constant temperature of 298 K using a water flow thermostat. The fluorescent probe was excited at the wavelength of 332 nm, and its concentration was 0.1 μM in the experiment. Before doing the spectral analysis, the instrumental setup involved monitoring the wavelength ranges between 350 to 450 nm and the slit widths at 14 and 2.5 nm for excitation and emission, respectively. The scan rate was fixed at 250 nm/min throughout the experiment. Among the five emission peaks of pyrene, the fluorescence was measured by taking the ratio of intensities of first (I_1) and third (I_3) vibronic peaks, at 373 and 383 nm, respectively.

2.2.4. Turbidimetry

The turbidity visualized in the study of oppositely charged pectin-C_nTABs interaction was measured in a UV-vis spectrophotometer (model Shimadzu 1601, Japan) at 298 K. Baseline correction was made in the preliminary step of each experiment using double-distilled water. The turbidimetric titration was carried out by adding C_nTABs progressively with the help of a Hamilton microsyringe into a quartz cuvette containing 2.5 mL of different % (w/v) pectin solution. After each addition, the solution was stirred and allowed for 2-3 minutes to get steady before taking the measurement. The spectral data were recorded in transmittance (% T) mode in the wavelength region of 200-800 nm. The absorbance (100 - %T) values taken at the midpoint of the experimental wavelength region i.e. λ = 500 nm were plotted against [C_nTABs].

2.2.5. Field emission scanning electron microscopy (FESEM)

The outer surface morphologies of pectin-C_nTABs samples were investigated by high resolution field emission scanning electron microscope (model Apreo S, Cam Scan Series-2, Cambridge Scanning Company, UK). Prior to measurements, a 2 µL drop of the experimental sample solution was placed onto a tiny glass slide by a 10 µL micropipette giving several hours for spreading and drying.

2.2.6. High resolution transmission electron microscopy (HR-TEM)

TEM images of C_nTABs-interacted pectin were taken using a JEOL JEM 2010 (Tokyo, Japan) high-resolution transmission electron microscope (HR-TEM) operating at an accelerating voltage of 200 kV. In order to prepare the TEM sample by drop casting method, the experimental solution drop was introduced onto a gold-coated copper grid, allowing some time for spreading. Following that, slow drying (for solvent removal) of the sample was applied for several hours under a vacuum to obtain more accurate morphological pattern during imaging process.

2.2.7. Fluorescence microscopy

Fluorescence imaging of the pectin-DTAB system was carried out using Olympus IX73 (one-deck system) inverted microscope. The fluorophore used in the experiment was DPH. The ethanolic DPH solution (0.1 mM) was added to the polymer-surfactant system, keeping the final mixture overnight before taking the images using FTIC filter.

3. Results and discussion

3.1. Pure C_nTAB in aqueous medium

A brief discussion of the amphiphilic behaviours of pure C_nTAB in the aqueous medium is necessary prior to analyzing their interactive nature in pectin environment. Increasing the alkyl groups (-CH_2) in the lengthened hydrocarbon chain of a surfactant tail is expected to substantially lower the critical micelle concentration (CMC) in aqueous solutions **[78, 79]**. The micellization of pure amphiphiles in the aqueous medium has been investigated by tensiometry, conductometry, and fluorimetry methods at 298 K. In Fig. 1A (a-c), 1B (a-c), 1C (a-c) and 1D (a-c), the experimental plots have been shown and the initial points of micellization have been pointed out in each instance. The measured CMC values closely match those reported in the literature **[80]**. According to tensiometric data, the CMC magnitude has decreased by a factor of ≈ 4 in both the cases of DTAB to TTAB and TTAB to CTAB, while it has decreased by a factor of ≈ 3.35 from CTAB to OTAB. Thus, elongating the hydrophobic chain length leads to a substantial decrease in the CMC values.

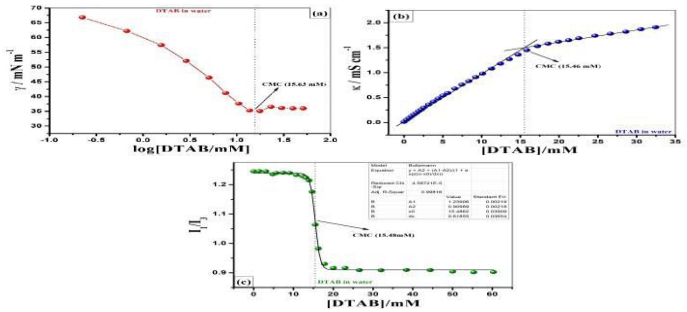

Figure 1A. Identification of the CMC of DTAB in aqueous medium at 298 K using (a) tensiometry, (b) conductometry, and (c) fluorimetry methods

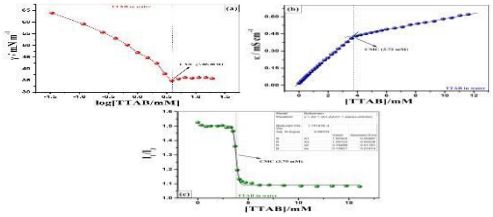

Figure 1B. Identification of the CMC of TTAB in aqueous medium at 298 K using (a) tensiometry, (b) conductometry, and (c) fluorimetry methods.

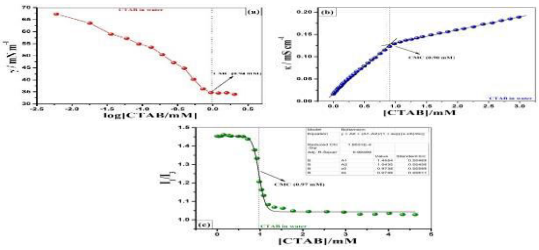

Figure 1C. Identification of the CMC of CTAB in aqueous medium at 298 K using (a) tensiometry, (b) conductometry, and (c) fluorimetry methods.

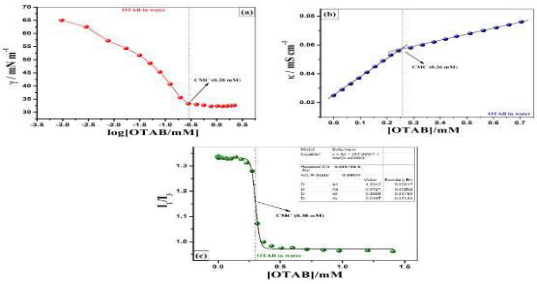

Figure 1D. Identification of the CMC of OTAB in aqueous medium at 298 K using (a) tensiometry, (b) conductometry, and (c) fluorimetry methods.

Table 2. Critical Micelle Concentration (CMC) values of pure C_nTAB in aqueous medium at 298 K, determined through Surface Tension (ST), Conductometry (Cond), and Steady-State Fluorescence (Flr) methods, including the corresponding interfacial and bulk parameters.

	CMC			γ_{CMC} $(mN\ m^{-1})$	π_{CMC} $(mN\ m^{-1})$	$-(\frac{d\gamma}{dlogC}\times 10^3)$	$\Gamma_{max}\times 10^6$ (mol/m^2)	A_{min} $(nm^2/molecule)$	G_{min} (KJ/mol)	β	$-\Delta G^0_{mic}$ (KJ/mol)	$-\Delta G^0_{Ads}$ (KJ/mol)	$\frac{\Delta G^0_{Ads}}{\Delta G^0_{mic}}$	$-\Delta G^0_{ef}$ (KJ/mol)	$p^{C_{20}}$	P
	ST	$cond$	Flr													
DTAB	15.63	15.46	15.48	35	36.4	30.87	2.70	0.61	12.86	0.73	35.04	48.52	1.38	13.48	2.51	0.343
TTAB	3.88	3.72	3.79	34.9	35.9	21.99	1.93	0.86	18.08	0.78	42.20	60.80	1.44	18.60	3.21	0.244

CTAB	0.94	0.90	0.97	34.7	37.1	24.82	2.17	0.76	15.88	0.75	47.64	64.73	1.36	17.09	3.79	0.276
OTAB	0.28	0.26	0.30	33.3	38	22.45	1.97	0.84	16.85	0.67	50.47	69.76	1.38	19.29	4.47	0.250

3.2. Interactional Behaviour of C_nTAB in an Aqueous Pectin Solution

3.2.1. Tensiometry

Tensiometry is a fundamental technique for probing the interactions between polymers and surfactants. This approach is particularly valuable as a key preliminary step that guides subsequent experimental procedures. When C_nTAB are subjected to binding with pectin, the scenario gets quite complex as compared to studying pure C_nTAB in an aqueous medium. In the combined pectin-C_nTAB systems, the amphiphiles experience both interfacial and bulk modifications. The tensiograms for the pectin-C_nTAB systems, as shown in Figures 2 (a), (b), and (c), are composed of four distinct interaction zones that arise due to variation in surface tension while raising the amphiphile concentration. The premicellar period produces three sharp transition points (cac, C_S, and C_f), and each one corresponds to the onset of a different mode of interaction. The γ −log [surfactant] profiles of these surfactants exhibit more or less uniform patterns, shaped by the pectin concentration (0.05, 0.1 and 0.2 % w/v) as well as the surfactant chain length. It has been observed that the γ value of an aqueous pectin solution (without surfactant) is slightly lower than that of pure water, which accounts for the mild surface activity of pectin polymer. At very low concentrations (Region I), C_nTAB monomers primarily adsorb onto the interface, causing a steep decrease in γ until it approaches a minimum point, known as the critical aggregation concentration (cac) **[81]**. This point is significant because it marks the onset of small micelle-like aggregates forming along the pectin chain. Importantly, the cac is considered analogous to the cmc, though it always occurs at a concentration manyfold lower than the cmc of pure amphiphiles. An increased alkyl chain length of the surfactants enhances hydrophobicity, which promotes the initiation of the complexation process and lowers the cac values from DTAB to OTAB. Comparing the cac values at the studied pectin concentrations, CTAB and TTAB show nearly close values, while DTAB has a markedly higher cac and OTAB a considerably lower one. A higher magnitude of cac suggests a relatively weaker association between the oppositely charged polymer and surfactant **[82]**. Considering this point of view, the strength of interaction between pectin and C_nTAB increases in the following order: DTAB < TTAB < CTAB < OTAB. The dependence of cac on [pectin] shows different trends: for DTAB and CTAB, it steadily increases, while for TTAB and OTAB, it decreases initially and eventually increases. With a further increase in [C_nTAB] beyond cac (Region II), the surface tension rises until the interaction is maximized with the appearance of either a hump or plateau-like shape **[83]**. In the post-cac region, the height of this rise shows no predictable correlation with [pectin], except in the cases of TTAB and CTAB, where it increases progressively. However, the alkyl chain length of the surfactants has an immense impact on the shape of this region in the tensiometric curves, as it is broadened from a single point or hump observed with DTAB and virtually

converted into a large plateau in the case of OTAB. Guzmán et al. **[74]** have comprehensively reviewed the appearance of both peak and flat regions in the tensiometric profile. The pectin chains act as the source of anionic sites, where the electrostatically induced small aggregates of C_nTAB get wrapped progressively to form complex ion pairs. These polymer-bound amphiphile aggregates are expelled from the interface and accumulate in the bulk, thereby reducing the surface activity of the medium. The second transition point is conventionally identified as the polymer saturation concentration (C_S) **[84]**, at which all the available anionic sites are occupied by the C_nTAB molecules. As the polymer concentration increases, more binding sites are exposed to the surfactant molecules. Consequently, the magnitude of C_S increases, which also aligns with our observations. Following the polymer saturation process, the newly introduced amphiphile molecules become trapped at the air-solution interface. This interfacial crowding brings about a second linear decline in the γ value on the tensiometric plots (Region III). Once the system reaches the third transition point, corresponding to the extended critical micelle concentration (C_f) **[85]**, free micelles start to form surrounding the saturated polymer backbone. The plateau-like behaviour observed in Region IV suggests a steady surface activity as more surfactant is added, akin to the independent micellization of pure amphiphiles. Thus, an oppositely charged polyanion slows down the micellization of C_nTAB, as a large number of surfactant monomers are involved in the complexation process (Regions I, II, and III). Similar to C_S, the C_f shows an increasing trend as [pectin] rises. The values of cac, C_S, and C_f are provided in Tables 3, 4, 5, and 6 for DTAB, TTAB, CTAB, and OTAB, respectively.

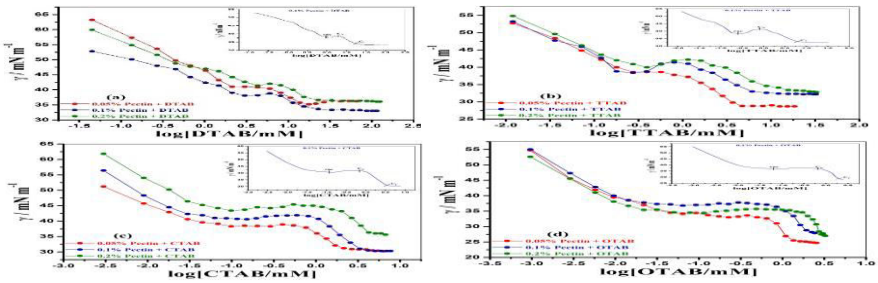

Figure 2A. Tensiometric profiles of Pectin-C_nTAB systems at various pectin concentrations (% w/v) at 298 K: (a) DTAB, (b) TTAB, (c) CTAB, and (d) OTAB. Inset: Transition points (cac, C_S, and C_f) for the respective 0.1% pectin-C_nTAB systems are marked.

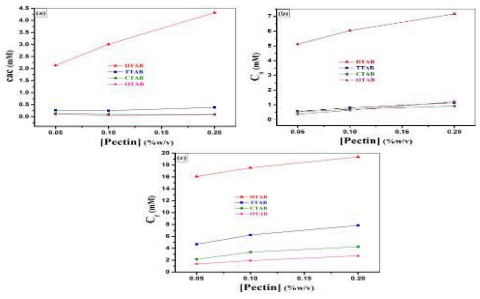

Figure 2B. Effect of hydrophobic alkyl chain length of C_nTAB surfactants on cac, C_S, and C_f in Pectin-C_nTAB systems: (a) 0.05%, (b) 0.1%, and (c) 0.2% pectin.

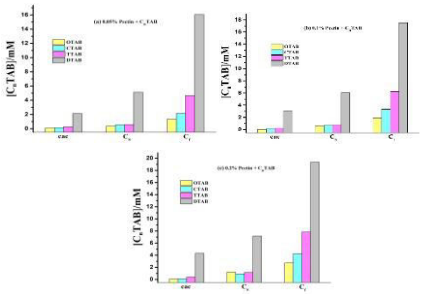

Figure 2C. Effect of varying pectin concentrations (0.05%, 0.1%, and 0.2%) on (a) cac, (b) C_S, and (c) C_f in Pectin-C_nTAB systems.

3.2.2. Conductometry

Conductometry is an effective technique for probing the interaction dynamics between oppositely charged polymers and surfactants in the bulk phase. The variation in specific conductance (κ) as a function of [C_nTAB] is depicted in Figure 3 (a-d). The CMC of the pure C_nTAB is identified as the single break point in the conductivity curve, determined by linear fitting to the pre- and post-micellar regions with different slopes. The conductometric results of C_nTAB interactions with pectin show two distinct break points, which closely match the C_S and C_f values obtained through tensiometry measurements. This approach lacks the detection of the initial break point (cac) since there is no significant deviation in linearity at very low amphiphile concentration. The ineffectiveness to detect the cac via conductometry is an extensively reported challenge in literature **[86, 87]**. It has been found that the conductance of DTAB, TTAB, CTAB, and OTAB is higher in the presence of aqueous pectin solutions (0.05%, 0.1%, and 0.2% w/v) than in pure water, and it also increases with polymer concentration. The first breakpoint corresponding to C_S is scarcely detectable, occurring when the polymer chain is fully saturated with small amphiphile aggregates. In this regime, the interaction shows little effect on the ion transport process, as evidenced by a lower slope. The post-C_S phase is characterized by a steeper slope, ensuring that no further binding occurs and the incoming surfactant monomers remain unbound to the polymer chain. As a result, the surfactant molecules can freely dissociate into surfactant ions (C_nTA^+) and counterions (Br^-). The second breakpoint at C_f, which is reasonably prominent, marks the micellization of free C_nTAB and the simultaneous movement of counterions (Br^-) from the bulk medium to the micellar interface. Thus, of the three distinct regions, the post-C_f phase shows the least slope.

The values of both C_S and C_f increase with increasing pectin concentration, a trend that is already validated by tensiometry results. The significant difference between the C_S and C_f for all C_nTAB surfactants is attributed to the strong electrostatic interactions between the oppositely charged components. However, the comparative evaluation of the data suggests that the interaction of pectin with DTAB is relatively weaker than with other cationic surfactants, irrespective of the polymer concentration.

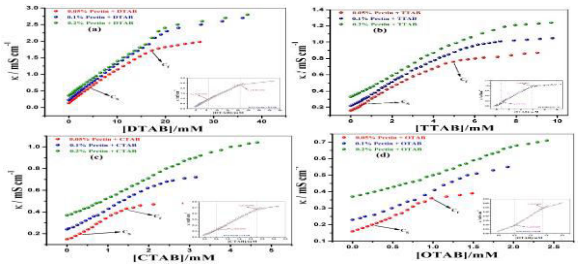

Figure 3. Plots of specific conductance (κ) as a function of [C_nTAB] in aqueous medium at 298 K: (a) DTAB, (b) TTAB, (c) CTAB, and (d) OTAB. Inset: Identification of the breakpoints (C_S and C_f) for the respective 0.1% Pectin-C_nTAB systems.

Table 3. Critical Concentration values Associated with Various Transitions in the Complexation of Pectin-DTAB Systems at 298 K, Determined Through Surface Tension, Conductometry, and Turbidimetry methods.

	Tensiometry			*Conductometry*		*Turbidimetry*		
[Pectin]/% (w/v)	cac	C_S	C_f	C_S	C_f	T_1	T_2	T_3
0.05	2.13	5.11	16.06	4.26	16.91	1.16	10.20	15.74
0.1	3.01	6.04	17.53	5.84	20.88	2.05	8.87	14.56
0.2	4.32	7.17	19.36	6.79	22.75	1.34	6.52	13.62

Table 4. Critical Concentration values Associated with Various Transitions in the Complexation of Pectin-TTAB Systems at 298 K, Determined Through Surface Tension, Conductometry, and Turbidimetry methods.

	Tensiometry			*Conductometry*		*Turbidimetry*		
[Pectin]/% (w/v)	cac	C_S	C_f	C_S	C_f	T_1	T_2	T_3
0.05	0.27	0.57	4.67	0.62	4.60	0.14	1.67	3.14
0.1	0.25	0.80	6.23	0.78	5.86	0.19	1.53	2.87
0.2	0.39	1.15	7.84	1.24	7.38	0.31	1.40	3.61

Table 5. Critical Concentration values Associated with Various Transitions in the Complexation of Pectin-CTAB Systems at 298 K, Determined Through Surface Tension, Conductometry, and Turbidimetry methods.

	Tensiometry			*Conductometry*		*Turbidimetry*		
[Pectin]/% (w/v)	cac	C_S	C_f	C_S	C_f	T_1	T_2	T_3
0.05	0.14	0.54	2.15	0.31	1.44	0.13	0.86	1.94
0.1	0.11	0.70	3.34	0.52	2.24	0.077	1.27	1.76
0.2	0.098	0.92	4.25	0.71	3.39	0.035	1.39	3.04

Table 6. Critical Concentration values Associated with Various Transitions in the Complexation of Pectin-OTAB Systems at 298 K, Determined Through Surface Tension, Conductometry, and Turbidimetry methods.

	Tensiometry			*Conductometry*		*Turbidimetry*		
[Pectin]/%	cac	C_S	C_f	C_S	C_f	T_1	T_2	T_3

(w/v)								
0.05	0.092	0.37	1.36	0.27	0.98	0.13	0.50	0.98
0.1	0.064	0.64	1.93	0.49	1.39	0.11	0.45	1.22
0.2	0.078	1.22	2.73	0.83	2.04	0.04	0.31	1.06

3.2.3. Thermodynamic Insights into the Micellization and Complexation Behaviour

This study has been using tensiometric and conductometric data to calculate a variety of relevant interfacial and bulk parameters, affording invaluable insights for understanding the complexation phenomenon. The estimated values for the pure C_nTAB and pectin-C_nTAB systems are summarized in Tables 2, 6, 7, and 8. Here, we address the underlying equations, point out the significance of the parameters in this context, and provide a detailed analysis of the observed results.

(a) Interfacial tension at cmc (γ_{CMC})

The γ_{CMC} value (reported in $mN\,m^{-1}$) represents the surface tension at the critical micelle concentration (CMC), indicating the tendency of surfactant monomers to accumulate at the air/water interface prior to self-assembling into micelles within the bulk medium. A higher γ_{CMC} value reflects a decline in the surface activity of the experimental solution. In general, lengthening the alkyl chain increases the hydrophobic nature of surfactants, causing γ_{CMC} to decrease **[88]**. For C_nTAB amphiphiles, the observed trend is consistent with expectations. However, the mixed systems do not exhibit a clear pattern.

(b) Surface pressure (π_{CMC})

At the interface saturation point, the surface pressure is denoted by the parameter π_{CMC}. The formula of π_{CMC} is based on surface tension readings at two distinct concentrations, as follows **[89]**:

$$\pi_{CMC} = \gamma_{iniial} - \gamma_{CMC/Cf} \quad (1)$$

Here, γ_{iniial} denotes the initial surface tension in the absence of amphiphiles, while $\gamma_{CMC/Cf}$ is the surface tension at either CMC or C_f in the presence of amphiphiles. In fact, π_{CMC} measures the maximum reduction in the surface tension observed in the surfactant-added solution. The individual surfactants show higher interfacial adsorption efficiency (π_{CMC}) compared to the polymer-surfactant mixtures (except for TTAB and OTAB at the lowest pectin concentration). This can be explained by the surfactant molecules being confined to the polymer segments, which reduces their ability to adsorb at the air-water interface. The

inclusion of π_{CMC} in the equation for ΔG^0_{Ads} calculation (addressed later) makes this parameter particularly important.

(c) Counterion binding (β)

The degree of counterion binding (β) measures the extent of counterions adsorbed onto the charged micelle. The mathematical expression for β is **[90]**:

$$\beta = 1 - \frac{S_2}{S_1} \quad (2)$$

where S_1 and S_2 are the conductivity slopes before and after the micellization, respectively. The post-micellar slope (S_2) is always lower in magnitude than the pre-micellar slope (S_1). Consequently, the ratio (S_2/S_1) is found less than unity and the numerical value of β is always a positive fraction **[91]**. For pure C_nTAB, the β values range from 0.67 to 0.78, indicating that 67% to 78% of the counterions (Br^-) are effectively bound to the micelles. An increase in hydrophobic alkyl chain length results in an increase in micellar surface area, which in turn reduces electrostatic repulsions. As a result, the β value is expected to decrease from DTAB to OTAB. However, no such tendency has been observed in this case. The β values of DTAB and TTAB show minimal changes in the presence of pectin, indicating that electrostatic interactions with pectin within the premicellar region are relatively weak. As a result, the cationic head group retains close proximity to its counterion. Compared to aqueous medium, the β values of both CTAB and OTAB show an initial increase at 0.05% pectin concentration, followed by a significant decline at higher pectin concentrations (0.1% and 0.2%). At low concentration, the polymer facilitates the accumulation of counterions around the micelles, leading to an increase in β. In contrast, at higher concentrations (0.1% and 0.2%), the polymer shields the surfactant charge and competes directly with the counterions for binding sites, causing a marked decrease in β.

(d) Maximum surface excess (Γ_{max})

The surface adsorption potential of C_nTAB monomers at the micellization concentration has been calculated from tensiometric data using Gibbs' adsorption equation and expressed in terms of maximum surface excess (Γ_{max}), as follows **[92]**:

$$\Gamma_{max} = -\frac{1}{2.303iRT} \lim_{[\mathrm{CnTAB}]\to CMC} \frac{d\gamma}{dlogC} \quad (3)$$

The symbol 'i' indicates the number of ionic species (i = 2) dissociated per C_nTAB monomer in the aqueous solution. The temperature (T) is measured in Kelvin scale, and 'R' stands for the molar gas constant ($Joule\ mol^{-1}\ K^{-1}$). The factor $d\gamma/\ dlogC$ is derived from the slope at cmc (or C_f) in the tensiometric plot (γ vs log C). The Γ_{max} values of pure C_nTAB follow the sequence: DTAB > CTAB >TTAB ≈ OTAB. The mixed systems have lower Γ_{max} values than the pure cationic surfactants, except for OTAB, which shows higher Γ_{max} values at pectin concentrations of 0.1% and 0.2% (w/v). The observed decrease in Γ_{max} may result from a reduced interfacial adsorption of the surfactant, likely due to the formation of electrostatic complexes.

(e) Minimum headgroup area (A_{min})

The minimum area enclosed by the head group of a surfactant molecule at a maximally saturated interface is calculated as follows **[93]**:

$$A_{min} = \frac{10^{18}}{N_A \Gamma_{max}} \quad (4)$$

'N_A' is well-known as the Avogadro's number. The parameter A_{min} is significant for understanding the interfacial distribution of surfactant molecules. The A_{min} values of pure surfactants and mixed systems usually follow a trend opposite to that of Γ_{max}. Among pure surfactants, DTAB has the smallest A_{min} value and, therefore, the highest surface activity. The observed increase in A_{min} for DTAB, TTAB, and CTAB in the presence of pectin suggests a relatively loose pacing of surfactant molecules at the air–solution interface. In other words, the addition of pectin reduces the number of surfactant molecules bound at the air/water interface, resulting in increased available space for each surfactant molecule within the interfacial zone.

(f) Minimum free energy of adsorption (G_{min})

A thermodynamic quantity has been formulated by Sugihara for the measurement of synergy in various mixed systems, and it is defined as **[94]**:

$$G_{min} = \gamma_{CMC}. A_{min}. N_A \quad (5)$$

Each term in the above equation has been clarified before. It measures the change in free energy that occurs when the components in the mixed solution move from the bulk to the interface. A lower value of G_{min} results in greater thermodynamic stability and enhanced surface activity. In other words, more effective synergistic interactions can take place. All surfactants, except OTAB, show an increase in their G_{min} values when pectin is present. This suggests that OTAB has the strongest synergistic interactions with pectin.

(g) Standard Gibbs free energy of micellization (ΔG^0_{mic})

The standard Gibbs free energy of micellization (ΔG^0_{mic}) can be represented as **[95]**:

$$\Delta G^0_{mic} = (1+\beta)\ \mathrm{RT} ln X_{CMC} \quad (6)$$

where X_{CMC} is cmc of C_nTAB in mole fraction scale. The free energy change associated with the micellization of surfactants is highly negative, both in the absence and presence of polymer, indicating that the process is spontaneous in all cases. For pure surfactants, the negative ΔG^0_{mic} values become increasingly more negative from DTAB to CTAB, suggesting that the hydrophobicity of the surfactants plays a controlling role in the micellization process. In the presence of pectin, the ΔG^0_{mic} values for DTAB and TTAB are comparable to those observed without the polymer; thus, the polymer has only a minor effect on the micellization of these surfactants. However, for CTAB and OTAB, the ΔG^0_{mic} values decrease in the presence of pectin, meaning that micellization becomes less favourable in the presence of the polymer.

(h) Standard Gibbs free energy of adsorption (ΔG^0_{Ads})

The standard Gibbs free energy change (ΔG^0_{Ads}) related to interfacial adsorption is represented by the following equation **[96]**:

$$\Delta G^0_{Ads} = \Delta G^0_{mic} - \frac{\pi_{cmc}}{\Gamma_{max}} \quad (7)$$

The ratio $\frac{\pi_{CMC}}{\Gamma_{max}}$ measures the amount of work needed to transfer an amphiphilic molecule from the interface to the micellar environment **[97]**. The more negative the ΔG^0_{Ads} value, the greater the ability of amphiphile molecules to adsorb at the interface. The pure surfactants show the same trends in ΔG^0_{Ads} values as those observed in ΔG^0_{mic}. In the pectin-C_nTAB system, the ΔG^0_{Ads} values for DTAB and TTAB increase in the presence of the polymer compared to the pure system. On the other hand, the ΔG^0_{Ads} values for CTAB and OTAB decrease in the presence of the polymer, except in the case of the 0.2% pectin-CTAB system.

(i) Effective Gibbs free energy (ΔG^0_{eff})

Amphiphile molecules exhibit a stronger tendency for interfacial adsorption rather than bulk micellization, as evidenced by the higher negative values of ΔG^0_{Ads} compared to ΔG^0_{mic} in both pure and mixed systems. The term "effective Gibbs free energy" (ΔG^0_{eff}) refers to the change in free energy associated with both adsorption and micellization, mathematically expressed as **[98]**:

$$\Delta G^0_{eff} = \Delta G^0_{Ads} - \Delta G^0_{mic} \quad (8)$$

It has been observed that the values of ΔG^0_{eff} for pure C_nTAB become higher in mixed systems, except for OTAB (0.1% and 0.2% pectin).

(j) Gibbs energy difference (ΔG^0_{ps})

In general, the cac value of a surfactant in a polymer-surfactant system is lower than the cmc in a polymer-free system. The interaction parameter, Gibbs energy difference (ΔG^0_{ps}), can be used to estimate the surfactant binding ability along a polymer chain, as follows **[99]**:

$$\Delta G^0_{ps} = RT\ ln\frac{cac}{cmc} \quad (9)$$

The more negative the ΔG^0_{ps} is, the more thermodynamically favourable the interactions will be. Accordingly, a lower (cac/cmc) ratio indicates stronger interactions between polymer and surfactant. For DTAB, CTAB, TTAB, and OTAB, the average ΔG^0_{ps} values are found to be - 4.07, - 6.36, - 5.21, and - 3.19 $kJ\ mol^{-1}$, respectively. These data indicate the extent of the interaction in the sequence: TTAB > CTAB > DTAB > OTAB.

(k) Efficiency of adsorption ($p^{C_{20}}$)

The physical parameter $p^{C_{20}}$ measures the adsorption capacity of a surfactant at the interface and is given by the following equation **[100]**:

$$p^{C_{20}} = - \log_{10} C_{20} \quad (10)$$

where C_{20} is the surfactant concentration (in molarity) necessary to lower the surface tension of the pure solvent by 20 mN m^{-1} and is estimated using the tensiometric plot. The higher the $p^{C_{20}}$, the better a surfactant can adsorb at the air-solution interface, reducing γ more effectively. Among pure surfactants, as the alkyl chain length increases, the $p^{C_{20}}$ value also increases, signifying an enhanced surface activity **[101]**. The presence of pectin results in higher $p^{C_{20}}$ values in the mixed systems compared to the respective pure systems, driven by strong electrostatic interactions that promote the formation of stable surface-active complexes. However, $p^{C_{20}}$ does not alter much at higher pectin concentrations.

(l) Packing parameter (P)

The packing parameter (P), proposed by Israelachvili **[102]**, can be used to predict the geometric shape of micelles. A micelle adopts a spherical shape when the P values are between 0 and 0.33 and a cylindrical shape when P values range from 0.33 to 0.5. In certain instances, the micelle can also form a lamellar structure, with P values falling between 0.5 and 1 **[103]**. It is calculated by applying the following equation **[104]**:

$$P = \frac{V}{l\, A0} \quad (11)$$

where v, l, and A_0 are the volume of the hydrophobic group, the length of the hydrophobic chain, and the surface area occupied by the hydrophilic head, respectively. The values of l and v are derived from Tanford's formulae **[105]**, as presented below:

$$l = (0.154 + 0.1265\ C_n)\ nm \quad (12)$$

$$v = (0.0274 + 0.0269\ C_n)\ nm^3 \quad (13)$$

C_n represents the number of carbon atoms in the hydrocarbon chain of C_nTAB surfactants, with values of 12, 14, 16, and 18 for DTAB, TTAB, CTAB, and OTAB, respectively. Accurately determining the value of A_0 is quite challenging; therefore, A_0 has been substituted with A_{min} **[106]**. In aqueous medium, all the surfactants self-assemble into spherical micelles, except for DTAB (P = 0.34), which shows a slight distortion from spherical arrangement. The presence of pectin lowers the P value of all surfactants (except OTAB), which is correlated to the corresponding increase in A_{min}. However, varying pectin concentrations have no effect on the spherical micellar shape of the surfactants **[107]**.

Table 7. Interfacial and Thermodynamic Parameters of DTAB Micellization at Various Pectin Concentrations (0.05%, 0.1%, and 0.2% w/v) at 298 K.

[Pectin]/% (w/v)	γ_{CMC} $(mN\ m^{-1})$	π_{CMC} $(mN\ m^{-1})$	$-(\frac{d\gamma}{dlogC} \times 10^3)$	$\Gamma_{max} \times 10^6$ (mol/m^2)	A_{min} $(nm^2/molecule)$	G_{min} (KJ/mol)	β	$-\Delta G^0_{mic}$ (KJ/mol)	$-\Delta G^0_{Ads}$ (KJ/mol)	$\frac{\Delta G^0_{Ads}}{\Delta G^0_{mic}}$	$-\Delta G^0_{eff}$ (KJ/mol)	ΔG^0_{ps} (KJ/mol)	$p^{C_{20}}$	P
0	35	36.4	30.87	2.70	0.61	12.86	0.73	35.04	48.52	1.38	13.48	-	2.51	0.343
0.05	35.4	34.4	17.35	1.52	1.09	23.24	0.71	34.52	57.15	1.65	22.63	4.94	3.34	0.192
0.1	34.2	31.1	14.08	1.23	1.35	27.80	0.77	35.35	60.63	1.71	25.28	4.08	3.25	0.155

0.2	36.9	31.7	11.49	1.00	1.66	36.89	0.78	35.11	66.81	1.90	31.7	3.19	3.32	0.126

Table 8. Interfacial and Thermodynamic Parameters of TTAB Micellization at Various Pectin Concentrations (0.05%, 0.1%, and 0.2% w/v) at 298 K.

[Pectin]/% (w/v)	γ_{CMC} $(mN\ m^{-1})$	π_{CMC} $(mN\ m^{-1})$	$-(\frac{d\gamma}{dlogC} \times 10^3)$	$\Gamma_{max} \times 10^6$ (mol/m^2)	A_{min} $(nm^2/molecule)$	G_{min} $(KJ/mol$	β	$-\Delta G^0_{mic}$ (KJ/mol)	$-\Delta G^0_{Ads}$ (KJ/mol)	$\frac{\Delta G^0_{Ads}}{\Delta G^0_{mic}}$	$-\Delta G^0_{eff}$ (KJ/mol)	ΔG^0_{ps} (KJ/mol)	$p^{C_{20}}$	P
0	34.9	35.9	21.99	1.93	0.86	18.08	0.78	42.20	60.80	1.44	18.60	-	3.21	0.244
0.05	28.8	39.3	14.98	1.31	1.27	22.03	0.79	41.62	71.62	1.72	30.00	6.60	4.42	0.165
0.1	33	34.2	12.31	1.08	1.54	30.60	0.82	41.01	72.67	1.77	31.66	6.79	4.35	0.136
0.2	34.9	31.1	16.76	1.47	1.13	23.75	0.83	40.19	61.35	1.53	21.16	5.69	4.12	0.185

Table 9. Interfacial and Thermodynamic Parameters of CTAB Micellization at Various Pectin Concentrations (0.05%, 0.1%, and 0.2% w/v) at 298 K.

[Pectin]/% (w/v)	γ_{CMC} $(mN\ m^{-1})$	π_{CMC} $(mN\ m^{-1})$	$-(\frac{d\gamma}{dlogC} \times 10^3)$	$\Gamma_{max} \times 10^6$ (mol/m^2)	A_{min} $(nm^2/molecule)$	G_{min} (KJ/mol)	β	$-\Delta G^0_{mic}$ (KJ/mol)	$-\Delta G^0_{Ads}$ (KJ/mol)	$\frac{\Delta G^0_{Ads}}{\Delta G^0_{mic}}$	$-\Delta G^0_{eff}$ (KJ/mol)	ΔG^0_{ps} (KJ/mol)	$p^{C_{20}}$	P
0	34.7	37.1	24.82	2.17	0.76	15.88	0.75	47.64	64.73	1.36	17.09	-	3.79	0.276
0.05	31.2	32.4	14.32	1.25	1.33	24.99	0.84	46.31	72.23	1.56	25.92	4.72	4.82	0.158
0.1	30.8	35	18.92	1.66	1.00	18.55	0.66	39.97	61.05	1.53	21.08	5.31	4.85	0.210
0.2	36.3	34.7	21.18	1.86	0.89	19.46	0.55	36.40	55.06	1.51	18.66	5.60	4.81	0.236

Table 10. Interfacial and Thermodynamic Parameters of OTAB Micellization at Various Pectin Concentrations (0.05%, 0.1%, and 0.2% w/v) at 298 K.

[Pectin]/% (w/v)	γ_{CMC} $(mN\ m^{-1})$	π_{CMC} $(mN\ m^{-1})$	$-(\frac{d\gamma}{dlogC} \times 10^3)$	$\Gamma_{max} \times 10^6$ (mol/m^2)	A_{min} $(nm^2/molecule)$	G_{min} (KJ/mol)	β	$-\Delta G^0_{mic}$ (KJ/mol)	$-\Delta G^0_{Ads}$ (KJ/mol)	$\frac{\Delta G^0_{Ads}}{\Delta G^0_{mic}}$	$-\Delta G^0_{eff}$ (KJ/mol)	ΔG^0_{ps} (KJ/mol)	$p^{C_{20}}$	P
0	33.3	38	22.45	1.97	0.84	16.85	0.67	50.47	69.76	1.38	19.29	-	4.47	0.250
0.05	25.5	42.4	20.63	1.80	0.92	14.13	0.74	45.77	69.32	1.51	23.55	2.76	5.66	0.228
0.1	28.8	37.1	27.96	2.45	0.68	11.79	0.54	39.17	54.31	1.39	15.14	3.66	5.45	0.309
0.2	28.4	34.7	26.13	2.29	0.72	12.31	0.51	37.11	52.26	1.41	15.15	3.17	5.37	0.292

3.2.4. Turbidimetry

In the context of oppositely charged polymer-surfactant systems, turbidity measurements are significant in visualizing the complexation behaviour in the bulk phase. In fact, the degree of turbidity relates directly to the extent of complexation, driven by the electrostatic attraction between components with opposite charges. Turbidity occurs due to the gradual formation of

coacervates in the medium, and it is measured quantitatively by the intensity of light transmitted through the polymer-surfactant aggregate. The turbidimetric profiles (100–T % vs. [C_nTAB]) of pectin-C_nTAB interactions are shown in Figures 4 (a-d). All the turbidity curves show significant changes, identifying four distinct regions. The inflection points, marked as T_1, T_2, and T_3 (where 'T' stands for turbidity), indicate phase transitions at various stages of the complexation process. In each region, both turbidity levels and aggregate sizes vary markedly. Also, the plots follow a distinctly different pattern depending on the nature of the amphiphiles. At low surfactant concentrations, the solution remains visually clear with minimal turbidity until reaching T_1, where turbidity starts to appear. For DTAB and TTAB, this region appears as a minor plateau, while for CTAB and OTAB, it shows an upward trend. Thereafter, the turbidity experiences a sharp increase, causing the solution to turn cloudy. This signals the onset of coacervation **[108, 109]**, as evidenced by liquid-liquid phase separation upon standing. As the surfactant concentration increases further, the population of the larger aggregates leads to a continual rise in turbidity, eventually reaching a maximum. For CTAB, the maximum turbidity point is identified as T_2. In contrast, for other surfactants, T_2 marks the initiation point of coacervation, while the point of maximum turbidity is designated as T_3. As can be seen, the turbidity maximum remains largely unaffected by increasing polymer concentration. Afterward, the coacervates of DTAB and TTAB undergo only partial solubilization, resulting in a slow decline in turbidity. In contrast, for OTAB, the coacervates remain insoluble even at higher surfactant concentrations, maintaining a stable turbidity plateau **[110]**. Also, separation of a small quantity of white precipitate is observed at the bottom of the cuvette after a prolonged period of standing. However, CTAB follows a more complex behaviour: after attaining a plateau, it experiences a sudden drop in turbidity above T_3 **[111]**. Thus, the measured turbidity reduces to a large extent in the post-T_3 stage. Notably, TTAB and CTAB exhibit opposite behaviour at the lowest pectin concentration (0.05%) compared to higher concentrations (0.1 and 0.2%), as turbidity does not change after reaching maximization. Therefore, both the surfactant hydrophobicity and the polymer concentration must be considered key factors in coacervate-based formulations.

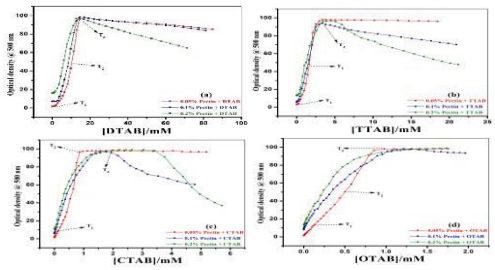

Figure 4. Variation in turbidity (100 - %T) of Pectin-C_nTAB systems at various pectin concentrations (% w/v) at 298 K: (a) DTAB, (b) TTAB, (c) CTAB, and (d) OTAB.

3.2.7. Field emission scanning electron microscopy (FESEM)

To gain a deeper understanding of the morphological features of the formed complexes, FESEM analysis has been performed on 0.1% (w/v) pectin-C_nTAB complexes at C_f. As

expected, the resultant morphographs showcase striking variations in the aggregate size, shape, surface texture, and structural organization depending on the extent of complexation. As depicted in Figure 5(a), the interaction between pectin and DTAB induces agglomeration, resulting in the formation of predominantly grainy clusters, alongside some elongated, irregular, sheet-like structures. The compact architecture of these assemblies suggests a core-shell configuration, where the polymer forms the core, encapsulated by surfactant molecules due to strong electrostatic interactions. The random particle distribution may be attributed to incomplete phase separation. The microstructure of pectin-TTAB complexes (Figure 5(b)) displays irregular, flake-like formations with overlapping and interlocking patterns. The layers exhibit a rough, textured appearance, characterized by prominent cracks and crevices, likely formed due to phase separation during the complexation process. Moreover, a uniform dispersion of fine spherical particles is evident across the surface, potentially indicating the presence of surfactant micelles embedded within the polymeric matrix. However, in the case of CTAB (Figure 5(c)), a well-defined lamellar structure is found, marked by distinct sheet-like layers with uneven, jagged edges. The presence of smaller pore-like voids is observed within the lamellar framework, suggesting loose connectivity and partial heterogeneity within the system. The behaviour of OTAB (Figure 5(d)) in the formation of a highly wrinkled, interconnected, network-like morphology is quite different from the rest. The development of the curvilinear ridges and valleys clearly demonstrates the formation of a self-assembled architecture. Based on the previous discussion, it is reasonable to compare the findings, as pectin exhibits different interactional behaviour with each surfactant, leading to significant variations in their complex structures.

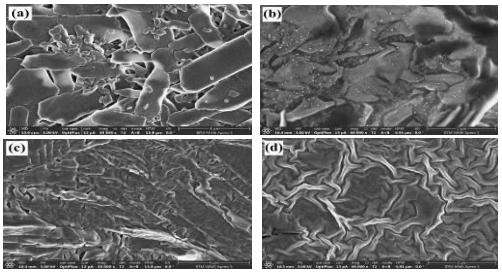

Figure 5. FESEM images of Pectin (0.1% w/v) + C_nTAB samples: (a) DTAB, (b) TTAB, (c) CTAB, and (d) OTAB; [C_nTAB] = C_f.

3.2.8. High resolution transmission electron microscopy (HR-TEM)

The HRTEM analysis reveals striking morphological variations in the pectin-C_nTAB aggregates formed with DTAB, TTAB, CTAB, and OTAB surfactants. These differences are mainly dictated by the alkyl chain length of the surfactant, which modulates the strength of both electrostatic and hydrophobic interactions. The pectin-DTAB system (Figure 6 (a)) forms large, irregular, and loosely packed aggregates ranging from 50 to 200 nm in size, indicating weak hydrophobic interactions and low stability. The scattered, non-uniform morphology further reflects poor aggregate cohesion and weak electrostatic binding. In the

pectin-TTAB system (Figure 6 (b)), predominantly spherical and compact aggregates of intermediate size (50–120 nm) are observed. The longer alkyl chain length strengthens hydrophobic interactions compared to DTAB, leading to the formation of more stable and denser aggregates. The pectin-CTAB system (Figure 6 (c)) produces the smallest and most uniformly dispersed aggregates, with sizes ranging from 5 to 50 nm. The pectin-CTAB system produces the smallest and most finely dispersed aggregates, with sizes ranging from 5 to 50 nm. This exceptional dispersion and uniformity result from the optimized balance of electrostatic and hydrophobic forces. Although OTAB features the longest alkyl chain, its aggregates (Figure 6 (d)) are slightly larger (30–80 nm) and less compact than those formed by CTAB. Although OTAB features the longest alkyl chain, the resulting aggregates are somewhat larger (30–80 nm) and less compact than CTAB. This is likely due to steric hindrance from the elongated chain, which limits the tight packing observed in CTAB. However, the aggregates are still well-distributed and exhibit excellent stability. In conclusion, the study highlights the significant impact of surfactant chain length on the structural and stabilizing properties of polymer-surfactant systems. The findings emphasize the importance of tuning surfactant properties to achieve desired aggregate characteristics for specific applications. Among the studied systems, CTAB stands out as the most effective, due to its ability to form stable, well-defined aggregates with ideal morphology and dispersion.

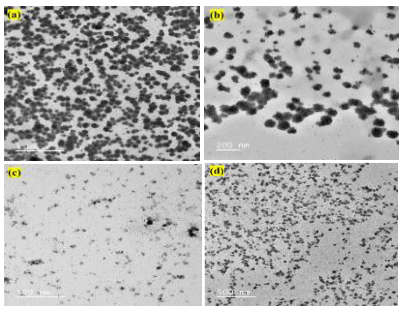

Figure 6. HR-TEM images of Pectin (0.1% w/v) + C_nTAB samples: (a) DTAB, (b) TTAB, (c) CTAB, and (d) OTAB; [C_nTAB] = C_f.

3.2.9. Fluorescence microscopy

The study of the fluorescence microscopy images has further supported the evidence for electrostatic complex formation between oppositely charged polymer and surfactant. The binding of DTAB in the presence of 0.1% (w/v) pectin has been analysed using DPH dye as a probe, with the findings illustrated in Figure 7(a) and (b). The formation of coacervates is clearly identified through the visualization of shiny yellow-coloured spots. Experimental findings suggest that at lower DTAB concentrations, the entry of dye molecules into smaller aggregates is not facilitated. Below C_S, DPH dye is practically ineffective in detecting the complexation behaviour of the pectin-DTAB system, resulting in no observable visualization at the pre-C_S stage **[112]**. Coacervates have been observed to accumulate only slightly as the

concentration of DTAB approaches C_S. However, when the DTAB concentration is increased further to C_f, smaller coacervates coalesce into larger ones, resulting in the formation of a more compact and structured assembly.

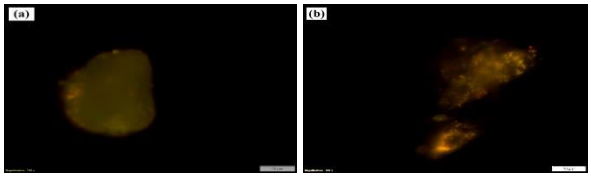

Figure 7. Fluorescence microscopy images of Pectin-DTAB complex coacervates captured at (a) C_S (6.04 mM), (b) C_f (17.53 mM); [Pectin] = 0.1% (w/v), Scale bar = 10 μm.

4. Conclusions

This manuscript provides a comprehensive analysis of the structural and interaction dynamics between the anionic polymer pectin and four cationic surfactants, DTAB, TTAB, CTAB, and OTAB, in aqueous solution. By conducting a systematic series of experiments, the study aims to compare and elucidate the impact of polymer concentration and surfactant hydrophobic chain length on their complexation behaviour. Among these techniques, surface tension is highly sensitive for detecting interactions even at extremely low surfactant concentrations, whereas turbidity measurements reveal whether the formed complexes are soluble or insoluble, based on the relative composition of the mixture. Coacervation, or the two-phase region, is primarily centred around a balanced charge ratio (1:1) between the surfactant and polymer. The key factor driving this coacervation process is the maintenance of electroneutrality within the polymer-surfactant complexes. These interaction mechanisms have also been validated through detailed visual analysis of the complexes using FESEM, HRTEM, and fluorescence microscopy imaging. The observed morphologies display clear behavioural differences, attributed to the varying degrees of interaction between them.

The complexation is originated due to the electrostatic forces between the negatively charged carboxyl groups of pectin and the positively charged surfactant head groups. In addition, hydrophobic interactions take place between the surfactant's alkyl chains and the hydrophobic segments of pectin molecules. Electrostatic interactions primarily govern the formation of neutral ion-pairs, which then undergo hydrophobic-driven growth, leading to the formation of micelles. Thus, in the pectin-cationic surfactant systems, three key modes of interaction have been observed: electrostatic forces, hydrophobic interactions, and polymer-driven micellization. Negative Gibbs free energy values further provide strong evidence for the existence of these interactions.

The ternary system of polymer, surfactant, and water features three major interaction points: cac, C_S, and C_f. While cac is independent, both C_S and C_f are controlled by the concentration of pectin. The interaction begins at the cac point, which is significantly lower than the cmc of the polymer-free surfactant. The accumulation of surfactant molecules near the polymer chain

promotes hydrophobic interactions, which can lead to their self-aggregation. The increase in critical concentrations (C_S and C_f) with higher polyelectrolyte concentrations indicates a higher polymer density in the solution, which in turn provides a greater number of surfactant-binding sites along the polymer chain. As the alkyl chain length of the surfactants increases, the cac value decreases, indicating a stronger interaction with the anionic polymer. Therefore, the surfactants with longer alkyl chains bind more tightly to pectin compared to those with shorter chains, owing to their enhanced hydrophobicity. Though direct comparison is difficult, the surface properties of these charge-associated complexes are largely governed by the anionic charge density and the length of the hydrophobic chain.

Based on the information available, no systematic and comprehensive study has investigated the effects of polymer charge density and surfactant tail length on the interfacial and bulk behaviour, as well as the micellar parameter, in pectin-C_nTAB systems. Herein, we have delved into multiple dimensions of the interaction phenomenon, offering insightful interpretations and well-founded speculations, which may contribute to a deeper understanding of the underlying mechanisms. Further experiments, including zeta potential, DLS, FTIR, NMR, etc., would be valuable in helping to characterize the nature of aggregates and strengthen the evidence for the suggested interaction pathways. A key beneficial outcome of the current research is its potential to accelerate advancements in pectin-based formulations, particularly for food and pharmaceutical applications.

References

[1] Deshpande TM, Shi H, Pietryka J, Hoag SW, Medek A. Investigation of polymer/surfactant interactions and their impact on itraconazole solubility and precipitation kinetics for developing spray-dried amorphous solid dispersions. Molecular pharmaceutics. 2018 Jan 18;15(3):962-74.

[2] Pal N, Babu K, Mandal A. Surface tension, dynamic light scattering and rheological studies of a new polymeric surfactant for application in enhanced oil recovery. Journal of Petroleum Science and Engineering. 2016 Oct 1;146:591-600.

[3] Hamouma M, Delbos A, Dalmazzone C, Colin A. Polymer surfactant interactions in oil enhanced recovery processes. Energy & Fuels. 2021 May 13;35(11):9312-21.

[4] Ramos GA, Akanji LT, Afzal W. A novel surfactant–polymer/alkaline–surfactant–polymer formulation for enhanced oil recovery (eor) processes. Energy & Fuels. 2020 Jan 10;34(2):1230-9.

[5] Gradzielski M. Polyelectrolyte–surfactant complexes as a formulation tool for drug delivery. Langmuir. 2022 Oct 24;38(44):13330-43.

[6] França MT, Pereira RN, Riekes MK, Pinto JM, Stulzer HK. Investigation of novel supersaturating drug delivery systems of chlorthalidone: The use of polymer-surfactant complex as an effective carrier in solid dispersions. European Journal of Pharmaceutical Sciences. 2018 Jan 1;111:142-52.

[7] Sharma M, Bharatiya B, Mehta K, Shukla A, Shah DO. Novel strategy involving surfactant–polymer combinations for enhanced stability of aqueous Teflon dispersions. Langmuir. 2014 Jun 24;30(24):7077-84.

[8] Stanimirova RD, Kralchevsky PA, Danov KD, Xu H, Ung YW, Petkov JT. Oil drop deposition on solid surfaces in mixed polymer-surfactant solutions in relation to hair-and skin-care applications. Colloids and Surfaces A: Physicochemical and Engineering Aspects. 2019 Sep 20;577:53-61.

[9] Bradbury R, Penfold J, Thomas RK, Tucker IM, Petkov JT, Jones C. Manipulating perfume delivery to the interface using polymer–surfactant interactions. Journal of colloid and interface science. 2016 Mar 15;466:220-6.

[10] Bellmann C. Surface modification by adsorption of polymers and surfactants. In Polymer Surfaces and Interfaces: Characterization, Modification and Applications 2008 Jan 26 (pp. 235-259). Berlin, Heidelberg: Springer Berlin Heidelberg.

[11] Gradzielski M. Polymer-Surfactant Interaction for Controlling the Rheological Properties of Aqueous Surfactant Solutions. Current Opinion in Colloid & Interface Science. 2022 Nov 26:101662.

[12] Saxena A, Pathak AK, Ojha K. Synergistic effects of ionic characteristics of surfactants on aqueous foam stability, gel strength, and rheology in the presence of neutral polymer. Industrial & Engineering Chemistry Research. 2014 Dec 10;53(49):19184-91.

[13] García ÁG, Nagelkerke MM, Tuinier R, Vis M. Polymer-mediated colloidal stability: On the transition between adsorption and depletion. Advances in colloid and interface science. 2020 Jan 1;275:102077.

[14] Zhao H, Kang W, Yang H, Huang Z, Zhou B, Sarsenbekuly B. Emulsification and stabilization mechanism of crude oil emulsion by surfactant synergistic amphiphilic polymer system. Colloids and Surfaces A: Physicochemical and Engineering Aspects. 2021 Jan 20;609:125726.

[15] Kirby SM, Anna SL, Walker LM. Effect of surfactant tail length and ionic strength on the interfacial properties of nanoparticle–surfactant complexes. Soft Matter. 2018;14(1):112-23.

[16] Sardar N, Kamil M. Interaction between nonionic polymer hydroxypropyl methyl cellulose (HPMC) and cationic gemini/conventional surfactants. Industrial & engineering chemistry research. 2012 Jan 25;51(3):1227-35.

[17] Mondal BB, Banik R, Ghosh S. Detailed physicochemical study and thermodynamic aspects of the interaction between nonionic cellulose derivative hydroxyethyl cellulose and anionic surfactant sodium N-dodecanoyl sarcosinate in aqueous media. Journal of the Taiwan Institute of Chemical Engineers. 2023 Aug 1;149:104982.

[18] Ortona O, D'Errico G, Paduano L, Vitagliano V. Interaction between cationic, anionic, and non-ionic surfactants with ABA block copolymer Pluronic PE6200 and with BAB reverse block copolymer Pluronic 25R4. Journal of colloid and interface science. 2006 Sep 1;301(1):63-77.

[19] Mafi A, Hu D, Chou KC. Complex formations between surfactants and polyelectrolytes of the same charge on a water surface. Langmuir. 2017 Aug 15;33(32):7940-6.

[20] Shrivastava S, Dey J. Interaction of anionic surfactant with polymeric nanoparticles of similar charge. Journal of colloid and interface science. 2010 Oct 1;350(1):220-8.

[21] Li D, Wagner NJ. Universal binding behavior for ionic alkyl surfactants with oppositely charged polyelectrolytes. Journal of the American Chemical Society. 2013 Nov 20;135(46):17547-55.

[22] Chiappisi L, Hoffmann I, Gradzielski M. Complexes of oppositely charged polyelectrolytes and surfactants–recent developments in the field of biologically derived polyelectrolytes. Soft Matter. 2013;9(15):3896-909.

[23] Burke SE, Palepu RM, Hait SK, Moulik SP. Physicochemical investigations on the interaction of cationic cellulose ether derivatives with cationic amphiphiles in an aqueous environment. InAqueous Polymer—Cosolute Systems: Special Issue in Honor of Dr. Shuji Saito 2003 (pp. 47-55). Springer Berlin Heidelberg.

[24] Petkova R, Tcholakova S, Denkov ND. Foaming and foam stability for mixed polymer–surfactant solutions: effects of surfactant type and polymer charge. Langmuir. 2012 Mar 20;28(11):4996-5009.

[25] Miyake M. Recent progress of the characterization of oppositely charged polymer/surfactant complex in dilution deposition system. Advances in Colloid and Interface Science. 2017 Jan 1;239:146-57.

[26] Feng R, Chen M, Fang Y, Fan Y, Xia Y. Supramolecular interactions in the pseudo-polyanions of polyvinylpyrrolidone complexed with various anionic surfactants. Colloids and Surfaces A: Physicochemical and Engineering Aspects. 2023 Aug 20;671:131585.

[27] Shyichuk A, Ziółkowska D, Szulc J. Coagulation of Hydrophobic Ionic Associates of Cetyltrimethylammonium Bromide and Carrageenan. Molecules. 2023 Nov 14;28(22):7584.

[28] Banerjee T, Samanta A, Mandal A. Mathematical regression models for rheological behavior of interaction between polymer-surfactant binary mixtures and electrolytes. Journal of Dispersion Science and Technology. 2022 Jul 1;43(9):1333-45.

[29] Patel D, Ray D, Tiwari S, Kuperkar K, Aswal VK, Bahadur P. SDS triggered transformation of highly hydrophobic Pluronics® nanoaggregate into polymer-rich and surfactant-rich mixed micelles. Journal of Molecular Liquids. 2022 Jan 1;345:117812.

[30] Tajik B, Sohrabi B, Amani R, Hashemianzadeh SM. The study of polymer–surfactant interaction in catanionic surfactant mixtures. Colloids and Surfaces A: Physicochemical and Engineering Aspects. 2013 Sep 5;436:890-7.

[31] Khademi M, Wang W, Reitinger W, Barz DP. Zeta potential of poly (methyl methacrylate)(PMMA) in contact with aqueous electrolyte–surfactant solutions. Langmuir. 2017 Oct 10;33(40):10473-82.

[32] Vijaya B, Murali R. Interaction of polyvinyl alcohol with cetyltrimethylammonium bromide surfactant and its effect on electrochemical property. Materials Today: Proceedings. 2022 Jan 1;68:602-11.

[33] Samwang T, Watanabe NM, Okamoto Y, Umakoshi H. Exploring the Influence of Morphology on Bipolaron–Polaron Ratios and Conductivity in Polypyrrole in the Presence of Surfactants. Molecules. 2024 Mar 7;29(6):1197.

[34] Prameela GK, Kumar BP, Subramanian J, Tsuchiya K, Pan A, Aswal VK, Abe M, Mandal AB, Moulik SP. Interaction between sodium dodecylsulfate (SDS) and pluronic L61 in aqueous medium: assessment of the nature and morphology of the formed mixed

aggregates by NMR, EPR, SANS and FF-TEM measurements. Physical Chemistry Chemical Physics. 2021;23(23):13170-80.

[35] Cao M, Hai M. Investigation on the interaction between sodium dodecyl sulfate and polyethylene glycol by electron spin resonance, ultraviolet spectrum, and viscosity. Journal of Chemical & Engineering Data. 2006 Sep 14;51(5):1576-81.

[36] Gutiérrez-Fernández E, Ezquerra TA, Rebollar E, Cui J, Marina S, Martín J, Nogales A. Photophysical and structural modulation of poly (3-hexylthiophene) nanoparticles via surfactant-polymer interaction. Polymer. 2021 Mar 18;218:123515.

[37] Ferreira MO, Pereira LO, Chaiben S, Lima KO, Edler KJ, Percebom AM. Oppositely charged polymer-surfactant nanoparticles stabilized by triblock copolymers for enhanced oil loading. Colloids and Surfaces A: Physicochemical and Engineering Aspects. 2025 Jan 5;704:135427.

[38] Llamas S, Guzmán E, Akanno A, Fernández-Peña L, Ortega F, Campbell RA, Miller R, Rubio RG. Study of the liquid/vapor interfacial properties of concentrated polyelectrolyte–surfactant mixtures using surface tensiometry and neutron reflectometry: equilibrium, adsorption kinetics, and dilational rheology. The Journal of Physical Chemistry C. 2018 Mar 1;122(8):4419-27.

[39] Fernández-Peña L, Guzmán E, Fernández-Pérez C, Barba-Nieto I, Ortega F, Leonforte F, Rubio RG, Luengo GS. Study of the dilution-induced deposition of concentrated mixtures of polyelectrolytes and surfactants. Polymers. 2022 Mar 25;14(7):1335.

[40] Najafi H, Jerri HA, Valmacco V, Petroff MG, Hansen C, Benczedi D, Bevan MA. Synergistic polymer–surfactant-complex mediated colloidal interactions and deposition. ACS applied materials & interfaces. 2020 Mar 3;12(12):14518-30.

[41] Babaev MS, Lobov AN, Shishlov NM, Kolesov SV. pH-sensitive particles of polymer-surfactant complexes based on a copolymer of N, N′-diallyl-N, N′-dimethylammonium chloride with maleic acid and sodium dodecyl sulfate. Reactive and Functional Polymers. 2022 Sep 1;178:105359.

[42] Feitosa E, Winnik FM. Interaction between Pluronic F127 and dioctadecyldimethylammonium bromide (DODAB) vesicles studied by differential scanning calorimetry. Langmuir. 2010 Dec 7;26(23):17852-7.

[43] Mohnen D. Pectin structure and biosynthesis. Current opinion in plant biology. 2008 Jun 1;11(3):266-77.

[44] Joshi N, Rawat K, Bohidar HB. Influence of structure, charge, and concentration on the pectin–calcium–surfactant complexes. The Journal of Physical Chemistry B. 2016 May 12;120(18):4249-57.

[45] Noreen A, Akram J, Rasul I, Mansha A, Yaqoob N, Iqbal R, Tabasum S, Zuber M, Zia KM. Pectins functionalized biomaterials; a new viable approach for biomedical applications: A review. International journal of biological macromolecules. 2017 Aug 1;101:254-72.

[46] Li DQ, Li J, Dong HL, Li X, Zhang JQ, Ramaswamy S, Xu F. Pectin in biomedical and drug delivery applications: A review. International Journal of Biological Macromolecules. 2021 Aug 31;185:49-65.

[47] Christiaens S, Van Buggenhout S, Houben K, Jamsazzadeh Kermani Z, Moelants KR, Ngouémazong ED, Van Loey A, Hendrickx ME. Process–structure–function relations of pectin in food. Critical Reviews in Food Science and Nutrition. 2016 Apr 25;56(6):1021-42.

[48] Chelfouh N, Coquil G, Rousselot S, Foran G, Briqueleur E, Shoghi F, Caradant L, Dolle M. Apple Pectin-Based Hydrogel Electrolyte for Energy Storage Applications. ACS Sustainable Chemistry & Engineering. 2022 Nov 16;10(48):15802-12.

[49] Perumal P, Selvin PC, Selvasekarapandian S, Sivaraj P. Structural and electrical properties of bio-polymer pectin with LiClO4 solid electrolytes for lithium ion polymer batteries. Materials Today: Proceedings. 2019 Jan 1;8:196-202.

[50] Khorasani AC, Shojaosadati SA. Pectin-non-starch nanofibers biocomposites as novel gastrointestinal-resistant prebiotics. International journal of biological macromolecules. 2017 Jan 1;94:131-44.

[51] Carrion CC, Nasrollahzadeh M, Sajjadi M, Jaleh B, Soufi GJ, Iravani S. Lignin, lipid, protein, hyaluronic acid, starch, cellulose, gum, pectin, alginate and chitosan-based nanomaterials for cancer nanotherapy: Challenges and opportunities. International Journal of Biological Macromolecules. 2021 May 1;178:193-228.

[52] Günter EA, Popeyko OV, Melekhin AK, Belozerov VS, Martinson EA, Litvinets SG. Preparation and properties of the pectic gel microparticles based on the Zn2+, Fe3+ and Al3+ cross-linking cations. International journal of biological macromolecules. 2019 Oct 1;138:629-35.

[53] Celus M, Kyomugasho C, Van Loey AM, Grauwet T, Hendrickx ME. Influence of pectin structural properties on interactions with divalent cations and its associated functionalities. Comprehensive Reviews in Food Science and Food Safety. 2018 Nov;17(6):1576-94.

[54] Wang R, Liang R, Dai T, Chen J, Shuai X, Liu C. Pectin-based adsorbents for heavy metal ions: A review. Trends in Food Science & Technology. 2019 Sep 1;91:319-29.

[55] Asker D, Weiss J, McClements DJ. Analysis of the interactions of a cationic surfactant (lauric arginate) with an anionic biopolymer (pectin): isothermal titration calorimetry, light scattering, and microelectrophoresis. Langmuir. 2009 Jan 6;25(1):116-22.

[56] Chang Y, McLandsborough L, McClements DJ. Interactions of a cationic antimicrobial (ε-polylysine) with an anionic biopolymer (pectin): An isothermal titration calorimetry, microelectrophoresis, and turbidity study. Journal of agricultural and food chemistry. 2011 May 25;59(10):5579-88.

[57] Liang LI, Luo Y. Casein and pectin: Structures, interactions, and applications. Trends in Food Science & Technology. 2020 Mar 1;97:391-403.

[58] Liu Y, Zheng D, Ma Y, Dai J, Li C, Xiao S, Liu K, Liu J, Wang L, Lei J, He J. Self-assembled nanoparticles platform based on pectin-dihydroartemisinin conjugates for codelivery of anticancer drugs. ACS Biomaterials Science & Engineering. 2017 Nov 20;4(5):1641-50.

[59] Ropers MH, Meister A, Blume A, Ralet MC. Pectin− Lipid Assembly at the Air–Water Interface: Effect of the Pectin Charge Distribution. Biomacromolecules. 2008 Apr 14;9(4):1306-12.

[60] Lopez-Pena C, Arroyo-Maya IJ, McClements DJ. Interaction of a bile salt (sodium taurocholate) with cationic (ε-polylysine) and anionic (pectin) biopolymers under simulated gastrointestinal conditions. Food Hydrocolloids. 2019 Feb 1;87:352-9.

[61] Batista KA, Purcena LL, Alves GL, Fernandes KF. A pectin–lipase derivative as alternative copolymer for lipase assay. Journal of Molecular Catalysis B: Enzymatic. 2014 Apr 1;102:25-32.

[62] Calce E, Mignogna E, Bugatti V, Galdiero M, Vittoria V, De Luca S. Pectin functionalized with natural fatty acids as antimicrobial agent. International Journal of Biological Macromolecules. 2014 Jul 1;68:28-32.

[63] McClements DJ. Isothermal titration calorimetry study of pectin− ionic surfactant interactions. Journal of agricultural and food chemistry. 2000 Nov 20;48(11):5604-11.

[64] Wei Z, Yi D, Hu X, Sun C, Long Y, Zheng H. Determining the critical micelle concentrations of cationic surfactants based on the visible-light-induced oxidase-like activity of fluorescein. Colloids and Surfaces A: Physicochemical and Engineering Aspects. 2020 Jun 20;595:124698.

[65] Esfandyari H, Rahimi AM, Esmaeilzadeh F, Davarpanah A, Mohammadi AH. Amphoteric and cationic surfactants for enhancing oil recovery from carbonate oil reservoirs. Journal of Molecular Liquids. 2021 Jan 15;322:114518.

[66] Binks BP, Rodrigues JA, Frith WJ. Synergistic interaction in emulsions stabilized by a mixture of silica nanoparticles and cationic surfactant. Langmuir. 2007 Mar 27;23(7):3626-36.

[67] Yamada H, Urata C, Higashitamori S, Aoyama Y, Yamauchi Y, Kuroda K. Critical roles of cationic surfactants in the preparation of colloidal mesostructured silica nanoparticles: control of mesostructure, particle size, and dispersion. ACS applied materials & interfaces. 2014 Mar 12;6(5):3491-500.

[68] Hegazy MA, El-Etre AY, El-Shafaie M, Berry KM. Novel cationic surfactants for corrosion inhibition of carbon steel pipelines in oil and gas wells applications. Journal of Molecular Liquids. 2016 Feb 1;214:347-56.

[69] Tehrani-Bagha AR, Singh RG, Holmberg K. Solubilization of two organic dyes by cationic ester-containing gemini surfactants. Journal of colloid and interface science. 2012 Jun 15;376(1):112-8

[70] Li Z, Ma Y, Zhao K, Zhang C, Gao Y, Du F. Regulating droplet impact and wetting behaviors on hydrophobic weed leaves by a double-chain cationic surfactant. ACS Sustainable Chemistry & Engineering. 2021 Feb 8;9(7):2891-901.

[71] Brinatti C, Huang J, Berry RM, Tam KC, Loh W. Structural and energetic studies on the interaction of cationic surfactants and cellulose nanocrystals. Langmuir. 2016 Jan 26;32(3):689-98.

[72] Schulze-Zachau F, Braunschweig B. C n TAB/polystyrene sulfonate mixtures at air–water interfaces: effects of alkyl chain length on surface activity and charging state. Physical Chemistry Chemical Physics. 2019;21(15):7847-56.

[73] Raffa P, Wever DA, Picchioni F, Broekhuis AA. Polymeric surfactants: synthesis, properties, and links to applications. Chemical reviews. 2015 Aug 26;115(16):8504-63.

[74] Guzmán E, Llamas S, Maestro A, Fernández-Peña L, Akanno A, Miller R, Ortega F, Rubio RG. Polymer–surfactant systems in bulk and at fluid interfaces. Advances in colloid and interface science. 2016 Jul 1;233:38-64.

[75] Voronov S, Kohut A, Tarnavchyk I, Voronov A. Advances in reactive polymeric surfactants for interface modification. Current opinion in colloid & interface science. 2014 Apr 1;19(2):95-121.

[76] Bureiko A, Trybala A, Kovalchuk N, Starov V. Current applications of foams formed from mixed surfactant–polymer solutions. Advances in colloid and interface science. 2015 Aug 1;222:670-7.

[77] Chatterjee S, Prajapati R, Bhattacharya A, Mukherjee TK. Microscopic evidence of "necklace and bead"-like morphology of polymer–surfactant complexes: a comparative study on poly (vinylpyrrolidone)–sodium dodecyl sulfate and poly (diallyldimethylammonium chloride)–sodium dodecyl sulfate systems. Langmuir. 2014 Aug 19;30(32):9859-65.

[78] Tetteh J, Bai S, Kubelka J, Piri M. Wettability reversal on oil-wet calcite surfaces: Experimental and computational investigations of the effect of the hydrophobic chain length of cationic surfactants. Journal of Colloid and Interface Science. 2022 Aug 1;619:168-78.

[79] Shen X, Wang S, Guo J, Chen F, Xu B, Wang Z, Liu Y. Effect of carbon chain lengths of cationic surfactant on inhibition rate of acid-rock reaction. Journal of Petroleum Science and Engineering. 2021 Jan 1;196:107793.

[80] Seres L, Varga N, Juhász Á, Csapó E. Novel approaches to monitoring the formation of self-assembled colloids composed of cationic surfactants and alginate polysaccharide. Surfaces and Interfaces. 2024 Jun 1;49:104430.

[81] Hinnant KM, Brown LC, Daniels GC, Capps JR, Weise NK, Giordano BC. Solution and foam properties of polyethylene oxide-lauryl acrylate random comb polymers and aggregation behavior with alkylpolyglycoside surfactants. Colloids and Surfaces A: Physicochemical and Engineering Aspects. 2024 Nov 20;701:134667.

[82] Ansari AA, Kamil M, Kabir-ud-Din. Polymer-surfactant interactions and the effect of tail size variation on micellization process of cationic ATAB surfactants in aqueous medium. Journal of dispersion science and technology. 2013 May 1;34(5):722-30.

[83] Bahramian A, Thomas RK, Penfold J. The adsorption behavior of ionic surfactants and their mixtures with nonionic polymers and with polyelectrolytes of opposite charge at the air–water interface. The Journal of Physical Chemistry B. 2014 Mar 13;118(10):2769-83.

[84] Khan N, Brettmann B. Intermolecular interactions in polyelectrolyte and surfactant complexes in solution. Polymers. 2018 Dec 31;11(1):51.

[85] Keshavarzi B, Schwarzenberger K, Huang M, Javadi A, Eckert K. Formation of Structured Membranes by Coacervation of Xanthan Gum with C n TAB Surfactants. Langmuir. 2019 Sep 24;35(42):13624-35.

[86] Dan A, Ghosh S, Moulik SP. Physicochemistry of the interaction between inulin and alkyltrimethylammonium bromides in aqueous medium and the formed coacervates. The Journal of Physical Chemistry B. 2009 Jun 25;113(25):8505-13.

[87] Das S, Mondal S, Ghosh S. Interaction of cationic gemini surfactant tetramethylene-1, 4-bis (dimethyltetradecylammonium bromide) with anionic polyelectrolyte sodium

carboxymethyl cellulose, with two different molar masses, in aqueous and aquo-organic (isopropanol) media. RSC advances. 2016;6(37):30795-803.

[88] Gaudin T, Lu H, Fayet G, Berthauld-Drelich A, Rotureau P, Pourceau G, Wadouachi A, Van Hecke E, Nesterenko A, Pezron I. Impact of the chemical structure on amphiphilic properties of sugar-based surfactants: A literature overview. Advances in Colloid and Interface Science. 2019 Aug 1;270:87-100.

[89] Zhao X, An D, Ye Z. Adsorption and thermodynamic properties of dissymmetric gemini imidazolium surfactants with different spacer length. Journal of Dispersion Science and Technology. 2017 Feb 1;38(2):296-302.

[90] Mahbub S, Islam M, Masum A, Akter P, Hoque MA, Kumar D, Khan F, Rub MA, Alfaifi SY, Asiri AM. Role of carbonate electrolytes on interaction of quinolone drug with anionic surfactant at various temperatures: a conductometric study. Journal of Physical Organic Chemistry. 2021 Jan;34(1):e4121.

[91] Di Michele A, Brinchi L, Di Profio P, Germani R, Savelli G, Onori G. Effect of head group size, temperature and counterion specificity on cationic micelles. Journal of colloid and interface science. 2011 Jun 1;358(1):160-6.

[92] Singh G, Singh G, Kang TS. Effect of alkyl chain functionalization of ionic liquid surfactants on the complexation and self-assembling behavior of polyampholyte gelatin in aqueous medium. Physical Chemistry Chemical Physics. 2016;18(37):25993-6009.

[93] Das S, Mondal S, Ghosh S. Physicochemical studies on the micellization of cationic, anionic, and nonionic surfactants in water–polar organic solvent mixtures. Journal of Chemical & Engineering Data. 2013 Sep 12;58(9):2586-95.

[94] Nabi A, Tasneem S, Jesudason CG, Lee VS, Zain SB. Study of interaction between cationic surfactant (CTAB) and paracetamol by electrical conductivity, tensiometric and spectroscopic methods. Journal of Molecular Liquids. 2018 Apr 15;256:100-7.

[95] Basu Ray G, Chakraborty I, Ghosh S, Moulik SP, Holgate C, Glenn K, Palepu RM. Studies on binary and ternary amphiphile combinations of tetradecyltrimethylammonium bromide (C14TAB), tetradecyltriphenylphosphonium bromide (C14TPB), and tetradecylpyridinium bromide (C14PB). A critical analysis of their interfacial and bulk behaviors. The Journal of Physical Chemistry B. 2007 Aug 23;111(33):9828-37.

[96] Kumar D, Rub MA, Azum N, Asiri AM. Mixed micellization study of ibuprofen (sodium salt) and cationic surfactant (conventional as well as gemini). Journal of Physical Organic Chemistry. 2018 Jan;31(1):e3730.

[97] Padasala S, Kanoje B, Kuperkar K, Bahadur P. Mixed micellization study of alkyltrimethylammonium and alkyltriphenylphosphonium bromides in aqueous solution. Journal of Surfactants and Detergents. 2016 Mar;19:389-98.

[98] Shah SK, Bhattarai A. Interfacial and micellization behavior of cetyltrimethylammonium bromide (CTAB) in water and methanol-water mixture at 298.15 to 323.15 K. Journal of Chemistry. 2020;2020(1):4653092.

[99] Loh W, Teixeira LA, Lee LT. Isothermal calorimetric investigation of the interaction of poly (N-isopropylacrylamide) and ionic surfactants. The Journal of Physical Chemistry B. 2004 Mar 11;108(10):3196-201.

[100] Zdziennicka A, Szymczyk K, Krawczyk J, Jańczuk B. Activity and thermodynamic parameters of some surfactants adsorption at the water–air interface. Fluid Phase Equilibria. 2012 Mar 25;318:25-33.

[101] Lv J, Qiao W, Xiong C. Synthesis and surface properties of a pH-regulated and pH-reversible anionic gemini surfactant. Langmuir. 2014 Jul 22;30(28):8258-67.

[102] Das S, Naskar B, Ghosh S. Influence of temperature and organic solvents (isopropanol and 1, 4-dioxane) on the micellization of cationic gemini surfactant (14-4-14). Soft Matter. 2014;10(16):2863-75.

[103] Rub MA, Azum N, Asiri AM. Interaction of cationic amphiphilic drug nortriptyline hydrochloride with TX-100 in aqueous and urea solutions and the studies of physicochemical parameters of the mixed micelles. Journal of Molecular Liquids. 2016 Jun 1;218:595-603.

[104] Bhattarai A. Studies of aggregation properties of surfactant with and without polyelectrolyte in water and binary mixture of methanol-water from the surface tension measurements. Journal of Molecular Liquids. 2020 Aug 15;312:113438.

[105] Liang Z, Qiu X, Li J, Pan H, Liu H. An investigation on the hydrophobic binding stability of Azithromycin to the hydrocarbon chains of Tween: Based on micellization thermodynamics. Journal of Molecular Liquids. 2024 Mar 15;398:124279.

[106] Parekh P, Varade D, Parikh J, Bahadur P. Anionic–cationic mixed surfactant systems: micellar interaction of sodium dodecyl trioxyethylene sulfate with cationic gemini surfactants. Colloids and Surfaces A: Physicochemical and Engineering Aspects. 2011 Jul 20;385(1-3):111-20.

[107] Banipal TS, Kaur H, Banipal PK, Sood AK. Effect of head groups, temperature, and polymer concentration on surfactant—Polymer interactions. Journal of Surfactants and Detergents. 2014 Nov;17:1181-91.

[108] Singh AN, Yethiraj A. Liquid–liquid phase separation as the second step of complex coacervation. The Journal of Physical Chemistry B. 2021 Mar 18;125(12):3023-31.

[109] Castelletto V, Seitsonen J, Pollitt A, Hamley IW. Minimal peptide sequences that undergo liquid–liquid phase separation via self-coacervation or complex coacervation with ATP. Biomacromolecules. 2024 Jul 27;25(8):5321-31.

[110] Mukherjee S, Dan A, Bhattacharya SC, Panda AK, Moulik SP. Physicochemistry of interaction between the cationic polymer poly (diallyldimethylammonium chloride) and the anionic surfactants sodium dodecyl sulfate, sodium dodecylbenzenesulfonate, and sodium N-dodecanoylsarcosinate in water and isopropyl alcohol− water media. Langmuir. 2011 May 3;27(9):5222-33.

[111] Dan A, Ghosh S, Moulik SP. Interaction of cationic hydroxyethylcellulose (JR400) and cationic hydrophobically modified hydroxyethylcellulose (LM200) with the amino-acid based anionic amphiphile Sodium N-Dodecanoyl Sarcosinate (SDDS) in aqueous medium. Carbohydrate polymers. 2010 Mar 25;80(1):44-52.

[112] Jiao L, Zhang L, Guan W, Lu C. Fluorescence visualization of interactions between surfactants and polymers. RSC advances. 2016;6(92):88954-8.

CHAPTER-V

Colloidal Self-Assembly of Amphiphilic imidazolium ionic liquid (C_{16}MImCl) in the Presence of Hyaluronic acid (HA): An Integrated Multi-Technique Spectroscopic and Structural Analysis

Colloidal Self-Assembly of Amphiphilic imidazolium ionic liquid (C_{16}MImCl) in the Presence of Hyaluronic acid (HA): An Integrated Multi-Technique Spectroscopic and Structural Analysis

ABSTRACT

This article explores the complexation between the sodium salt of hyaluronic acid (HA), an anionic polyelectrolyte (PE), and 1-hexadecyl-3-methyl imidazolium chloride (C_{16}MImCl), a surface-active ionic liquid (SAIL) featuring an imidazolium cation moiety, in an aqueous medium, has been explored. The characterization of the PE-SAIL colloidal complex has necessitated a detailed analysis, addressing its surface activity, electrical mobility, coacervation behavior, size, and morphology. Various experimental methods, such as tensiometry, conductometry, turbidimetry, steady state and time-resolved fluorescence spectroscopy, dynamic light scattering (DLS), ζ-potential, FTIR-ATR, FESEM, HR-TEM, and fluorescence microscopy have been employed to unravel the complex interactions between oppositely charged PE and SAIL. The relevant thermodynamic parameters provide deep physicochemical understanding of the fundamental forces driving both interfacial and bulk complexation phenomena. The tensiometric findings illustrate the dynamic interaction between HA and C_{16}MImCl, giving rise to three key transition points, namely critical aggregation concentration (CAC), concentration of saturation (C_S), and extended critical micelle concentration (C_f), which emerge chronologically from lower to higher concentrations. A satisfactory correlation has been established between the experimental data and visual analysis of HA-C_{16}MImCl frameworks, supporting the validity of the observations and interpretations. In addition to the electrostatic interactions, which are supposed to be predominant, hydrophobic effects also contribute significantly during PE-IL binding processes. The ongoing research endeavour promises to be extremely beneficial in deeply understanding the fundamentals of the interactional behaviour between PEs and SAILs, as well as in the development of novel colloidal formulations for biomedical applications.

1. Introduction

The growing utilization of imidazolium-based ionic liquids for charge neutralization **[1]** in anionic polyelectrolytes represents a fascinating trend in modern colloid chemistry, holding both theoretical importance and potential practical benefits. Polyelectrolytes, which leverage the dual assets of polymeric and electrolytic functions, dissociate in an ionizing medium to release oppositely charged polyions and counterions. The polyelectrolyte backbone, abundant in polarized and dissociable functional groups, provides multiple intermolecular binding sites for effective interactions with surface-active agents. The colloidal formulations based on the oppositely charged PE-SAIL conjugates have been designed for advanced material development, finding applications in drug delivery **[2]**, protein encapsulation **[3]**, cosmetics **[4]**, enhanced oil recovery **[5]**, and many others. The key beneficial feature of PE-SAIL interacting systems is their exceptional ability to improve the solubilization of hydrophobic substances **[6]**, making a transformative impact on pharmaceutical science. The stability and physicochemical activities of these colloidal aggregates are primarily dictated by the polyelectrolyte charge **[7]** and the functional attributes of the SAIL alkyl chain **[8]**. In a recent

study, Das et al. **[9]** (2022) conducted a systematic investigation into the interaction dynamics of an imidazolium-based ionic liquid (C_{16}MImCl) and a phosphonium-based cationic surfactant (C_{16}TPB) with the anionic polyelectrolyte, sodium alginate (NaAlg), providing a detailed comparative analysis of their associative behavior. A few years ago, Singh et al. **[10]** (2018) explored the complexation behavior of three structurally distinct imidazolium-based ionic liquids (C_{12}MImCl, C_{12}AMImCl, and C_{12}EMImCl) with anionic sodium carboxymethylcellulose (NaCMC).

Hyaluronic acid (HA) is a linear, unbranched heteropolysaccharide from the glycosaminoglycans family that occurs naturally in the connective tissues of the human body and serves as a key component of the extracellular matrix (ECM) **[11]**. Based on the structural analysis of HA, the disaccharide building blocks consist of two monomeric units: D-glucuronic acid (containing a free carboxyl group) and N-acetyl-D-glucosamine (containing an N-acetyl group) **[12]**. HA is widely categorized as a polyanion, considering the dissociation of its carboxyl group imparts a net negative charge to the polymeric backbone over a broad p^H range **[13]**. With its excellent qualities, including biological compatibility **[14]**, biological degradability **[15]**, chemical modifiability **[16]**, viscoelasticity **[17]**, and biological availability **[18]**, this PE has earned a strong reputation in pharmaceutical research, being recognized as the "biomaterial of the near future **[19]**." The ability of HA to interact with various macromolecules, such as polymers **[20]** and proteins **[21]**, further enhances its versatility in biomedical applications (e.g., cancer therapy **[22]**, drug delivery **[23]**, wound dressings **[24]**, and tissue engineering **[25]**). Accordingly, researchers have engineered a variety of HA-based materials, including hydrogels **[26]**, nano-emulsions **[27]**, nanofibers **[28]**, dermal fillers **[29]**, microspheres **[30]**, nanocarriers **[31]**, and nanocomposites **[32]**. Polyelectrolyte-surfactant colloidal formulations for hydrophobic drug delivery can be optimized by applying positively charged surfactants to counteract the negative charge of the strongly hydrophilic surface of HA, a process driven by a combination of ionic and hydrophobic interactions [33]. So far, HA has been accepted as a suitable candidate for minimizing the cytotoxic actions of cationic surfactants (CTAB, Septonex) **[34]**. Until now, a number of publications addressing the interactions of HA with oppositely charged vesicles **[35]**, surfactants **[36-39]** are available in the literature. To the best of our knowledge, the colloidal behavior of HA in the presence of SAILs has yet to be studied, nor have the underlying mechanisms been elucidated.

Ionic liquids (ILs), better known as surface-active ionic liquids (SAILs) **[40]** within the colloidal science community, have attracted extensive scholarly interest across chemical, biological, and materials science disciplines due to their intrinsic amphiphilicity and exceptional interfacial properties. ILs are chemically identified as organic salts with melting points below 100^0C, composed of bulky organic cations such as imidazolium **[41]**, pyridinium **[42]**, pyrazolium **[43]**, piperidinium **[44]**, pyrrolidinium **[45]**, triazolium **[46]**, thiazolium **[47]**, sulfonium **[48]**, guanidium **[49]**, and morpholinium **[50]**, coupled with relatively smaller organic or inorganic anions. The unique physicochemical attributes of ILs are exemplified by their superb solvating power **[51]**, good heat stability **[52]**, high electrical conductivity **[53]**, non-volatility **[54]**, recyclability **[55]**, and potent antimicrobial activity **[56]**. Their structural flexibility allows fine-tuning of interfacial activity and other features

through strategic modulation of their cation-anion arrangement, earning them the title of "designer solvents" **[57]**. So far, ILs have been evaluated as "solvents of the future" **[58]** due to their wide range of applications in organic synthesis **[59]**, drug formulations **[60]**, nanotechnology **[61]**, and electrosynthesis **[62]**. In recent years, the solution thermodynamics of amphiphilic ILs, specifically 1-alkyl-3-methylimidazolium chloride (C_nMImCl, n=8-16), featuring a π-electron-stabilized aromatic imidazolium cation moiety, has been reported extensively in literature **[63, 64]**. These SAILs exhibit superior amphiphilic performance and a significantly lower CMC, outperforming traditional homologous ionic surfactants **[65]** and making them highly impactful in colloid and interface science. The SAIL used in this study is 1-hexadecyl-3-methylimidazolium chloride (C_{16}MImCl), which carries an imidazole ring as the hydrophilic head and a long hexadecyl chain as the hydrophobic tail. The enhanced hydrophobicity of the long alkyl chain, in tandem with the bulky imidazolium ring, effectively minimizes electrostatic repulsions between the cationic head groups, thereby facilitating the micellization process. A review of the published literature unveils elaborate discussions on the micellar dynamics of C_{16}MImCl in the presence of additives, including salts **[66]** and solvents **[67]**. Furthermore, substantial studies have explored its contribution to inducing vesicular self-assembly **[68]** and mix-micellization phenomenon **[69]**. The potential of C_{16}MImCl to form complexes with proteins **[70]** and drugs **[71]** has sparked increasing focus on its interactions with PEs. While the molecular interactions between conventional surfactants and PEs have been well-established, the intricate behaviour of SAILs with PEs has received comparatively less attention.

As articulated in the foregoing discourse, the interfacial dynamics of PE-SAIL conjugates remain inherently ambiguous due to the conspicuous paucity of systematic scholary investigations in this domain. This research embarks on a comprehensive exploration of the colloidal aggregation phenomena of the imidazolium-based SAIL, 1-hexadecyl-3-methyl imidazolium chloride (C_{16}MImCl), in conjunction with the anionic polyelectrolyte, hyaluronic acid (HA) in an aqueous medium, employing a state-of-the-art multi-technique analytical approach. The empirical data and microscopic observations of the HA-C_{16}MImCl complex demonstrate a high degree of synergistic convergence. The selection of PE and SAIL pairs is primarily dictated by their intrinsic biological functionalities. The colloidal behavior characterized in this study has, whenever necessary, been correlated with relevant literature to fortify our motif.

2. Experimental section

2.1. Materials

The anionic polyelectrolyte, hyaluronic acid sodium salt (HA), extracted from streptococcus equi sp., was the product of Sigma Aldrich (USA). The cationic surface-active ionic liquid (SAIL), 1-hexadecyl-3-methyl imidazolium chloride (C_{16}MImcl), was purchased from Acros Organics (Germany). No further purification protocols were undertaken for any of these samples. Scheme 1 illustrates the molecular structures of HA and C_{16}MImCl. AR-grade pyrene (a steady state fluorescence probe), coumarin 153 (a time-resolved fluorescence probe), and 1,6-diphenyl-1,3,5-hexatriene (DPH; a fluorescence microscopy probe) were

sourced from Sigma Aldrich (USA) and immediately utilized upon receipt to ensure molecular stability and uphold analytical precision. All experimental solutions were carefully prepared using double-distilled water. The concentration of HA in the aqueous medium was deliberately selected at 0.005%, 0.01%, and 0.02 % (w/v). Over the course of the experimental period, the aqueous polyelectrolyte solutions maintained remarkable physicochemical stability, with no detectable modifications in their structural attributes. Each experiment was conducted at a carefully controlled temperature of 298 K.

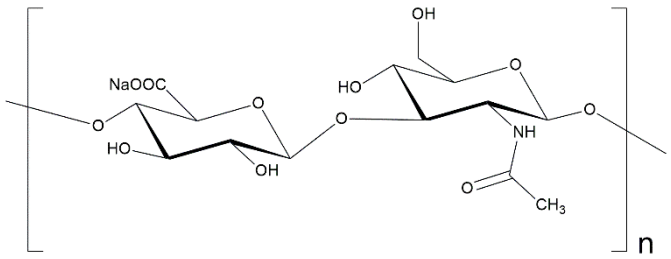

Hyaluronic acid

1-hexadecyl-3-methyl imidazolium chloride

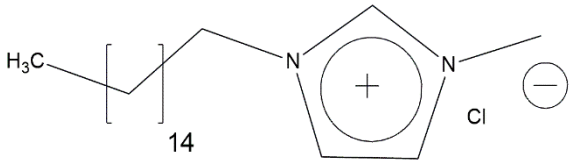

Scheme 1. Chemical structures of hyaluronic acid (left) and 1-hexadecyl-3-methyl imidazolium chloride (right).

2.2. Methods

2.2.1. Tensiometry

A calibrated tensiometer (Krüss, Germany) was used to analyze the surface behaviour of the HA-C_{16}MImcl system at the air/solution interface. Based on the ring (platinum) detachment technique, tensiometric measurements were conducted to ensure accurate characterization of interfacial dynamics. Prior to each experiment, the platinum ring was subjected to a rigorous purification procedure involving sequential cleansing with double-distilled water and acetone. It was then exposed to a high-temperature pyrolytic treatment in a pure ethanol flame until glowing, ensuring the complete thermal decomposition and volatilization of residual organic impurities. The experimental protocol was initiated by transferring 5 mL of aqueous polyelectrolyte solutions (0.005, 0.01 and 0.02% w/v) into a smoothly cleaned double-walled glass apparatus. A concentrated C_{16}MImcl solution (15 mM) was then progressively added to the polyelectrolyte stock solution using a Hamiltonian micro syringe, in exact accordance with the specified experimental requirements. Before taking each measurement, the polyelectrolyte-ionic liquid mixture was homogenized and allowed to settle for 10 minutes (equilibration time) to achieve a stable phase. The entire system was coupled to a thermostatic water bath to facilitate thermal regulation and maintain a constant temperature of 298 K. The accuracy of the measured tensiometric data was within a margin of $\pm$ 0.1 $mN\ m^{-1}$.

2.2.2. Conductometry

The specific conductance (κ) values were systematically measured using a Systronics 304 digital conductivity meter (India) equipped with a cell constant of 1.0 cm^{-1}. An initial aliquot of 6 mL of the polyelectrolyte solution was introduced into a thermostatic glass container, followed by the stepwise titration of the ionic liquid in accordance with the methodological framework detailed in Section 2.2.1. The dilution effect was effectively minimized by applying a very high concentration (≈ 15 times the CMC value) of the ionic liquid. The κ values maintained an accuracy within a ± 0.5% tolerance range.

2.2.3. Turbidimetry

A Shimadzu 1601 (Japan) UV-VIS spectrophotometer, operating in dual-beam mode under thermo-stated conditions at 298 K, was employed to probe the turbidity evolution. Prior to spectrophotometric analysis, double-distilled water was placed into two identical quartz cuvettes (1 cm optical path length) to standardize the experimental baseline. The turbidimetric titration process entailed the stepwise injection of a concentrated IL solution using a Hamiltonian micro-syringe to a cuvette containing 2.5 mL of the polyelectrolyte solution. The PE-SAIL solution was thoroughly agitated and given 2-3 minutes to attain equilibrium before recording absorbance data. The absorbance spectra were examined within the UV-visible spectral domain (200-800 nm) in percent transmittance (% T) mode. The turbidity index (100 - %T) of the polyelectrolyte solution was quantified at λ = 500 nm (the midpoint of the experimental wavelength range) and plotted against [IL]. The experimental errors ranged within ± 5%.

2.2.4. Zeta potential

The surface ζ-potential was analyzed using a Nano ZS Zetasizer (Malvern, UK) equipped with a gold-coated electrode at 298 K. A He-Ne laser beam, operating at a wavelength (λ) of 332 nm, was employed at a 90° scattering angle. To minimize interference from particulate contaminants and ensure optimal sample purity, the solutions underwent multiple filtrations (3–4 cycles) through cellulose acetate paper (0.45 μm pore size).

2.2.5. Fluorescence emission study

Steady-state fluorescence emission spectra were recorded using a Perkin-Elmer fluorimeter (LS 55, USA). Fluorimetric titrations were conducted by the gradual addition of a concentrated IL (≈ 15 mM) solution to different (w/v) % PE solutions. The measurements were carried out in a transparent quartz cuvette (10 mm path length) containing an initial sample volume of 2.5 ml. During the experiment, a tiny magnet bar was continuously actuated by an oscillating electromagnetic field within the cuvette, ensuring enhanced solute distribution. The thermal stability of the system was maintained at 298 K through a water flow thermostat. In this study, pyrene functioned as a fluorescent hydrophobic probe, exhibiting an excitation wavelength of 332 nm, while the emission spectra were recorded within the 350-450 nm spectral window. The excitation and emission slit bandwidths were calibrated to 14 and 2.5 nm, respectively, with spectral acquisition executed at a scanning rate of 250 nm/min. The pyrene concentration was maintained constant ($1 \times 10^{-4}\ mM$) in both the PE and IL solutions. For pyrene fluorescence analysis, the intensities of the first (I_1 at 373

nm) and third (I_3 at 383 nm) vibronic peaks were selected from the five well-defined vibronic emission bands. The molecular interactions of PE-IL complexes at various binding stages were investigated by plotting (I_1/I_3) against [IL] following the standard approach.

The effect of PE concentration on the aggregation number (N_{agg}) of SAIL micelles was studied using the static fluorescence quenching (SFQ) method, with pyrene ($1 \times 10^{-4}\ mM$) as the probe and 1-hexadecylpyridinium chloride (CPC) as the quencher. Using a Hamiltonian microsyringe, CPC was added dropwise to the pyrene-containing sample solution. After each addition, the fluorescence intensity spectra of the probe were recorded and subjected to quantitative analysis.

2.2.6. Time-resolved fluorescence

Time-resolved fluorescence lifetime measurements of C_{16}MImCl and HA-C_{16}MImCl systems were performed using a HORIBA-Jobin-Yvon TCSPC instrument at 298 K. Coumarin 153 was used as the fluorescent probe, excited at 450 nm with a NanoLED (IBH, UK), and its emission decay was recorded at 544 nm via a TBX photon detection module. Decay profiles for pure SAIL and SAIL-titrated HA solutions were analyzed with IBH DAS-6 software, following the titration method detailed in Section 2.2.5. A micellar SDS solution was used as a scatterer to calibrate the lamp profile, and χ^2 values were optimized near unity to ensure accurate fittings.

2.2.7. FTIR spectroscopy

Infrared spectral analysis was conducted using a Perkin Elmer (USA) FTIR spectrophotometer with an attenuated total reflectance (ATR) setup and a $LiTaO_3$ detector. Spectra were recorded over the 400–4000 cm^{-1} range. Pure HA and C_{16}MImCl were analyzed in solid form. The complex was prepared by dissolving 0.98 mM C_{16}MImCl in a 0.01 g% HA solution, followed by prolonged sonication. After settling, the coacervate was filtered, vacuum-dried, and analyzed via FTIR spectroscopy.

2.2.8. Dynamic light scattering (DLS)

The size of PE and PE-SAIL aggregates was measured using dynamic light scattering (DLS) with a Malvern Nano-ZS Zetasizer (Malvern, UK) at a constant 298 K. A He-Ne laser (λ = 632 nm) was directed at a 90-degree scattering angle. Prior to analysis, samples were sonicated for uniformity and filtered through 0.45 μm cellulose acetate paper to eliminate impurities. Reported size values represent the average of duplicate measurements.

2.2.9. Field emission scanning electron microscopy (FESEM)

The nanoscale surface morphology of SAIL-interacted HA samples was analyzed using a field emission scanning electron microscope (ZEISS EVO-18, 5.00 kV, Germany). Each FESEM sample was prepared by applying a 2 μL drop of the experimental solution onto a tiny transparent glass slide, enabling uniform surface coverage, followed by controlled solvent evaporation over several hours to enhance imaging resolution.

2.2.10. High resolution transmission electron microscopy (HR-TEM)

TEM images of pure HA and HA-C_{16}MImcl complex were examined using a JEOL JEM-2100 Plus (Tokyo, Japan) electron microscope operated at 200 kV. Sample preparation followed the drop-casting method, where a drop of the liquid sample was deposited onto a gold-coated Cu grid and left to dry slowly in a silica gel desiccator overnight, allowing residual solvent to dissipate entirely.

2.2.11. Fluorescence microscopy

Fluorescence imaging of the PE-IL samples was performed using an Olympus IX73 (one-deck system) inverted microscope. DPH was used as the fluorophore for the investigation, and its solution was prepared in absolute ethanol. A small amount of DPH was added to the PE-IL system, with the final concentration in the mixture being 0.1 mM. Prior to measurement, the experimental solution underwent thorough homogenization in an ultrasonic sonicator bath for several hours, followed by an overnight equilibration period. The instrument was outfitted with an FTIC filter to capture the high-resolution PE-IL binding images.

3. Results and discussions

3.1. Tensiometry

Tensiometric analysis enables an accurate assessment of the interfacial complexation dynamics within the HA-C_{16}MImCl colloidal system. Surface tension is inherently an interfacial property rather than a bulk characteristic. However, during tensiometric titration, a dynamic equilibrium is established between the interfacial and bulk structures through steady measurements, offering profound insights into the bulk-phase molecular interactions. Figure 2 (a-b) depicts the surface activity behaviour (γ vs. log C) of C_{16}MImCl in aqueous HA solutions. To evaluate their binding interactions, γ has been measured over a wider range of [C_{16}MImCl] in the HA-containing medium. The manifestation of multiple well-defined surface-active regimes substantiates the likelihood of strong molecular associations between HA and C_{16}MImCl. In the presence of HA, the tensiometric profile reveals three critical phase transitions: the critical aggregation concentration (CAC), polymer saturation concentration (C_s), and extended CMC (C_f). Accordingly, the overall interactional behaviour of the HA-C_{16}MImCl system can be segmented into four distinct interfacial zones, each corresponding to a varying degree of complexation. For pure IL, the surface tension plot (Figure 1 (a)) follows the expected interfacial response, marked by a distinct inflection point indicative of a singular phase shift. The hydrophobic tail of the SAIL withdraws from the aqueous environment to reduce repulsion from water molecules, while the hydrophilic head remains preferentially in the aqueous phase, guided by favourable solvation energetics. The competitive accumulation of SAIL monomers at the interface disrupts the cohesive H-bonding network in the water medium, significantly lowering surface tension as [SAIL] increases and ultimately leading to interfacial saturation **[72]**. The onset of micellization is indicated by the emergence of a minimum in the plot, with the corresponding [SAIL]

defining the critical micelle concentration (CMC) of pure SAIL. Thereafter, any additional SAIL molecules spontaneously self-assemble into thermodynamically stable micellar structures within the bulk solution. These micelles exhibit a well-organized amphiphilic architecture, wherein the bulky polar head groups form a sterically stabilized interfacial shell and effectively encapsulate the hydrophobic alkyl chain within the micellar core. At this stage, the interfacial monolayer reaches saturation and remains practically inert to further monomer adsorption, ensuring that the surface activity of the experimental solution remains unaffected. Micellar particles are recognized as forming an entirely different colloidal phase, which can dramatically alter the physicochemical nature of the solution. The self-aggregation behaviour and related thermodynamic aspects of C_{16}MImCl have already been discussed in the literature. The measured CMC value (0.85 mM) falls within the range of literature-reported data **[73]**. Table 1 provides a comprehensive summary of the concentration values corresponding to the observed transitions (CAC, C_S, and C_f) in the HA-C_{16}MImCl systems, along with the CMC of pure C_{16}MImCl, as determined through various analytical techniques. The appearance of three inflection points highlights the complex and multifaceted interaction pathways between C_{16}MImCl and HA. In our previous study **[74]**, the absence of both CAC and C_S in the weakly interacting HEC-SDDS system is likely due to the lack of electrostatic forces. In that case, their binding is induced only by hydrophobic interactions. The aqueous solution of HA exhibits surface activity **[75]**, as indicated by its ability to lower the γ of water from 71.8 $mN\ m^{-1}$ to 63, 63.2, and 62.9 $mN\ m^{-1}$ at concentrations of 0.005%, 0.01%, and 0.02% (w/v), respectively. However, within this concentration range, no significant change in γ is observed, indicating that its surface-active effect has attained saturation.

Initially, the addition of a small amount of C_{16}MImCl to the HA solution causes a sharp reduction in γ, marking the first noticeable breakpoint at CAC. The interactions between opposing charges ($C_{16}MIm^+$ and COO^-) drive the early-stage self-assembly of C_{16}MImCl, even at a concentration far below its CMC. This suggest that the cooperative binding is activated at CAC. The observed tensiometric trend in Zone I can be ascribed to the spontaneous formation of highly surface-active HA-C_{16}MImCl monomer complexes. Another possible reason for the initial rapid decrease in γ is a consequence of the predominant interfacial adsorption of C_{16}MImCl during the binding process. As evidenced in other PE-SAIL systems, [HA] exerts a negligible influence on CAC values, causing only a marginal increase. In the post-CAC zone (Zone II), the aggregates show a strong affinity for the polymeric backbone, minimizing the adsorption of C_{16}MImCl at the interface. This implies that complex formation is more favoured in the bulk phase than at the interfacial region. Consequently, surface activity in this zone remains largely unperturbed, resulting in the development of a large-scale plateau. As the [HA] increases from 0.005% to 0.02%, the plateau gradually widens. However, with the further addition of C_{16}MImCl, it abruptly disappears, followed by a steady decrease in γ. This transition occurs at a specific concentration, referred to as C_S. At this point, the anionic HA backbone becomes fully occupied by electrostatic-induced small C_{16}MImCl aggregates, indicating the completion of the complexation between HA and C_{16}MImCl. Notably, electrostatic and hydrophobic interactions work synergistically, exerting a dual influence within this interaction zone. The appearance of a plateau between the CAC and C_S regions in the tensiographs is highly

unusual, with only a few cases reported in the literature, such as the inulin-OTAB **[76]** and NaCMC-GS (14-1-14) **[77]** systems. In this section of the graph, most patterns display a trough followed by a maximum, creating a hump-like shape **[78]**, with the maxima point identified as C_S. Increasing [HA] expands the polymeric surface area available for binding with C_{16}MImCl, which is reflected in the substantial rise in C_S values to 0.086, 0.20, and 0.38 mM for 0.005, 0.01, and 0.02% HA, respectively. This trend underscores the impact of PE concentration in modulating binding interactions. As detailed in Section 3.3., coacervates begin to nucleate just beyond CAC and remain partially solubilized even at higher [C_{16}MImCl]. The visualization of this early-stage phase separation strongly indicates the dominance of electrostatic interactions. In the post-C_S region (Zone III), the gradual accumulation of C_{16}MImCl molecules congests the interface, leading to a continuous decline in γ until full saturation is achieved. As illustrated in Figure 1, Zone I exhibits a steeper slope than Zone III. Upon reaching the final break point at C_f, C_{16}MIMCl monomers readily micellize in the bulk, bringing about a stabilization of interfacial activity in Zone IV. The resulting plateau-like shape closely mirrors the micellization behaviour of pure C_{16}MImCl. The data in Table 1 clearly shows that the C_f values increase with [HA]. Thereby, an increase in PE concentration slows down the onset of micellization in surfactant systems. This finding is consistent with trends observed in the literature **[79]**. Dan et al. **[80]** have provided an explanation for the increase in C_S and C_f with PE concentration, drawing attention to the relevance of 'mass balance consideration'. In an aqueous HA environment, the C_f values tend to increase relative to the CMC of pure SAIL, except at the lowest [HA], where a slight decrease is seen. In fact, at 0.005% HA, the C_f value (0.71 mM) falls below the CMC (0.82 mM) of pure C_{16}MImCl. However, as [HA] increases from 0.01% to 0.02%, the C_f values rise by ~1.2 and ~1.5 folds, respectively, compared to the normal CMC of C_{16}MImCl. It is plausible to predict a marked increase in the C_f values for both SAILs and conventional surfactants within an aqueous PE solution, as a large excess of SAIL or surfactant monomers is requisite to saturate the PE backbone before free micellization can take place.

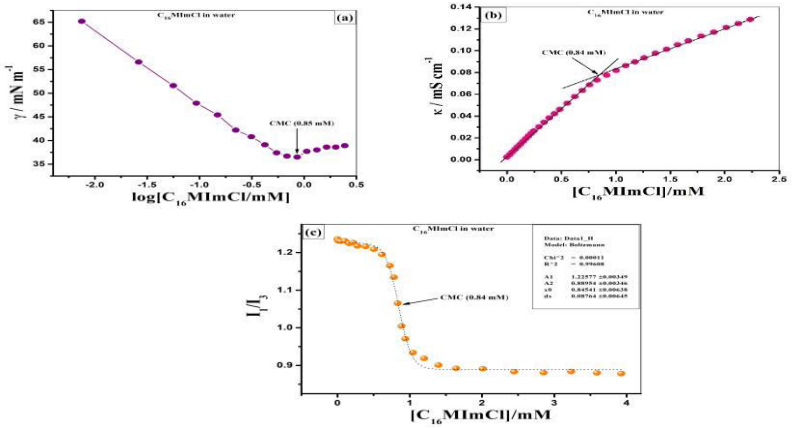

Figure 1. Experimental identification of the critical micelle concentration (CMC) of C_{16}MImCl in an aqueous system at 298 K using (a) tensiometry, (b) conductometry, and (c) fluorimetry.

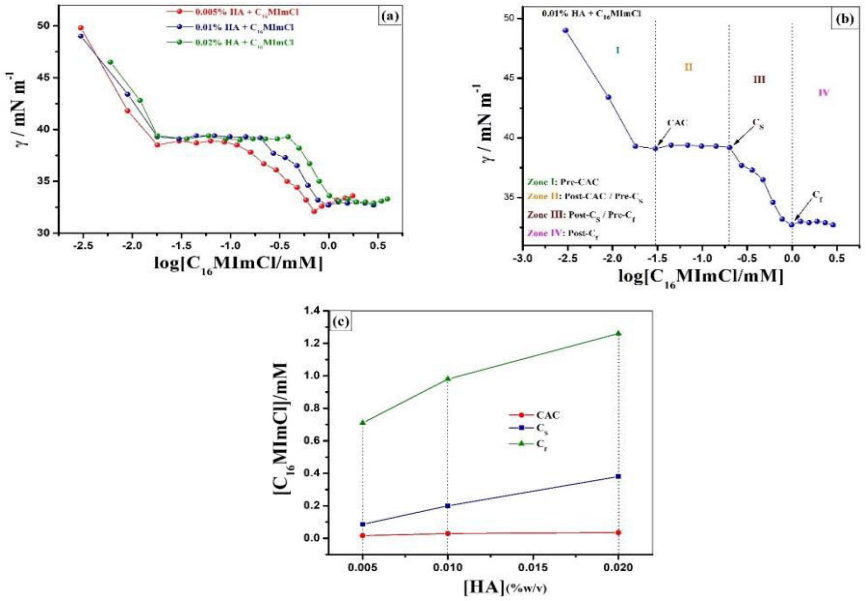

Figure 2. (a) Tensiometric curves of HA-C_{16}MImCl systems at different HA concentrations (% w/v) in aqueous solution at 298 K; (b) Transition points (CAC, C_S, and C_f) marked for the 0.01% HA solution; (c) Effect of varying PE concentrations (0.005%, 0.01%, and 0.02%) on CAC, C_S, and C_f in HA-C_{16}MImCl systems.

3.2. Conductometry

Conductometry is a potential approach for analyzing the bulk complexation mediated by charged species. Figure 3 displays conductometric plots depicting the variation in specific conductance slope as a function of [SAIL] in aqueous HA solutions. In all cases, electrical conductivity exhibits a non-uniform rise with increasing [SAIL]. Table 1 presents the concentrations measured at key transition points during conductometric titrations. As predicted for pure SAIL, a sudden conductivity transition is observed at the CMC (Figure 1 (b)). In an aqueous solution, SAIL monomers behave as strong electrolytes, fully dissociating into their constituent ions ($C_{16}MIm^+$ and Cl^-). The resulting plot perfectly fits into a pair of straight lines with different slopes, intersecting at the CMC. This distinguishes the pre- and post-micellar zones in the plot. Since the former zone is steeper than the latter, it suggests a decrease in the rate of conductivity enhancement following the micellization process. In the pre-micellar zone, the increase in conductivity is primarily driven by the combined ion transport of free monomers ($C_{16}MIm^+$) and counterions (Cl^-) of SAIL molecules. At the micellization point, an equilibrium is established, where free monomers, counterions, and newly formed micelles coexist. In the post-micellar zone, the restricted transport of charged species in the bulk is attributed to the formation of larger micelles (aggregated monomers) and the condensation of counterions onto the micellar interface. As a result, the overall count

of charge carriers decreases, which in turn slows the conductivity growth, even at higher [SAIL]. There is a strong agreement between the observed CMC values of pure SAIL obtained through tensiometry (0.85 mM) and conductometry (0.84 mM).

The interaction between SAIL and HA produces two clear break points, which closely resemble the C_S and C_f values achieved via tensiometry. The conductometric plot, however, fails to detect a distinct break point near the CAC. At extremely low [SAIL], the conductance values are very close, making it difficult to locate the subtle slope changes surrounding the CAC region. The absence of the first break point in conductometry, in contrast to tensiometry, has been mentioned by several authors in their systems **[81]**. This discrepancy is likely due to the fact that conductometry registers a major shift only after considerable coacervation has occurred in the bulk, while tensiometry, being more sensitive, tracks the initial formation of the surface-active HA-$C_{16}MIM^+$ complex at a much earlier stage. The analysis of the interaction process using tensiometry focuses on the interfacial properties, whereas conductometry probes bulk physico-chemistry. Thus, identical conclusions may or may not be obtained while studying a specific system using different methods. The initial mild break point, corresponding to C_S, results from the gradual binding of small SAIL aggregates to the PE chain. During this phase, stronger interactions between PE and SAIL have little impact on the solution conductivity, as reflected in the lower slope value. At this juncture, the PE chain is fully enriched with SAIL. In the post-C_S stage, the PE-SAIL complex no longer exhibits any affinity for incoming SAIL. Therefore, increasing [SAIL] introduces SAIL monomers as the only charge carriers, leading to a sharp rise in conductivity with a much steeper slope. The second and final break point, identified as C_f, which signals the onset of micelle formation, is fairly prominent. Following the identical micellization pathway as pure SAIL, the counterions from the bulk tend to accumulate at the electrical double layer of micellar assembly. This significantly lowers the number of available charge carriers, resulting in a reduced conductivity slope. Table 1 shows that increasing the PE content is accompanied by a rise in both C_S and C_f values.

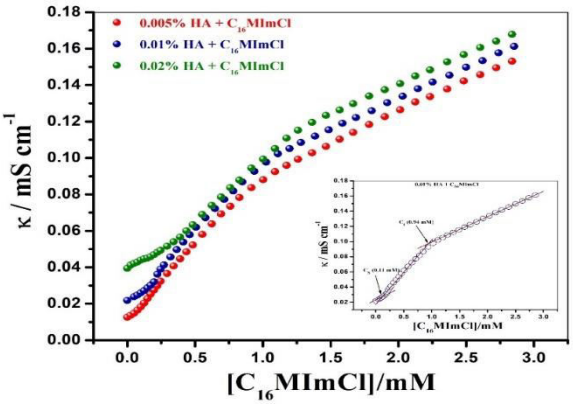

Figure 3. Variation of specific conductance (κ) with [C_{16}MImCl] in an aqueous medium at different HA concentrations (% w/v). Inset: Identification of breakpoints (C_S and C_f) for the 0.01% HA-C_{16}MImCl system.

Table 1. Critical Concentrations for Various Stages of HA-C_{16}MImCl Complex Formation in Aqueous Solution at 298 K, Measured Through Surface Tension, Conductometry, Turbidimetry, and Fluorimetry Techniques.

	Tensiometry			Conductometry		Turbidimetry			Fluorimetry		
[HA]/% (w/v)	CAC	C_S	C_f	C_S	C_f	T_1	T_2	T_3	CAC	C_S	C_f
0	-	-	0.85	-	0.84	-	-	-	-	-	0.84
0.005	0.017	0.086	0.71	0.069	0.86	0.034	0.27	0.99	0.014	0.17	0.98
0.01	0.029	0.20	0.98	0.11	0.94	0.067	0.39	1.09	0.030	0.35	1.10
0.02	0.035	0.38	1.26	0.26	1.22	0.084	0.61	1.34	0.039	0.40	1.50

3.3. Thermodynamics of interfacial and bulk complexation

Tensiometric and conductometric results have been used to quantify and characterize several fundamental interfacial and bulk physicochemical parameters. Table 2 encapsulates a comprehensive summary of the computed parameters for both pure SAIL and PE-SAIL systems. The underlying mathematical formulations, the paramount significance of these parameters within this analytical framework, and a meticulous exegesis of the observed phenomena are discussed below.

(a) Interfacial tension at CMC (γ_{CMC})

Phenomenologically, the CMC signifies interfacial saturation in the tensiometric curve. Thus, after exceeding this specific concentration, the γ value does not alter much. The parameter γ_{CMC} (in $mN\,m^{-1}$) represents the relevant surface tension value at CMC, which gives a measure of the propensity of the SAIL monomers to crowd at the air/solution interface prior to micelle formation in the bulk. In this study, compared to HA-free SAIL system, the values of γ_{CMC} are somewhat lower in the presence of HA. A decrease in the γ_{CMC} value indicates enhanced interfacial activity of the experimental solution. The tensiometric analysis (Section 3.1.) has already established the mild surface-active nature of HA. Thus, HA can impact the surface properties as well as γ_{CMC} of the HA-SAIL systems. However, according to Table 2, the γ_{CMC} increases as the HA concentration does. The most plausible explanation is that at higher PE concentrations, the incoming SAIL molecules preferentially tend to interact with SAIL-saturated PE in the bulk instead of accumulating at the interface.

(b) Surface pressure (π_{CMC})

There exists a strong interrelation between surface tension and surface pressure. Thus, the concept of surface pressure provides an estimation of the interfacial behavior of the SAIL

molecules. By introducing surface tension values at two distinguished intervals, the following formula has been applied for the measurement of π_{CMC} **[82]**:

$$\pi_{CMC} = \gamma_{iniial} - \gamma_{CMC/Cf} \quad (1)$$

Where, π_{CMC} represents the surface pressure at the interfacial saturation point (CMC), γ_{iniial} defines the interfacial tension of the SAIL-free surface (e.g., double-distilled water or aqueous PE solution), and $\gamma_{CMC/Cf}$ corresponds to the interfacial tension under the influence of SAIL at CMC or C_f. Here, γ_{CMC} pertains to the micellization of pure SAIL, while γ_{Cf} is ascertained for PE-SAIL systems at varying PE concentrations. In the presence of SAIL, the surface tension of the relevant colloidal systems is minimized at CMC or C_f. Thus, the value of π_{CMC} denotes the maximum decrement in surface tension of the experimental system. The value of π_{CMC} for pure SAIL exhibits a decreasing trend with increasing PE concentration. Accordingly, the effectiveness of surface tension minimization in the PE-SAIL systems, as evaluated, demonstrates an inverse correlation with $\gamma_{CMC/Cf}$. This parameter serves as a valuable metric for evaluating the surface activity of SAIL in both aqueous and PE media. Another salient aspect of this parameter is its integration in the equation involving ΔG^0_{Ads}.

(c) The surface excess concentration at CMC (Γ_{max})

This interfacial parameter characterizes the preferential adsorption of SAIL molecules at the interface, quantifying their excess accumulation relative to the bulk-phase equilibrium state. In this regard, the interfacial thickness is assumed to be infinitesimally small. The quantity Γ_{max} is derived from the Gibbs adsorption isotherm equation and is therefore termed Gibbs surface excess. The following equation provides a mathematical explanation for the natural tendency of surface-active agents to lower the medium surface tension **[83]**:

$$\Gamma_{max} = -\left(\frac{1}{2.303iRT}\right) \lim_{[SAIL]\rightarrow CMC(\mathrm{Cf})} \left(\frac{d\gamma}{dlogC}\right) \quad mol\, m^{-2} \quad (2)$$

Here, the term 'i' represents the effective stoichiometric dissociation factor of ionic species per SAIL monomer adsorbed at the air/solution interface. For the studied SAIL, i = 2 ($C_{16}MIm^+$ and Cl^-) in both aqueous and polyelectrolyte environments. The symbol 'R' is the universal gas constant (8.314 joule $mol^{-1}K^{-1}$), and 'T' is the absolute temperature, set at 298 K. The differential factor $\left(\frac{d\gamma}{dlogC}\right)$ represents the premicellar slope near the saturation point, and it is derived through a second-order polynomial regression in the tensiometric plot (γ vs. log [SAIL]). For pure SAIL, the slope is evaluated within the pre-CMC phase, extending to the micellization onset. However, in the HA-SAIL system, the pre-micellar region lies between C_S and C_f, extending up to C_f. The Γ_{max} of the SAIL shows a slight increase at lower PE concentrations (0.005% and 0.01%) but declines sharply at the higher concentration (0.002%). The large reduction in Γ_{max} results from the stronger electrostatic association of SAIL molecules in a highly ionic atmosphere with increased PE charge density, which limits the availability of SAIL molecules for interfacial adsorption.

(d) Minimum headgroup area (A_{min})

The limiting headgroup area of a surfactant molecule at a maximally packed interface is determined as follows **[84]**:

$$A_{min} = \frac{10^{18}}{N_A \Gamma_{max}} \quad (3)$$

Here, 'N_A' denotes Avogardo's constant, while the exponential factor 10^{18} arises from the unit conversion of m^2 to nm^2, given that 1 nm = 10^{-9} nm. A_{min} is essential for deciphering the interfacial arrangement of SAILs, determining whether the molecules exhibit a high or low packing density at the interface. As expected, the trend in A_{min} values is exactly the opposite to that observed for Γ_{max}.

(e) Counterion binding (β)

As determined by electrochemical measurements, κ vs. [SAIL] plots show distinct slope variations reflecting the linear dependence of specific conductivity on SAIL concentration. It is well-known that the bulk counterions (Cl^- in the case of C_{16}MImCl micelles) are the primary drivers for the sharp decline in slope observed beyond the CMC. The charge disparity between the micellar interface and the counterions induces the ionic micelles to electrostatically capture and bind the surrounding counterions. Above the CMC, incoming SAIL monomers dissociate to release more counterions, which accelerates the binding process at higher SAIL concentrations. The extent of counterion adsorption on the charged micellar surface is quantitatively assessed using the slope ratio method via conductometry. This approach is widely favoured for β measurements due to its simplicity, precision, and extensive validation in the literature **[85]**. According to the definition, the degree of counterion binding (β) represents the fraction of counterions that associate with the micellar surface and is mathematically expressed as:

$$\beta = 1-\alpha \quad (4)$$

In this context, α denotes the degree of dissociation, expressed as the ratio of the slopes of the post-micellar (S_2) and pre-micellar (S_1) phases. Accordingly, the following equation serves as an alternative means of introducing β **[86]**:

$$\beta = 1 - \frac{S_2}{S_1} \quad (5)$$

Considering that S_2 is less than S_1, the experimental value of β is expected to be within the range of 0 to 1, i.e., $0 < \beta < 1$. For pure SAIL, a single break point (CMC) with two distinct slopes has been detected. On the other hand, two break points (C_S and C_f) with three distinct slopes are produced when SAIL is introduced into the polyelectrolyte medium. In the PE-SAIL system, the post-micellization phase takes place between the C_S and C_f regions. The values of β show slight variation in the presence of HA, indicating that the high charge density of HA effectively screens the electrostatic interactions between the cationic headgroups and the counterions.

(f) Minimum free energy of adsorption (G_{min})

Sugihara has proposed a thermodynamic variable termed the minimum Gibbs free energy of adsorption (G_{min}) to evaluate synergistic interactions in composite systems. This variable is computed utilizing a designated mathematical expression **[87]**:

$$G_{min} = \gamma_{CMC}. A_{min}. N_A \quad (6)$$

Each symbol in the equation has been described previously. It determines the variation in free energy associated with the migration of the mixture components from the interior to the surface. The calculated $Gmin$ values for C_{16}MImCl decrease consistently at HA concentrations of 0.005% and 0.01% compared to the aqueous medium but show a marked increase at 0.02%.

(g) Standard Gibbs free energy of micellization (ΔG^0_{mic})

The Gibbs free energy change associated with micellar aggregation can be quantitatively determined through the utilization of the pseudophase model formulation **[88]**:

$$\Delta G^0_{mic} = (1+\beta)\ RT ln X_{CMC} \quad (7)$$

In this equation, X_{CMC} corresponds to the cmc or C_f quantified on a mole-fraction basis. The free energy change related to SAIL micellization is considerably negative, irrespective of the presence or absence of PE, thereby confirming that the process is inherently spontaneous from a thermodynamic perspective in all scenarios. The high negative value of ΔG^0_{mic} for the pure SAIL further increases in the presence of 0.005% and 0.01% HA but decreases at 0.02% HA. In the case of the mixed systems, the value of ΔG^0_{mic} becomes progressively less negative as the concentration of PE increases. This analytical finding suggests that the micellization in mixed PE-SAIL colloidal system is thermodynamically more favourable at lower PE concentrations.

(h) Standard Gibbs free energy of adsorption (ΔG^0_{Ads})

Rosen and Aronson **[89]** have formulated an equation that establishes a thermodynamic correlation between ΔG^0_{mic} and ΔG^0_{Ads} as follows:

$$\Delta G^0_{Ads} = \Delta G^0_{mic} - \frac{\pi_{CMC}}{\Gamma_{max}} \quad (8)$$

A more negative ΔG^0_{Ads} value signifies an enhanced thermodynamic propensity of the SAIL molecules to interfacially adsorb. In the present study, ΔG^0_{mic} and ΔG^0_{Ads} do not necessarily follow the same trend. The negative value of ΔG^0_{Ads} for the SAIL shifts lower at 0.005% and 0.01% HA but increases at 0.02% HA. This indicates that adsorption in mixed systems becomes more energetically favourable at higher PE content.

(i) Effective Gibbs free energy (ΔG^0_{eff})

The dominance of ΔG^0_{Ads} over ΔG^0_{mic} suggests that amphiphilic molecules are more likely to adsorb at interfaces than to spontaneously self-assemble into micelles in the bulk phase. The concept of "effective Gibbs free energy" denotes the thermodynamic divergence between ΔG^0_{Ads} and ΔG^0_{mic} **[90]**:

$$\Delta G^0_{eff} = \Delta G^0_{Ads} - \Delta G^0_{mic} \quad (9)$$

In both pure and mixed systems, the ΔG^0_{Ads} values invariably exceed the ΔG^0_{mic} values, with a ratio ($\frac{\Delta G^0_{Ads}}{\Delta G^0_{mic}}$) ranging from 1.59 to 2.15. This substantiates that adsorption process is energetically more advantageous than micellization phenomenon.

(j) Gibbs energy difference (ΔG^0_{ps})

The cac of the PE-SAIL system, at which micelle-analogous aggregates begin to nucleate along the PE chain, is always lower in magnitude than the CMC of pure SAIL. The ratio of these values enables a rigorous assessment of the PE-SAIL interaction strength via the parameter known as excess Gibbs free energy or Gibbs energy difference. This metric delineates the relative thermodynamic stability of PE-induced aggregates in contrast to free SAIL micelles. The equation requisite is as follows **[91]**:

$$\Delta G^0_{ps} = RT\ ln\frac{cac}{cmc} \quad (10)$$

A more negative ΔG^0_{ps} value indicates a greater thermodynamic propensity for interaction. Hence, a reduced (cac/CMC) ratio reflects more potent and cohesive molecular synergism between the polymer and surfactant. The ΔG^0_{ps} values corresponding to 0.005%, 0.01%, and 0.02% HA are determined to be – 9.24, - 8.72, and – 8.87 $kJ\ mol^{-1}$, respectively, thereby illustrating the sequential predominance of interaction: 0.005% > 0.02% > 0.01%.

(k) Efficiency of adsorption ($p^{C_{20}}$)

The interfacial adsorption metric $p^{C_{20}}$ characterizes the amphiphile's propensity for accumulation at the interface and is mathematically articulated by the following equation **[92]**:

$$p^{C_{20}} = - \log_{10} C_{20} \quad (11)$$

Here, C_{20} denotes the molar concentration of the SAIL molecules to diminish the interfacial tension of the initial solvent by an amount of 20 mN m^{-1}, as derived from the tensiometric plot. A higher $p^{C_{20}}$ value signifies enhanced interfacial accumulation at the air-liquid interface, culminating in a substantial diminution of surface tension. In the mixed systems, the introduction of HA induces an elevation in $p^{C_{20}}$ values relative to the pure system. This is attributed to the robust electrostatic interactions between HA and SAIL, which strengthen the formation of thermodynamically stable surface-active complexes. However, with a gradual increase in PE content, a simultaneous decrease in $p^{C_{20}}$ is observed within the mixed systems.

(l) Packing parameter (P)

The packing parameter (P), conceptualized by Israelachvili **[93]**, serves as a quantitative determinant in governing the self-assembled geometric architectures of micelles. A micelle can adopt a spheroidal conformation when P values range from 0 to 0.33, a cylindrical shape between 0.33 and 0.5, and a lamellar structure between 0.5 and 1 **[94]**. It is determined through the utilization of the following mathematical expression **[95]**:

$$P = \frac{V}{l A0} \quad (12)$$

where v, l, and A_0 correspond to the intrinsic molecular volume of the hydrophobic moiety, the theoretical maximum extension of the aliphatic chain, and the effective interfacial area per hydrophilic headgroup, respectively. The parameters l and v are systematically derived using Tanford's empirical correlations **[96]**, as elaborated below:

$$l = (0.154 + 0.1265\ C_N)\ nm \quad (13)$$

$$v = (0.0274 + 0.0269\ C_N)\ nm^3 \quad (14)$$

C_N quantifies the carbon atom count within the fully saturated alkyl hydrocarbon backbone of the SAIL. Due to the complexities associated with precisely measuring A_0, the literature suggests using A_{min} as a replacement in the equation **[97]**. In this study, the P values in all four cases are found well below 0.33, corresponding to the formation of spherical micelles.

Table 2. Interfacial and Thermodynamic Profiles of C_{16}MImCl Micellization as a Function of HA Concentration at 298 K.

[HA]/ % (w/v)	γ_{CMC} $(mN\ m^{-1})$	π_{CMC} $(mN\ m^{-1})$	$-(\frac{dy}{dlogC} \times 10^3)$	$\Gamma_{max} \times 10^6$ (mol/m^2)	A_{min} $(nm^2/molecule)$	G_{min} (KJ/mol)	β	$-\Delta G^0_{mic}$ (KJ/mol)	$-\Delta G^0_{Ads}$ (KJ/mol)	$\frac{\Delta G^0_{Ads}}{\Delta G^0_{mic}}$	$-\Delta G^0_{eff}$ (KJ/mol)	ΔG^0_{ps} (KJ/mol)	$p^{C_{20}}$	P
0	36.5	35.3	11.20	0.98	1.69	37.15	0.56	42.85	78.87	1.84	36.02		4.26	0.124
0.005	32.1	30.9	11.58	1.01	1.64	31.70	0.57	43.82	74.41	1.70	30.59	9.24	5.12	0.128
0.01	32.7	30.5	13.69	1.19	1.39	27.38	0.59	43.11	68.74	1.59	25.63	8.72	5.03	0.151
0.02	33.1	29.8	7.34	0.64	2.59	51.63	0.52	40.27	86.83	2.15	46.56	8.87	4.92	0.081

3.4. Turbidimetry

Turbidimetric titrations (100 - %T vs. [C_{16}MImCl]) provide a visual means to monitor the stepwise formation of coacervates during the bulk complexation of the HA-C_{16}MImCl system. The resulting curves (Figure 4) display three inflection points (T_1, T_2, and T_3), which indicate key phase transitions in the aggregation behavior of PE-SAIL complexes. Tiny solubilized particles barely scatter light, keeping solutions optically clear with minimal turbidity. In contrast, bulky insoluble aggregates strongly deflect light, producing highly turbid suspensions. Accordingly, turbidity-based measurement aids in determining the effective bulk composition of colloidal dispersions. Table 1 lists the quantitative parameters of the HA-C_{16}MImCl system at different [HA]. Turbidity remains visually undetectable until the first inflection point, T_1. At [SAIL] below T_1, the reduction in PE surface charge density is insufficient to disrupt solution homogeneity, resulting in the formation of soluble complexes. Consequently, the system persists as a monophasic solution, with no visible transitions. Within this narrow-concentration range, the solution composition carries a high net negative charge (as discussed in Section 3.4). The first transition (T_1) marks the onset of electrostatic association of SAIL molecules with the PE backbone, wherein monomeric $C_{16}MIm^+$ initiates adsorption onto the HA surface via charge interactions. After exceeding T_1, turbidity becomes visually apparent for the first instance and then rises sharply until reaching

the second transition point, T_2. Between T_1 and T_2, increasing [SAIL] enhances adsorption affinity at the PE interface through both electrostatic and hydrophobic interactions, accelerating the growth of the complexes and driving coacervation. At higher [SAIL], the reinforcement in hydrophobic interaction occurs as progressive charge neutralization diminishes the net negative zeta potential of the complexes. The sudden agglomeration of macroscopic colloidal particles induces a distinct biphasic separation, concomitant with a diminution in electrical mobility (elaborated in Section 3.2). The increase in turbidity is primarily due to the enlargement of both particle size and quantity in the medium. The emergence of T_2 signifies the point of maximum SAIL adsorption. The increasing trend in T_2 values (Table 1) with PE concentration confirms that a larger surface area enhances the molecular entrapment of SAIL. These observations show a strong correlation with both tensiometric and conductometric results. Thereafter, any additional SAIL contributes only marginally to turbidity until it attains a maximum at T_3. However, both the height and location of the turbidity maximum are shaped by PE concentration. As the initial HA concentration increases, both the peak turbidity and the corresponding SAIL concentration at which this peak is observed exhibit a concurrent rise. Specifically, at HA concentrations of 0.005%, 0.01%, and 0.02%, the maximum turbidity reaches approximately 36%, 79%, and 91%, respectively. The final inflection point corresponds to the optimal phase for liquid/solid separation, allowing the complete precipitation and maximum isolation of the PE-SAIL complex following an extended period of standing. As predicted, the complex electrical charges approach zero in the vicinity of maximum turbidity, which is reflected in the reduced stability of the colloidal complexes. After the T_3 stage, a slight fall in turbidity is observed **[98]**, as the [SAIL] is high enough to introduce free micelles into the bulk. This causes the coacervates to partially dissolve within the micellar environment. The values of T_1, T_2, and T_3 can be correlated with the inflection points, CAC, C_S, and C_f, respectively, observed in tensiometry. Here, it is noteworthy that different techniques are characterized by different modes of interaction mechanisms. In comparison to CAC, the T_1 values are considerably higher in magnitude. On the other hand, the values of T_2 and T_3 align closely with C_S and C_f, respectively. The only exception is observed at 0.005% (w/v) HA, where T_2 is much higher than the corresponding C_S value.

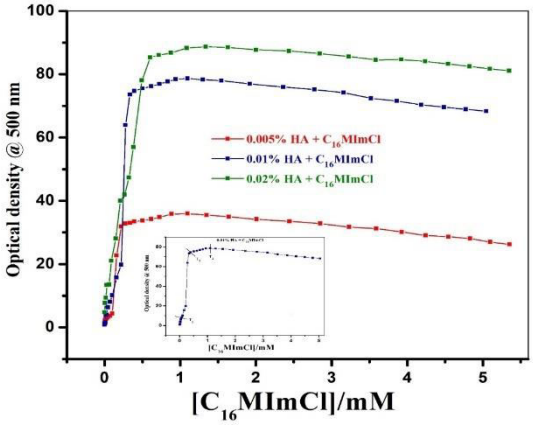

Figure 4. Measured turbidity (100 - %T) in HA-C_{16}MImCl mixtures at varying HA concentrations (% w/v); Inset: Detection of transition points (T_1, T_2, and T_3) for the 0.01% HA solution.

3.5. Zeta potential

The colloidal electrostatic stability of mixed PE-SAIL systems can be evaluated through ζ-potential measurements. Molecular associations within such formulations follow fundamental ion-exchange kinetics **[99]**, where electrostatic forces mediate the selective entrapment of surface-active cations around macroionic frameworks. As presumed, native 0.01% (w/v) HA carries a highly negative ζ-potential (-43.5 mV) **[100]** in the experimental solution, ascribed to the ionized carboxylate (COO^-) moieties along its polysaccharide backbone. The stepwise complexation of $C_{16}MIm^+$ with the HA backbone diminishes its anionic character, achieving electrostatic neutrality at ≈ 0.35 mM [C_{16}MImCl] (SAIL-to-PE mass ratio ≈ 1.26:1). Beyond this, excess SAIL induces charge inversion, yielding a highly cationic system. The ζ-potential curve (Figure 5) for [C_{16}MImCl] exhibits three distinct transitions, namely, ϕ_1, ϕ_2, and ϕ_3, comparable with tensiometric results. At very low concentrations, the introduction of cationic SAIL leads to a steady rise in ζ-potential until ϕ_1 (0.047 mM). With the continued addition of SAIL, the surface charge continues to increase but at a slower rate, reaching ϕ_2 (0.27 mM), where the PE chain becomes fully saturated. Throughout these transitions, electrostatic interactions between imidazolium and carboxyl groups of HA dominate. While electrostatic interactions contribute to charge modulation, hydrophobic forces play a crucial role in molecular association and surface charge stabilization. Beyond ϕ_3 (>1.13 mM), excess counterions bind to positively charged "HA-stabilized" micelles, with little impact on overall electrical properties. A deeper understanding of charge dynamics in these complexes is essential for unraveling the colloidal stability of the oppositely charged PE-SAIL system.

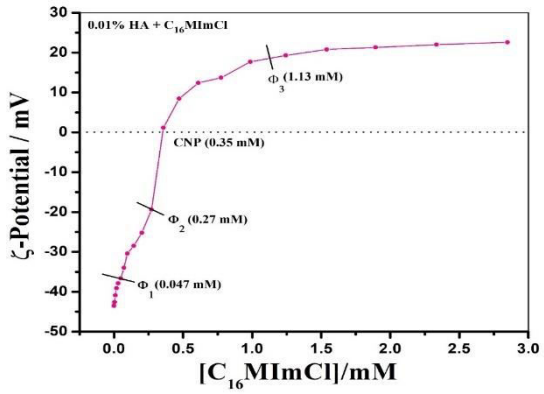

Figure 5. Changes in ζ-potential (electrical charge) of an aqueous 0.01% (w/v) HA-C_{16}MImCl solution as a function of C_{16}MImCl concentration at 298 K. Charge neutralization of HA takes place at 0.35 mM C_{16}MImCl (CNP). Transition points (ϕ_1, ϕ_2, and ϕ_3) are marked by arrows.

3.6. Fluorescence emission study

Fluorescence spectroscopy is employed to investigate further the role of micropolarity in HA-C_{16}MImCl complexation in light of bulk microenvironment dynamics. Fluorescence analysis substantiates the validity of prior observations, with pyrene **[101]** serving as a polarity-sensitive hydrophobic probe. Despite its low water solubility, pyrene reliably detects SAIL micellization and PE-SAIL interactions. The aromatic structure of pyrene consists of four highly conjugated planar rings, with an emission spectrum featuring five vibrational peaks (I_1, I_2, I_3, I_4, and I_5) **[102]**. Fluorescence spectral analysis primarily focuses on I_1 and I_3, where I_1 varies with medium polarity, but I_3 does not. The micropolarity index (I_1/I_3) **[103]** monitors the environmental polarity sensed by adjacent probe molecules, with values above and below unity corresponding to polar and non-polar atmospheres, respectively. The variation of (I_1/I_3) depending on [C_{16}MImCl] in HA-containing media is displayed in Figure 6 (a-c).

In an aqueous solution, pure SAIL exhibits a decreasing (I_1/I_3) ratio as [SAIL] increases. This behavior is widely used to study amphiphile micellization, with sigmoidal fitting **[104]** of (I_1/I_3) vs. [SAIL] (Figure 1 (c)) determining its CMC. At low [SAIL], with few monomers available, pyrene molecules remain un-associated, maintaining steady polarity in the premicellar zone. As micelles start forming, polarity drops suddenly, as pyrene preferentially binds to the micellar hydrophobic regions. In the post-micellar zone, excess micelles redistribute pyrene with minimal polarity change, forming the final plateau. Consequently, the (I_1/I_3) ratio remains fairly stable, unaffected by [SAIL] or probe molecules.

In contrast to the micellization behaviour of pure C_{16}MImCl, the HA-C_{16}MImCl system displays an unusual fluorimetric pattern, deviating from the typical sigmoidal shape. Table 1 provides the [C_{16}MImCl] values for the three transitions, each corresponding to different interactions. The (I_1/I_3) ratio serves as an indicator to compare the hydrophobicity of the complexes formed at different stages. At low [SAIL], the (I_1/I_3) ratio exhibits a rapid and uninterrupted decline, devoid of an initial plateau. In the early stages, charge interactions between the HA backbone and surrounding C_{16}MImCl monomers drive the formation of hydrophobic microdomains, resulting in a steady lowering in polarity. In all cases, the midpoint of the nearly vertical line has been identified as the CAC. Just beyond this sharp transition, the local polarity remains relatively invariant, as indicated by the consistent (I_1/I_3) values that persist over a narrow concentration window until the second critical juncture (C_S) is reached. Within the CAC–C_S region, coacervate assemblies progressively coalesce, shielding probe molecules from their surroundings and maintaining constant (I_1/I_3) values until the PE chain is fully saturated. Afterward, micropolarity briefly drops to a minimum (C_f), followed by a slight rise before stabilizing at a constant value. Beyond C_f, the system enters a state of polarity saturation, and any further addition of SAIL no longer affects the medium's polarity. A well-defined minimum is observed for 0.005% HA, while the minima for 0.01% and 0.02% HA are less prominent. Exploiting the observed hydrophobicity in conjunction with the aforementioned techniques has obtained conclusive information about the colloidal behaviour of the HA-C_{16}MImCl complex.

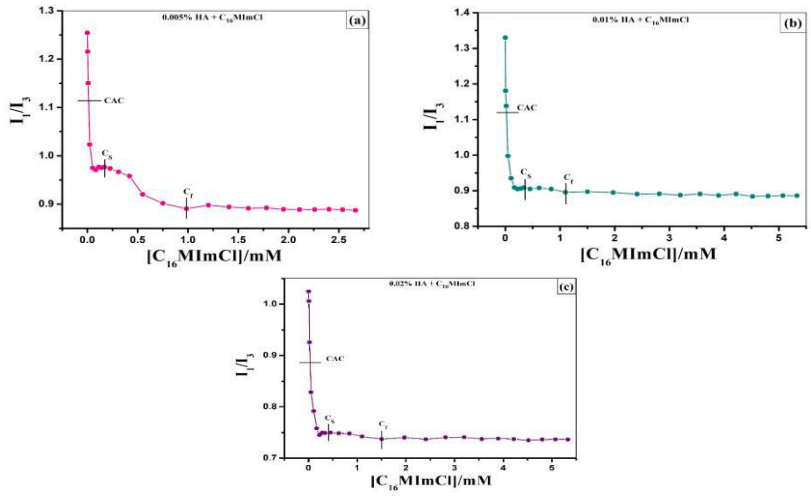

Figure 6. Pyrene fluorescence intensity ratio (I_1/I_3) plotted as a function of [C_{16}MImCl] for different HA concentrations: (a) 0.005%, (b) 0.01%, and (c) 0.02% (w/v).

3.7. Aggregation number

The aggregation number (N_{agg}) of PE-bound SAIL colloidal systems is a key determinant of micellar size. To investigate the influence of PE on SAIL micellar self-assembly, the N_{agg} is quantified via the SFQ method, based on the following equation:

$$\ln\left(\frac{I_0}{I}\right) = \frac{N_{agg}\ [CPC]}{[\text{SAIL}] - \text{CMC (Cf)}}$$

Here, I_0 and I correspond to the fluorescence intensities pre- and post-quenching, respectively, while [SAIL] specifies its bulk concentration in solution, with [CPC] denoting the quencher concentration. The N_{agg} is derived from the slope of the linear regression of the ln(I_0/I) vs. [CPC] plot (Figure 7 (a-d)). In all measurements, [SAIL] (~10 mM) is kept well above the corresponding CMC or C_f values. The N_{agg} of pure SAIL micelles in aqueous solution is 49. The addition of PE leads to an increase in the N_{agg} of HA-interacting SAIL micelles, with calculated values of 54, 51, and 56 in the presence of 0.005%, 0.01%, and 0.02% (w/v) HA, respectively. This increase is likely due to enhanced hydrophobicity around the micellar surface.

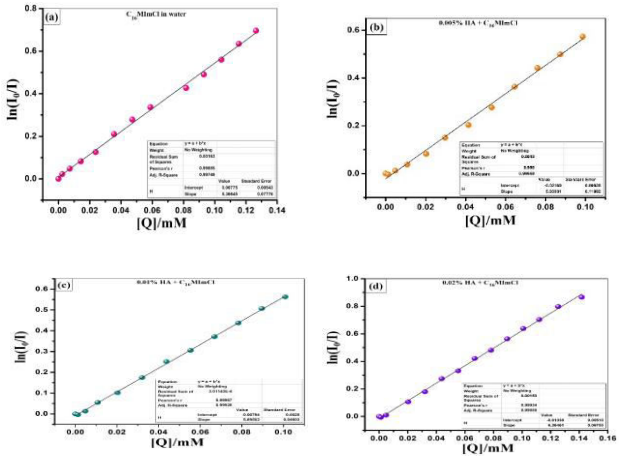

Figure 7. Plot of ln (I_0/I) vs. [Q] for C_{16}MImCl in the absence and presence of different (w/v) % HA in aqueous solutions at 298 K.

3.8. Time-resolved fluorescence

Time-resolved fluorescence quenching (TRFQ) **[105]** serves as a complementary technique for probing the complex dynamics of PE-SAIL interactions. Titrimetric average lifetime (τ_{av}) measurements of the coumarin 153 dye probe in both aqueous and HA (0.01%) media provide quantitative insights into microenvironmental changes during the self-assembly of C_{16}MImCl. In pure SAIL, the τ_{av} initially measures ~1.42 ns, rising sharply with increasing C_{16}MImCl concentration before stabilizing at ~3.26 ns. The data follow a well-defined sigmoidal (S-shaped) trend, fitting perfectly to the Boltzmann equation (Adj. R^2 = 0.98244) **[106]**. From this analysis, the CMC of C_{16}MImCl in water is estimated at ~0.78 mM. The resultant plot of the HA–C_{16}MImCl system identifies three critical points (τ_1, τ_2, and τ_3), corresponding to the critical concentrations CAC, C_S, and C_f, marking distinct aggregation phases. The initial sharp rise in τ_{av} suggests early HA-SAIL interactions, likely due to small aggregate formation that traps fluorophores, enhancing fluorescence and resulting in the observed peak. This peak may represent an optimal interaction point associated with CAC. Thereafter, τ_{av} declines, indicating structural reorganization, and stabilizes near the charge neutralization point, where HA binding sites reach saturation (C_S). Following this, τ_{av} undergoes a more rapid decline before reaching a final stable plateau. The breakpoint C_f signifies the stage at which the PE accommodates larger micellar structures, beyond which additional SAIL molecules no longer significantly affect the microenvironment.

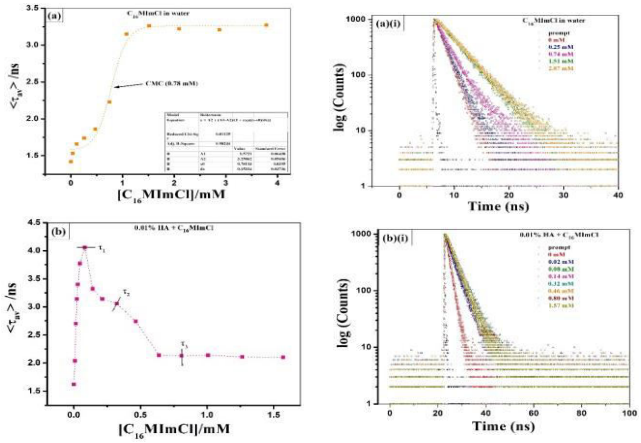

Figure 8. Time-resolved fluorescence lifetime curves of C_{16}MImCl in (a) water and (b) 0.01% (w/v) HA, measured using coumarin 153 as a probe. The associated decay profiles are illustrated in (a) (i) and (b) (i), respectively.

3.9. DLS size measurement

DLS measurements are conducted to examine the size distribution of aggregates formed between HA and SAIL. Figure 9 (a) depicts the structural transitions as a function of [SAIL] in a 0.01% aqueous HA solution. The hydrodynamic diameter (D_h) of unbound HA, which measures ≈ 257.5 nm initially, undergoes a sharp reduction to ≈ 89.23 nm at 0.042 mM [SAIL], matching the CAC threshold. This shrinkage likely results from electrostatic charge neutralization in HA–SAIL (monomer) complexes, which reduces intramolecular repulsion and compacts the PE structure **[107]**. A further rise in [SAIL] stimulates the growth of the SAIL-mediated PE complex, resulting in a steady increase in D_h. However, beyond 0.20 mM, accumulating turbidity interferes with precise size measurements.

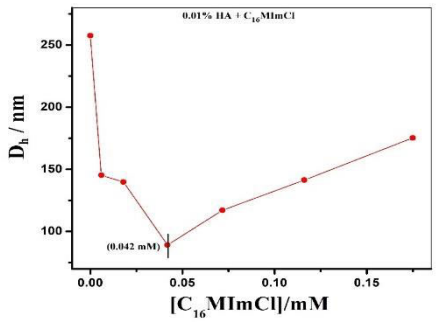

Figure 9(a). Effect of C_{16}MImCl concentration on the hydrodynamic diameter of 0.01% (w/v) HA + C_{16}MImCl aqueous solutions at 298 K.

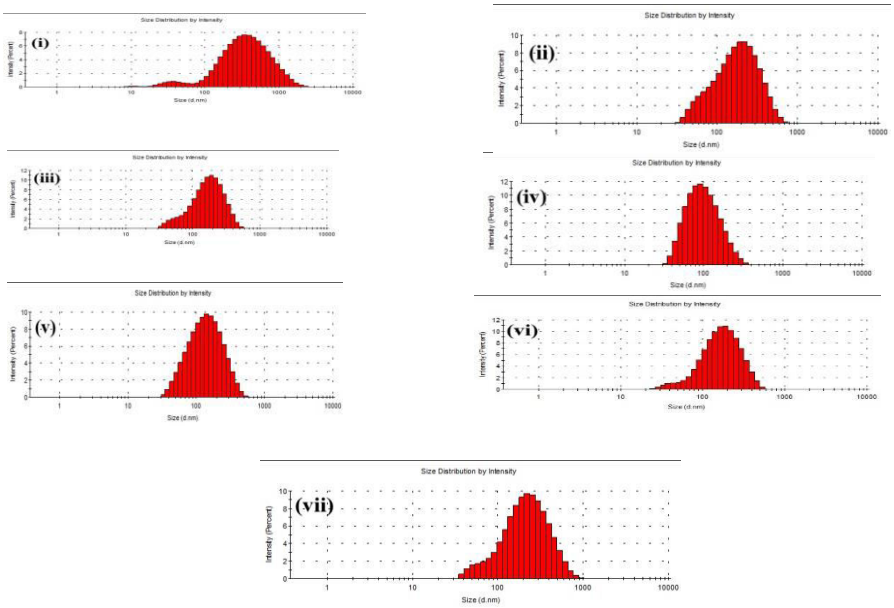

Figure 9 (b). Comparison of Particle Size Distribution (PSD) patterns for 0.01% (w/v) HA at 298 K: (i) pure HA and HA-C_{16}MImCl complexes at C_{16}MImCl concentrations of (ii) 0.006 mM, (iii) 0.0018 mM, (iv) 0.042 mM, (v) 0.072 mM, (vi) 0.116 mM, and (vii) 0.174 mM.

3.10. FTIR spectroscopy

The molecular structure of the complex is characterized using FTIR spectroscopy. Significant spectral transformations, including peak shifts, the emergence of new vibrational bands, and the depletion or fading of existing ones, provide compelling evidence of complexation between HA and C_{16}MImCl. Figure 10 presents the FTIR spectra of HA, C_{16}MImCl, and their coacervate, while Table 5 summarizes the associated vibrational modes. The broad peak at 3351 cm^{-1} in the HA-C_{16}MImCl complex corresponds to O-H stretching **[108]**, indicating hydrogen bonding, primarily between hydroxyl (-OH) groups of HA and the imidazolium cation ($C_{16}MIm^{+}$). The asymmetric and symmetric C-H stretching vibrations of the alkyl chain, originally at 2915 and 2850 cm^{-1} in C_{16}MImCl **[109]**, shift to 2924 and 2854 cm^{-1}, suggesting hydrophobic interactions between the aliphatic components of C_{16}MImCl and HA. The shift of the HA carboxylate ($-COO^{-}$) asymmetric stretching peak from 1606 cm^{-1} **[110]** to 1633 cm^{-1} indicates strong electrostatic interactions with $C_{16}MIm^{+}$. The 1410 cm^{-1} peak (shifted from 1398 cm^{-1}) **[111]** confirms further electrostatic interactions between carboxylate groups and the imidazolium cation. The 1166 cm^{-1} peak, attributed to C-N stretching of the imidazolium ring (shifted from 1175 cm^{-1}) **[9]**, suggests interactions with HA that weaken the C-N bond. Moreover, the peak at 1042 cm^{-1}, shifted from 1025 cm^{-1} in pure HA **[112]**, implies perturbation of the polysaccharide backbone upon interaction with the SAIL. Several characteristic peaks observed in C_{16}MImCl and HA profiles, including those at 1574, 1637, 3054, and 3087 cm^{-1} for the C_{16}MImCl and 1557 cm^{-1} for HA, are absent in the complex spectrum, indicating structural modifications. Notably, the peaks at 3084 cm^{-1} and 3051 cm^{-1}, corresponding to C-H stretching vibrations of the imidazolium ring in the C_{16}MImCl **[9]**, disappear in the complex, possibly due to their merging with other spectral features. These spectral shifts evidence stable complex formation between HA and C_{16}MImCl, driven by electrostatic, hydrophobic, and hydrogen bonding interactions, leading to a modified structural environment.

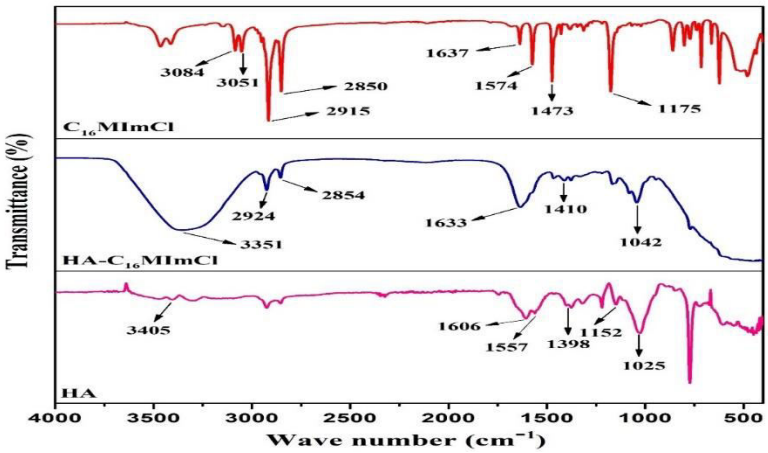

Figure 10. FTIR spectra of pure HA, pure C_{16}MImCl, and HA -C_{16}MImCl complex.

3.11. Field emission scanning electron microscopy (FESEM)

Direct visualization of the complexation phenomenon is essential for corroborating the conclusions drawn from the preceding physicochemical analyses, as well as the underlying assumptions. A careful study of FESEM morphographs provides valuable insights into their broader implications within the realm of surface science. FESEM measurements enable the high-resolution characterization of surface topology and a fine-grained analysis of the micro-aggregation behaviour of the PE-SAIL complex. Accordingly, FESEM imaging has been employed to examine the morphological transformations of the PE surface induced by SAIL aggregation. Figure 11 (a-c) presents FESEM images of pure HA and its complexes with C_{16}MImCl at two different concentrations (below and at C_f). While pure HA exhibits a smooth surface with a leaf-like particle arrangement, its interaction with SAIL has witnessed a significant modification in the overall texture of the exterior morphology. The electrostatic bridging between PE and SAIL establishes a highly interconnected network within the interfacial structure. Below C_f, a new kind of rosette-like cluster develops on the PE surface, suggesting that cationic SAIL molecules are compactly arranged and firmly stuck to the oppositely charged backbone. When SAIL reaches C_f, a higher degree of agglomeration occurs, possibly due to phase separation effects. However, the core rosette-like structural pattern remains intact. Thus, as supported by the FESEM findings, the SAIL concentration strongly affects the complexation behaviour. The functionalization of SAIL with a natural polysaccharide can undoubtedly lead to the development of colloidal formulations for diverse biological activities.

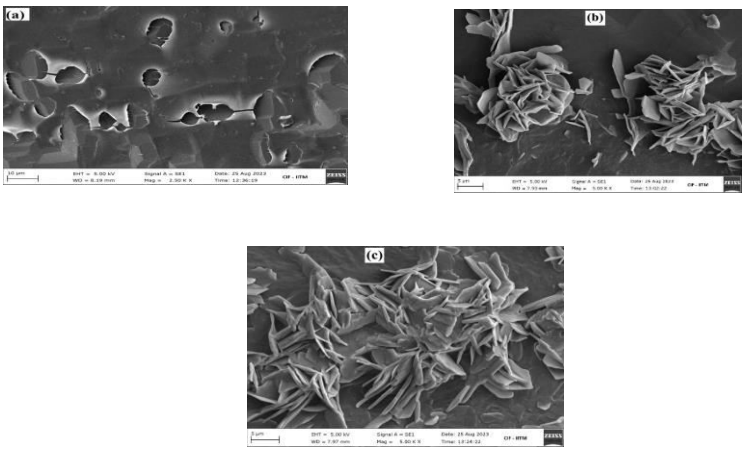

Figure 11. FESEM images of (a) pure 0.1% (w/v) HA; HA-C_{16}MImCl complexes (b) below C_f, and (c) at C_f.

3.12. High resolution transmission electron microscopy (HR-TEM)

HRTEM imaging provides a detailed view of the morphological transformation of HA induced by C_{16}MImCl. These images clearly demonstrate the inclusion of the host-guest complex on the HA surface. Figure 12(a) depicts pristine HA, characterized by loosely packed, leaf-like sheets. Before the micellization period, the complexation of HA with C_{16}MImCl leads to partial structural disruption, resulting in irregular, dispersed aggregates (Figure 12 (b)). The increased electron density in localized regions suggests electrostatic interactions between HA and the ionic liquid, though micelle formation has not yet occurred. At the C_f, as shown in Figure 12(c), dense, spherical micellar structures emerge, indicating successful self-assembly driven by amphiphilic interactions. The increased contrast and compact morphology further emphasize the stabilizing role of C_{16}MImCl in micelle formation.

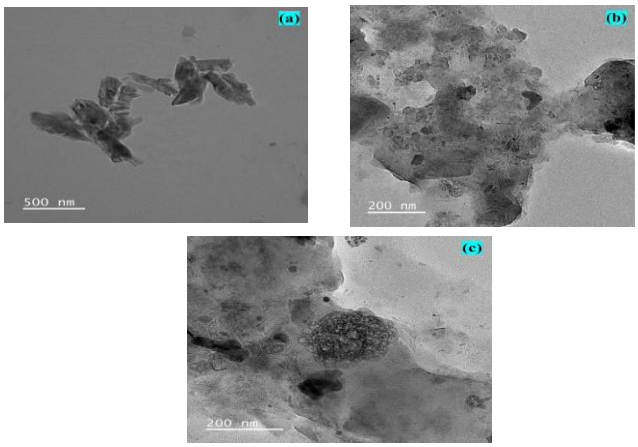

Figure 12. (a), (b), and (c) present HR-TEM images of the same samples previously analyzed using FESEM.

3.13. Fluorescence microscopy

The FESEM and HR-TEM findings have been established to be extremely useful in the analysis of the surface morphographs of the PE-SAIL complexation. However, it is still lacking in some aspects to gain insights into the structural patterns and spatial distributions of the PE-SAIL aggregates. The conception of a visualization approach for understanding the interactions between oppositely charged PE and SAIL has been simplified by fluorescence image analysis. The introduction of fluorescence imaging can provide new prospects for interpreting the structure and composition of PE-SAIL binding, as well as the molecular process underlying the complexation phenomenon. Earlier, Jiao et al. **[113]** has noticed the appearance of bright luminous dots during the interaction study of cationic polymer chitosan and anionic surfactant TPE-SDS. Through PL microscopy, Chatterjee et al. **[114]** has visualized the formation of ring-shaped complex between neutral polymer PVP and anionic surfactant SDS. According to Das et al. [9], anionic polyelectrolyte (NaAlg) can form a more aggregated ring-shaped complex with cationic SAIL (C_{16}MImCl) than cationic surfactant (C_{16}TPB), based on the fluorescence microscopy study. It follows that the observation of binding patterns of the HA-C_{16}MImCl system at different stages is expected to be feasible so

as to impart strong visual evidence in favor of their propensity towards complex formation. Accordingly, the experiments have been carried out using different SAIL concentrations in the presence of 0.01% (w/v) HA, including free HA. The fluorophore DPH can selectively sense the aggregated structures, making it unable to locate the free polyelectrolyte structure. At low SAIL concentrations below CAC, no apparent complexation develops, and thus DPH molecules cannot get into the interior of such smaller aggregates. Above CAC, the SAIL concentrations are sufficient to form larger micelle-like agglomeration of SAIL coated on PE chains, which can readily trap the probe molecules. Hence, the measurements of the PE-SAIL system below CAC and the free polyelectrolyte are not shown here. Figure 13 (a-d) displays the microscopy images of the investigated compositions of the HA-C_{16}MImCl system. On the whole, it represents better visibility of the presence of coacervation at different stages of the binding process. The non-uniform PE-SAIL aggregates can be discriminated in terms of shape, size, and compactness depending on the SAIL concentration. Between CAC and C_S (Figure 13 (a)) the coacervation slowly starts to become visible, which enlarges at C_S (Figure 13 (b)). The completion of saturation of SAIL monomers along PE chains leads to growth of the aggregates. Thereafter, free SAIL monomers accumulate to initiate PE-induced micelle formation at C_f, and the micellized forms assume the largest aggregated size (Figure 13 (c)). When the SAIL concentration is much above the C_f, the observations of relatively smaller aggregation (Figure 13 (d)) can be explained by considering the dissolution of the larger aggregates in the post-micellar state (discussed in 3.4.). Moreover, it can be clearly observed from the proposed images that the intensity of aggregated structures becomes more prominent at higher SAIL concentrations. The fluorescence microscopy images of the PE-SAIL complex obtained in this study at a wide range of SAIL concentrations are quite phenomenal. Very few reports in the literature provide as much detail on the microscopy study using the oppositely charged PE-SAIL system.

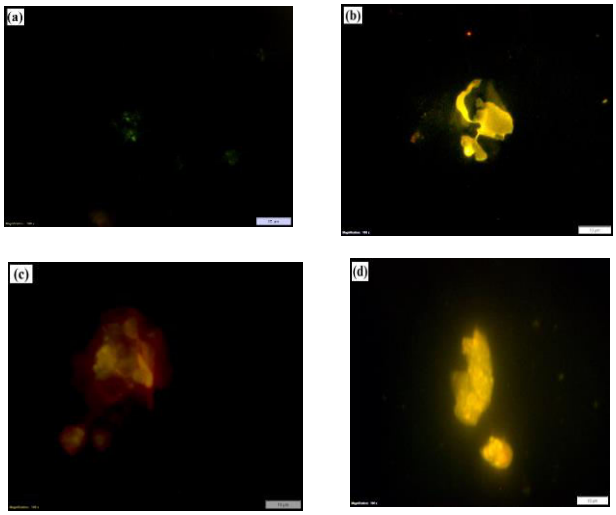

Figure 13. Fluorescence microscopy images of HA-C_{16}MImCl complexes: (a) between CAC and C_S; (b) at C_S; (c) at C_f; (d) >> C_f; [HA] = 0.01% (w/v), Scale bar = 10 μm.

4. Conclusions

This study explores the molecular interactions between hyaluronic acid (HA), an anionic polyelectrolyte (PE), and 1-hexadecyl-3-methyl imidazolium chloride (C_{16}MImCl), a surface-active ionic liquid (SAIL). Through a multi-technique approach including tensiometry, conductometry, turbidimetry, zeta potential analysis, and fluorescence spectroscopy, we demonstrate the ability of SAIL molecules to interact with HA, resulting in the formation of colloidal complexes with distinct structural and interfacial properties.

The interaction mechanism is primarily governed by a combination of electrostatic forces, hydrogen bonding, and hydrophobic interactions. Electrostatic neutralization of HA triggers coacervation, followed by the growth of hydrophobically stabilized complexes. Tensiometric analysis reveals the presence of critical aggregation concentration (CAC), saturation concentration (C_S), and extended critical micelle concentration (C_f), with all three increasing as PE concentration rises. FTIR spectroscopy confirms the role of hydrogen bonding in complex stabilization, while DLS measurements characterize the size of the complexes. Furthermore, FESEM and HR-TEM imaging capture the morphological evolution of HA upon complexation with SAIL. Fluorescence microscopy visually supports the formation of stable colloidal aggregates.

Given the widespread biomedical applications of HA, this study opens new possibilities for designing novel HA-based formulations with enhanced functional properties. The findings can be extended to other biopolymer-ionic liquid systems, which are integral to colloidal science and material chemistry. Advanced experimental methodologies coupled with computational modeling will be pivotal in deciphering the complex physicochemical principles underlying these interactions.

References

(1) Zhang J, Yin J, Zhang X, Ran H, Zhang Y, Zhu L, Jiang W, Li H, Li H, Zhang M. Constructing protic porous ionic liquids via one-step coupling neutralization reaction for extraction-adsorption coupled desulfurization. Journal of Colloid and Interface Science. 2023 Dec 15;652:1836-47.

(2) Gradzielski M. Polyelectrolyte–surfactant complexes as a formulation tool for drug delivery. Langmuir. 2022 Oct 24;38(44):13330-43.

(3) McTigue WC, Perry SL. Design rules for encapsulating proteins into complex coacervates. Soft Matter. 2019;15(15):3089-103.

(4) Llamas S, Guzman E, Ortega F, Baghdadli N, Cazeneuve C, Rubio RG, Luengo GS. Adsorption of polyelectrolytes and polyelectrolytes-surfactant mixtures at surfaces: A physico-chemical approach to a cosmetic challenge. Advances in colloid and interface science. 2015 Aug 1;222:461-87.

(5) Cheng J, Xu J, Yang J, Lv W, Lian C, Liu H. Enhanced oil recovery by sacrificing polyelectrolyte to reduce surfactant adsorption: A classical density functional theory study. Chemical Engineering Science. 2022 Nov 2;261:117957.

(6) Seres L, Csapó E, Varga N, Juhász Á. The Effect of Concentration, Temperature, and pH on the Formation of Hyaluronic Acid–Surfactant Nanohydrogels. Gels. 2023 Jun 29;9(7):529.

(7) Carrascosa-Tejedor J, Tummino A, Fehér B, Kardos A, Efstratiou M, Skoda MW, Gutfreund P, Maestro A, Lawrence MJ, Campbell RA, Varga I. Effects of Charge Density on Spread Hyperbranched Polyelectrolyte/Surfactant Films at the Air/Water Interface. Langmuir. 2023 Oct 15;39(42):14869-79.

(8) Del Sorbo GR, Cristiglio V, Clemens D, Hoffmann I, Schneck E. Influence of the Surfactant Tail Length on the Viscosity of Oppositely Charged Polyelectrolyte/Surfactant Complexes. Macromolecules. 2021 Feb 12;54(5):2529-40.

(9) Das S, Ghosh S. A detailed assessment on the interaction of sodium alginate with a surface-active ionic liquid and a conventional surfactant: a multitechnique approach. Physical Chemistry Chemical Physics. 2022;24(22):13738-62.

(10) Singh G, Singh G, Kang TS. Colloidal systems of surface active ionic liquids and sodium carboxymethyl cellulose: physicochemical investigations and preparation of magnetic nano-composites. Physical Chemistry Chemical Physics. 2018;20(27):18528-38.

(11) Wang D, Guo Y, Zhu J, Liu F, Xue Y, Huang Y, Zhu B, Wu D, Pan H, Gong T, Lu Y. Hyaluronic acid methacrylate/pancreatic extracellular matrix as a potential 3D printing bioink for constructing islet organoids. Acta biomaterialia. 2023 Jul 15;165:86-101.

(12) Zakani B, Bose A, Grecov D. Yield stress analysis of cellulose nanocrystals (CNCs) in hyaluronic acid suspensions. Carbohydrate Polymers. 2024 Feb 15;326:121650.

(13) Casadidio C, Mayol L, Biondi M, Scuri S, Cortese M, Hennink WE, Vermonden T, De Rosa G, Di Martino P, Censi R. Anionic polysaccharides for stabilization and sustained release of antimicrobial peptides. International Journal of Pharmaceutics. 2023 Apr 5;636:122798.

(14) Zhang D, Ren Y, He Y, Chang R, Guo S, Ma S, Guan F, Yao M. In situ forming and biocompatible hyaluronic acid hydrogel with reactive oxygen species-scavenging activity to improve traumatic brain injury repair by suppressing oxidative stress and neuroinflammation. Materials Today Bio. 2022 Jun 1;15:100278.

(15) Shi M, Dong R, Hu J, Guo B. Conductive self-healing biodegradable hydrogel based on hyaluronic acid-grafted-polyaniline as cell recruitment niches and cell delivery carrier for myogenic differentiation and skeletal muscle regeneration. Chemical Engineering Journal. 2023 Feb 1;457:141110.

(16) Raza H, Ashraf A, Shamim R, Manzoor S, Sohail Y, Khan MI, Raza N, Shakeel N, Gill KA, El-Marghany A, Aftab S. Synthesis and characterization of Hyaluronic Acid (HA) modified polymeric composite for effective treatment of wound healing by transdermal drug delivery system (TDDS). Scientific Reports. 2023 Aug 17;13(1):13425.

(17) Marinelli L, Cacciatore I, Eusepi P, Di Biase G, Morroni G, Cirioni O, Giacometti A, Di Stefano A. Viscoelastic behaviour of hyaluronic acid formulations containing carvacrol prodrugs with antibacterial properties. International Journal of Pharmaceutics. 2020 May 30;582:119306.

(18) Šimek M, Turková K, Schwarzer M, Nešporová K, Kubala L, Hermannová M, Foglová T, Šafránková B, Šindelář M, Šrůtková D, Chatzigeorgiou S. Molecular weight and gut microbiota determine the bioavailability of orally administered hyaluronic acid. Carbohydrate Polymers. 2023 Aug 1;313:120880.

(19) Sauerová P, Verdánová M, Mravec F, Pilgrová T, Venerová T, Kalbáčová MH, Pekař M. Hyaluronic acid as a modulator of the cytotoxic effects of cationic surfactants. Colloids and Surfaces A: Physicochemical and Engineering Aspects. 2015 Oct 20;483:155-61.

(20) Van Le H, Dulong V, Picton L, Le Cerf D. Polyelectrolyte complexes of hyaluronic acid and diethylaminoethyl dextran: Formation, stability and hydrophobicity. Colloids and Surfaces A: Physicochemical and Engineering Aspects. 2021 Nov 20;629:127485.

(21) Song G, Zhou L, Zhao L, Wang D, Yuan T, Li L, Gong J. Analysis of non-covalent interaction between β-lactoglobulin and hyaluronic acid under ultrasound-assisted treatment: Conformational structures and interfacial properties. International Journal of Biological Macromolecules. 2024 Jan 1;256:128529.

(22) Yang M, Zhang Y, Hu Z, Xie H, Tian W, Liu Z. Application of hyaluronic acid-based nanoparticles for cancer combination therapy. International Journal of Pharmaceutics. 2023 Sep 29:123459.

(23) Zhang F, Zhang S, Lin R, Cui S, Jing X, Coseri S. Injectable multifunctional carboxymethyl chitosan/hyaluronic acid hydrogel for drug delivery systems. International Journal of Biological Macromolecules. 2023 Sep 30;249:125801.

(24) Zarei N, Hassanzadeh-Tabrizi SA. Alginate/hyaluronic acid-based systems as a new generation of wound dressings: A review. International Journal of Biological Macromolecules. 2023 Oct 5:127249.

(25) Serafin A, Culebras M, Collins MN. Synthesis and evaluation of alginate, gelatin, and hyaluronic acid hybrid hydrogels for tissue engineering applications. International journal of biological macromolecules. 2023 Apr 1;233:123438.

(26) Luo Y, Tan J, Zhou Y, Guo Y, Liao X, He L, Li D, Li X, Liu Y. From crosslinking strategies to biomedical applications of hyaluronic acid-based hydrogels: A review. International Journal of Biological Macromolecules. 2023 Jan 17:123308.

(27) Ding X, Li S, Tian M, Yang P, Ding Y, Wang Y, Duan G, Zhang D, Chen B, Tan Q. Facile preparation of a novel nanoemulsion based hyaluronic acid hydrogel loading with Poria cocos triterpenoids extract for wound dressing. International Journal of Biological Macromolecules. 2023 Jan 31;226:1490-9.

(28) Sun J, Perry SL, Schiffman JD. Electrospinning nanofibers from chitosan/hyaluronic acid complex coacervates. Biomacromolecules. 2019 Oct 15;20(11):4191-8.

(29) Heo Y, Shin SW, Kim DS, Lee S, Park SY, Baek SW, Lee JK, Kim JH, Han DK. Bioactive PCL microspheres with enhanced biocompatibility and collagen production for functional hyaluronic acid dermal fillers. Biomaterials Science. 2022;10(4):947-59.

(30) He S, Liu A, Zhang J, Liu J, Shao W. Preparation of ε-polylysine and hyaluronic acid self-assembled microspheres loaded bacterial cellulose aerogels with excellent antibacterial activity. Colloids and Surfaces A: Physicochemical and Engineering Aspects. 2022 Dec 5;654:130114.

(31) Anbardan MA, Alipour S, Mahdavinia GR, Rezaei PF. Synthesis of magnetic chitosan/hyaluronic acid/κ-carrageenan nanocarriers for drug delivery. International Journal of Biological Macromolecules. 2023 Dec 31;253:126805.

(32) Dey N, Mohny FP, Reshma GB, Rao D, Ganguli M, Santhiya D. Bioinspired synthesis of bioactive glass nanocomposites for hyaluronic acid delivery to bone and skin. International Journal of Biological Macromolecules. 2023 Dec 31;253:127262.

(33) Payne WM, Svechkarev D, Kyrychenko A, Mohs AM. The role of hydrophobic modification on hyaluronic acid dynamics and self-assembly. Carbohydrate polymers. 2018 Feb 15;182:132-41.

(34) Sauerová P, Pilgrová T, Pekař M, Kalbáčová MH. Hyaluronic acid in complexes with surfactants: The efficient tool for reduction of the cytotoxic effect of surfactants on human cell types. International Journal of Biological Macromolecules. 2017 Oct 1;103:1276-84.

(35) Havlikova M, Jugl A, Krouska J, Szabová J, Mravcova L, Venerova T, Chang CH, Pekar M, Mravec F. Interactions between Cationic Ion Pair Amphiphile Vesicles and Hyaluronan—A Physicochemical Study. Langmuir. 2021 Jul 2;37(28):8525-33.

(36) Holínková P, Mravec F, Venerová T, Chang CH, Pekař M. Hyaluronan interactions with cationic surfactants–Insights from fluorescence resonance energy transfer and anisotropy techniques. International Journal of Biological Macromolecules. 2022 Jun 30;211:107-15.

(37) Pilgrová T, Venerová T, Mravec F, Pekař M. Interactions of hyaluronan with oppositely charged surfactants in very diluted solutions in water. International journal of biological macromolecules. 2018 Jun 1;112:241-9.

(38) Krouská J, Pekař M, Klučáková M, Šarac B, Bešter-Rogač M. Study of interactions between hyaluronan and cationic surfactants by means of calorimetry, turbidimetry, potentiometry and conductometry. Carbohydrate polymers. 2017 Feb 10;157:1837-43.

(39) Bračič M, Hansson P, Pérez L, Zemljic LF, Kogej K. Interaction of sodium hyaluronate with a biocompatible cationic surfactant from lysine: a binding study. Langmuir. 2015 Nov 10;31(44):12043-53.

(40) Buettner CS, Cognigni A, Schroeder C, Bica-Schröder K. Surface-active ionic liquids: A review. Journal of Molecular Liquids. 2022 Feb 1;347:118160.

(41) Wang D, He J, Xiao Z, Wang J. Effect of molar ratio and alkyl chain length on the aggregation behavior of imidazolium-based ionic liquid surfactants/SDS systems. Colloids and Surfaces A: Physicochemical and Engineering Aspects. 2024 Jan 5;680:132636.

(42) Xu R, Mu J, Zhang L, Gao J, Ma Y, Xu D, Wang Y. Experimental determination of liquid-liquid equilibrium and interaction insights for ternary mixtures 2, 2, 2-trifluoroethanol+ water+ pyridinium-based ionic liquids. Journal of the Taiwan Institute of Chemical Engineers. 2024 Feb 1;155:105275.

(43) Ndayambaje JD, Shabbir I, Zhao Q, Dong L, Su Q, Cheng W. Controlling dual-positively charged pyrazolium ionic liquids for efficient catalytic conversion of CO 2 into carbonates under mild conditions. Catalysis Science & Technology. 2024.

(44) Panja SK, Kumar S. Weak intra and intermolecular interactions via aliphatic hydrogen bonding in piperidinium based ionic Liquids: Experimental, topological and molecular dynamics studies. Journal of Molecular Liquids. 2023 Apr 1;375:121354.

(45) Liu X, Wang Y, Liu R, Lv P, Xue W, Guo J, Wei H, Yang Y. Selective and Efficient Gold Extraction from E-Waste by Pyrrolidinium-Based Ionic Liquids with Various N-Substituents. ACS Sustainable Chemistry & Engineering. 2023 Jan 4;11(2):638-48.

(46) Sun X, Li G, Zeng S, Yuan L, Bai L, Zhang X. Ultra-high NH3 absorption by triazole cation-functionalized ionic liquids through multiple hydrogen bonding. Separation and Purification Technology. 2023 Feb 15;307:122825.

(47) Kaur G, Mehra S, Kumar H, Kumar A. Exploring the aggregation behaviour and antibiotic binding ability of thiazolium-based surface-active ionic liquids; Understanding transportation of poorly water-soluble drug. Colloids and Surfaces A: Physicochemical and Engineering Aspects. 2023 May 5;664:131195.

(48) Sampaio AM, Fileti EE, Siqueira LJ. Atomistic study of the physical properties of sulfonium-based ionic liquids as electrolyte for supercapacitors. Journal of Molecular Liquids. 2019 Dec 15;296:112065.

(49) Rauber D, Philippi F, Becker J, Zapp J, Morgenstern B, Kuttich B, Kraus T, Hempelmann R, Hunt P, Welton T, Kay CW. Anion and ether group influence in protic guanidinium ionic liquids. Physical Chemistry Chemical Physics. 2023;25(8):6436-53.

(50) Viradiya RA, Patel N, Aswal VK, Patel VK, Panjabi SH. Investigating the Influence of Aromatic Counterions on the Micellar Structure and Aggregation Behavior of Morpholinium-Based Surface-Active Ionic Liquids in an Aqueous Solution. Langmuir. 2023 Aug 7;39(33):11684-93.

(51) Yalcin D, Drummond CJ, Greaves TL. Solvation properties of protic ionic liquids and molecular solvents. Physical Chemistry Chemical Physics. 2020;22(1):114-28.

(52) Wang L, Li L, Fan Q, Chu T, Wang Y, Xu Y. Thermal stability and flammability of several quaternary ammonium ionic liquids. Journal of Molecular Liquids. 2023 Jul 15;382:121920.

(53) Dong Y, Steinhart M, Butt HJ, Floudas G. Conductivity of Ionic Liquids In the Bulk and during Infiltration in Nanopores. The Journal of Physical Chemistry B. 2023 Jul 27;127(31):6958-68.

(54) Huang K, Liu R, Liu X, Yin X, Zhang J, Yang Y. Simultaneous leaching and separating of palladium from spent palladium catalyst by tribromide ionic liquids as non-volatile oxidizing solvents. Journal of Molecular Liquids. 2023 Oct 15;388:122754.

(55) Karadaghi LR, Pan B, Baddour FG, Malmstadt N, Brutchey RL. A techno-economic approach to guide the selection of flow recyclable ionic liquids for nanoparticle synthesis. RSC Sustainability. 2023;1(7):1861-73.

(56) Michalski J, Odrzygóźdź C, Mester P, Narożna D, Cłapa T. Defeat undefeatable: Ionic liquids as novel antimicrobial agents. Journal of Molecular Liquids. 2023 Jan 1;369:120782.

(57) Jha D, Maheshwari P, Singh Y, Haider MB, Kumar R, Balathanigaimani MS. A comparative review of extractive desulfurization using designer solvents: Ionic liquids & deep eutectic solvents. Journal of the Energy Institute. 2023 Jun 25:101313.

(58) Quintana AA, Sztapka AM, Santos Ebinuma VD, Agatemor C. Enabling sustainable chemistry with ionic liquids and deep eutectic solvents: a fad or the future?. Angewandte Chemie. 2022 Sep 12;134(37):e202205609.

(59) Migowski P, Lozano P, Dupont J. Imidazolium based ionic liquid-phase green catalytic reactions. Green Chemistry. 2023;25(4):1237-60.

(60) Zhang Y, Liu C, Wang J, Ren S, Song Y, Quan P, Fang L. Ionic liquids in transdermal drug delivery system: Current applications and future perspectives. Chinese Chemical Letters. 2023 Mar 1;34(3):107631.

(61) Ray P, Pilania M. The application and influence of ionic liquids in nanotechnology. Materials Today: Proceedings. 2021 Jan 1;47:2835-8.

(62) Kathiresan M, Velayutham D. Ionic liquids as an electrolyte for the electro synthesis of organic compounds. Chemical Communications. 2015;51(99):17499-516.

(63) Sanchora P, Pandey DK, Kagdada HL, Materny A, Singh DK. Impact of alkyl chain length and water on the structure and properties of 1-alkyl-3-methylimidazolium chloride ionic liquids. Physical Chemistry Chemical Physics. 2020;22(31):17687-704.

(64) El Seoud OA, Pires PA, Abdel-Moghny T, Bastos EL. Synthesis and micellar properties of surface-active ionic liquids: 1-Alkyl-3-methylimidazolium chlorides. Journal of colloid and interface science. 2007 Sep 1;313(1):296-304.

(65) Galgano PD, El Seoud OA. Micellar properties of surface active ionic liquids: a comparison of 1-hexadecyl-3-methylimidazolium chloride with structurally related cationic surfactants. Journal of Colloid and Interface Science. 2010 May 1;345(1):1-1.

(66) Das S, Patra N, Banerjee A, Das B, Ghosh S. Studies on the self-aggregation, interfacial and thermodynamic properties of a surface active imidazolium-based ionic liquid in aqueous solution: effects of salt and temperature. Journal of Molecular Liquids. 2020 Dec 15;320:114497.

(67) Tan X, Zhang J, Luo T, Sang X, Liu C, Zhang B, Peng L, Li W, Han B. Micellization of long-chain ionic liquids in deep eutectic solvents. Soft Matter. 2016;12(24):5297-303.

(68) Dutta R, Ghosh S, Banerjee P, Kundu S, Sarkar N. Micelle-vesicle-micelle transition in aqueous solution of anionic surfactant and cationic imidazolium surfactants: Alteration of the location of different fluorophores. Journal of colloid and interface science. 2017 Mar 15;490:762-73.

(69) Das S, Ghosh S, Das B. Formation of mixed micelle in an aqueous mixture of a surface active ionic liquid and a conventional surfactant: experiment and modeling. Journal of Chemical & Engineering Data. 2018 Sep 10;63(10):3784-800.

(70) Kundu S, Banerjee C, Sarkar N. Inhibiting the fibrillation of serum albumin proteins in the presence of surface active ionic liquids (SAILs) at low pH: spectroscopic and microscopic study. The Journal of Physical Chemistry B. 2017 Jul 19;121(32):7550-60.

(71) Azum N, Alotaibi MM, Ali M, Rub MA, Marwani HM, Alamry KA, Asiri AM. Investigation of an anaesthetic drug (tetracaine hydrochloride) in the presence of ionic fluid and surfactant: Mixed micellization & spectroscopic studies. Journal of Molecular Liquids. 2023 Jan 15;370:121057.

(72) Perinelli DR, Cespi M, Lorusso N, Palmieri GF, Bonacucina G, Blasi P. Surfactant self-assembling and critical micelle concentration: one approach fits all?. Langmuir. 2020 May 6;36(21):5745-53.

(73) Pathan T, Girase M, Patel K, Pillai SA, Pathan S, Parekh P, Kuperkar K, Patel VI. Synergistic self-assembly in a surface-active ionic liquid and an anionic surfactant mixed system: a comprehensive physicochemical analysis. Industrial & Engineering Chemistry Research. 2024 May 22;63(22):9688-700.

(74) Mondal BB, Banik R, Ghosh S. Detailed physicochemical study and thermodynamic aspects of the interaction between nonionic cellulose derivative hydroxyethyl cellulose and anionic surfactant sodium N-dodecanoyl sarcosinate in aqueous media. Journal of the Taiwan Institute of Chemical Engineers. 2023 Aug 1;149:104982.

(75) Snetkov P, Zakharova K, Morozkina S, Olekhnovich R, Uspenskaya M. Hyaluronic acid: The influence of molecular weight on structural, physical, physico-chemical, and degradable properties of biopolymer. Polymers. 2020 Aug 11;12(8):1800.

(76) Dan A, Ghosh S, Moulik SP. Physicochemistry of the interaction between inulin and alkyltrimethylammonium bromides in aqueous medium and the formed coacervates. The Journal of Physical Chemistry B. 2009 Jun 25;113(25):8505-13.

(77) Das S, Mondal S, Ghosh S. Interaction of cationic gemini surfactant tetramethylene-1, 4-bis (dimethyltetradecylammonium bromide) with anionic polyelectrolyte sodium carboxymethyl cellulose, with two different molar masses, in aqueous and aquo-organic (isopropanol) media. RSC Advances. 2016;6(37):30795-803.

(78) Varga I, Campbell RA. General physical description of the behavior of oppositely charged polyelectrolyte/surfactant mixtures at the air/water interface. Langmuir. 2017 Jun 13;33(23):5915-24.

(79) Mukherjee S, Dan A, Bhattacharya SC, Panda AK, Moulik SP. Physicochemistry of interaction between the cationic polymer poly (diallyldimethylammonium chloride) and the anionic surfactants sodium dodecyl sulfate, sodium dodecylbenzenesulfonate, and sodium N-dodecanoylsarcosinate in water and isopropyl alcohol− water media. Langmuir. 2011 May 3;27(9):5222-33.

(80) Dan A, Ghosh S, Moulik SP. Interaction of cationic hydroxyethylcellulose (JR400) and cationic hydrophobically modified hydroxyethylcellulose (LM200) with the amino-acid based anionic amphiphile Sodium N-Dodecanoyl Sarcosinate (SDDS) in aqueous medium. Carbohydrate polymers. 2010 Mar 25;80(1):44-52.

(81) Mitra D, Bhattacharya SC, Moulik SP. Physicochemical studies on the interaction of gelatin with cationic surfactants alkyltrimethylammonium bromides (ATABs) with special focus on the behavior of the hexadecyl homologue. The Journal of Physical Chemistry B. 2008 May 29;112(21):6609-19.

(82) Alam MS, Mandal AB. Thermodynamic studies on mixed micellization of amphiphilic drug amitriptyline hydrochloride and nonionic surfactant Triton X-100. Journal of Molecular Liquids. 2012 Apr 1;168:75-9.

(83) Singh G, Singh G, Kang TS. Effect of alkyl chain functionalization of ionic liquid surfactants on the complexation and self-assembling behavior of polyampholyte gelatin in aqueous medium. Physical Chemistry Chemical Physics. 2016;18(37):25993-6009.

(84) Singh G, Singh G, Kang TS. Micellization behavior of surface active ionic liquids having aromatic counterions in aqueous media. The Journal of Physical Chemistry B. 2016 Feb 18;120(6):1092-105.

(85) Zehner B, Schmidt F, Korth W, Cokoja M, Jess A. Determination of the critical micelle concentration of imidazolium ionic liquids in aqueous hydrogen peroxide. Langmuir. 2019 Nov 13;35(49):16297-303.

(86) Patra N, Ray D, Aswal VK, Ghosh S. Exploring physicochemical interactions of different salts with sodium N-dodecanoyl sarcosinate in aqueous solution. ACS omega. 2018 Aug 16;3(8):9256-66.

(87) Rub MA, Azum N, Asiri AM. Interaction of cationic amphiphilic drug nortriptyline hydrochloride with TX-100 in aqueous and urea solutions and the studies of physicochemical parameters of the mixed micelles. Journal of Molecular Liquids. 2016 Jun 1;218:595-603.

(88) Kumar D, Farkaš Agatić Z, Popović K, Poša M. Binary mixed micelles of hexadecyltrimethylammonium bromide–sodium deoxycholate and dodecyltrimethylammonium bromide–sodium deoxycholate: Thermodynamic stabilization and mixed micelle solubilization capacity of daidzein (isoflavonoid). Industrial & Engineering Chemistry Research. 2024 Feb 8;63(7):3336-48.

(89) Szymczyk K, Zdziennicka A, Jańczuk B. Properties of some nonionic fluorocarbon surfactants and their mixtures with hydrocarbon ones. Advances in Colloid and Interface Science. 2021 Jun 1;292:102421.

(90) Bhattarai A. Studies of aggregation properties of surfactant with and without polyelectrolyte in water and binary mixture of methanol-water from the surface tension measurements. Journal of Molecular Liquids. 2020 Aug 15;312:113438.

(91) Loh W, Teixeira LA, Lee LT. Isothermal calorimetric investigation of the interaction of poly (N-isopropylacrylamide) and ionic surfactants. The Journal of Physical Chemistry B. 2004 Mar 11;108(10):3196-201.

(92) Gong C, Zhao T, Zhao Y, Zhang G. Effects of oxyethylene groups on the adsorption behavior and application performance of long alkyl chain phosphate surfactants. Journal of Molecular Liquids. 2022 Jan 1;345:117044.

(93) Kulkarni CV. Calculating the ‘chain splay’of amphiphilic molecules: Towards quantifying the molecular shapes. Chemistry and Physics of Lipids. 2019 Jan 1;218:16-21.

(94) Contini C, Hu W, Elani Y. Manufacturing polymeric porous capsules. Chemical Communications. 2022;58(28):4409-19.

(95) Mandal B, Ghosh S, Moulik SP. Interaction between a bio-tolerable amino-acid based amphiphile (N-dodecanoylsarcosinate, SDDS) and modified cationic polymers, hydroxyethylcelluloses (JR 400, and LM 200) in isopropanol-water medium. Colloids and Surfaces A: Physicochemical and Engineering Aspects. 2019 Apr 5;566:156-65.

(96) Viradiya RA, Aswal VK, Patel N, Patel VK, Solanki JD, Soni SS, Vashi AS, Panjabi SH. Surface-active ionic liquids with morpholinium cations and aromatic counterions: experimental and DFT approach to study their profound effect on micelle formation. Colloid and Polymer Science. 2024 Dec 30:1-5.

(97) Parekh P, Varade D, Parikh J, Bahadur P. Anionic–cationic mixed surfactant systems: micellar interaction of sodium dodecyl trioxyethylene sulfate with cationic gemini surfactants. Colloids and Surfaces A: Physicochemical and Engineering Aspects. 2011 Jul 20;385(1-3):111-20.

(98) Patra N, Mal A, Das S, Ghosh S. Detailed physicochemical interaction of inulin with some conventional surfactants and surface active ionic liquid. Journal of Molecular Liquids. 2021 Oct 15;340:116849.

(99) Li W, Liu W, Liu W, Kou W. Removal of copper and iron cyanide complex from cyanide solution by polymer-surfactant aggregates. Colloids and Surfaces A: Physicochemical and Engineering Aspects. 2024 Nov 5;700:134788.

(100) Chen S, Sun C, Wang Y, Han Y, Dai L, Abliz A, Gao Y. Quercetagetin-loaded composite nanoparticles based on zein and hyaluronic acid: Formation, characterization, and physicochemical stability. Journal of agricultural and food chemistry. 2018 Jun 13;66(28):7441-50.

(101) Wang H, Zhang J, Zhang Y. Effects of mono-substituents on the polarity-sensitive fluorescent probe properties of pyrene. Spectrochimica Acta Part A: Molecular and Biomolecular Spectroscopy. 2025 Mar 13:126049.

(102) Gopi A, Vindhyasarumi A, Yoosaf K. Electrostatically driven self-assembly of CdTe nanoparticles with organic chromophores probed via Ham effect. RSC Advances. 2015;5(59):47813-9.

(103) Tănase MA, Raducan A, Oancea P, Diţu LM, Stan M, Petcu C, Scomoroşcenco C, Ninciuleanu CM, Nistor CL, Cinteza LO. Mixed pluronic—Cremophor polymeric micelles as nanocarriers for poorly soluble antibiotics—The influence on the antibacterial activity. Pharmaceutics. 2021 Mar 24;13(4):435.

(104) Mondal BB, Banik R, Ghosh S. Impact of 2, 2, 2-trifluoroethanol (TFE) on hydrophobicity enhancement in the aggregation of sodium N-dodecanoyl sarcosinate (SDDS) with nonionic hydroxyethyl cellulose. Colloids and Surfaces A: Physicochemical and Engineering Aspects. 2024 Jan 20;681:132781.

(105) Mora AK, Singh PK, Nath S. Controlled sequestration of DNA intercalated drug by polymer–surfactant supramolecular assemblies. The Journal of Physical Chemistry B. 2016 May 5;120(17):4143-51.

(106) Biswas B, Shah D, Cox-Vázquez SJ, Vázquez RJ. Sensing cholesterol-induced rigidity in model membranes with time-resolved fluorescence spectroscopy and microscopy. Journal of Materials Chemistry B. 2024;12(27):6570-6.

(107) Kong L, Cao M, Hai M. Investigation on the interaction between sodium dodecyl sulfate and cationic polymer by dynamic light scattering, rheological, and conductivity measurements. Journal of Chemical & Engineering Data. 2007 May 10;52(3):721-6.

(108) Zhao Y, Wang N, Pang SF, Zhang YH. In-situ micro-FTIR spectroscopic observation on the hydration process of Poria cocos. Spectrochimica Acta Part A: Molecular and Biomolecular Spectroscopy. 2016 Jul 5;164:61-6.

(109) Thomas E, Thomas D, Bhuvaneswari S, Vijayalakshmi KP, George BK. 1-Hexadecyl-3-methylimidazolium chloride: structure, thermal stability and decomposition mechanism. Journal of Molecular Liquids. 2018 Jan 1;249:404-11.

(110) Ekici S, Ilgin P, Butun S, Sahiner N. Hyaluronic acid hydrogel particles with tunable charges as potential drug delivery devices. Carbohydrate Polymers. 2011 Apr 2;84(4):1306-13.

(111) Vasi AM, Popa MI, Butnaru M, Dodi G, Verestiuc L. Chemical functionalization of hyaluronic acid for drug delivery applications. Materials Science and Engineering: C. 2014 May 1;38:177-85.

(112) Manju S, Sreenivasan K. Conjugation of curcumin onto hyaluronic acid enhances its aqueous solubility and stability. Journal of colloid and interface science. 2011 Jul 1;359(1):318-25.

(113) Jiao L, Zhang L, Guan W, Lu C. Fluorescence visualization of interactions between surfactants and polymers. RSC Advances. 2016;6(92):88954-8.

(114) Chatterjee S, Prajapati R, Bhattacharya A, Mukherjee TK. Microscopic evidence of “necklace and bead”-like morphology of polymer–surfactant complexes: a comparative study on poly (vinylpyrrolidone)–sodium dodecyl sulfate and poly (diallyldimethylammonium chloride)–sodium dodecyl sulfate systems. Langmuir. 2014 Aug 19;30(32):9859-65.

Summary and Conclusions

The first chapter examines the interaction between hydroxyethyl cellulose (HEC), a non-ionic biopolymer, and sodium N-dodecanoyl sarcosinate (SDDS), an anionic surfactant. The interaction observed between them is solely hydrophobic, and the strength of this association increases with polymer concentration. The CMC values of SDDS decrease with increasing HEC concentration, indicating rapid aggregation.

The second chapter provides a detailed analysis of the aggregation behaviour of SDDS with HEC in two different environments: pure water and a TFE-water binary mixture. We observe that SDDS effectively binds to HEC through hydrophobic interactions. The cosurfactant-like role of TFE intensifies hydrophobicity, leading to a reduction in the CMC. The decrease in micellar charge density on the surfactant head groups facilitates closer packing among them.

In the third chapter, experiments and visual techniques are employed to investigate the coacervate formation between anionic biopolymer pectin and cationic alkyltriphenylphosphonium bromides (C_nTPB) surfactants. This interaction is controlled by the balance of electrostatic attraction and hydrophobic binding. The resulting aggregates exhibit concentration-dependent modifications in surface activity, ionic transport, turbidity, polarity, viscosity, charge, and morphology.

The fourth chapter presents a comparative study of interactions between pectin with homologous cationic surfactants (DTAB, TTAB, CTAB, and OTAB). Their interactions primarily originate from electrostatic forces between the anionic carboxylate group and the cationic head group. In addition to the electrostatic forces, hydrophobic interactions are also evident. These interactions involve the binding of the surfactant alkyl chains to the hydrophobic regions of the pectin macromolecule.

In Chapter five, the molecular interactions between hyaluronic acid (HA), an anionic polyelectrolyte, and 1-hexadecyl-3-methyl imidazolium chloride (C16MImCl), a surface-active ionic liquid, are analysed. These interactions are shaped by electrostatic attraction, hydrogen bonding, and hydrophobic effects. Coacervation is triggered by charge neutralization of HA, followed by the growth of aggregates stabilized predominantly through hydrophobic forces.

Appendix

Basic Data

Chapter I

1.1. Tensiometric data for the CMC determination of SDDS in the absence and presence of different [HEC] at 298 K.

Water		0.05 g% HEC		0.1 g% HEC		0.2 g% HEC	
log[SDDS/mM]	γ/mNm^{-1}	log[SDDS/mM]	γ/mNm^{-1}	log[SDDS/mM]	γ/mNm^{-1}	log[SDDS/mM]	γ/mNm^{-1}
--	72.1	--	65.8	--	61	--	58.1
-0.85405	68.5	-0.85405	64.6	-0.85405	60.8	-0.85405	55.3
-0.37727	58.4	-0.37727	62.5	-0.37727	57.4	-0.37727	50
-0.07676	51.8	-0.07676	56.3	-0.07676	51.9	-0.07676	45.2
0.14439	46.7	0.14439	49.3	0.14439	46.4	0.14439	40.9
0.31962	42.5	0.31962	44	0.31962	41.6	0.31962	36.1
0.46471	38.7	0.46471	37.9	0.46471	37.9	0.46471	32.7
0.59605	36	0.59605	36.4	0.59605	34.7	0.59605	30.8
0.72495	33.7	0.72495	33.1	0.72495	32.7	0.72495	28.3
0.86529	31.7	0.84493	31.9	0.84493	29.4	0.86529	25.8
0.97008	28.9	0.95436	28.2	0.97008	27	1.02757	23.2
1.06594	27.8	1.05355	26.2	1.08964	24.4	1.18184	23.8
1.1534	26.4	1.14345	26	1.19973	25.2	1.33213	24.8
1.23326	26.9	1.22514	26.7	1.29964	26	1.48404	25.2
1.30636	27.5	1.29964	27.7	1.39519	26.6	1.62054	25.4
1.379	28	1.37345	28	1.48818	27	1.75748	25.8
1.44919	28.3	1.44459	28.4	1.59412	27.4		
1.51586	28.7	1.51203	29				
1.58485	29	1.5817	29.5				
		1.66545	29.9				

1.2. Conductometric data for the CMC determination of SDDS in the absence and presence of different [HEC] at 298 K.

Water		0.05 g% HEC		0.1 g% HEC		0.2 g% HEC	
[SDDS/mM]	κ/mS cm^{-1}	[SDDS/mM]	κ/mS cm^{-1}	[SDDS/mM]	κ/mS cm^{-1}	[SDDS/mM]	κ/mS cm^{-1}
0	0.008	0	0.053	0	0.098	0	0.24
0.32097	0.039	0.21398	0.067	0.21398	0.105	0.21398	0.26
0.64103	0.066	0.42735	0.08	0.42735	0.121	0.42735	0.27
0.96017	0.092	0.64011	0.098	0.64011	0.137	0.64011	0.29
1.27841	0.117	0.85227	0.113	0.85227	0.151	0.85227	0.3
1.59574	0.141	1.06383	0.129	1.06383	0.163	1.06383	0.31
1.91218	0.166	1.27479	0.143	1.27479	0.179	1.27479	0.33
2.22772	0.191	1.48515	0.16	1.48515	0.194	1.48515	0.34

2.85614	0.24	1.69492	0.174	1.69492	0.21	1.69492	0.36
3.48101	0.28	1.90409	0.188	1.90409	0.22	1.90409	0.37
4.10238	0.33	2.11268	0.2	2.11268	0.23	2.11268	0.38
4.72028	0.37	2.52809	0.23	2.52809	0.26	2.52809	0.41
5.33473	0.41	2.94118	0.26	2.94118	0.29	2.94118	0.44
6.25	0.47	3.35196	0.29	3.35196	0.31	3.35196	0.47
7.15768	0.53	3.76045	0.32	3.76045	0.34	3.76045	0.49
8.05785	0.59	4.16667	0.34	4.16667	0.37	4.16667	0.52
8.95062	0.65	4.57064	0.37	4.57064	0.4	4.57064	0.54
9.83607	0.71	4.97238	0.39	4.97238	0.42	4.97238	0.57
11.00543	0.78	5.3719	0.42	5.3719	0.45	5.3719	0.6
12.16216	0.85	5.76923	0.44	5.76923	0.47	5.76923	0.62
13.30645	0.92	6.16438	0.47	6.16438	0.5	6.16438	0.65
14.4385	0.98	6.75307	0.51	6.75307	0.53	6.75307	0.68
15.55851	1.03	7.33696	0.54	7.33696	0.57	7.33696	0.72
16.66667	1.08	7.9161	0.58	7.9161	0.61	7.9161	0.76
18.03548	1.14	8.49057	0.62	8.49057	0.64	8.49057	0.79
19.38642	1.19	9.0604	0.66	9.0604	0.68	9.0604	0.83
20.71984	1.24	9.62567	0.69	9.62567	0.72	9.62567	0.86
22.03608	1.29	10.18642	0.73	10.18642	0.75	10.18642	0.89
23.59335	1.35	10.74271	0.76	10.74271	0.79	10.74271	0.93
25.1269	1.4	11.29458	0.8	11.29458	0.82	11.29458	0.96
26.63728	1.45	11.84211	0.83	11.84211	0.85	11.84211	0.98
28.125	1.5	12.56545	0.88	12.56545	0.88	12.56545	1.02
29.59057	1.56	13.28125	0.92	13.28125	0.92	13.28125	1.05
31.27306	1.62	13.98964	0.95	13.98964	0.96	13.98964	1.09
32.92683	1.67	14.69072	0.99	14.69072	0.99	14.69072	1.12
34.5526	1.73	15.38462	1.02	15.38462	1.03	15.38462	1.15
36.15108	1.79	16.07143	1.05	16.07143	1.06	16.07143	1.17
37.72295	1.84	16.75127	1.08	16.75127	1.08	16.75127	1.2
		17.42424	1.11	17.42424	1.11	17.42424	1.22
		18.09045	1.14	18.09045	1.13	18.09045	1.25
		18.75	1.16	18.75	1.16	18.75	1.27
		19.56522	1.2	19.56522	1.19	19.56522	1.3
		20.37037	1.23	20.37037	1.22	20.37037	1.33
		21.16564	1.26	21.16564	1.25	21.16564	1.36
		21.95122	1.29	21.95122	1.28	21.95122	1.38
		22.72727	1.31	22.72727	1.3	22.72727	1.41
		23.49398	1.34	23.49398	1.33	23.49398	1.44

1.3. Calorimetric data for the CMC determination of SDDS in the absence and presence of different [HEC] at 298 K.

Water		0.05 g% HEC		0.1 g% HEC		0.2 g% HEC	
[SDDS/mM]	ΔH^0 (kJ.mol^{-1})	[SDDS/mM]	ΔH^0 (kJ.mol^{-1})	[SDDS/mM]	ΔH^0 (kJ.mol^{-1})	[SDDS/mM]	ΔH^0 (kJ.mol^{-1})
0	--	0	--	0	--	0	--
0.79592	-1.22497	0.37856	-0.97761	0.36594	-0.86373	0.36594	-2.75847
3.96016	-1.20447	1.88355	-0.92122	1.82076	-0.85878	1.82076	-2.75317
7.09325	-1.16662	3.37372	-0.89031	3.26126	-0.78961	3.26126	-2.73091
10.19519	-1.06391	4.84908	-0.90059	4.68745	-0.75349	4.68745	-2.67495
13.26599	-0.98276	6.30963	-0.81914	6.09931	-0.74772	6.09931	-2.51603
16.30565	-0.88059	7.75536	-0.76857	7.49685	-0.71775	7.49685	-2.42666
19.31417	-0.72358	9.18629	-0.7663	8.88008	-0.68087	8.88008	-2.32913
22.29154	-0.61263	10.60239	-0.78272	10.24898	-0.67854	10.24898	-2.22391
25.23776	-0.6022	12.00369	-0.7197	11.60357	-0.60115	11.60357	-2.12771
28.15284	-0.5739	13.39017	-0.46242	12.94384	-0.42414	12.94384	-1.94181
31.03678	-0.54138	14.76184	-0.22242	14.26978	-0.24039	14.26978	-1.70553
33.88957	-0.53732	16.1187	-0.08665	15.58141	-0.10964	15.58141	-1.5648
36.71122	-0.52981	17.46075	-0.02335	16.87872	-0.02925	16.87872	-1.45561
39.50173	-0.53527	18.78798	-0.01169	18.16171	-0.01954	18.16171	-1.41533
42.26109	-0.51924	20.1004	0.00747	19.43039	-0.02572	19.43039	-1.35624
44.9893	-0.50629	21.398	0.00414	20.68474	-0.01424	20.68474	-1.339
47.68638	-0.49594	22.6808	0.02746	21.92477	-0.0107	21.92477	-1.30508
50.35231	-0.50462	23.94878	-0.00336	23.15049	7.82452E-4	23.15049	-1.26137
52.98709	-0.50142	25.20195	0.0133	24.36188	-0.0054	24.36188	-1.24161

1.4. Fluorimetric data for the CMC determination of SDDS in the absence and presence of different [HEC] at 298 K.

Water		0.05 g% HEC		0.1 g% HEC		0.2 g% HEC	
[SDDS/mM]	I_1/I_3	[SDDS/mM]	I_1/I_3	[SDDS/mM]	I_1/I_3	[SDDS/mM]	I_1/I_3
0	1.45835	0	1.33822	0	1.33158	0	1.42245
0.11995	1.45658	0.11995	1.33654	0.2997	1.32881	0.2997	1.42519
0.47923	1.45719	0.35957	1.33209	0.74813	1.32148	0.89731	1.41831
1.07613	1.45351	0.95694	1.32925	1.64097	1.3145	1.49254	1.41346
2.2628	1.45233	1.90779	1.32347	3.11727	1.30971	2.38095	1.4072
5.76697	1.43484	3.08789	1.31026	4.57903	1.29874	3.55731	1.39864
9.18961	1.39547	5.42027	1.28198	6.02646	1.27188	5.01475	1.39239
13.63116	1.24895	7.71629	1.24938	7.45978	1.25442	7.88705	1.35593
18.99588	1.0465	11.09399	1.19568	8.87918	1.22924	10.70395	1.20776

24.1633	1.02205	15.478	1.0044	10.28489	1.18294	13.46705	1.12054
32.04716	1.01479	20.77439	0.90798	13.05595	1.12912	16.17786	1.0451
41.2901	1.00732	25.87719	0.90107	15.77451	1.03086	24.01104	1.01488
49.91664	1.00726	30.79684	0.89314	21.05997	1.01191	28.99729	1.01308
57.98645	1.00721	38.31124	0.89597	23.62966	1.00961	36.14776	1.00885
65.55173	1.00262	47.13419	0.88837	33.4518	1.005	47.26201	1.00836
72.65838	1.0014	55.3816	0.88515	40.37213	1.00148	66.89977	1.00808
85.65304	0.99375	63.10802	0.88639	51.14061	1.0037	91.23173	1.00721
		70.3613	0.88021	61.05137	1.00039		
		83.61223	0.88129	86.55283	1.00137		
		95.41735	0.87687				

1.5. Quenching of pyrene by [CPC] at micellar SDDS solution in absence and presence of different [HEC] at 298K.

Water		0.05 g% HEC		0.1 g% HEC		0.2 g% HEC	
[SDDS]/mM	$\ln(I_0/I)$	[SDDS]/mM	$\ln(I_0/I)$	[SDDS]/mM	$\ln(I_0/I)$	[SDDS]/mM	$\ln(I_0/I)$
0	0	0	0	0	0	0	0
0.0024	0.00855	0.0012	0.00252	0.0024	0.0142	0.0012	0.00127
0.00599	0.03186	0.0036	0.01128	0.00479	0.02367	0.0036	0.04119
0.00957	0.04069	0.00957	0.06574	0.00838	0.02826	0.00599	0.0485
0.01552	0.06395	0.01552	0.09552	0.01433	0.06355	0.00957	0.06872
0.02145	0.08691	0.02145	0.12102	0.02026	0.09218	0.01433	0.10018
0.02735	0.09369	0.02735	0.15385	0.02735	0.12555	0.01908	0.14178
0.03557	0.13403	0.03323	0.18337	0.03557	0.15243	0.02381	0.15877
0.04375	0.15777	0.04142	0.209	0.04492	0.20297	0.0297	0.18442
0.05189	0.17884	0.04957	0.24256	0.0542	0.24734	0.03791	0.21784
0.06343	0.23355	0.05882	0.27457	0.06573	0.29055	0.04608	0.26434
0.07488	0.26535	0.06802	0.3092			0.0542	0.29118
		0.0783	0.34023			0.06458	0.34849
		0.08851	0.37259			0.07488	0.38611
		0.09977	0.40329				
		0.11094	0.43886				
		0.12203	0.47537				

Chapter II

2.1. Tensiometric data for the CMC determination of SDDS in water and water/TFE mixtures at 298 K.

Water		5% TFE		10% TFE		15% TFE	
log[SDDS/mM]	γ/mNm^{-1}	log[SDDS/mM]	γ/mNm^{-1}	log[SDDS/mM]	γ/mNm^{-1}	log[SDDS/mM]	γ/mNm^{-1}
--	71.3	--	41.6	--	32.5	--	26.2
-0.86993	64.1	-0.86993	42	-0.86993	33.3	-0.64825	27.3
-0.44439	56.3	-0.39333	41	-0.39333	34.1	-0.20187	27.7
-0.14406	49.5	-0.09308	38	-0.11781	35	0.09795	28.4
0.08224	44.2	0.14189	34.9	0.09795	36.9	0.32125	28.8
0.26245	38.7	0.32125	32.5	0.27283	35.3	0.49835	29.1
0.41163	34.9	0.46706	30.1	0.41897	33.3	0.64492	27.3
0.54403	31.4	0.59971	28	0.54941	30.9	0.77525	25.8
0.6734	28.9	0.7291	25	0.67736	28.2	0.90234	25
0.81365	25.6	0.86914	22.4	0.81647	25.5	1.03978	25.1
0.97504	22.3	1.02996	20.3	0.97715	23.6	1.19678	25.2
1.1452	19.6	1.19905	20.7	1.13143	23.8	1.36068	25.3
1.28714	21	1.33961	21	1.27755	23.9	1.49582	25.3
1.46808	22.8	1.51792	21.4	1.46241	24.2		
1.63038	24	1.67669	21.8	1.62688	24.3		
1.7624	24.9	1.80468	22	1.76009	24.6		
1.86692	25.7						

2.2. Conductometric data for the CMC determination of SDDS in water and water/TFE mixtures at 298 K.

Water		5% TFE		10% TFE		15% TFE	
[SDDS/mM]	κ/mS cm^{-1}	[SDDS/mM]	κ/mS cm^{-1}	[SDDS/mM]	κ/mS cm^{-1}	[SDDS/mM]	κ/mS cm^{-1}
0	0.012	0	0.01	0	0.0079	0	0.0049
0.21398	0.024	0.21398	0.0195	0.32097	0.03	0.21398	0.0191
0.42735	0.035	0.42735	0.033	0.64103	0.052	0.42735	0.035
0.64011	0.046	0.64011	0.046	0.96017	0.07	0.64011	0.05
0.85227	0.057	0.85227	0.06	1.27841	0.09	0.85227	0.064
1.06383	0.068	1.06383	0.073	1.59574	0.109	1.06383	0.079
1.27479	0.079	1.27479	0.086	1.91218	0.131	1.27479	0.093
1.48515	0.089	1.48515	0.098	2.22772	0.154	1.48515	0.108
1.90409	0.109	1.69492	0.111	2.85614	0.192	1.69492	0.122
2.32068	0.13	1.90409	0.123	3.48101	0.23	1.90409	0.136
2.73492	0.149	2.11268	0.136	4.10238	0.27	2.11268	0.151

3.14685	0.17	2.52809	0.159	4.72028	0.3	2.52809	0.178
3.55649	0.19	2.94118	0.183	5.33473	0.34	2.94118	0.2
3.96384	0.22	3.35196	0.21	6.25	0.39	3.35196	0.23
4.36893	0.23	3.76045	0.23	7.15768	0.44	3.76045	0.26
4.97238	0.26	4.16667	0.25	8.05785	0.48	4.16667	0.28
5.57084	0.29	4.57064	0.28	8.95062	0.53	4.57064	0.31
6.16438	0.31	4.97238	0.3	9.83607	0.57	4.97238	0.33
6.75307	0.34	5.3719	0.32	11.00543	0.63	5.3719	0.36
7.33696	0.37	5.76923	0.34	12.16216	0.68	5.76923	0.38
7.9161	0.4	6.16438	0.37	13.30645	0.74	6.16438	0.4
8.49057	0.42	6.75307	0.4	14.4385	0.79	6.75307	0.44
9.24933	0.46	7.33696	0.43	15.55851	0.84	7.33696	0.47
10	0.49	7.9161	0.46	16.66667	0.89	7.9161	0.51
10.74271	0.52	8.49057	0.49	18.03548	0.94	8.49057	0.54
11.47757	0.55	9.0604	0.52	19.38642	1	9.0604	0.56
12.20472	0.59	9.62567	0.54	20.71984	1.05	9.62567	0.59
13.103	0.62	10.18642	0.57	22.03608	1.11	10.18642	0.62
13.98964	0.66	10.74271	0.59	23.59335	1.17	10.74271	0.64
14.86486	0.7	11.29458	0.62	25.1269	1.23	11.29458	0.67
15.7289	0.73	11.84211	0.64	26.63728	1.3	11.84211	0.69
16.58196	0.77	12.7451	0.68	28.125	1.36	12.7451	0.73
17.59142	0.81	13.63636	0.72	29.59057	1.41	13.63636	0.77
18.58573	0.85	14.51613	0.76	31.27306	1.48	14.51613	0.81
19.56522	0.88	15.38462	0.8	32.92683	1.54	15.38462	0.85
20.53021	0.92	16.24204	0.84	34.5526	1.6	16.24204	0.88
21.48103	0.96	17.08861	0.88	36.15108	1.67	17.08861	0.92
22.57282	1	17.92453	0.92	37.72295	1.73	17.92453	0.95
23.64621	1.05	18.75	0.96			18.75	0.99
24.70167	1.09	19.56522	1			19.56522	1.02
25.73964	1.13	20.37037	1.04			20.37037	1.05
26.76056	1.16	21.48103	1.09			21.48103	1.1
27.76484	1.2	22.57282	1.13			22.57282	1.14
28.89273	1.24	23.64621	1.18			23.64621	1.18
30	1.28	24.70167	1.23			24.70167	1.23
31.0872	1.32	25.73964	1.27			25.73964	1.27
32.15488	1.36	26.90504	1.32			26.90504	1.31
33.20356	1.4	28.04878	1.37			28.04878	1.36
34.48845	1.44	29.17146	1.42			29.17146	1.4
35.74538	1.48	30.27366	1.47			30.27366	1.44
36.97524	1.52	31.35593	1.51			31.35593	1.49
38.17891	1.56	32.68156	1.57			32.68156	1.54

39.35722	1.6	33.9779	1.62			33.9779	1.59
40.51095	1.64	35.2459	1.67			35.2459	1.64
		36.48649	1.72			36.48649	1.69
		37.70053	1.77			37.70053	1.73
						38.88889	1.78

2.3. Calorimetric data for the CMC determination of SDDS in water and water/TFE mixture at 298 K.

Water		10% TFE	
[SDDS/mM]	ΔH^0 (kJ.mol^{-1})	[SDDS/mM]	ΔH^0 (kJ.mol^{-1})
0	--	0	--
0.42224	-4.05704	0.51323	5.36207
2.10088	-4.00979	6.57414	4.81687
3.763	-3.96799	9.53682	2.85271
5.40859	-3.88258	12.45431	1.65953
7.03766	-3.80262	15.32661	0.5134
8.65021	-3.683	18.15373	0.33958
10.24624	-3.5173	20.93566	0.20648
11.82575	-3.26511	23.67241	0.13059
13.38873	-3.21839	26.36397	0.05276
14.93519	-3.01754	29.01034	0.00536
16.46513	-2.81218	32.46856	0.03238
17.97855	-2.65589		
19.47545	-2.37806		
20.95582	-2.37113		
22.41968	-2.34992		
23.86701	-2.26692		
25.29781	-2.09711		
26.7121	-2.10135		
28.10986	-2.02377		

2.4. Fluorimetric data for the CMC determination of SDDS in water and water/TFE mixtures at 298 K.

Water		5% TFE		10% TFE		15% TFE	
[SDDS/mM]	I_1/I_3	[SDDS/mM]	I_1/I_3	[SDDS/mM]	I_1/I_3	[SDDS/mM]	I_1/I_3
0	1.44467	0	1.45992	0	1.48223	0	1.44805
0.33699	1.43443	0.67298	1.458	0.53871	1.48116	0.4491	1.44441
0.89641	1.43432	1.67494	1.45618	1.34195	1.47953	1.34195	1.44732

1.78571	1.44041	3.32512	1.451	2.40404	1.45631	2.66798	1.43732
6.1284	1.419	6.5534	1.41625	3.63046	1.45691	4.41176	1.40852
11.62873	1.32381	12.73585	1.07825	6.1284	1.41583	6.5534	1.29216
14.32584	1.21848	15.69767	1.03796	10.9589	1.09394	8.65385	1.16027
15.60028	1.13236	18.57798	1.0223	17.81768	1.01367	10.71429	1.09834
16.85939	1.06009	21.38009	1.01097	26.30696	0.99585	14.71963	1.05519
18.10345	1.04118	28.06346	1.00018	35.9879	0.98802	22.2973	1.02076
20.64033	1.01881	40.19507	0.98682	44.7693	0.98017	29.34783	1.00787
26.5873	1.00792	60.46618	0.98058	52.77097	0.98129	39.04959	0.99643
32.19794	1.00148	95.87518	0.96626	60.09235	0.98016	53.24427	0.97896
42.59222	0.99857			66.81665	0.96735	75.99338	0.96571
60.34577	0.99506			78.74415	0.9642	93.42105	0.95461
81.32184	0.9916			88.99903	0.96947		
				97.91008	0.96515		
				105.72519	0.9586		

2.5. Quenching of pyrene by [CPC] at micellar SDDS solution in water and water/TFE mixtures at 298 K.

Water		5% TFE		10% TFE		15% TFE	
[SDDS]/mM	$\ln(I_0/I)$	[SDDS]/mM	$\ln(I_0/I)$	[SDDS]/mM	$\ln(I_0/I)$	[SDDS]/mM	$\ln(I_0/I)$
0	0	0	0	0	0	0	0
0.0012	0.00723	0.0024	0.00814	0.0024	0.02505	0.0024	0.00888
0.0024	0.0155	0.00599	0.01768	0.00598	0.0411	0.00479	0.02033
0.0036	0.02097	0.01195	0.04921	0.01076	0.048	0.00718	0.02259
0.00599	0.03117	0.01789	0.07092	0.0167	0.07688	0.00957	0.03832
0.00838	0.03863	0.02381	0.09775	0.02263	0.09751	0.01314	0.03901
0.01076	0.04922	0.0297	0.10962	0.02971	0.11982	0.01908	0.0536
0.01433	0.06291	0.03791	0.14014	0.03792	0.14618	0.02499	0.07506
0.01789	0.07779	0.04608	0.16164	0.04724	0.17725	0.03088	0.09043
0.02145	0.09103	0.0542	0.19027	0.05767	0.20747	0.04259	0.12166
0.02735	0.11312	0.06228	0.22096	0.06917	0.24477	0.0542	0.15157
0.03323	0.13074						

2.6. Tensiometric data for 0.01 g% HEC-SDDS interaction in water and water/TFE mixtures at 298 K.

Water		5% TFE		10% TFE		15% TFE	
log[SDDS/mM]	γ/mNm^{-1}	log[SDDS/mM]	γ/mNm^{-1}	log[SDDS/mM]	γ/mNm^{-1}	log[SDDS/mM]	γ/mNm^{-1}
--	59.4	--	41.7	--	34.1	--	29.3
-0.74507	57.9	-0.74507	41.2	-0.86993	35.8	-0.74507	30.7
-0.30635	55	-0.30635	34.8	-0.34766	36.6	-0.26865	31.7
-0.00627	48.9	-0.00627	30.3	-0.04749	37.3	0.03134	31.1
0.21821	43.6	0.21821	27.3	0.18175	35.2	0.25181	29.4
0.38882	39	0.38882	25.4	0.35638	32.9	0.42618	27.4

0.53307	35	0.53307	23.9	0.50434	30.9	0.57026	26
0.66538	31.8	0.66538	22.6	0.63601	29.2	0.70033	24.9
0.79334	29.2	0.79334	21.4	0.76247	27	0.82756	23.9
0.9309	25.7	0.9309	20.4	0.90005	25	0.96543	23.3
1.08971	22.6	1.06326	19.9	1.03161	23.7	1.12369	23.5
1.2573	23.2	1.18256	20.2	1.15131	23.8	1.27252	23.6
1.39608	23.6	1.30442	20.7	1.25822	24	1.4154	23.7
1.53516	23.8	1.42865	21.1	1.36493	24.1	1.55692	23.9
1.65845	24.3	1.55692	21.5	1.46454	24.3	1.68075	24
1.77917	24.4	1.67308	21.7	1.57367	24.5		
1.88235	24.6	1.78858	22	1.67694	24.6		

2.7. Conductometric data for 0.01 g% HEC-SDDS interaction in water and water/TFE mixtures at 298 K.

Water		5% TFE		10% TFE		15% TFE	
[SDDS/mM]	κ/mS cm^{-1}	[SDDS/mM]	κ/mS cm^{-1}	[SDDS/mM]	κ/mS cm^{-1}	[SDDS/mM]	κ/mS cm^{-1}
0	0.195	0	0.136	0	0.12	0	0.074
0.21398	0.2	0.21398	0.143	0.21398	0.131	0.21398	0.088
0.42735	0.22	0.42735	0.155	0.42735	0.145	0.42735	0.106
0.64011	0.23	0.64011	0.167	0.64011	0.158	0.64011	0.12
0.85227	0.24	0.85227	0.181	0.85227	0.171	0.85227	0.132
1.06383	0.26	1.06383	0.194	1.06383	0.184	1.06383	0.148
1.27479	0.28	1.27479	0.21	1.27479	0.197	1.27479	0.159
1.48515	0.29	1.48515	0.22	1.48515	0.21	1.48515	0.174
1.69492	0.3	1.69492	0.23	1.69492	0.22	1.90409	0.193
1.90409	0.32	1.90409	0.24	1.90409	0.23	2.32068	0.22
2.11268	0.33	2.11268	0.26	2.11268	0.25	2.73492	0.24
2.52809	0.36	2.52809	0.28	2.52809	0.27	3.14685	0.26
2.94118	0.39	2.94118	0.3	2.94118	0.3	3.55649	0.28
3.35196	0.41	3.35196	0.33	3.35196	0.32	3.96384	0.3
3.76045	0.44	3.76045	0.35	3.76045	0.34	4.36893	0.33
4.16667	0.47	4.16667	0.37	4.16667	0.36	4.97238	0.36
4.57064	0.5	4.57064	0.39	4.57064	0.39	5.57084	0.39
4.97238	0.52	4.97238	0.42	4.97238	0.41	6.16438	0.42
5.3719	0.55	5.3719	0.44	5.3719	0.43	6.75307	0.45
5.76923	0.58	5.76923	0.46	5.76923	0.45	7.33696	0.48
6.16438	0.6	6.16438	0.48	6.16438	0.48	7.9161	0.51
6.75307	0.64	6.75307	0.51	6.75307	0.51	8.49057	0.53
7.33696	0.68	7.33696	0.54	7.33696	0.54	9.24933	0.56
7.9161	0.71	7.9161	0.57	7.9161	0.57	10	0.59

8.49057	0.75	8.49057	0.6	8.49057	0.6	10.74271	0.62
9.0604	0.78	9.0604	0.62	9.0604	0.62	11.47757	0.65
9.62567	0.82	9.62567	0.65	9.62567	0.65	12.20472	0.68
10.18642	0.85	10.18642	0.67	10.18642	0.67	13.103	0.71
10.74271	0.89	10.74271	0.7	10.74271	0.69	13.98964	0.74
11.29458	0.92	11.29458	0.72	11.29458	0.71	14.86486	0.77
11.84211	0.95	11.84211	0.75	11.84211	0.73	15.7289	0.8
12.56545	0.99	12.7451	0.78	12.7451	0.77	16.58196	0.83
13.28125	1.03	13.63636	0.82	13.63636	0.81	17.59142	0.86
13.98964	1.06	14.51613	0.86	14.51613	0.84	18.58573	0.89
14.69072	1.09	15.38462	0.9	15.38462	0.87	19.56522	0.93
15.38462	1.12	16.24204	0.94	16.24204	0.9	20.53021	0.96
16.07143	1.15	17.08861	0.97	17.08861	0.93	21.48103	0.99
16.75127	1.18	17.92453	1.01	17.92453	0.96	22.57282	1.03
17.42424	1.21	18.75	1.04	18.75	0.99	23.64621	1.06
18.09045	1.23	19.56522	1.07	19.56522	1.02	24.70167	1.1
18.75	1.26	20.37037	1.1	20.37037	1.05	25.73964	1.13
19.56522	1.29	21.32353	1.13	21.32353	1.09	26.76056	1.17
20.37037	1.31	22.26277	1.17	22.26277	1.13	27.90698	1.2
21.16564	1.34	23.18841	1.21	23.18841	1.16	29.03226	1.24
21.95122	1.37	24.10072	1.25	24.10072	1.19	30.13699	1.28
		25	1.28	25	1.22	31.22172	1.32
		25.88652	1.32	25.88652	1.25	32.287	1.35
		26.76056	1.36	26.76056	1.28	33.59202	1.39
		27.62238	1.39	27.62238	1.31	34.86842	1.42
		28.47222	1.43	28.47222	1.34	36.11714	1.47
		29.31034	1.46	29.31034	1.37	37.33906	1.51
		30.41002	1.51	30.41002	1.41	38.53503	1.54
		31.48984	1.56	31.48984	1.45	39.70588	1.58
		32.55034	1.6	32.55034	1.49	40.85239	1.62
		33.59202	1.64	33.59202	1.53	41.97531	1.65
		34.61538	1.68	34.61538	1.56	43.07536	1.69
		35.62092	1.72	35.86957	1.6	44.15323	1.72
		36.60907	1.76	37.09677	1.64		
		37.5803	1.79	38.29787	1.68		
		38.53503	1.83	39.47368	1.72		
		39.47368	1.86	40.625	1.76		
				41.75258	1.81		
				42.85714	1.85		
				43.93939	1.89		
				45	1.93		

				46.0396	1.97		

2.8. Calorimetric data for 0.01 g% HEC-SDDS interaction in water and water/TFE mixture at 298 K.

Water		10% TFE	
[SDDS/mM]	ΔH^0 (kJ.mol^{-1})	[SDDS/mM]	ΔH^0 (kJ.mol^{-1})
0	--	0	--
0.23866	0.15427	0.27446	1.17729
1.18745	0.14175	1.36557	1.14253
2.12691	0.13056	2.44595	1.11815
3.05703	0.105	3.51558	1.11513
3.97781	0.0949	4.57448	1.07847
4.88925	0.09856	5.62264	1.03145
5.79135	0.09682	6.66006	0.95145
6.68412	0.08301	7.68674	0.88942
7.56754	0.07845	8.70268	0.79415
8.44163	0.06006	9.70788	0.71084
9.30638	0.04402	10.70234	0.64131
10.16179	0.02327	11.68606	0.58825
11.00786	0.00767	12.65904	0.51533
11.8446	0.0235	13.62129	0.45207
12.67199	0.29203	14.57279	0.41857
13.49005	0.4982	15.51355	0.38649
14.29876	0.53168	16.44358	0.34573
15.09814	0.46837	17.36286	0.31998
15.88818	0.41916	18.27141	0.32381

2.9. Fluorimetric data for 0.01 g% HEC-SDDS interaction in water and water/TFE mixtures at 298 K.

Water		5% TFE		10% TFE		15% TFE	
[SDDS/mM]	I_1/I_3	[SDDS/mM]	I_1/I_3	[SDDS/mM]	I_1/I_3	[SDDS/mM]	I_1/I_3
0	1.47636	0	1.45212	0	1.47648	0	1.46011
0.17986	1.47343	0.67298	1.44292	0.53871	1.47645	0.67298	1.45567
0.53871	1.46255	1.34195	1.45164	1.60842	1.4735	2.00694	1.4521
0.98566	1.46731	2.66798	1.44455	3.36879	1.47254	5.27344	1.38013
1.87426	1.46682	4.62782	1.4436	5.10164	1.46239	11.52751	1.11851
3.63046	1.46479	7.1878	1.36983	8.4873	1.3149	17.43542	1.04984
7.06122	1.37613	10.30534	1.23756	11.77028	1.16878	23.02513	1.02726

11.20296	1.35264	16.28015	1.08148	18.04636	1.04166	33.34753	1.00107
15.19023	1.12277	21.93141	1.05096	23.96355	1.0112	42.66613	0.99743
19.03149	1.00453	32.36301	1.0195	32.23098	0.99593	55.06042	0.97976
22.73463	0.98685	46.14467	0.99335	44.59589	0.98107	72.35414	0.97349
26.30696	0.98404	65.19886	0.98129	55.47016	0.97203	73.89187	0.97363
29.75529	0.98332	80.58408	0.97705	65.10802	0.96453	76.87623	0.96684
36.30493	0.97104	93.26698	0.95889	73.70898	0.96274	101.30566	0.95625
42.42941	0.96656	103.90205	0.95772	81.43185	0.95957		
48.16881	0.98676	112.94821	0.94794	88.40457	0.94542		
53.55837	0.98878	120.73679	0.94714	100.49801	0.94999		
58.6291	0.9904			110.62424	0.93945		
				119.22715	0.94125		
				126.62644	0.93601		

2.10. Quenching of pyrene by [CPC] at micellar 0.01 g% HEC-SDDS solution in water and water/TFE mixtures at 298 K.

Water		5% TFE		10% TFE		15% TFE	
[SDDS]/mM	$\ln(I_0/I)$	[SDDS]/mM	$\ln(I_0/I)$	[SDDS]/mM	$\ln(I_0/I)$	[SDDS]/mM	$\ln(I_0/I)$
0	0	0	0	0	0	0	0
0.0012	-0.00886	0.0012	0.00716	0.0024	0.01624	0.00478	0.0046
0.0024	0.00134	0.0024	0.01264	0.00478	0.02811	0.01077	0.01395
0.00479	0.02204	0.0036	0.01655	0.00838	0.02883	0.0167	0.02597
0.00718	0.0367	0.00599	0.02862	0.01433	0.04216	0.02381	0.03627
0.01314	0.07695	0.00838	0.03766	0.02145	0.0672	0.03088	0.04676
0.01908	0.09147	0.01076	0.04619	0.02852	0.08418	0.03908	0.0597
0.03088	0.12291	0.01433	0.05538	0.03674	0.10029	0.04841	0.07104
0.04259	0.17346	0.01789	0.06937	0.04609	0.12479	0.05767	0.08542
0.0542	0.22866	0.02145	0.08546	0.05536	0.14319	0.06802	0.09568
0.07146	0.26946	0.02735	0.1006	0.06688	0.1673	0.07944	0.11328
0.08851	0.33879	0.03323	0.11442	0.07831	0.19166		

Chapter III

3.1. Tensiometric data for the CMC determination of pure C_nTPB in aqueous medium at 298 K.

$C_{12}TPB$		$C_{14}TPB$		$C_{16}TPB$	
log[$C_{12}TPB$/mM]	γ/mNm^{-1}	log[$C_{14}TPB$/mM]	γ/mNm^{-1}	log[$C_{16}TPB$/mM]	γ/mNm^{-1}
--	70.6	--	70.8	--	70.6
-1.92099	61.2	-2.77478	63.3	-2.92099	61.4
-1.44422	57.6	-2.29783	58.3	-2.44422	56
-1.14371	55.7	-1.99706	55.3	-2.14371	52.9
-0.92255	53.2	-1.5999	51.5	-1.92255	50.7
-0.74733	51.3	-1.25903	48.2	-1.71947	49.5
-0.57253	49.1	-1.05499	45.3	-1.4709	47
-0.41949	47.5	-0.86276	42.8	-1.20166	44.8
-0.20969	44.5	-0.69534	40.8	-1.0134	43.2
-0.04478	41.4	-0.48448	38.3	-0.85009	42.5
0.11122	38.9	-0.3188	37.8	-0.71066	42.2
0.26269	36.9	-0.20305	37.5	-0.52895	41.4
0.41543	37	-0.07752	37	-0.36193	41.1
0.55246	36.8	0.04118	36.4	-0.22268	40.5
0.68979	36.4	0.16474	35.8	-0.1097	40.3
0.81094	36.1	0.27678	35.2	-0.01848	40
		0.37281	35	0.06402	39.7
		0.45321	34.8		

3.2. Conductometric data for the CMC determination of pure C_nTPB in aqueous medium at 298 K.

$C_{12}TPB$		$C_{14}TPB$		$C_{16}TPB$	
[$C_{12}TPB$]/mM	κ/mS cm^{-1}	[$C_{14}TPB$]/mM	κ/mS cm^{-1}	[$C_{16}TPB$]/mM	κ/mS cm^{-1}
0	0.006	0	0.0024	0	0.058
0.03852	0.01	0.01198	0.0037	0.00855	0.059
0.07692	0.015	0.02393	0.005	0.0255	0.061
0.11522	0.019	0.03585	0.0062	0.04225	0.063
0.15341	0.024	0.04773	0.0075	0.05882	0.065
0.19149	0.028	0.05957	0.009	0.07521	0.066
0.22946	0.032	0.07139	0.0103	0.09141	0.068
0.26733	0.037	0.08317	0.0116	0.10744	0.07
0.30508	0.041	0.09492	0.0127	0.12329	0.072
0.38028	0.049	0.10663	0.0138	0.13896	0.074
0.45506	0.057	0.11831	0.0151	0.15447	0.075
0.52941	0.064	0.14157	0.0177	0.16981	0.077
0.60335	0.072	0.16471	0.02	0.18876	0.078
0.67688	0.08	0.18771	0.023	0.20745	0.08
0.78641	0.091	0.21058	0.025	0.22589	0.082
0.89503	0.102	0.23333	0.027	0.24409	0.083
1.00275	0.112	0.25596	0.03	0.26206	0.084
1.10959	0.123	0.27845	0.032	0.27979	0.086
1.21555	0.133	0.30083	0.034	0.2973	0.087
1.3555	0.147	0.32308	0.037	0.31458	0.088
1.49393	0.16	0.34521	0.039	0.33164	0.089
1.63087	0.173	0.37817	0.042	0.34848	0.09
1.76636	0.184	0.41087	0.045	0.36842	0.092
1.9004	0.194	0.4433	0.048	0.38806	0.093
2.06596	0.203	0.47547	0.051	0.40741	0.095

2.22936	0.212	0.50738	0.054	0.42647	0.096
2.39063	0.221	0.53904	0.056	0.44526	0.097
2.54981	0.23	0.57044	0.059		
2.70694	0.24	0.60159	0.061		
2.89286	0.25	0.6325	0.063		
3.07595	0.26	0.66316	0.065		
3.25628	0.27	0.71373	0.069		
3.43392	0.28	0.76364	0.072		
3.60891	0.29	0.8129	0.076		
		0.86154	0.079		
		0.90955	0.082		
		0.95696	0.085		
		1.00377	0.088		
		1.05	0.091		
		1.09565	0.094		
		1.14074	0.097		

3.3. Fluorimetric data for the CMC determination of pure C_nTPB in aqueous medium at 298 K.

$C_{12}TPB$		$C_{14}TPB$		$C_{16}TPB$	
$[C_{12}TPB]$/mM	I_1/I_3	$[C_{14}TPB]$/mM	I_1/I_3	$[C_{16}TPB]$/mM	I_1/I_3
0	1.45508	0	1.43672	0	1.46358
0.40369	1.45551	0.00839	1.43574	0.00419	1.46053
0.95418	1.45547	0.09139	1.43714	0.01394	1.46252
1.25574	1.448	0.17277	1.43436	0.02087	1.46081
1.62016	1.36517	0.29189	1.41528	0.03191	1.46291
2.04009	1.1798	0.44545	1.25119	0.06593	1.46208
2.57248	1.08081	0.62942	1.14247	0.15775	1.38835
3.19736	1.07433	0.83924	1.07165	0.19562	1.26316
3.78124	1.06279	1.102	1.03713	0.24479	1.16093
4.84118	1.05678	1.40583	1.01731	0.30424	1.09819
5.32368	1.05635	1.68537	1.00646	0.39496	1.0652
5.7782	1.06138	1.94343	1.00413	0.50137	1.02735
		2.40428	0.99252	0.60073	1.0152
		2.80373	0.99386	0.69371	1.00745
		3.31217	0.99015	0.78092	1.0107
		3.73592	0.98305	0.86287	1.00264
		4.09452	0.9758		

3.4. Tensiometric data for pectin-$C_{12}TPB$ interaction at different [pectin] at 298K.

0.05% (w/v)		0.1% (w/v)		0.2% (w/v)	
$\log[C_{12}TPB/mM]$	γ/mNm^{-1}	$\log[C_{12}TPB/mM]$	γ/mNm^{-1}	$\log[C_{12}TPB/mM]$	γ/mNm^{-1}
--	68.4	--	66.7	--	66.8
-2.26769	56.1	-2.26769	55.3	-2.26769	55.7
-1.79075	51.3	-1.79075	50.8	-1.79075	48.8
-1.48998	47.3	-1.48998	47.4	-1.48998	45.9
-1.26847	46.2	-1.26847	44.6	-1.26847	43.6
-1.09282	44.6	-1.09282	43.7	-1.09282	42.1
-0.90787	42.2	-0.90787	41.9	-0.94721	41.5
-0.75195	41.2	-0.75195	41.2	-0.80772	41
-0.59051	41.2	-0.59051	39.9	-0.67992	40.1
-0.44096	41.1	-0.44096	39.7	-0.53988	40.1
-0.28481	40.3	-0.28481	40.4	-0.40475	41.3
-0.13955	39.6	-0.13955	40.2	-0.25951	41.4
-0.00948	38.5	-0.00948	39.5	-0.12157	41.9

0.13785	37.1	0.13785	38.3	0.00366	41.3
0.2674	35.4	0.2674	36.6	0.14697	40.9
0.40391	34.3	0.40391	34.9	0.27394	39.8
0.53024	34.1	0.53024	34	0.40844	38.2
0.64141	34.2	0.65966	33.7	0.5334	36.5
0.73735	33.6	0.77564	33.3	0.66178	35.4
0.82956	33.5	0.87423	33.4	0.77707	35
0.91203	33.4	0.95632	33.1	0.87521	34.5
0.98322	33.4	1.03222	33	0.957	34.4
1.05091	33.2	1.09732	33	1.03269	34.3
1.11027	33.2	1.14352	32.8	1.0865	34.1
				1.13562	34

3.5. Tensiometric data for pectin-C_{14}TPB interaction at different [pectin] at 298K.

0.05% (w/v)		0.1% (w/v)		0.2% (w/v)	
log[C_{14}TPB/mM]	γ/mNm^{-1}	log[C_{14}TPB/mM]	γ/mNm^{-1}	log[C_{14}TPB/mM]	γ/mNm^{-1}
--	68.7	--	67.8	--	68.4
-2.77478	54.9	-2.47383	48	-2.77478	58.6
-2.29783	47.6	-1.99706	41	-2.29783	50.8
-1.99706	45.1	-1.69655	37.3	-1.99706	45.8
-1.77556	42.9	-1.47539	35.3	-1.77556	43.4
-1.5999	41.5	-1.30017	35.4	-1.5999	42.3
-1.41496	40.8	-1.15507	35.2	-1.45429	41.8
-1.25903	40.3	-1.02374	35.7	-1.3148	40.5
-1.0976	40.3	-0.89484	36.1	-1.187	41.2
-0.94805	40.3	-0.77486	36.2	-1.04696	42
-0.79189	40.6	-0.63456	36.6	-0.91184	42.5
-0.64664	40.8	-0.50775	36.8	-0.7666	42.6
-0.51656	40.5	-0.33396	36.8	-0.62866	42.7
-0.36923	40.5	-0.16606	36.2	-0.50342	42.6
-0.23969	38.9	-0.01962	35.2	-0.36011	42.6
-0.10317	37.3	0.1244	33.1	-0.23315	42.6
0.02316	34.9	0.23675	31.7	-0.06298	42.2
0.15257	33.7	0.32712	31	0.09686	41.5
0.26856	33.4	0.40827	30.8	0.2319	39.7
0.36715	33.2	0.47855	30.5	0.34239	38
0.44923	33	0.54552	30.1	0.43206	37
0.52514	32.8	0.60437	29.9	0.51345	36.5
0.59024	32.7			0.58227	36.3
				0.63061	36
				0.66664	35.8

3.6. Tensiometric data for pectin-C_{16}TPB interaction at different [pectin] at 298K.

0.05% (w/v)		0.1% (w/v)		0.2% (w/v)	
log[C_{16}TPB/mM]	γ/mNm^{-1}	log[C_{16}TPB/mM]	γ/mNm^{-1}	log[C_{16}TPB/mM]	γ/mNm^{-1}
--	67.9	--	67.5	--	67.2
-3.22194	61.7	-3.22194	62	-2.92099	53
-2.74499	48	-2.74499	52	-2.44422	44.5
-2.44422	42.3	-2.44422	45.2	-2.14371	38.9
-2.22272	39.9	-2.22272	42.7	-1.92255	38.1
-2.04706	39.3	-2.04706	40.5	-1.74733	38
-1.86211	38.2	-1.86211	39	-1.5272	38.4
-1.70619	36.2	-1.70619	36.9	-1.32565	38.7
-1.54476	35.4	-1.54476	36.9	-1.11905	39.1
-1.39521	35.9	-1.39521	37.4	-0.87965	39.4
-1.23905	35.9	-1.23905	38	-0.62421	39.3

-1.09379	36	-1.09379	38.8	-0.41771	39.3
-0.96372	36.2	-0.96372	38.4	-0.25726	39.1
-0.81639	36.5	-0.81639	38.9	-0.1322	38.8
-0.68684	36.6	-0.68684	39	-0.03371	38.5
-0.55033	36.7	-0.55033	39	0.05385	37.2
-0.424	36.2	-0.424	39.2	0.12674	36.5
-0.29458	35	-0.29458	39	0.17739	35
-0.1786	33.7	-0.1786	38.5	0.21486	34
-0.08001	31.2	-0.08001	36.8	0.24381	33.4
0.00207	30.6	0.00207	35.2	0.26689	33.3
0.07798	30.4	0.07798	33.1	0.28575	33.2
0.13191	30.2	0.13191	32.2	0.30146	33
		0.17687	32	0.31476	32.9
		0.21447	31.9	0.32617	32.8
		0.2435	31.7		

3.7. Conductometric data for pectin-C_{12}TPB interaction at different [pectin] at 298K.

0.05% (w/v)		0.1% (w/v)		0.2% (w/v)	
[C_{12}TPB]/mM	κ/mS cm^{-1}	[C_{12}TPB]/mM	κ/mS cm^{-1}	[C_{12}TPB]/mM	κ/mS cm^{-1}
0	0.13	0	0.19	0	0.33
0.07692	0.14	0.19149	0.2	0.19149	0.34
0.19149	0.15	0.38028	0.22	0.38028	0.35
0.26733	0.16	0.56643	0.24	0.56643	0.37
0.34274	0.17	0.75	0.26	0.75	0.39
0.41772	0.18	0.93103	0.29	0.93103	0.41
0.49229	0.19	1.10959	0.31	1.10959	0.43
0.56643	0.2	1.3555	0.35	1.3555	0.46
0.64017	0.21	1.59677	0.39	1.59677	0.5
0.82271	0.24	1.83356	0.43	1.83356	0.53
1.00275	0.27	2.06596	0.47	2.06596	0.56
1.18033	0.3	2.29412	0.5	2.29412	0.59
1.3555	0.33	2.6129	0.54	2.6129	0.64
1.5283	0.36	2.92357	0.57	2.92357	0.67
1.6988	0.38	3.22642	0.6	3.22642	0.71
1.93369	0.41	3.52174	0.62	3.52174	0.74
2.16426	0.44	3.80982	0.64	3.80982	0.77
2.39063	0.46	4.09091	0.65	4.09091	0.8
2.6129	0.48	4.63314	0.67	4.63314	0.82
2.8312	0.49	5.15029	0.68	5.15029	0.84
3.13636	0.51	5.64407	0.7	5.64407	0.86
3.43392	0.52	6.11602	0.72	6.11602	0.87
3.72414	0.53	6.56757	0.73	6.56757	0.88
4.0073	0.54	7	0.74	7	0.89
4.28365	0.55	7.41451	0.75	7.41451	0.9
4.8169	0.57	7.81218	0.76	7.81218	0.91
5.32569	0.59				
5.81166	0.61				

3.8. Conductometric data for pectin-C_{14}TPB interaction at different [pectin] at 298K.

0.05% (w/v)		0.1% (w/v)		0.2% (w/v)	
[C_{14}TPB]/mM	κ/mS cm^{-1}	[C_{14}TPB]/mM	κ/mS cm^{-1}	[C_{14}TPB]/mM	κ/mS cm^{-1}
0	0.14	0	0.21	0	0.37
0.11831	0.16	0.11831	0.22	0.11831	0.38
0.23333	0.18	0.23333	0.23	0.23333	0.39
0.34521	0.2	0.34521	0.24	0.34521	0.4
0.45405	0.22	0.45405	0.25	0.45405	0.41

0.56	0.25	0.56	0.27	0.56	0.42
0.66316	0.28	0.66316	0.28	0.66316	0.44
0.76364	0.3	0.76364	0.3	0.76364	0.45
0.86154	0.33	0.86154	0.32	0.86154	0.46
0.95696	0.35	0.95696	0.33	0.95696	0.47
1.05	0.36	1.05	0.35	1.05	0.48
1.22927	0.39	1.22927	0.39	1.22927	0.51
1.4	0.4	1.4	0.42	1.4	0.54
1.79326	0.41	1.56279	0.44	1.56279	0.56
2.46061	0.42	1.71818	0.46	1.71818	0.59
		1.86667	0.48	1.86667	0.62
		2.0087	0.49	2.0087	0.64
		2.33814	0.5	2.14468	0.66
		3.15	0.51	2.275	0.68
				2.4	0.7
				2.52	0.71
				2.69126	0.73
				2.87605	0.74
				3.17663	0.75
				3.49785	0.76
				3.92743	0.77
				4.23834	0.78
				4.50596	0.79
				4.74783	0.8

3.9. Conductometric data for pectin-C_{16}TPB interaction at different [pectin] at 298K.

0.05% (w/v)		0.1% (w/v)		0.2% (w/v)	
[C_{16}TPB]/mM	κ/mS cm^{-1}	[C_{16}TPB]/mM	κ/mS cm^{-1}	[C_{16}TPB]/mM	κ/mS cm^{-1}
0	0.14	0	0.22	0	0.33
0.08333	0.15	0.08333	0.23	0.12329	0.34
0.16216	0.16	0.2	0.24	0.30769	0.35
0.23684	0.17	0.30769	0.25	0.46988	0.36
0.30769	0.19	0.40741	0.26	0.61364	0.37
0.375	0.2	0.5	0.27	0.74194	0.38
0.43902	0.21	0.58621	0.28	0.85714	0.39
0.5	0.23	0.66667	0.29	0.96117	0.4
0.55814	0.24	0.74194	0.3	1.05556	0.41
0.61364	0.26	0.8125	0.32	1.14159	0.42
0.66667	0.28	0.87879	0.33	1.22034	0.43
0.74194	0.3	0.94118	0.34	1.29268	0.44
0.8125	0.31	1	0.35	1.35937	0.45
0.87879	0.32	1.07339	0.37	1.42105	0.46
0.98077	0.33	1.14159	0.38	1.53147	0.47
1.15038	0.34	1.29268	0.39	1.62745	0.48
1.28827	0.35	1.42105	0.4	1.75	0.49
1.42572	0.36	1.5906	0.41	1.91192	0.5
		1.74251	0.42	2.07895	0.51
				2.25795	0.52

3.10. Turbidimetric data for pectin-C_{12}TPB interaction at different [pectin] at 298K.

0.05% (w/v)		0.1% (w/v)		0.2% (w/v)	
[C_{12}TPB]/mM	100 - % T	[C_{12}TPB]/mM	100 - % T	[C_{12}TPB]/mM	100 - % T
0	3.943	0	7.849	0	17.444
0.012	4.431	0.012	8.557	0.012	18.506
0.02398	4.651	0.02398	8.801	0.02398	19.043

0.03596	4.749	0.03596	8.96	0.03596	19.385
0.04792	4.907	0.04792	9.216	0.04792	19.641
0.07183	5.017	0.07183	9.485	0.07183	19.983
0.09569	5.139	0.09569	10.352	0.09569	20.215
0.15519	5.2	0.15519	10.205	0.15519	20.422
0.2499	11.157	0.2499	11.707	0.2499	33.142
0.36744	24.133	0.36744	28.296	0.36744	40.649
0.48406	37.439	0.48406	33.899	0.48406	57.458
0.59976	54.089	0.59976	48.223	0.59976	67.627
0.82847	66.931	0.71456	63.351	0.71456	74.451
1.05365	86.169	0.82847	77.747	0.82847	81.372
1.27537	96.033	1.05365	89.905	1.05365	87.915
1.60167	98.95	1.27537	95.801	1.27537	93.616
2.02536	98.804	1.60167	99.365	1.60167	98.254
2.53753	98.853	2.02536	99.622	2.02536	99.548
3.12791	98.853	2.53753	99.524	2.53753	99.731
3.8767	98.84	3.12791	99.426	3.12791	99.573
4.75597	98.792	3.8767	99.341	3.8767	99.353
5.57799	98.755	4.75597	99.255	4.75597	99.158
6.34816	98.633	5.57799	99.133	5.57799	98.938
		6.34816	99.023	6.34816	98.743

3.11. Turbidimetric data for pectin-C_{14}TPB interaction at different [pectin] at 298K.

0.05% (w/v)		0.1% (w/v)		0.2% (w/v)	
[C_{14}TPB]/mM	100 - % T	[C_{14}TPB]/mM	100 - % T	[C_{14}TPB]/mM	100 - % T
0	4.858	0	6.885	0	15.503
0.00336	5.908	0.00336	7.764	0.01007	19.092
0.00671	6.47	0.00671	8.276	0.03017	25.879
0.01007	6.738	0.01007	8.936	0.06019	34.705
0.01342	7.788	0.01677	9.119	0.1	42.847
0.02011	7.739	0.02345	9.485	0.14941	47.314
0.02679	9.802	0.03013	11.108	0.24706	53.613
0.0368	11.279	0.04678	12.463	0.3907	60.645
0.0501	11.841	0.06336	19.226	0.62281	72.876
0.06667	14.075	0.11271	23.389	1.06154	88.928
0.09304	14.16	0.14528	28.381	1.46926	99.402
0.12577	20.239	0.1776	31.006	1.84915	99.707
0.17438	28.613	0.20967	34.045	2.20396	99.512
0.23832	33.948	0.24149	37.256	2.84768	99.06
0.33239	39.014	0.33548	47.241	3.41633	98.84
0.42431	54.236	0.39695	54.504		
0.54366	66.406	0.45749	62.854		
0.65949	88.989	0.51712	67.798		
0.79957	97.473	0.57586	71.399		
0.96111	99.377	0.66234	80.444		
1.1661	99.353	0.74694	85.461		
1.40699	99.402	0.8297	94.421		
1.63236	99.451	0.9107	97.119		
1.84365	99.438	0.98998	98.621		
2.04214	99.426	1.09311	99.28		
2.40514	99.402	1.19341	99.609		
2.72892	99.377	1.291	99.585		
		1.38597	99.548		
		1.50118	99.5		
		1.61267	99.426		
		1.72061	99.39		
		1.92651	99.39		
		2.1201	99.402		

		2.30244	99.39		
		2.47449	99.377		

3.12. Turbidimetric data for pectin-C_{16}TPB interaction at different [pectin] at 298K.

0.05% (w/v)		0.1% (w/v)		0.2% (w/v)	
[C_{16}TPB]/mM	100 - % T	[C_{16}TPB]/mM	100 - % T	[C_{16}TPB]/mM	100 - % T
0	4.053	0	5.4	0	11.975
0.0012	4.541	0.00252	5.945	0.00252	13.904
0.0024	5.139	0.00504	8.545	0.00504	16.26
0.0036	5.273	0.01006	11.255	0.01006	18.75
0.00479	6.067	0.01508	12.817	0.01508	20.703
0.00718	6.006	0.0226	14.954	0.0226	24.182
0.00957	6.616	0.03259	17.102	0.04504	27.356
0.01314	7.202	0.04504	20.886	0.08943	34.412
0.01789	8.167	0.06485	22.656	0.11383	38.391
0.02381	10.986	0.08943	24.28	0.16204	41.431
0.03323	13.184	0.11383	26.746	0.20951	47.559
0.04492	14.514	0.16204	29.529	0.27936	50.928
0.06228	17.578	0.20951	32.483	0.34762	53.833
0.08511	20.068	0.27936	34.668	0.64673	68.555
0.1076	22.9	0.34762	39.148	0.84262	74.316
0.14068	28.577	0.43626	45.642	1.02539	87.964
0.17301	32.556	0.54342	51.733	1.19631	93.713
0.215	37.878	0.64673	61.401	1.3565	97.278
0.25576	43.42	0.84262	87.268	1.50694	98.34
0.30507	48.572	1.02539	97.656	1.78193	99.438
0.36194	55.444	1.19631	99.084	2.02708	99.683
0.43414	70.264	1.3565	99.194	2.24699	99.426
0.51902	89.868	1.50694	98.816		
0.59846	98.853	1.78193	97.986		
0.67298	99.341	2.02708	97.461		
0.743	99.255	2.24699	96.899		
0.87113	99.292	2.44537	95.776		
0.9855	99.341	2.62524	95.227		

Chapter IV

4.1. Tensiometric data for the CMC determination of pure C_nTAB in aqueous medium at 298 K.

DTAB		TTAB		CTAB		OTAB	
log[DTAB/mM]	γ/mNm^{-1}	log[TTAB/mM]	γ/mNm^{-1}	log[CTAB/mM]	γ/mNm^{-1}	log[OTAB/mM]	γ/mNm^{-1}
--	71.4	--	70.8	--	71.8	--	71.3
-0.64825	66.8	-1.47013	63.9	-2.22202	67.3	-3.01782	65
-0.172	62.2	-0.92649	59.1	-1.74525	63.5	-2.54087	62.5
0.19425	57.4	-0.59619	55.6	-1.44474	59	-2.11533	57.2
0.46052	52.1	-0.37521	53	-1.22358	57.2	-1.76402	54.3
0.70403	46.4	-0.17238	50.2	-1.04836	54.9	-1.50207	51.7
0.88131	41.2	0.00199	46.9	-0.87356	53.5	-1.29803	48.7
1.0216	37.6	0.17551	44.7	-0.71557	50.4	-1.1058	45.3
1.13775	35.3	0.33181	42.3	-0.55333	47.1	-0.90528	40.7
1.24617	35.1	0.46893	37.8	-0.40412	44.8	-0.70747	35.6
1.36561	36.5	0.58887	34.9	-0.27149	40.2	-0.54855	33.3
1.47993	36.1	0.70722	35.7	-0.13794	36.2	-0.39061	33
1.60004	36	0.81724	36.2	-0.026	34.7	-0.25029	32.7
1.70973	36	0.93801	36	0.07938	34.5	-0.1106	32.3
		1.0533	36.2	0.19622	34.6	0.01208	32.4
		1.17418	36.2	0.30866	34	0.11494	32.3
		1.2844	35.8			0.19979	32.4
						0.27772	32.5
						0.3442	32.6

4.2. Conductometric data for the CMC determination of pure C_nTAB in aqueous medium at 298 K.

DTAB		TTAB		CTAB		OTAB	
[DTAB]/mM	κ/mS cm^{-1}	[TTAB]/mM	κ/mS cm^{-1}	[CTAB]/mM	κ/mS cm^{-1}	[OTAB]/mM	κ/mS cm^{-1}
0	0.013	0	0.017	0	0.016	0	0.025
0.32097	0.053	0.08559	0.026	0.0214	0.02	0.03191	0.029
0.64103	0.089	0.17094	0.039	0.04274	0.023	0.06338	0.033
0.96017	0.126	0.25605	0.048	0.06401	0.027	0.09441	0.037
1.27841	0.159	0.34091	0.059	0.08523	0.03	0.125	0.041
1.59574	0.193	0.42553	0.07	0.10638	0.032	0.15517	0.045
1.91218	0.23	0.50992	0.08	0.12748	0.035	0.18493	0.049
2.22772	0.26	0.59406	0.09	0.14851	0.039	0.21429	0.053
2.54237	0.3	0.67797	0.1	0.16949	0.042	0.24324	0.056
3.16901	0.36	0.84507	0.119	0.21127	0.047	0.28877	0.058
3.79213	0.42	1.01124	0.137	0.25281	0.052	0.33333	0.06
4.41176	0.48	1.17647	0.155	0.29412	0.057	0.37696	0.062
5.02793	0.54	1.34078	0.174	0.3352	0.061	0.41969	0.064
5.64067	0.59	1.50418	0.193	0.37604	0.067	0.46154	0.066
6.5534	0.68	1.74757	0.22	0.43689	0.073	0.51266	0.068
7.45856	0.76	1.98895	0.24	0.49724	0.079	0.5625	0.07
8.35626	0.83	2.22834	0.27	0.55708	0.086	0.61111	0.072
9.24658	0.91	2.46575	0.29	0.61644	0.093	0.65854	0.074
10.1296	0.98	2.70123	0.32	0.67531	0.098	0.70482	0.076
11.29579	1.08	3.01221	0.35	0.75305	0.107		
12.44939	1.18	3.31984	0.38	0.82996	0.115		
13.5906	1.27	3.62416	0.41	0.90604	0.123		
14.71963	1.36	3.92523	0.43	0.98131	0.129		
15.83665	1.45	4.22311	0.44	1.07427	0.133		
17.21636	1.53	4.59103	0.45	1.16601	0.137		

18.57798	1.58	4.95413	0.46	1.25654	0.139		
19.92188	1.62	5.3125	0.47	1.3459	0.142		
21.24838	1.65	5.66624	0.48	1.43411	0.145		
22.55784	1.69	6.01542	0.49	1.57289	0.149		
24.61832	1.74	6.56489	0.5	1.70886	0.153		
26.63728	1.78	7.10327	0.51	1.84211	0.156		
28.61596	1.82	7.63092	0.53	1.9727	0.16		
30.55556	1.87	8.14815	0.54	2.10074	0.163		
32.45721	1.91	8.65526	0.55	2.25728	0.167		
		9.27536	0.56	2.41007	0.173		
		9.88067	0.58	2.55924	0.176		
		10.4717	0.59	2.70492	0.181		
		11.04895	0.61	2.84722	0.185		
		11.6129	0.62	2.98627	0.189		

4.3. Fluorimetric data for the CMC determination of pure C_nTAB in aqueous medium at 298 K.

DTAB		TTAB		CTAB		OTAB	
[DTAB]/mM	I_1/I_3	[TTAB]/mM	I_1/I_3	[CTAB]/mM	I_1/I_3	[OTAB]/mM	I_1/I_3
0	1.24546	0	1.52533	0	1.45423	0	1.33876
1.34195	1.24582	0.35785	1.50643	0.04188	1.45207	0.00192	1.3334
3.10651	1.24547	0.8284	1.49675	0.08946	1.45336	0.00575	1.33055
4.84344	1.23531	1.29159	1.5	0.14851	1.46165	0.01149	1.33205
5.70175	1.23937	1.97292	1.5	0.26523	1.45851	0.01912	1.33438
7.39845	1.24039	2.41843	1.50404	0.3229	1.45383	0.02863	1.3332
9.0691	1.23935	2.85714	1.48928	0.49323	1.45294	0.04376	1.3312
10.71429	1.23281	3.28922	1.49159	0.60461	1.45147	0.05879	1.33217
12.33459	1.22891	3.50282	1.46467	0.71429	1.4379	0.07745	1.32798
13.13559	1.22359	3.71482	1.36017	0.87571	1.37864	0.10516	1.32901
13.93058	1.21425	3.92523	1.19467	0.92871	1.33291	0.14161	1.33555
14.71963	1.17578	4.13408	1.1314	0.98131	1.20653	0.18639	1.32617
15.50279	1.06379	4.34137	1.11682	1.03352	1.16278	0.23031	1.31194
16.28015	0.98262	4.75138	1.10803	1.08534	1.13153	0.27341	1.27974
17.81768	0.93011	5.35519	1.10398	1.18785	1.08268	0.3157	1.07194
20.08197	0.91662	6.14004	1.09058	1.3388	1.06815	0.36541	0.99899
23.02513	0.9169	7.08995	1.09127	1.53501	1.06261	0.43001	0.98332
26.5873	0.90896	8.54202	1.08755	1.77249	1.04824	0.50815	0.97485
32.03259	0.90839	10.24876	1.08351	2.13551	1.0448	0.59832	0.97604
38.43284	0.90959	11.84591	1.08061	2.56219	1.04397	0.71281	0.96968
44.42215	0.90918	13.3437	1.08216	2.96148	1.04126	0.84743	0.96712
50.03888	0.9041	14.75113	1.08431	3.33593	1.02965	0.97347	0.9637
55.31674	0.90181	16.07613	1.07992	3.68778	1.02997	1.20288	0.96469
60.28551	0.90234			4.01903	1.03489	1.40633	0.96158
				4.33144	1.02841		
				4.62656	1.02806		

4.4. Tensiometric data for pectin- DTAB interaction at different [pectin] at 298K.

0.05% (w/v)		0.1% (w/v)		0.2% (w/v)	
log[DTAB /mM]	γ/mNm^{-1}	log[DTAB /mM]	γ/mNm^{-1}	log[DTAB /mM]	γ/mNm^{-1}
--	69.8	--	65.3	--	68.6
-1.34687	63.2	-1.34687	52.8	-1.34687	59.9
-0.86993	57.3	-0.86993	50.1	-0.86993	54.8
-0.56916	53.6	-0.56916	48	-0.56916	51.6
-0.34766	49.7	-0.34766	46.9	-0.34766	48.8
-0.172	48.1	-0.172	44.2	-0.172	47.7

0.01295	46.4	0.01295	42.3	0.01295	47
0.16887	43.2	0.16887	41.4	0.16887	46.2
0.3303	41	0.3303	39	0.3303	44.2
0.47985	41	0.47985	38.1	0.47985	42.6
0.63601	40.8	0.63601	38.2	0.63601	41.4
0.78127	40.4	0.78127	38.8	0.78127	42
0.91134	39	0.91134	38	0.91134	41.5
1.02664	37.4	1.05867	35.7	1.05867	40
1.14149	35.7	1.18822	34.5	1.18822	37.6
1.24899	35.2	1.36083	33.6	1.36083	36.6
1.33225	35.4	1.52221	33.3	1.52221	36.5
1.42922	35.9	1.65817	33.4	1.65817	36.4
1.52645	36.4	1.7692	33.2	1.7692	36.3
1.63248	36.2	1.85921	33.2	1.85921	36.4
1.7322	36.3	1.94085	33	1.94085	36.3
1.81992	36.2	2.00984	33	2.00984	36.2
		2.05827	33	2.05827	36.1
				2.09435	36.1

4.5. Tensiometric data for pectin- TTAB interaction at different [pectin] at 298K.

0.05% (w/v)		0.1% (w/v)		0.2% (w/v)	
log[TTAB /mM]	γ/mNm^{-1}	log[TTAB /mM]	γ/mNm^{-1}	log[TTAB /mM]	γ/mNm^{-1}
--	68.1	--	67.2	--	66
-1.92091	52.7	-1.92091	53.2	-1.92091	54.8
-1.44396	48.4	-1.44396	47.7	-1.44396	49.6
-1.14319	44.8	-1.14319	45.9	-1.14319	46.3
-0.92169	42.2	-0.92169	42.7	-0.92169	43.6
-0.74603	40	-0.74603	38.8	-0.74603	42
-0.56108	38.6	-0.56108	38.4	-0.56108	40.9
-0.40516	38.6	-0.40516	38.8	-0.40516	40
-0.24373	38.6	-0.24373	41	-0.24373	40.8
-0.09418	37.8	-0.09418	41.4	-0.09418	41.9
0.06198	37.2	0.06198	41	0.06198	42.2
0.20724	35.5	0.20724	39.3	0.20724	41.9
0.33731	33.7	0.33731	38.4	0.33731	40.5
0.45261	31.7	0.48464	36.4	0.48464	39.9
0.56746	29.8	0.61419	34.8	0.61419	38.4
0.67496	28.8	0.7868	33	0.7868	35.9
0.7936	28.8	0.94818	32.6	0.94818	34.6
0.90735	28.8	1.08414	32.4	1.08414	34.1
1.00997	29	1.19517	32.3	1.19517	33.4
1.10008	28.7	1.28518	32.3	1.28518	33.3
1.18781	28.7	1.36682	32.2	1.36682	33.2
1.26705	28.7	1.4358	32.3	1.4358	33
		1.48424	32.2	1.48424	32.9
		1.50704	32.2	1.51385	32.8

4.6. Tensiometric data for pectin- CTAB interaction at different [pectin] at 298K.

0.05% (w/v)		0.1% (w/v)		0.2% (w/v)	
log[CTAB /mM]	γ/mNm^{-1}	log[CTAB /mM]	γ/mNm^{-1}	log[CTAB /mM]	γ/mNm^{-1}
--	63.6	--	65.8	--	71
-2.52297	51.2	-2.52297	56.4	-2.52297	61.8
-2.04602	45.7	-2.04602	48.3	-2.04602	54
-1.74525	42.9	-1.74525	44.5	-1.74525	50.2
-1.52375	40.6	-1.52375	42.3	-1.52375	46.4
-1.34809	39.6	-1.34809	41.9	-1.34809	45.2

-1.16314	39.1	-1.20248	41	-1.16314	44.2
-1.00722	38.3	-1.06299	40.9	-1.00722	43.4
-0.84579	38.5	-0.93519	40.7	-0.84579	43.7
-0.69624	38.4	-0.81972	40.6	-0.69624	44.5
-0.54008	38.3	-0.70903	40.9	-0.54008	44.2
-0.39482	38.9	-0.59579	41.5	-0.39482	44.6
-0.26475	38.6	-0.46838	41.7	-0.26475	45.4
-0.11742	37.9	-0.3431	41.8	-0.14945	45
0.01213	36	-0.22655	41.9	-0.0346	45
0.1251	34.3	-0.09067	41.6	0.0729	44.6
0.22979	32.1	0.03141	40.7	0.19154	43.8
0.33307	31.2	0.16206	38.3	0.30529	43.2
0.42825	30.9	0.28436	35.5	0.42495	41
0.51312	30.8	0.4107	33	0.53432	38.5
0.59672	30.8	0.52463	31	0.62859	36.3
0.67294	30.5	0.62189	30.5	0.70782	36
0.73972	30.4	0.7031	30.3	0.77377	36
0.80396	30.2	0.77836	30.3	0.82855	35.6
		0.84302	30.3		
		0.88895	30.3		

4.7. Tensiometric data for pectin- OTAB interaction at different [pectin] at 298K.

0.05% (w/v)		0.1% (w/v)		0.2% (w/v)	
log[OTAB /mM]	γ/mNm^{-1}	log[OTAB /mM]	γ/mNm^{-1}	log[OTAB /mM]	γ/mNm^{-1}
--	67.9	--	65.9	--	63.1
-3.01782	54.7	-3.01782	55	-3.01782	52.6
-2.54087	45.6	-2.54087	47.3	-2.54087	45.5
-2.2401	41.9	-2.2401	42.8	-2.2401	41
-2.0186	39.5	-2.0186	40	-2.0186	38.1
-1.84294	38.6	-1.84294	38.5	-1.84294	36.7
-1.65799	37	-1.65799	37.8	-1.65799	35.4
-1.50207	35.4	-1.50207	37.3	-1.50207	35.5
-1.34064	34.5	-1.34064	37.2	-1.29803	34.6
-1.19109	34.1	-1.19109	36.8	-1.1058	34.5
-1.03493	34.4	-1.03493	37	-0.93838	34.4
-0.88967	33.7	-0.88967	37.1	-0.79446	34.9
-0.7596	33.3	-0.7596	37.5	-0.67015	35.1
-0.6443	33	-0.6443	37.3	-0.54855	35.4
-0.52945	33.2	-0.52945	37.8	-0.43625	35.6
-0.42195	33.6	-0.42195	37.6	-0.31356	35.7
-0.30331	33	-0.30331	37.3	-0.19688	35.6
-0.18956	32.6	-0.18956	37.1	-0.09224	35.5
-0.0699	31	-0.0699	36.4	-7.29826E-4	35.4
0.03947	26.9	0.03947	35	0.08808	35.3
0.13374	25.5	0.13374	33.4	0.16811	34.8
0.21297	25.2	0.21297	30.5	0.23759	34.6
0.27892	25.1	0.28676	28.8	0.30395	33.4
0.3337	24.9	0.35041	28.2	0.36237	32.3
0.37481	24.8	0.38774	27.9	0.4046	30.7
0.40695	24.7			0.4367	28.4
				0.46198	27.5
				0.48244	27.8
				0.49936	27.2
				0.51359	27

4.8. Conductometric data for pectin- DTAB interaction at different [pectin] at 298K.

0.05% (w/v)		0.1% (w/v)		0.2% (w/v)	
[DTAB]/mM	κ/mS cm^{-1}	[DTAB]/mM	κ/mS cm^{-1}	[DTAB]/mM	κ/mS cm^{-1}
0	0.14	0	0.23	0	0.36
0.32097	0.18	0.29957	0.26	0.32097	0.4
0.64103	0.22	0.59829	0.3	0.64103	0.43
0.96017	0.25	0.89616	0.34	0.96017	0.47
1.27841	0.29	1.19318	0.37	1.27841	0.51
1.59574	0.33	1.48936	0.41	1.59574	0.54
1.91218	0.36	1.7847	0.44	1.91218	0.58
2.22772	0.39	2.07921	0.47	2.22772	0.61
2.54237	0.42	2.37288	0.5	2.54237	0.64
3.16901	0.49	2.66573	0.54	3.16901	0.7
3.79213	0.55	2.95775	0.57	3.79213	0.77
4.41176	0.61	3.53933	0.63	4.41176	0.83
5.02793	0.68	4.11765	0.69	5.02793	0.89
5.64067	0.74	4.69274	0.75	5.64067	0.95
6.5534	0.83	5.26462	0.81	6.5534	1.05
7.45856	0.92	5.83333	0.87	7.45856	1.14
8.35626	1	6.6805	0.95	8.35626	1.22
9.24658	1.08	7.52066	1.05	9.24658	1.31
10.1296	1.15	8.35391	1.14	10.1296	1.4
11.29579	1.25	9.18033	1.23	11.29579	1.51
12.44939	1.35	10	1.31	12.44939	1.61
13.5906	1.45	11.08254	1.42	13.5906	1.71
14.71963	1.54	12.15343	1.52	14.71963	1.81
15.83665	1.63	13.21285	1.62	15.83665	1.9
17.21636	1.72	14.26099	1.71	17.21636	2.1
18.57798	1.78	15.29801	1.8	18.57798	2.3
19.92188	1.82	16.57895	1.91	19.92188	2.4
21.24838	1.85	17.84314	2.1	22.55784	2.5
22.55784	1.88	19.09091	2.2	27.63158	2.6
24.10714	1.92	20.32258	2.3	32.45721	2.7
25.63291	1.95	22.73885	2.4	37.05251	2.8
27.13568	1.98	27.3913	2.5		
		31.81818	2.6		
		36.0355	2.7		

4.9. Conductometric data for pectin- TTAB interaction at different [pectin] at 298K.

0.05% (w/v)		0.1% (w/v)		0.2% (w/v)	
[TTAB]/mM	κ/mS cm^{-1}	[TTAB]/mM	κ/mS cm^{-1}	[TTAB]/mM	κ/mS cm^{-1}
0	0.16	0	0.22	0	0.33
0.08559	0.17	0.08559	0.23	0.08559	0.34
0.17094	0.18	0.17094	0.24	0.17094	0.35
0.25605	0.19	0.25605	0.25	0.25605	0.36
0.34091	0.2	0.34091	0.26	0.34091	0.37
0.42553	0.21	0.42553	0.27	0.42553	0.38
0.50992	0.23	0.50992	0.28	0.59406	0.4
0.59406	0.24	0.59406	0.3	0.76164	0.42
0.67797	0.25	0.67797	0.31	0.92827	0.44
0.84507	0.28	0.76164	0.32	1.09397	0.46
1.01124	0.31	0.84507	0.33	1.25874	0.49
1.17647	0.33	1.01124	0.36	1.50418	0.52
1.34078	0.36	1.17647	0.38	1.74757	0.55
1.50418	0.38	1.34078	0.41	1.98895	0.59
1.74757	0.42	1.50418	0.44	2.22834	0.62
1.98895	0.45	1.66667	0.46	2.46575	0.66

2.22834	0.48	1.82825	0.49	2.77929	0.7
2.46575	0.51	1.98895	0.51	3.08943	0.75
2.70123	0.54	2.14876	0.54	3.39623	0.8
3.01221	0.58	2.30769	0.56	3.69973	0.84
3.31984	0.61	2.46575	0.58	4	0.87
3.62416	0.64	2.70123	0.61	4.37086	0.92
3.92523	0.67	2.93478	0.65	4.73684	0.96
4.22311	0.7	3.16644	0.68	5.09804	0.99
4.59103	0.74	3.39623	0.7	5.45455	1.03
4.95413	0.76	3.62416	0.73	5.80645	1.06
5.3125	0.78	3.85027	0.76	6.36015	1.11
5.66624	0.79	4.07457	0.78	6.90265	1.15
6.01542	0.8	4.29708	0.81	7.43429	1.19
6.42857	0.81	4.51783	0.83	7.95539	1.21
7.10327	0.82	4.73684	0.85	8.46626	1.22
7.76119	0.84	5.02618	0.88	9.09091	1.23
8.40295	0.86	5.3125	0.91	9.7006	1.24
9.02913	0.87	5.59585	0.93		
		5.87629	0.95		
		6.15385	0.97		
		6.42857	0.98		
		6.70051	0.99		
		6.9697	1		
		7.23618	1.01		
		7.89082	1.02		
		8.52941	1.03		
		9.15254	1.04		
		9.76077	1.05		

4.10. Conductometric data for pectin- CTAB interaction at different [pectin] at 298K.

0.05% (w/v)		0.1% (w/v)		0.2% (w/v)	
[CTAB]/mM	κ/mS cm^{-1}	[CTAB]/mM	κ/mS cm^{-1}	[CTAB]/mM	κ/mS cm^{-1}
0	0.15	0	0.24	0	0.37
0.10638	0.16	0.04274	0.25	0.10638	0.38
0.21127	0.18	0.14851	0.26	0.21127	0.4
0.31469	0.2	0.25281	0.28	0.31469	0.41
0.41667	0.22	0.35565	0.3	0.41667	0.43
0.51724	0.24	0.45706	0.32	0.51724	0.44
0.61644	0.26	0.55708	0.34	0.61644	0.46
0.71429	0.29	0.65574	0.36	0.71429	0.48
0.81081	0.31	0.75305	0.37	0.81081	0.49
0.94378	0.34	0.8871	0.4	0.94378	0.52
1.07427	0.37	1.01864	0.43	1.07427	0.54
1.20237	0.39	1.14776	0.46	1.20237	0.56
1.32813	0.41	1.27451	0.49	1.32813	0.59
1.45161	0.43	1.39896	0.51	1.45161	0.61
1.6242	0.44	1.52118	0.54	1.59004	0.64
1.79245	0.46	1.64122	0.56	1.72566	0.66
2.11656	0.47	1.80905	0.59	1.85857	0.69
2.86127	0.48	1.9727	0.62	1.98885	0.71
		2.13235	0.64	2.11656	0.74
		2.28814	0.66	2.27273	0.77
		2.44019	0.68	2.42515	0.8
		2.58865	0.69	2.57396	0.82
		2.87529	0.71	2.7193	0.84
		3.14898	0.72	2.86127	0.87
				3	0.89
				3.13559	0.9

				3.26816	0.92
				3.52459	0.95
				3.77005	0.97
				4.00524	1
				4.23077	1.01
				4.44724	1.03
				4.65517	1.04

4.11. Conductometric data for pectin- OTAB interaction at different [pectin] at 298K.

0.05% (w/v)		0.1% (w/v)		0.2% (w/v)	
[OTAB]/mM	κ/mS cm^{-1}	[OTAB]/mM	κ/mS cm^{-1}	[OTAB]/mM	κ/mS cm^{-1}
0	0.16	0	0.23	0	0.37
0.06338	0.17	0.09441	0.24	0.09441	0.38
0.125	0.18	0.15517	0.25	0.18493	0.39
0.18493	0.19	0.27181	0.26	0.27181	0.4
0.24324	0.2	0.38235	0.28	0.35526	0.41
0.3	0.21	0.48726	0.3	0.43548	0.42
0.35526	0.22	0.58696	0.32	0.51266	0.43
0.40909	0.23	0.68182	0.34	0.58696	0.44
0.46154	0.24	0.77219	0.35	0.65854	0.45
0.53774	0.26	0.9	0.38	0.75	0.46
0.61111	0.27	1.01934	0.41	0.83721	0.47
0.68182	0.29	1.13102	0.44	0.92045	0.49
0.75	0.31	1.23575	0.46	1	0.5
0.81579	0.33	1.33417	0.48	1.07609	0.51
0.9	0.34	1.42683	0.5	1.16667	0.53
0.98045	0.36	1.54225	0.51	1.25258	0.54
1.16667	0.37	1.74891	0.53	1.33417	0.56
1.33417	0.38	1.92857	0.55	1.41176	0.57
1.48565	0.39			1.5	0.59
				1.58333	0.6
				1.66216	0.62
				1.73684	0.63
				1.80769	0.64
				1.875	0.66
				1.95968	0.67
				2.03906	0.68
				2.18382	0.69
				2.2972	0.7
				2.41391	0.71

4.12. Turbidimetric data for pectin- DTAB interaction at different [pectin] at 298K.

0.05% (w/v)		0.1% (w/v)		0.2% (w/v)	
[DTAB]/mM	100 - % T	[DTAB]/mM	100 - % T	[DTAB]/mM	100 - % T
0	1.672	0	6.97	0	15.808
0.08996	1.721	0.08996	7.239	0.08996	16.138
0.17986	1.819	0.17986	7.312	0.17986	16.028
0.35942	1.77	0.35942	7.361	0.35942	16.162
0.53871	1.794	0.53871	7.336	0.53871	16.528
0.7177	1.868	0.7177	7.141	0.7177	16.309
1.16395	1.855	1.16395	7.068	0.89641	16.858
1.60842	2.661	1.60842	7.031	1.34195	16.711
2.05113	3.223	2.05113	7.007	1.78571	18.262
2.93131	5.554	2.93131	8.191	2.66798	21.301
3.80456	7.556	3.80456	12.122	3.54331	25.732

4.67098	9.766	4.67098	17.7	4.41176	34.497
5.53063	13.049	5.53063	23.987	5.27344	43.091
6.3836	16.785	6.3836	30.481	6.1284	51.697
8.0698	25.952	8.0698	45.203	7.81853	69.25
9.7302	42.896	9.7302	64.001	9.48276	80.53
11.36536	61.682	11.36536	81.262	11.12167	88.989
12.97588	84.229	12.97588	94.238	12.73585	96.704
14.56229	96.252	14.56229	98.364	14.32584	97.424
16.89789	97.595	16.89789	97.949	16.66667	95.972
19.18222	96.985	19.18222	97.156	18.95604	94.543
22.1511	96.375	22.1511	96.167	21.93141	92.566
25.03555	95.825	25.03555	95.508	24.82206	90.723
28.52777	95.154	28.52777	94.8	28.32168	88.684
31.9001	94.519	31.9001	94.226	31.70103	86.707
35.15862	94.031	35.15862	93.555	34.96622	84.888
38.30899	93.555	38.30899	93.054	38.12292	82.776
44.30614	92.896	44.30614	91.943	41.17647	80.798
49.92997	92.09	49.92997	90.979	46.99367	78.174
55.21431	91.174	55.21431	90.332	52.45399	75.22
60.18898	90.564	60.18898	89.526	57.58929	72.327
64.88044	89.514	64.88044	88.293	62.42775	69.91
69.31221	88.55	69.31221	87.341	66.99438	67.395
73.50525	87.83	73.50525	85.986	71.31148	65.027
77.47836	87	77.47836	85.132		
81.2484	86.023	81.2484	83.887		
84.83055	85.193				

4.13. Turbidimetric data for pectin- TTAB interaction at different [pectin] at 298K.

0.05% (w/v)		0.1% (w/v)		0.2% (w/v)	
[TTAB]/mM	100 - % T	[TTAB]/mM	100 - % T	[TTAB]/mM	100 - % T
0	3.113	0	5.847	0	12.915
0.02399	3.479	0.02399	6.421	0.02399	13.55
0.04796	3.247	0.04796	6.555	0.04796	13.635
0.09585	3.125	0.09585	6.702	0.09585	13.989
0.14366	3.516	0.14366	7.361	0.14366	14.05
0.26284	4.236	0.19139	7.141	0.19139	13.977
0.38156	6.885	0.31039	9.119	0.31039	15.344
0.4998	8.74	0.42891	12.28	0.42891	19.531
0.73489	13.806	0.66456	20.728	0.54697	22.388
0.96812	18.616	0.89835	27.234	0.78168	34.436
1.19953	26.392	1.1303	37.476	1.01455	46.57
1.42913	36.401	1.36044	43.652	1.24559	50.134
1.65694	47.937	1.58879	53.052	1.47483	58.74
2.10729	83.496	2.04019	69.666	1.70229	68.677
2.55075	92.969	2.48466	90.088	2.15195	78.015
2.98746	96.423	2.92237	92.688	2.59472	85.779
3.41758	98.059	3.35347	94.019	3.03076	93.25
3.84126	97.961	3.77811	92.761	3.46023	95.935
4.46501	97.876	4.40326	91.968	3.88328	96.362
5.07506	97.754	5.01466	90.759	4.5061	96.802
5.86792	97.681	5.61276	89.27	5.11526	95.74
6.63821	97.607	6.19799	87.927	5.90696	92.688
7.57078	97.522	7.14588	86.401	6.67615	85.925
8.47132	97.437	8.06094	85.107	7.6074	81.567
10.18266	97.29	8.94486	83.862	8.50669	77.6
11.78399	97.131	10.62541	82.019	9.37563	75.453
13.28558	96.985	12.19885	80.298	10.21573	73.621
14.69647	96.753	13.67511	78.601	11.0284	70.264

16.02463	96.558	15.06291	76.917	12.57667	66.577
17.27713	96.338	16.36998	75.525	14.03003	63.013
18.46026	96.094	17.60317	74.255	15.39697	59.705
		18.76855	72.388	16.68496	56.677
		19.87159	71.423	17.90065	53.735
		20.91714	70.068	19.04996	51.331
				20.13819	49.292
				21.17008	47.876

4.14. Turbidimetric data for pectin- CTAB interaction at different [pectin] at 298K.

0.05% (w/v)		0.1% (w/v)		0.2% (w/v)	
[CTAB]/mM	100 - % T	[CTAB]/mM	100 - % T	[CTAB]/mM	100 - % T
0	1.392	0	5.847	0	10.852
0.006	1.77	0.006	6.519	0.006	11.353
0.01199	2.222	0.01199	6.787	0.01199	11.597
0.02396	2.966	0.02396	7.983	0.02396	11.707
0.03591	3.198	0.03591	9.778	0.03591	13.342
0.04785	4.163	0.04785	10.803	0.06571	15.881
0.0776	5.872	0.0776	12.927	0.09539	21.362
0.10723	7.629	0.10723	16.357	0.15439	28.613
0.13674	9.033	0.13674	20.715	0.21293	35.84
0.19542	12.671	0.19542	26.233	0.27101	42.468
0.25364	16.431	0.25364	31.592	0.32864	50.293
0.3114	20.605	0.3114	38.562	0.38581	55.444
0.36871	24.414	0.36871	43.884	0.49884	63.977
0.42557	29.785	0.42557	50.256	0.61013	71.301
0.53799	44.434	0.53799	58.447	0.71973	76.77
0.64868	55.359	0.64868	64.844	0.82766	81.055
0.75769	84.485	0.75769	71.167	0.93398	84.717
0.86506	96.521	0.86506	76.147	1.0905	90.491
0.97082	97.168	0.97082	80.701	1.24358	93.86
1.12653	97.681	1.12653	87.292	1.39332	95.581
1.27881	97.791	1.27881	93.237	1.53984	96.802
1.4278	97.827	1.4278	94.91	1.77715	98.047
1.57358	97.9	1.57358	95.789	2.00624	98.694
1.76315	97.913	1.76315	96.741	2.22752	98.901
1.94744	97.913	1.94744	95.789	2.44139	98.926
2.17072	97.791	2.17072	92.554	2.64822	98.95
2.38648	97.717	2.38648	86.646	3.04209	98.938
2.5951	97.668	2.5951	81.116	3.41162	98.083
2.99232	97.546	2.79694	77.905	3.75899	91.064
3.36488	97.388	2.99232	75.549	4.08615	78.491
3.71502	97.253	3.18153	71.716	4.3948	69.092
4.0447	97.93443	3.54262	69.739	4.68647	57.392
4.35566	96.985	3.8823	67.09	4.96253	49.609
4.64946	96.887	4.20242	64.038	5.22419	44.531
4.92748	96.741	4.50462	61.719	5.47256	40.125
5.19095	96.545	4.79036	60.388	5.70862	37.048

4.15. Turbidimetric data for pectin- OTAB interaction at different [pectin] at 298K.

0.05% (w/v)		0.1% (w/v)		0.2% (w/v)	
[OTAB]/mM	100 - % T	[OTAB]/mM	100 - % T	[OTAB]/mM	100 - % T
0	1.404	0	7.874	0.00192	13.098
0.00192	1.367	0.00192	8.777	0.00384	13.44
0.00384	1.55	0.00384	10.095	0.00767	14.172

0.00767	2.039	0.00575	10.071	0.01149	14.832
0.01149	2.527	0.00958	10.962	0.01531	15.991
0.01531	2.991	0.0134	11.267	0.02483	18.518
0.02483	3.772	0.02293	12.634	0.03431	20.203
0.03431	4.419	0.03242	14.392	0.04376	21.35
0.04376	5.469	0.04187	15.918	0.06253	24.951
0.06253	6.824	0.06066	18.469	0.08116	28.162
0.08116	8.24	0.07931	21.472	0.11799	34.338
0.09965	10.754	0.09781	23.535	0.13618	37.219
0.11799	12.415	0.11616	25.928	0.17216	39.465
0.13618	13.684	0.13437	29.871	0.20758	46.228
0.17216	17.261	0.17037	31.238	0.24246	52.197
0.20758	20.337	0.20582	36.755	0.31066	59.375
0.24246	23.315	0.24073	40.749	0.36049	67.371
0.27682	27.161	0.27511	43.127	0.40922	72.302
0.32739	31.445	0.30898	47.241	0.47256	78.113
0.37685	35.925	0.35885	53.223	0.53409	81.555
0.44112	43.433	0.40761	57.324	0.60859	86.182
0.50354	50.452	0.45532	61.084	0.68054	88.721
0.57911	58.887	0.50201	64.172	0.81726	92.444
0.65206	70.813	0.56271	69.775	0.9452	94.116
0.72253	80.249	0.62173	73.206	1.06517	95.142
0.79064	90.991	0.69322	78.613	1.17791	96.497
0.85652	96.509	0.76231	81.873	1.28403	97.424
0.98199	98.145	0.82912	85.706	1.38412	97.827
1.09972	98.23	0.89375	90.417	1.47866	98.242
1.21041	98.291	0.95631	91.992	1.56811	98.523
1.31467	98.315	1.0169	95.349	1.65287	98.779
1.41304	98.328	1.07561	96.704	1.7333	98.95
1.50601	98.34	1.13252	97.217		
1.59402	98.352	1.22005	97.778		
1.67744	98.34	1.3035	97.839		
1.75663	98.315	1.40249	97.29		
		1.49604	96.484		
		1.58457	95.215		
		1.66848	94.946		
		1.74812	94.141		
		1.82381	94.116		
		1.89584	93.909		
		1.96446	93.616		

Chapter V

5.1. Tensiometric data for the CMC determination of pure C_{16}MImCl in aqueous medium at 298 K.

log[C_{14}TPB/mM]	γ/mNm^{-1}
--	71.8
-2.12511	65.2
-1.58148	56.6
-1.25118	51.6
-1.03019	47.9
-0.82737	45.4
-0.653	42.2
-0.50387	40.8
-0.37515	39.1
-0.26271	37.4
-0.16341	36.7
-0.06612	36.5
0.02585	37.7
0.122	38
0.21546	38.6
0.30296	38.6
0.38839	38.9

5.2. Conductometric data for the CMC determination of pure C_{16}MImCl in aqueous medium at 298 K.

[C_{16}MImCl]/mM	κ/mS cm^{-1}
0	0.0024
0.02496	0.0046
0.04983	0.0071
0.07463	0.0096
0.09934	0.012
0.12397	0.0143
0.14851	0.0168
0.17298	0.0193
0.19737	0.0217
0.22167	0.0241
0.2459	0.0264
0.29412	0.0302
0.34202	0.0343
0.38961	0.0383
0.43689	0.0422
0.48387	0.0461
0.55377	0.0518
0.623	0.0579
0.69157	0.0635
0.75949	0.0687
0.82677	0.073
0.91549	0.0775
1.00311	0.0819
1.08964	0.0863
1.17512	0.0897
1.25954	0.0934
1.36364	0.0977
1.46617	0.1013
1.56716	0.1055
1.66667	0.1091

1.78414	0.1134
1.89956	0.117
2.01299	0.1213
2.12446	0.1248
2.23404	0.1287

5.3. Fluorimetric data for the CMC determination of pure C_{16}MImCl in aqueous medium at 298 K.

[C_{16}MImCl]/mM	I_1/I_3
0	1.23605
0.01199	1.23129
0.04188	1.22965
0.10131	1.23093
0.16027	1.22402
0.21876	1.2262
0.2768	1.21742
0.39151	1.21608
0.50445	1.20873
0.61565	1.19484
0.72516	1.16497
0.77929	1.13424
0.83302	1.0652
0.88634	1.0046
0.93926	0.97071
1.04392	0.93403
1.19801	0.91871
1.39826	0.9009
1.64054	0.89216
2.01074	0.89129
2.4456	0.8834
2.85228	0.88098
3.23345	0.88397
3.59142	0.88007
3.92826	0.87836

5.4. Tensiometric data for HA-C_{16}MImCl interaction at different [HA] at 298K.

0.005% (w/v)		0.01% (w/v)		0.02% (w/v)	
log[C_{16}MImCl /mM]	γ/mNm^{-1}	log[C_{16}MImCl /mM]	γ/mNm^{-1}	log[C_{16}MImCl /mM]	γ/mNm^{-1}
--	63	--	63.2	--	62.9
-2.52297	49.8	-2.52297	49	-2.22202	46.5
-2.04602	41.8	-2.04602	43.4	-1.92117	42.8
-1.74525	38.5	-1.74525	39.3	-1.74525	39.4
-1.52375	38.9	-1.52375	39.1	-1.44474	39.1
-1.34809	38.7	-1.34809	39.4	-1.22358	39.4
-1.20248	38.9	-1.16314	39.4	-1.04836	39.1
-1.06299	38.8	-1.00722	39.3	-0.90326	39
-0.93519	38.5	-0.84579	39.3	-0.77193	39.1
-0.79515	37.8	-0.69624	39.2	-0.64303	39.1
-0.66003	36.7	-0.5624	37.7	-0.52305	39.1
-0.53576	36.1	-0.44353	37.3	-0.41362	39.3
-0.42335	35	-0.32462	36.5	-0.30204	38.2
-0.32205	34.4	-0.21262	34.6	-0.19539	36.7
-0.23062	33.2	-0.1098	33.2	-0.09646	35
-0.14779	32.1	-0.00473	32.7	0.00547	33.6
-0.07243	32.6	0.09555	33	0.10338	33.1

0.0021	32.8	0.18816	32.9	0.19422	33.3
0.08304	33.2	0.27761	33	0.2823	33
0.16425	33.4	0.36875	32.9	0.37231	33
0.24224	33.6	0.45489	32.7	0.45758	32.9
				0.53523	33.1
				0.59564	33.3

5.5. Conductometric data for HA-C_{16}MImCl interaction at different [HA] at 298K.

0.005% (w/v)		0.01% (w/v)		0.02% (w/v)	
[C_{16}MImCl]/mM	κ/mS cm^{-1}	[C_{16}MImCl]/mM	κ/mS cm^{-1}	[C_{16}MImCl]/mM	κ/mS cm^{-1}
0	0.0126	0	0.0219	0	0.0395
0.02496	0.0137	0.04983	0.0238	0.02496	0.0412
0.04983	0.0148	0.07463	0.0248	0.04983	0.0421
0.07463	0.0165	0.09934	0.026	0.07463	0.0429
0.09934	0.0183	0.12397	0.0272	0.09934	0.044
0.12397	0.0204	0.14851	0.0287	0.12397	0.0447
0.14851	0.0228	0.17298	0.0302	0.14851	0.0451
0.17298	0.0253	0.19737	0.032	0.17298	0.0459
0.19737	0.0275	0.22167	0.0362	0.19737	0.0469
0.22167	0.0299	0.2459	0.039	0.22167	0.0482
0.2459	0.0324	0.27005	0.0413	0.2459	0.0493
0.29412	0.0366	0.31811	0.0457	0.29412	0.0516
0.34202	0.0407	0.36585	0.0497	0.34202	0.054
0.38961	0.0447	0.41329	0.0538	0.38961	0.0566
0.43689	0.0485	0.46042	0.0579	0.43689	0.06
0.48387	0.0523	0.50725	0.062	0.48387	0.0634
0.55377	0.0581	0.57692	0.0672	0.55377	0.069
0.623	0.0639	0.64593	0.0722	0.623	0.074
0.69157	0.0693	0.71429	0.0772	0.69157	0.0786
0.75949	0.0735	0.78199	0.0819	0.75949	0.0837
0.82677	0.0783	0.84906	0.0869	0.82677	0.0879
0.91549	0.0837	0.9375	0.0927	0.91549	0.0945
1.00311	0.0881	1.02484	0.0977	1.00311	0.0994
1.08964	0.0925	1.11111	0.1023	1.08964	0.1052
1.17512	0.0959	1.19632	0.1052	1.17512	0.1109
1.25954	0.0993	1.28049	0.1085	1.25954	0.1152
1.36364	0.1028	1.38427	0.112	1.36364	0.1195
1.46617	0.1064	1.48649	0.1154	1.46617	0.1234
1.56716	0.1103	1.58718	0.119	1.56716	0.1263
1.66667	0.114	1.68639	0.1222	1.66667	0.1298
1.78414	0.1184	1.80352	0.1259	1.78414	0.134
1.89956	0.1227	1.9186	0.1304	1.89956	0.1374
2.01299	0.1264	2.0317	0.1339	2.01299	0.1408
2.12446	0.1307	2.14286	0.138	2.12446	0.145
2.23404	0.1337	2.25212	0.1417	2.23404	0.1484
2.35955	0.1378	2.37728	0.1454	2.35955	0.1528
2.48261	0.1423	2.5	0.1498	2.48261	0.1567
2.60331	0.1457	2.62036	0.1534	2.60331	0.1606
2.72169	0.1495	2.73842	0.1577	2.72169	0.1641
2.83784	0.1531	2.85425	0.1612	2.83784	0.1678

5.6. Turbidimetric data for HA-C_{16}MImCl interaction at different [HA] at 298K.

0.005% (w/v)		0.01% (w/v)		0.02% (w/v)	
[C_{16}MImCl]/mM	100 - % T	[C_{16}MImCl]/mM	100 - % T	[C_{16}MImCl]/mM	100 - % T
0	1.404	0	0.867	0	4.761

0.006	2.136	0.006	1.16	0.006	7.69
0.01199	2.563	0.01199	1.636	0.01798	9.338
0.01798	2.686	0.01798	3.882	0.02994	13.342
0.02994	2.93	0.02994	3.992	0.05976	13.574
0.04188	3.271	0.04188	6.311	0.08946	21.033
0.07166	3.65	0.07166	8.093	0.14851	28.113
0.10131	4.382	0.10131	10.181	0.2071	40.015
0.16027	22.754	0.16027	15.735	0.26523	41.907
0.21876	31.86	0.21876	19.812	0.3229	47.327
0.2768	32.8	0.2768	63.928	0.38012	56.946
0.33438	33.008	0.33438	73.608	0.49323	78.04
0.39151	33.423	0.39151	74.719	0.60461	85.291
0.50445	33.752	0.50445	75.5	0.71429	86.023
0.61565	34.204	0.61565	76.184	0.87571	86.743
0.72516	34.814	0.72516	76.929	1.08534	88.269
0.88634	35.84	0.83302	77.686	1.3388	88.696
1.09566	35.95	0.93926	78.43	1.63102	88.489
1.34874	35.498	1.09566	78.662	2.00173	87.744
1.64054	34.949	1.29887	78.271	2.43719	87.366
2.01074	34.155	1.54467	78.015	2.84441	86.536
2.4456	33.484	1.92013	76.965	3.22606	85.645
2.85228	32.837	2.36097	75.964	3.58447	84.558
3.23345	31.677	2.77307	75.171	3.92171	84.644
3.59142	31.25	3.15914	74.182	4.2396	84.058
3.92826	30.164	3.52158	72.4	4.53975	83.252
4.24577	29.041	3.86249	71.57	4.82361	82.483
4.54558	28.65	4.18373	70.349	5.09247	81.726
4.82913	28.076	4.48696	69.604	5.34749	81.091
5.0977	26.953	4.77366	68.909		
5.35246	26.208	5.04513	68.311		

List of Publications and Reprints

For Thesis:

1. Detailed physicochemical study and thermodynamic aspects of the interaction between nonionic cellulose derivative hydroxyethyl cellulose and anionic surfactant sodium N- dodecanoyl sarcosinate in aqueous media; **B. B. Mondal**, R. Banik, S. Ghosh; ***Journal of the Taiwan Institute of Chemical Engineers***, **2023**, 149, 104982.

2. Impact of 2, 2, 2-trifluoroethanol (TFE) on hydrophobicity enhancement in the aggregation of sodium N-dodecanoyl sarcosinate (SDDS) with nonionic hydroxyethyl cellulose; **B. B. Mondal**, R. Banik, S. Ghosh; ***Colloids and Surfaces A: Physicochemical and Engineering Aspects***, **2024**, 681, 13278

Other Publications:

3. Comparative Study of the Aggregation Behavior of Some Ionic Surfactants with Nonionic Triton X-114 in Water and a Water/2, 2, 2-Trifluoroethanol Mixture; R. Banik, **B. B. Mondal**, R. Sardar and S. Ghosh; ***Industrial & Engineering Chemistry Research***, **2024**, 63 (7), 3057-3071.

4. A physicochemical investigation on the complex formation by β-Cyclodextrin with Triton X-100 and Triton X-114 and their aggregation behaviour in aqueous solution: an experimental approach; R. Banik, R. Sardar, **B. B. Mondal** and S. Ghosh; **Physical Chemistry Chemical Physics**, 2025, 27, 3782-3795.

Poster Presentation:

- **Presented a poster** at the National Seminar on Chemical Sciences: Today and Tomorrow (CSTT-2019) on March, 2019 organized by Department of Chemistry, Jadavpur University. (**Topic: Colloid Chemistry**)
- **Presented a poster** at the International Seminar on Emerging Trends in Chemical Sciences Towards Sustainability & Interdisciplinarity (ETCSTSI-2025) on 10-11 January, 2025 organized by The Bhawanipur Education Society College. (**Topic: Analysis of the interaction of cationic surfactants with anionic biopolymer pectin**).

Journal of the Taiwan Institute of Chemical Engineers 149 (2023) 104982

Contents lists available at ScienceDirect

Journal of the Taiwan Institute of Chemical Engineers

journal homepage: www.journals.elsevier.com/journal-of-the-taiwan-institute-of-chemical-engineers

Detailed physicochemical study and thermodynamic aspects of the interaction between nonionic cellulose derivative hydroxyethyl cellulose and anionic surfactant sodium N-dodecanoyl sarcosinate in aqueous media

Bipin Bihari Mondal, Rajesh Banik, Soumen Ghosh *

Centre for Surface Science, Physical Chemistry Section, Department of Chemistry, Jadavpur University, Kolkata, West Bengal 700 032, India

ARTICLE INFO

Keywords:
Biopolymer
Anionic surfactant
Hydrophobic synergism
Aggregation number
Physicochemical methods

ABSTRACT

Background: The scheme of this work was to study the interaction between hydroxyethyl cellulose (HEC), a non-ionic, water soluble biopolymer and sodium N-dodecanoyl sarcosinate (SDDS), a novel, environmentally friendly amino acid-based anionic surfactant in aqueous medium. The study of this type of interaction is relatively less complicated compared to that between a polymer and a surfactant with opposite charges.

Methods: The critical micelle concentration (CMC) of HEC-induced SDDS has been determined by various physicochemical methods such as tensiometry, conductometry, fluorimetry and microcalorimetry. Several thermodynamic and surface parameters related to the binding of SDDS with HEC have been assessed. The aggregation number (N_{agg}) of SDDS micelles in the presence of non-ionic HEC polymer has been measured by the steady-state fluorescence method. The hydrodynamic diameter (D_h) and zeta potential (ζ) of the polymer-surfactant aggregate have been measured by the dynamic light scattering method. The interaction study has further been amplified by detecting the change in the surface morphology of the polymer due to surfactant binding using Field Emission Scanning Electron Microscopy (FESEM) and high resolution transmission electron microscopy (HR-TEM) imaging in solvent-free state, as well as visualization of the HEC-SDDS micelle in the solution phase using fluorescence microscopy technique.

Significant findings: From a physicochemical point of view, hydrophobic synergism seems to be important for understanding the interaction pattern of HEC-SDDS combination. In each scenario, the CMC of SDDS decreases with an increase in weight percentage of HEC. The aggregation number (N_{agg}) of SDDS micelles is also found to decrease with an increase in weight percentage of HEC in the medium. The hydrodynamic diameter (D_h) and zeta potential (ζ) of the polymer-surfactant aggregate, these two parameters have been found to be strongly dependent on the amphiphile concentration. Finally, investigations of the surface morphologies by taking Field Emission Scanning Electron Microscopy (FESEM), high resolution transmission electron microscopy (HR-TEM) and fluorescence microscopy techniques assist the experimental data.

1. Introduction

Over the course of several decades, many research works have been studied with the polymer-surfactant interactions. The advancement of this course of investigation still continues to generate a great deal of interest due to the intricacy of the mechanisms for interpreting the nature of interactions involved and the divergence of applications in different fields, such as, pharmaceutical science [1–3], enhanced oil recovery [4–10], colloidal stability [11,12], surface modification [13], drug encapsulation [14–17], paint formulation [18] etc. The polymer-surfactant interacted gels can be used as templates for nanomaterials synthesis [19–22]. Surfactant molecules can self-assemble to form micelles [23–25] both in aqueous medium as well as in aqueous polymer solution. The key factor of this study when choosing polymers and surfactants to various possible combinations is based on their physicochemical properties and the strength of interactions has been found to be highly dependent on the intrinsic properties of both polymers and surfactants, such as, nature of charges, molecular compositions etc. The polymer-surfactant binding can be stabilized to a large extent by strong electrostatic force for oppositely charged pairs and weak hydrophobic force when one of them is uncharged. For non-ionic polymers, the more recommended combination

* Corresponding author.
E-mail address: gsoumen70@hotmail.com (S. Ghosh).

https://doi.org/10.1016/j.jtice.2023.104982
Received 1 February 2023; Received in revised form 17 May 2023; Accepted 9 June 2023
Available online 26 June 2023

for the investigation of interaction features has been found with anionic surfactants than other conventional surfactants [26]. The physicochemical interactions between them can either induce or prevent the binding of surfactant molecules at the polymer interface. Previous studies [27,28] suggest that the nature and charges of both polymers and surfactants have a significant impact on the nature of the interactions between them. There are strong hydrophobic interactions between non-ionic polymers and anionic surfactants [29–31]. In the case of polymer and surfactant with opposing charges [32–34], both electrostatic and hydrophobic interactions have been established. Comparatively to oppositely charged polymer-surfactant systems, the former types of polymer-surfactant interactions are simpler to investigate. The hydrophobic synergism has been established experimentally in this work, operates between the anionic surfactant tail and the non-ionic polymeric lipophilic domain. According to a recent publication [35], it has been reported that the enlargement of the surfactant tail using sodium dodecyl sulfate (SDS) and sodium tetradecyl sulfate (TSDS), two anionic surfactants, can induce polymer-surfactant binding with hydrophobically modified non-ionic hydroxypropyl cellulose (HPC) polymer.

Naturally occurring cellulose is the most abundant 'biopolymer'. This polymer is prepared by the treatment of cellulose with ethylene oxide in the presence of sodium hydroxide in an esterification process [36]. Cellulose derivative, hydroxyethyl cellulose (HEC) is water soluble and non-ionic carbohydrate based polymer. Three hydroxyl groups (-OH) present in each unit of cellulose are esterified with hydroxyethyl groups (-CH_2CH_2OH) in the HEC skeleton, making it excellently soluble in water. The interaction of this polymer with amphiphilic molecules and its industrial applications on a large scale make it one of the most important materials for researchers. It has spacious uses in pharmaceutical fields [37], waste water treatment [38,39], drug delivery [40], paint industry [41], plasma expansion [42], thickening [43], dyeing [44,45], membrane preparation [46–49], etc. It is extensively used for grafting with other polymers [50]. The HEC grafted material is becoming an invaluable resource for researchers. Prior to the present study, several non-ionic cellulose polymers have been interacted with different amphiphiles [51,52].

Sodium N-dodecanoyl sarcosinate (SDDS) is the sodium salt of sarcosine (derivative of the amino acid glycine), a derivative of lauric acid. Thus, it belongs to one of the most significant naturally occurring amino acid-based surfactants [53,54]. Due to its high biodegradability [55,56] and biocompatibility [57], extremely low toxicity [58], and environmental designation as a 'novel' [59] and 'green' surfactant [60], modern research in the field of surface chemistry has been enormously interested in working with this surface active substance [61]. Due to its ability to control dental decay in humans, SDDS is used as one of the ingredients of tooth paste [62]. In many cosmetic products, such as, shaving, shampoo, wash products etc., it is used as a foamy ingredient and a cleansing agent [63]. It has antimicrobial activity [64], antibacterial [65] and anti-corrosive properties [66]. It is also used in anaerobic digestion of waste sludge [67] to remove organic matters (e.g., methane), wettability [68], drug release [69] etc. Self-aggregation of anionic amphiphile SDDS in aqueous medium has already been reported [70]. The effect of different solvents [71–73], salts [74] and mixed-micellization properties [75] of SDDS have been discussed. The interaction behaviour of anionic SDDS with various polymers [76,77], proteins [78,79], dyes [80,81] and drugs [82] has been investigated, but its interaction with the non-ionic polymer hydroxyethyl cellulose remains unexplored.

The majority of the previously reported pertinent works involve the study of hydrophobically modified non-ionic cellulose derivatives with anionic surfactants in order to identify the binding patterns between them using commonly used surface tension, fluorimetry, and viscosity methods. To understand the compositions and the mechanisms of polymer-surfactant binding as determined by physicochemical approaches, it is still imperative to develop a direct view of the polymer-surfactant complex using FESEM, HR-TEM, and fluorescence microscopy imaging. Furthermore, sodium dodecyl sulphate (SDS) has been used mostly as an anionic surfactant with non-ionic polymers [83]. Here, in the field of interaction study, the use of both of these materials, unmodified hydroxyethyl cellulose and SDDS, is quite unique as both have received significantly less attention with respect to earlier published reports. The focus of the present exertion is to explore the detailed reports on physicochemistry between HEC and an anionic surfactant, sodium N-dodecanoyl sarcosinate (SDDS) in aqueous medium using a number of technical methods, including tensiometry, conductometry, microcalorimetry, and fluorimetry at 298K. The zeta potential of the HEC-SDDS system is measured at varying concentrations of surfactant. The size and surface morphology of the polymer-surfactant aggregate has been illustrated by using DLS and FESEM instruments.

Ultimately, an attempt to correlate the physicochemistry and thermodynamics of the widely investigated polymer-surfactant interaction has been made (Scheme 1).

2. Experimental section

2.1. Materials

Hydroxyethyl cellulose (Scheme 2) with molecular weight of 90,000 g mol^{-1} was purchased from Sigma. The average degree of substitution (α) of the polymer used was 1.5. The anionic surfactant, sodium N-dodecanoyl sarcosinate (SDDS, purity > 97%) (Scheme 2) was from Fluka, Germany. Pyrene, used as the fluorescence probe, was obtained from Sigma-Aldrich. All the experimental solutions were prepared in double distilled water. All these materials were used without any further purification. The polymer solutions were prepared in (w/v) percentage as the concentration unit. All these experiments were performed maintaining the constant temperature of 298 K.

2.2. Methods

2.2.1. Tensiometry

The surface tension (γ) values of the experimental solutions were taken by using a calibrated du Noüy tensiometer (Krüss, Germany). The values were measured by ring detachment method. A 5 mL initial volume of aqueous HEC solution of different concentrations were taken for the measurements to which aqueous concentrated SDDS solution was added in steps using Hamilton microsyringe. Thermal equilibration was done with 10-minute intervals between each measurement. The accuracy in the measurement was ±0.1mN m^{-1}.

2.2.2. Conductometry

A Jenway (UK) conductometer in a conductivity cell (cell constant 1.0 cm^{-1}) was used to measure the conductance values. A 7 mL initial volume of polymer solution of experimental concentration was taken in a thermostated container. Concentrated SDDS solution (~ 15 times that of CMC) was added step-by-step for the experiment. As the concentration used in the prepared aqueous solution of SDDS for conductometric titration was very high, the dilution impact was minimized. The measured values were accurate within ±0.5%.

2.2.3. Isothermal titration calorimetry (ITC)

An omega ITC micro calorimeter (Microcal, USA) was used for the thermometric studies. During measurements, temperature was maintained constant at 298K throughout the experimental process by using a Nesleb RTE 100 circulating water bath. A concentrated SDDS solution was added gradually into 0.2 mL of the polymer solution with time duration of 30 seconds in the calorimeter cell having equal time intervals of 210 seconds in multiple successive steps (20-30 additions) under constant stirring (300 rpm) conditions. The amount of heat involved during the micellization of SDDS in the absence and presence of HEC after each step of addition of SDDS was recorded, and the value of enthalpy change per mole of the injectant was calculated using ITC

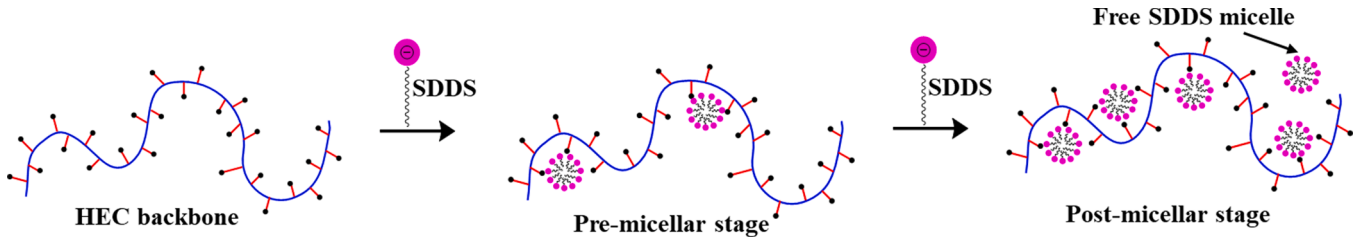

Scheme 1. Schematic illustration of HEC/SDDS interaction at different [SDDS].

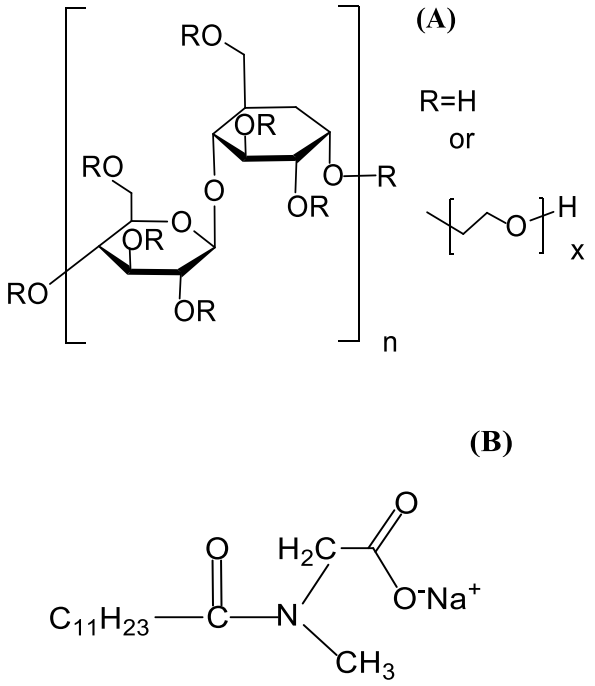

Scheme 2. Structures of (A) Hydroxyethyl cellulose, (B) Sodium N-dodecanoyl sarcosinate (SDDS).

software. The reproducibility was verified by repeating the experiments.

2.2.4. Fluorimetry

The fluorimetric emissions were measured in a Perkin-Elmer fluorimeter (LS 55, USA) in a quartz cuvette having path length of 1cm. Pyrene was taken as the hydrophobic probe in fluorescence emission spectra to determine the CMC of SDDS in polymer solutions. The temperature was kept constant at 298 K with the help of a water flow thermostat. Concentrated aqueous solution of SDDS (225 mM) was used initially and added progressively in the sample cell containing polymer solution of three different concentrations. The excitation wavelength of the probe was 332 nm. The emission spectra were taken in the wavelength range of 350 to 450 nm. The slit widths for excitation and emission were taken at 14 nm and 2.5 nm respectively. The scan time was 250 nm / min. The CMC of the polymer-surfactant combinations were measured by plotting (I_1/I_3) vs. [SDDS], where, I_1 and I_3 are the intensities of first (373 nm) and third (383 nm) vibronic peaks of pyrene.

The aggregation numbers of both surfactant micelle and polymer-induced surfactant micelles were determined by the static fluorescence quenching (SFQ) study using tryptophan as the probe. 1-hexadecylpyridinium chloride (CPC) was taken as the quencher. The concentration of the probe was maintained very low in the micelle assembly. Quencher, CPC was added stepwise into the experimental solution containing tryptophan probe using a Hamiltonian microsyringe and the intensity spectra were collected for data analysis. Hence, two different probes were used. Pyrene was used for the determination of CMC while tryptophan was used for the determination of aggregation number.

2.2.5. Dynamic light scattering (DLS)

Dynamic light scattering experiments were performed in a Malvern zetasizer Nano-zs (Malvern, UK) instrument at 173°scattering angle using He-Ne laser source of wavelength 632 nm at 298 K. All the experimental solutions were filtered 3-4 times through cellulose acetate paper of pore size 0.45 μm to remove unwanted extraneous particles. All the experiments were duplicated and the mean values were taken for analysis of the size of the polymer-surfactant aggregates in the aqueous solution.

2.2.6. Zeta potential

The same DLS instrument was used for zeta potential measurements using a gold coated copper electrode in the cell at 298 K. Before the experiment, the solutions were filtered as mentioned above. The experiments were performed twice and the mean values were reported.

2.2.7. Field emission scanning electron microscopy (FESEM)

High resolution field emission scanning electron microscope (FESEM, model FEI INSPECT F50, Japan) was used to study the surface morphology of the surfactant interacted polymer samples. The surface images were taken at two different surfactant concentrations (CMC and ≫ CMC). 2 μL drops of the experimental solutions were taken by a 10 μL micro pipette on a glass slide for drying and spreading of the samples. The sputtering technique was introduced by supplying 5.5 mA current with 1 min time duration of these dried samples for gold plating.

2.2.8. High resolution transmission electron microscopy (HR-TEM)

TEM imaging of HEC and HEC-SDDS combination were carried out in JEOL JEM 2010 (Tokyo, Japan) high-resolution transmission electron microscope (HR-TEM) under 200 kV. Prior to measurements, the respective TEM samples were prepared by drop casting method of the desired solutions onto a copper grid (gold-coated) and the samples were kept overnight for drying (solvent removal).

2.2.9. Fluorescence microscopy

Olympus IX73 (one-deck system) inverted microscope was introduced for fluorescence imaging of the polymer-surfactant system. The experiment was carried out by taking DPH as the fluorophore. DPH was dissolved in absolute ethanol. A small drop of DPH solution was added to HEC-SDDS system prepared in 10% TFE solvent, surfactant concentration was taken much above CMC. In the final mixture, concentration of DPH was fixed at 0.1 mM. The experimental polymer-surfactant system containing DPH was well sonicated and kept overnight before the measurement. FITC filter included in the instrument was used for taking the required image.

3. Results and discussion

3.1. Tensiometry

The tensiometry is one of the most sophisticated methods and this method has the effectiveness to serve as an indicator in the polymer-

surfactant interaction behaviour. The micellization of pure SDDS amphiphile in aqueous medium has been summarized in Fig. 1(A-D) providing tensiometry, conductometry, microcalorimetry and fluorimetry plots at 298 K. In each case, the location of CMC has been recognized. From microcalorimetry, the obtained value of CMC is slightly higher than other methods. The inconsistency in the magnitudes of CMCs in various methods is due to the fact that there are some systematic differences between these methods [78]. It should also be mentioned here, that CMC does not study a particular concentration, rather it covers a small range of concentration, and different methods generate slightly different values. CMC represents the point of inflection meaning interfacial saturation of the amphiphile and in tensiometry, it is visualized by plotting surface tension (γ) vs. log [SDDS] (Fig. 1A).

In the tensiometric profile of pure SDDS, surface tension (γ) decreases with the stepwise addition of the aqueous solution of the surfactant into water. This decrease is due to the preferential adsorption of SDDS molecules on water surface which overcomes the strong intermolecular hydrogen bonding between water molecules that result in high surface tension value of water [84]. The decrease continues until 14.23 mM [SDDS] is reached. This specific concentration is termed as CMC showing minima in the plot. From this specific concentration, micelle formation is started. This phenomenon is related to interfacial saturation of the SDDS micelles in the aqueous medium. Beyond CMC, the surface tension of experimental solution slightly increases. This increase may be attributed to the higher affinity of the surfactant molecules to form micelle in the bulk at higher concentration that results more number of micelles in the bulk [74]. Other surfactants generally show almost constant nature of γ values beyond CMC in the tensiometric plots [85]. The determined CMC values of pure amphiphile in these above mentioned techniques are fairly satisfying the literature values (Table 1) [71,86].

The nature of the interaction of the anionic amphiphile SDDS with non-ionic polymer HEC in terms of tensiometry plots has been attested in Fig. 2.

In general, the surfactant starts binding with the polymer at lower surfactant concentration called critical aggregation concentration (CAC)

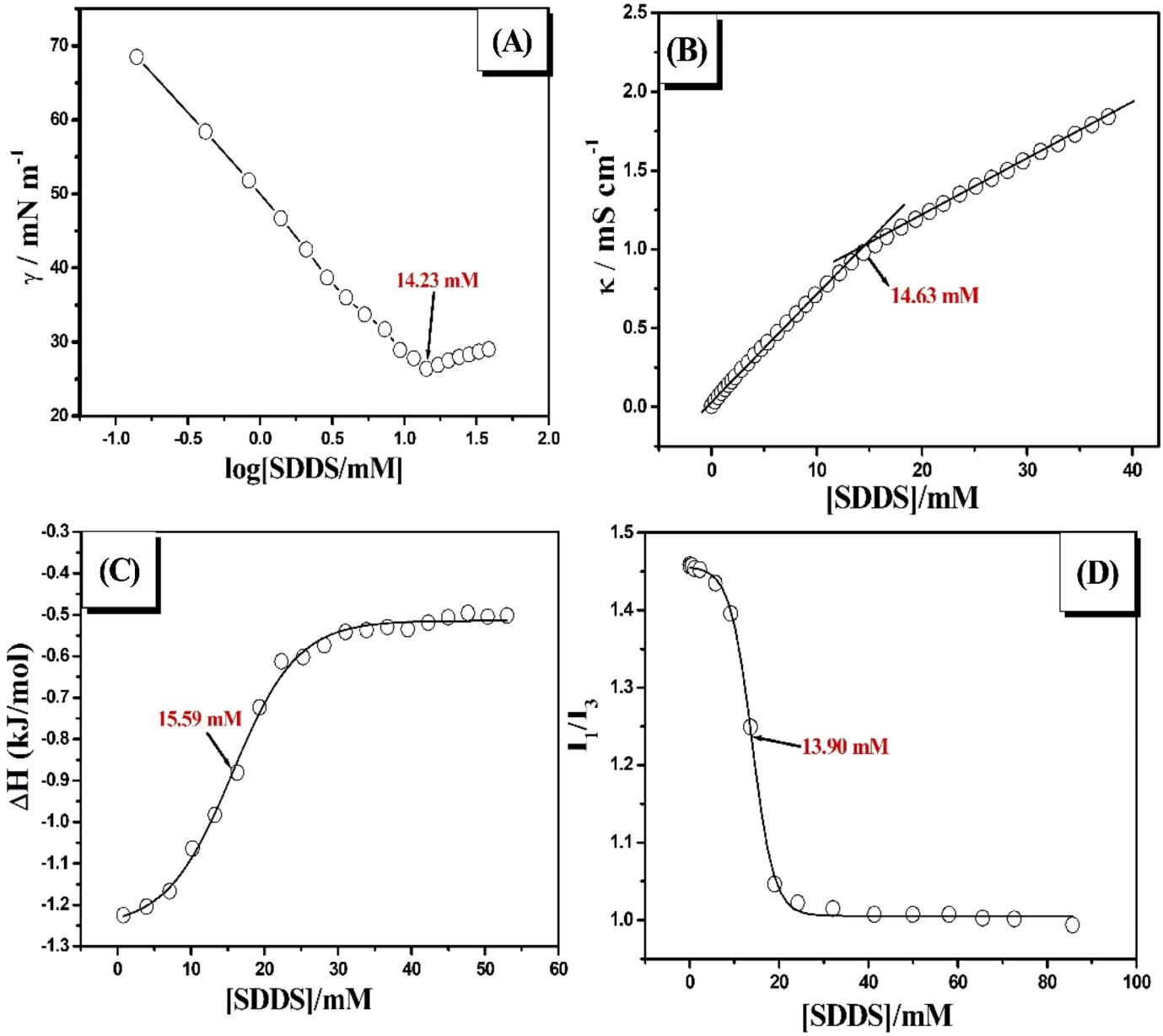

Fig. 1. Determination of CMC of pure SDDS surfactant in aqueous medium from (A) tensiometry, (B) conductometry, (C) microcalorimetry, (D) fluorimetry methods at 298 K.

Table 1
Determination of CMC by tensiometric method, interfacial parameters and thermodynamics of micellization of SDDS interacting with different HEC concentrations in aqueous medium at 298 K.

[HEC]/ g %	CMC (mM)	γ_{CMC} (mN m^{-1})	Γ_{max} $\times 10^6$ (mol/ m^{-2})	A_{min} (nm^2/ molecule)	β	$-\Delta G^0_{mic}$ (kJ/ mol)	$-\Delta G^0_{Ads}$ (kJ/ mol)
0	14.23	26.4	1.66	1.00	0.465	40.98	68.51
0.05	13.91	26	1.68	0.99	0.377	40.89	64.58
0.1	12.29	24.4	1.73	0.96	0.385	40.87	62.02
0.2	10.65	23.2	1.64	1.01	0.400	42.62	63.90

Standard deviations: CMC (6%), Γ_{max} (8%), A_{min} (6%), ΔG^0_{mic} (7%), ΔG^0_{Ads} (3%).

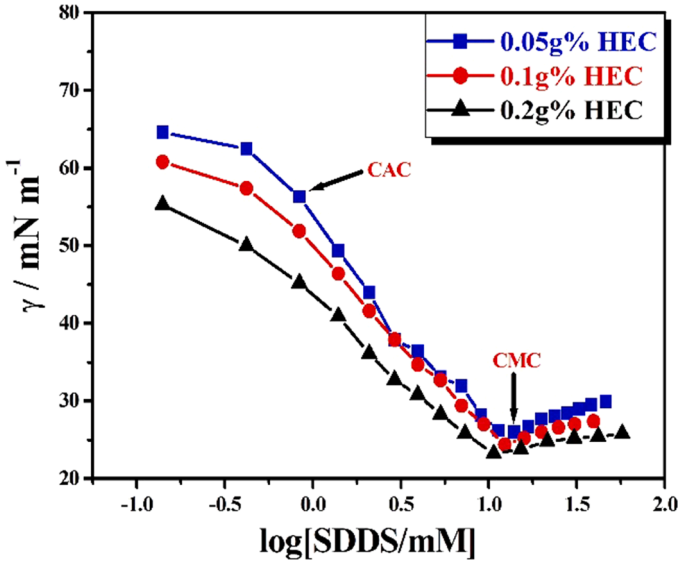

Fig. 2. Tensiometric profile for HEC-SDDS interaction with different polymer concentrations in aqueous medium at 298 K.

[28,32]. In this study, CAC is detected only at the lowest polymer concentration used in the experiment. It is not observed at higher polymer concentrations. With successive addition of the surfactant, surface tension (γ) of the polymer solution decreases linearly up to a transition point. This point is the CMC of the HEC-SDDS aggregate. The CMCs of the polymer-surfactant systems were found at lower surfactant concentration compared to pure SDDS. The measured values decrease noticeably with increasing weight percentage of polymer concentration. Few publications have documented such a decline in CMCs in the analysis of polymer-surfactant systems [87,88]. In this study, concentration of saturation (C_s) is not detected suggesting only hydrophobic synergism and electrostatic interaction is absent. Hence, the presence of polymer enhances the surfactant monomer association ability by hydrophobic binding between the SDDS tails and the HEC lipophilic domain. As a result, micellization of surfactant monomer in the presence of polymer becomes more favourable and CMC decreases. Presence of HEC reduces the interfacial tension in the aqueous medium, and this reduction is enhanced with increasing HEC concentration. The reason behind this fact is that HEC polymer acts typically as long-chain alkane and tends to shift towards the surface of water from the bulk to reduce the surface tension of aqueous HEC solution with respect to pure water [89]. Consequently, the surface tension of combined HEC-SDDS system also diminishes with increase in HEC concentration at the same SDDS concentration. It is observed that the tensiometric profiles of oppositely charged systems are much more complex to study due to the existence of strong electrostatic interaction [90]. The CMC values measured in different techniques of polymer-surfactant couple are slightly different due to the difference in sensitivity of different techniques. However, the trends of decreasing nature of CMCs are found in all methods. The initial surface tension readings for pure polymer solutions at various concentrations differ slightly. This suggests that HEC is feebly surface active [91,92].

3.2. Conductometry

Conductometry is another promising method for understanding the combination pattern and bulk property of the anionic amphiphile with the non-ionic polymer. The study of such method is comparatively less sensitive to the presence of any impurity than the other conventional methods [93]. However, presence of ionic impurities may cause difficulty in CMC measurement by this method as the conductivity produced by ionic amphiphile is low compared to the ionic impurities [94]. All the materials taken for this conductometric titration are pure and double distilled water has been used to make the required solutions (Section 2.1.), hence, the interference from ionic contaminants has been minimized in this study. The conductometric titrations of the polymer-surfactant system are presented in Fig. 3.

The CMCs of SDDS amphiphile in the absence and presence of polymer are determined from the inflection point of the conductometric plots of specific conductance vs. [SDDS] (Table 2). In both cases, the specific conductance (κ) increases linearly upon stepwise addition of SDDS. Two zones, known as the pre-micellar and the post-micellar regions, can be found on the conductometric plots before and after the inflection point. The slope of the former is greater than that of the latter indicating that after the micellization of the surfactant, the rate of increase of specific conductance decreases. The ratio of these two slopes (S_2/S_1) can give the nature of the counter-ion binding (β). This parameter is useful for the determination of the energetics of micellization. This conductometric method can also find single major break point termed as CMC of the polymer-surfactant couple as it is found in the previous mentioned method. It is observed from Fig. 3, the slopes are almost equal for 0.05 and 0.1 (w/v) % of HEC. This implies the same specific conductivity for non-ionic polymer at lower concentration. Although HEC is a non-ionic polymer, it exhibits changes in conductivity at higher concentration. The hydroxyl groups present in HEC have a strong propensity to form hydrogen bonds with water, which boosts its capacity as a proton donor [95] in aqueous media and thus, HEC exhibits better conductivity at higher concentration. Now, comparing the

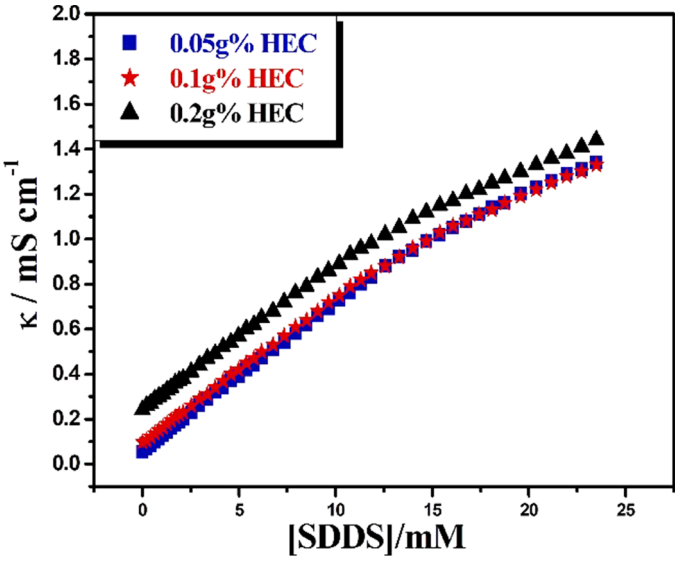

Fig. 3. Conductometic plots for HEC-SDDS interaction with different [HEC] in aqueous medium at 298 K.

Table 2
Determination of CMC (mM) of SDDS with different (w/v) % of HEC in aqueous medium from tensiometry, conductometry, microcalorimetry, and fluorimetric methods at 298 K.

[HEC]/ g %	Tensiometry	Conductometry	Fluorimetry	Microcalorimetry
0	14.23	14.63	13.90	15.59
0.05	13.91	13.54	12.75	13.57
0.1	12.29	12.83	10.75	13.05
0.2	10.65	11.15	10.90	11.94

Standard deviation in CMC measurement: 6%

conductometric results for pure SDDS (Fig. 1B) and HEC-SDDS systems (Fig. 3), it is seen that solutions of HEC-SDDS systems display higher conductivity than pure SDDS solution. The increase in conductivity of the SDDS solution in presence of HEC can be justified on the basis of the higher mobility of the counter ion, Na^+ of the amphiphile in the solution [96]. In HEC-SDDS systems, DDS^- can bind hydrophobically with HEC backbone allowing Na^+ to be freer than the solution containing only SDDS. As a result, Na^+ ion gets higher mobility in combined HEC-SDDS systems, whereas, its mobility gets lowered in pure SDDS solution by pairing strongly with anionic DDS^- through charge attraction. The characteristic results observed in the conductometric plots are the indirect evidence of the interaction between HEC and SDDS and also the micellization of SDDS in presence of HEC. The value of CMC of the interacted polymer-surfactant system decreases as the weight percentage of polymer increases. Upon stepwise addition of anionic surfactant into non-ionic polymer in aqueous medium, the shape of the resultant conductometric curve is nearly identical to that of the pure SDDS. This similarity causes only for hydrophobic interaction between the polymer and the surfactant in terms of physicochemistry in the bulk. Two linear regions with inconsistent slopes can be attributed to the monomeric and micellar aggregates of SDDS in aqueous polymeric medium. This clearly evidences the change in the nature of the charge carriers or ionic mobility from pre-CMC region to post-CMC region. The first region can be ascribed to the existence of SDDS monomers in the bulk whereas the second region corresponds to the formed free SDDS micelles in the aqueous polymeric solution. The Na^+ counter-ion is concentrated in the ionic atmosphere termed as electrical double layer of micellar aggregates which cause a reduction of the ionic mobility in the post-micellar state [84].

3.3. Discussion of interfacial and thermodynamic parameters

For the calculation of Gibbs surface excess (Γ_{max}), minimum amphiphile head group area (A_{min}), standard Gibbs free energy change of micellization (ΔG^0_{mic}), counter ion binding (β), standard free energy change of adsorption (ΔG^0_{Ads}) for both pure SDDS and HEC-SDDS systems, the following five equations have been introduced [Eqs. (1)–(5)]

$$\Gamma_{max} = -\frac{1}{2.303iRT}\lim_{[SDDS]\to cmc}\frac{d\gamma}{dlogC} \quad (1)$$

where, 'i' is designated as the no. of ionic species per SDDS molecule (n = 2) in solution. Γ_{max} gives the information about the relative amount of SDDS adsorption at the interface compared to the bulk in the solution.

$$A_{min} = \frac{10^{18}}{N_A\Gamma_{max}} \quad (2)$$

'N_A' is the Avogadro's number and A_{min} represents the area of excursion per monomeric SDDS.

$$\Delta G_{mic} = (1+\beta)\mathrm{RT}lnX_{CMC} \quad (3)$$

'T' is absolute temperature (in Kelvin scale) and 'R' is universal gas constant (in $Jmol^{-1}K^{-1}$). X_{CMC} is (the mole-fraction of the amphiphile at CMC) calculated from tensiometry method.

$$\beta = 1 - \frac{S_2}{S_1} \quad (4)$$

The fraction of counter ion that is bound to the micellar aggregate is expressed in terms of β. It is determined by conductometric slope ratio method, where, S_1 and S_2 are the slopes in the pre- and post-cmc regions. The equation related to the change in standard Gibbs free energy of adsorption (ΔG^0_{Ads}) is:

$$\Delta G^0_{Ads} = \Delta G^0_{mic} - \frac{\pi_{CMC}}{\Gamma_{max}} \quad (5)$$

where, π_{CMC} is the surface pressure at CMC calculated by the following equation:

$$\pi_{CMC} = \gamma_{iniial} - \gamma_{CMC} \quad (6)$$

Hence, π_{CMC} is measured by taking difference of the surface tension (γ)values of the initial aqueous polymer solution and the polymer-surfactant system at CMC.

Γ_{max}, A_{min}, ΔG^0_{mic}, and ΔG^0_{Ads} are expressed in mol m^{-2}, $nm^2molecule^{-1}$, $kJmol^{-1}$ and kJ mol^{-1} repectively. The negative values of free energy change indicate the spontaneity of both micellization and adsorption of surfactant molecules on the polymeric interface.

All the calculated values are arranged in Table 1.

3.4. Isothermal titration calorimetry

Calorimetry is another potential method for demonstrating the thermodynamic aspects of the polymer-surfactant binding process. The titrations are carried out by the stepwise injection of concentrated SDDS solution into aqueous solution of HEC in a cell at constant temperature (298K). The isothermal titration calorimetry (ITC) results for the pure SDDS and the interaction of SDDS with HEC of different weight percentage are shown in Figs. 1C and 4 respectively. The measured net standard enthalpy change depends on heat from several factors including the dissociation of SDDS micelles to monomers, the binding of SDDS onto HEC. However, enthalpy change from the dilution effect is negligible in this experiment as the other enthalpy changes are too high. In each case, the plots of standard enthalpy change vs. concentration of the surfactant are fitted as sigmoidal curve [97]. The CMCs of the pure surfactant and the polymer-interacted surfactant solutions are determined (Table 2) from sigmoidal Boltzmann equation [28]. An abrupt increase at an inflection point in the intermediate region provides the quantitative measurement of CMC. The resulting sigmoidal ITC curves exhibit three distinct concentration zones [98] in the endothermic enthalpograms as SDDS micellizes both with and without HEC. The enthalpy changes in the pre- and post-micellar regimes are nearly constant and virtually plateau-like, whereas, the intermediate micellization zone between two shows a sharp increase. Initially, in the pre-micellar condition, the addition of concentrated SDDS micellar solution to the medium induces micellar breakdown into monomers with subsequent dilution of the monomers. Dilution of both free micelles and monomers occurs in the post-micellar stage (Scheme 3), at high SDDS concentration [99]. The heat change when CMC is achieved in the transition region essentially corresponds to a fractional dissociation of micelles into monomers. There is a sharp upward line in this micellization zone and from the inflection point, CMC is measured. Again, the quantitative information about the standard net enthalpy change of micellization (ΔH^0_{mic}) is the integrated enthalpy change for each step of injection per mole of the surfactant. In the sigmoidal curve, it is obtained by measuring the difference of enthalpy in the pre- and post-micellar regions as identified by two horizontal parts [100]. The micellization process of pure SDDS in aqueous solution and the binding process of SDDS with HEC both are found to be endothermic in nature. Different polymer-surfactant systems are investigated on the basis of microcalorimetric study.

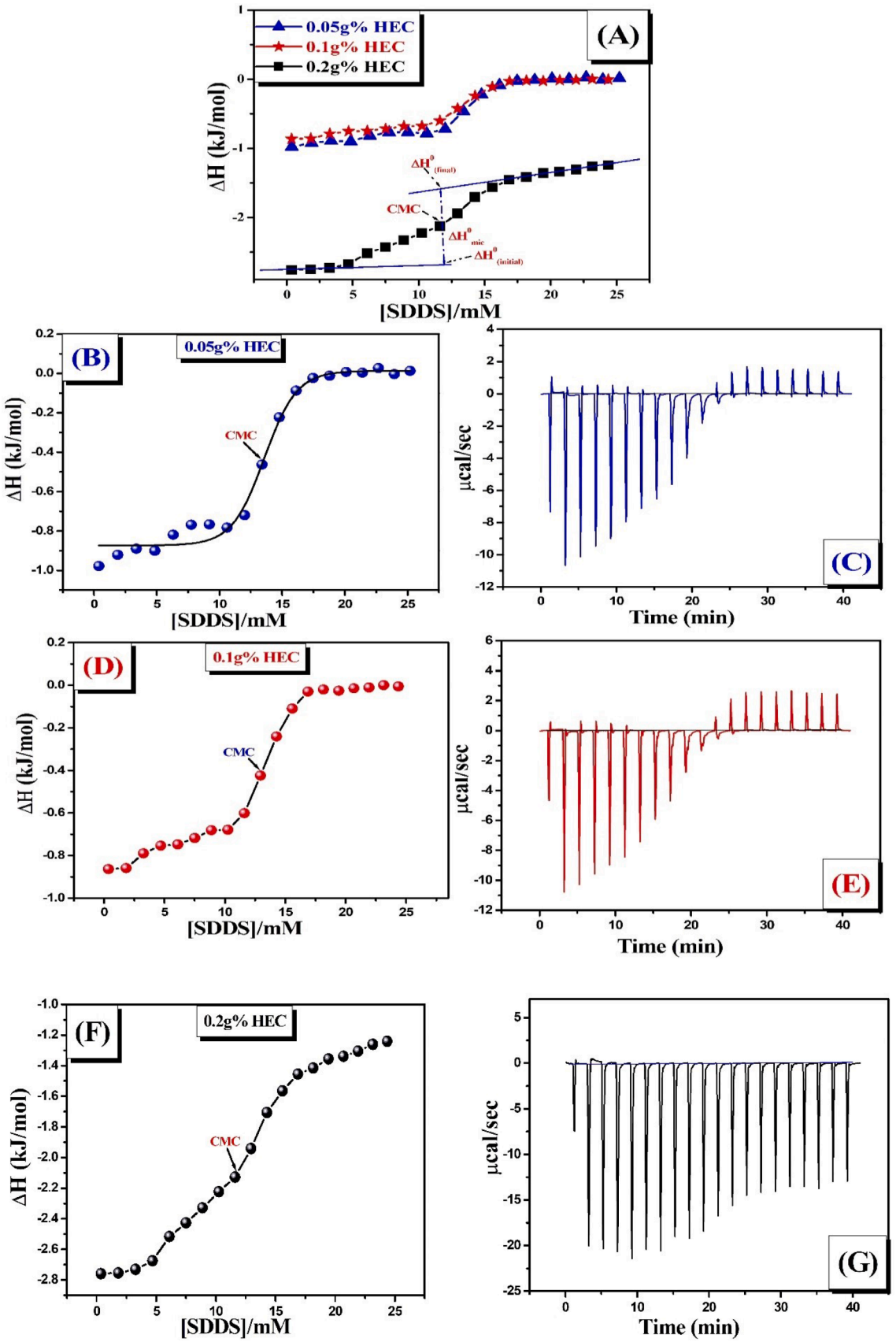

Fig. 4. (A), (B), (D) and (F) Enthalpy profiles of interaction of HEC with SDDS at different HEC concentrations at 298 K. (C), (E) and (G) represent enthalpograms for 0.05, 0.1 and 0.2 (w/v) % HEC interacting with aqueous SDDS solution respectively.

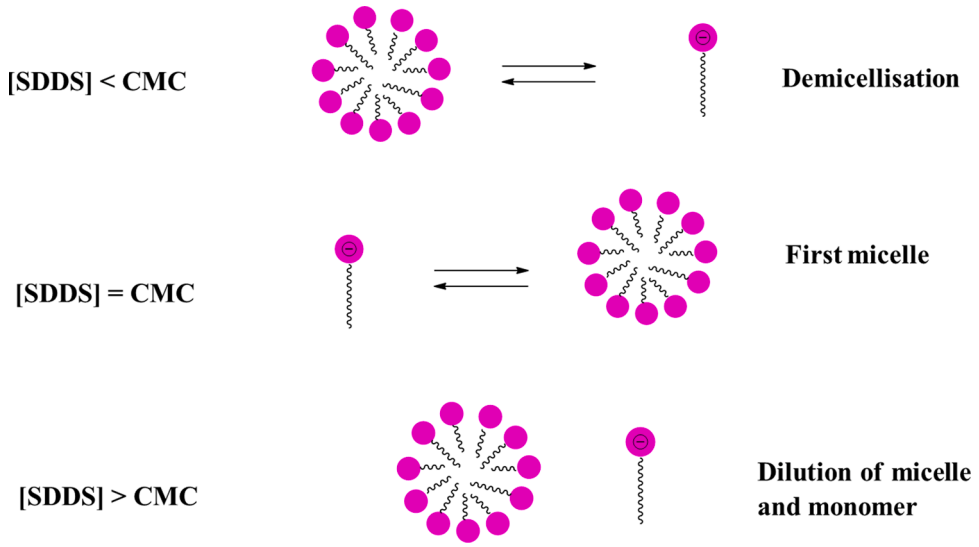

Scheme 3. Schematic presentation of mechanism of micellization in ITC experiment.

3.5. Micropolarity

The study of interaction of HEC-SDDS system has become more diverse through further exploration of the micro environment of the micellar behaviour in the bulk medium by efficient fluorescence probe method. Here, pyrene is preferentially used as spectroscopic probe as its molecules can easily bind to the hydrophobic environment of the molecular assembly [101]. Pyrene molecule has thus, photophysical property, as it is highly sensitive to the polarity of the investigated system [102,103]. Pyrene is an aromatic compound containing four extensively conjugated planar aromatic rings. The emission spectrum of pyrene in the vibrational pattern consists of five peaks (viz. I_1, I_2, I_3, I_4, and I_5). Among these five fine emission peaks, intensities of I_1 and I_3 were used in the present study (where I_1 and I_3 are the intensity values of first and third vibronic peaks) as I_1 increased with medium polarity but I_3 was polarity insensitive. The intensity ratio (I_1/I_3), known as micro polarity index, of hydrophobic pyrene was used for qualitative analysis of micro polarity sensed by probe molecules in the environment of the investigated system [104]. This micro polarity index (I_1/I_3) is an important parameter as it is highly sensitive to any change in the micro polarity of the medium relating to the change in micellar aggregation behaviour. This intensity ratio (I_1/I_3) is highly dependent on surfactant concentration confirming the change in polarity of the medium with surfactant addition. The ratio (I_1/I_3) having values less than unity and greater than unity reveals the non-polar and polar environment surrounding the probe respectively. By using this method, CMC values of both pure SDDS and HEC-SDDS system (Table 2) in aqueous medium are determined. The values of CMC are calculated by sigmoidal fitting of the plot (I_1/I_3) vs. [SDDS] for both the systems [105] (Figs. 1D and 5), which are comparable with those determined by other methods.

The identical orientation of decreasing trend of CMC of SDDS with increasing weight percentage of HEC in aqueous medium is also followed here similar to the other methods. In case of pure SDDS, an initial plateau is observed. This plateau region signifies unchanged nature of polarity of medium with increasing surfactant concentration. The value of (I_1/I_3) decreases sharply indicating the micellization of the surfactant molecules. Slight different types of plateau are observed in case of polymer-surfactant systems. HEC-SDDS systems experience a sudden drop in polarity which proves strong hydrophobic interaction between them and after that, the polarity of the medium practically remains unchanged with respect to surfactant concentration.

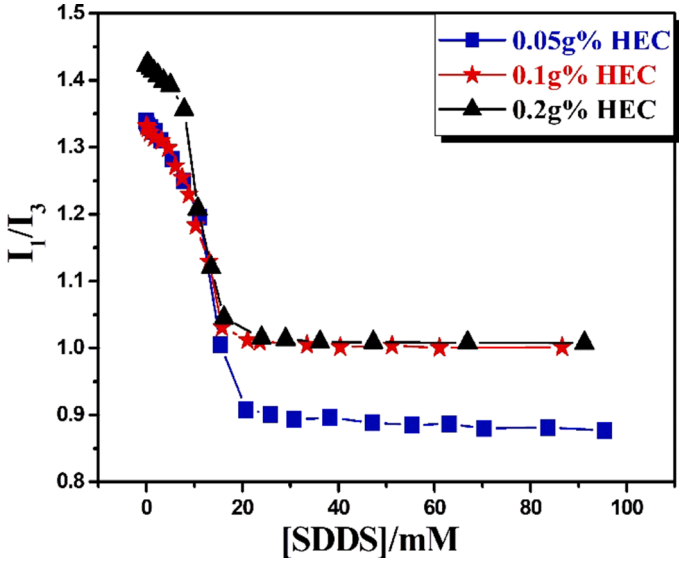

Fig. 5. Fluorimetric profiles for HEC-SDDS interaction at different HEC concentrations in aqueous medium at 298 K.

3.6. Aggregation number

Comparative measurement of aggregation number of polymer bound surfactant micelle is another useful parameter for the conception of interaction between polymer and surfactant. This parameter can give an idea about micellar size. There are many methods available to determine the aggregation number. Here, the effect of polymer on SDDS micellar structure is determined by calculating the aggregation number by SFQ method using the following eq. [106,107]:

$$\ln\left(\frac{I_0}{I}\right) = \frac{n_{agg}\,[CPC]}{[SDDS] - CMC}$$

Where, I and I_0 are the quenched and non-quenched fluorescence intensities respectively. [SDDS] and [CPC] are the concentrations of the surfactant SDDS and the quencher (Q) used CPC respectively. The slope of the plot of ln $(\frac{I_0}{I})$ *vs* [CPC] is used to calculate N_{agg}(Fig. 6) by linear fitting of the plot. In all measurements, [SDDS] is taken much higher than the corresponding CMC values. The $N_{agg}$of pure SDDS micelles is found as 51 in aqueous medium [53]. The aggregation number of

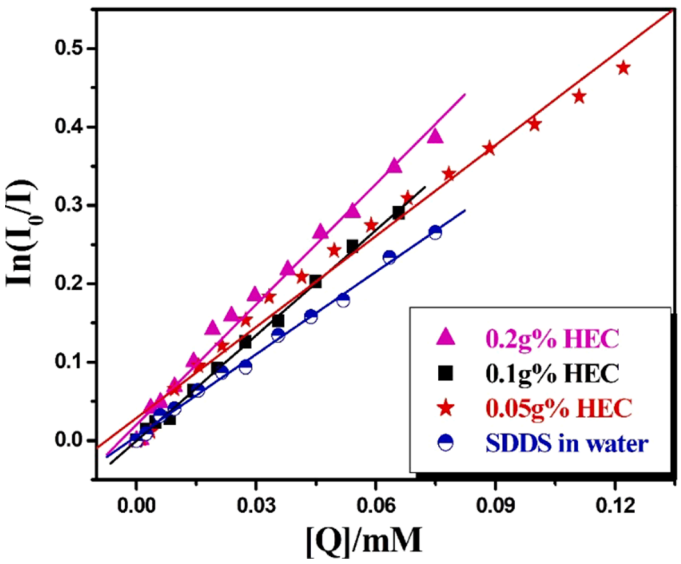

Fig. 6. Plot of ln (I_0/I) vs. [Q] for pure SDDS and in presence of different [HEC] in aqueous medium at 298 K.

HEC-bound micelles of SDDS is found to decrease with increasing HEC concentration. The calculated N_{agg} values are 45, 39 and 35 with changed [HEC] of 0.05, 0.1 and 0.2 g% respectively. Hence, more is the hydrophobicity, less is the number of SDDS monomers associated with the micelle in the system. Many authors have previously claimed the decreasing trend of aggregation number of the ionic amphiphilic micelle in the presence of non-ionic polymer systems [108,109].

3.7. DLS size measurement

DLS study for 0.1 g% HEC and its interaction with SDDS in aqueous medium at different [SDDS] involves the measurement of both the hydrodynamic diameter (D_h) and polydispersity index (PDI). The diffusion of colloidal particles in the polymer-surfactant system is measured by hydrodynamic radius. Such size distributions are shown in Fig. 7. The presentation of measured values is shown in Table 3. Two discrete

Table 3
Hydrodynamic diameter (D_h) and polydispersity index (PDI) for 0.1(w/v) % of HEC interacting with various SDDS concentrations at 298 K.

0.1 g % HEC+ SDDS system		
[SDDS]	Hydrodynamic diameter($D_h^{I,II}$)/nm	Polydispersity Index(PDI)
0	28.2, 122.4	0.470
<CMC	37.8, 141.8	0.382
CMC	37.8, 190.1	0.389
>>CMC	43.8, 342.0	0.671

The errors in measuring D_h and PDI are within 7% and 9% respectively.

hydrodynamic diameters (D_h^I) and (D_h^{II}) are observed in each case ($D_h^{II} \gg D_h^I$). The DLS study of 0.1 g% pure HEC in water shows distinct bimodal distribution. The resulting two peaks correspond to the behaviour of monomeric or unassociated and aggregated states of HEC polymer in aqueous medium. The tendency of carbohydrate based neutral polymer to form aggregates in aqueous medium has been reported earlier [110]. It is found that both diameters are highly dependent on [SDDS] and increased with increasing concentration of SDDS (except at CMC and less than CMC, D_h^I values are found equal) due to aggregation of the surfactant molecules in the aqueous polymer system. The noticeable changes in the hydrodynamic diameters of the polymer-surfactant aggregates with respect to surfactant concentration are the result of surfactant aggregation assisted by non-ionic polymer. Hence, the presence of the amphiphile can change the configuration of the polymer. The measured PDI values are quite high (larger than 0.30), suggesting multidispersity of the studied systems [111]. The polydispersity of non-ionic HEC is essentially due to the polymer aggregation at the concentration of 0.1 g% (w/v) in aqueous medium. The PDI value at this concentration has been found 0.470. The development of the polymer aggregation is relevant to the TEM morphographs (Section 3.10.) of pure HEC polymer [112].

3.8. Zeta potential

Measurement of zeta potential (ζ) is a significant parameter associated with the surface charge of the colloidal system. Its magnitude depends on the stability of the colloidal particles within the polymer-

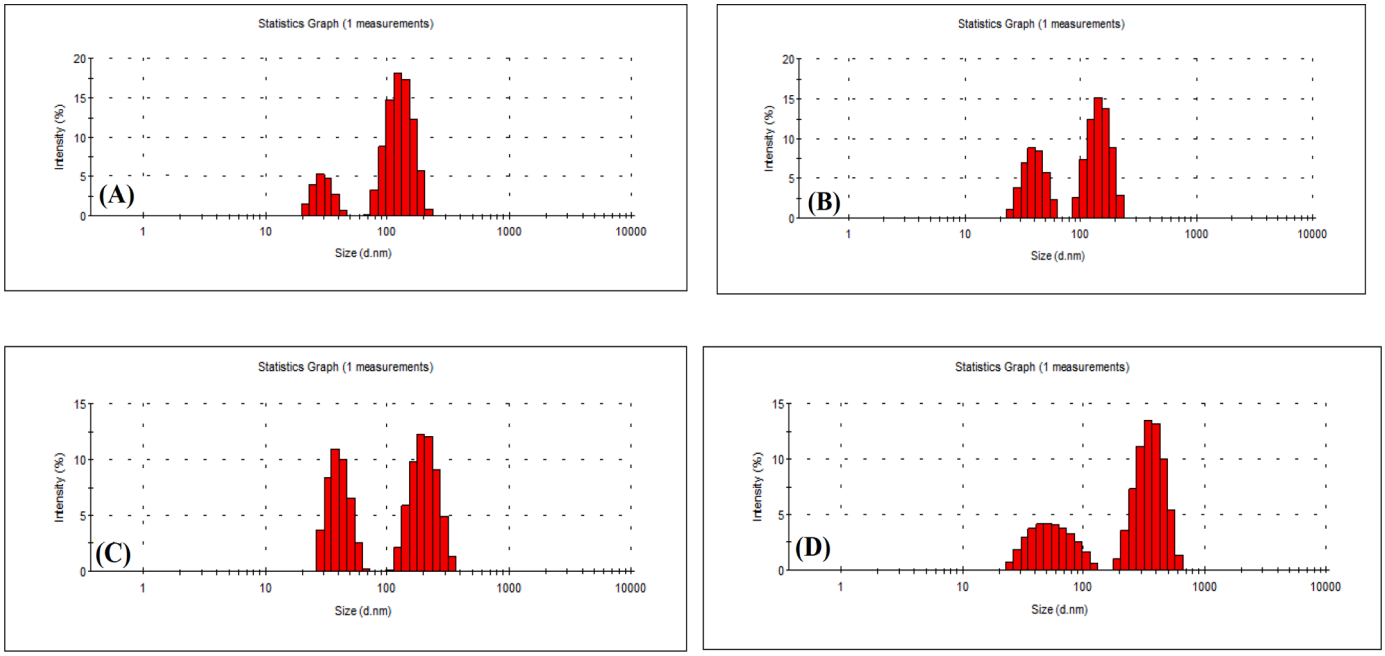

Fig. 7. DLS size distribution curves of (A) pure 0.1g% HEC; (B) with [SDDS]<CMC; (C) with [SDDS] at CMC; (D) with [SDDS]>>CMC in aqueous medium at 298K.

surfactant system. The zeta potential is measured as the electrostatic potential of the interfacial electrical double layer of the colloidal system. In general, the physical stability of colloid is considered to have zeta potential magnitude $|\zeta| > 30$[113]. In the present study, both the zeta potential and the electrophoretic mobility of the HEC- SDDS system have been measured at four different [SDDS] (Fig. 8). The measured values are presented in Table 4. In each case, the negative zeta potential is attributed to the negative surface charge of the colloidal particles in the system. The magnitudes of zeta potential sharply become more and more negative with increasing [SDDS] until the system reaches up to critical micelle concentration of HEC-SDDS system. At CMC, maximum charge accumulation is expected [114] and thereafter, in between CMC and 2 CMC, there occurs very slow rate of increasing in negative value of the zeta potential. Study of zeta potential measurement of polymer-surfactant systems has been reported earlier [115].

Table 4
Zeta potential (ζ) and electrophoretic mobility (μ) for 0.1 (w/v) % of HEC-SDDS system using various SDDS concentrations at 298 K.

0.1 g % HEC+ SDDS system		
[SDDS]	ζ /mV	$10^8 \mu/m^{-2}V^{-1}s^{-1}$
¼ CMC	− 7.31	− 0.57
½ CMC	− 9.34	− 0.73
CMC	− 33.7	− 2.63
2CMC	− 38.3	− 3.04

The error is within ± 10% in measuring zeta potential (ζ).

3.9. Field emission scanning electron microscopy (FESEM)

In order to characterise the scientific eye-catching change in the surface morphology and topography of the polymer-surfactant aggregates from the pure polymer material via complexation with anionic surfactant and the analysis of microstructure of the aggregates, FESEM images have been displayed in Fig. 9 (A-C). The FESEM images of 0.1% (w/v) pure HEC polymer and its complexes with anionic SDDS surfactant (at CMC and >> CMC) have been reported in this study. All these taken images (in the solvent-free states) having own distinguished entities are different in shapes and sizes from each other. It is clearly observed that the particles of pure HEC polymer (Fig. 9A) have been aggregated on the surface. The aggregated particles are arranged to form branched fern tree-like structures. Similar type of FESEM findings have been noticed during investigation of the microstructure imaging of pure hydroxypropyl cellulose (HPC) polymer [35]. A striking surface morphological change is detected when HEC polymer is subjected to interact with anionic SDDS surfactant at two different 5concentrations. The wrecking of the branched fern tree-like structures is observed in both occasions due to the very strong binding of the surfactant molecules on the surface of the polymer. The two polymer-surfactant aggregated structures have different patterns of coating of the surfactant molecules on the polymeric interface. Consequently, such interactions are strongly dependent on the concentration of surfactant. At CMC, porosity is developed and the particles of the polymer are distributed with the surfactant molecules reconstructing a new patterned morphology (Fig. 9B). The aggregates are looking like perforated non-uniform spherical bodies. Further, at higher concentration of SDDS (>> CMC), more surfactant molecules are held back strongly by the polymer backbone and it forms homogeneous like aggregates (Fig. 9C). Different types of surface morphologies due to interaction between cationic gemini surfactant (14-4-14) with anionic polymer NaCMC in aqueous and aquo-isopropanol media can also be cited for our study [116]. Hence, the strong association of the polymer-surfactant is highly recommended by such surface morphological change via FESEM imaging.

3.10. High resolution transmission electron microscopy (HR-TEM)

The surface morphological analysis in this interaction study has been further elaborated by HRTEM measurements. The resulting HRTEM morphographs of pure HEC (0.1 g%) and HEC-SDDS binding at sufficiently high [SDDS] (≫ CMC) have been illustrated in Fig. 10(A-D). Pure HEC shows similar branched fern tree-like morphology as found in FESEM characterization. But, the morphology has been completely changed in case of HEC-SDDS aggregation. It looks as some accumulation of stones like appearance of varied shapes and sizes. The multidispersity of the HEC-SDDS binding beyond CMC from DLS results can

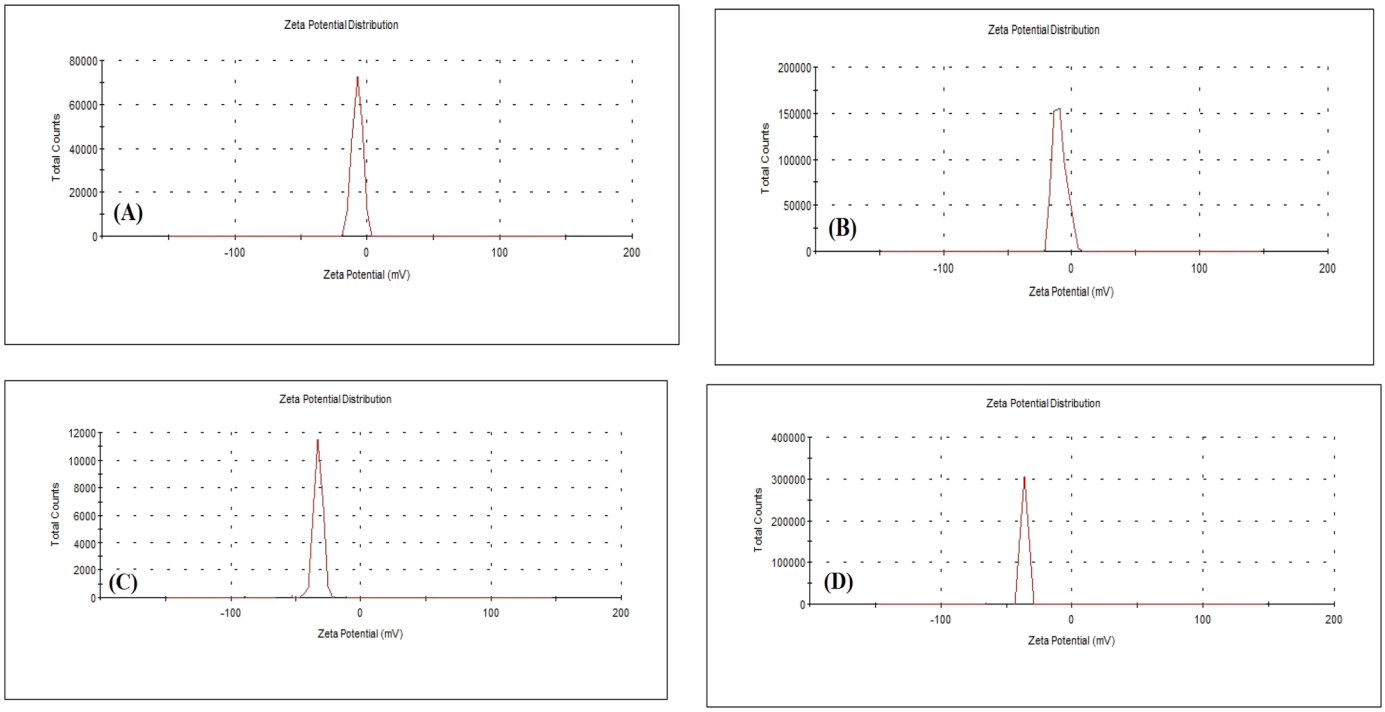

Fig. 8. Zeta potential distribution curves of HEC-SDDS interaction measured at [SDDS] (A) ¼ CMC; (B) ½ CMC; (C) CMC; (D) 2 CMC in aqueous medium at 298K.

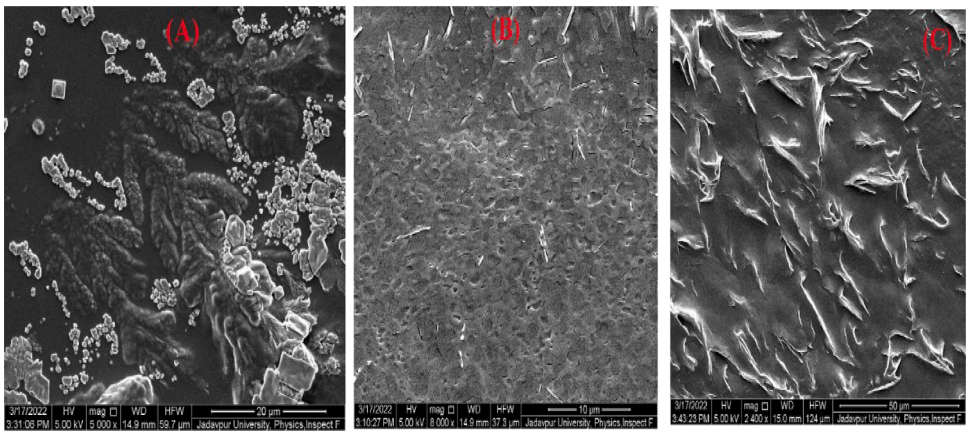

Fig. 9. FESEM images of (A) pure 0.1g% HEC; in presence of (B) [SDDS] at CMC; (C) [SDDS] > CMC.

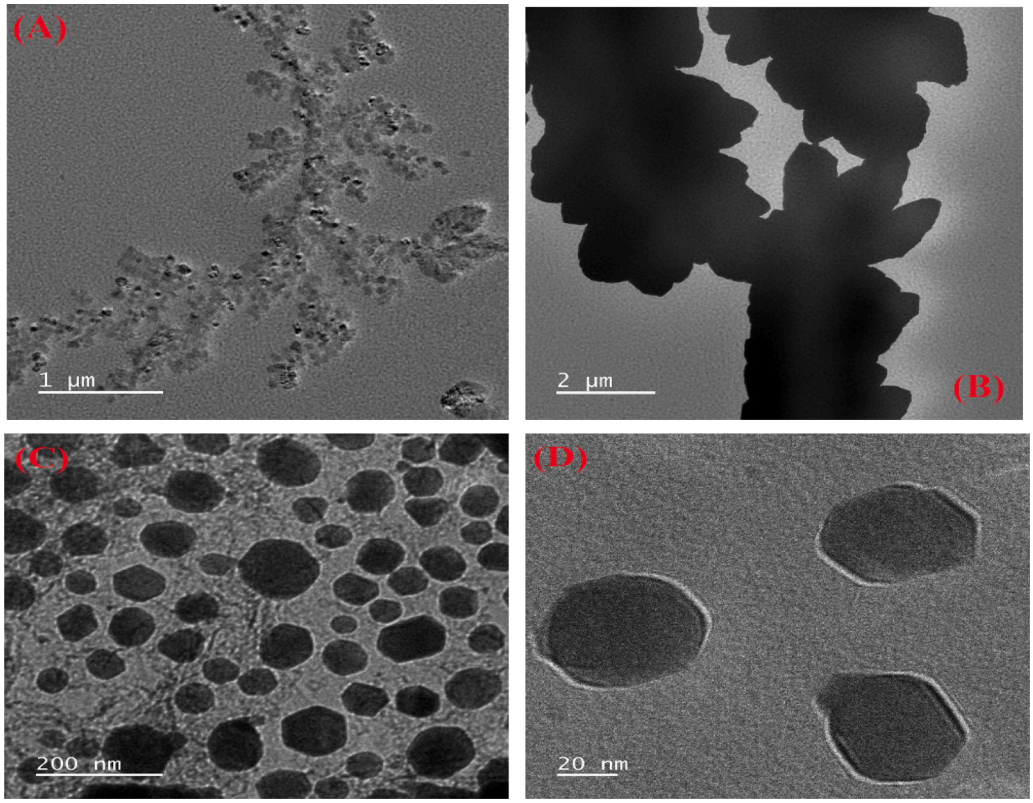

Fig. 10. HRTEM images of (A-B) pure 0.1g% HEC; (C-D) with [SDDS] > CMC.

be verified in HRTEM detection. The HRTEM analysis thus can be supportive in conjunction with FESEM findings as it imparts competence to distinguish between the morphologies of HEC and SDDS micellized HEC.

3.11. *Fluorescence microscopy*

The binding pattern of anionic SDDS with non-ionic HEC has been supported by fluorescence technique. Such images are solid visual evidences for HEC-SDDS interaction. In this manuscript, FESEM (Section 3.10.) and HR-TEM (Section 3.11.) images have already been proved to be immensely effectual for the visualization of SDDS micelles that aggregate in presence of HEC. In the present fluorescence microscopy investigation, it is only reported the image of HEC-SDDS binding beyond critical micelle concentration (CMC) of the experimental system. The micellar aggregates are showed (Fig. 11) by observing fluorescence intensity as bright green coloured fluorescent dots (10μm) probed by DPH dye. In this case, the fluorescence microscopy images of HEC-SDDS system have been studied at different stages of polymer-surfactant binding including free HEC. But, fluorescence probe DPH cannot visualize effective micelle-like aggregates at low or moderate SDDS concentration. It is obvious that at pre-CMC stage, DPH molecules are not able to enter into the core of the micellar aggregates in such insufficient SDDS concentration. Beyond CMC, when SDDS concentration is large enough, HEC-SDDS micelles (i.e. aggregated SDDS micelles wrapped by HEC polymer chains) can be easily trapped by DPH probe [117]. Hence, the fluorescence microscopy images of free HEC and HEC-SDDS micelles at lower SDDS concentration are not reported in the present study.

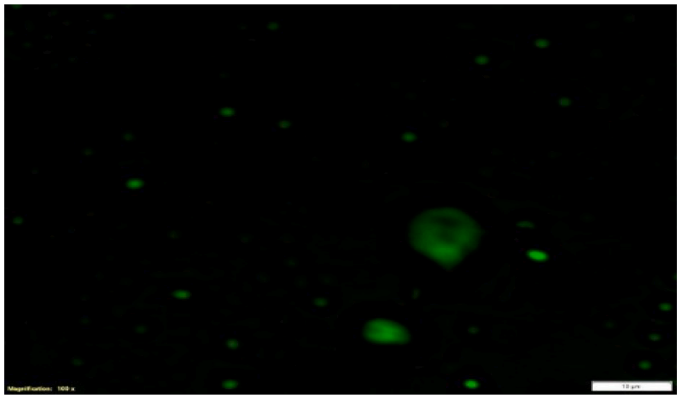

Fig. 11. Fluorescence microscopy image of 0.1g% HEC – SDDS binding ([SDDS] > CMC). Scale bar = 10 μm.

4. Conclusions

Owing to versatile applications in multidimensional fields as mentioned above, polymer-surfactant interaction study is still taking a significant place in modern research. Due to the complexity of the types of interactions existing between them, such area of research is still quite intriguing. The current research plan that led to the selection of this particular field is to break the complicity of the interaction behaviour between the non-ionic polymer and the anionic surfactant in aqueous medium through clear understanding via usage of multi technical approaches. Several works have been reported prior to this study to investigate the interaction characteristics of non-ionic cellulose derivatives with anionic amphiphilic molecules. Most often, non-ionic cellulose ethers, e.g., hydroxypropyl cellulose (HPC) and methyl cellulose (MC) and their derivatives; ethyl derivative and hydrophobically modified form (both cationic and anionic) of hydroxyethyl cellulose (HEC) etc. have been studied for understanding the interaction behaviour with anionic surfactants. These reports on pure HEC are, however, largely unexplored. At the same time, anionic SDDS has been only rarely studied with non-ionic polymer.

Anionic sodium dodecyl sulphate (SDS) has typically been reported with non-ionic polymer in this kind of study. In this paper, it has been tried to investigate the interaction by using multimethods such as tensiometry, conductometry, microcalorimetry and fluorimetry. The change in aggregation number of SDDS micelles in the presence of HEC has been determined. Both size and zeta potential of HEC-SDDS systems has been measured by dynamic light scattering method. FESEM, HR-TEM, and fluorescence microscopy images are taken to analyse the surface morphology. Finally, the key observations can be summarised as:

The nature of the interaction found between them is purely hydrophobic and the tenacity of such interaction leads in higher polymer concentration. The CMC values of SDDS are found to decrease with increase in HEC concentration denoting quick aggregation. This is extremely rare in literature. The negative value of ΔG^0_{mic} confirms the spontaneity of the micellization process of the surfactant in the presence of polymer and the feasibility of interaction between them. Endothermic enthalpy change (ΔH^0_{mic}) during micellization process is supported by ITC plots. The values of $N_{agg}$of SDDS micelles are lowered in the presence of polymer and it decreases with increasing hydrophobicity of the medium. The hydrodynamic diameter (D_h) of the HEC-SDDS system is found to increase with [SDDS] in aqueous medium. Zeta potential (ζ) of HEC-SDDS system acquires fairly negative charge value. After reaching CMC, the zeta potential of the system only slightly increases with [SDDS]. Both FESEM and HR-TEM analysis produces significant changes in surface morphology and affirms their interactive behaviour. Development of HEC-SDDS micelle structure in fluorescence microscopy imaging provides fundamental concepts of SDDS micellization induced by HEC. All of these experimental findings are consistent with the existence of hydrophobic forces that act significantly between the SDDS tails and the lipophilic region of HEC, which lead to HEC-SDDS binding and micelle formation at lower SDDS concentration in non-ionic HEC compared to free SDDS micellization.

The interaction between HEC and SDDS leads to the development of a typical polymer-surfactant complex with a distinct composition and morphology. We can get the conclusion that studying such systems is a challenging issue. A variety of interaction phenomenon traits have been shown, discussed, and some interpretations have been made. A mixed HEC/SDDS system may give rise to a variety of beneficial features. In addition to the potential applications of both HEC and SDDS in drug delivery and cosmetic formulations, we believe that the environment-friendly HEC-SDDS complexes are potential candidates for enhanced oil recovery as well as templates for nanomaterials synthesis.

Optimistically, our little effort can be innovating and encouraging for the upcoming researchers to expand the practical applications of this prominent field by formulating new and more advanced ideas in diverse directions.

Declaration of Competing Interest

The authors declare that they have no known competing financial interests or personal relationships that could have appeared to influence the work reported in this paper.

The authors declare the following financial interests/personal relationships which may be considered as potential competing interests:

The authors declare that they have no known competing financial interests or personal relationships that could have appeared to influence the work reported in this paper.

Acknowledgement

B.B.M. and R.B. thank CSIR, India, for senior research fellowship.

References

[1] Deshpande TM, Shi H, Pietryka J, Hoag SW, Medek A. Investigation of polymer/surfactant interactions and their impact on itraconazole solubility and precipitation kinetics for developing spray-dried amorphous solid dispersions. Mol Pharm 2018;15(3):962–74.
[2] Zhang W, Hate SS, Russell DJ, Hou HH, Nagapudi K. Impact of surfactant and surfactant-polymer interaction on desupersaturation of clotrimazole. J Pharm Sci 2019;108(10):3262–71.
[3] Mdlovu NV, Lin KS, Chen Y, Juang RS, Chang TW. Mdlovu NB. Formulation and characterization of multifunctional polymer modified-iron oxide magnetic nanocarrier for doxorubicin delivery. J Taiwan Inst Chem Eng 2019;104:260–72.
[4] Zhao G, Li J, Gu C, Li L, Sun Y, Dai C. Dispersed particle gel-strengthened polymer/surfactant as a novel combination flooding system for enhanced oil recovery. Energy Fuels 2018;32(11):11317–27.
[5] Raffa P, Broekhuis AA, Picchioni F. Polymeric surfactants for enhanced oil recovery: a review. J Pet Sci Eng 2016;145:723–33.
[6] Saleem SM, Hernandez A. Enhanced oil recovery of acidic crudes by caustic cosurfactant-polymer flooding. J Surface Sci Technol 1987;3(1):1–10.
[7] Maurya NK, Kushwaha P, Mandal A. Studies on interfacial and rheological properties of water soluble polymer grafted nanoparticle for application in enhanced oil recovery. J Taiwan Inst Chem Eng 2017;70:319–30.
[8] Pal N, Vajpayee M, Mandal A. Cationic/nonionic mixed surfactants as enhanced oil recovery fluids: Influence of mixed micellization and polymer association on interfacial, rheological, and rock-wetting characteristics. Energy Fuels 2019;33(7):6048–59.
[9] Pal N, Mandal A. Enhanced oil recovery performance of gemini surfactant-stabilized nanoemulsions functionalized with partially hydrolyzed polymer/silica nanoparticles. Chem Eng Sci 2020;226:115887.
[10] Pal N, Babu K, Mandal A. Surface tension, dynamic light scattering and rheological studies of a new polymeric surfactant for application in enhanced oil recovery. J Pet Sci Eng 2016;146:591–600. Oct 1.
[11] Li C, Li G, Liu S, bai J, zhang A. Spherical hydroxyapatite with colloidal stability prepared in aqueous solutions containing polymer/surfactant pair. Colloids Surf A 2010;366(1-3):27–33.
[12] Sakai T, Oishi T. Colloidal stabilization of surfactant-free emulsion by control of molecular diffusion among droplets. J Taiwan Inst Chem Eng 2018;92:123–8.

[13] Michael FM, Khalid M, Walvekar R, Siddiqui H, Balaji AB. Surface modification techniques of biodegradable and biocompatible polymers. Biodegradable and biocompatible polymer composites: processing, properties and applications. Shimpi NG Ed 2018:33–54.

[14] Qi S, Roser S, Edler KJ, Pigliacelli C, Rogerson M, Weuts I, Dycke FV, Stokbroekx S. Insights into the role of polymer-surfactant complexes in drug solubilisation/stabilisation during drug release from solid dispersions. Pharm Res 2013;30(1):290–302.

[15] Pokharkar V, Patil V, Mandpe L. Engineering of polymer–surfactant nanoparticles of doxycycline hydrochloride for ocular drug delivery. Drug Deliv 2015;22(7): 955–68.

[16] Shagholani H, Ghorbani M, Nikpay A, Soltani M. Chitosan nanocapsule-mounted cellulose nanofibrils as nanoships for smart drug delivery systems and treatment of avian trichomoniasis. J Taiwan Inst Chem Eng 2019;95:290–9.

[17] Nachari Y, Jabbari M. A case study on the partitioning of pharmaceutical compound naproxen in edible oil-water system in the presence of ionic and non-ionic surfactants. J Taiwan Inst Chem Eng 2021;119:1–5.

[18] Tam KC, Wyn-Jones E. Insights on polymer surfactant complex structures during the binding of surfactants to polymers as measured by equilibrium and structural techniques. Chem Soc Rev 2006;35(8):693–709.

[19] Capek I. Preparation and functionalization of gold nanoparticles. J Surface Sci Technol 2013;29(3-4):1–18.

[20] Yu M, Liang C, Liu M, Liu X, Yuan K, Cao H, Che R. Yolk–shell Fe 3 O 4@ ZrO 2 prepared by a tunable polymer surfactant assisted sol–gel method for high temperature stable microwave absorption. J Mater Chem C 2014;2(35):7275–83.

[21] Duan P, Su R, Xu X, Li Q, Gao B. Preparation of Cu2O-Fe3O4@ carbon nanocomposites derived from natural polymer hydrogel template for organic pollutants degradation. J Taiwan Inst Chem Eng 2019;102:456–64.

[22] Pal N, Mandal A. Compositional simulation model and history-matching analysis of surfactant-polymer-nanoparticle (SPN) nanoemulsion assisted enhanced oil recovery. J Taiwan Inst Chem Eng 2021;122:1–3.

[23] Chakraborty T, Ghosh S. A unique survey of applicability of theories of mixed adsorbed film and mixed micellization. J Surfactants Deterg 2008;11:323–34.

[24] Perinelli DR, Cespi M, Lorusso N, Palmieri GF, Bonacucina G, Blasi P. Surfactant self-assembling and critical micelle concentration: one approach fits all? Langmuir 2020;36(21):5745–53.

[25] Zhou M, Li S, Zhang Z, Luo G, Zhao J. Synthesis of oligomer betaine surfactant (DDTPA) and rheological properties of wormlike micellar solution system. J Taiwan Inst Chem Eng 2016;66. 1-1.

[26] Khan MY, Samanta A, Ojha K, Mandal A. Interaction between aqueous solutions of polymer and surfactant and its effect on physicochemical properties. Asia-Pac J Chem Eng 2008;3(5):579–85.

[27] Ghosh S, Mal A, Chakraborty T, De GC, Marangoni DG. Interaction of a cationic surfactant with an oppositely charged polymer. J Surface Sci Technol 2016;32(3-4):107–14.

[28] Das S, Ghosh S. A detailed assessment on the interaction of sodium alginate with a surface-active ionic liquid and a conventional surfactant: a multitechnique approach. Phys Chem Chem Phys 2022;24:13738–62.

[29] Rangaraj A, Rakshit AK. Solution properties of mixed nonionic surfactant-polymer systems. J Surface Sci Technol 2000;16(1-4):246–65.

[30] Chauhan S, Singh R, Sharma K, Kumar K. Interaction study of anionic surfactant with aqueous non-ionic polymers from conductivity, density and speed of sound measurements. J Surfactants Deterg 2015;18(2):225–32.

[31] Burman AD, Ghosh S, Das AR. Behavior of cationic and anionic surfactants including bile salts in presence of hydroxy propyl cellulose (HPC). J Nanofluids 2014;3:140–53.

[32] Chakraborty T, Chakraborty I, Ghosh S. Sodium carboxymethylcellulose−CTAB interaction: a detailed thermodynamic study of polymer− surfactant interaction with opposite charges. Langmuir 2006;22(24):9905–13.

[33] Asker D, Weiss J, McClements DJ. Analysis of the interactions of a cationic surfactant (lauric arginate) with an anionic biopolymer (pectin): isothermal titration calorimetry, light scattering, and microelectrophoresis. Langmuir 2009; 25(1):116–22.

[34] Tseng HW, Chen PC, Tsui HW, Wang CH, Hu TY, Chen LJ. Effect of molecular weight of poly (acrylic acid) on the interaction of oppositely charged ionic surfactant–polyelectrolyte mixtures. J Taiwan Inst Chem Eng 2018;92:50–7.

[35] Mondal S, Pyne P, Patra A, Mitra RK, Ghosh S. Effect of surfactant tail length on the hydroxypropyl cellulose-mediated premicellar aggregation of sodium n-alkyl sulfate surfactants. Langmuir 2021;37(20):6168–77.

[36] Giudice FD, Tassieri M, Oelschlaeger C, Shen AQ. When microrheology, bulk rheology, and microfluidics meet: Broadband rheology of hydroxyethyl cellulose water solutions. Macromolecules 2017;50(7):2951–63.

[37] Sehaqui H, Morimune S, Nishino T, Berglund LA. Stretchable and strong cellulose nanopaper structures based on polymer-coated nanofiber networks: an alternative to nonwoven porous membranes from electrospinning. Biomacromolecules 2012;13(11):3661–7.

[38] Mukerabigwi JF, Lei S, Fan L, Wang H, Luo S, Ma X, Qin J, Huang X, Cao Y. Eco-friendly nano-hybrid superabsorbent composite from hydroxyethyl cellulose and diatomite. RSC Adv 2016;6(38):31607–18.

[39] Mdlovu NV, Lin KS, Chen ZW, Liu YJ, Mdlovu NB. Treatment of simulated chromium-contaminated wastewater using polyethylenimine-modified zero-valent iron nanoparticles. J Taiwan Inst Chem Eng 2020;108:92–101.

[40] Angadi SC, Manjeshwar LS, Aminabhavi TM. Interpenetrating polymer network blend microspheres of chitosan and hydroxyethyl cellulose for controlled release of isoniazid. Int J Biol Macromol 2010;47(2):171–9.

[41] Maestro A, González C, Gutiérrez JM. Interaction of surfactants with thickeners used in waterborne paints: a rheological study. J Colloid Interface Sci 2005;288 (2):597–605.

[42] Mahmoud KH. Optical properties of hydroxyethyl cellulose film treated with nitrogen plasma. Spectrochim Acta Part A 2016;157:153–7.

[43] Li MX, Wang XW, Yang YQ, Chang Z, Wu YP, Holze R. A dense cellulose-based membrane as a renewable host for gel polymer electrolyte of lithium ion batteries. J Membr Sci 2015;476:112–8.

[44] Chen P, Liu X, Jin R, Nie W, Zhou Y. Dye adsorption and photo-induced recycling of hydroxypropyl cellulose/molybdenum disulfide composite hydrogels. Carbohydr Polym 2017;167:36–43.

[45] Liang Y, Liu X, Fang K, An F, Li C, Liu H, Qiao X, Zhang S. Construction of new surface on linen fabric by hydroxyethyl cellulose for improving inkjet printing performance of reactive dyes. Prog Org Coat 2021;154:106179.

[46] Chanachai A, Jiraratananon R, Uttapap D, Moon GY, Anderson WA, Huang RY. Pervaporation with chitosan/hydroxyethylcellulose (CS/HEC) blended membranes. J Membr Sci 2000;166(2):271–80.

[47] Gu J, Xu S, Lu X, Ma R, Zhang S, Zheng S, Wang H, Shen H. Study on the membrane formation mechanism of PVDF/PVDF-CTFE blends. J Taiwan Inst Chem Eng 2023:104655.

[48] Dirin AChen PM, Saljoughi E, Mousavi SM, Kiani S. Pervaporation separation of isopropylbenzene from water using four different polymeric membranes: Membrane preparation, modification, characterization, and performance evaluation. J Taiwan Inst Chem Eng 2020;114:67–80.

[49] da Rocha HD, Reis ES, Ratkovski GP, da Silva RJ, Gorza FD, Pedro GC, de Melo CP. Use of PMMA/(rice husk ash)/polypyrrole membranes for the removal of dyes and heavy metal ions. J Taiwan Inst Chem Eng 2020;110:8–20.

[50] Noreen A, Zia KM, Tabasum S, Khalid S, Shareef R. A review on grafting of hydroxyethylcellulose for versatile applications. Int J Biol Macromol 2020;150: 289–303.

[51] Lo JT, Yen HT, Tsai CC, Chen BH, Hou SS. Interaction between hydrophobically modified 2-hydroxyethyl cellulose and sodium dodecyl sulfate studied by viscometry and two-dimensional NOE NMR spectroscopy. J Phys Chem B 2014; 118(24):6922–30.

[52] Villegas-Pañeda X, Pérez-Casas S, Hernández-Baltazar E, Chávez-Castellanos AE. Study of interactions between octyl-β-D-glucopyranoside and the hydroxyethyl-cellulose biopolymer in aqueous solution. J Chem Thermodyn 2014;79:69–75.

[53] Tripathy DB, Mishra A, Clark J, Farmer T. Synthesis, chemistry, physicochemical properties and industrial applications of amino acid surfactants: a review. C R Chim 2018;21(2):112–30.

[54] Bordes R, Holmberg K. Amino acid-based surfactants–do they deserve more attention? Adv Colloid Interface Sci 2015;222:79–91.

[55] Bourkaib MC, Delaunay S, Framboisier X, Hôtel L, Aigle B, Humeau C, Guiavarc'h Y, Chevalot I. N-acylation of L-amino acids in aqueous media: Evaluation of the catalytic performances of Streptomyces ambofaciens aminoacylases. Enzyme Microb Technol 2020;137:109536.

[56] Akter N, Radiman S, Mohamed F, Rahman IA, Reza MI. Ternary phase behaviour and vesicle formation of a sodium N-lauroylsarcosinate hydrate/1-decanol/water system. Sci Rep 2011;1(1):71.

[57] Pinazo A, Pons R, Pérez L, Infante MR. Amino acids as raw material for biocompatible surfactants. Ind Eng Chem Res 2011;50(9):4805–17.

[58] Katiyar SS, Kushwah V, Dora CP, Patil RY, Jain S. Design and toxicity evaluation of novel fatty acid-amino acid-based biocompatible surfactants. AAPS PharmSciTech 2019;20(5):186.

[59] Brito RO, Silva SG, Fernandes RM, Marques EF, Enrique-Borges J, do Vale ML. Enhanced interfacial properties of novel amino acid-derived surfactants: Effects of headgroup chemistry and of alkyl chain length and unsaturation. Colloids Surf B 2011;86(1):65–70.

[60] Morán MC, Pinazo A, Pérez L, Clapés P, Angelet M, García MT, Vinardell MP, Infante MR. Green" amino acid-based surfactants. Green Chem 2004;6(5): 233–40.

[61] Zhou M, Zhang Z, Xu D, Hou L, Zhao W, Nie X, Zhou L, Zhao J. Synthesis of three gemini betaine surfactants and their surface active properties. J Taiwan Inst Chem Eng 2017;74:7–13.

[62] Rajstein J, Fuks M, Markitziu A, Gedalia I. Solubility of enamel powder following treatment with a sodium-n-lauroyl sarcosinate containing toothpaste in the presence and absence of fluoride. J Oral Rehabil 1983;10(6):469–71.

[63] Ananthapadmanabhan KP. Amino-acid surfactants in personal cleansing. Tenside Surfactants Deterg 2019;56(5):378–86.

[64] Pinazo A, Manresa MA, Marques AM, Bustelo M, Espuny MJ, Pérez L. Amino acid–based surfactants: New antimicrobial agents. Adv Colloid Interface Sci 2016; 228:17–39.

[65] Yapar S, Ateş M, Özdemir G. Preparation and characterization of sodium lauroyl sarcosinate adsorbed on cetylpyridinium-montmorillonite as a possible antibacterial agent. Appl Clay Sci 2017;150:16–22.

[66] Yu Y, Zhang D, Zeng H, Xie B, Gao L, Lin T. Synergistic effects of sodium lauroyl sarcosinate and glutamic acid in inhibition assembly against copper corrosion in acidic solution. Appl Surf Sci 2015;355:1229–37.

[67] Du W, Huang X, Zhang J, Wang D, Yang Q, Li X. Enhancing methane production from anaerobic digestion of waste activated sludge with addition of sodium lauroyl sarcosinate. Bioresour Technol 2021;336:125321.

[68] Xu C, Wang D, Wang H, Ma L, Zhu X, Zhu Y, Zhang Y, Liu F. Experimental investigation of coal dust wetting ability of anionic surfactants with different structures. Process Saf Environ Prot 2019;121:69–76.

[69] Zhang M, Zhao SX, Ding B, Zhang YQ. Sodium N-lauryl amino acids derived from silk protein can form catanionic aggregates with cytarabine as novel anti-tumor drug delivery systems. Drug Deliv 2020;27(1):482–90.
[70] Ray GB, Ghosh S, Moulik SP. Physicochemical studies on the interfacial and bulk behaviors of sodium N-dodecanoyl sarcosinate (SDDS). J Surfactants Deterg 2009;12(2):131–43.
[71] Das S, Mondal S, Ghosh S. Physicochemical studies on the micellization of cationic, anionic, and nonionic surfactants in water–polar organic solvent mixtures. J Chem Eng Data 2013;58(9):2586–95.
[72] Shah RA, Chat OA, Rather GM, Dar AA. Volumetric properties of sodium lauroylsarcosinate in aqueous alcohol solutions of methanol, ethanol, and 1-propanol. J Chem Eng Data 2017;62(10):3015–24.
[73] Ren ZH, Huang J, Luo Y, Zheng YC, Mei P, Yu WC, Lai L, Chang YL, Li FX. Effect of isopropanol on the micellization of binary mixture containing amino sulfonate amphoteric surfactant in aqueous solution: mixing with sodium dodecylbenzene sulfonate. J Taiwan Inst Chem Eng 2016;65:482–7.
[74] Patra N, Ray D, Aswal VK, Ghosh S. Exploring physicochemical interactions of different salts with sodium N-dodecanoyl sarcosinate in aqueous solution. ACS Omega 2018;3(8):9256–66.
[75] Bagheri A, Jafari-Chashmi P. Study of aggregation behavior between N-lauryl sarcosine sodium and dodecyltrimethylammonium bromide in aqueous solution, using conductometric and spectrophotometric techniques. J Mol Liq 2019;282:466–73.
[76] Dan A, Ghosh S, Moulik SP. Interaction of cationic hydroxyethylcellulose (JR400) and cationic hydrophobically modified hydroxyethylcellulose (LM200) with the amino-acid based anionic amphiphile Sodium N-Dodecanoyl Sarcosinate (SDDS) in aqueous medium. Carbohydr Polym 2010;80(1):44–52.
[77] Naskar B, Ghosh S, Moulik SP. Interaction of normal and reverse pluronics (L44 and 10R5) and their mixtures with anionic surfactant sodium N-dodecanoylsarcosinate. J Colloid Interface Sci 2014;414:82–9.
[78] Rudra S, Dasmandal S, Mahapatra A. Binding interaction of sodium-N-dodecanoyl sarcosinate with hemoglobin and myoglobin: Physicochemical and spectroscopic studies with molecular docking analysis. J Colloid Interface Sci 2017;496:267–77.
[79] Mandal B, Ghosh S, Moulik SP. Detailed characterization of lysozyme (Lyz)–surfactant (SDDS) interaction and the structural transitions. New J Chem 2016;40(5):4617–24.
[80] Owoyomi O, Junaid OZ, Olaoye OE. Spectroscopic investigation of the interaction between crystal-violet and sodium dodecanoylsarcosinate. Phys Chem Liq 2022;60(1):129–40.
[81] Mondal S, Doloi B, Ghosh S. Spectroscopic studies of interaction of safranine T with ionic surfactants. Fluid Phase Equilib 2013;360:180–7.
[82] Azum N, Rub MA, Khan A, Alotaibi MM, Asiri AM. Synergistic interaction and binding efficiency of tetracaine hydrochloride (anesthetic drug) with anionic surfactants in the presence of NaCl solution using surface tension and UV–visible spectroscopic methods. Gels 2022;8(4):234.
[83] Banerjee T, Samanta A, Mandal A. Mathematical regression models for rheological behavior of interaction between polymer-surfactant binary mixtures and electrolytes. J Dispersion Sci Technol 2022;43(9):1333–45.
[84] Chakraborty T, Chakraborty I, Ghosh S. The methods of determination of critical micellar concentrations of the amphiphilic systems in aqueous medium. Arab J Chem 2011;4(3):265–70.
[85] Elarbi FM, Janger AA, Abu-sen LM, Ettarhouni ZO. Determination of CMC and interfacial properties of anionic (SDS) and cationic (CPB) surfactants in aqueous solutions. Am J Eng Res 2020;9:118–26.
[86] Mandal B, Ghosh S, Moulik SP. Interaction between a bio-tolerable amino-acid based amphiphile (N-dodecanoylsarcosinate, SDDS) and modified cationic polymers, hydroxyethylcelluloses (JR 400, and LM 200) in isopropanol-water medium. Colloids Surf A 2019;566:156–65.
[87] Niranjan PS, Upadhyay SK. Interaction of polyacrylamide with conventional anionic and gemini anionic surfactants. J Dispersion Sci Technol 2010;32(1):109–13.
[88] Besra L, Sengupta DK, Roy SK, Ay P. Flocculation and dewatering of kaolin suspensions in the presence of polyacrylamide and surfactants. Int J Miner Process 2002;66(1-4):203–32.
[89] Li Q, Ye L, Cai Y, Huang R. Study of rheological behavior of hydrophobically modified hydroxyethyl cellulose. J Appl Polym Sci 2006;100(4):3346–52. May 15.
[90] Mal A, Saha A, Dinda G, Ghosh S. Effect of carbohydrate based polymers on worm-like micelles of cetyltrimethylammonium p-toluenesulfonate in aqueous media: Detail physicochemical and antimicrobial properties survey. J Mol Liq 2020;299:112153.
[91] McNally EJ, Gau CS, Zografi G. Effects of hydroxypropyl cellulose and hydroxyethyl cellulose adsorption on the wetting of low energy solid surfaces. J Adhes Sci Technol 1992;6(4):445–54.
[92] Božič M, Elschner T, Tkaučič D, Bračič M, Hribernik S, Kleinschek KS, Kargl R. Effect of different surface active polysaccharide derivatives on the formation of ethyl cellulose particles by the emulsion-solvent evaporation method. Cellulose 2018;25(12):6901–22.
[93] Petrović LB, Sovilj VJ, Milanović JL, Katona JM. A conductometric investigation of hydroxypropylmethyl cellulose/sodium dodecyl sulfate/nonionic surfactant systems. J Serb Chem Soc 2014;79(11):1421–32.
[94] Carey E, Patil SR, Stubenrauch C. Conductivity measurements as a method for studying ionic technical grade surfactants. Tenside Surfactants Deterg 2008;45(3):120–5.
[95] Zhang P, Zhang J, Wang D, Zhang F, Zhao Y, Yan M, Zheng C, Wang Q, Long M, Chen C. Modification of g-C3N4 with hydroxyethyl cellulose as solid proton donor via hydrogen bond to enhance H2O2 production. Appl Catal B 2022;318:121749.
[96] Winnik MA, Bystryak SM, Chassenieux C, Strashko V, Macdonald PM, Siddiqui J. Study of interaction of poly (ethylene imine) with sodium dodecyl sulfate in aqueous solution by light scattering, conductometry, NMR, and microcalorimetry. Langmuir 2000;16(10):4495–510.
[97] Loh W, Brinatti C, Tam KC. Use of isothermal titration calorimetry to study surfactant aggregation in colloidal systems. Biochim Biophys Acta 2016;1860(5):999–1016.
[98] Majhi PR, Moulik SP. Energetics of micellization: reassessment by a high-sensitivity titration microcalorimeter. Langmuir 1998;14(15):3986–90.
[99] Bouchemal K, Agnely F, Koffi A, Djabourov M, Ponchel G. What can isothermal titration microcalorimetry experiments tell us about the self-organization of surfactants into micelles? J Mol Recognit 2010;23(4):335–42.
[100] Das S, Patra N, Banerjee A, Das B, Ghosh S. Studies on the self-aggregation, interfacial and thermodynamic properties of a surface active imidazolium-based ionic liquid in aqueous solution: Effects of salt and temperature. J Mol Liq 2020;320:114497.
[101] Piñeiro L, Novo M, Al-Soufi W. Fluorescence emission of pyrene in surfactant solutions. Adv Colloid Interface Sci 2015;215:1–12.
[102] Howarth AJ, Majewski MB, Wolf MO. Photophysical properties and applications of coordination complexes incorporating pyrene. Coord Chem Rev 2015;282-283:139–49.
[103] Ottonelli M, Piccardo M, Duce D, Thea S, Dellepiane G. Tuning the photophysical properties of pyrene-based systems: A theoretical study. J Phys Chem A 2012;116(1):611–30.
[104] Dar AA, Garai A, Das AR, Ghosh S. Rheological and fluorescence investigation of interaction between hexadecyltrimethylammonium bromide and methylcellulose in the presence of hydrophobic salts. J Phys Chem A 2010;114(15):5083–91.
[105] Halasová T, Krouská J, Mravec F, Pekař M. Hyaluronan-surfactant interactions in physiological solution studied by tensiometry and fluorescence probe techniques. Colloids Surf A 2011;391(1):25–31.
[106] Ghosh S, Mondal S. Spectroscopic study on the interaction of medicinal pigment, curcumin with various surfactants: an overview. J Surface Sci Technol 2012;28(3-4):179–95.
[107] Alargova RG, Kochijashky II, Sierra MR, Zana R. Micelle aggregation numbers of surfactants in aqueous solutions: a comparison between the results from steady-state and time-resolved fluorescence quenching. Langmuir 1998;14(19):5412–8.
[108] Turro NJ, Baretz BH, Kuo PL. Photoluminescence probes for the investigation of interactions between sodium dodecylsulfate and water-soluble polymers. Macromolecules 1984;17(7):1321–4.
[109] Mylonas Y, Staikos G, Lianos P. Investigation of the poly (N-isopropylacrylamide)-sodium dodecyl sulfate complexation with viscosity, dialysis, and time-resolved fluorescence-quenching measurements. Langmuir 1999;15(21):7172–5.
[110] Dan A, Ghosh S, Moulik SP. Physicochemical studies on the biopolymer inulin: A critical evaluation of its self-aggregation, aggregate-morphology, interaction with water, and thermal stability. Biopolym Orig Res Biomol 2009;91(9):687–99.
[111] Mandal B, Moulik SP, Ghosh S. Influence of aquo-organic solvent media on the self-aggregation of sodium dodecyl sulfate (SDS) and its interaction with polyvinylpyrrolidone (PVP). Colloid Polym Sci 2014;292(10):2485–95.
[112] Naskar B, Dan A, Ghosh S, Moulik SP. Characteristic physicochemical features of the biopolymer inulin in solvent added and depleted states. Carbohydr Polym 2010;81(3):700–6.
[113] Honary S, Zahir F. Effect of zeta potential on the properties of nano-drug delivery systems-a review (Part 2). Trop J Pharm Res 2013;12(2):265–73.
[114] Nizri G, Lagerge S, Kamyshny A, Major DT, Magdassi S. Polymer–surfactant interactions: Binding mechanism of sodium dodecyl sulfate to poly (diallyldimethylammonium chloride). J Colloid Interface Sci 2008;320(1):74–81.
[115] Nambam JS, Philip J. Effects of interaction of ionic and nonionic surfactants on self-assembly of PEO–PPO–PEO triblock copolymer in aqueous solution. J Phys Chem B 2012;116(5):1499–507.
[116] Das S, Mondal S, Ghosh S. Interaction of cationic gemini surfactant tetramethylene-1, 4-bis (dimethyltetradecylammonium bromide) with anionic polyelectrolyte sodium carboxymethyl cellulose, with two different molar masses, in aqueous and aquo-organic (isopropanol) media. RSC Adv 2016;6(37):30795–803.
[117] Jiao L, Zhang L, Guan W, Lu C. Fluorescence visualization of interactions between surfactants and polymers. RSC Adv 2016;6(92):88954–8.

Colloids and Surfaces A: Physicochemical and Engineering Aspects 681 (2024) 132781

Contents lists available at ScienceDirect

Colloids and Surfaces A: Physicochemical and Engineering Aspects

journal homepage: www.elsevier.com/locate/colsurfa

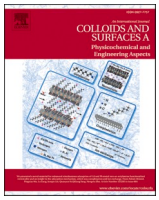

Impact of 2,2,2-trifluoroethanol (TFE) on hydrophobicity enhancement in the aggregation of sodium N-dodecanoyl sarcosinate (SDDS) with nonionic hydroxyethyl cellulose

Bipin Bihari Mondal, Rajesh Banik, Soumen Ghosh *

Centre for Surface Science, Physical Chemistry Section, Department of Chemistry, Jadavpur University, Kolkata 700032, India

HIGHLIGHTS

- Effect of TFE solvent on the hydrophobic interaction between non-ionic HEC and anionic SDDS.
- Analysis of the related bulk and interfacial parameters.
- Estimation of the micellar aggregation number of HEC-SDDS aggregate.
- Visualization of the surface morphologies.

GRAPHICAL ABSTRACT

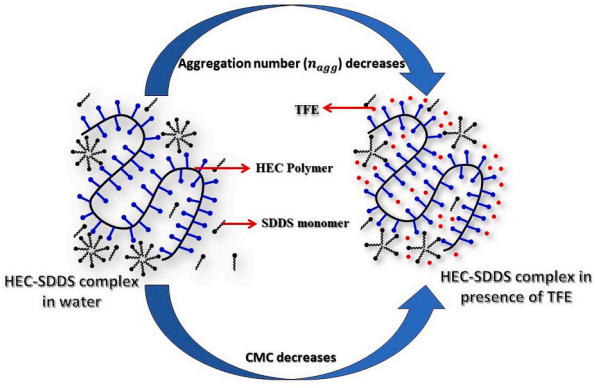

ARTICLE INFO

Keywords:
Cosurfactant
Anionic surfactant
Biopolymer
Conventional methods
Aggregation number

ABSTRACT

An organic solvent has the ability to improve the extent of hydrophobicity in a mixed polymer-surfactant system. The carbohydrate-based polymers, having spacious applications in food and pharmaceutical industries, can interact effectively with anionic surfactants in a hydrophobic fashion. Over the past few decades, such interaction behaviour has been used in surface modification process in the fields of human health care and cosmetics. This article has been highlighted to gain perception about the effect of 'cosurfactant' like organic solvent 2,2,2-trifluoroethanol (TFE) on the self-aggregation of anionic surfactant sodium N-dodecanoyl sarcosinate (SDDS), and its interaction with non-ionic biopolymer hydroxyethyl cellulose (HEC). In this work, the interaction behaviour has been detailed by the use of some conventional methods, such as, tensiometry, conductometry, fluorimetry and microcalorimetry in mixed aquo-alcohol solution. Understanding the binding pattern of the HEC-SDDS system, it appears to be dependent on hydrophobic interaction. From tensiometry, TFE exhibits a fair extent of surface activity and thus, it further enhances the hydrophobicity of the medium. An increased alcohol percentage in the water medium has resulted in a significant reduction in the critical micelle concentration (CMC). TFE promotes micellization of the ionic surfactants at a lower concentration by lowering the charge intensity on the polar head groups of the micelles. Thus, the micellization becomes favoured in TFE solvent. The

* Corresponding author.
E-mail address: gsoumen70@hotmail.com (S. Ghosh).

https://doi.org/10.1016/j.colsurfa.2023.132781
Received 4 July 2023; Received in revised form 23 October 2023; Accepted 12 November 2023
Available online 15 November 2023

related thermodynamic and surface parameters have been estimated to get an insight into the bulk and interfacial properties of the anionic amphiphile on the polymeric interface in mixed aquo-alcohol solution. The decreasing trend of aggregation number (N_{Agg}) in TFE solvent has been discussed with the aid of steady state fluorescence spectroscopic technique. Dynamic light scattering (DLS) study has been used for the measurement of hydrodynamic size (D_h) and polydispersity index (PDI) of HEC polymer in the presence of varying percentage of TFE. All these observations have been displayed and explored conceptually and in stepwise fashion. Further, HEC-SDDS aggregate has been visualized from field emission scanning electron microscopy (FESEM) imaging. A striking change in the morphology has been seen in the TFE environment. As an additive, TFE is opted because of its unique properties as a solvent and also vast applications in the field of biological and pharmaceutical industry. The system chosen in this study is completely new in the field of surface chemistry and each of the experimental results provided below is distinct. At higher TFE contents, the micellization of SDDS is not feasible.

1. Introduction

The study of quaternary interacting systems containing polymer-surfactant-water-additive are rarely found in literatures. This topic has been extremely fascinated for continuously growing research interest to understand the fundamental mechanisms of interactions among them. The researchers are able to take advantages of such interacted systems in diverse fields of modern science, such as pharmaceutics [1], drug encapsulation [2,3], cosmetics [4] and many other industrial applications [5,6]. An amphiphile can undergo micellization not only in aqueous medium [7], but also in the presence of additives such as salts [8,9], non-aqueous solvents [10,11] etc. Depending upon the chemical nature of such additives, physicochemical modification of micellization process can be possible by introducing further complexity in such systems. Among different additives, use of alcohols is most frequently reported in literatures. Alcohol is characterized by their hydrogen bonding abilities, solubilisation, dielectric constant values etc. [12]. The mixtures of certain surfactants and alcohols have the potential to display synergism and improve individual qualities, e.g., surface activity, foaming, wetting, and many others [13]. Both the nature and concentration of the alcohol modify the features of the surfactant formulations. Among all the surfactants, anionic sodium dodecyl sulphate (SDS) is the most widely studied in mixed aquo-alcohol solvents by different research groups [14–18]. Fatima et al. [19] has recently conducted a comparative study between TFE and ethanol, while studying their effects on the thermophysical properties of an ionic liquid (1-ethyl-3--methylimidazolium dicyanamide) in binary alcohol mixture. In an another study, Patidar et al. [20] has compared the effects of TFE with various alcohols (ethanol, 1-butanol, 1-hexanol, 1-octanol, etc.) on the clouding behaviour of two block copolymers, finding a decreasing trend of clouding points with [TFE]. The most interesting aspects about the alcohols is that they can act either as 'cosurfactants' [21,22] or 'cosolvents' [23] depending on their concentration in the mixture to decrease or increase the critical micelle concentration (CMC) of the surfactant respectively during the micelle formation. The widely used alcohol, ethanol, works as a 'cosurfactant' at lower concentration, but as a 'cosolvent' at higher concentration [24]. We have shown that isopropanol (IP) functions as a cosurfactant below 6.62% to lower the CMC of sodium dodecylsulfate (SDS), and as a cosolvent above that [17]. Instead, TFE serves only as a 'cosurfactant' in the present study by lowering the CMC of SDDS at the studied concentration ranges. The TFE solvent molecules can easily enter into the micellar palisade layer, and undergo co-aggregation with SDDS micelles. The micellization behaviour of surfactants also gets affected by the hydrocarbon chain length of the alcohol being used. When the chain length is larger, the alcohol becomes more hydrophobic and its hydrophobicity causes the CMC to fall more rapidly [25]. The appearance of alcohols in the field of colloid chemistry has immense impact for their properties of structure making or breaking [26,27] of water in water-alcohol mixture. The micellization of surfactant can also be modified in a polymer/surfactant mixture, resulting in either increase or decrease in the CMC value. Using polymer or surfactant alone is insufficient for the development of several beneficial features, but their mixture does [28,29]. For instance, rheological control and colloidal stability are provided by the polymer, whereas the surfactant aids in emulsification and interfacial tension control. The surfactants are commonly known to bind with polymers through either electrostatic or hydrophobic interactions or both depending upon their physicochemical characteristics and electrical charges. The interaction between anionic surfactant (SDDS) and neutral polymer (HEC) is hydrophobic in nature. The driving force responsible for their interaction is to minimize the interfacial territory that exists between the non-polar segments of the polymer and the hydrophobic parts of the surfactant in the solvent medium. For interactions to be effective, the non-ionic polymer and the anionic surfactant must have different chemical affinities. Further, the interaction behavior can be controlled by several factors, such as, presence of additives (solvent, salt, etc.), hydrophobic chain of the surfactant, and the rigidity of the polymer backbone. The presence of additive is very much effective to induce their mutual interactions as well as their individual fundamental properties. Because of this, the interaction study appears to still be developing.

Cellulose is known as the most abundant natural biopolymer. Non-ionic hydroxyethyl cellulose (HEC) is carbohydrate based, cellulose derivative with high molecular weight. Industrially, this polymer is synthesized [30] using cellulose in sodium hydroxide and ethylene oxide. High water solubility of HEC makes this polymer as an important material both in industry and academic research. The biodegradability, biocompatibility, and low immunogenicity of the carbohydrate-based polymers make them particularly attractive [31–33]. In recent times, the cellulose polymers have been turned into excellent research materials as they are widely used in grafting [34,35] with different polymers and also their physicochemical changes in presence of various surface active agents [36,37]. In a recent publication, we haves examined the aggregation of two different anionic surfactants in the presence of a cellulose polymer (HPC) as well as the effect of their tail length on the formation of premicellar polymer-surfactant complexes (PS) [38]. The biomedical and industrial importance of hydroxyethyl cellulose has already been reported in a variety of areas, including treatment of waste water [39,40], paint formulation [41,42], plasma expansion [43], drug delivery [44], membrane preparation [45], etc.

Sodium N-dodecanoyl sarcosinate (SDDS) is one of the most important amino acid surfactants. Now-a- days, novel amino acid surfactants [46] have immense impact on modern surface chemistry research over a large scale due to their biocompatible [47] and biodegradable [48] nature. Furthermore, attention has been drawn to this naturally occurring anionic surface active agent due to its antimicrobial [49] and antibacterial [50] properties. It is a derivative of lauric acid. In human dental system, it is used in tooth paste production to regulate dental caries [51]. In cosmetics industry (e.g. shampoo, shaving cream, wash products etc.), it is largely used for its foaming and cleansing actions [52]. A number of detailed physicochemical studies have been reported on the micellization of this amphiphile [53]. The amphiphilic behaviour of SDDS in presence of salts [54], solvents [55], polymers [56,57], proteins [58,59], drugs [60], etc. has also been the subject of numerous earlier research. The study of biopolymer with surfactant is important because it resembles the protein-surfactant interaction, in which the surfactant can induce protein denaturation. Recently, we have explored

the impact of solvent IP on the SDDS-modified HEC system (cationic JR 400, and LM 200) [61]. In a related work, Moulik et al. [62] has made a comparative study on the interaction between cationic polymer PDADMAC with various anionic surfactants (SDS, SDBS, and SDDS) in water and IP-water media. However, there is no such reported work involving SDDS and non-ionic polymer in aqueous organic media.

2,2,2-Trifluoroethanol (TFE), a classical fluorinated alcohol [63,64], has a large-scale demand for the researchers both in academic and biophysical fields [65] for its unique physicochemical properties. Owing to its excellent water miscibility [66], TFE can act as an efficient cosolvent with water for the biological research studies of proteins and peptides [67–69] and also as a solvent medium in many organic synthesis reactions [70–73]. It is prepared commercially from acid chloride derivative of trifluoroacetic acid by catalytic hydrogenation [74]. The trifluoromethyl group (-CF_3), due to its strong electron withdrawing nature, makes TFE a superior proton donor [α(TFE) = 1.51] [75] compared to proton acceptor in the formation of hydrogen bonds with water molecules. It also makes TFE significantly more acidic ($p^{K_a} = 12.4$) [76] than other commonly used conventional alcohols. The lower dielectric constant value ($\epsilon = 27$)[66] of TFE in comparison to water may be responsible for the reduced polarity in TFE-water mixture. At the same time, hydrophobic part of TFE molecule, i.e., trifluoromethyl group definitely may impart some hydrophobicity in the medium and also increases the hydrogen bonding ability [77,78] with water in the duo solvent mixture. Owing to this interesting behaviour, there is a great deal of curiosity to study the micellar properties of amphiphiles and ionic liquids taking TFE as an additive in water medium and only a few research works [79–81] have been done in this motive. Hence, TFE has been chosen as an additive for its interesting solvent character [82] in the present survey to investigate the amphiphilic behaviour of SDDS alone and in HEC-SDDS systems. The micellization of anionic surfactants in solution and their interaction with non-ionic polymers are both significantly influenced by the short chain alcohols [17]. A multi physicochemical techniques (tensiometry, conductometry, fluorimetry and microcalorimetry) have been applied for designing the focus of this work. The influence of TFE solvent on polymer size has been revealed by dynamic light scattering (DLS) method. Development of FESEM imaging helps us to elucidate the composition and surface morphology of HEC-SDDS complex in TFE-water solvent mixture. There have been some excellent review articles published in the past ten years that cover everything from fundamental concepts to further modern advances in the behaviour of polymer-surfactant aggregation [83–85].

2. Experimental section

2.1. Materials

Hydroxyethyl cellulose (HEC) (molar mass = 90,000 $g\ mol^{-1}$, degree of substitution (α) = 1.5), a carbohydrate based polymer, has been purchased from Sigma Aldrich (USA). The anionic surfactant, Sodium N-dodecanoyl sarcosinate (SDDS) (AR-grade quality, purity> 97%), has been obtained from Fluka, Germany. Pyrene (fluorescence probe for polarity index (I_1/I_3) determination), cetylpyridinium chloride (CPC, fluorescence quencher) and tryptophan (fluorescence probe for the determination of micellar aggregation number) are the products of Sigma Aldrich (USA). All these materials are used in the experiment without any further purification. The solvent 2,2,2-trifluoroethanol (TFE) (purity 99%), an AR-grade product, has been received from SRL, India. Double-distilled water (specific conductance (κ) ~1.0 $\mu S\ cm^{-1}$) has been used to prepare all the experimental solutions. A constant temperature of 298 K has been strictly maintained throughout all the measurements. HEC having 0.01 g% (w/v) concentration has been taken in this investigation. The concentration of TFE has been expressed in % (v/v). In this study, 5%, 10% and 15% (v/v) TFE solutions were prepared in double-distilled water. The structures of HEC, SDDS and TFE are presented in Scheme 1.

2.2. Methods

2.2.1. Tensiometry

The surface tension data were collected from calibrated Krüss du Noüy tensiometer (Germany) using platinum ring detachment technique at 298 K. A 5 mL of the experimental solution was taken in a double-walled container to which surfactant solution was added stepwise. Hamilton microsyringe was used for the addition process. All the equipment required for the experiment were properly cleaned using double distilled water and dried with acetone before each experiment. The platinum ring was further burned in ethanol flame. The concentration of the stock surfactant solution was taken as 225 mM (15 times of CMC). The temperature of the system was kept constant (accuracy of ± 0.1 K) throughout the experiment using a thermostatic water bath. Each data was collected by allowing time interval of 10 min for equilibration. In all experiments, the accuracy was maintained as ± 0.1 mN m^{-1}.

2.2.2. Conductometry

The specific conductance values were collected by using Jenway (UK) conductometer (cell constant 1.0 cm^{-1}). The experiment was initiated by taking 7 mL of experimental solution in a double-walled glass container. The whole system was kept in a thermostatic water bath to maintain temperature accuracy of ± 0.1 K. The surfactant solution (225 mM) was added into the experimental solution using a Hamilton microsyringe. The error in the specific conductance measurement was maintained within ± 0.5%.

2.2.3. Isothermal titration calorimetry (ITC)

An Omega ITC-200 microcalorimeter (Microcal, USA) instrument was used for carrying ITC measurements. The experimental system was kept in a Neslab RTE 100 circulating water bath for the maintenance of constant temperature at 298 K. The titration was carried out by adding surfactant solution (10–15 times of CMC) with the help of a micro syringe in 20–30 successive additions taking a time interval of 210 s for each addition with constant stirring (300 rpm). The heat change involved in each step of the surfactant addition was recorded in ITC software.

2.2.4. Fluorimetry

Steady state fluorimetric emission measurements were performed in a Perkin Elmer LS 55 (USA) spectrofluorimeter. The CMC of both surfactant and polymer-surfactant systems were determined using pyrene as a hydrophobic probe. For maintaining constant temperature of the experimental system at 298 K, a water flow thermostat was applied. The hydrophobic pyrene was excited at 332 nm. The wavelength range was 350–450 nm for measuring emission spectra. The slit widths were fitted at 14 and 2.5 nm for excitation and emission respectively. The scan rate was maintained 250 nm/min for each experiment. The polymer solutions prepared in both aqueous medium and in presence of different (v/v)% of TFE were taken in quartz cuvette having path length of 10 mm. The surfactant concentration was 225 mM. During fluorimetric measurement, surfactant solution (prepared in both aqueous and aquo-organic media) was added stepwise by a Hamilton micro syringe and the consequent change in intensity ratio of the first (I_1) and third (I_3) vibrational peak of the probe was taken for the determination of CMC.

On the other hand, aggregation number (n_A) of the same systems were calculated by static fluorescence quenching (SFQ) method. Here, tryptophan and 1-hexadecylpyridinium chloride (CPC) were used as the probe and quencher respectively, and quencher CPC was added with Hamilton micro syringe to the studied system to measure fluorescence intensity. The concentration of the surfactant used in the experiment was much above their measured CMC and that of tryptophan was used in

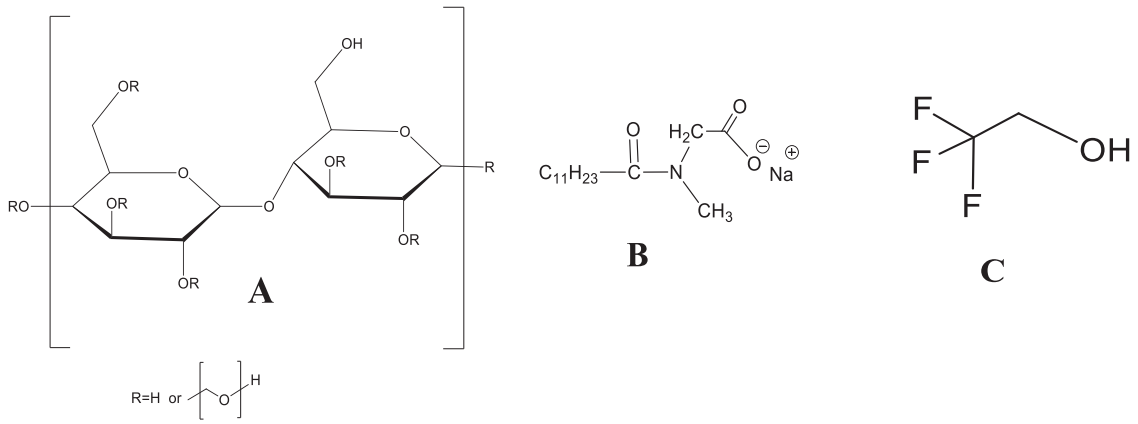

Scheme 1. Structures of (A) Hydroxyethyl Cellulose (HEC), (B) Sodium N-Dodecanoyl Sarcosinate (SDDS), (C) 2,2,2-Trifluoroethanol (TFE).

very low amount.

2.2.5. Dynamic light scattering

DLS size measurements of HEC polymer in aqueous solution and water-TFE medium were taken using Malvern Nano ZS Zetasizer (United Kingdom) instrument at 173° angle in He-Ne laser source (wavelength 632.8 nm) at 298 K. All these solutions before experiment were filtered through cellulose acetate paper for 3–4 times to remove unwanted dust particles. Each measurement was duplicated for reproducibility and the mean values were reported for analysis.

2.2.6. Field emission scanning electron microscopy (FESEM)

The images of surface morphology of experimental systems were taken from high resolution field emission scanning electron microscope (FEI INSPECT F50, Japan). A 2 μL drop of the investigated systems was placed on a tiny square glass slide followed by overnight drying (solvent removal) and spreading of the samples. The samples were then processed for gold coating via sputtering method with time duration of 1 min and applied 5.5 mA current.

3. Results and discussion

3.1. Effect of TFE on self-aggregation of SDDS

The amphiphilic nature of SDDS in TFE-water medium has been investigated via tensiometry, conductometry, microcalorimetry and fluorimetric measurements. The resultant plots are displayed in Fig. 1(A-E). The CMC values, and the related interfacial and thermodynamic parameters have been represented in Tables 1 and 2 respectively. The appearance of CMC evidences the self-aggregation of SDDS in TFE solvent. Using the concept of CMC, it is feasible to measure several thermodynamic parameters that can be used to ascribe the thermodynamic stability of the micelles. It is found that the CMC of anionic SDDS surfactant has been decreased markedly with increasing (v/v)% of TFE solvent. At 15% TFE, the value of CMC has been decreased by about 43%. Hence, TFE acts as the 'co-surfactant' in the aqueous environment [21]. When TFE molecules interact with ionic surfactants, they are more likely to get into the micellar surface layer, which reduces the micellar charge density by lengthening the average distance between the polar head groups [86]. At higher TFE percentage, due to higher solubilization of TFE molecules in the micellar surface, the CMC decreases. Addition of TFE solvent to water medium can act in two different ways. In one hand, TFE serves for making water structure to decrease CMC of SDDS amphiphile. At the same time, TFE decreases the medium polarity (ϵ_{TFE} = 27) [66] to increase CMC. The decrease in medium polarity is opposed by the way of making water structure. The overall result tends to decrease in CMC. For non-ionic TX-100, an exception is observed. García-Blanco et al. [81] has outlined a tendency towards increase in the CMC value with the increase in [TFE], and at 0.83 M TFE, the CMC has reached only 30% higher, which is compatible with a slight rise in solubility of TX-100 micelles in higher [TFE]. In another investigation, Civera et al. [80] has examined the effect of TFE on CMC and CP of non-ionic TX-165 micelles, both are found to decrease with an increase in [TFE] because of an enhancement in hydrophobicity. Beyond 15% TFE, SDDS surfactant shows difficulty in micelle formation and no inflection point is found in either tensiometric or conductometric plot. When TFE exceeds 15%, either the tensiometric plots scatter too much or the conductometric plots are insensitive to detect the observable slope change before and after the micellization. In fact, the micellization of amphiphiles cannot be defined above a certain alkanol percentage, which is also seen in the present system. Therefore, the highest concentration of TFE is taken to be 15% (v/v) to accurately present and compare data in this study. We have observed that above 20% IP, micellization of SDDS becomes non-existent [61]. In another investigation, We have reported the same about the micellization of zwitterionic amphiphile CHAPS above 10% IP [87]. Again, in case of cationic gemini surfactant (14−4−14), micelle formation is not possible above 15% IP [88].

Gibbs adsorption equation represents the surface excess of SDDS surfactant at CMC in Eq. 1.

$$\Gamma_{max} = -\frac{1}{2.303iRT}\lim_{[S]\to CMC}\frac{d\gamma}{dlogC} \quad (1)$$

where, i represents the number of dissociated species per amphiphile molecule in solution. For SDDS molecule, i = 2. T is the temperature in Kelvin scale and R is the molar gas constant ($Joule\ mol^{-1}\ \ K^{-1}$).

The following equation (Eq. 2) represents the expression ofA_{min}, i.e., minimum surface area per SDDS molecule.

$$A_{min} = \frac{10^{18}}{N_A\Gamma_{max}} \quad (2)$$

N_A is called Avogadro's constant.

The changes in standard Gibbs free energy of both micellization (ΔG^0_{mic}) and adsorption (ΔG^0_{Ads}) are represented in Eqs. 3 and 4 respectively.

$$\Delta G_{mic} = (1+\beta)RT\ln X_{CMC} \quad (3)$$

$$\Delta G^0_{Ads} = \Delta G^0_{mic} - \frac{\pi_{CMC}}{\Gamma_{max}} \quad (4)$$

The units used for Γ_{max}, A_{min}, $\Delta G^0_{mic}$and ΔG^0_{Ads} are $mol\ m^{-2}$, $nm^2 molecule^{-1}$, $kJ\ mol^{-1}$ and $kJ\ mol^{-1}$ respectively.

where, β is known as counter ion binding calculated from the ratio of post- and pre-micellar regions in the conductometric plots subtracted from unity. The value of slope in pre-CMC region (S_1) is higher than that

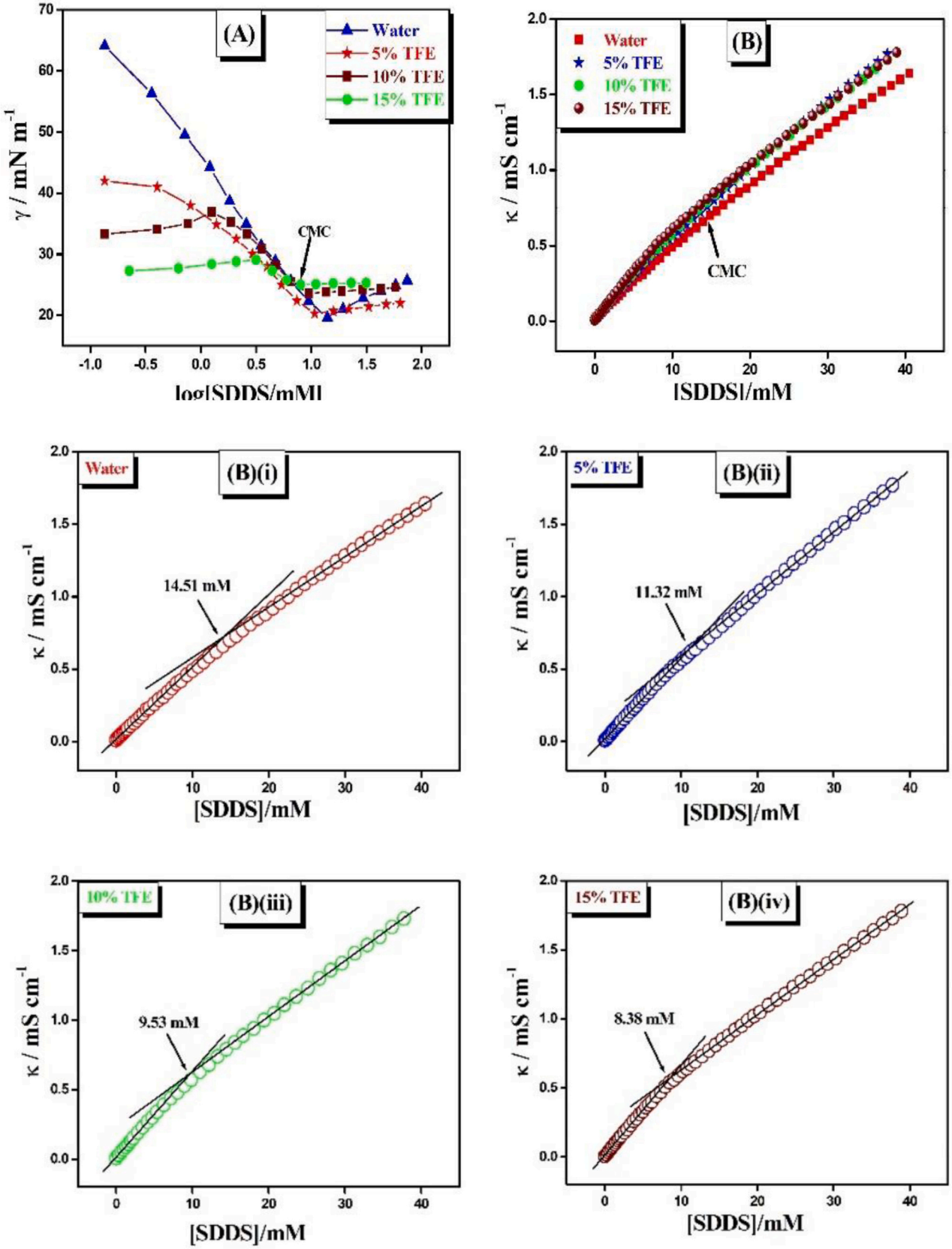

Fig. 1. Determination of CMC of SDDS in water and TFE-water media from (A) Tensiometry, (B) Conductometry: [(B)(i) Water, (B)(ii) 5% TFE, (B)(iii) 10% TFE, (B)(iv) 15% TFE], (C)(i) and D(i) Microcalorimetry in water and 10% TFE-water media respectively, (C)(ii) and (D)(ii) indicate corresponding enthalpograms, (E) Fluorimetry methods at 298 K.

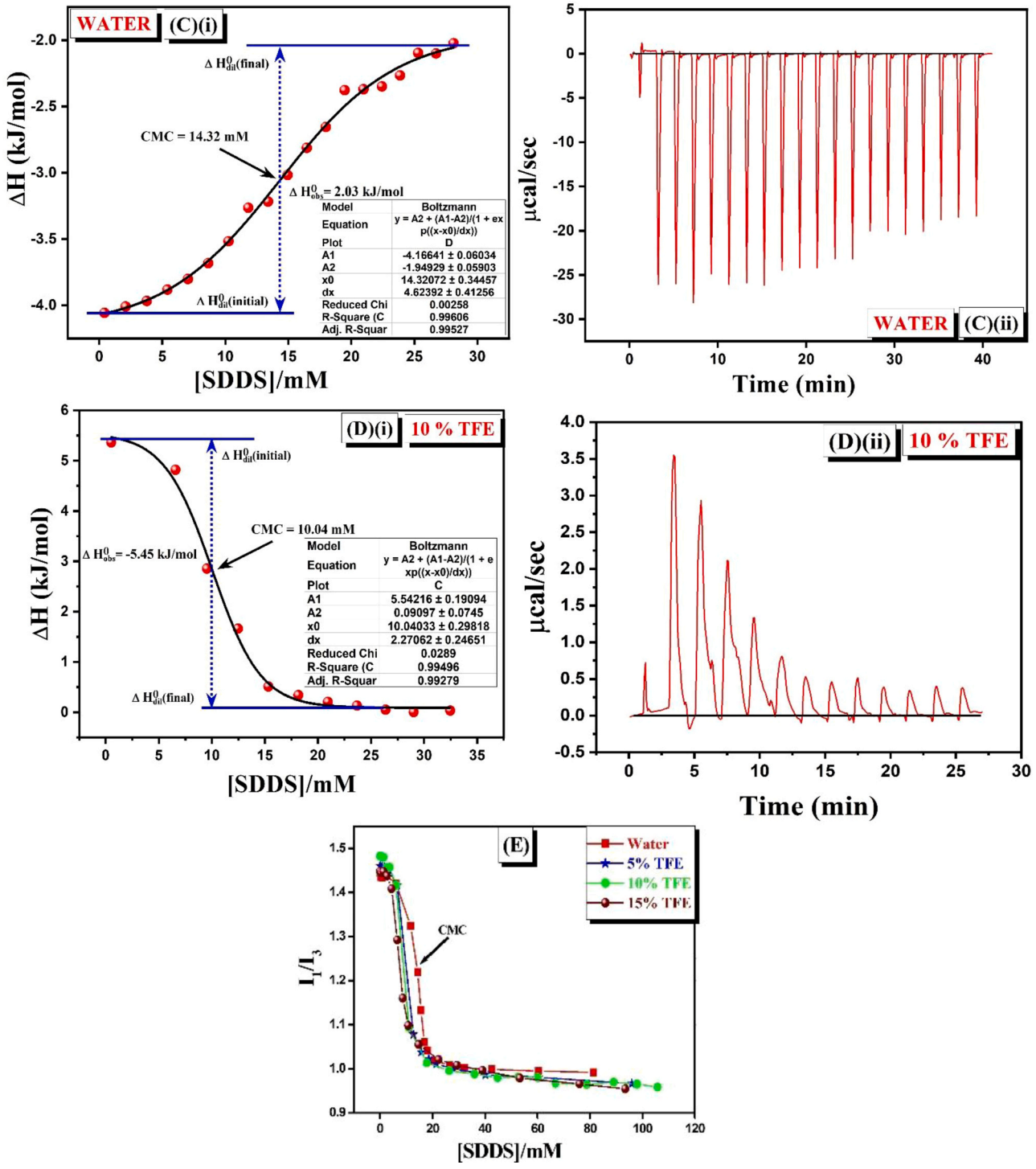

Fig. 1. (*continued*).

Table 1
Determination of the CMC of SDDS in Water and Different % TFE-Water Media from Tensiometry, Conductometry, Microcalorimetry, and Fluorimetric Methods at 298 K.

%TFE	*CMC(mM)*			
(v/v)	*Tensiometry*	*Conductometry*	*Fluorimetry*	*ITC*
0	13.97	14.51	13.96	14.32
5	10.71	11.32	10.25	–
10	9.48	9.53	9.08	10.04
15	7.98	8.38	7.73	–

found in post-CMC region (S_2). Consequently, the numerical value of β is found lower than unity (Eq. 5).

$$\beta = 1 - \frac{S_2}{S_1} \tag{5}$$

The term X_{CMC} denotes the fraction of moles of SDDS at CMC in tensiometric profiles and π_{CMC} is calculated from the following equation. It is the surface excess pressure measured at CMC.

$$\pi_{CMC} = \gamma_{iniial} - \gamma_{CMC} \tag{6}$$

The surfactants are recognized for surface activity properties. When

Table 2
Determination of Interfacial Parameters, and Thermodynamics of Micellization of SDDS in Water and Different % TFE-Water Media at 298 K.

%*TFE* (v/v)	γ_{CMC} ($mN\ m^{-2}$)	$\Gamma_{max} \times 10^6$ (mol/m^{-2})	A_{min} (nm^2/molecule)	β	$-\Delta G^0_{mic}$ (kJ/mol)	$-\Delta G^0_{Ads}$ (kJ/mol)
0	19.6	1.79	0.92	0.21	24.85	53.73
5	20.3	1.64	1.01	0.20	25.44	38.42
10	23.6	1.44	1.15	0.29	27.74	33.92
15	25	0.52	3.19	0.36	29.82	31.12

surface active agents are added to aqueous medium, the surface tension value is reduced due to the adsorption of the surfactant molecules at the air-water interface. The surfactants are aggregated to form micelles beyond a threshold concentration. This particular concentration is known as CMC [89]. The term γ_{CMC} is the numerical value of surface tension at the CMC. In this experiment, the values of γ_{CMC} are found considerably low. The values are 19.6, 20.3, 23.6 and 25 mN m^{-2} for SDDS at 0%, 5%, 10% and 15% TFE-water media respectively. We have also found quite low values of γ_{CMC} in the micellization of SDDS in IP/water media [61]. The reported values are 17.4, 22.8, 25.8, 26.1, 28.3 and 30.9 mN m^{-2} at 0%, 2%, 5%, 7%, 10% and 15% IP-water media respectively. These values in each instance increase with solvent concentration, which is another similarity.

The value of Γ_{max} decreases with increasing percentage of TFE solvent, as a result A_{min} increases. The increase in A_{min} indicates the presence of surface active TFE solvent which enhances the minimum head group area of SDDS amphiphile at CMC. Maximum increase of A_{min} per SDDS molecule is observed in presence of 15% TFE (Table 2) where CMC is minimum (Table 1). The value of A_{min} increases with TFE percentage due to less tendency of SDDS molecules to populate at the air-water interface at higher TFE concentration. The value of β, i.e., the part of the counter-ions that are bound to micelle increases with volume % of TFE (except at 5% TFE, β slightly decreases). At higher TFE percentage, due to greater solubilization of TFE solvent at the micellar surface, the micellar surface charge density decreases. As a result, the value of β increases at higher TFE contents [88]. The negative change in both ΔG^0_{mic} and ΔG^0_{Ads} confirms about the spontaneity of SDDS micellization and interfacial adsorption in the presence of TFE solvent. The higher negative value of ΔG^0_{Ads} than ΔG^0_{mic} means greater spontaneity of interfacial adsorption than micellization process.

3.2. Interaction of SDDS with HEC in TFE-water medium

Further, the solvent effect of TFE on the physicochemical interaction between SDDS and non-ionic HEC has been assessed. In this experiment, [HEC] is taken as 0.01 g%. The details of the results are provided below.

3.2.1. Tensiometry

In case of polymer-surfactant systems, tensiometric measurements are very much fruitful for the determination of both bulk and interfacial parameters. The tensiometric profiles for 0.01 g% HEC-SDDS interaction in both aqueous and TFE-water media have been illustrated in Fig. 2. The values of CMC for each of these have been calculated from surface tension (γ) vs log [SDDS] plot by visualizing the sharp break point. From this inflection point, SDDS molecules started micellization. Several combinations are feasible between polymers and surfactants in their interaction study, viz., non-ionic polymer/non-ionic surfactant [90,91], non-ionic polymer/cationic or anionic surfactant [92–95], and polymer and surfactant of opposite or similar charges [96–98]. The relative charge and hydrophobicity of the polymer-surfactant pairs have a significant impact on their interaction aspects. For oppositely charged polymer-surfactant systems, both electrostatic attraction and hydrophobic effect work in collaboration to strengthen their interactions [99]. In other cases, only hydrophobic effect operates. Joshi et al. [100] has made a comparative study of the strength of interaction of an anionic polymer (pectin) with different charged surfactants, and the sequence has been found as: cationic (CTAB, DTAB) > non-ionic (TX-100)

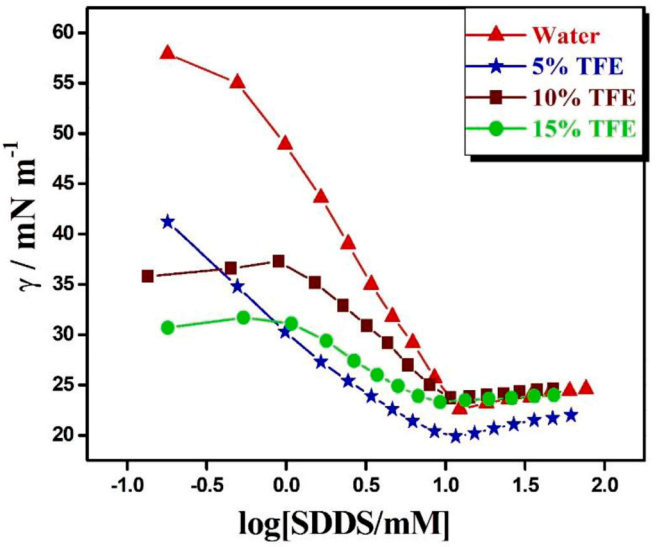

Fig. 2. Tensiometric profile for 0.01 g% HEC-SDDS interaction in water and different % TFE-water media at 298 K.

> anionic (SDS). Polymer-surfactant system of opposite charges is much more complicated to study than non-ionic polymer/ionic surfactant system in terms of physicochemical interaction [101]. Following several investigations, the non-ionic polymers are found to have a much stronger interaction with anionic surfactants than cationic or non-ionic surfactants [102]. In aqueous non-ionic polymer medium, the hydrophobic interaction causes reduction in the CMC of SDDS micelles. In HEC-SDDS system, the association ability of SDDS monomers is enhanced owing to the hydrophobic interaction between the hydrophobic tails of SDDS and the lipophilic domain of non-ionic HEC [103]. As a result, the micellization of SDDS occurs at a lower [SDDS] and the CMC is decreased. Beyond CMC, the free SDDS micelles can coexist with the HEC-SDDS aggregates supported on HEC backbone. When surface active TFE [104] is added, the tensiometric plots become slightly different than that found in aqueous medium. In the presence of TFE, the surface tension values have been lowered (Figs. 1A and 2), that corresponds to the water structure making ability of TFE solvent [80]. Here, with increasing TFE percentage in the medium, adsorption of TFE molecules also increases significantly at the water-air interface. This tends to diminution of surface tension at higher TFE concentration. A similar propensity is shown by other alcohols such as methanol, ethanol and propanol [13]. In case of 10% and 15% TFE, with stepwise addition of SDDS, the surface tension values first increase slightly, then decrease sharply until CMC is reached. However, in 2% and 5% TFE, the tensiometry plots look as in the aqueous medium. In this investigation, TFE further promotes micellization of SDDS at a lower surfactant concentration in presence of non-ionic polymer solution. Hence, CMC of HEC-SDDS system has been reduced with increasing TFE percentage in water. At 15% TFE, the CMC value of HEC-SDDS system in aqueous medium is reduced by about 25%. Previously, it has been mentioned (Section 3.1.) that exceeding a certain alkanol percentage as a solvent in the medium, micellization of amphiphile becomes difficult [87]. In this study, it has been observed that above 15% TFE, micellization of SDDS

becomes non-existent and the measured surface tension values are so scattered to find a definite break point needed for CMC detection Table 3.

3.2.2. Conductometry

Conductometry is another significant conventional method which can be useful for the investigation of non-ionic polymer and anionic surfactant aggregation. This method is dependent on the transport capacity of charged species present in the bulk. The conductometric titration in this study is correlated to the linear change of specific conductance (κ) of the investigated system with the concentration of anionic surfactant. During stepwise addition of SDDS in the HEC solution, DDS^- ions progressively bind with HEC backbone hydrophobically that allows Na^+ counter ions to be free in the medium. As a result, conductivity steeply increases. Now, CMC of HEC-SDDS system is ascertained from the intersection point lying between two straight lines both in aqueous and aquo-TFE media (Fig. 3). Hence, in such conductometric plots, two regions before and after CMC with different slopes have been found, viz., pre-micellar and post-micellar regions. In the pre-micellar region, only SDDS monomers present in the bulk move freely and the specific conductance increases more rapidly with SDDS concentration. In the post-micellar region, SDDS monomers spontaneously aggregate to form micelles resulting in lesser rate of increase in ion conductivity. Hence, post-micellar part has comparatively smaller value of slope than pre-micellar one. The term counter-ion binding (β) [105, 106] measures the strength of micelle ionization following Eq. 5 (Table 4). When binding with non-ionic HEC in aqueous environment, less SDDS monomers are needed for micellization, i.e., CMC is decreased. Therefore, the presence of polymer reduces CMC similar to tensiometric results. In this case, above 15% TFE, the conductometric plots are going up steeply showing no change in the slope and detection of CMC becomes not possible (no break point is observed).

3.2.3. Isothermal titration calorimetry

Isothermal titration calorimetry (ITC) provides basic thermodynamics of micellar aggregation of amphiphile. This method is highly sensitive to heat changes during micellization of the amphiphile alone or in presence of polymer. The gradual binding of SDDS with HEC corresponds to different rates of enthalpy change in the enthalpograms. Both the values of CMC and net heat change of micellization measurements are possible from the resulting ITC plots. Interaction of SDDS with HEC are studied in aqueous and 10% TFE medium and the plots are showed in Fig. 4(A-D). The determined CMC values are displayed in Table 4. In each case, the plots are found to be sigmoidal [107] and the CMCs are calculated from the inflection point in the intermediate zone of the respective enthalpograms [108,109] using Boltzmann-sigmoidal fitting [110]. The calorimetric profile can be assumed to have three separate concentration zones: (i) premicellar zone, where the concentrated surfactant solution is diluted, and the micellar breakdown leads to the formation of monomers (demicellization process), (ii) intermediate zone, where a sudden change in the enthalpy value (either a drop or an increase) is seen as a result of a portion of micelles dissolving into free monomers, while the rest continue to be in the micellar form (micellization process), (iii) post micellar zone, where both micelles and monomers are diluted. The CMC is obtained from the midpoint of the intermediate zone. The initial enthalpy of dilution (at premicellar zone), $\Delta H^0_{dil}(initial)$is found at the point where the vertical line across the CMC intersects the premicellar line, and the final enthalpy of dilution (at post micellar zone), $\Delta H^0_{dil}(final)$is determined at the point where this vertical line across the CMC intersects the post micellar line. The net enthalpy change during the micellization (at intermediate zone), $\Delta H^0_{obs}$is obtained from the difference between $\Delta H^0_{dil}(final)$ and$\Delta H^0_{dil}(initial)$ values [111]. The calculated values of both CMC and ΔH^0_{obs} are shown in Fig. 1(C)(i), 1 (D)(i), 4(A) and 4(C) for the relevant systems. In aqueous medium, in the micellization of SDDS alone and its binding with HEC are found endothermic, i.e., net positive enthalpy change ($\Delta H^0_{obs}>0$). In 10% TFE, both SDDS micellization and HEC-SDDS binding becomes exothermic ($\Delta H^0_{obs}<0$). The micellization of SDDS in IP/water media has been observed to follow a similar trend, and at 10% IP, it becomes exothermic. [61]. In Fig. 4A, the first data point in the premicellar zone has been found below zero value. During the titration, the concentrated SDDS solution experiences ready demicellization after the first injection to the sample cell containing aqueous HEC, and the enthalpy change in the first step becomes negative. Such inconsistency of the first data point in the sigmoidal-type ITC plot has been reported by Rajarathnam et al., [112] while studying membrane protein-ligand binding. The resulting CMC values from microcalorimetry are compatible with the tensiometric and conductometric data.

3.2.4. Fluorescence study

The solvent effect of TFE on the micellization behaviour of SDDS in absence and presence of non-ionic HEC has been described by steady-state fluorescence measurement. The value of CMC of anionic surfactant has been determined by varying TFE percentage without and with 0.01 g% HEC by this method. The values of CMC obtained from fluorescence intensity measurements are found close to those obtained from tensiometric and conductometric results. The difference in sensitivity of the experimental techniques used can be a justification for the slight difference in measured CMC values. To succeed this procedure, it is essential to select an efficient fluorescent probe to obtain invaluable information about the polarity change of the experimental system as a consequence of surfactant addition. Pyrene, already well established in literatures as a spectroscopic probe [113,114], is employed in our study to detect the micellization of SDDS alone as well as its aggregation behaviour with HEC in TFE solvent. In spite of its low water solubility, the pyrene molecules can introduce adequate fluorescence signal to identify the medium polarity. The fluorescence spectrum of pyrene can emit with five vibrational peaks [115]. Among these five emission bands, the relative intensity ratio (I_1/I_3) or 'micropolarity index' [116] (where, I_1 and I_3 are the fluorescence intensities of pyrene emission spectra), an important parameter providing details of the change in microstructural properties during the assembly of micelles, has been used for qualitative measurement of micropolarity experienced by the probe molecules surrounding it. During the experiment, hydrophobic pyrene molecules bind themselves to the hydrophobic region of gradually added surfactant molecules. Thus, the surfactant concentration has an extensive effect on the polarity of the system as well as on the intensity ratio(I_1/I_3). The micropolarity index(I_1/I_3) having values greater and less than unity accounts for the polar and non-polar environments respectively surrounding pyrene molecules [117]. The medium becomes more non-polar as TFE concentration is increased, and as a result, pyrene molecules perceive more non-polar environments, as evidenced by the decline in the CMC value. The early plateau region in the plot at very

Table 3
Determination of Interfacial Parameters, and Thermodynamics of Micellization of HEC-SDDS Interaction in Water and Different % TFE-Water Media at 298 K.

%TFE (v/v)	γ_{CMC} ($mN\ m^{-1}$)	$\Gamma_{max} \times 10^6 (mol/m^{-2})$	A_{min} ($nm^2/molecule$)	β	$-\Delta G^0_{mic}$ (kJ/mol)	$-\Delta G^0_{Ads}$ (kJ/mol)
0	22.6	1.89	0.87	0.40	29.19	48.66
5	19.9	0.47	3.53	0.23	25.83	72.21
10	23.7	1.22	1.36	0.34	28.39	36.91
15	23.3	0.41	4.05	0.38	29.75	44.38

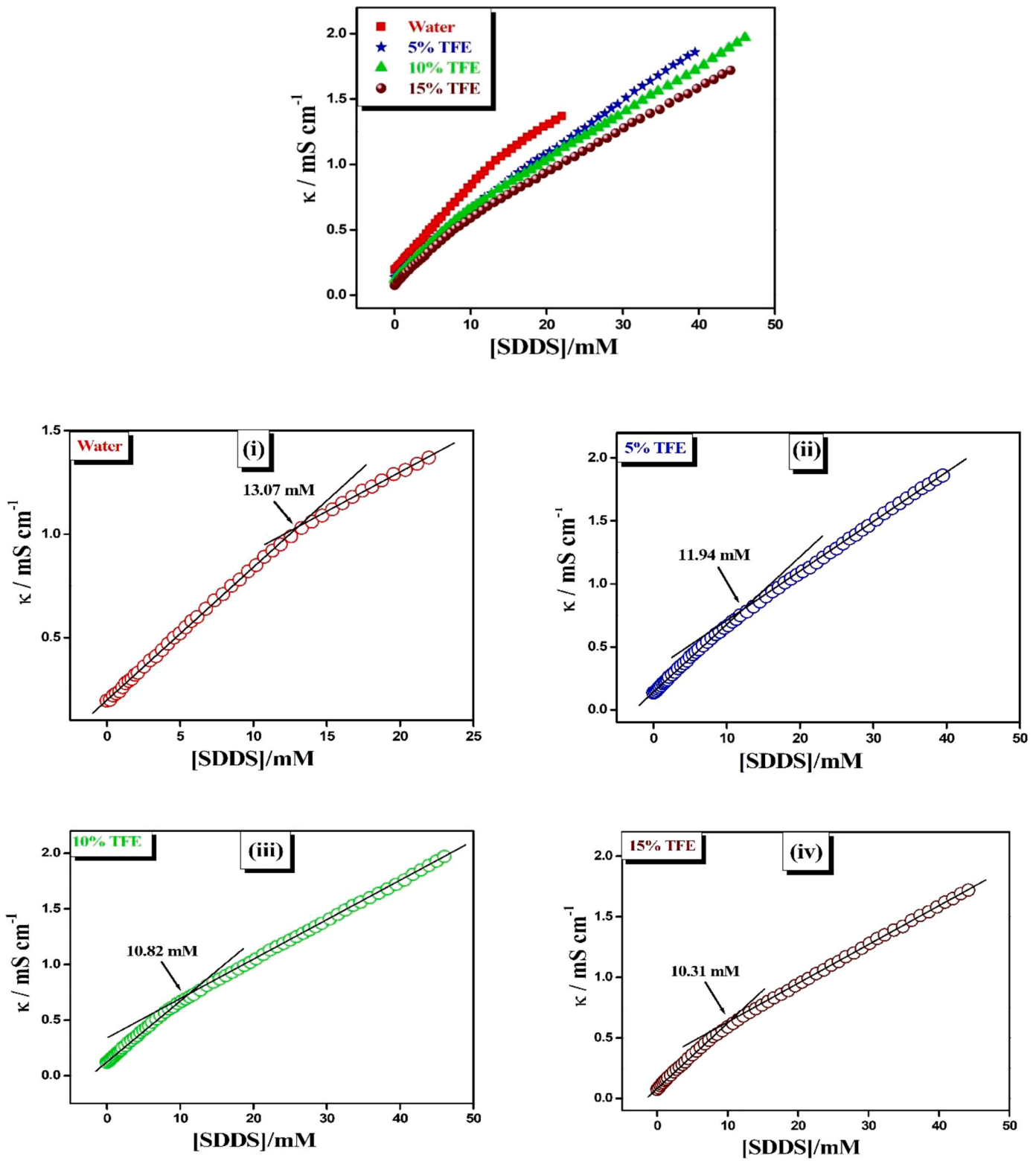

Fig. 3. Conductometric plots for 0.01 g% HEC-SDDS interaction in water and different % TFE-water media at 298 K: (i) Water, (ii) 5% TFE, (iii) 10% TFE, (iv) 15% TFE.

low [SDDS] is an indication of nearly constant value of(I_1/I_3) and non-micellization of SDDS molecules on HEC chains. Thereafter, the abrupt decrease in micropolarity is a consequence of the feasibility in the micellization process at intermediate [SDDS]. The saturation of SDDS micelles on HEC chain gives rise to further constant nature of micropolarity at higher amphiphile concentration. The values of CMC of the experimental systems have been detected from(I_1/I_3) vs [SDDS] plots. The resultant plots have been fitted as sigmoidal to quantify the single prominent break point Figs. 5 and 6.

3.2.5. *Aggregation number (n_{Agg})*

Comparative study of mean aggregation number (n_{Agg}) determina-

Table 4
Interaction Characteristic of HEC-SDDS Interaction in Water and Different % TFE-Water Media from Tensiometry, Conductometry, Microcalorimetry, and Fluorimetric Methods at 298 K.

% TFE	*CMC*(*mM*)			
(v/v)	*Tensiometry*	*Conductometry*	*Fluorimetry*	*ITC*
0	12.29	13.07	13.31	12.61
5	11.56	11.94	11.23	–
10	10.75	10.82	10.62	9.50
15	9.23	10.31	8.56	–

tion of amphiphile is a useful method which gives an idea about the size of the micelle [118] formed. In this work, the effect of TFE solvent has been performed on the aggregation number of pure SDDS and HEC-SDDS systems. Here, static fluorescence quenching technique has been applied. The quenching of tryptophan (an efficient fluorescence probe) has been measured with the help of CPC, used as a quencher, throughout the experiment [119]. The following Eq. 7 has been utilised to calculate the aggregation number (n_{Agg}) [120].

$$\ln\left(\frac{I_0}{I_1}\right) = \frac{n_{Agg}\ [CPC]}{[SDDS] - CMC} \tag{7}$$

where, I_0 and I_1 are the measured fluorescence intensities of tryptophan probe in the absence and presence of CPC quencher respectively. [SDDS] is taken as much higher than the corresponding CMC values in each experiment. [CPC] is the concentration of the quencher (3 mM). In this titrimetric method, the slope has been evaluated by linear fitting of $\ln(\frac{I_0}{I_1})$ *vs* [CPC] plot to quantify the aggregation number. The aggregation number of SDDS has been found 52 in water medium [55]. The added TFE causes a reduction in the polarity of the medium. In aquo-TFE media, the value of n_{Agg} has been lowered and decreases with increasing percentage of TFE. The calculated values of n_{Agg} are found as 47, 44 and 37 in 5%, 10% and 15% TFE in water respectively. At 15% TFE, the n_{Agg} value of SDDS found in the aqueous medium is reduced by about 29%. The decreasing order of aggregation number of amphiphile by non- aqueous alcoholic solvent in water has been affirmed by many authors [80,81] previously. In the presence of TFE, lowering of n_{Agg} of SDDS is caused by the cosurfactant nature of TFE in the medium.

Further, in the presence of non-ionic polymer HEC, hydrophobicity of the system is increased. Hence, n_{Agg} of HEC-bound SDDS micelle is lower than pure SDDS. The values of n_{Agg} of 0.01 g% HEC-SDDS system are 51, 46, 31 and 19 in 0%, 5%, 10% and 15% TFE respectively. At 15% TFE, the n_{Agg} value of HEC-SDDS system in the aqueous medium has been reduced by about 63%. According to literature [121], the aggregation number of anionic surfactant has been reduced during binding with non-ionic polymer.

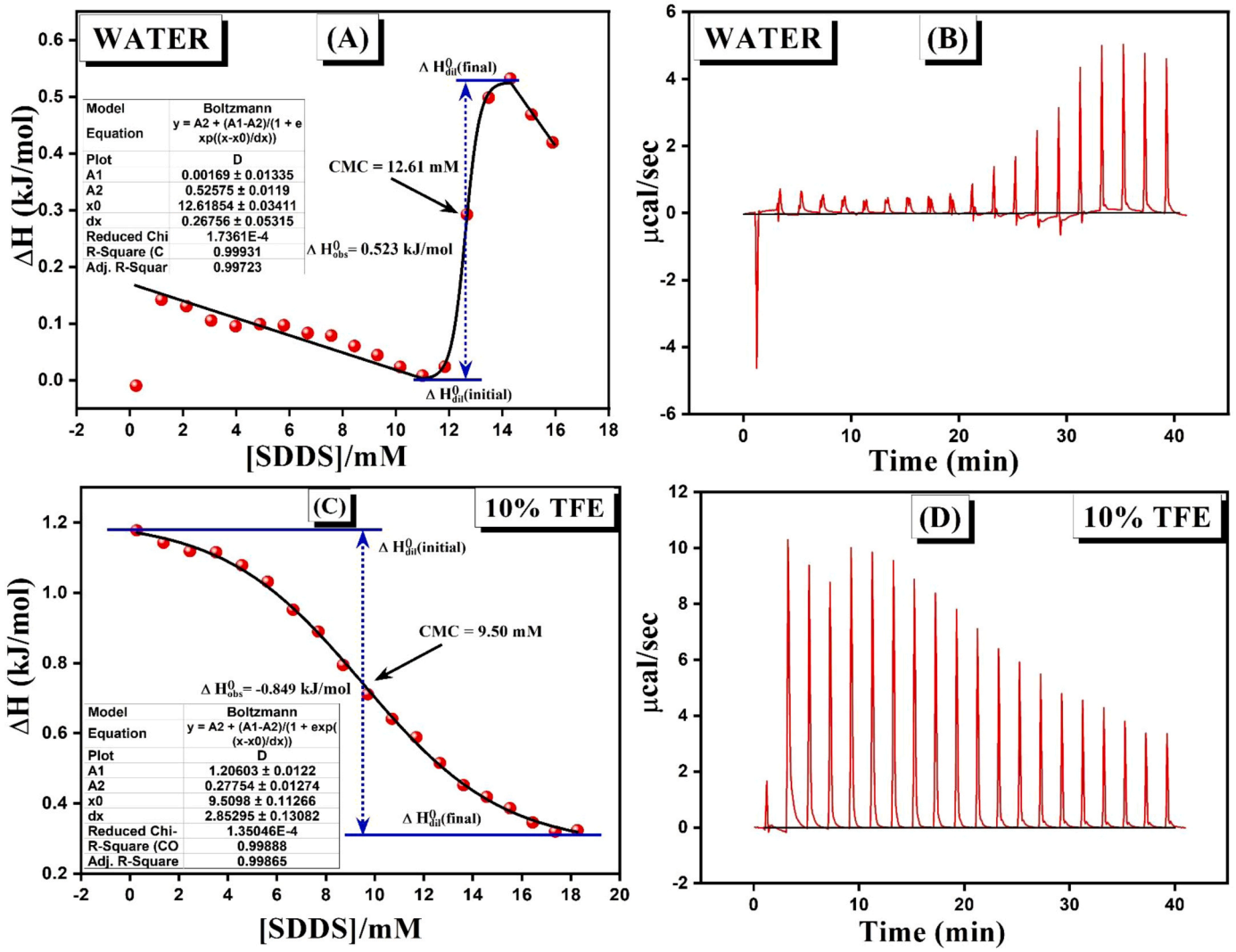

Fig. 4. ITC plots of 0.01 g% HEC-SDDS interaction in (A) water, (C) 10% TFE at 298 K. (B) and (D) represent corresponding enthalpograms.

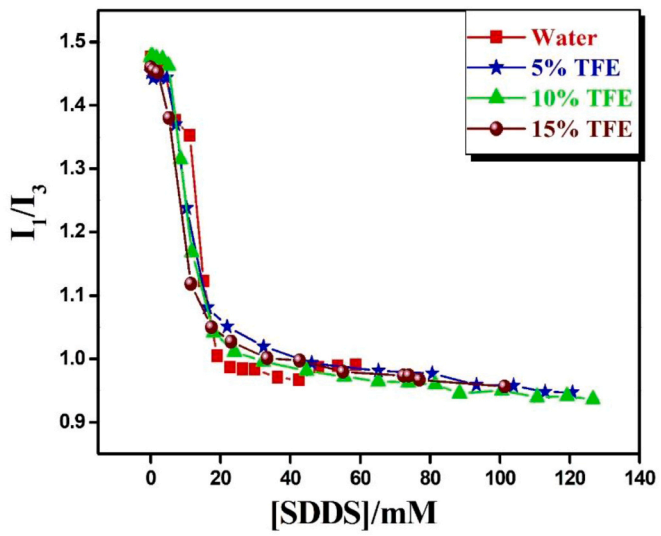

Fig. 5. Fluorimetric profile for 0.01 g% HEC-SDDS interaction in water and different % TFE-water media at 298 K.

3.2.6. *Dynamic light scattering*

DLS is the most effective technique for the analysis of particle size (in solution state) in the nanometer (nm) range. DLS measurements of HEC (0.01 g %) in aqueous solution as well as in TFE-water solvent media have been performed. Both hydrodynamic diameter (D_h) and polydispersity index (PDI) are studied. The calculated values of both D_h and PDI are presented in Table 5. In case of water and 5% TFE media, two hydrodynamic diameters (D_h^I, D_h^{II}) are observed. But three discrete diameters (D_h^I, D_h^{II} andD_h^{III}) are found in 10% and 15% TFE solutions. In general, the DLS distribution of polymers shows one or two peaks [122]. Here, the D_h values depend on TFE percentage. For each distribution, first one is assumed to be in monomeric state and the others are in aggregated states. The aggregated form is definitely larger than the monomeric form ($D_h^{III} > D_h^{II} > D_h^I$). The PDI values follow an irregular trend with TFE composition. Each measurement shows that PDI values are much larger than 0.30. Hence, the distributions are multidisperse.

3.2.7. *FESEM Imaging*

Surface morphology images of 0.01 g% HEC without and with SDDS are taken by FESEM technique. The images are depicted in Fig. 7(A-D). The experimental sample solutions are prepared in water and 10% TFE-water. To observe the morphological change of HEC in the presence of SDDS, concentration of SDDS has been taken much higher than CMC. In water, HEC forms fern-tree like clusters [123] with wide branching (Fig. 7A). In 10% TFE, HEC shows relatively smaller cluster with somewhat elongated branching (Fig. 7B), but the main structure remains same. In the presence of SDDS, the fern-like pattern of HEC has been destroyed and SDDS micelles are aggregated on the surface of HEC polymer (Fig. 7C). The morphology looks like flower like cluster. On the other hand, in 10% TFE, on further addition of SDDS, HEC polymer cluster turns into leafy canopy like morphology (Fig. 7D).

4. Conclusion

Reports on polymer-surfactant interactions are noteworthy and therefore, valuable research materials with potential applications in the aforementioned areas of modern science. Thus, a research strategy in this discipline needs an overview of previous and related investigations as well as an amplification of the observed findings. In order to develop distinct analogy, it is important to choose newer systems, and investigate their interactions using a variety of measurement approaches. In this manuscript, an effort has been made to coordinate between polymer and surfactant in presence of an alcoholic solvent. The quaternary combination discussed here belongs to a completely new category in this field, where the solvency effect of aquo-alcohol mixture on the polymer-surfactant system has been reported. The complexity of studying such quaternary systems deserves greater emphasis. It has become more intriguing in the presence of TFE because of its unique solvent properties as compared to other ordinary alcohols, as well as the fact that it has never been studied as an additive in the polymer-surfactant aggregation process. Furthermore, the effect of TFE on the self-aggregation of surfactants has gained scant attention in the literature. The non-ionic cellulose derivatives are most often used in the hydrophobically modified

Table 5
Hydrodynamic Diameter (D_h) and Polydispersity Index (PDI) for 0.01 g% HEC in Water and Different % TFE-Water Media at 298 K.

%*TFE* (v/v)	D_h/*nm*	*PDI*
0	32.6, 190.1	0.621
5	58.7, 396.1	0.722
10	7.5, 50.7, 255	0.544
15	28.2, 105.7, 615.1	0.666

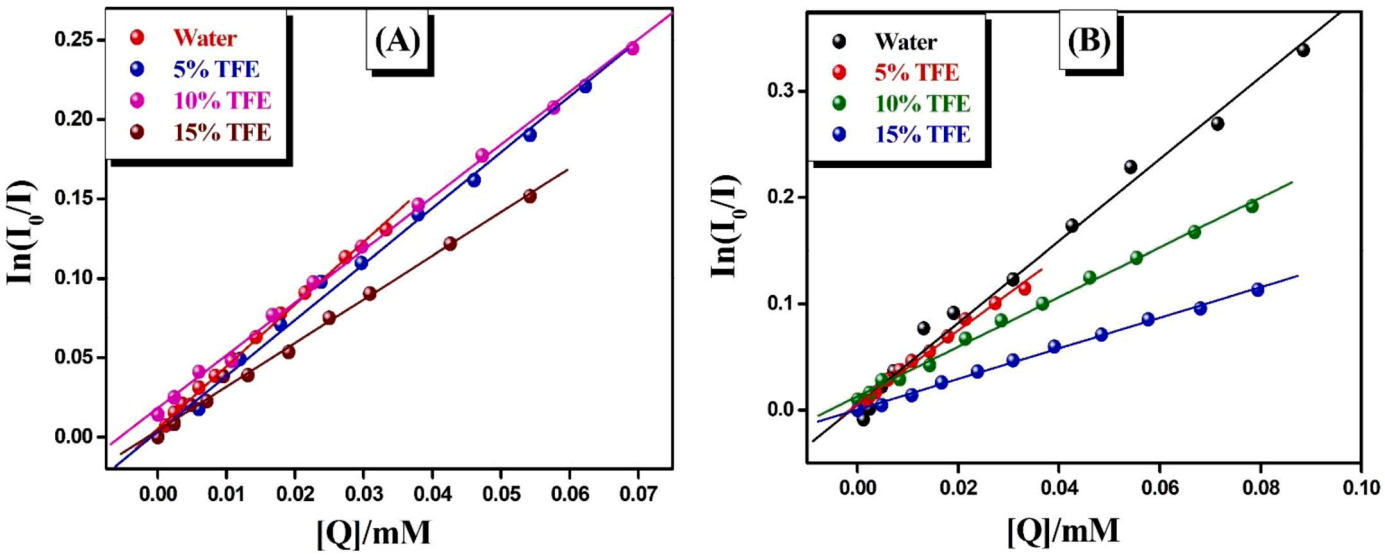

Fig. 6. Plot of $\ln(I_0/I)$ vs [Q] for (A) SDDS, (B) 0.01 g% HEC-SDDS interaction in water and different % TFE-water media at 298 K.

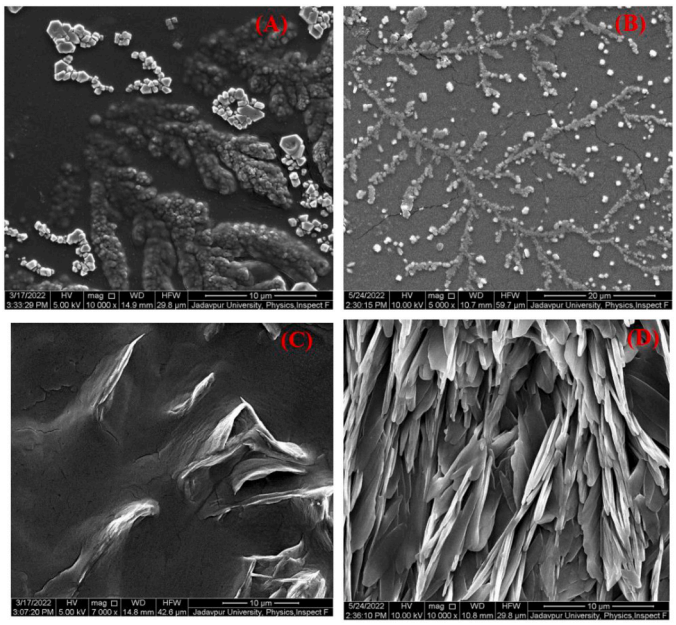

Fig. 7. FESEM images of pure 0.01 g% HEC in (A) water, (B) 10% TFE, (C) 0.01 g% HEC-SDDS in water, and (D) 10% TFE at [SDDS] > CMC.

form in terms of interaction with anionic surfactant, while using it in the form of pure HEC is rather uncommon. Similarly, the amino acid-based green surfactant SDDS has also received limited attention relevant to such studies. In most instances, Sodium dodecyl sulfate (SDS) as the anionic surfactant has conventionally been interacted with a non-ionic polymer. This article has comprehensively discussed the aggregation of SDDS with HEC in water and TFE-water media through a comparative study. It has been attempted to interpret the interaction features using some assumptions. Further investigation in this field employing a variety of experimental approaches would be beneficial. A step-by-step presentation of the summary of this manuscript has been made:

(1) Typical hydrophobic interactions have been established between non-ionic HEC and anionic SDDS. The 'cosurfactant' nature of TFE solvent further reinforces the hydrophobicity in the medium to reduce the CMC, observed experimentally using tensiometry, conductometry, fluorimetry and ITC techniques. The decrease in micellar charge density of the polar head groups can be used to explain the phenomenon of lowering CMC in the presence of TFE. At 15% TFE, the CMC value of pure SDDS has been reduced by about 43%, but when SDDS is bound with HEC, it is reduced by about 25% (tensiometry).
(2) Endothermic heat change during micellization of SDDS has been switched to exothermic nature both in the absence and presence of HEC in 10% TFE solvent.
(3) TFE causes a decline in micellar aggregation number (n_{Agg}) as a consequence of decreasing polarity in the medium. At 15% TFE, this decrease is about 29% for pure SDDS; but for HEC-SDDS system, it is decreased by about 63%.
(4) The change in HEC polymer configuration in TFE solvent has been justified in dynamic light scattering (DLS) method.
(5) The spontaneity of SDDS micellization has been affirmed by negative ΔG^0_{mic} values in each measurement.
(6) Finally, the changes in surface morphologies of pure HEC and HEC-SDDS binding have been recognized in 10% TFE from FESEM images.

The literature survey finds that the structures of proteins and peptides are much more complex to study. Analogous to biological aggregates, surfactant-induced micelles feature a hydrophilic part that remains exposed while the hydrophobic part stays away from the aqueous environment. Keeping in mind the importance of TFE in the conformational analysis of proteins and peptides, the present work is relevant, and thus it merits attention.

CRediT authorship contribution statement

Authors have equal contributions for doing experiments, writing the manuscript and finally reviewing and editing this one.

Declaration of Competing Interest

The Authors declare here that they have no conflict of interest with anybody for publication of this work.

Data Availability

No data was used for the research described in the article.

Acknowledgement

B.B.M. and R.B. thank CSIR,Govt. of India, for senior research fellowship.

References

[1] M.D. Chavanpatil, A. Khdair, Y. Patil, H. Handa, G. Mao, J. Panyam, Polymer-surfactant nanoparticles for sustained release of water-soluble drugs, J. Pharm. Sci. 96 (12) (2007) 79–3389.
[2] S. Decato, T. Bemis, E. Madsen, S. Mecozzi, Synthesis and characterization of perfluoro-tert-butyl semifluorinated amphiphilic polymers and their potential application in hydrophobic drug delivery, Polym. Chem. 5 (22) (2014) 6461–6471.
[3] V.P. Torchilin, Structure and design of polymeric surfactant-based drug delivery systems, J. Control. Release 73 (2–3) (2001) 137–172.
[4] P. Somasundaran, S. Chakraborty, Q. Qiang, P. Deo, J. Wang, R. Zhang, Surfactants, polymers and their nanoparticles for personal care applications, J. Cosmet. Sci. 55 (2004) S1.
[5] M.A. Villetti, C.I. Bica, I.T. Garcia, F.V. Pereira, F.I. Ziembowicz, C.L. Kloster, C. Giacomelli, Physicochemical properties of methylcellulose and dodecyltrimethylammonium bromide in aqueous medium, J. Phys. Chem. B 115 (19) (2011) 5868–5876.
[6] P. Raffa, D.A. Wever, F. Picchioni, A.A. Broekhuis, Polymeric surfactants: synthesis, properties, and links to applications, Chem. Rev. 115 (16) (2015) 8504–8563.
[7] S.P. Moulik, S. Ghosh, Surface chemical and micellization behaviours of binary and ternary mixtures of amphiphiles (Triton X-100, Tween-80 and CTAB) in aqueous medium, J. Mol. Liq. 72 (1997) 145–161.
[8] B. Šarac, M. Bešter-Rogač, Temperature and salt-induced micellization of dodecyltrimethylammonium chloride in aqueous solution: a thermodynamic study, J. Colloid Interface Sci. 338 (1) (2009) 216–221.
[9] Z.H. Ren, Mechanism of the salt effect on micellization of an aminosulfonate amphoteric surfactant, Ind. Eng. Chem. Res. 54 (40) (2015) 9683–9688.
[10] A. Saha, A. Mal, S. Ghosh, An elaborate investigation on the transition of rod-like micelle of cetyltrimethylammonium p-toluenesulfonate in presence of different additives, J. Mol. Liq. 309 (2020), 113084.
[11] A. Dey, N. Patra, A. Mal, S. Ghosh, Impact of organic polar solvents (DMSO and DMF) on the micellization and related behavior of an anionic (AOT), cationic (CEM2AB) and cationic gemini surfactant (16-5-16), J. Mol. Liq. 244 (2017) 85–96.
[12] S. Aslanzadeh, A. Yousefi, The effect of ethanol on nanostructures of mixed cationic and anionic surfactants, J. Surfactants Deterg. 17 (2014) 709–716.
[13] A. Zdziennicka, Surface behavior of Triton X-165 and short chain alcohol mixtures, Langmuir 26 (3) (2010) 1860–1869.
[14] A. Das Burman, S. Ghosh, A.R. Das, Behavior of cationic and anionic surfactants including bile salts in presence of hydroxypropyl cellulose (HPC), J. Nanofluids 3 (2014) 140–153.
[15] N. Dubey, Micellar properties and related thermodynamic parameters of aqueous anionic surfactants in the presence of monohydric alcohols, J. Chem. Eng. Data 56 (8) (2011) 3291–3300.
[16] A. Rodríguez, M.D. Graciani, M.L. Moyá, Effects of addition of polar organic solvents on micellization, Langmuir 24 (22) (2008) 12785–12792.
[17] A. Dan, I. Chakraborty, S. Ghosh, S.P. Moulik, Interfacial and bulk behavior of sodium dodecyl sulfate in isopropanol– water and in isopropanol– poly (vinylpyrrolidone)– water media, Langmuir 23 (14) (2007) 7531–7538.

[18] C. Totland, A.M. Blokhus, Swollen micelles and alcohol–surfactant co-adsorption: structures and mechanisms from liquid-and solid-state ^{1}H–^{1}H NMR spectroscopy, Phys. Chem. Chem. Phys. 19 (11) (2017) 7708–7713.

[19] U. Fatima, Riyazuddeen, P. Dhakal, J.K. Shah, Comparative study of influence of ethanol and 2, 2, 2-trifluoroethanol on thermophysical properties of 1-ethyl-3-methylimidazolium dicyanamide in binary mixtures: experimental and MD simulations, J. Chem. Eng. Data 66 (1) (2020) 101–115.

[20] P. Patidar, A. Bahadur, Modulating effect of different biomolecules and other additives on cloud point and aggregation of amphiphilic linear and starblock copolymer, J. Mol. Liq. 249 (2018) 219–226.

[21] M. Handa, R.R. Ujjwal, N. Vasdev, S.J. Flora, R. Shukla, Optimization of surfactant-and cosurfactant-aided pine oil nanoemulsions by isothermal low-energy methods for anticholinesterase activity, ACS Omega 6 (1) (2020) 559–568.

[22] J. Santhanalakshmi, A. Parameswari, Studies on the effect of cosurfactant on the phase behaviour of water in oil (CCl_4/water/Triton X – 100/n-alkanol) microemulsions, J. Surf. Sci. Technol. 13 (2–4) (1997) 113–129.

[23] H. Jiang, G. Beaucage, K. Vogtt, M. Weaver, The effect of solvent polarity on wormlike micelles using dipropylene glycol (DPG) as a cosolvent in an anionic/zwitterionic mixed surfactant system, J. Colloid Interface Sci. 509 (2018) 25–31.

[24] S.K. Shah, S.K. Chatterjee, A. Bhattarai, Micellization of cationic surfactants in alcohol—water mixed solvent media, J. Mol. Liq. 222 (2016) 906–914.

[25] T. Sidim, G. Acar, Alcohols effect on critic micelle concentration of polysorbate 20 and cetyl trimethyl ammonium bromine mixed solutions, J. Surfactants Deterg. 16 (2013) 601–607.

[26] P. Parekh, K. Singh, D.G. Marangoni, P. Bahadur, Effect of alcohols on aqueous micellar solutions of PEO–PPO–PEO copolymers: a dynamic light scattering and ^{1}H NMR study, J. Mol. Liq. 165 (2012) 49–54.

[27] S. MacLennan, D.G. Marangoni, Thermodynamics of glyme-sodium dodecyl sulfate (SDS) mixed micelle formation via isoperibol solution calorimetry: temperature, and concentration effects, J. Indian Chem. Soc. 100 (5) (2023) 100980–100990.

[28] M. Gradzielski, Polymer-surfactant interaction for controlling the rheological properties of aqueous surfactant solutions, Curr. Opin. Colloid Interface Sci. (2022), 101662.

[29] A. Bureiko, A. Trybala, N. Kovalchuk, V. Starov, Current applications of foams formed from mixed surfactant–polymer solutions, Adv. Colloid Interface Sci. 222 (2015) 670–677.

[30] F. Del Giudice, M. Tassieri, C. Oelschlaeger, A.Q. Shen, When microrheology, bulk rheology, and microfluidics meet: broadband rheology of hydroxyethyl cellulose water solutions, Macromolecules 50 (7) (2017) 2951–2963.

[31] T. Jiang, Q. Duan, J. Zhu, H. Liu, L. Yu, Starch-based biodegradable materials: challenges and opportunities, Adv. Ind. Eng. Polym. Res. 3 (1) (2020) 8–18.

[32] N. Dabholkar, S. Gorantla, T. Waghule, V.K. Rapalli, A. Kothuru, S. Goel, G. Singhvi, Biodegradable microneedles fabricated with carbohydrates and proteins: Revolutionary approach for transdermal drug delivery, Int. J. Biol. Macromol. 170 (2021) 602–621.

[33] K. Liu, X. Jiang, P. Hunziker, Carbohydrate-based amphiphilic nano delivery systems for cancer therapy, Nanoscale 8 (36) (2016) 16091–16156.

[34] A. Noreen, K.M. Zia, S. Tabasum, S. Khalid, R. Shareef, A review on grafting of hydroxyethylcellulose for versatile applications, Int. J. Biol. Macromol. 150 (2020) 289–303.

[35] M. Oprea, S.I. Voicu, Recent advances in composites based on cellulose derivatives for biomedical applications, Carbohydr. Polym. 247 (2020), 116683.

[36] J.T. Lo, H.T. Yen, C.C. Tsai, B.H. Chen, S.S. Hou, Interaction between hydrophobically modified 2-hydroxyethyl cellulose and sodium dodecyl sulfate studied by viscometry and two-dimensional NOE NMR spectroscopy, J. Phys. Chem. B 118 (24) (2014) 6922–6930.

[37] U. Kästner, H. Hoffmann, R. Dönges, R. Ehrler, Interactions between modified hydroxyethyl cellulose (HEC) and surfactants, Colloids Surf. A: Physicochem. Eng. Asp. 112 (2–3) (1996) 209–225.

[38] S. Mondal, P. Pyne, A. Patra, R.K. Mitra, S. Ghosh, Effect of surfactant tail length on the hydroxypropyl cellulose-mediated premicellar aggregation of sodium n-alkyl sulfate surfactants, Langmuir 37 (20) (2021) 6168–6177.

[39] B. Peng, Z. Yao, X. Wang, M. Crombeen, D.G. Sweeney, K.C. Tam, Cellulose-based materials in wastewater treatment of petroleum industry, Green. Energy Environ. 5 (1) (2020) 37–49.

[40] M. Akter, M. Bhattacharjee, A.K. Dhar, F.B. Rahman, S. Haque, T.U. Rashid, S. F. Kabir, Cellulose-based hydrogels for wastewater treatment: a concise review, Gels 7 (1) (2021) 30.

[41] S.S. Gwebu, H. Chirirriwa, The effect of hydroxyl ethyl cellulose (HEC) and hydrophobically–modified alkali soluble emulsions (HASE) on the properties and quality of water based paints, Int J. Appl. Chem. 13 (2017) 1–3.

[42] A. Maestro, C. González, J.M. Gutiérrez, Interaction of surfactants with thickeners used in waterborne paints: a rheological study, J. Colloid Interface Sci. 288 (2) (2005) 597–605.

[43] K.H. Mahmoud, Optical properties of hydroxyethyl cellulose film treated with nitrogen plasma, Spectrochim. Acta Part A: Mol. Biomol. Spectrosc. 157 (2016) 153–157.

[44] S.C. Angadi, L.S. Manjeshwar, T.M. Aminabhavi, Interpenetrating polymer network blend microspheres of chitosan and hydroxyethyl cellulose for controlled release of isoniazid, Int. J. Biol. Macromol. 47 (2) (2010) 171–179.

[45] P.R. Choudhury, S. Majumdar, G.C. Sahoo, S. Saha, P. Mondal, High pressure ultrafiltration CuO/hydroxyethyl cellulose composite ceramic membrane for separation of Cr (VI) and Pb (II) from contaminated water, Chem. Eng. J. 336 (2018) 570–578.

[46] R.O. Brito, S.G. Silva, R.M. Fernandes, E.F. Marques, J. Enrique-Borges, M.L. do Vale, Enhanced interfacial properties of novel amino acid-derived surfactants: effects of headgroup chemistry and of alkyl chain length and unsaturation, Colloids Surf. B: Biointerfaces 86 (1) (2011) 65–70.

[47] A. Pinazo, R. Pons, L. Pérez, M.R. Infante, Amino acids as raw material for biocompatible surfactants, Ind. Eng. Chem. Res. 50 (9) (2011) 4805–4817.

[48] M.C. Bourkaib, S. Delaunay, X. Framboisier, L. Hôtel, B. Aigle, C. Humeau, Y. Guiavarc'h, I. Chevalot, N-acylation of L-amino acids in aqueous media: evaluation of the catalytic performances of Streptomyces ambofaciens aminoacylases, Enzym. Microb. Technol. 137 (2020), 109536.

[49] A. Pinazo, M.A. Manresa, A.M. Marques, M. Bustelo, M.J. Espuny, L. Pérez, Amino acid–based surfactants: new antimicrobial agents, Adv. Colloid Interface Sci. 228 (2016) 17–39.

[50] C.M. Lee, S.Y. Kim, S.H. Yoon, J.B. Kim, Y.S. Yeo, J.S. Sim, B.S. Hahn, D.G. Kim, Characterization of a novel antibacterial N-acyl amino acid synthase from soil metagenome, J. Biotechnol. 294 (2019) 19–25.

[51] J. Rajstein, M. Fuks, A. Markitziu, I. Gedalia, Solubility of enamel powder following treatment with a sodium-n-lauroyl sarcosinate containing toothpaste in the presence and absence of fluoride, J. Oral. Rehabil. 10 (6) (1983) 469–471.

[52] K.P. Ananthapadmanabhan, Amino-acid surfactants in personal cleansing, Tenside Surfactants Deterg. 56 (5) (2019) 378–386.

[53] G.B. Ray, S. Ghosh, S.P. Moulik, Physicochemical studies on the interfacial and bulk behaviors of sodium N-dodecanoyl sarcosinate (SDDS), J. Surfactants Deterg. 12 (2) (2009) 131–143.

[54] N. Patra, D. Ray, V.K. Aswal, S. Ghosh, Exploring physicochemical interactions of different salts with sodium N-dodecanoyl sarcosinate in aqueous solution, ACS Omega 3 (8) (2018) 9256–9266.

[55] S. Das, S. Mondal, S. Ghosh, Physicochemical studies on the micellization of cationic, anionic, and nonionic surfactants in water–polar organic solvent mixtures, J. Chem. Eng. Data 58 (9) (2013) 2586–2595.

[56] A. Dan, S. Ghosh, S.P. Moulik, Interaction of cationic hydroxyethylcellulose (JR400) and cationic hydrophobically modified hydroxyethylcellulose (LM200) with the amino-acid based anionic amphiphile Sodium N-Dodecanoyl Sarcosinate (SDDS) in aqueous medium, Carbohydr. Polym. 80 (1) (2010) 44–52.

[57] B. Naskar, S. Ghosh, S.P. Moulik, Interaction of normal and reverse pluronics (L44 and 10R5) and their mixtures with anionic surfactant sodium N-dodecanoylsarcosinate, J. Colloid Interface Sci. 414 (2014) 82–89.

[58] M.A. Alsenaidy, Biophysical evaluation of amyloid fibril formation in bovine cytochrome c by sodium lauroyl sarcosinate (sarkosyl) in acidic conditions, J. Mol. Liq. 241 (2017) 722–729.

[59] S. Mondal, M.L. Raposo, A. Ghosh, G. Prieto, S. Ghosh, Physicochemical and conformational studies on interaction of myoglobin with an amino-acid based anionic surfactant, sodium N- dodecanoyl sarcosinate (SDDS), Colloids Surf. A Physicochem. Eng. Asp. 577 (2019) 167–174.

[60] N. Azum, M.A. Rub, A. Khan, M.M. Alotaibi, A.M. Asiri, Synergistic interaction and binding efficiency of tetracaine hydrochloride (Anesthetic Drug) with anionic surfactants in the presence of NaCl solution using surface tension and UV–visible spectroscopic methods, Gels 8 (4) (2022) 234.

[61] B. Mandal, S. Ghosh, S.P. Moulik, Interaction between a bio-tolerable amino-acid based amphiphile (N-dodecanoylsarcosinate, SDDS) and modified cationic polymers, hydroxyethylcelluloses (JR 400, and LM 200) in isopropanol-water medium, Colloids Surf. A Physicochem. Eng. Asp. 566 (2019) 156–165.

[62] S. Mukherjee, A. Dan, S.C. Bhattacharya, A.K. Panda, S.P. Moulik, Physicochemistry of interaction between the cationic polymer poly (diallyldimethylammonium chloride) and the anionic surfactants sodium dodecyl sulfate, sodium dodecylbenzenesulfonate, and sodium N-dodecanoylsarcosinate in water and isopropyl alcohol– water media, Langmuir 27 (9) (2011) 5222–5233.

[63] A. Berkessel, J.A. Adrio, D. Hüttenhain, J.M. Neudörfl, Unveiling the "booster effect" of fluorinated alcohol solvents: aggregation-induced conformational changes and cooperatively enhanced H-bonding, J. Am. Chem. Soc. 128 (26) (2006) 8421–8426.

[64] S. Khaksar, Fluorinated alcohols: a magic medium for the synthesis of heterocyclic compounds, J. Fluor. Chem. 172 (2015) 51–61.

[65] D.P. Hong, M. Hoshino, R. Kuboi, Y. Goto, Clustering of fluorine-substituted alcohols as a factor responsible for their marked effects on proteins and peptides, J. Am. Chem. Soc. 121 (37) (1999) 8427–8433.

[66] R. Chitra, P.E. Smith, Properties of 2, 2, 2-trifluoroethanol and water mixtures, J. Chem. Phys. 114 (1) (2001) 426–435.

[67] B. Chaubey, A. Dey, A. Banerjee, N. Chandrakumar, S. Pal, Assessment of the role of 2, 2, 2-trifluoroethanol solvent dynamics in inducing conformational transitions in melittin: an approach with solvent 19F low-field NMR relaxation and overhauser dynamic nuclear polarization studies, J. Phys. Chem. B 124 (28) (2020) 5993–6003.

[68] D. Mohanta, M. Jana, Can 2, 2, 2-trifluoroethanol be an efficient protein denaturant than methanol and ethanol under thermal stress? Phys. Chem. Chem. Phys. 20 (15) (2018) 9886–9896.

[69] V.L. Anderson, W.W. Webb, A desolvation model for trifluoroethanol-induced aggregation of enhanced green fluorescent protein, Biophys. J. 102 (4) (2012) 897–906.

[70] C. Yu, J. Sanjosé-Orduna, F.W. Patureau, M.H. Pérez-Temprano, Emerging unconventional organic solvents for C–H bond and related functionalization reactions, Chem. Soc. Rev. 49 (6) (2020) 1643–1652.

[71] D. Gimenez, A. Dose, N.L. Robson, G. Sandford, S.L. Cobb, C.R. Coxon, 2, 2, 2-Trifluoroethanol as a solvent to control nucleophilic peptide arylation, Org. Biomol. Chem. 15 (19) (2017) 4081–4085.

[72] S. Lu, W. Chen, Q. Shen, Friedel-Crafts trifluoromethylthiolation of electron-rich (hetero) arenes with trifluoromethylthio-saccharin in 2, 2, 2-trifluoroethanol (TFE), Chin. Chem. Lett. 30 (12) (2019) 2279–2281.

[73] H. Abe, H. Amii, K. Uneyama, Pd-catalyzed asymmetric hydrogenation of α-fluorinated iminoesters in fluorinated alcohol: a new and catalytic enantioselective synthesis of fluoro α-amino acid derivatives, Org. Lett. 3 (3) (2001) 313–315.

[74] G. Siegemund, W. Schwertfeger, A. Feiring, B. Smart, F. Behr, H. Vogel, B. McKusick, P. Kirsch, Fluorine compounds, organic, Ullmann's Encycl. Ind. Chem. 11 (2016) 361.

[75] J.P. Begue, D. Bonnet-Delpon, B. Crousse, Fluorinated alcohols: a new medium for selective and clean reaction, Synlett 2004 (01) (2004) 18–29.

[76] I.A. Shuklov, N.V. Dubrovina, A. Boerner, Fluorinated alcohols as solvents, cosolvents and additives in homogeneous catalysis, Synthesis 2007 (19) (2007) 2925–2943.

[77] M. Matsugami, R. Yamamoto, T. Kumai, M. Tanaka, T. Umecky, T. Takamuku, Hydrogen bonding in ethanol–water and trifluoroethanol–water mixtures studied by NMR and molecular dynamics simulation, J. Mol. Liq. 217 (2016) 3–11.

[78] S. Mondal, B. Biswas, T. Nandy, P.C. Singh, Understanding the role of hydrophobic terminal in the hydrogen bond network of the aqueous mixture of 2, 2, 2-trifluoroethanol: IR, molecular dynamics, quantum chemical as well as atoms in molecules studies, J. Phys. Chem. B 122 (25) (2018) 6616–6626.

[79] M.R. Islam, F. Warsi, A.B. Khan, T. Kausar, I. Khan, M. Ali, Solvatochromism of binary mixtures of 2, 2, 2-trifluoroethanol+ ionic liquid [bmim][Tf2N]: a comparative study with molecular solvents, J. Chem. Eng. Data 64 (3) (2019) 1140–1154.

[80] C. Civera, C. Arias, M.A. Elorza, B. Elorza, F. García-Blanco, P.A. Galera-Gómez, Hydrophobicity enhancement in micelles of Triton X-165 by the presence of the cosolvent 2, 2, 2 trifluoroethanol (TFE), J. Mol. Liq. 199 (2014) 29–34.

[81] F. García-Blanco, M.A. Elorza, C. Arias, B. Elorza, I. Gómez-Escalonilla, C. Civera, P.A. Galera-Gómez, Interactions of 2, 2, 2-trifluoroethanol with aqueous micelles of Triton X-100, J. Colloid Interface Sci. 330 (1) (2009) 163–169.

[82] A. Burakowski, J. Gliński, B. Czarnik-Matusewicz, P. Kwoka, A. Baranowski, K. Jerie, H. Pfeiffer, N. Chatziathanasiou, Peculiarity of aqueous solutions of 2, 2, 2-trifluoroethanol, J. Phys. Chem. B 116 (1) (2012) 705–710.

[83] R.P. Gawade, S.L. Chinke, P.S. Alegaonkar, Polymers in cosmetics. In Polymer science and innovative applications, Elsevier, 2020, pp. 545–565.

[84] F.M. Michael M. Khalid R. Walvekar H. Siddiqui A.B. Balaji. Surface modification techniques of biodegradable and biocompatible polymers. Biodegradable and Biocompatible Polymer Composites: Processing, Properties and Applications; Shimpi, NG, Ed. 2018:33–54.

[85] S. Llamas, E. Guzman, F. Ortega, N. Baghdadli, C. Cazeneuve, R.G. Rubio, G. S. Luengo, Adsorption of polyelectrolytes and polyelectrolytes-surfactant mixtures at surfaces: a physico-chemical approach to a cosmetic challenge, Adv. Colloid Interface Sci. 222 (2015) 461–487.

[86] I.V. Rao, E. Ruckenstein, Micellization behavior in the presence of alcohols, J. Colloid Interface Sci. 113 (2) (1986) 375–387.

[87] B. Naskar, S. Ghosh, S. Nagadome, G. Sugihara, S.P. Moulik, Behavior of the amphiphile CHAPS alone and in combination with the biopolymer inulin in water and isopropanol–water media, Langmuir 27 (15) (2011) 9148–9159.

[88] S. Das, B. Naskar, S. Ghosh, Influence of temperature and organic solvents (isopropanol and 1, 4-dioxane) on the micellization of cationic gemini surfactant (14-4-14), Soft Matter 10 (16) (2014) 2863–2875.

[89] D.R. Perinelli, M. Cespi, N. Lorusso, G.F. Palmieri, G. Bonacucina, P. Blasi, Surfactant self-assembling and critical micelle concentration: one approach fits all? Langmuir 36 (21) (2020) 5745–5753.

[90] R. Fijan, S. Šostar-Turk, R. Lapasin, Rheological study of interactions between non-ionic surfactants and polysaccharide thickeners used in textile printing, Carbohydr. Polym. 68 (4) (2007) 708–717.

[91] O. Ortona, G. D'Errico, L. Paduano, V. Vitagliano, Interaction between cationic, anionic, and non-ionic surfactants with ABA block copolymer Pluronic PE6200 and with BAB reverse block copolymer Pluronic 25R4, J. Colloid Interface Sci. 301 (1) (2006) 63–77.

[92] A. Dan, S. Ghosh, S.P. Moulik, Physicochemistry of the interaction between inulin and alkyltrimethylammonium bromides in aqueous medium and the formed coacervates, J. Phys. Chem. B 113 (25) (2009) 8505–8513.

[93] N. Patra, A. Mal, S. Das, S. Ghosh, Detailed physicochemical interaction of inulin with some conventional surfactants and surface active ionic liquid, J. Mol. Liq. 340 (2021), 116849.

[94] N. Sardar, M. Kamil, Interaction between nonionic polymer hydroxypropyl methyl cellulose (HPMC) and cationic gemini/conventional surfactants, Ind. Eng. Chem. Res. 51 (3) (2012) 1227–1235.

[95] R.M. Altman, G.L. Richmond, Coming to order: adsorption and structure of nonionic polymer at the oil/water interface as influenced by cationic and anionic surfactants, Langmuir 36 (8) (2020) 1975–1984.

[96] M. Miyake, Recent progress of the characterization of oppositely charged polymer/surfactant complex in dilution deposition system, Adv. Colloid Interface Sci. 239 (2017) 146–157.

[97] D. Asker, J. Weiss, D.J. McClements, Analysis of the interactions of a cationic surfactant (lauric arginate) with an anionic biopolymer (pectin): isothermal titration calorimetry, light scattering, and microelectrophoresis, Langmuir 25 (1) (2009) 116–122.

[98] S. Shrivastava, J. Dey, Interaction of anionic surfactant with polymeric nanoparticles of similar charge, J. Colloid Interface Sci. 350 (1) (2010) 220–228.

[99] H.D. Burrows, M.J. Tapia, C.L. Silva, A.A. Pais, S.M. Fonseca, J. Pina, J. Seixas de Melo, Y. Wang, E.F. Marques, M. Knaapila, A.P. Monkman, Interplay of electrostatic and hydrophobic effects with binding of cationic gemini surfactants and a conjugated polyanion: experimental and molecular modeling studies, J. Phys. Chem. B 111 (17) (2007) 4401–4410.

[100] N. Joshi, K. Rawat, H.B. Bohidar, Influence of structure, charge, and concentration on the pectin–calcium–surfactant complexes, J. Phys. Chem. B 120 (18) (2016) 4249–4257.

[101] T. Chakraborty, I. Chakraborty, S. Ghosh, Sodium carboxymethylcellulose−CTAB interaction: a detailed thermodynamic study of polymer − surfactant interaction with opposite charges, Langmuir 22 (24) (2006) 9905–9913.

[102] M.Y. Khan, A. Samanta, K. Ojha, A. Mandal, Interaction between aqueous solutions of polymer and surfactant and its effect on physicochemical properties, Asia-Pacific J. Chem. Eng. 3 (5) (2008) 579–585.

[103] B.B. Mondal, R. Banik, S. Ghosh, Detailed physicochemical study and thermodynamic aspects of the interaction between nonionic cellulose derivative hydroxyethyl cellulose and anionic surfactant sodium N-dodecanoyl sarcosinate in aqueous media, J. Taiwan Inst. Chem. Eng. 149 (2023), 104982.

[104] G. Gente, C. La Mesa, Water—trifluoroethanol mixtures: some physicochemical properties, J. Solut. Chem. 29 (11) (2000) 1159–1172.

[105] T. Chakraborty, I. Chakraborty, S. Ghosh, The methods of determination of critical micellar concentrations of the amphiphilic systems in aqueous medium, Arab. J. Chem. 4 (3) (2011) 265–270.

[106] G. Sugihara, M. Hisatomi, Roles of counterion binding in the micelle formation of ionic surfactants in water, J. Jpn. Oil Chem. ' Soc. 47 (7) (1998) 661–683.

[107] H. Piekarski, K. Łudzik, A microcalorimetric titration study on the micelle formation of alkanediyl-α, ω-bis (dimethylalkylammonium bromide) surfactants at a 283.15–343.15 K temperature range, J. Therm. Anal. Calorim. 110 (1) (2012) 263–271.

[108] W. Loh, C. Brinatti, K.C. Tam, Use of isothermal titration calorimetry to study surfactant aggregation in colloidal systems, Biochim. Et. Biophys. Acta (BBA)-Gen. Subj. 1860 (5) (2016) 999–1016.

[109] K. Beyer, D. Leine, A. Blume, The demicellization of alkyltrimethylammonium bromides in 0.1 M sodium chloride solution studied by isothermal titration calorimetry, Colloids Surf. B: Biointerfaces 49 (1) (2006) 31–39.

[110] C. Brinatti, L.B. Mello, W. Loh, Thermodynamic study of the micellization of zwitterionic surfactants and their interaction with polymers in water by isothermal titration calorimetry, Langmuir 30 (21) (2014) 6002–6010.

[111] S. Das, N. Patra, A. Banerjee, B. Das, S. Ghosh, Studies on the self-aggregation, interfacial and thermodynamic properties of a surface active imidazolium-based ionic liquid in aqueous solution: effects of salt and temperature, J. Mol. Liq. 320 (2020), 114497.

[112] K. Rajarathnam, J. Rösgen, Isothermal titration calorimetry of membrane proteins—progress and challenges, Biochim. Et. Biophys. Acta (BBA)-Biomembr. 1838 (1) (2014) 69–77.

[113] M. Osa, Y. Itoda, Y. Suzuki, T. Yumoto, A. Yoshida, A fluorescence probe study on the effects of surfactants on cloud points in aqueous poly (N-isopropylacrylamide) solutions, Polym. J. 47 (1) (2015) 59–65.

[114] N.P. Barry, B. Therrien, Pyrene: The guest of honor. Inorganic Nanoreactors, Academic Press, 2016, pp. 421–461.

[115] J.R. Ritter, M.J. Caldas, T.J. da Silva, A. Calzolari, M.D. McCluskey, Surface effects on pyrene luminescence excitation, ACS Appl. Electron. Mater. 2 (9) (2020) 2806–2812.

[116] A. Băran, G. Stîngă, D.F. Anghel, A. Iovescu, M. Tudose, Comparing the spectral properties of pyrene as free molecule, label and derivative in some colloidal systems, Sens. Actuators B Chem. 197 (2014) 193–199.

[117] T. Wu, J. Oake, Z. Liu, C. Bohne, N.R. Branda, Probing the microenvironments in a polymer-wrapped core–shell nanoassembly using pyrene chromophores, ACS Omega 3 (7) (2018) 7673–7680.

[118] P.A. Kralchevsky, K.D. Danov, S.E. Anachkov, G.S. Georgieva, K. P. Ananthapadmanabhan, Extension of the ladder model of self-assembly from cylindrical to disclike surfactant micelles, Curr. Opin. Colloid Interface Sci. 18 (6) (2013) 524–531.

[119] S. Wu, M. Tachiya, Z. Yan, An improved procedure for determination of the mean aggregation number of micelles, Spectrochim. Acta Part A Mol. Biomol. Spectrosc. 138 (2015) 807–810.

[120] R.G. Alargova, I.I. Kochijashky, M.L. Sierra, R. Zana, Micelle aggregation numbers of surfactants in aqueous solutions: a comparison between the results from steady-state and time-resolved fluorescence quenching, Langmuir 14 (19) (1998) 5412–5418.

[121] N.J. Turro, B.H. Baretz, P.L. Kuo, Photoluminescence probes for the investigation of interactions between sodium dodecylsulfate and water-soluble polymers, Macromolecules 17 (7) (1984) 1321–1324.

[122] B. Mandal, S.P. Moulik, S. Ghosh, Influence of aquo-organic solvent media on the self-aggregation of sodium dodecyl sulfate (SDS) and its interaction with polyvinylpyrrolidone (PVP), Colloid Polym. Sci. 292 (10) (2014) 2485–2495.

[123] S. Das, S. Mondal, S. Ghosh, Interaction of cationic gemini surfactant tetramethylene-1, 4-bis (dimethyltetradecylammonium bromide) with anionic polyelectrolyte sodium carboxymethyl cellulose, with two different molar masses, in aqueous and aquo-organic (isopropanol) media, RSC Adv. 6 (37) (2016) 30795–30803.

I&EC research
Industrial & Engineering Chemistry Research
pubs.acs.org/IECR
Article

Comparative Study of the Aggregation Behavior of Some Ionic Surfactants with Nonionic Triton X-114 in Water and a Water/2,2,2-Trifluoroethanol Mixture

Rajesh Banik, Bipin Bihari Mondal, Raju Sardar, and Soumen Ghosh*

Cite This: *Ind. Eng. Chem. Res.* 2024, 63, 3057−3071

ABSTRACT: The influence of 2,2,2-trifluoroethanol (TFE) on the micellar properties of ionic surfactants hexadecyltrimethylammonium bromide (CTAB), hexadecyltrimethylammonium *p*-toluenesulfonate (CTAT), sodium dodecyl sulfate (SDS), *N*-lauroylsarcosine sodium salt (SDDS), and nonionic surfactant Triton X-114 (TX-114) in aqueous solutions was studied using tensiometry, electrical conductivity, fluorimetry, time-resolved fluorescence, and microcalorimetry. With increasing concentrations of TFE, the micellar charge densities of the ionic head groups decrease, causing a decrease in the critical micelle concentration (CMC) of ionic-surfactant solutions (SDS, SDDS, CTAB, and CTAT) in micellar solutions. However, for nonionic surfactant TX-114, the polar headgroup undergoes some conformational changes causing an increase in the value of CMC. Time-resolved fluorescence decay measurements were done to get evidence of penetration of TFE molecules into the stern layer of the micelle. The micellar aggregation number declines with increasing concentration of solvent, indicating a higher concentration of mixed solvent reducing the number of monomers needed for micellization for ionic surfactants, whereas for nonionic TX-114, it indicates some structural changes of the molecule forming the micelle in the presence of TFE.

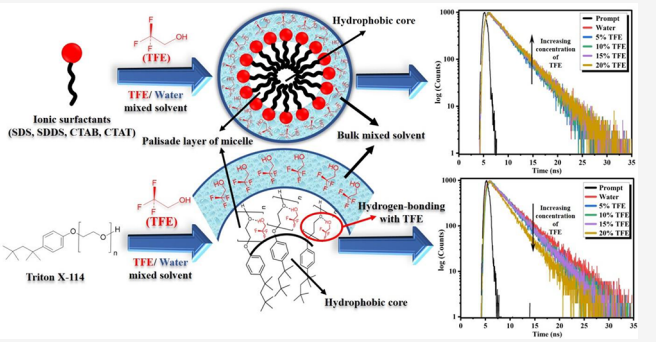

1. INTRODUCTION

In recent years, a broad community of surface chemists has shown a great deal of scientific interest in the physicochemical modifications of surface-active agents in an attempt to improve the functionality of surfactant formulations. In this context, various additives, including salts,[1] solvents,[2] polymers,[3] drugs,[4] etc., have been introduced to the micellar environment of amphiphilic systems to achieve the desired features with various industrial importance in cosmetics,[5] food products,[6] enhanced oil recovery,[7] and pharmaceuticals.[8] Among all the additives, nonaqueous alcohol solvents have been examined mostly in amphiphile-water-solvent ternary systems using both theoretical and experimental approaches.[9−17] The exceptional solubilizing and hydrogen bonding potential of alcohols distinguish them as solvents of choice.[18] Moreover, alcohols possess a dual character of serving as either cosurfactants or cosolvents as a motif to modify the critical micelle concentration (CMC) in the self-assembly of amphiphilic systems.[19] The present study has opted to use 2,2,2-trifluoroethanol (TFE), a fluorinated alcohol,[20,21] due to its great demand as a cosolvent in molecular biology, particularly during the denaturation process of proteins.[22,23] More importantly, TFE has been extensively reported in the literature in elucidation of the secondary structures of biological macromolecules, including polypeptides and proteins.[24,25] The presence of electron-withdrawing trifluoromethyl (CF_3) group in TFE imparts unique qualities as a solvent compared to other conventional alcohols.[26−28] TFE has the advantage of being highly soluble in water, irrespective of having a hydrophobic $-CF_3$ terminal. Fatima et al.[29] has performed a comparative analysis to investigate the effects of TFE and ethanol solvents on the thermal stability of an ionic liquid 1-ethyl-3-methylimidazolium dicyanamide ([EMIM]-[DCA]) in a TFE/ethanol binary mixture. TFE has been reported as a solvent medium in many organic synthesis reactions.[30,31] Nevertheless, there has not been substantial attention on surfactant aggregation in TFE solvent.[32,33]

Surfactants,[34,35] also known as surface-active agents, are widely recognized for their ability to self-assemble into various

Received: June 16, 2023
Revised: January 22, 2024
Accepted: January 22, 2024
Published: February 12, 2024

PCCP

ROYAL SOCIETY OF CHEMISTRY

PAPER

View Article Online
View Journal

Cite this: DOI: 10.1039/d4cp03264k

A physicochemical investigation of the complex formation by β-cyclodextrin with Triton X-100 and Triton X-114 and their aggregation behaviour in aqueous solution: an experimental approach

Rajesh Banik, Raju Sardar, Bipin Bihari Mondal and Soumen Ghosh *

The complexation behavior and binding affinity of Triton X-100 (TX-100) and Triton X-114 (TX-114) with β-cyclodextrin (β-CD) were extensively studied in an aqueous medium using a comprehensive suite of experimental techniques. These techniques allowed for the evaluation of key physicochemical parameters, including critical micelle concentration (cmc), aggregation number (N_{agg}), Stern–Volmer constant, and particle size distribution. These metrics were instrumental in understanding the underlying mechanism of the host–guest interaction between β-CD and Triton-X. Dynamic light scattering (DLS) data provided strong evidence for the formation of inclusion complexes, demonstrating significant hydrophobic interactions between the hydrophobic regions of Triton-X and the cavity of β-CD. The disruption of micellar structures, caused by β-CD encapsulating the hydrophobic moieties of the surfactants, was clearly observed. This process also resulted in an increased CMC, further underscoring the impact of β-CD on the aggregation behavior of the surfactants. To quantify the interaction, the Benesi–Hildebrand method was utilized to determine the stoichiometry and binding constants of the β-CD/Triton-X complexes. The results confirmed a well-defined 1 : 1 binding mode, indicating the precise incorporation of the surfactant's hydrophobic tails into the β-CD cavity while leaving the hydrophilic regions exposed to the aqueous environment. This selective binding mechanism alters the thermodynamics of micellization and disrupts the native micellar equilibrium of the surfactant systems. This systematic and comparative investigation is among the few studies that thoroughly examine the interactions between Triton-X surfactants and β-CD. Such research not only enhances our understanding of these complexes, but also reveals their significant potential for various applications. In drug delivery, for example, β-CD/Triton-X complexes can improve the solubility, stability, and bioavailability of hydrophobic drugs. In supramolecular chemistry, these complexes serve as model systems for studying host–guest interactions and self-assembly processes. Furthermore, their ability to modulate surfactant behaviour opens avenues for their use in material science, cosmetics, and industrial formulations, where precise control over micelle formation and aggregation is essential. This study underscores the versatility and utility of β-CD in interacting with non-ionic surfactants, offering insights that can be applied to other amphiphilic systems and paving the way for innovative applications in diverse fields.

Received 19th August 2024,
Accepted 23rd January 2025

DOI: 10.1039/d4cp03264k

rsc.li/pccp

Introduction

Cyclodextrins (CDs) are macrocyclic oligosaccharides which are linked by α-1,4glucosidic bonds.[1] Discovered by French chemist Antoine Villiers in 1891 as a potato-starch fermentation by-product, cyclodextrins are truncated cone-shaped oligosaccharides classified as α-, β-, or γ-CDs, containing six, seven, or eight α-(1–4) D-glucopyranose units, respectively. β-Cyclodextrin (β-CD), with seven glucose units, has a toroidal shape and a hydrophilic exterior.[2] Cyclodextrins possess unique structural properties that enable them to selectively bind organic molecules within their cavities, forming stable host–guest inclusion complexes with exceptional molecular and enantioselectivity.[3] These oligosaccharides have a cone-shaped structure with an internal cavity size ranging from 4 to 8 Å, depending on the number of glucose units in the macrocycle. The structure consists of two rims: the smaller, referred to as the primary rim or head, and the larger, known as the secondary rim or tail. The outer surface is hydrophilic due to the presence of hydroxyl (O–H) groups, while the inner cavity is hydrophobic, characterized by inward-oriented C–H bonds. Additionally, the non-bonding electron pairs of oxygen atoms in the glycosidic bonds

Centre for Surface Science, Physical Chemistry Section, Department of Chemistry, Jadavpur University, Kolkata-700032, West Bengal, India.
E-mail: gsoumen70@hotmail.com